PETROLOGY AND PETROGENESIS OF BATHOLITHIC ROCKS, SAN JACINTO MOUNTAINS, SOUTHERN CALIFORNIA

Thesis by

Robert Ian Hill

In Partial Fulfillment of the Requirements

for the Degree of

Doctor of Philosophy

California Institute of Technology

Pasadena, California

1984

(Submitted January 4, 1984)

ACKNOWLEDGEMENTS

First, thanks must go to Professor Leon T. Silver, without whose encouragement, scientific knowledge and enthusiasm, and, at times, patience, this project would not have been possible.

Dr B.W. Chappell at the Australian National University, Canberra, kindly provided major and trace element data for over 100 rock samples; this thesis benefited greatly from access to these data. Professor L.P. Gromet at Brown University kindly made available unpublished REE analyses for two rocks from the study area. Strontium and oxygen isotopic data presented herein were collected in the laboratories of Professors L.T. Silver and H.P. Taylor, Jr., respectively. L. Peter Gromet, Dolly Pearson, Gerry Silver, Victor Nenow, Rico Dagonel, Peter Larson, Dave Beaty, Sally Rigden and Art Chodos variously assisted with learning the use of the isotope laboratories and the electron microprobe. For their patience they deserve much thanks.

The California Department of Parks and Recreation kindly allowed sample collecting within Mount San Jacinto State Park. They and the United States Forest Service also deserve much gratititude for their excellent management of the "high country" of the San Jacintos. Working in this area has truly been a pleasure, and the unspoilt beauty of these mountains owes much to the management skills and enthusiasm of the personnel of these two often maligned agencies. The U.S. Forest Service and the Lake Hemet Municipal Water District kindly allowed access to lands normally closed to public entry.

Various people have contributed much through scientific discussion and suggestion. Professors L.T. Silver and H.P. Taylor, Jr., introduced the author to the geology, geochemistry and contradictions of the Peninsular Ranges batholith. Without the regional perspective allowed by their previous work this thesis would not have been possible. Stimulating discussion with Drs B.W. Chappell, W. Compston and D. Walker, introduced the author respectively to the problems of isotopic heterogeneity within single plutons, the implications allowed by major and trace element geochemical data, and the probable complexities of a recharging, crystallizing, assimilating and convecting(!) magma chamber.

Lastly, my sincere thanks go to my wife Sally for her encouragement and support throughout the progress towards this thesis.

Financial support for field and laboratory work was provided by NSF Grants EAR 76-23153 and EAR 77-23507 to Professor L.T. Silver; laboratory support was provided by DOE Contract DE-AC13-76 GJO 1664, Bendix Field Engineering Corporation sub-contract No. 79-384-E, and a grant from Atlantic Richfield Corporation in support of Professor L.T. Silver's research; and by NSF Grant EAR 78-16874 to Professor H.P. Taylor, Jr.. Support was also provided by a Conoco Fellowship and by the Division of Geological and Planetary Sciences, California Institute of Technology.

ABSTRACT

A combined field and laboratory study of plutonic rocks from the San Jacinto Mountains of southern California was conducted in order to investigate the nature and origins of strontium and oxygen isotope heterogeneities within batholithic rocks.

Geological mapping has allowed differentiation of three major and many minor masses of plutonic rock. Contacts between units are offset up to 6 km by faults of the Neogene San Jacinto fault system, which has a total right-lateral displacement of 29±1 km. The early small intrusives range from olivine gabbro through granite. They were intruded by three larger plutons of relatively homogeneous biotite-hornblende-titanite tonalite. The oldest major intrusive unit, Unit I, is an elongate body of dimensions 40x8 km. Before complete solidification it was intruded by Unit II, an irregular tabular mass 25 km long and a few kilometers wide. Unit III, in turn, intruded Unit II before it was completely solidified, producing a roughly rectangular mass 20x12 km that appears to funnel in downwards.

Mineral foliations and banding, schlieren, and xenolith orientations within each unit usually parallel the nearest contact. Alignment of foliations and apparent flow-sorting and scour features seem to reflect flow patterns within each chamber. Mafic synplutonic dikes (quartz diorite to tonalite) intruded into the tonalites, and were commonly broken up and redistributed as linearly extensive xenolith trains. From these relationships it is interpreted that: 1) magma adjacent to pluton walls had considerable yield strength, as it could fracture to allow dike emplacement; 2) magmatic flow adjacent to pluton walls was capable

of moving material some distances (up to km) to create the xenolith trains; and 3), that the dikes are potentially the feeders through which material was added to the inflating magma chambers. Each major tonalite unit spans a limited compositional range of from mafic tonalite (Colour Index > 15) to low-K granodiorite (Colour Index < 10). Volumetrically minor felsic differentiates extend the compositional range through to granodiorite. Units I and II average slightly more mafic overall compositions than does Unit III. All units are comprised of plagioclase (An_{30-40})[50-55%], quartz[20-30%], K-feldspar[1-8%], biotite [10-15%], hornblende[0-5%], titanite[0-2%] and accessory zircon, apatite, allanite and ilmenite. Variations in mineral abundances are geographically systematic only within Unit III, which grades from marginal mafic tonalite to central low-K granodiorite.

Mineral compositions throughout the major tonalites are remarkably uniform. The An content of the bulk plagioclase falls from $An_{40} \pm 1$ in the most mafic tonalites to An_{30} in low-K granodiorites; Mg/(Mg + Fe) of biotite and hornblende drop similarly from 0.44 to 0.36. The entire observed range of plagioclase compositions within the major tonalites is An_{44} to An_{25} (and to An_{47} in mafic xenoliths). The sole opaque mineral is almost pure ilmenite. This homogeneity of mineral compositions implies remarkable stability of physico-chemical conditions throughout crystallization of each unit.

Major and trace element abundances reflect the general homogeneity of these rocks. Most have SiO_2 in the range 63-68 wt.%; minor felsic differentiates extend to 71 wt.%. 60% of analyzed samples from Unit III fall in the restricted compositional range 66-68 wt.% SiO_2; the

majority of samples from Units I and II are more mafic than this. Major elements (excepting K_2O) define excellent linear arrays on Harker diagrams. K_2O shows a diffuse curvilinear pattern. Trace elements generally considered "compatible" (including the transition metals), and Sr also define linear arrays on Harker diagrams. Other trace elements, especially Ba, Rb, Pb, Th, U and REE show more complex behaviour. "Mafic" tonalites, (<65.5 wt.% SiO2) have simply covarying trace element endowments. Minor felsic differentiates, collected on the basis of field evidence for *in situ* fractionation, have higher Si, K, Rb, Ba, U and Th. "Normal" tonalites ($66.5<SiO_2<70.0$) have trace element and K endowments intermediate between the mafic tonalites and the felsic differentiates.

Mafic tonalites, comprising about half the exposed rocks, crystallized from liquids which derived their geochemical characteristics before injection into the high-level magma chambers. The minor felsic differentiates are considered end-products of fractional crystallization within the magma chamber; the "normal" tonalites are interpreted as crystallizing from liquids of intermediate character, *i.e.*, mixtures of "primitive" and fractionated liquids.

Measured primary $\delta^{18}O$ values vary from +9.0 to +10.6. Metasedimentary country rocks have $\delta^{18}O$ values of +11.5 to +13.5. Exchange of oxygen between plutons and country rock is minor and limited to narrow border zones. Within Unit III primary $\delta^{18}O$ correlates with position. A marginal zone of variable values (+9.0–+10.0) gives way to regularly increasing values (+10.0–+10.5) inwards. Primary $\delta^{18}O$ correlates with Colour Index. Within the central part of Unit III the observed range in $\delta^{18}O$ values can be explained by crystallization of modally variable rocks

from a liquid of constant $^{18}O/^{16}O$ (to±0.2 per mil). The $\delta^{18}O$ values of the more mafic marginal rocks (and of mafic rocks from Units I and II) also correlate with Colour Index; lower SiO_2 rocks have lower $\delta^{18}O$. This correlation cannot simply result from varying mineral abundances, but must reflect variations in $\delta^{18}O$ values of the liquids from which these rocks crystallized.

Calculated initial $^{87}Sr/^{86}Sr$ (Sr_i) varies substantially among rocks from each major tonalite unit (Unit I: 0.7060-0.7076; Unit II: 0.7060-0.7074; Unit III: 0.7058-0.7073). These variations appear geographically regular at the kilometer scale within each pluton. The complex patterns, however, differ fundamentally from the general regular west-to-east increase in Sr_i reported for the batholith (Early and Silver, 1973), and observed in the small early intrusives from the San Jacinto Mountains (0.7057-0.7077). Sr_i within these rocks shows no identified correlation with other geochemical and petrological parameters.

The Sr isotope data indicate that melt production, transport, and crystallization processes <u>combined</u> were not capable of completely homogenizing initial variations in Sr_i within the liquids from which these rocks crystallized. This further implies that <u>either</u> the time scale for convection was large compared to that for crystallization, or that the length scale for convection was small compared to the size of the plutons. Field evidence suggests considerable flow within the magma chamber; estimation of rheological parameters suggest that flow was within a laminar flow convective regime.

The combined observations are compatible with crystallization from an intermittently recharged, continuously fractionating system.

Recharge tended to buffer both the thermal and chemical properties of liquids within the magma chamber; it gave a mechanism for introducing isotopic variations that are incorporated into this continuously crystallizing system. The mafic dikes are suggested to be conduits through which some of these liquids were injected into the various magma chambers. Chemical buffering by continued recharge is also compatible with the observation that the majority of these rocks have geochemical features interpreted as resulting from the action of processes prior to injection of liquids into the high-level magma chambers.

Rocks with low Sr_i (0.7058-0.7068) generally have intermediate $\delta^{18}O$ values (+9.7-+10.3), and fall near the low-$\delta^{18}O$ side of the batholithic trend defined by Taylor and Silver (1978). Rocks with high Sr_i (>0.7072) cover the entire observed range in $\delta^{18}O$ values (+9.0-+10.6), and overlap the field defined for the San Jacinto - Santa Rosa Mountains block by Taylor and Silver. These data require involvement of material from three isotopically distinct source materials in the generation of these rocks. Two of these components (one with low Sr_i, low $\delta^{18}O$; one with high Sr_i, high $\delta^{18}O$) are common to the bulk of the batholith to the south and west. The third (high Sr_i, low $\delta^{18}O$) seems unique to the San Jacinto - Santa Rosa Mountains block; its relative importance within the San Jacinto rocks appears to correlate negatively with SiO_2, suggesting that it was associated with relatively mafic liquids. The oxygen isotopic data imply that as much as 35% of this component may be present in some rocks. This component has isotopic and inferred geochemical characteristics compatible with old, slightly enriched (in Rb relative to Sr) subcontinental lithosphere. The low-Sr_i, low-$\delta^{18}O$ component appears to be either (or both) normal depleted mantle or (subducted) oceanic crust.

The oxygen data imply that the third (high-Sr_i, high-$\delta^{18}O$) component has had a prior history at the Earth's surface; it could be either sediment, or igneous material altered at low temperatures such as hydrothermally altered oceanic crust. Geochemical features (K, Rb, LREE abundances) appear more compatible with sedimentary material.

These data are compatible with, but do not prove, a model for this source region as being a mixture of normal depleted mantle, oceanic crust, old slightly enriched "subcontinental lithosphere", and subducted sediment. This model source contains variously 0-35% (oxygen atom basis) subcontinental lithosphere, up to 25% sedimentary component, and apparently requires material of both basaltic (oceanic crust) and depleted mantle composition to balance isotope systematic systematics.

The combined data show 1) that the source volumes for the batholithic rocks were heterogeneous at the scale of hundreds of meters or greater, 2) that the effects of these source heterogeneities were at least partially preserved throughout melt production, transport, and crystallization, and 3) that the net effect of a persistent recharge - fractional crystallization process within the magma chambers was to buffer the composition of the bulk of the rock near that of the early-crystallizing solids.

TABLE OF CONTENTS

		Page
1	INTRODUCTION	1
	1.1 OVERVIEW	1
	1.1.1 SCOPE OF THIS PROJECT	4
	1.2 REVIEW	6
	1.2.1 ASYMMETRIC BATHOLITHS	6
	Transverse assymetries within the Peninsular Ranges Batholith	7
	1.2.2 ISOTOPIC VARIABILITY WITHIN A SINGLE PLUTON	10
	1.2.3 GRANITOIDS AS IMAGES OF THEIR SOURCE ROCKS	13
2	A RB, SR, AND $^{87}Rb/^{86}SR$ STUDY OF METASEDIMENTARY ROCKS, NORTHERN PENINSULAR RANGES	18
	2.1 INTRODUCTION	18
	2.2 GEOLOGY	19
	2.2.1 CALIFORNIA CONTINENTAL BORDERLAND	25
	2.2.2 VOLCANIC-VOLCANICLASTIC BELT	28
	2.2.3 SHALE-SANDSTONE BELT	30
	2.2.4 EASTERN QUARTZ-RICH SEQUENCES	34
	2.3 RB-SR GEOCHRONOLOGY OF SEDIMENTARY ROCKS	39
	2.3.1 STRONTIUM ISOTOPE DATA AS A DISCRIMINANT BETWEEN SEDIMENTARY UNITS	43
	2.3.2 METAMORPHIC EFFECTS	43
	2.4 RB, SR, AND $^{87}SR/^{86}SR$ WITHIN PRE-BATHOLITHIC ROCKS OF THE PENINSULAR RANGES	51
	2.4.1 PREVIOUS WORK	51
	2.4.2 SAMPLING AND ANALYTIC PROCEDURES	53
	2.5 RESULTS	57
	2.5.1 METAMORPHIC EFFECTS	57
	2.5.2 RELATIVELY NON-RADIOGENIC GROUP	61
	South of the San Jacinto Fault	61
	Alisitos Formation	61

Shale-Sandstone and Graywacke Sequences of Northern Batholith 61
Northeast of the San Jacinto Fault 66
2.5.3 RELATIVELY RADIOGENIC GROUP 67
Samples from the Upper Plate Assemblage 67
Samples from the Lower Plate Assemblages 68

2.6 DISCUSSION 75

2.6.1 REGIONAL IMPLICATIONS 76
2.6.2 STROTIUM ISOTOPE DATA FROM PRE-CENOZOIC SEDIMENTARY AND METASEDIMENTARY ROCKS OF WESTERN NORTH AMERICA 77
2.6.3 POSSIBLE CORRELATIVES OF THE NON-RADIOGENIC ("?MESOZOIC") GROUP 79

2.7 CONCLUSIONS 83

3 GEOLOGY OF THE SAN JACINTO MOUNTAINS
PART I: PREVIOUS WORK AND STRATIGRAPHY 86

3.1 INTRODUCTION 86

3.2 PREVIOUS WORK 89

3.3 ROCK UNITS 92

3.3.1 PRE-BATHOLITHIC ROCKS 92
3.3.2 WINDY POINT METAMORPHICS 93
Distribution 93
Lithology 94
Protolith 95
Age 95
3.3.3 DESERT DIVIDE GROUP 96
Distribution 96
Lithology 97
Metamorphic Conditions 98
Protolith 106
Age 106
3.3.4 RELATIONS BETWEEN THE WINDY POINT METAMORPHICS AND THE DESERT DIVIDE GROUP 106

3.4 BATHOLITHIC ROCKS 107

3.4.1 EARLY INTRUSIVES 107
Olivine Gabbro of Thomas Mountain 108
Quartz Diorite of Lucky Deer Mine 109
Tonalite of Herkey Creek 110
Tonalite of Snow Creek 111
Granodiorite of Poppet Creek 112
Granodiorite of Apple Canyon 114
Granite dike, Little Thomas Mountain 115

Granite of Penrod Canyon 115
3.4.2 LATE TONALITES 116

3.5 TERTIARY DEPOSITS 120

3.5.1 MOUNT EDEN FORMATION 121
3.5.2 TERRESTRIAL SEDIMENTARY DEPOSITS 121

3.6 QUATERNARY DEPOSITS 126

3.6.1 POSSIBLE QUATERNARY GLACIAL DEPOSITS 126
3.6.2 ACTIVE ALLUVIAL MATERIALS 127

4 GEOLOGY OF THE SAN JACINTO MOUNTAINS
PART II: STRUCTURE 128

4.1 INTRODUCTION 128

4.1.1 STRUCTURAL SETTING 129

4.2 YOUNG (POST-BATHOLITHIC) STRUCTURES 133

4.2.1 THE SAN JACINTO FAULT SYSTEM 134
San Jacinto Fault 136
Hot Spring Fault 136
Thomas Mountain and related faults 137
Un-named faults 139
Total displacement across the San Jacinto Fault system 140
Timing of motion 141
Development of Garner Valley as a pull-apart basin 142
4.2.2 LAWRENCE FAULT 148
4.2.3 SOUTH BOUNDING FAULT OF BANNING PASS 149
4.2.4 POTRERO FAULT FIELD 150

4.3 A PRE-TERTIARY RECONSTRUCTION OF THE SAN JACINTO MOUNTAINS 150

4.4 EASTERN PENINSULAR RANGES MYLONITE ZONE 150

4.5 PRE-BATHOLITHIC STRUCTURES 155

4.5.1 WINDY POINT METAMORPHICS 155
4.5.2 DESERT DIVIDE GROUP 156

4.6 IGNEOUS STRUCTURES 157

4.6.1 EXTERNAL AND CONTACT RELATED STRUCTURES 157
Contact relations of early intrusives 165
4.6.2 INTERNAL STRUCTURES 168
Igneous foliations and lineations 168

Schlieren and other mineral layering 171
Xenoliths 176
Dikes and sills intruding the major tonalite plutons 181
Mafic dikes 181
Aplites 184
Pegmatites 184
Feldspar-rich mafic tonalites 184
K-feldspar granodiorite dikes 185

4.7 RELATIONSHIP OF MAFIC DIKES AND XENOLITHS 185

4.8 DISCUSSION 192

4.8.1 GEOMETRIC RELATIONS OF FOLIATIONS AND LINEATIONS WITHIN INDIVIDUAL INTRUSIVES 193
Unit I 193
Unit II 193
Unit III 196

5 GEOLOGY OF THE SAN JACINTO MOUNTAINS
PART III: PETROGRAPHY OF IGNEOUS ROCKS 201

5.1 INTRODUCTION 201

5.2 EARLY INTRUSIVES 201

5.2.1 QUARTZ DIORITE OF LUCKY DEER MINE 201
5.2.2 TONALITE OF HERKEY CREEK 204
5.2.3 TONALITE OF SNOW CREEK 207
5.2.4 TONALITES AND GRANODIORITES NORTHEAST OF TAHQUITZ PEAK 207
5.2.5 GRANODIORITE OF POPPET CREEK 208
Petrographic peculiarities of the granodiorite of Poppet Creek 213
5.2.6 PORPHYRITIC GRANODIORITE OF APPLE CANYON 214
5.2.7 GRANITE DIKE FROM LITTLE THOMAS MOUNTAIN 216
5.2.8 GRANITE OF PENROD CANYON 216

5.3 MAJOR TONALITES 221

5.3.1 TITANITE DISTRIBUTIONS AND TEXTURAL RELATIONSHIPS 231
5.3.2 MINERAL PARAGENESES WITHIN THE MAJOR TONALITES 242
5.3.3 XENOLITHS AND DIKE ROCKS 243

5.4 SUMMARY 252

6 MINERAL CHEMISTRY 255

6.1 INTRODUCTION 255

6.2 MINERAL COMPOSITIONS AND TEXTURAL RELATIONS 257
6.2.1 PLAGIOCLASE 257
6.2.2 K-FELDSPAR 264
6.2.3 BIOTITE 266
6.2.4 HORNBLENDE 266
6.2.5 TITANITE 280
6.2.6 ILMENITE 282
6.2.7 APATITE 289
6.2.8 ALLANITE-EPIDOTE 291

6.3 CONCLUSIONS 291

7 GEOCHEMISTRY 294

7.1 INTRODUCTION 294

7.2 ANALYTICAL PROCEDURES 295

7.3 ANALYTICAL RESULTS 298

7.3.1 MAJOR TONALITES 317
Trace elements 322
Felsic "differentiates" 327
Na, Ca, and Sr - elements associated with feldspars 330
Biotite - K, Rb, and Ba 336
Elements controled by a polymineralic assemblage - Ti, V 351
Rare earth element behavior 355

7.4 EARLY INTRUSIVES 362

7.5 SAMPLES FROM NORTH AND EAST OF TAHQUITZ PEAK, AND THE ROLE OF SEDIMENT CONTAMINATION 363

7.6 SUMMARY 364

8 OXYGEN ISOTOPE RESULTS 366

8.1 INTRODUCTION 366

8.2 RESULTS 367

8.2.1 ANALYTIC PROCEDURES 367

8.3 DISCUSSION 369

8.3.1 METAMORPHIC EFFECTS 369

8.3.2 PRIMARY IGNEOUS $^{18}O/^{16}O$ 381

8.4 ORIGIN OF THE $\delta^{18}O$ CHARACTERISTICS OF THE SAN JACINTO ROCKS 386

8.4.1 $^{18}O/^{16}O$ VARIATIONS IN IGNEOUS ROCKS 386
8.4.2 CAUSES OF PRIMARY $^{18}O/^{16}O$ VARIATIONS IN IGNEOUS ROCKS 389
Fractionation processes 389
8.4.3 $^{18}O/^{16}O$ VARIATIONS IN THE PENINSULAR RANGES BATHOLITH 395
8.4.4 δ^{18} O IN SAN JACINTO ROCKS 404

8.5 CONCLUSIONS 412

9 STRONTIUM ISOTOPE RESULTS 416

9.1 INTRODUCTION 416

9.1.1 SAMPLING PROCEDURES 417

9.2 STRONTIUM ISOTOPIC RESULTS 420

9.3 DISCUSSION 424

9.3.1 INTRUSIVE - WALL-ROCK INTERACTION 430
9.3.2 RB AND SR CONCENTRATIONS, AND RB-SR COVARIATION 434

9.4 OBSERVATIONS ON INITIAL STRONTIUM ISOTOPE COMPOSITION 449

9.4.1 POSSIBLE SOURCES OF ERROR IN CALCULATION OF SR_i 450
9.4.2 GEOGRAPHICAL VARIATION OF SR_i 468
9.4.3 RELATION OF SR_i TO $^{87}RB/^{86}SR$ AND SR CONCENTRATION 471

9.5 COMPARISON OF RB, SR, AND $^{87}SR/^{86}SR$ DATA FROM THE SAN JACINTO MOUNTAINS WITH DATA FROM THE REST OF THE PENINSULAR RANGES BATHOLITH 482

9.6 CONCLUSIONS 494

10 SUMMARY OF DATA FROM THE SAN JACINTO MOUNTAINS AND ADJOINING REGION IMPORTANT IN CONTRAINING BATHOLITH DEVELOPMENT 498

10.1 INTRODUCTION 498

10.1.1 GEOLOGICAL AND PETROGRAPHIC OBSERVATIONS 499
10.1.2 GEOCHEMICAL OBSERVATIONS 501
10.1.3 ISOTOPIC DATA 505
10.1.4 REGIONAL CONSIDERATIONS 507

11 MAGMA CHAMBER PROCESSES 511

11.1 INTRODUCTION 511

11.2 RHEOLOGICAL AND MINERAL PROPERTIES OF CRUSTAL MAGMA CHAMBERS 514
Density 514
Viscosity 514
Yield Strength 516
Rheological Parameters 520

11.3 PHYSICO-CHEMICAL CONSIDERATIONS 522
Possible kinetic control of trace element partitioning 522
Crystallization Rate 528
Diffusivity 528
Equilibrium distribution coefficients 529

11.4 MODELLING TRACE ELEMENT BEHAVIOUR IN SILICATE LIQUIDS 534

11.4.1 MODELLING TRACE ELEMENT BEHVIOUR DURING CRYSTALLIZATION 536

11.4.2 LINEAR ELEMENT-ELEMENT COVARIATIONS IN CALC-ALKALINE ROCKS 538

11.5 APPLICATIONS TO THE SAN JACINTO IGNEOUS COMPLEX 540

11.6 CONCLUSIONS

12 PETROGENESIS OF BATHOLITHIC ROCKS, SAN JACINTO MOUNTAINS 557

12.1 INTRODUCTION 557

12.2 REVIEW OF WORK PERTINENT TO UNDERSTANDING THE GENESIS OF THE CALC-ALKALINE ROCK SUITES 558

12.2.1 OCEANIC AND CONTINENTAL MARGIN ARCS 558
A-, I-, and S- type granites 561
Domains, suites and series - the case for uniqueness of segments of an arc 562
12.2.2 GEOCHEMISTRY 563
Major and trace element abundance patterns 563

Isotope geochemistry 566
Strontium 566
Lead 569
Neodymium 573
Oxygen 578
12.2.3 EXPERIMENTAL PETROLOGY 580
12.2.4 MASS BALANCE CONSIDERATIONS 584
12.2.5 CONCLUSIONS 587

12.3 A MODEL FOR THE GENERATION OF IGNEOUS ROCKS OF THE SAN JACINTO MOUNTAINS 590

12.3.1 IMPLICATIONS FOR TRACE ELEMENT ABUNDANCES OF DERIVATIVE LIQUIDS 603

12.4 CONCLUSIONS 612

REFERENCES CITED 616

APPENDIX 1: ANALYTICAL PROCEDURES 647

APPENDIX 2: LOCATIONS AND DESCRIPTIONS OF META-SEDIMENTARY ROCK SAMPLES 649

APPENDIX 3: USE OF GRID REFERENCES 652

APPENDIX 4: COMPARISON OF ALTERNATE METHODS (ID, XRF) FOR DETERMINATION OF RB AND SR 653

TABLES

		Page
2.1	Rb, Sr and $^{87}Sr/^{86}Sr$ data for metasedimentary wall rocks, northern Peninsular Ranges batholith	56
3.1	Metamorphic mineral assemblages, Desert Divide Group	100
3.2	Microprobe analyses of selected minerals from sample SCB 747D	101
3.3	Microprobe analyses of selected minerals from sample SCB 747A	102
4.1	Estimated displacements across individual strands of the San Jacinto fault zone	140
5.1	Modal data for quartz diorite of Lucky Deer Mine	202
5.2	Modal data for tonalite of Herkey Creek	205
5.3	Modal data for granodiorite of Poppet Creek	209
5.4	Modal data for granodiorite of Apple Canyon	215
5.5	Modal data for granite of Penrod Canyon	217
5.6	Modal data for major tonalites	222
5.7	Modal data for a mafic xenolith and a mafic dike	245
6.1	Microprobe analyses for selected feldspars	260
6.2	Microprobe analyses for selected feldspars	265
6.3	Representative microprobe analyses of biotite	267
6.4	Representative microprobe analyses of hornblende (1)	272
6.5	Representative microprobe analyses of hornblende (2)	272
6.6	Electron microprobe analyses of titanite	283
6.7	Microprobe analyses of ilmenite-hematite	286
6.8	Electron microprobe analyses of apatite	290
6.9	Microprobe analyses of allanite-epidote	292

		Page
7.1	Comparison of duplicate analyses of LTS 152	297
7.2	Analytical data for Unit I	300
7.3	Analytical data for mafic xenoliths from Unit I	302
7.4	Analytical data for Unit II	303
7.5	Analytical data for Unit III	304
7.6	Analytical data for two marginal samples from Unit III	307
7.7	Analytical data for four mafic xenoliths from Unit III	308
7.8	Analytical data for a mafic dike intrusive into Unit III	309
7.9	Analytical data for the tonalite of Snow Creek	310
7.10	Analytical data for the granodiorite of Poppet Creek	311
7.11	Analytical data from five early intrusives	312
7.12	Analytical data for the granite of Penrod Canyon	313
7.13	Analytical data for samples east and northeast of Taquitz Rock	314
7.14	Analytical data for metasediments of the Desert Divide Group	315
7.15	Analytical data for metasediments of Windy Point	316
7.16	Calcium apportionment among the phases	331
7.17	Apportionment of K and Rb between mineral phases	337
7.18	Analytical data for rare earth elements	356
8.1	Oxygen isotope analyses	370
8.2	Mineral-mineral fractionations for the Bonsall Tonalite	407
9.1	Sr isotopic analyses of igneous country rocks	421

		Page
9.2	Sr isotopic analyses of contaminated rocks, Red Taquitz area	431
9.3	Rb, Sr and $^{8}/Sr/^{8}$ Sr data for minerals	452
9.4	Regression analyses of Rb/Sr and Sr isotopic data	483
11.1	Calculated liquid densities for three San Jacinto rock compositions	515
11.2	Estimates of crystallization rate for Unit III	528
12.1	Strontium isotopes in volcanic rocks from converging plate margins	567
12.2	Parameters used in mixing model calculations	596
12.3	Comparison of sedimentary composites from the French Valley Fm. (PRB) and the "Calaveras" (SNB)	598
12.4	Geochemical parameters of a 50:25:25 mix of depleted mantle, oceanic crust, and model subducted sediment	601
12.5	Assumed REE concentrations for model components	604
12.6	Typical values for partition coefficients	608

FIGURES

		Page
1.1	Mesozoic and Early Cenozoic batholithic rocks of western North America	2
1.2	Distribution of igneous rocks of the Peninsular Ranges batholith and older igneous and metamorphic rocks	3
2.1	Lithotectonic belts of the northern Peninsular Ranges and adjacent Sonora, palinspastic base	20
2.2	Index to locations mentioned in text	22
2.3	Summary of age relations within Peninsular Ranges and some adjoining geological provinces	26
2.4	Isochron diagram showing results from several published Rb-Sr studies on shales	44
2.5	An example of metamorphic resetting of Rb-Sr isotopic systems	47
2.6	Diagram illustrating systematics of metamorphic resetting of Rb-Sr isotopic systems	49
2.7	Sample locations	54
2.8	Isochron diagram showing data from this study	58
2.9	Isochron diagram showing inferred metamorphic redistribution in schist samples	60
2.10	Summary of Rb-Sr isotopic data from Mesozoic and inferred Mesozoic metasedimentary sequences from the northern Peninsular Ranges	62
2.11	Isochron diagram for three rocks from the Coyote Mountains	69
2.12	Isochron diagram for eleven samples from the San Jacinto Mountains	70
2.13	Diagrammatic stratagraphic column for metasedimetary rocks of the Desert Divide	73
3.1	Previous geological studies in the San Jacinto Mountains	91

3.2	Pressure-temperature grid showing inferred metamorphic conditions for San Jacinto rocks	104
3.3ab	Photomicrographs of igneous and metamorphic glass in terrestrial sedimentary deposits	122
4.1	Structural setting of the San Jacinto Mountains	130
4.2	Located earthquake epicenters in San Jacinto Mountains region	131
4.3	Mapped and inferred faults in San Jacinto Mountains region	135
4.4	Simplified geological map of Garner Valley and vicinity	144
4.5	Schematic illustration of model for development of Garner Valley as a pull-apart basin	146
4.6	Palinspastic reconstruction of the San Jacinto Mountains prior to tertiary faulting	151
4.7	Map showing eastern Peninsular Ranges mylonite zone	153
4.8	Attitudes of imposed foliations within rocks other than major tonalites, palinspastic base	158
4.9ab	Photographs showing contact relations between Unit III and metasedimentary country rocks	160
4.10	Geologic map of the northeastern contact of Unit I	162
4.11ab	Photographs of contact relations within the early intusives	166
4.12	Summary of structural data for the major tonalite units	169
4.13	Textural photograph of mafic tonalite	170
4.14	Representative examples of Schleiren and mineral banding	172
4.15	Representative examples of mineral layering	174
4.16	Mineral layering in dike rock	177
4.17	Representative examples of xenolith trains	179
4.18	Mafic dike intruding low-K granodiorite	183
4.19	Plagioclase-rich dike cutting mafic tonalite	186

4.20	Synplutonic dike intruding xenolith rich tonalite of Unit III	187
4.21ab	Stages of disaggregation of a mafic dike	188
4.22abcdef	Diagrammatic illustration of inferred relationship between mafic dikes and xenolith trains	190
4.23ab	Double foliation within Unit I tonalite	194
4.24	Flat-lying pegmatite sheets within roof-zone of Unit III	197
4.25	Exploded block diagram of San Jacinto major tonalite, Unit III	199
5.1	Classification of early intrusives	203
5.2	Photomicrograph of granite of Penrod Canyon	218
5.3	Classification of five representative major tonalite samples	223
5.4ab	Photographs illustrating range of varition within major tonalites	224
5.5	Hornblende and biotite abundances of major tonalites	227
5.6	Intergrown hornblende and titanite in sample LTS 360	229
5.7	Photomicrograph of textural relatins between plagioclase, quartz, allanite and K-feldspar, sample LTS 217	230
5.8ab	Illustrative examples of textural relations of allanites from major tonalites	233
5.9ab	Illustrative examples of textural relations of titanites from mafic tonalites	236
5.10ab	Illustrative examples of textural relations of titanites from mafic tonlites	238
5.11ab	Photomicrographs of a typical mafic xenolith	246
5.12ab	Photomicrographs of a mafic dike	248
6.1	Histograms of plagioclase composition for eleven rocks and two xenoliths	258
6.2	Triangular diagram plot of analyzed plagioclases and K-feldspars	262

6.3	Histograms of $Mg/(Mg+Fe^{2+}+Mn)$ for analyzed mafic minerals	268
6.4	Histograms of $Fe^{3+}/(Fe^{2+}+Fe^{3+})$ for amphiboles from samples LTS 290 and LTS 291	274
6.5ab	Al^{IV} versus (Na+K) and $(Al^{VI}+Fe^{3+}+Ti)$ for selected amphiboles from the San Jacinto Mountains	276
6.6	$Mg/(Mg+\Sigma Fe+Mn)$ for analyzed hornblendes, biotites and a single chlorite	281
6.7	Structural Al versus F for analysed titanites	284
6.8	Ilmenite analyses plotted in the TiO_2-(Fe,Mn)O-$1/2Fe_2O_3$ triangle	287
6.9	Ilmenite analyses plotted in the $(Mn,Mg)TiO_3$-$FeTiO_3$-Fe_2O_3 triangle	288
7.1	Harker variation diagrams for K_2O	299
7.2	Harker variation diagrams for selected major elements, major tonalite units	318
7.3	Histogram showing distibution of SiO_2 abundance	320
7.4	Harker variation diagrams for selected trace elements	325
7.5	Harker variation diagrams for selected trace elements	326
7.6	Harker variation diagrams for selected trace elements	327
7.7	K_2O versus Rb, Ba, TiO_2 and Zr	328
7.8	Sr-Ca variation for major tonalites	334
7.9ab	Biotite-Rb (a) and Biotite-K_2O (b) variation for major tonalites	338
7.10	K/Rb versus K_2O for major tonalites	340
7.11	Rb versus K_2O showing available mineral data	344
7.12ab	K_2O-Rb (a) and K_2O-U variation for major tonalites	349
7.13	U-Th variation for major tonalites	352
7.14	REE patterns for two rocks from major tonalites	358
7.15	Ce/Y-Ce variation for major tonalites	360
8.1	Location of analysed samples	372

8.2	Histogram of observed $\delta^{18}O$ values	374
8.3	Illustration of plagioclase-mineral and plagioclase-water oxygen isotope fractionation as a function of temperature	377
8.4	Geographic distribution of measured $\delta^{18}O$ values	382
8.5	Correlation between Colour Index and measured $\delta^{18}O$ for tonalites and low-K granodiorites	384
8.6	Observed $\delta^{18}O$ values of igneous rocks for a wide variety of localities	387
8.7	Relationship between $\delta^{18}O$ and percent solidified for a simple Rayleigh distillation model	390
8.8	Histogram of $\delta^{18}O$ values for rocks of the northern Peninsular Ranges batholith	397
8.9	Contoured $\delta^{18}O$ values for the northern Peninsular Ranges batholith	398
8.10	Contoured $\delta^{18}O$ values for the northern Peninsular Ranges batholith (palinspastic base)	400
8.11	Correlation of Sr_i and $\delta^{18}O$ for the northern Peninsular Ranges batholith	402
8.12	Colour Index versus $\delta^{18}O$ for altered rocks from the San Jacinto Mountains	409
9.1	Regional variation of Sr_i in the Peninsular Ranges batholith	418
9.2	Location of samples analysed for Sr isotopes	426
9.3	Histogram of Sr_i San Jacinto Mountains samples	428
9.4	Histogram of Sr and Rb concentrations, San Jacinto Mountains	432
9.5	Geographic distribution of Rb and Sr, palinspastic base	433
9.6	Contoured Sr concentration for Unit III	437
9.7	Rb versus Sr: all data from San Jacinto Mountains	438
9.8	Rb-Sr diagram for Unit I	440
9.9	Rb-Sr diagram for Unit II	442

9.10	Rb-Sr diagram for Unit III	444
9.11	Isochron diagram for mineral data from two rocks	454
9.12	Calculated Sr_i for San Jacinto igneous rocks	458
9.13	Contoured Sr_i (at 97 m.y.) for early intrusives	460
9.14	Contoured Sr_i for Unit I	462
9.15	Contoured Sr_i for Unit II	464
9.16	Contoured Sr_i for Unit III	466
9.17	Geographic variation in Sr content for Unit III	470
9.18	Calculated Sr_i versus Sr concentration, major tonalites	472
9.19	Sr_i versus Sr for Unit I	474
9.20	Sr_i versus Sr for Unit II	476
9.21	Sr_i versus Sr for Unit III	478
9.22	Isochron diagram for San Jacinto samples	480
9.23	Sr_i versus $\delta^{18}O$, San Jacinto Mountains	486
9.24	Sr_i versus $\delta^{18}O$, Peninsular Ranges batholith	488
9.25	Sr_i versus $\delta^{18}O$, San Jacinto samples and remainder of Peninsular Ranges batholith	490
11.1	Viscosity of orogenic andesite as a function of T	517
11.2	Relationship of particle radius, density contrast, and yield strength	518
11.3	Variation of apparent distribution coefficient (K^*) with the function $V\delta/D$	526
11.4	Interrelationship of chemical diffusivity, K^*, and the function $V\delta/D$	530
11.5	An RFC model for Rb-Sr behaviour in the San Jacinto rocks	542
11.6ab	Variation of Ce/Y with Ce	544
11.7	Variation of K/Rb with Rb	548
11.8	Sr_i versus K_2O	550

11.9	Sr_i versus Sr	552
12.1	Chemical composition of andesite	564
12.2	Lead isotopic composition of selected Cenozoic andesite suites	570
12.3	Isotopic composition of Nd for rocks from various tectonic environments	574
12.4	$\varepsilon_{Nd} - \varepsilon_{Sr}$ diagram for the Peninsular Range and Sierra Nevada batholiths	576
12.5	Diagram showing in cartoon form a model for the origin of the igneous rocks of the San Jacinto Mtns	592
12.6	$\varepsilon_{Nd} - \varepsilon_{Sr} - \delta^{18}O$ for mixtures of depleted mantle, oceanic crust, and model subducted sediment	594
12.7ab	Assumed REE patterns for model source components (a), and for various mixtures (b)	605
12.8ab	REE patterns for liquids derivative from partial fusion, showing effects of differing residues	606
12.9ab	REE patterns for liquids derivative from fractional crystallization	610
A4.1	Comparison of ID and XRF data for Sr	654
A4.2	Comparison of ID and XRF data for Rb	656

CHAPTER 1

INTRODUCTION

1.1 OVERVIEW

An understanding of the origin of the great continental batholiths of the world is fundamental to the development of theories on the nature and origin of the continental crust. It has been suggested (e.g., Taylor, 1967, 1979) that island arcs are the major sites of formation of new continental crust. The continental batholiths, in contrast, have been inferred to largely involve the reprocessing of existing continental material (e.g., Gast, 1960; White and Chappell, 1977; DePaolo, 1981b). Many basic problems remain, however, and it is towards the elucidation of several of these that this thesis is addressed.

The area chosen for this study, the San Jacinto Mountains, lies at the northeastern extremity of the Peninsular Ranges about 100 km east of Los Angeles (Fig. 1.1). The igneous rocks exposed in the San Jacinto Mountains are part of the Late Mesozoic Peninsular Ranges batholith of southern and Baja California (Fig. 1.2). These rocks were chosen for a detailed geological-petrological-geochemical-isotopic study because:-

1. A regional context of geological, petrological, geochemical, isotopic and age relations is well understood following the work of L.T. Silver and his colleagues, and contributions by numerous other investigators (e.g., Larsen, 1948; Baird et al., 1974a,b, 1979; Gastil et al., 1975; Dibblee, 1981a).

2. This previous work suggested that the San Jacinto Mountains had some geochemical and isotopic characteristics intermediate between

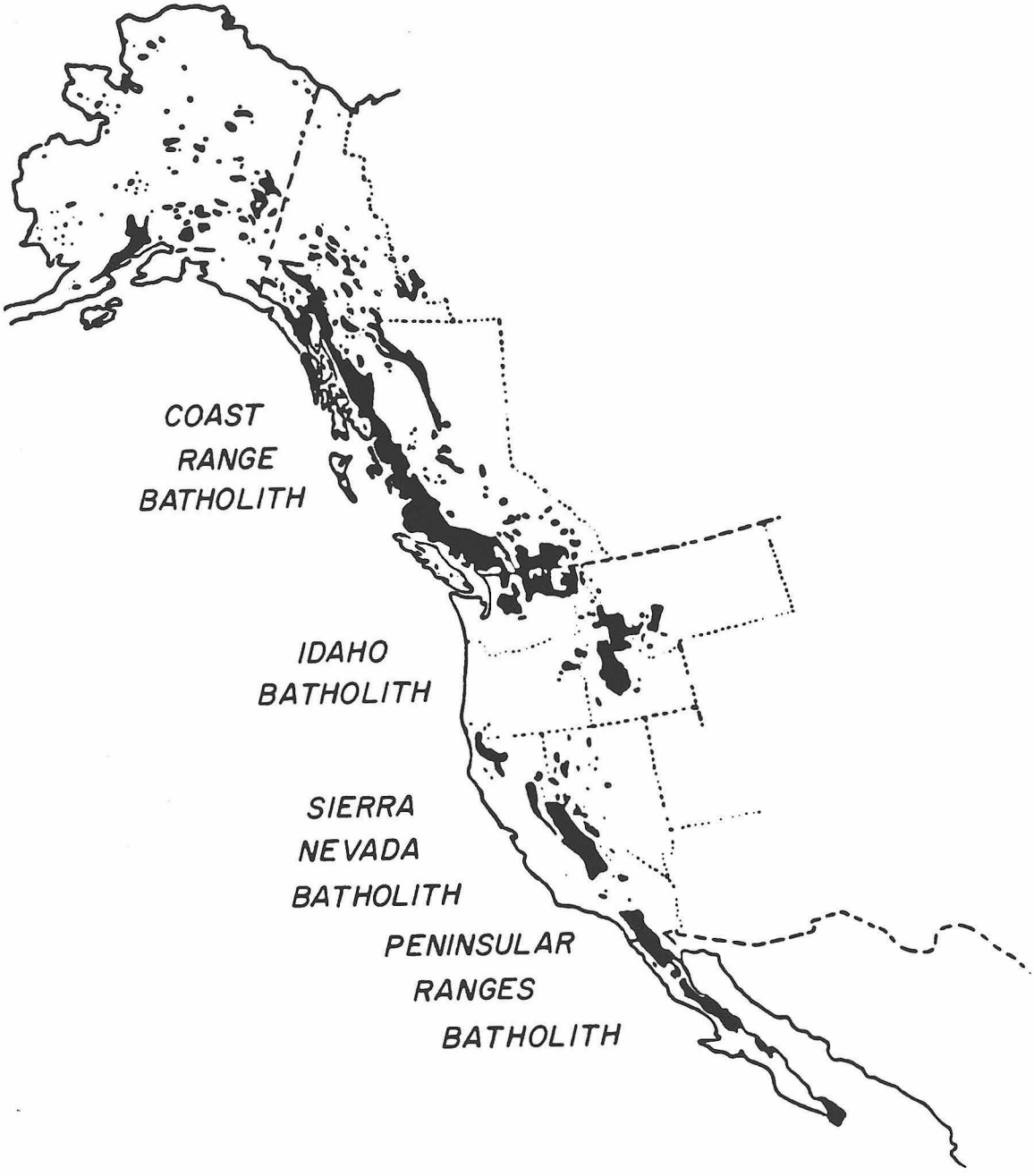

Figure 1.1. Mesozoic and Early Cenozoic batholithic rocks of western North America.

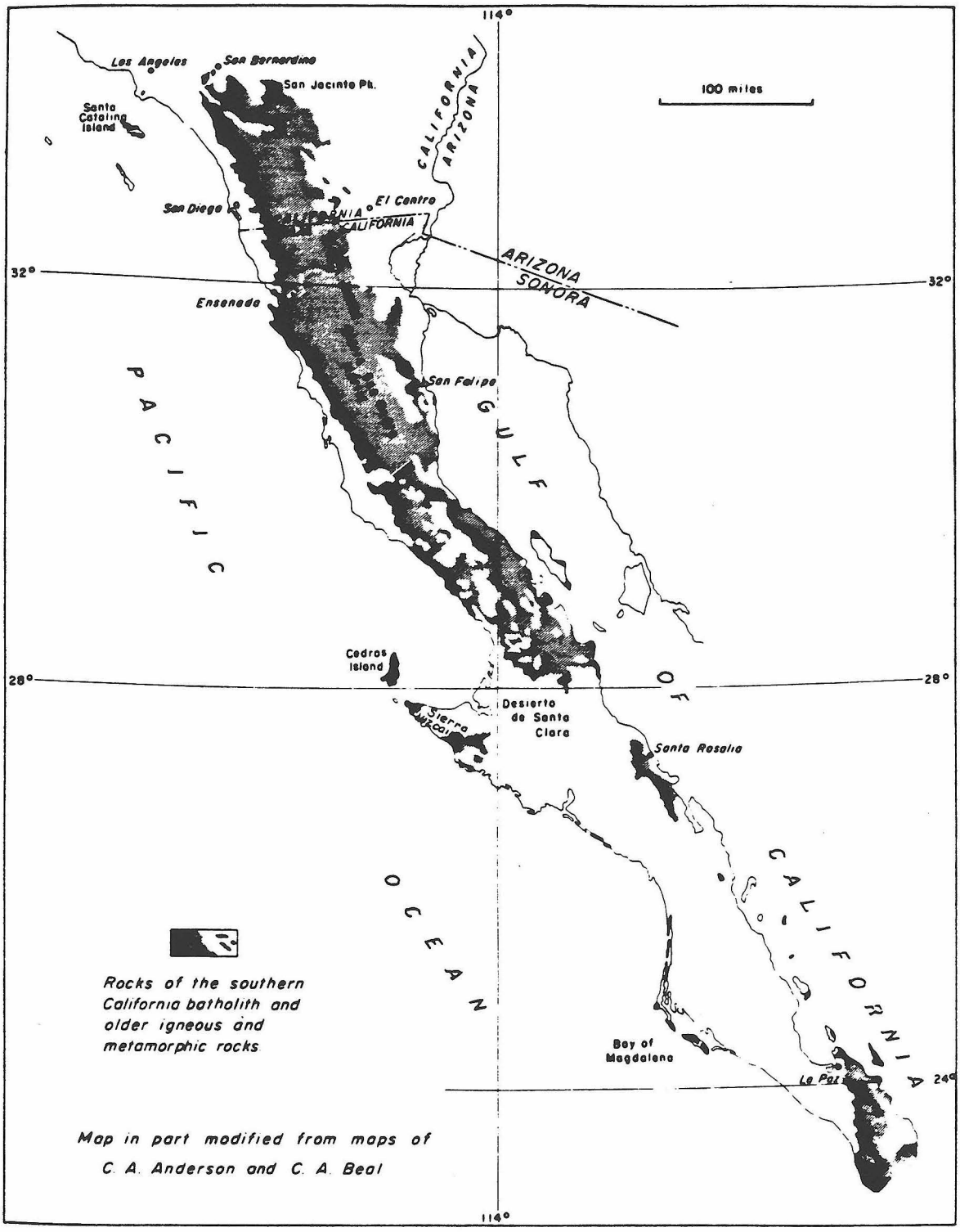

Figure 1.2. Distribution of igneous rocks of the Peninsular Ranges batholith and older igneous and metamorphic rocks (Jahns, 1954).

those of the main part of the Peninsular Ranges batholith to the south, and of the Sierra Nevada batholith 200 km to the north.

3. The large amount of relief within the San Jacinto Mountains (>3,000 meters) afforded an excellent opportunity to obtain three-dimensional details on the relationships both within and between plutons in considerable detail.

Three problems were specifically addressed from the beginning of the study. First, are there variations in the the isotopic properties of a single intrusive unit at the time of emplacement? If so, can these heterogeneities be used to constrain models of magma transport and magma chamber processes? Second, could detailed study of one or a few plutons within a well-constrained regional context be used to understand the genesis of those studied plutons? This question leads to the third problem addressed - how does the genesis of the studied plutons relate to the origin of the rest of the batholith, and to the tectonic environment prevailing at the time of magma generation and emplacement?

This chapter introduces these problems and gives a brief summary of work pertinent to the development of current understanding. For each subject delineated a rationale for development within the context of the present study is then outlined.

1.1.1 SCOPE OF THIS PROJECT

This thesis is comprised of three closely related parts. In an effort to better understand regional relationships within the metasedimentary wall rocks that host the batholith Rb, Sr, and $^{87}Sr/^{86}Sr$ data were collected for a suite of samples from north of the international border (between Mexico and the United States). These data are presented

in Chapter 2, and, in conjunction with published results, demonstrate that the bulk of the metasedimentary rocks exposed in the western and central San Jacinto Mountains differ substantially from those exposed elsewhere within the northern part of the batholith. Available data on the wall rocks to the batholith as a whole are also summarized in this chapter, and the possible relationships between these rocks and rocks of similar age elsewhere in western North America is briefly discussed.

Geological mapping of about 400 km^2 of largely igneous rock outcrops within the San Jacinto Mountains enabled the differentiation of three large, and many smaller intrusive units. Data on the stratigraphic, structural, petrological, geochemical and isotopic relations of the igneous rocks are presented in Chapters 3 through 9.

In the third section of this thesis important observations are summarized and then integrated into a model for the origin of the igneous rocks of the San Jacinto Mountains. Chapter 10 briefly reviews pertinent observational data presented in Chapters 2 through 9. These data allow significant inferences to be made about magma transport and magma chamber processes (Chapter 11). Finally, Chapter 12 considers the problem of the origin of these rocks using the data presented here in conjunction with previous observational, experimental and theoretical results, and presents a model for the genesis of the San Jacinto igneous rocks.

1.2 REVIEW

1.2.1 ASYMMETRIC BATHOLITHS

The rapid increase in the availability of geochemical data in the late 1960's and early 1970's, combined with an increased interest in detailed geological work in continental margin batholithic and volcanic complexes, led to a growing realization that petrological asymmetries are widespread, perhaps ubiquitous, in these terranes. These studies were spurred by twin impetii; the proposition from plate tectonic theory that the igneous belts inboard of oceanic trenches were one manifestation of the consumption of oceanic crust in the subduction zones, and by the increasing importance of the exploitation of mineral deposits (notably of the porphyry copper-gold-molybdenum type) that were demonstrably related to this igneous activity.

In fact, the west-to-east zonation within the major Cordilleran batholiths had been noted much earlier (Lindgren, 1915; Moore, 1959). However, it was the work within active volcanic arcs, particularly that of Kuno on the modern Japanese arc (e.g., Kuno, 1966), that first demonstrated the intimate relationship between the chemistry of the volcanic rocks and the depth to the Benioff Zone (and thus distance from the trench). Later workers showed comparable relationships for isotope systematics (e.g., Tatsumoto and Knight, 1969), trace element contents (e.g., Jakes and White, 1972) and even age (e.g., Gill, 1970). Recent summaries (e.g., Johnson et al., 1978; Arculus and Johnson, 1978; Gill, 1981) have tended to emphasize that each arc differs significantly in detail, and that the general relationships that had been postulated between the chemical composition and the inherently asymmetric geometry of the sub-

duction zone have probably been overstated. However, the demonstrable relationship between plate consumption and the presence of voluminous magmatic activity implies that these complex geological, chemical, isotopic, geophysical and temporal relationships are related genetically by some fundamental petrologic process or processes that take place during subduction [see Gill (1981) for a recent review].

The transverse variations across the volcanic arcs have batholithic analogues. Lindgren (1915) and Moore (1959) recognized petrological zonation within the Sierra Nevada batholith that was later quantified (Bateman and Dodge, 1970). Similar chemical variations have been reported in many other batholiths [e.g., Alaska-Aleutian Range batholith (Reed and Lanphere, 1974)], as have variations in emplacement age (e.g., Silver, 1971; Stern, 1981; Chen and Moore, 1982); in isotope chemistry (e.g., Early and Silver, 1973; Kistler and Peterman, 1973; Doe and Delevaux, 1973; Taylor and Silver, 1978; DePaolo, 1981b). Although the asymmetric zonations within these batholiths cannot be related to the depth to their now extinct Benioff Zones, they may in some cases be seen to vary systematically with distance from the position of an inferred trench, just as has been shown for several modern arc systems (e.g., Kuno, 1966).

An understanding of the origin of these asymmetric zonation patterns will add substantially to understanding of both the development of batholiths and of the processes operating in and above subduction zones.

Transverse Asymmetries within the Peninsular Ranges Batholith

The Peninsular Ranges batholith of southern California and northern Baja California is perhaps the simplest and best preserved of the thus far studied continental margin batholiths of the world. It was

intruded during a single prolonged period of magmatic activity during the Cretaceous (e.g., Silver et al., 1979), has largely escaped later thermal or tectonic disturbance, and has not been covered by large areas of post-batholithic sediment subsequent to unroofing. The magmatic arc of which the Peninsular Ranges batholith is part was once continuous into western continental Mexico, a point emphasized by L.T. Silver (e.g., Silver, 1975, 1982); present usage, however, limits the term "Peninsular Ranges batholith" to those exposures west of the sedimentary fill of the Gulf of California rift system.

Silver argues that the batholith was constructed by two closely related magmatic episodes; an older western static arc, and a younger eastern transgressive arc (Silver et al., 1979). Petrological, geochemical and isotopic asymmetries are largely independent of this bipartite (but continuous) emplacement history, showing simple west to east variation across the batholith. For the northern 600 kilometer segment of the batholith studied by Silver and his co-workers, the initial strontium isotopic composition becomes more radiogenic (increasing from <0.703 to >0.707; Early and Silver, 1973; Silver and Early, 1977), $\delta^{18}O$ increases (from +6 to +12 per mil; Taylor and Silver, 1978), neodymium becomes less radiogenic (ε(Nd) decreases from +8.0 to -6.4; DePaolo, 1981b), and lead becomes more radiogenic (Silver, 1982) from west to east, largely independent of age and rock type. Within rocks of broadly similar composition (tonalites and low-K granodiorites) the concentration o fLIL elements (including Rb, Sr, Ba, Pb, U and Th) increases systematically from west to east (Silver et al., 1979); this zonation does not appear to correlate with the pattern for K, which shows only modest enrichment, if any, eastward. Rare earth element (REE) behaviour also shows remark-

able zonation within the batholith (Gromet, 1979). Three zones of distinctive REE behaviour parallel the long axis of the batholith. A western zone shows nearly flat fractionation patterns, commonly with negative Eu anomalies. The central zone is characterized by tonalites with heavy REE (HREE) depletions and subdued Eu anomalies, if any. The eastern zone rocks are marked by the additional feature of light REE (LREE) enrichment along with the HREE depletion.

It is within the context of this earlier work that the present study was designed. The reported asymmetries are largely (though not entirely) based upon inter-plutonic observations. This posed the question: "Could detailed studies of several plutons or plutonic complexes from different tectonic environments within the batholith help elucidate the origin of the features that pertain to the batholith as a whole?" The effectiveness of conducting such detailed studies of intra-plutonic variability within the context of a much larger scale regional project has been amply demonstrated by P.C. Bateman and colleagues in their work on the Sierra Nevada batholith (e.g., Bateman and Nokleberg, 1978; Bateman and Chappell, 1979), and by B.W. Chappell and A.J.R. White, and co-workers, in southeastern Australia (e.g., Chappell, 1978; Chappell and White, 1976; Griffin et al., 1978; Hine et al., 1978; Compston and Chappell, 1979). Any model for the origin of a particular plutonic complex must be compatible with the regional pattern; conversely, any model that attempts to explain batholith-scale features must be at least consistent with the peculiar features of individual plutons, and with intra-pluton variability.

Although the plutons of the San Jacinto Mountains have many features in common with the rest of the batholith, several distinctive

features set them apart. These differences presumably relate to a different geologic setting for this part of the batholith compared with the immediately adjacent rocks to the south and west. In particular, the slightly more potassic nature, the more radiogenic strontium and the heavier oxygen of these plutons, along with slight traces of inherited zircon in some rocks led Taylor and Silver to suggest that these differences might be the result of the involvement of the extreme western edge of the North American craton (or its subjacent lithospheric root) in their genesis (Taylor and Silver, 1978).

1.2.2 ISOTOPIC VARIABILITY WITHIN A SINGLE PLUTON

The order of magnitude increase in the precision of an isotopic analysis made possible by the combination of on-line capability with the development of a new generation of mass spectrometers in the late 1960's (Arriens and Compston, 1968; Clement and Compston, 1969; Wasserburg *et al.*, 1969) opened new dimensions in the study of isotope systematics. The early workers had demonstrated that, within the limits of measurement available to them, plutons or plutonic complexes were homogeneous in their original isotopic properties (specifically for isotopes not involved in mass-dependent fractionation); this assumption of initial isotopic homogeneity was critical to the development of the Rb-Sr total rock method of age determination (Schreiner, 1958; Gast, 1960; Compston *et al.*, 1960; Riley and Compston, 1962; Pidgeon and Compston, 1965). Initial isotopic heterogeneity within a single, mappable intrusive unit was perhaps first unequivocably demonstrated by Roddick and Compston in their study of the Murrumbidgee Batholith of southeastern Australia (Roddick, 1974; Roddick and Compston, 1977). These workers found that within one large (65x15 km) intrusive unit, the Clear Range Granodiorite, a correlation existed

between Rb/Sr, $^{87}Sr/^{86}Sr$ and bulk chemistry, and they inferred that this correlation had been established by the time of crystallization of this igneous body. This pluton formed by partial melting of pre-existing sedimentary material within the crust (Joyce, 1973) and it was concluded that the correlation between Rb/Sr and $^{87}Sr/^{86}Sr$ at the time of formation reflected, at least in part, an earlier metamorphic re-equilibration event within this sedimentary source volume. This important study demonstrated that it was possible for an igneous system emplaced at a high level in the crust [the Murrumbidgee Batholith intrudes, in part, its own volcanic ejecta (Owen and Wyborn, 1979)] to inherit isotopic heterogeneity from its source region, albeit probably somewhat modified. This implies that the partial fusion, melt collection, melt transport, and any magma chamber processes combined were incapable of efficiently stirring this large volume of silica-rich magma.

It was considered that such isotopic heterogeneity may prove to be the rule rather than the exception within the large silica-rich plutons that comprise a substantial portion of the major batholiths of the world, and that, if present, such heterogeneities may retain some record of source properties and thus be useful in constraining models of magma genesis, as well as providing important information on processes during solidification of a large magma chamber.

The geochemical asymmetries characteristic of the Peninsular Ranges batholith are attributed to similar asymmetric variations in the properties of the source material(s) rather than to higher level processes (Early and Silver, 1973; Silver et al., 1979; Gromet, 1979; Gromet and Silver, 1983). The west to east variation of several isotopic properties is substantial (e.g., Silver and Early, 1973; Taylor and Silver, 1978) and

poses the question: "If a large pluton comprises 20% of the width of the batholith at a particular latitude, will it contain 20% of the cross-batholithic isotopic variation also?" Such a large pluton (diameter 25 km) would be predicted to show as much as a 1.2 per mil variation in $\delta^{18}O$, or a 0.001 variation in initial strontium isotopic composition. These predicted variations are some twenty times the analytical errors for the respective techniques, and should be easily resolvable. Several plutons within the batholith are of such dimensions, and thus become ideal candidates for detailed study.

Any data gathered on the isotopic heterogeneity (or lack thereof) within a single, mappable igneous unit can be used to constrain models of magma chamber dynamics. Substantial isotopic heterogeneity within such a chamber would necessarily imply that mixing, by whatever processes, is inefficient. If convection is the dominant transport process within the magma chamber this would further imply that the length scale for convection is small compared to the dimensions of the magma chamber, and/or that the time scale for convection is large compared to the time scale for crystallization. Such conclusions are contrary to those obtained by mathematical analysis of simulated fluid systems (e.g., Shaw, 1965; Bartlett, 1969; Spera et al., 1982)

A combination of recent theoretical, experimental and geological observations suggest that the various transport processes operating within a large magma chamber might be considerably more complex than has generally envisioned by most geologists (e.g., McBirney and Noyes, 1979; Sparks et al., 1980; Turner, 1980; Huppert and Sparks, 1980a,b; McBirney, 1980; Huppert and Turner, 1981). Much of the relation of theoretical work to observed geological relationships completed to date has involved

basaltic systems (e.g. McBirney and Noyes, 1979; Sparks et al., 1980) which may have considerably different physical properties (density, temperature, viscosity, yield strength) to the more silica-rich rocks studied here. Many of the studies cited above imply that a magma chamber is a highly dynamic environment, and evidence for the existence (or non-existence) of relative motions within the exhumed magma chambers of the San Jacinto Mountains was sought as part of this project.

1.2.3 GRANITOIDS AS IMAGES OF THEIR SOURCE ROCKS

The composition and nature of the lower crust and of the mantle can be estimated only indirectly. Historically, rocks with mineral assemblages thought to have crystallized at high pressures have been inferred to be samples of lower crustal or mantle material, and have been used to estimate the properties of these regions. Such samples usually arrive at the surface by tectonic accident; because of their small total volume and this accidental means of occurrence they need not necessarily be representative samples of the regions from which they originate. An alternate method of sampling these regions could have great importance in the development of theories of the origin of the crust, particularly of the continental crust.

B.W. Chappell and A.J.R. White and their co-workers in south-eastern Australia have developed the thesis (Chappell, 1966; Presnall and Bateman, 1973) that some granitoids are mixtures of a granitic liquid and refractory residual source material ("restite") (Chappell, 1978; White and Chappell, 1977; Chappell and Compston, 1979). This model states explicitly that a granitoid images its source material. Detailed analysis of the petrogenesis of a granitoid body may, according to this model,

enable estimation of the composition of the source material, its age, and perhaps some of its prehistory. Using this approach, Compston and Chappell (1979) modelled the lower crust of part of southeastern Australia as being initially a late Precambrian island arc construct that had continued to receive mantle-derived contributions until the time of granitoid formation some 400 m.y. ago. Other plutons in this general area are thought to be derived from predominantly metasedimentary source regions (Chappell and White, 1974; Hine et al., 1978; L. Wyborn, 1977). D. Wyborn (1982) has suggested that modelling of the composition of these sedimentary source regions enables determination of the maturity (first cycle, second cycle, etc.) of the sediments from which individual plutons are derived, thus allowing significant inference about the provenance and depositional environment of these otherwise hidden materials. The geochemical and isotopic data from the Murrumbidgee Batholith (Joyce, 1973; Roddick and Compston, 1977), for instance, can be interpreted as imaging facies variation within the source volumes of these tonalitic and granodioritic plutons. If constraints can be placed on the location of these source volumes within the crust, either by experimental, mineral equilibration (Wyborn et al., 1981), seismic (Finlayson et al., 1980) or empirical (Rickard and Ward, 1981) means, a three-dimensional picture of a large section of crust can be developed.

The studies quoted above are interpreted as demonstrating that the crust underlying much of southeastern Australia is considerably older and more complex than previously believed, contains major tectonic boundaries, and developed over a long period of time. The implications for larger scale problems are only beginning to be explored: "It is clear that the model is also capable of being applied to more general questions

relating to the geochemical and isotopic evolution of the crust." (Compston and Chappell, 1979, p. 423).

Although the restite model does not appear to be applicable to the origin of many of the Cordilleran plutonic rocks (e.g., Bateman and Chappell, 1979; Gromet, 1979; Gromet and Silver, 1983; this work), the philosophy developed by the workers in southeastern Australia is. The use of igneous rocks as probes of their source regions is, of course, not new, and has proved critical to, for example, development of current ideas of basalt genesis (e.g., Faure and Hurley, 1963; Gast, 1968; O'Nions and Pankhurst, 1974) and of mantle structure (e.g., Gast, 1960; DePaolo and Wasserburg, 1976; Jacobsen and Wasserburg, 1980).

Within the Cordillera several groups have used data from the igneous rocks to solve or constrain larger scale tectonic problems, or to identify very general source materials ("oceanic"; "lower crustal"; "cratonic"; and etc) for these igneous rocks. They have not, in general, addressed the problem of detailed crustal structure and evolution, an exceedingly difficult proposition in this complex geological terrain. Kistler and Peterman (1973) used strontium isotope data to model the origin of the Sierra Nevada batholith and to infer the general nature and position of pre-existing materials immediately prior to batholithic development. They have since used an enlarged data base to further develop models for the reconstruction of southern California prior to Neogene faulting (Kistler et al., 1973; Kistler and Peterman, 1978). D.J. DePaolo, using new neodymium and strontium isotope and trace element data in combination with published oxygen, strontium and lead isotope data, and age data, developed a model for the origin of the southern Cordilleran batholiths (the Sierra Nevada and Peninsular Ranges batho-

liths; DePaolo, 1981b) in terms of general reservoirs ("mantle"; "crustal"), but did not further investigate the processes involved in the development of these identified materials. The origin of one of these probable source volumes (the "crustal" reservoir) has been the focus of many independent studies (e.g., Wasserburg et al., 1959; Lanphere et al., 1963; Anderson and Silver, 1970; Silver, 1974; Silver et al., 1977).

Attempts to develop an integrated picture of the development of western North America have been hampered by the need to remove the effects of large scale tectonic disruptions that occurred both during and after crustal development. A coherent picture is only beginning to emerge, and involves tectonic accretion, large scale lateral displacements, and considerable horizontal dislocation as well as magma genesis and sedimentation (Silver and Anderson 1974, 1983; Silver, 1982; Saleeby, 1982). These workers have found that an essential key to understanding the development of the various terranes in which they have worked is an understanding of the igneous and metamorphic histories of the various plutonic and volcanic belts present (see especially Silver, 1982, and Saleeby, 1982).

This project was planned with the above considerations in mind. Was it possible to identify specific source materials that were involved in the genesis of one or a group of plutons, and, if so, what could be inferred about the age and/or development of these identified materials? If such inferences could be made, how did these identified materials relate to the development of the North American continent?

The San Jacinto mountains were chosen as the area for study because they were postulated to provide a link between the main Peninsular

Ranges batholith, which appeared to have formed on a largely oceanic substrate, and the presumed extension of this igneous arc northwards and eastwards onto the continent (Taylor and Silver, 1978). It appeared probable that an understanding of this transition region would have regional application, both in understanding batholithic development and in constraining tectonic reconstruction of the North American continental margin.

CHAPTER 2

A RB, SR, AND $^{87}SR/^{86}SR$ STUDY OF METASEDIMENTARY ROCKS, NORTHERN PENINSULAR RANGES

2.1 INTRODUCTION

The age, provenance, and sedimentary and tectonic environments of the rocks into which a large batholith is emplaced may yield information critical to interpretation of batholithic development. Unfortunately, the intense thermal and stress fields which may be associated with rising igneous bodies tend to obliterate the fossil record and, in extreme cases, even the original characters of the rocks themselves. Alternately, the country rocks themselves may be of a type or age not conducive to fossil occurrence or to fossil preservation. A combination of these and other factors has made the the age, and, to a lesser extent, the origin of the metasedimentary wall rocks to the northern Peninsular Ranges batholith somewhat of an enigma.

In the course of a mapping and geochemical project in the northwestern San Jacinto Mountains strontium isotope data were obtained for samples of the schists and gneisses that host the Cretaceous batholithic rocks. The extremely radiogenic character of these rocks differed sufficiently from the values obtained elsewhere in the pre-batholithic materials by other workers (Early and Silver, 1973; Criscione *et al.*, 1978) that sampling was extended in an attempt to identify possible *isotopic provinces* within the metasedimentary sequences of the northern Peninsular Ranges.

2.2 GEOLOGY

Three gross subdivisions of the pre-batholithic rocks of the Peninsular Ranges have been proposed (e.g., Gastil et al., 1975; Gastil and Miller, 1981). A fourth unit, apparently unaffected by Cretaceous plutonic activity, lies immediately to the west of the present coastline except where it crops out on the Vizcaino and Palos Verdes Peninsulas, and on offshore islands. The geographic distribution of these four lithological belts is shown on Fig. 2.1.

Neither temporal nor structural relations between these proposed belts are well understood (e.g., Jones et al., 1976; Howell and Vedder, 1981). It has been suggested by a number of workers (e.g., Jones et al., 1982; Howell et al., 1982a,b; Gastil and Miller, 1983) that there has been major relative displacements both between and within these belts. An important implication of these proposals is that the different belts may in fact have no temporal or genetic relationship to each other - they have been merely juxtaposed by syn- or post-depositional tectonic events.

Gastil's subdivision is largely a lithologic one. The apparent consistency of pre-batholithic lithology over large areas of the northern Peninsular Ranges in elongate belts that parallel the long axis of the batholith may be, at least in part, an artefact of the current level of exposure. In general, the pre-batholithic rocks become more intensely metamorphosed eastwards, suggesting greater unroofing of the more easterly part of the batholith (e.g., Silver et al., 1956, 1963; Schwarcz, 1969; Gastil et al., 1975). Within the limits of these provisos, Gastil's proposed belts form a useful framework for a brief description of the pre-batholithic rocks types. From west to east these lithological

Figure 2.1. Lithotectonic belts of the northern Peninsular Ranges and adjacent Sonora, palinspastic base. CONTINENTAL BORDERLAND, VOLCANOGENIC BELT, SHALE SANDSTONE BELT and EASTERN QUARTZ-RICH SEQUENCES from Gastil et al., 1975. Position of MOJAVE-SONORA MEGASHEARS from Anderson and Silver, 1979, and L.T. Silver, written communication, 1982. CRATON I AND CRATON II are, in part, diagrammatic, and are meant to show only that there could be considerable complexity in the craton immediately to the east of the Peninsular Ranges.

Restoration of Gulf of California using pole positions of Chase, quoted in Larson et al., 1972, and maximum closure of Gulf. Although this restoration may over-estiamte the amount of separation after rifting commenced, it potentially allows for a small amount of crustal extension prior to the initiation of the active rift system.

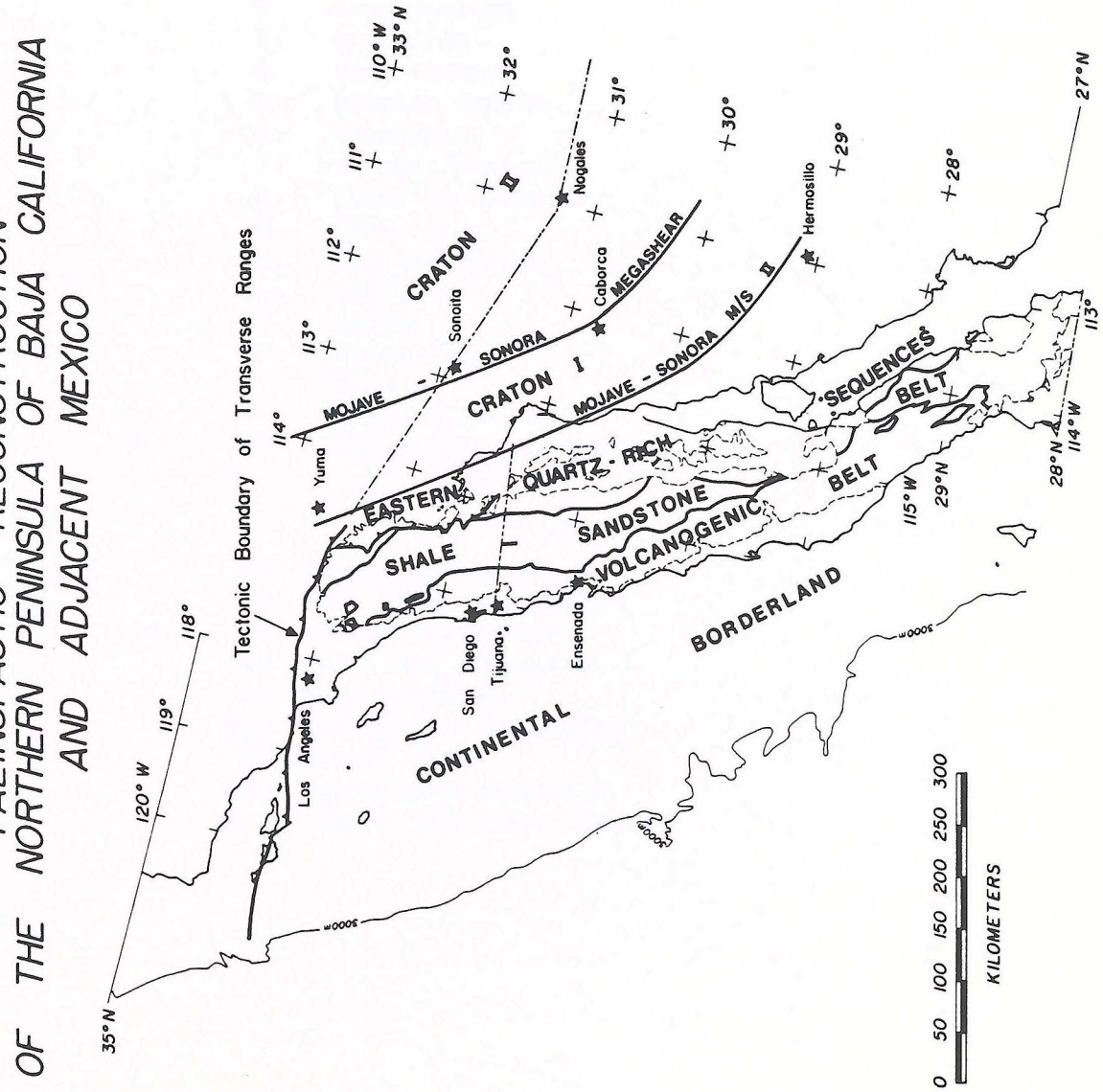
PALINSPASTIC RECONSTRUCTION
OF THE NORTHERN PENINSULA OF BAJA CALIFORNIA
AND ADJACENT MEXICO
Tectonic Boundary of Transverse Ranges
MOJAVE - SONORA M/S II
MOJAVE - SONORA
MEGASHEAR
CRATON
CRATON I
EASTERN
QUARTZ - RICH
SHALE
SANDSTONE
VOLCANOGENIC
BELT
SEQUENCES
BELT
CONTINENTAL
BORDERLAND
Los Angeles
San Diego
Tijuana
Ensenada
Yuma
Sonoita
Caborca
Nogales
Hermosillo
3000m
KILOMETERS
0 50 100 150 200 250 300

Figure 2.1.

Figure 2.2. Index to locations mentioned in the text.

1. Banning
2. Palm Springs
3. Riverside
4. Ladd Canyon
5. McBride Canyon
6. Winchester
7. Thomas Mountain
8. Cahuilla Mountain
9. Anza
10. Borrego Valley
11. Julian
12. Banner
13. Coyote Wells
14. Tecate
15. Valle Guadalupe
16. San Marcos (El Burro)

CM Coyote Mountains
FCM Fish Creek Mountains
JM Jurupa Mountains
SAM Santa Ana Mountains
SJ Sierra Juarez
SJM San Jacinto Mountains
SP Sierra Pinta
SRM Santa Rosa Mountains
SSPM Sierra San Pedro Martir

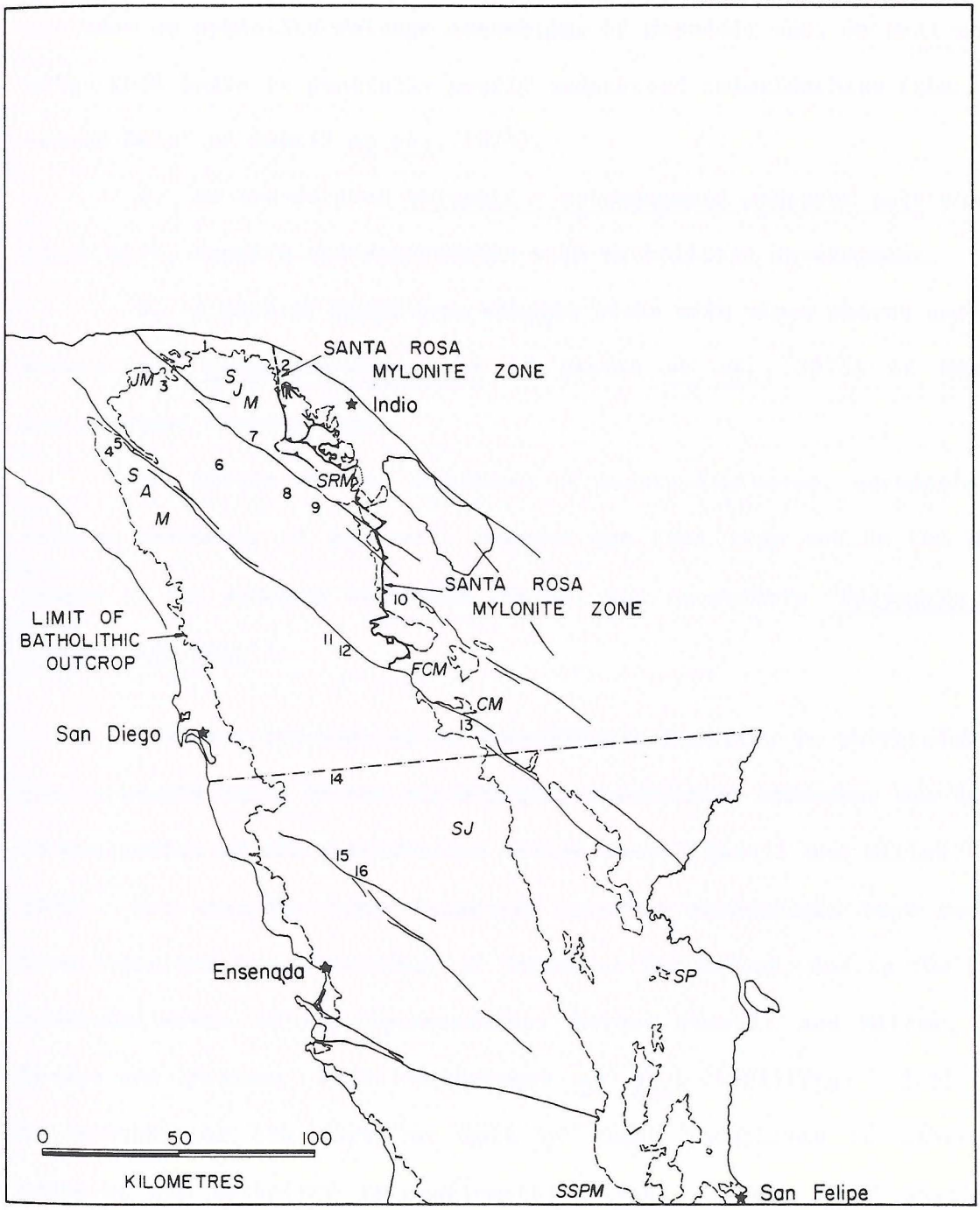
SANTA ROSA
MYLONITE ZONE
Indio
JM
SJM
SAM
SRM
SANTA ROSA
MYLONITE ZONE
LIMIT OF
BATHOLITHIC
OUTCROP
FCM
CM
San Diego
SJ
Ensenada
SP
SSPM
San Felipe
0
50
100
KILOMETRES

Figure 2.2

subdivisions are (modified from Gastil et al., 1975):-

1. The California Continental Borderland, a complex terrain which includes an ophiolite-melange assemblage of Mesozoic age, as well as many other rock units in generally poorly understood relationships (the 'Franciscan Belt' of Gastil et al., 1975).

2. An arc-derived volcanic - volcanogenic sediment belt that, in large part, appears contemporaneous with batholithic development.

3. A unit of flysh-type clastic rocks with minor cherts and limestones (the sandstone-shale belt of Gastil et al., 1975) of Mesozoic and presumed Mesozoic age.

4. Little studied sequences of quartz-dominated, carbonate containing sediments of generally unknown age that crop out in the desert ranges of the eastern peninsula (Gastil and co-workers 'Paleozoic metasedimentary belt').

Recent discoveries of identifiable fossils, in particular from the carbonate units of the eastern quartz-dominated sequences are forcing re-evaluation of the subdivisions listed above (Gastil and Miller, 1981, 1983). For example, lower Paleozoic conodont assemblages have recently been described from south-west of Tecate at San Marcos, and in the Coyote Mountains north of the international border (Gastil and Miller, 1981; Dockum and Miller, 1982; Lothringer et al., 1982)[Fig. 2.2]. The relationship of the rocks at both of these localities to other rock units of the batholith is problematical (e.g., Sharp, 1979; Gastil and Miller, 1981).

Strontium isotope data have been reported previously for sedimentary rock samples from the volcanic-volcanogenic sediment belt (Early

and Silver, 1973), and from the shale-sandstone belt (Early and Silver, 1973; Criscione et al., 1978). Samples analysed in this study are from the shale-sandstone belt and the eastern quartz-dominated sequences. The interpretation of these data requires an understanding of the geological relationships between the rocks of these various lithologic packages; following is a brief summary of the lithological and paleontological character of each belt. These relationships are summarized on Fig. 2.3.

2.2.1 CALIFORNIA CONTINENTAL BORDERLAND

The best exposures of rocks from the California Continental Borderland Province (D.G. Moore, 1969) are on the Vizcaino Peninsula and nearby Isla Cedros, and on Isla Catalina and Isla Santa Cruz; these localities are separated by over 700 km of geologically poorly known terrain. Two ophiolite sequences have been described from the Vizcaino Peninsula (e.g., Jones et al., 1976). The pillowed basalts of one contain interbedded late medial to late Triassic cherts; the basalts are overlain by more chert, and then by a sequence containing limestones, breccias, and volcanogenic litharenite. A thick limestone unit low in the sequence is of medial late Triassic (late Norian) age (Jones et al., 1976; Finch and Abbott, 1977). The second ophiolite is depositionally overlain by sediments containing abundant Upper Jurassic (Tithonian) fossils (Jones et al., 1976; Barnes and Berry, 1979; T.E. Moore, 1979). This sequence has been correlated with the Coast Range ophiolite and overlying Great Valley Sequence of central California (Jones et al., 1976). Similar ophiolitic-type rocks that crop out on nearby Isla Cedros are overlain by Middle Jurassic (Callovian - Bajocian) cherts, siltstones, conglomerates and tuffs, all of which structurally overlie a glaucophane- and

Figure 2.3. Summary of age relations within the Peninsular ranges and some adjoining geological provinces. Radiometric time scale of Harland et al., 1982.

Data from:

Peninsular Ranges Radiometric data: Zircon U-Pb (solid circle), Silver et al., 1969; Total Rock Rb-Sr (open squares), Criscione et al., 1978. Paleontologic data: Allison, 1955; Silver et al., 1956, 1963; Silberling et al., 1961; Imlay, 1963, 1964; Fife et al., 1967; Minch, 1969; D.L. Jones et al., 1976; D.L. Jones, quoted in Gastil et al., D.A. Jones et al., 1983.

Coast Ranges Radiometric data: Zircon U-Pb (solid circles), Xenophontos and Bond, 1978; Hopson et al., 1981; Total Rock Rb-Sr (solid square), McJunkin et al., 1979. Paleontologic data: Hopson et al., 1981.

Sierran Foothills Jones et al., 1976.

Peninsular Ranges Batholith Age ranges of western static arc and eastern transgressive arc from Silver et al., 1979.

Mojave-Sonora Megashear Timing from Silver and Anderson, 1983.

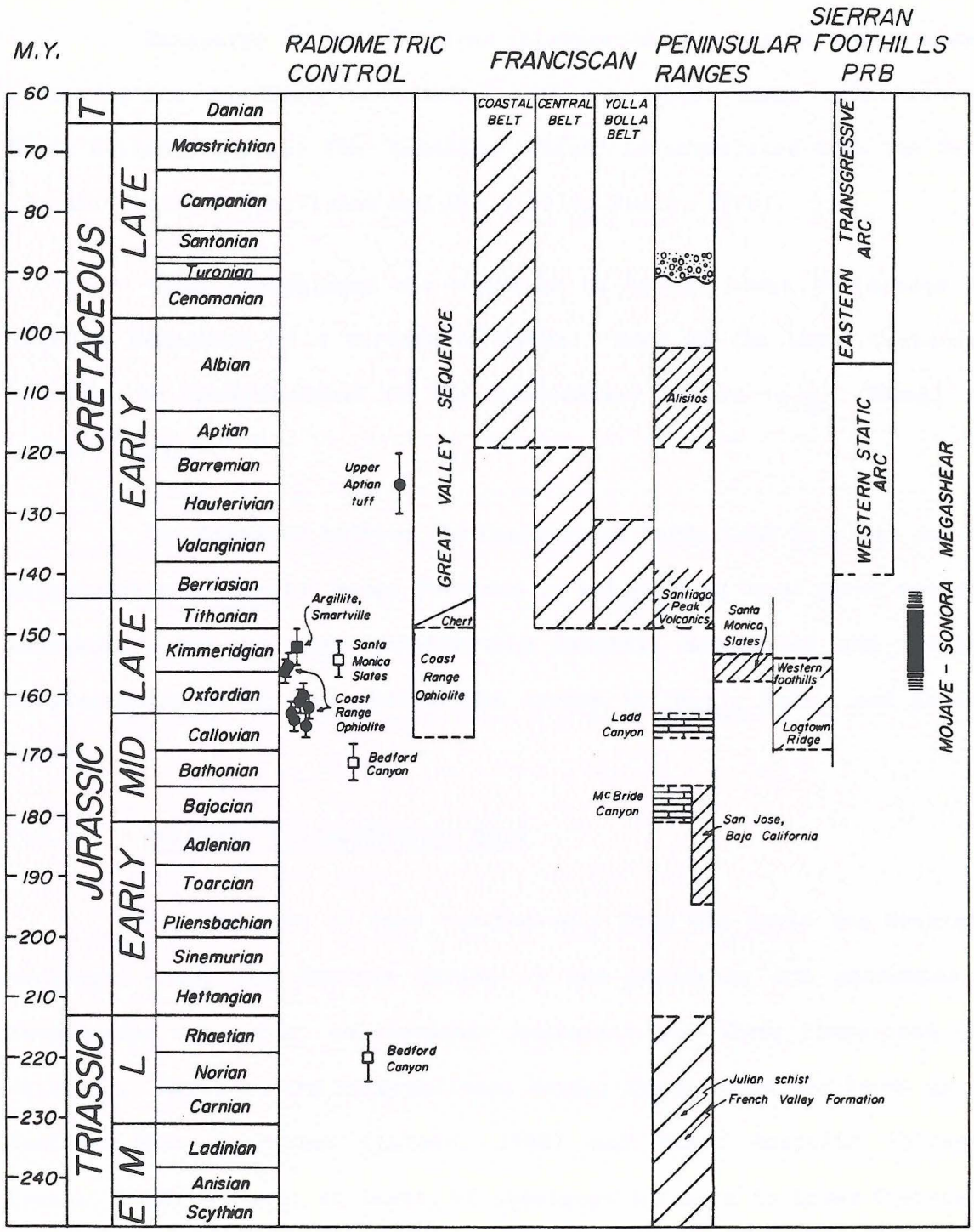
M.Y.
RADIOMETRIC CONTROL
FRANCISCAN
PENINSULAR RANGES
SIERRAN FOOTHILLS PRB
60
70
80
90
100
110
120
130
140
150
160
170
180
190
200
210
220
230
240
CRETACEOUS
JURASSIC
TRIASSIC
T
LATE
EARLY
LATE
MID
EARLY
L
M
E
Danian
Maastrichtian
Campanian
Santonian
Turonian
Cenomanian
Albian
Aptian
Barremian
Hauterivian
Valanginian
Berriasian
Tithonian
Kimmeridgian
Oxfordian
Callovian
Bathonian
Bajocian
Aalenian
Toarcian
Pliensbachian
Sinemurian
Hettangian
Rhaetian
Norian
Carnian
Ladinian
Anisian
Scythian
Upper Aptian tuff
Argillite, Smartville
Santa Monica Slates
Coast Range Ophiolite
Bedford Canyon
Bedford Canyon
GREAT VALLEY SEQUENCE
Chert
Coast Range Ophiolite
COASTAL BELT
CENTRAL BELT
YOLLA BOLLA BELT
Alisitos
Santiago Peak Volcanics
Ladd Canyon
Mc Bride Canyon
Santa Monica Slates
Western foothills
Logtown Ridge
San Jose, Baja California
Julian schist
French Valley Formation
EASTERN TRANSGRESSIVE ARC
WESTERN STATIC ARC
MOJAVE - SONORA MEGASHEAR

actinolite-schist bearing melange correlated with the Franciscan Formation of central California (Jones et al., 1976).

Exposures on Isla Catalina interpreted as parts of a dismembered ophiolite are similarly correlated with the Coast Range ophiolite and Great Valley Sequence; the 'Catalina schist' is correlated with the Franciscan Formation (Mattinson and Hill, 1976; Platt, 1976).

These assemblages are overlain by latest Lower Cretaceous and Tertiary sediments of a variety of types. Much of the Lower Cretaceous seems to be unrepresented in the sedimentary record (e.g., Howell and Vedder, 1981).

The boundary between the Continental Borderland Province and the neighbouring Peninsular Range Province is believed to be of great tectonic complexity, and may have considerable lateral, horizontal and vertical displacements of several generations across it (e.g., Howell and Vedder, 1981).

2.2.2 VOLCANIC-VOLCANICLASTIC BELT

Exposed more or less continuously from the Santa Ana Mountains southward along the western margin of the peninsula are sequences of interbedded volcanics, volcanogenic sediments and minor limestones (and marbles). North of the international border these rocks are known as the Santiago Peak Volcanics (Larsen, 1948) and Black Mountain Volcanics (Hanna, 1926) and are, at least, of uppermost Jurassic to Lower Cretaceous (Tithonian to Hauterivian) age (Fife et al., 1967; D.L. Jones et al., 1976; D.A. Jones et al., 1983). South of the international border the

immense thicknesses of volcanogenic sediments and volcanics and minor interbedded carbonates of the Alisitos Formation are of Lower Cretaceous (Aptian-Albian) age where fossiliferous (Allison, 1955; Silver et al., 1956, 1963). Considerable portions of the Alisitos Formation are unfossiliferous, and could be older (e.g., Silver et al., 1963).

Relationships between the volcanogenic rocks and apparently underlying shale-sandstone and graywacke sequences are unclear. The Santiago Peak Volcanics are reported to be unconformable upon Jurassic (Callovian and older) Bedford Canyon Formation (Larsen, 1948; Gray, 1961). Engel (1959), however, reports the presence of andesite flows interbedded with the slates of the Bedford Canyon Formation. More recent work in this relatively inaccessible terrain suggests that the contacts may be tectonic, gradational, or both (T.E. Davis, personal communication, 1982; L.T. Silver, personal communication, 1983;). In Arroyo San Jose, some 400 km southeast of Tijuana, fossiliferous volcanogenic sediments and volcanics of Lower to Medial Jurassic (Toarcian - Bajocian) age are reported to be unconformably overlain by the Aptian-Albian Alisitos Formation (Minch, 1969; Jones et al., 1976). The only other locality where the base of the Alisitos Formation has been suggested to be exposed is in Valle Guadelupe (Fig. 2.2), where a volcanic-volcaniclastic sequence is reported to lie unconformably upon metamorphosed graywacke and shale, with thin carbonate layers (Bell, 1969, reported in Gastil et al., 1975). Relationships at this locality have not been well documented, and other interpretations of the exposures are possible (L.T. Silver, personal communication, 1983). In San Diego County the pre-batholithic sequences are reported to be of dominantly volcanogenic or volcanic origin as far east as Mount Laguna (Todd and Shaw, 1979).

A 127±5 m.y. U-Pb date on zircon from a tuff interbedded with fossiliferous Alisitos sediments has been reported (Silver et al., 1969). These paleontologic and geochronologic data are at odds with currently used geochronological time scales (e.g., Harland et al., 1982) and imply that the absolute time scale used in Fig. 2.3 is in error by about 10 m.y. for the Aptian. More work is obviously needed to resolve this problem.

Silver and his co-workers also report field evidence that batholithic rocks were intruded contemporaneously with and even predate deposition of some of the Mesozoic volcanic rocks (Silver et al., 1969). Support for this comes from zircon U-Pb data interpreted as giving crystallization ages that range from 105 to 140 m.y. for plutons from the western part of the batholith (Silver et al., 1979; L.T. Silver, personal communication, 1983), indicating contemporaneity of volcanism (Alisitos Formation) and plutonism (Peninsular Ranges batholith).

2.2.3 SHALE-SANDSTONE BELT

East of the volcanic-volcaniclastic belt crop out many exposures of flysh-type clastic rocks with minor chert and limestone lenses. This unit includes the Bedford Canyon formation (Larsen, 1948), the French Valley formation (Schwarcz, 1969), large parts of the Julian schists of southern California, and the Santa Eulalia formation of northern Baja California (Woodford and Harriss, 1938) as well as many un-named sedimentary sequences on both sides of the international border (e.g., Gastil et al., 1975).

The Bedford Canyon formation of the northern Santa Ana Mountains is a sequence of mildly metamorphosed slates and argillites with some

feldspathic quartzites and a very few thin lenses of limestone and conglomerate. Sedimentary structures indicate that a significant portion is overturned (Larsen, 1948; Moscoso, 1967, quoted in Gastil et al., 1975). Recent work suggests that at least some of the limestones are probably tectonic blocks or penecontemporaneous slump blocks incorporated into the unit during deformation (Criscione et al., 1978). A few small pods of serpentinite suggested by Larsen to be a hydrothermally altered granodiorite (Larsen, 1948, p.41) have been re-interpreted as tectonically emplaced blocks of ophiolitic materials, the serpentinite replacing harzburgite (Criscione et al., 1978). These later workers interpret the Bedford Canyon Formation as an accretionary prism.

Fossils obtained from the limestone lenses were originally assigned to the Triassic (Smith, 1898, 1914; Mendenhall, in Willis, 1912; Larsen, 1948; Engel, 1959) but are considered to be Jurassic (Bajocian and Callovian) by more recent workers (Silberling et al., 1961; Imlay, 1963, 1964). Many of the earlier localities have not been recollected, and the possibility remains that Triassic material was indeed recovered. Microfossils of both Triassic and Jurassic age have recently been recovered from the northern Santa Ana Mountains (T.E. Davis, personal communication, 1982; D.L. Jones, quoted in Gastil et al., 1981). On the basis of age similarities Jones and his co-workers correlate the Bedford Canyon Formation with the eastern metamorphic belt of the Sierran foothills (Jones et al., 1976), although they note that the predominant graywackes and slates of the Bedford Canyon formation are quite unlike the siliceous volcanics and volcanogenic sediments of the Sierran rocks.

Relations between the Bedford Canyon formation and the apparently overlying Santiago Peak Volcanics are uncertain, and have been discussed above.

Interlayered schist, feldspathic to arkosic quartzite, amphibolite, meta-chert and meta-conglomerate exposed in the Winchester area east of the Santa Ana Mountains (Fig 2.2) have been described and named the French Valley Formation (Schwarcz, 1969). These metasedimentary rocks were characterised by abundant thick arkoses which show relict textures with very poor sorting and "shale-chip" conglomerates. Schwarcz considered the original sediments to have been deposited in a marginal basin (in the sense of Krumbein and Sloss, 1963, p.418) flanking a cratonic highland and possibly transitional on the west into a eugeosyncline. The French Valley formation was thought to be conformable with, and gradational downwards into the Bedford Canyon Formation. Sedimentary structures found by Schwarcz indicate that the whole sequence is in normal upright position.

Fossil pelecypods discovered by Murphy (reported in Schwarcz, 1969, p.21) from west of the sequences studied by Schwarcz are from rocks similar in lithology to, and apparently represent an extension of, the French Valley formation (Schwarcz, 1969). These fossils have been tentatively identified as Triassic or older (Lamb, 1970); if this assignment is correct, the French Valley formation and underlying "Bedford Canyon formation" is older than at least the fossiliferous parts of the Bedford Canyon formation in Ladd and McBride Canyons (see Fig. 2.2 for locations).

Metasedimentary rocks dominated by quartz-mica schists and quartzites that crop out 100 km southeast of Winchester have been termed the Julian schists, after the township of Julian (Fig. 2.2)[Hudson, 1922; Donnelly, 1934; Creasey, 1946; Merriam, 1946; Miller, 1946]. Many of these rocks are perhaps better described as gneisses than schists (Todd and Shaw, 1979; L.T. Silver, personal communication, 1983). Although predominantly mica-schist in which quartz+feldpars commonly comprises 50% of the rock (Creasey, 1946), quartzites, meta-conglomerates, and sillimanite and cordierite bearing schists, as well as minor calc-silicate lenses, crystalline limestones and amphibolites are also present (Merriam, 1946; Miller, 1946). Hudson reported the discovery of an ammonite imprint on the surface of an angular pebble of dark gray, quartzitic rock from the sequence of quartz-mica schists, sillimanite schists, and quartzites south-east of Banner (Fig 2.2). It was identified by J.P. Smith (in Hudson, 1922, p.190) as "a slender ammonite that is without much doubt Triassic". Unfortunately, the material has been lost (see Gastil et al., 1975, p.22) and the identification cannot be reconfirmed.

Schwarcz tentatively correlated his French Valley formation with the Julian schists on the basis of lithology. The scant fossil evidence suggesting that both units may be, at least in part, Triassic, is not in conflict with such a correlation.

Similar schists and quartzites with minor amounts of metacarbonate rock crop out in the Sierra Juarez of Baja California (Gastil et al., 1975). Further south again, in the Sierra San Pedro Martir, the Santa Eulalia Formation (Woodford and Harriss, 1938) has been suggested to be "migmatized" Julian schist (Gastil et al., 1975). These latter

authors report the presence of quartzite-phyllite sequences that are lithologically similar to Julian schist and that extend for another 300 km south of the Sierra San Pedro Martir. Without age control the suggested correlations of these various sequences must be considered tentative at best. However, this graywacke-dominated shale-sandstone lithofacies (Gastil's shale-sandstone belt), of whatever ages and correlation, apparently persists as a north-north-west trending belt for some considerable distance into Baja California.

2.2.4 EASTERN QUARTZ-RICH SEQUENCES

Quartz-rich, carbonate-containing sequences that crop out in the desert ranges of southern California, and in the San Jacinto and Santa Rosa Mountains along the western margin of the Salton Depression have, until recently, been generally presumed to be of Carboniferous age. With a few local exceptions, these rocks have been studied in reconnaissance only. The pre-batholithic rocks of the San Jacinto and Santa Rosa Mountains have been described by Fraser (1931), Miller (1944, 1946) and Dibblee (1954, 1981a). These workers describe a series of highly metamorphosed sedimentary rocks, including quartzites, schists and crystalline limestones. Protoliths are interpreted to have been sandstones, argillaceous sandstones, feldspathic sandstones, limestones, and shales. Dibblee (1954), Brooks and Ellis (1954), and Sharp (1967) describe carbonate-containing sequences in the Fish Creek and Coyote Mountains, in the desert ranges south and south-west of Coyote Wells, and around Borrego Valley.

More detailed studies have been made of selected local areas of well-exposed rock on the eastern scarp of the San Jacinto Mountains, and

in the Santa Rosa Mountains. Wright (1946), in his study of the Santa Rosa Mountains described a sequence of bedded phyllites, ferruginous phyllites and shales containing minor limestone lenses and a hornblende-mica schist, all of which were in thrust contact with a sequence of phyllites and schists that contained a thick (200 m) quartzite unit. Brown (1968, 1981) mapped an area immediately northwest of that mapped by Wright, and described a thick sequence of schists, marbles and quartzites, all regionally metamorphosed to almandine-amphibolite facies assemblages. Similar rocks occur elsewhere in the San Jacinto Mountains, particularly in roof pendants on Thomas Mountain (this work, Ch. 3) and in the areas of metasedimentary rock south and southwest of Banning (Dibblee, 1981a,b,c,d,e,f). The quartz-dominated nature of the clastic rocks in these sections in general, combined with the presence of a thick quartzite unit associated with mica-schists and marbles, is a unifying feature of these several areas. A similar assemblage of schists and gneisses containing a thick quartzite unit (600 m) and minor recrystallized limestone lenses crops out in the Jurupa Mountains northwest of Riverside. It has been described by MacKevett (1951), who correlated it with the Bedford Canyon Formation of the nearby Santa Ana Mountains on the basis of proximity and because of the similar size and proportion of limestone lenses in the two units. MacKevett recognised lithological disparities between the two sections, but attributed them to differences in the degree of metamorphism in the two areas.

The age of these quartz-rich sequences has long been a subject of debate. Miller (1944) reported finding Paleozoic crinoidal remains in his "Palm Canyon Series" south of Palm Springs, but later considered this material to be of non-biogenic origin (Miller, 1946). Other reports

of upper Paleozoic fossils from the Peninsular Ranges north of the international border (Webb, 1939; Mueller and Condie, 1964) are either unconfirmed, undocumented, or otherwise controversial (Schwarcz, 1969; R.V. Sharp, quoted in Gastil and Miller, 1981, p.828).

South of the international border Upper Paleozoic fossils are known from several localities (Gastil and Miller, 1981). They include fossils of Permian age found in a block of limestone and quartzite in a melange on Isla Cedros (Kilmer, 1979); unidentified brachiopods and crinoidal material of "definitely late Paleozoic" age (R. Langenheim, quoted in Gastil et al., 1981) from limestone in the Sierra Pinta, north of San Felipe (Fig. 2.2; McEldowney, 1970); and Permian fusulinids found in limestone boulders in a conglomerate of Miocene or older age near El Marmol, south of San Felipe (Gastil et al., 1973). Fossils from recrystallized limestone found near El Volcan some 250 km south-south-west of the Sierra Pinta originally thought to be Paleozoic (Gastil et al., 1975) are now reported to be most likely of Triassic age (D.V. LaMone, quoted in Gastil et al., 1981). Gastil and Miller (1983) report the discovery of an upper Paleozoic sequence near El Marmol.

The host rocks from Isla Cedros are considered part of the "Franciscan belt" (Kilmer, 1979), and the fusulinid-containing boulders are thought to have been derived from Permian limestones that crop out east of the Gulf of California, in western Sonora (Gastil et al., 1973). The Sierra Pinta is a small isolated range in an area of considerable tectonic complexity (Gastil et al., 1975) and extrapolation of age data obtained here to sequences elsewhere in the Peninsula must be made with some caution.

The recent discovery of Lower Paleozoic fossils at two localities within the Peninsular Ranges re-opens the question of the age of the thick metasedimentary sequences of the eastern part of the Peninsula. The recovery an early Ordovician (medial Arenig) conodont fauna from a section of carbonate, quartzite, bedded chert, and subordinate slate exposed in a tectonic package at San Marcos (Fig. 2.2) has recently been reported (Lothringer et al., 1982; Gastil and Miller, 1981). Preliminary mapping suggests that these rocks were tectonically emplaced over the sandstone-slate turbidite deposits. Emplacement pre-dated batholithic development.

A thick sequence of metasedimentary rocks crops out in the Coyote Mountains of western Imperial County and eastern-most San Diego County (Dibblee, 1954). Dockum and Miller (1982) reported the discovery of late Early Ordovician to early Medial Ordovician (late Arenig to early Llanvirn) conodont faunas in a sample of marble from the eastern end of the range. The metasedimentary sequence from which the conodonts were recovered consists of marbles and dolomitic marbles (85%), and quartz-muscovite schist and quartzite (15%)(Dockum and Miller, 1982).

Mapping by Sharp (1967, 1979) and Theodore (1966, 1970) has delineated a major mylonite zone, roughly north-south trending, that post-dates the emplacement of the Middle Cretaceous plutons of the eastern Peninsular Ranges (Fig. 2.2). This mylonite zone is cut by even lower angle thrust faults with similar regional trends (Sharp, 1979) and is continuous from near Palm Springs southward for at least 120 km (Sharp, 1979). Part of this thrust system in the Santa Rosa Mountains was first recognized by Wright (1946). Displacement on the thrust faults cutting

the mylonite is constrained to be approximately west-vergent with displacements of at least 11-15 km (Sharp, 1979). The amount of shortening across the mylonite zone has been suggested to be of order 50-100 km (Silver, 1982, 1983; Engel and Engel, 1982). Relationships within the thrust stack are interpreted as indicating in excess of 30 km of east-west shortening, as well as at least 25 km of north-south shortening and left-lateral slip. This complex movement history is suggested to be the result of Late Cretaceous to Eocene supra- to mesocrustal transport, first to the west, then to the north-northwest over and along the developing Peninsular Range - Salton Trough interface (Engel, 1983). Recognition of the earlier events is complicated by the development of east-directed detachment faults in Miocene time. These detachment faults cut the older north- and west-vergent structures (E. Frost, personal communication, 1983; Engel, 1983). Some of the detachment surfaces had been previously mapped, but their movement history had not been discussed (Sharp, 1979).

The previously cited observations and interpretations suggest that the mylonite zone divides the metasedimentary rock sequences of the eastern batholith into upper and lower plate assemblages that may have been juxtaposed from quite disparate original positions. It is thus possible to recognize an eastern upper plate metasedimentary assemblage, a mylonite zone assemblage with probable considerable complexity, and a western lower plate assemblage. The Ordovician section of the Coyote Mountains is apparently part of the eastern upper plate assemblage. The metasedimentary rocks of the San Jacinto Mountains studied by Brown (1968, 1981), Sydnor (1975), and in this work (Ch. 3) are all part of the western lower plate assemblage, as are the quartzites and schists mapped by Wright (1946) to the southwest of his thrust. Rocks apparently similar

to these are reported to occur in the Jurupa Mountains northwest of Riverside and on Cahuilla Mountain, west of Anza (Fig. 2.2). With the exception of the section of schists and marbles that crop out in the Chino Canyon - Windy Point area north-west of Palm Springs (Fraser, 1931; Syndor, 1975), the rocks of this lower plate assemblage are characterized by the dominance of quartz in the clastic materials; feldspars and mafic minerals are subordinate except where the metamorphic grade is sufficiently high to have produced potassium feldspar from the breakdown of muscovite in pelitic protoliths.

2.3 RB - SR GEOCHRONOLOGY OF SEDIMENTARY ROCKS

Understanding the Sr isotopic properties of sedimentary rocks involves complex considerations that are still not well understood. In principle several types of information might be obtained from such data. Of particular interest to geologists are estimates of age, and the use of the ratio $^{87}Sr/^{86}Sr$ at the time of sedimentation as a provenance indicator. Some authors have reported some success and considerable internal consistency in the application of strontium isotope techniques to the dating of shales (e.g., Compston and Pidgeon, 1962; Compston et al., 1966; Obradovich and Peterman, 1968; Bofinger et al., 1970; Clauer, 1973; Criscione et al., 1978), yet these and other studies have also reported indeterminate or conflicting results (e.g., Compston and Pidgeon, 1962; Chaudhuri and Brookins, 1969; Chaudhuri, 1976). The existence of isochron ages that appear to approximate very closely the time of either sedimentation or diagenesis is evidence that, at least in some cases, weathering, transport, sedimentation and compaction are capable of homogenizing $^{87}Sr/^{86}Sr$ over some indeterminate volume within the developing sedimentary

pile.

How these processes operate is not clear. Dasch and his co-workers have studied the Rb, Sr and $^{87}Sr/^{86}Sr$ systematics of Holocene sediments from the ocean basins and conclude that there is little interaction between the Sr of the sediments and sea-water Sr during transport and deposition (Dasch et al., 1966; Dasch, 1969; Biscaye and Dasch, 1971). These authors also report a correlation between $^{87}Sr/^{86}Sr$ and Rb/Sr in recently deposited sediments that they interpret as a characteristic inherited from the source area(s) of the sediment, albeit modified by physical processes such as winnowing and differential sedimentation. If age significance was attached to the slope of this correlation, apparent 'ages' of 200 to 400 m.y. are obtained for Holocene sediments from different depositional basins (Biscaye and Dasch, 1971). The Rb/Sr of all their samples was quite low (maximum $^{87}Sr/^{86}Sr=4.38$; maximum $^{87}Sr/^{86}Sr=0.7304$) compared to values commonly observed for argillaceous sedimentary rocks ($^{87}Sr/^{86}Sr\approx6-20+$). More recent work (e.g., Clauer, 1973) suggests that the high Rb/Sr characteristic of argillaceous sediments is at least in part the result of diagenetic processes that result in the fixing of Rb in authigenic minerals.

Biscaye and Dasch (1971) stress that no simple interpretation of their samples (to give an inherited isochron) is possible. Rather, the linear arrays are mixing lines generated by physically mixing components having low Rb/Sr and low $^{87}Sr/^{86}Sr$ with components having higher Rb/Sr and $^{87}Sr/^{86}Sr$ during transport and sedimentation.

It appears that considerable homogenization of $^{87}Sr/^{86}Sr$ can take place within the sedimentary pile during diagenesis. This seems

particularly true if there has been large-scale development of authigenic minerals such as glauconite or illite. Compston et al. (1966) demonstrated that illite could itself give valid results, and Obradovich and Peterman (1968) showed that glauconite and whole rock data from almost unmetamorphosed Belt Series rocks were internally consistent. The glauconites appeared to have been in isotopic equilibrium with sea-water strontium, while the shales were not.

Clauer et al. (1975) show that $^{87}Sr/^{86}Sr$ changes as a function of depth in the pore waters of recent sediments, indicating some degree of exchange between clays and interstitial waters. Clauer has also shown that by means of careful separation of authigenic mineral species from unmetamorphosed sedimentary rocks it is possible to accurately and precisely date sedimentary sequences (Clauer, 1973). These techniques are now in routine use in several laboratories (e.g. Ma et al., 1980; Zhang et al., 1982) and appear to hold considerable promise for precise age determination within suitable materials.

Apparently conversely, Perry and Turekian (1974) found that incomplete isotope homogenization had occurred within samples of Miocene shale from a deep (5800 m) drill hole in south-western coastal Louisiana. Chaudhuri and Brookins (1969) and Chaudhuri (1976) report similar phenomena from Permian shales from the mid-continent region of the U.S.A.. It is unclear why equilibration has not occurred in these samples. A common factor is, however, the presence of carbonate in these specimens that is not in isotopic equilibrium with the silicate component of the rock (Perry and Turekian, 1974; Chaudhuri and Brookins, 1969; Chaudhuri, 1976). This complication of the isotope systematics could conceivably lead to problems

in analysis of whole rock specimens, even if acid leaching techniques are used.

In summary, it appears that in carbonate-poor environments isotopic homogenization at the scale of a typical sample (tens to hundreds of cm^3) may be approached within the sedimentary pile. The mechanism appears to be via both the growth of new (authigenic) minerals in isotopic equilibrium with interstitial fluids and by exchange of Sr between mineral grains and interstitial fluids during diagenesis. Most of the Sr ultimately fixed in the sediments comes from detrital mineral grains; only low temperature authigenic minerals (including clays, glauconite and especially carbonate) may contain a significant fraction of strontium derived from sea-water. The isotopic composition of the strontium fixed within the sediment is thus a function of the provenance of that sediment, and of the amount of introduction of sea-water strontium to the sedimentary pile that has occurred. The studies cited above suggest that $^{87}Sr/^{86}Sr$ of sediments after diagenesis may vary from approximately 0.704 to 0.730 or higher; Rb/Sr may also vary widely but appears in general not to correlate with $^{87}Sr/^{86}Sr$. The work of Clauer and his colleagues (Clauer, 1973; Clauer et al., 1975) suggests that much of the homogenization of strontium that does occur within fine-grained sediment may take place within a few tens of centimeters of the sediment-water interface. The role and scale of later diagenetic processes is still poorly understood. Carbonate minerals precipitated from circulating pore fluids at low metamorphic (extreme diagenetic?) grades appear to commonly be not in isotopic equilibrium with other mineral species present (e.g., Perry and Turekian, 1974; Chaudhuri, 1976).

2.3.1 STRONTIUM ISOTOPE DATA AS A DISCRIMINANT BETWEEN SEDIMENTARY UNITS

A particular sedimentary layer (or related group of layers) may thus have two characteristics derived from Rb-Sr systematics that could serve to type it isotopically - its $^{87}Sr/^{86}Sr$ at or shortly after deposition (its "initial" or "depositional" $^{87}Sr/^{86}Sr$) and its slope on the isochron diagram (where measured $^{87}Sr/^{86}Sr$ is plotted against measured $^{87}Rb/^{86}Sr$). The slope is a function of age. This is illustrated using literature data on Fig. 2.4. The data from all units illustrated were believed by the authors to give geologically reasonable estimates of the time of deposition of these rocks (Compston et al., 1966; Obradovich and Peterman, 1968; Criscione et al., 1978). Note the wide range of apparent initial $^{87}Sr/^{86}Sr$ both between units, and, especially within the samples samples from one unit, the State Circle Shale. It is clear that, except at low Rb/Sr values, it would be possible to unequivocally distinguish between these particular units on the basis of their isotope characteristics alone.

2.3.2 METAMORPHIC EFFECTS

The redistribution of Rb and Sr, and Sr isotopes in response to metamorphic conditions is even less well understood than processes during sedimentation and diagenesis. Clauer (1974) demonstrated that the fine fractions ($<2\mu$) of argillaceous sediments can be reset by incipient metamorphism ("anchimetamorphism"); detrital components, however, may not be open to element redistribution until much more severe conditions are reached. In general, it appears that during the growth of new mineral assemblages the Sr isotope systems tend to be reset (e.g., Compston and

Figure 2.4. Isochron diagram showing results from several published studies on Rb, Sr, $^{87}Sr/^{86}Sr$ systematics of shales. Note complete separation of these three suites of rocks at high $^{87}Rb/^{86}Sr$.

Data from: Obradovich and Peterman, 1968; Bofinger *et al.*, 1970; Criscione *et al.*, 1978.

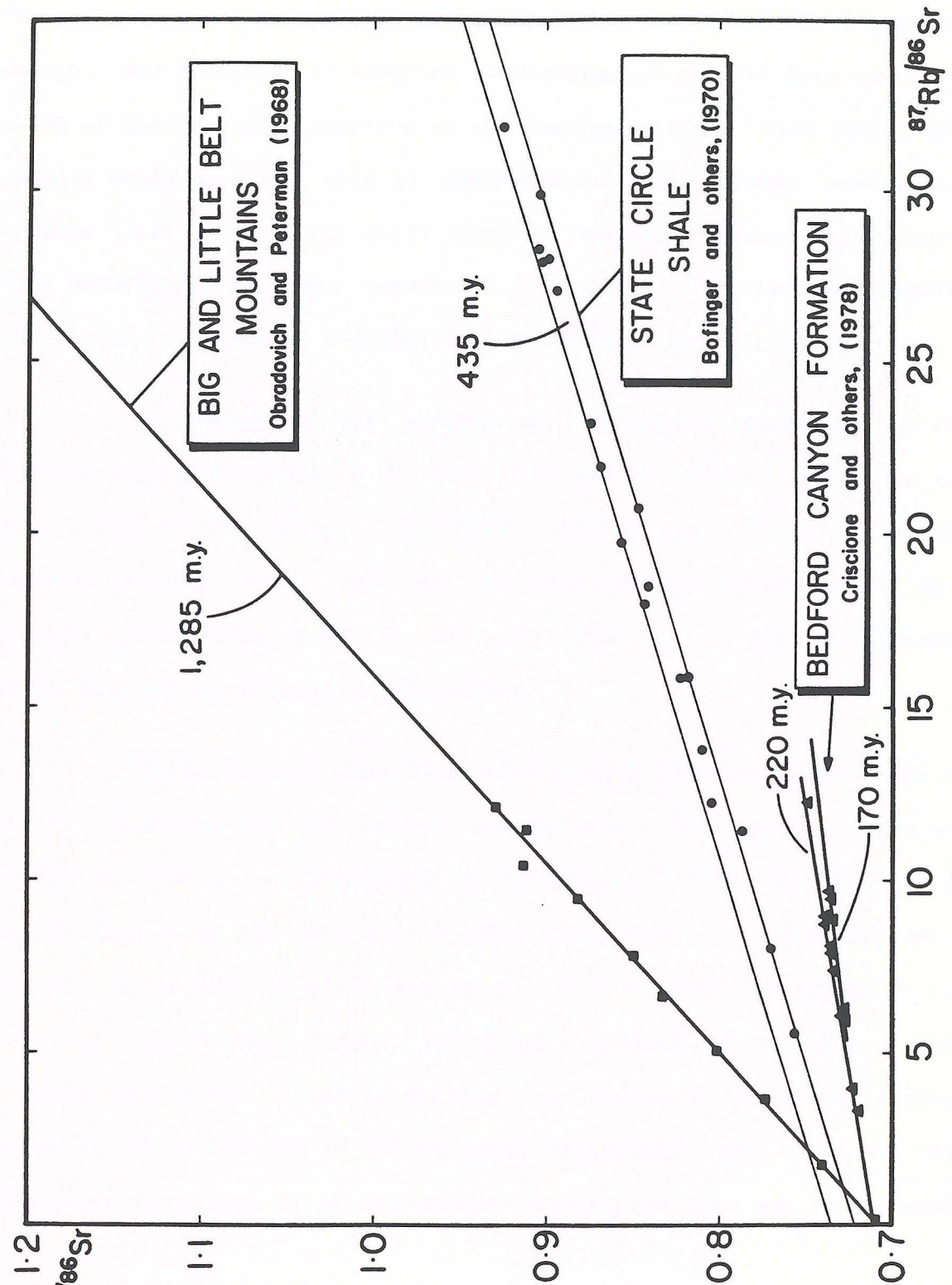
BIG AND LITTLE BELT MOUNTAINS
Obradovich and Peterman (1968)
1,285 m.y.
435 m.y.
STATE CIRCLE SHALE
Bofinger and others, (1970)
BEDFORD CANYON FORMATION
Criscione and others, (1978)
220 m.y.
170 m.y.
1·2
1·1
1·0
0·9
0·8
0·7
$^{87}Sr/^{86}Sr$
5
10
15
20
25
30
$^{87}Rb/^{86}Sr$

Pidgeon, 1962; Compston et al., 1966; Clauer, 1974; Black et al., 1979). The distance scale of complete re-equilibration must then affect sampling design. For instance, if complete redistribution results from the formation of mineralogical layering at the centimeter scale, then small (cm^3) samples would give the time of metamorphism whereas larger samples (of perhaps liter size) might still date the original sedimentation event. This possibility has been considered in detail by Roddick and Compston (1977) and developed as a dating tool by Black et al., (1979).

An example of the effects of metamorphic resetting of the isotope systems is shown in Fig 2.5. The samples used to define the 675 m.y. isochron are shales. The other samples are of biotite schists derived from the shales, and have had their isotope systems reset by a regional metamorphic event at 455 m.y. The age of this metamorphic event has been determined independently.

In the general case metamorphism will tend to redistribute Rb and Sr throughout the new mineral assemblages. Some general considerations pertaining to metamorphic disturbance of Rb-Sr systematics are illustrated using the isochron diagram (Fig. 2.6). In general, metamorphic redistribution of Rb and Sr will give a spread of points on the isochron diagram (Fig. 2.6c). Following evolution of the various subsystems (Fig. 2.6d) it may be difficult or impossible to extract information on either the age of the original sedimentary rock or on the time of metamorphism even if an appropriate sampling program can be designed.

Figure 2.5. An example of metamorphic resetting of Rb, Sr isotopic systems. Note movement of metamorphically disturbed systems to higher $^{87}Rb/^{86}Sr$. From Compston *et al.*, 1966

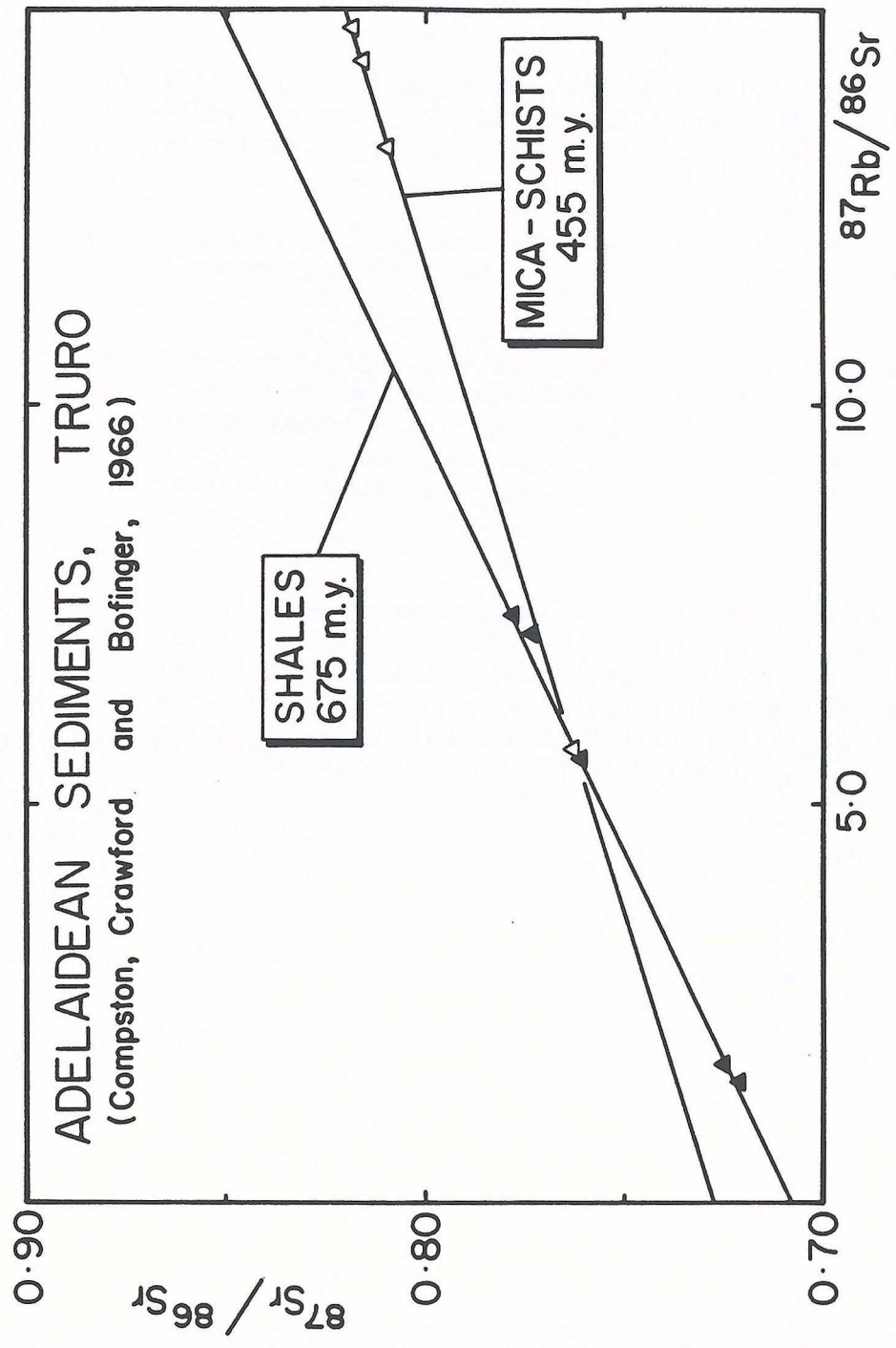
ADELAIDEAN SEDIMENTS, TRURO
(Compston, Crawford and Bofinger, 1966)
SHALES
675 m.y.
MICA-SCHISTS
455 m.y.
0·90
0·80
0·70
87Sr / 86Sr
5·0
10·0
87Rb/86Sr

Figure 2.6. Diagram illustrating systematics of metamorphic resetting of Rb, Sr isotope systems

(a) Deposition of sediments with a considerable range in $^{87}Rb/^{86}Sr$ and a relatively small range in $^{87}Sr/^{86}Sr$ at time $t=t_0$.

(b) Rotation of line because of acculmulated radiogenic Sr between time $t=t_0$ and $t=t_1$. Slope of line gives age.

(c) Development of new subsystems during metamorphism. Each subsystem has the $^{87}Sr/^{86}Sr$ of its parental volume, and different $^{87}Rb/^{86}Sr$ dependent on mineralogy. Lines joining samples from each subsystem have zero slope, indicating zero age (for the metamorphic redistribution event).

(d) Rotation of lines because of accumulation of radiogenic strontium between times $t=t_1$ and $t=t_2$. Slope of total rock line (circles) gives sedimentation age; slope of metamorphic subvolume line (squares) gives age of metamorphism. Note diffuse spread of points to the high $^{87}Rb/^{86}Sr$ side of the total rock line.

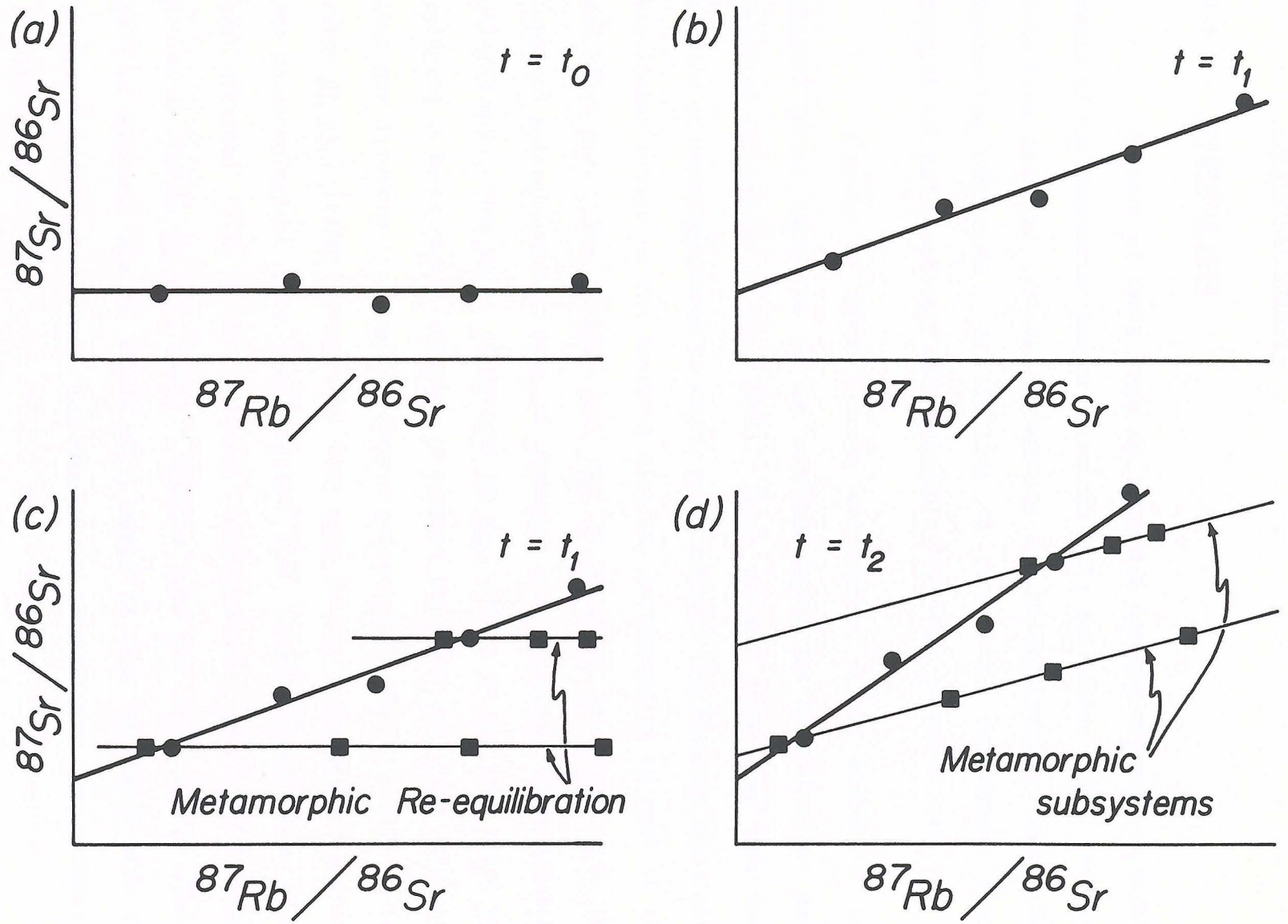
(a)
t = t_o
87Sr/86Sr
87Rb/86Sr
(b)
t = t_1
87Rb/86Sr
(c)
t = t_1
87Sr/86Sr
Metamorphic Re-equilibration
87Rb/86Sr
(d)
t = t_2
Metamorphic
subsystems
87Rb/86Sr

2.4 RB, SR AND $^{87}SR/^{86}SR$ WITHIN PRE-BATHOLITHIC ROCKS OF THE PENINSULAR RANGES

2.4.1 PREVIOUS WORK

As part of their study of strontium isotope systematics within rocks of the Peninsular Ranges batholith Early and Silver (1973) reported data from selected typical sedimentary and metasedimentary rocks that hosted the intrusives. At the time of batholithic development these samples all had relatively non-radiogenic $^{87}Sr/^{86}Sr$ (0.704-0.714).

A study of Rb-Sr isotope systematics within shales of the Bedford Canyon Formation of the northern Santa Ana Mountains has been reported (Criscione et al., 1978). These workers found that data from samples of unmetamorphosed to weakly metamorphosed argillaceous shale gave two linear arrays on the isochron diagram, corresponding to ages of 171±3 and 220±4 m.y. The younger age was in apparent agreement with the reported paleontological ages of Bajocian and Callovian (approximately 181-163 m.y., time scale of Harland et al., 1982); at the time there was believed to be no fossil evidence to support the older age (Late Triassic) (but see discussion of Bedford Canyon paleontology above, p.31). Criscione et al., (1978) interpreted both ages dating sedimentation events, and paleontological data that support this interpretation have since been obtained (T.E. Davis, personal communication, 1982; D.L. Jones, quoted in Gastil et al., 1981). Samples from the Santa Monica slates gave an apparent age of 153±14 m.y., again in good agreement with the paleontological age of Late Oxfordian-Early Kimmeridgian (approximately 158-150 m.y.).

These data are particularly important in that they apparently constrain deposition and subsequent isotopic homogenization of the argillaceous sediments, and the deposition of the carbonates to have occurred within a relatively short time interval. This apparent synchroneity of the palaeontological evidence (from the carbonates) and isotopic results (from the shales) implies that, although the carbonate lenses have been interpreted as tectonic or slump blocks, they might have formed nearly concurrently (perhaps within a few million years) with deposition of the siliceous material. If this is so, the limestone blocks may not be allochthonous as suggested by Moran (1976). Given the complexity of the Bedford Canyon formation, with fossils reportedly ranging in age from Triassic through Middle Jurassic (T.E. Davis, personal communication, 1982), much work remains to be done to clarify the interpretation of these Rb-Sr data.

The combined $^{87}Sr/^{86}Sr$ and Rb/Sr data were interpreted by Criscione *et al.*, (1978) as showing that the Bedford Canyon formation was derived from a different source terrain than the Santa Monica slates, and that a component of young igneous material not equilibrated with sea-water strontium was more important in the younger slates.

Data from two samples of sandstone from the Bedford Canyon Formation have lower $^{87}Sr/^{86}Sr$ at a particular Rb/Sr than do the shales, whilst data from obviously metamorphosed samples from the Santa Monica slates scatter about the linear array defined by the unmetamorphosed rocks. The lower $^{87}Sr/^{86}Sr$ of the sandstones was not discussed by Criscione *et al.*, (1978), but perhaps reflects less complete equilibration with sea-water strontium of the coarser mineral fraction (particularly

plagioclase) of these rocks.

2.4.2 SAMPLING AND ANALYTICAL PROCEDURES

Samples were selected in an attempt to delineate isotopically distinctive zones within the pre-batholithic rocks of the northern-most Peninsular Ranges. Data from three samples from Baja California, and two composite samples from southern California (Early and Silver, 1973; L.T. Silver, unpublished data), as well as the results of Criscione et al., (1978) were used in designing the sampling scheme. It was not expected that anything but the most general age information would be obtained in the present study. Geographic coverage and an attempt to collect material with a high Rb/Sr were the major considerations in later sample selection. The use of high Rb/Sr samples from high-grade metamorphic terrains poses a potential problem in that it may be difficult to distinguish between the metamorphosed equivalent of original argillaceous material and metamorphically produced layering.

Up to several hundred grams of selected chips were ground in a tungsten carbide lined SPEX "Shatterbox". Rb and Sr concentrations and $^{87}Sr/^{86}Sr$ were determined on an aliquot of this powder using standard isotope dilution procedures (Appendix 1). Analytical data for 33 samples are given in Table 2.1. Brief descriptions of these samples, and sample locations are given in an appendix (Appendix 2). Sample localities are shown on Fig. 2.7. $^{87}Sr/^{86}Sr$ is reported referenced to a value of 0.70800 for the Eimer and Armend $SrCO_3$ standard.

Figure 2.7. Sample localities. Circles, shale-sandstone belt; upright triangles, quartz-rich samples from San Jacinto Mountains; inverted triangle in San Jacinto Mountains, Windy Point' metamorphics; inverted triangles in Baja California, Alisitos Formation; squares, Coyote Mountains.

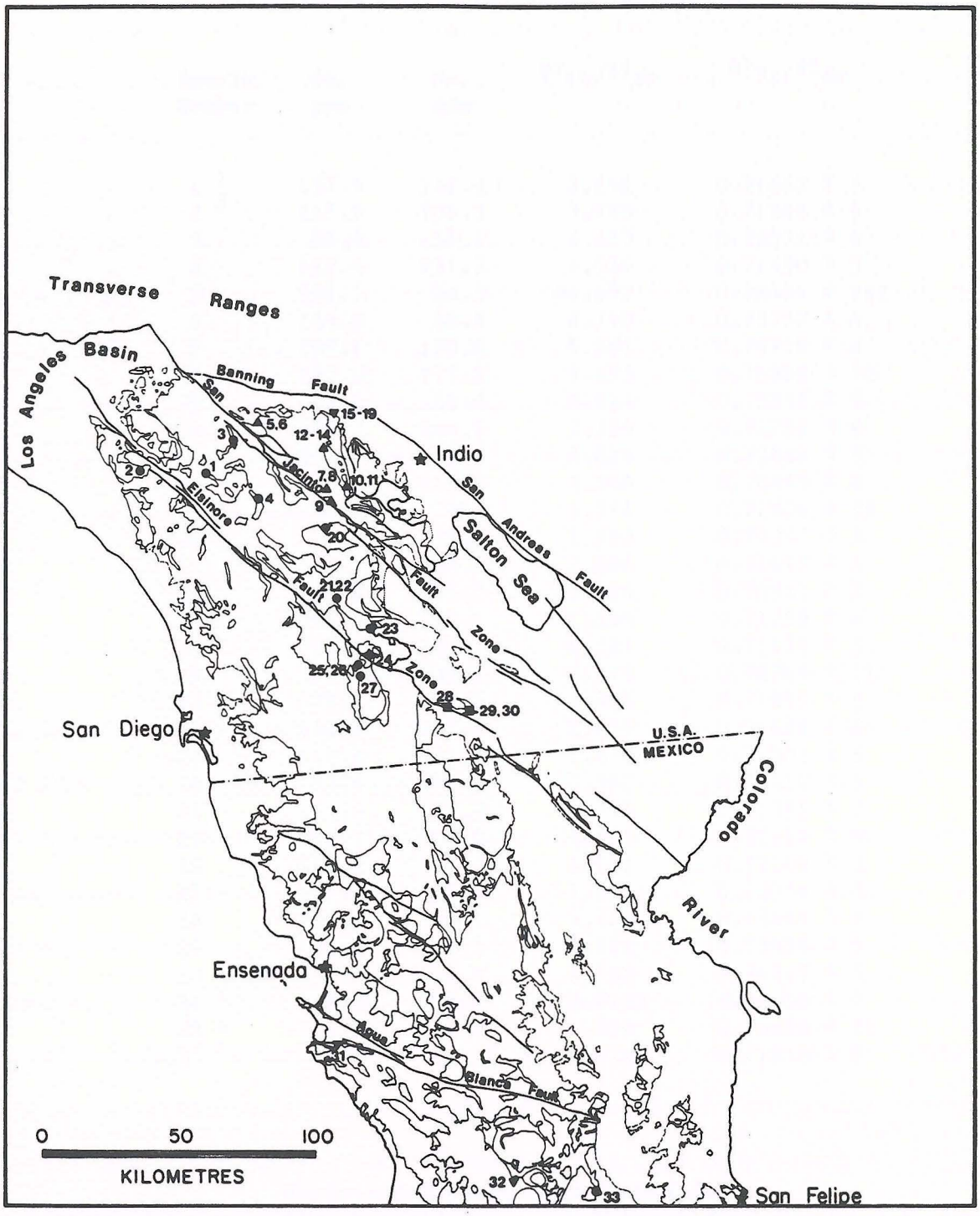
Transverse Ranges
Los Angeles Basin
San Banning Fault
15-19
5.6
12-14
3
1
2
Jacinto
7,8
10,11
9
4
Elsinore
Fault
20
21,22
23
24
25,26
27
Zone
28
29,30
Indio
San Andreas Fault
Salton Sea
Fault
Zone
San Diego
U.S.A.
MEXICO
Colorado
River
Ensenada
Agua
Blanca
Fault
32
33
San Felipe
0
50
100
KILOMETRES

TABLE 2.1

RB, SR, AND $^{87}SR/^{8}$ SR DATA FOR METASEDIMENTARY WALL ROCKS, NORTHERN PENINSULAR RANGES BATHOLITH

Sample Number	Rb, ppm	Sr, ppm	$^{87}Rb/^{86}Sr$	$^{87}Sr/^{86}Sr$
1 [1]	132.5	132.5	2.895	0.71663 ± 5
2 [2]	137.5	105.3	3.783	0.71949 ± 4
3	86.4	54.1	4.633	0.72571 ± 6
4	122.5	231.3	1.534	0.71580 ± 5
5	252.7	16.5	44.692	0.78494 ± 192
6	153.9	66.6	6.710	0.73797 ± 4
7	193.1	120.0	4.681	0.76729 ± 6
8	181.0	117.8	4.473	0.76989 ± 10
9	19.0	60.4	0.914	0.72531 ± 5
10	194.7	264.9	2.129	0.71729 ± 6
11	231.9	139.5	4.824	0.73924 ± 5
12	129.2	113.7	3.308	0.76843 ± 8
13	34.0	77.3	1.274	0.72906 ± 26
14	27.2	58.3	1.353	0.73397 ± 4
15	164.9	165.6	2.884	0.71417 ± 4
16	153.9	363.7	1.224	0.70911 ± 5
17	361.9	90.1	11.639	0.71789 ± 4
18	84.9	387.1	0.635	0.71121 ± 5
19	69.0	535.0	0.373	0.70769 ± 11
20	79.1	65.5	3.494	0.71837 ± 8
21	140.5	197.7	2.059	0.71663 ± 4
22	157.6	271.7	1.679	0.71202 ± 6
23	83.6	244.0	0.992	0.71410 ± 5
24	130.7	79.0	4.795	0.71985 ± 7
25	142.7	100.8	4.105	0.72155 ± 5
26	154.6	111.7	4.011	0.72162 ± 3
27	131.8	203.0	1.879	0.70959 ± 5
28	256.6	164.7	4.520	0.73644 ± 4
29	125.5	149.6	2.434	0.73658 ± 5
30	150.5	92.9	4.703	0.74243 ± 5
31 [1]	6.37	790.1	0.0233	0.70456 ± 7
32 [1]	54.6	81.8	1.929	0.70822 ± 21
33 [1]	73.5	72.8	2.920	0.71618 ± 6

[1] Early and Silver, unpublished data
[2] Gromet and Silver, unpublished data

2.5 RESULTS

These samples can be divided into two groups on the basis of their $^{87}Sr/^{86}Sr$ and $^{87}Rb/^{86}Sr$ (Fig. 2.8). A relatively radiogenic group includes samples from the San Jacinto and Coyote Mountains, and contains no samples from the "shale-sandstone belt" of Gastil *et al.*, (1975)[Fig. 2.1]. The second, relatively non-radiogenic group contains samples from the Alisitos Formation, from various units of the "shale-sandstone belt" (the Bedford Canyon, French Valley and Santa Eulalia Formations, and the Julian schists), from Windy Point in the north-eastern San Jacinto Mountains, as well as a single sample from the southern San Jacinto Mountains. After a brief review of metamorphic effects, relationships within these two groups will be discussed in detail.

2.5.1 METAMORPHIC EFFECTS

One of the problems inherent in selecting samples for an isotopic study within a high-grade metamorphic terrain is the development of mica-rich layers by metamorphic segregation that are difficult to distinguish from the metamorphosed equivalents of original argillaceous sedimentary units. Two such layers have probably been sampled in the present study, and a brief discussion of the Rb-Sr systematics of these samples is helpful at this point in understanding the effects of metamorphic redistribution of Rb and Sr within the other samples. Sample (5) is a biotite-muscovite-sillimanite schist (with very minor quartz) from a small roof pendant in a large tonalite that underlies much of the south-western San Jacinto Mountains. Sample (6), from within the same roof pendant, is mineralogically similar but contains some quartz. Samples (16) and (17) are, respectively, biotite-poor and biotite-rich

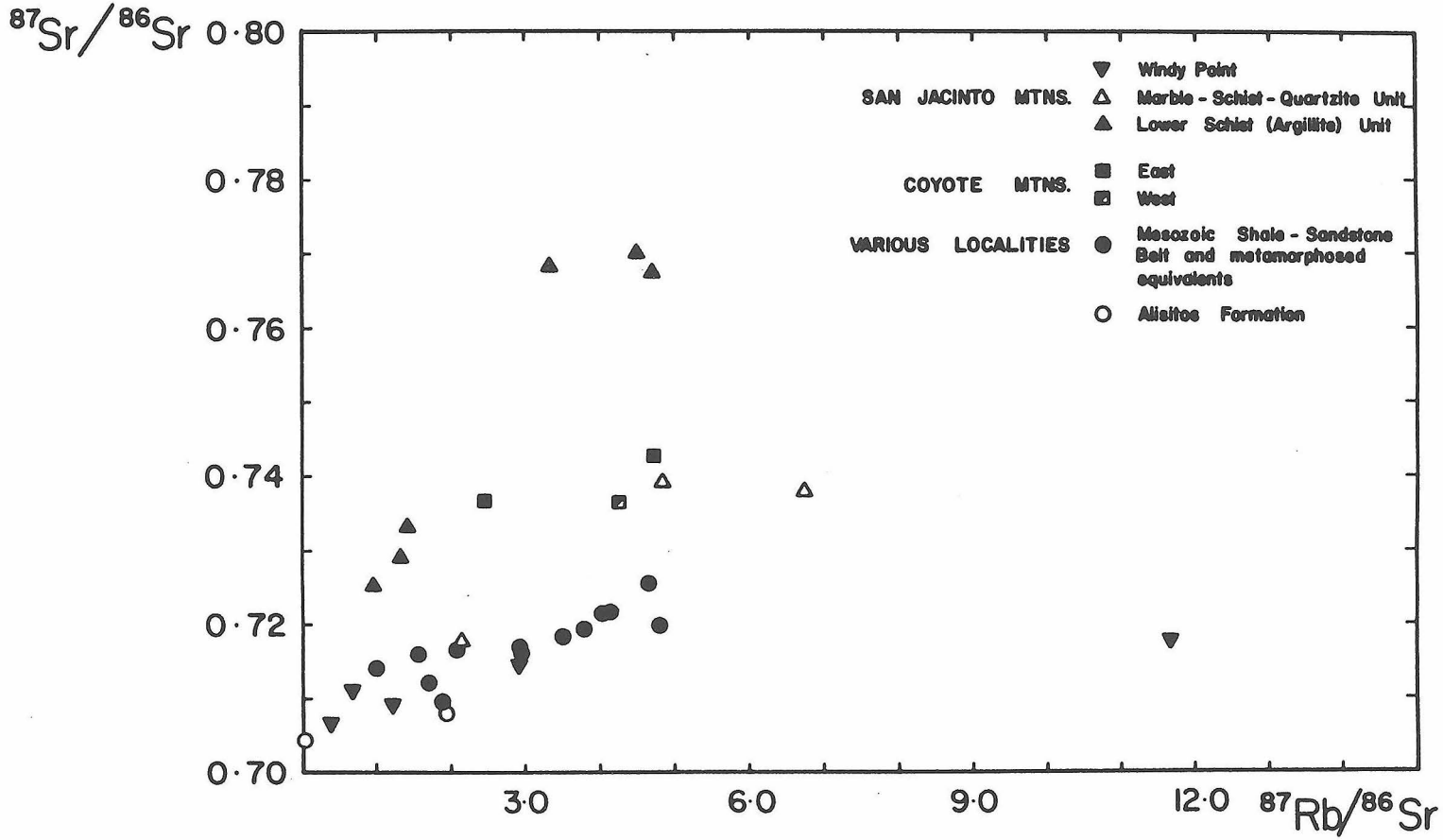

Figure 2.8. Isochron diagram showing data from this study (Table 2.1). Symbols as shown. Note that samples from the Mesozoic shale-sandstone belt (circles) have lower $^{87}Sr/^{86}Sr$ for a given $^{87}Rb/^{86}Sr$ than do quartz-rich samples from the San Jacinto and Coyote Mountains.

Windy Point at the north-eastern extremity of the San Jacinto Mountains. Data from these samples are shown plotted on the isochron diagram (Fig. 2.9).

The slopes of lines joining these two groups of points are approximately those expected if there has been complete or near complete equilibration of their strontium isotopes in Late Cretaceous time (≈60 -90 m.y.). The local intrusive rocks have been dated by U-Pb isotopes in zircons at 97±1 m.y. (L.T. Silver, personal communication). K-Ar ages from biotite and hornblende (Armstrong and Suppe, 1973) and fission track ages from a suite of minerals (Dokka and Frost, 1978) are lower than the zircon U-Pb results and have been interpreted (Krummenacher et al., 1975; Dokka and Frost, 1976; Silver et al., 1979) as demonstrating a prolonged thermal history for these rocks.

The Rb-Sr data obtained from the four schist samples (5,6,16,17) are thus consistent with disturbance of their isotope systems by thermal effects associated with emplacement of the Cretaceous plutons. Re-equilibration at the scale of the samples (a few tens of cm^3) has apparently been largely complete, and probably accompanied recrystallization to new mineral assemblages.

These samples illustrate the probable behaviour of Rb and Sr during metamorphism. $^{87}Sr/^{86}Sr$ tends to be equilibrated within subsystems having different Rb/Sr, with the scale of the redistribution being a function of the redistribution process. The net effect is to produce a scatter of points to the high Rb/Sr side of the isochron diagram.

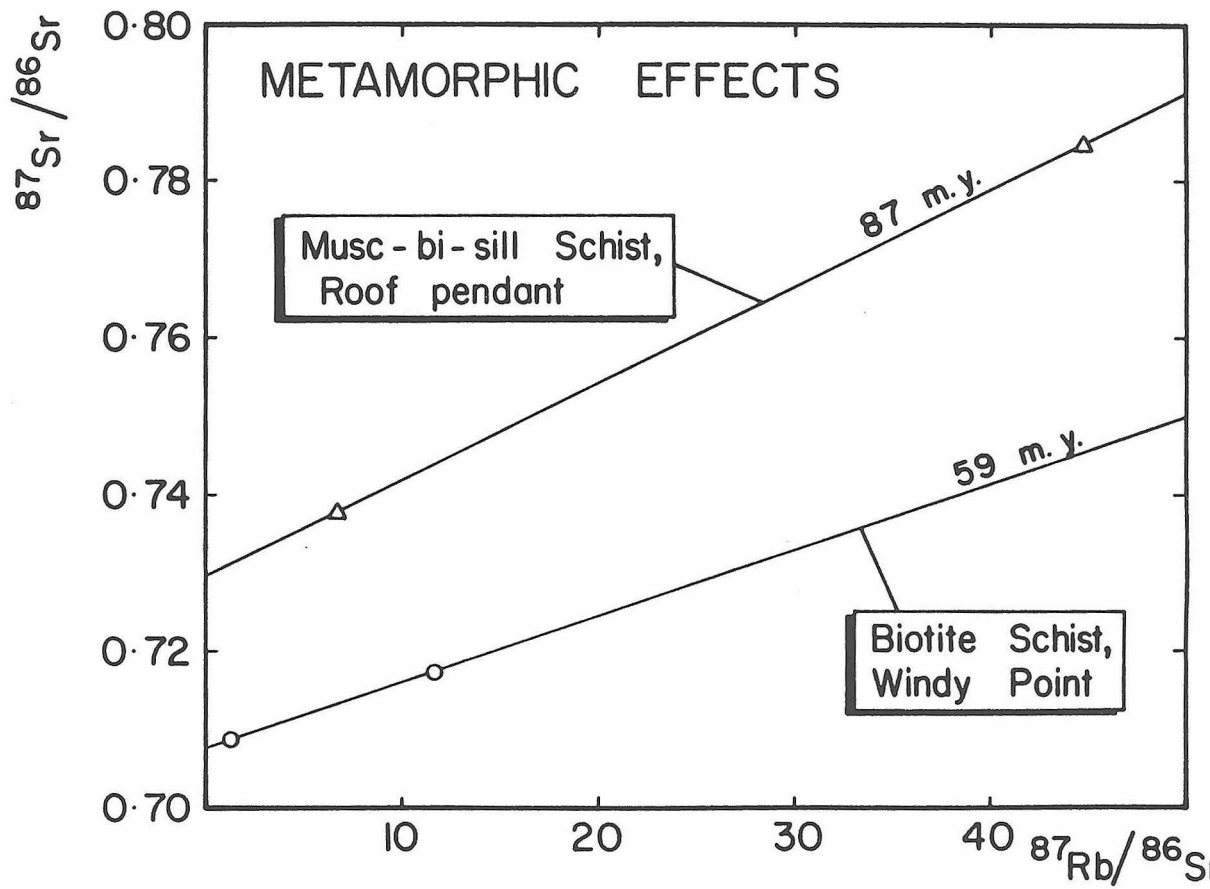

Figure 2.9. Isochron diagram showing inferred metamorphic redistribution in schist samples. 'Ages' are inferred to have no geological significance.

2.5.2 RELATIVELY NON-RADIOGENIC GROUP

South of the San Jacinto Fault

Alisitos Formation

Two samples from the Alisitos Formation of Baja California reported by Early and Silver (1973) have low measured $^{87}Sr/^{86}Sr$ and low $^{87}Rb/^{86}Sr$. A zircon U-Pb date of 125±5 m.y. has been reported from a tuff interbedded with fossiliferous Upper Aptian Alisitos strata (Silver et al., 1969). Early and Silver used this age to calculate apparent initial $^{87}Sr/^{86}Sr$ for these samples and obtained values of 0.7045 and 0.7047. These calculated initial Sr ratios are relatively insensitive to errors in the value taken for the age, and are completely consistent with derivation of these sedimentary rocks from the developing batholith and its associated volcanic ejecta (Silver et al., 1956, 1963, 1969; Early and Silver, 1973). The low values inferred for the initial $^{87}Sr/^{86}Sr$ are interpreted as resulting from little modification of these primitive igneous source materials; any exchange with sea-water strontium has been either minimal or has been buffered by the relatively huge reservoir of strontium contained within the developing sedimentary pile.

Shale-Sandstone and Graywacke Sequences of the Northern Batholith

Thirteen samples of sedimentary rock from the extensive shale-sandstone and graywacke sequences from both the western and central part of the batholith form a tight grouping on the isochron diagram (Fig. 2.10). Three of these samples (1,2,33) are composite samples collected by L.T. Silver to be representative of the sedimentary sequence at a

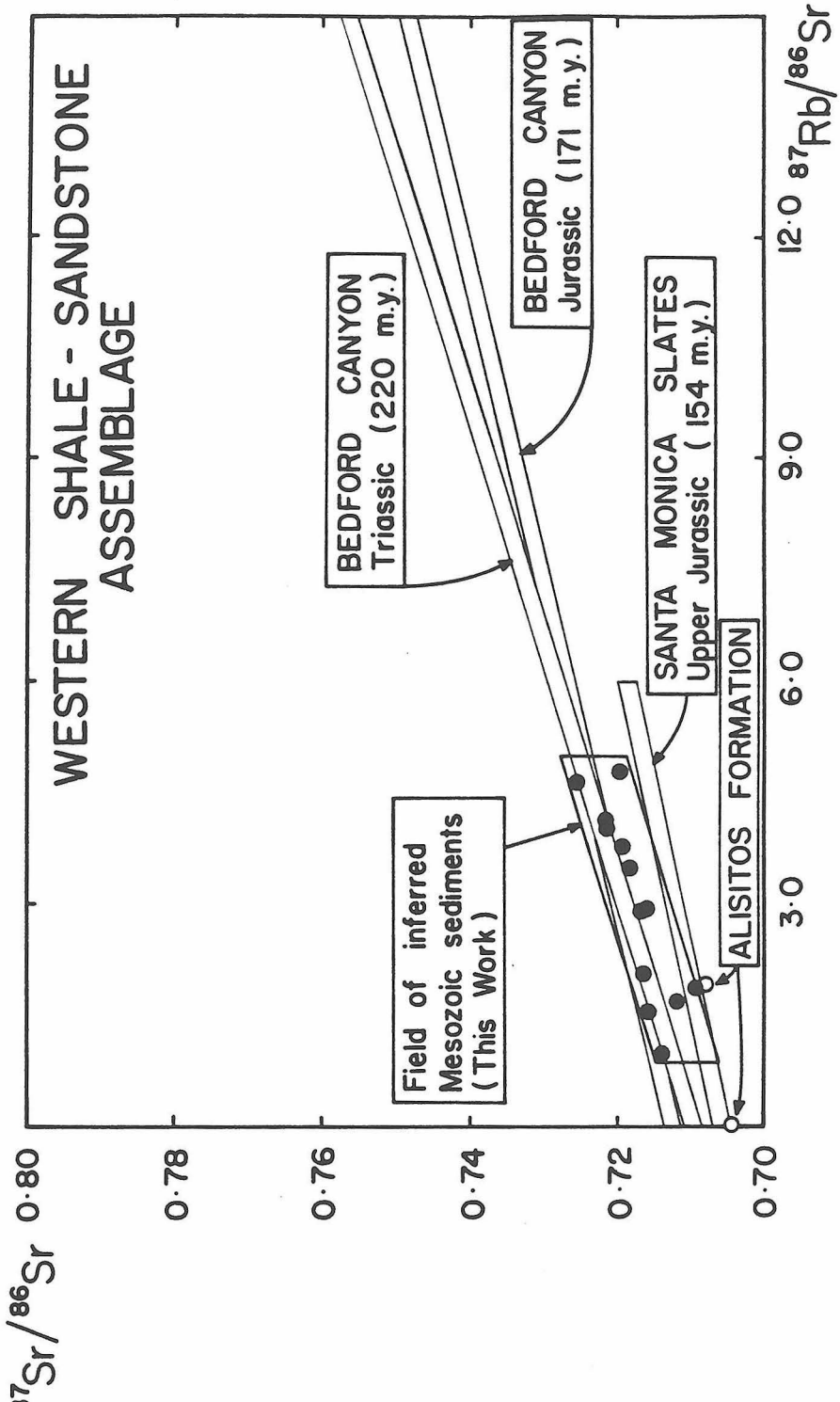

Figure 2.10. Summary of Rb, Sr isotopic data from Mesozoic and inferred Mesozoic metasedimentary sequences from the northern Peninsular Ranges.

particular locality. Data from two of these composite samples (1,33) have been presented previously (Early and Silver, 1973), where the results from the sedimentary rocks were compared to data obtained from samples of the batholithic intrusives. These workers concluded that there was no apparent relationship between the values of initial $^{87}Sr/^{86}Sr$ calculated for the plutonic rocks and the strontium isotope properties of their sedimentary and metasedimentary host rocks.

Samples collected for the current study were selected to give geographic coverage, to be as fresh as possible, and to have higher Rb/Sr. These rocks are meta-arenites (plagioclase+quartz+biotite±sillimanite± K-feldspar± muscovite±cordierite±graphite) except for (3,4 and 20) which are metaquartzites (quartz+biotite±sillimanite±muscovite± plagioclase). Two samples (25,26) also contain staurolite. None of these rocks would have had a predominantly argillaceous protolith. The data for these samples are plotted on Fig. 2.10, along with the fields for shales from the Bedford Canyon Formation and the Santa Monica slates reported by Criscione et al., (1978). Also shown are data for two samples of sandstone from the northern Santa Ana Mountains analysed by Criscione et al., (1978), and the two Alisitos Formation samples of Early and Silver (1973). The shales from the Bedford Canyon Formation analysed by Criscione et al., (1978) have higher Rb/Sr than the present samples, and also tend to be slightly more radiogenic. This latter feature perhaps reflects the presence of detrital micas in these finer-grained rocks.

All samples from this coherent suite of rocks (predominantly metamorphosed feldspathic graywackes, but with a few quartzites) form a tight grouping on the isochron diagram (Fig. 2.10). Such a relationship

and source terrain for all of these rocks. If such an inference is correct, the whole suite must have components of at least as disparate sedimentation age as the Bedford Canyon formation i.e., of at least from Late Triassic to latest Middle Jurassic. Such a range of paleontological ages suggests an absolute age range of some 70 m.y. - from perhaps 230 to 160 m.y. [time scale of Harland et al., (1982)]. If it is assumed that the Rb/Sr and $^{87}Sr/^{86}Sr$ for each sample was fixed immediately following deposition (but see discussion above), an apparent initial $^{87}Sr/^{86}Sr$ (at sedimentation) can be calculated for any assumed age. For an assumed age of 230 m.y., calculated deposition $^{87}Sr/^{86}Sr$ ranges from 0.703 to 0.711 [mean 0.7077±0.0024(1σ)]. For an assumed age of 160 m.y., calculated deposition $^{87}Sr/^{86}Sr$ would range from 0.705 to 0.715 [mean 0.7107±0.0024 (1σ)]. Over this same time interval, the $^{87}Sr/^{86}Sr$ ratio of sea-water appears to have decreased steadily, from ≈ 0.7077 at the beginning of the Late Triassic to ≈ 0.7068 at the end of the Middle Jurassic (Burke et al., 1982). Thus, if all samples are of Late Triassic age, these data might be interpreted as demonstrating that most of these samples apparently closely approached isotopic equilibrium with contemporaneous sea-water. Such an argument is, however, inconclusive; Clauer and his colleagues have demonstrated that equilibration of strontium in a developing sedimentary pile is probably buffered by the largest strontium reservoir present (usually the developing sedimentary sequence itself) rather than by sea-water strontium (Clauer et al., 1975). This is well demonstrated by the two samples from the Alisitos Formation analysed by Early and Silver (1973). The strontium isotopic composition of these rocks subsequent to deposition has been controlled by their relatively huge inherent strontium concentrations relative to any circulating fluids,

such as sea-water. The isotopic composition of strontium in marine sediments thus presents somewhat of a dilemna. These data might be interpreted as showing a similarity of both sedimentation age and protolith age. If the estimated $^{87}Sr/^{86}Sr$ at or shortly after deposition is not that of contemporaneous sea-water strontium, it is possible to argue that equilibration with sea-water has not been complete. If $^{87}Sr/^{86}Sr$ is identical to that of contemporaneous sea-water, then either equilibration has been complete or the inherent strontium isotopic composition of the developing sedimentary pile was similar to that of contemporaneous sea-water. Burke et al., (1982) argue that the strontium isotopic composition of sea-water has varied between limits of 0.7067 and 0.7091 over the past 500 m.y.. Many sediments probably have $^{87}Sr/^{86}Sr$ within this range (e.g., Biscaye and Dasch, 1971). It is clear that the use of depositional $^{87}Sr/^{86}Sr$ as a provenance indicator is fraught with difficulties unless extremes of isotopic composition (<0.706, >0.710) are represented in the sediments.

If these sediments were deposited more recently than Late Triassic, calculated depositional $^{87}Sr/^{86}Sr$ is proportionally higher. For instance, if the sediments are 160 m.y. old (Medial Jurassic), 10 of the 13 samples have calculated depositional $^{87}Sr/^{86}Sr$ of 0.710 or greater, apparently ruling out complete equilibration with contemporaneous sea-water (≈ 0.707). This would imply a significant contribution to the Sr balance of the sediments from somewhat older, more radiogenic materials. The scant fossil evidence is suggestive of an older (Triassic) rather than younger (Jurassic) assignment for the bulk of these rocks. However, until a more definite age assignment can be made, either by paleontological or geochronological means, little can be said about the provenance(s) for

these sediments other than that there is no direct evidence in the Sr isotopic data for the presence of either a major highly radiogenic component (probably older) or a major relatively non-radiogenic component (such as recently formed crust) within these rocks. These data do not, however, exclude the possibility of such components being present; the masking of such components by nearly complete equilibration between the Sr of the sediments and sea-water Sr cannot be discounted.

The data presented here, in combination with the data reported by Criscione et al., (1978), are consistent with, but do not prove, the possibility that all of these rocks were formed in Mesozoic time. The isotope data are thus in accord with the paleontological evidence summarized above, but extend the region underlain by rocks of probable Mesozoic (Jurassic and Triassic) age for some distance east and south of the known fossil occurrences, and into much more highly metamorphosed sections of the pre-batholithic sedimentary rocks where fossil preservation is less likely.

Northeast of the San Jacinto Fault

Six metasedimentary rock samples from the San Jacinto Mountains north-east of the San Jacinto Fault fall within the relatively non-radiogenic group. Five of these are from a thick section of carbonates, schists and gneisses exposed at Windy Point and described by Sydnor (1975). The other is a sample of quartz-biotite schist from the Bull Canyon Formation of Brown (1968, 1981) in the southern-most San Jacinto Mountains. This latter sample is from a sequence of rocks for which other samples plot in the radiogenic field (but scatter widely), and will be considered with these relatively radiogenic samples.

One of the samples from Windy Point (17) appears to have high Rb/Sr as a result of metamorphic differentiation processes, and has been discussed above. The other four samples are of highly metamorphosed relatively plagioclase-rich sediments, and have low $^{87}Sr/^{86}Sr$ and low Rb/Sr. These four samples have similar measured $^{87}Sr/^{86}Sr$ for a given Rb/Sr as do the samples discussed above, although their overall Rb/Sr tends to be lower (Fig. 2.8). Calculated $^{87}Sr/^{86}Sr$ at 160 m.y. is 0.706-0.710; at 230 m.y. it is 0.705-0.709. The calculation assumes no redistribution of Rb relative to Sr during post-sedimentation processes, perhaps an unwarranted simplification for these intensely metamorphosed rocks.

These data are, perhaps, most consistent with this sequence being a Mesozoic or latest Paleozoic sedimentary pile derived largely from synchronous or only slightly older additions to the continental crust.

2.5.3 RELATIVELY RADIOGENIC GROUP

Samples within the relatively radiogenic group come from two areas - the San Jacinto Mountains at the north end of the Peninsular Ranges, and the Coyote Mountains, an isolated range in the desert southwest of the Salton Sea (Fig. 2.2). These two localities are on opposite sides of the eastern Peninsular Ranges mylonite zone and associated cross-cutting thrusts (Sharp, 1979), and are thus from the lower and upper plates respectively (see Fig. 2.2).

Samples from the Upper Plate Assemblage

The samples from the Coyote Mountains are of cordierite-andalu-

site and muscovite-garnet schists. A late Early Ordovician to early Medial Ordovician conodont fauna has been described from meta-carbonates in the eastern Coyote Mountains (near samples 29 and 30); these rocks are thus probably between 470 and 490 million years old (Harland et al., 1982; Ross et al., 1982). The data are plotted with a 475 m.y. reference isochron on Fig. 2.11. Samples (30) and (31) are from a large slab of cordierite-andalusite schist criss-crossed by innumerable thin (< 1mm) quartz veins. It appears probable that there has been considerable redistribution of Rb and Sr during this metamorphism. This severely limits any inferences that might be made from these data regarding either the age of sedimentation (or diagenesis), or the provenance for the sedimentary materials. If the samples analysed are from part of the Ordovician sequence, it is most probable that they had relatively high (>0.710) $^{87}Sr/^{86}Sr$ at deposition. This is suggestive of the possibility that an older continental terrain was the source for much of the sedimentary material.

Samples from the Lower Plate Assemblages

Ten samples from seven localities within the San Jacinto Mountains are shown plotted on the isochron diagram (Fig. 2.12). The considerable scatter evident may reflect metamorphic effects, although this could also represent substantial variations in both age and provenance of the different samples.

The metamorphic rocks of the San Jacinto Mountains consist of thick sections of schists, gneisses, meta-carbonates and quartzites. The largest area of continuous outcrop is astride the Desert Divide between the southern San Jacinto Mountains and the northwestern Santa Rosa Moun-

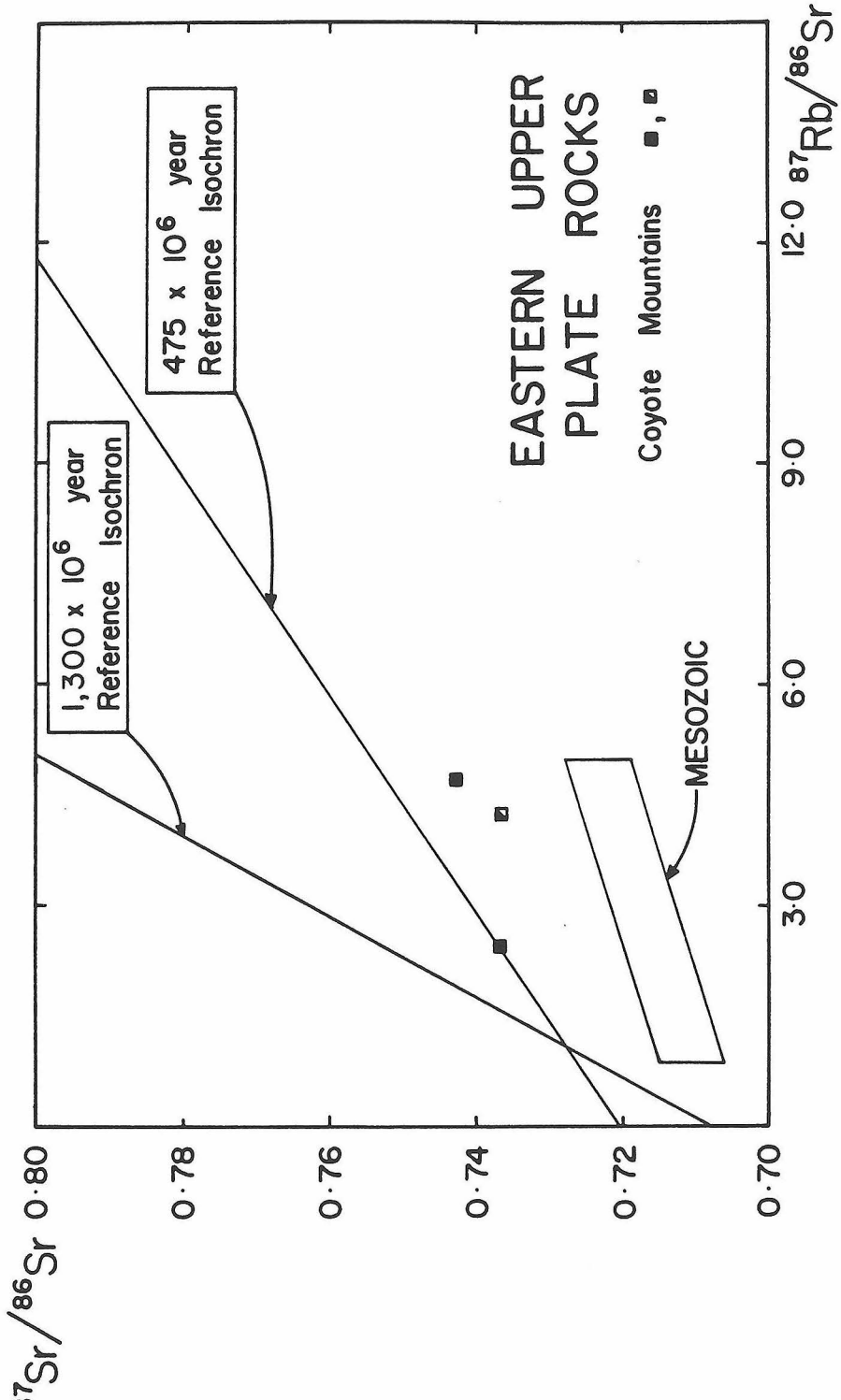

Figure 2.11. Isochron diagram for three rocks from the Coyote Mountains.

Figure 2.12. Isochron diagram for 11 samples from the San Jacinto Mountains. Filled upright triangles: Quartz-rich schists and gneisses from the Desert Divide Group of Brown, 1968, 1981; Filled inverted triangles: Plagioclase-rich schists from the Windy Point metamorphics (Sydnor, 1975); Open triangles: biotite muscovite- and biotite-tourmaline schists schists from the San Jacinto Mountains. These latter three samples are interpreted as showing considerable redistribution of Rb and Sr during metamorphism.

Fields for the Mesozoic shale-sandstone assemblage rocks, and for the Cretaceous Alisitos Formation rocks are shown for comparison. Note general separation between quartz-rich San Jacinto samples and relatively quartz-poor Mesozoic rocks.

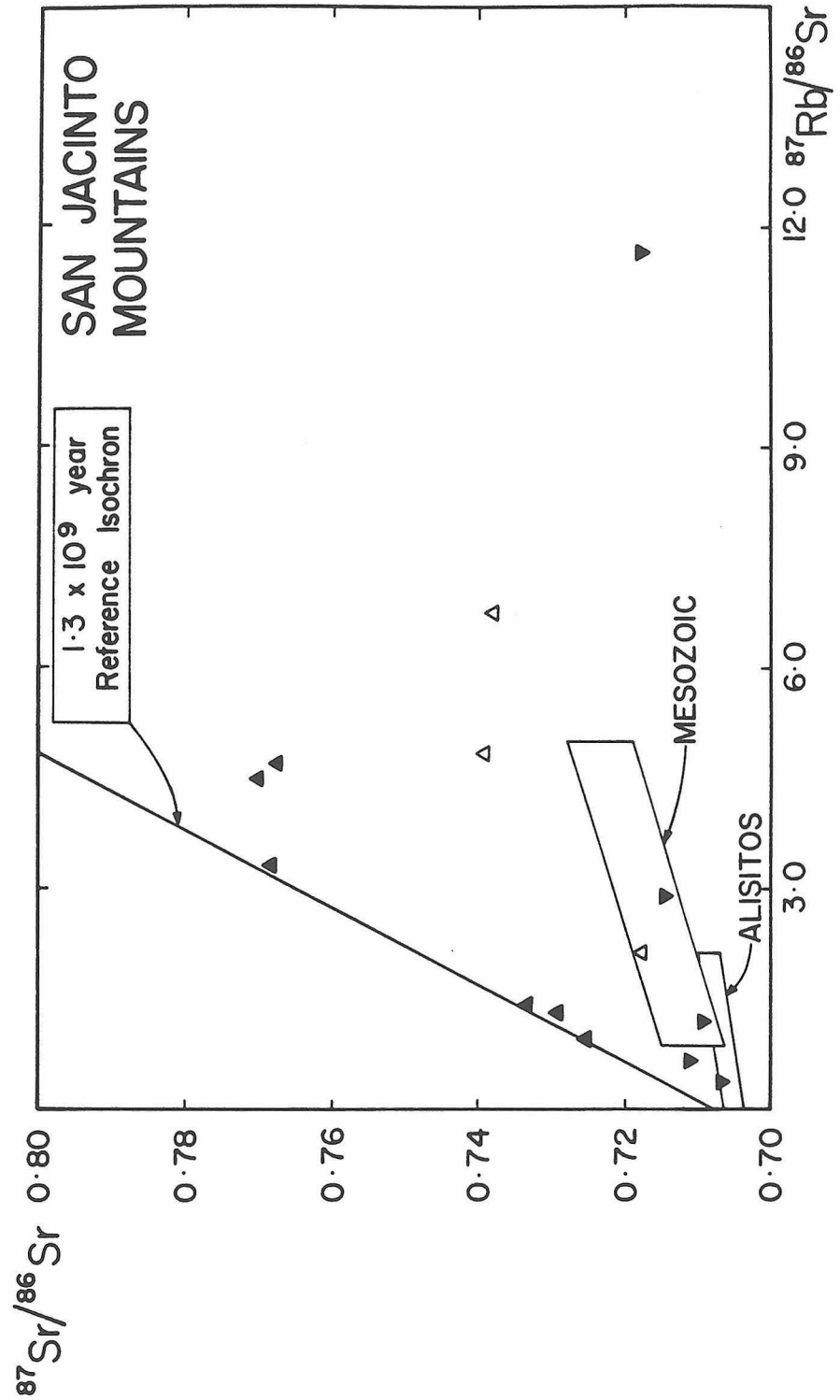
SAN JACINTO
MOUNTAINS
1·3 x 10⁹ year
Reference Isochron
MESOZOIC
ALISITOS
0·70
0·72
0·74
0·76
0·78
0·80
3·0
6·0
9·0
12·0
87Sr/86Sr
87Rb/86Sr

tains. A sequence with a structural thickness in excess of 4300 m has been mapped by Dibblee (1981e) and described by Brown (1968, 1981). Figure 2.13 is a generalized stratigraphic column (modified from Brown, 1981) and shows the relative location of several of the Rb/Sr samples within the sequence. The other samples analysed in the present study are from small screens and roof pendants, and their position within the sequence can only be estimated very approximately. Samples (9), (12) and (13) probably come from the schist-dominated lower third of the section, whereas (5) and (6) are from a sequence of interbedded schists, marbles, calc-silicates and quartzites, and thus are probably from near the structurally highest part of the column. Large variations in the thicknesses of distinctive units (such as the marbles and the quarzite) along strike attest to considerable lateral variation within the section. Apparent grading within individual quartzite layers near the base of the thick quartzite unit suggest that at least this part of the section is upward-facing. It is possible that materials of a variety of ages occur within this sequence. Although the gross asymmetry of the section studied by Brown is suggestive of no large-scale repetition within the sequence, the high metamorphic grade and the development of a prominent metamorphic fabric could mask substantial repetition at smaller scales (less than a few hundred meters).

Samples (12),(13) and (14) are schists collected from the inferred lowest part of the section. These samples were collected over a distance of a few meters from a sequence where regular lithological layering, probably original bedding, is preserved. Sample (9) is a biotite quartzite. These four samples do not show a penetrative schistosity, and may be the least disturbed of the San Jacinto Mountains

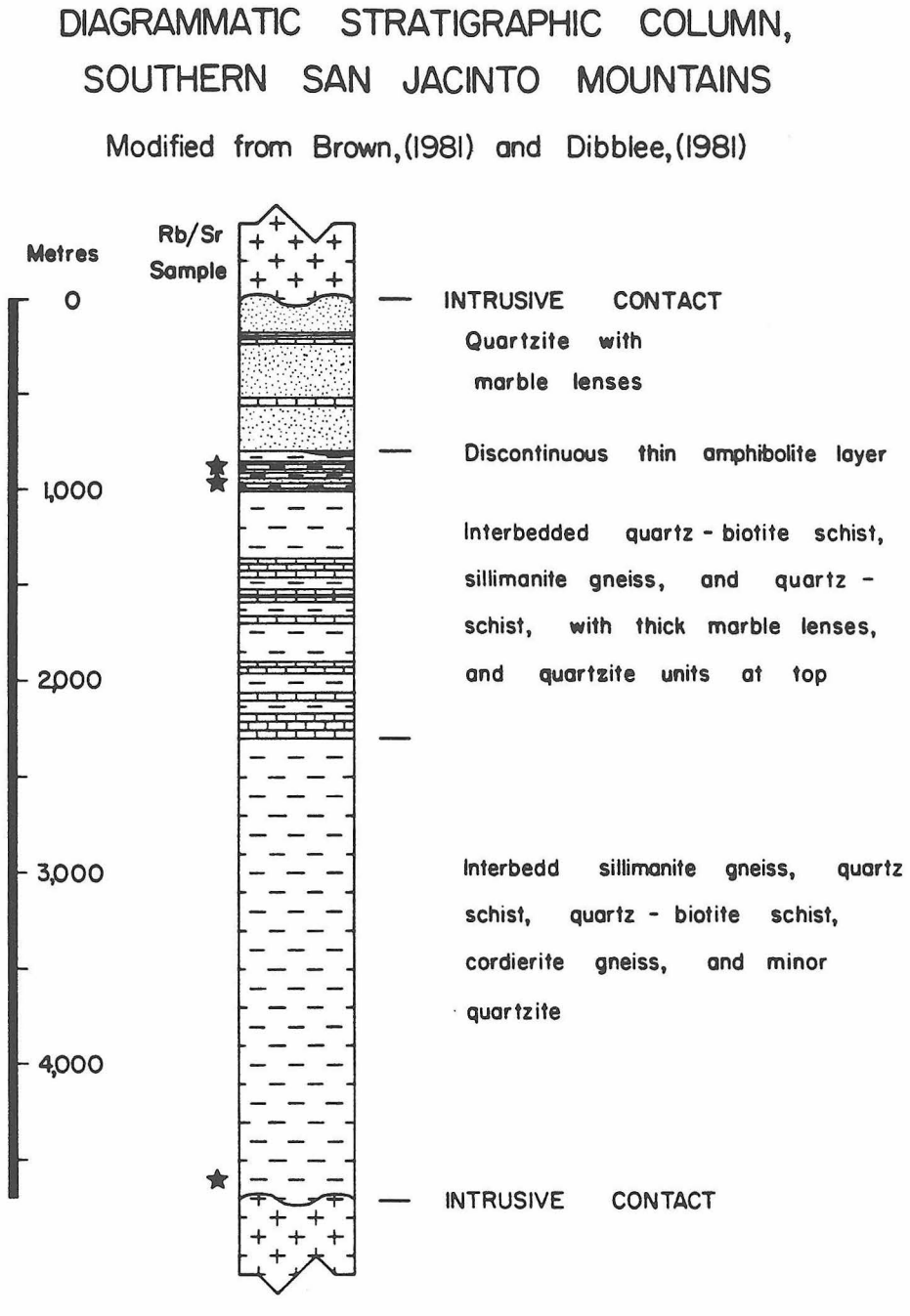

Figure 2.13. Diagrammatic stratigraphic column for metasedimentary rocks of the Desert Divide. Stars show relative sample locations.

samples. Metamorphic mineral assemblages imply equilibration at pressures of 3.2-3.5 kb. and temperatures of 620-660°C (Ch. 3.). These conditions are just below the 'granite minimum', and there is no evidence for melting in suitable compositions.

These samples form a linear array on the isochron diagram; the slope of this linear array corresponds to an age of $\approx 1.3 \times 10^9$ years, and implies an initial $^{87}Sr/^{86}Sr$ of 0.708. A 1.3×10^9 year reference isochron is shown on Fig. 2.12. Because of the low (0.708) intercept at Rb/Sr = 0, the slope of this line may be interpreted as indicating an upper limit to the possible age of these samples. The line could also be a mixing line between materials with different properties (such as source or age); if so, it would have no explicit age significance. These data are suggestive that the sequence could contain a Proterozoic component.

The other samples from the San Jacinto Mountains come from rocks that are either more intensely metamorphosed, or deformed, or both. Samples (7) and (8), for instance, are from a block of sillimanite-garnet schist cut by veins of granitic composition. These samples all apparently scatter to the higher Rb/Sr side of the isochron diagram, but define a field that is still largely distinct from that of the non-radiogenic group.

The highly radiogenic nature of these rocks is most simply interpreted as indicating the presence of components of old cratonic material within these sequences, or of the presence of old (?Precambrian) sediments. Studies of Sr isotope systematics during sediment transport and deposition (e.g., Biscaye and Dasch, 1971) suggest that there is

sufficient mixing of the various contributions to the sediment pile to limit $^{87}Sr/^{86}Sr$ to relatively low values (<0.730, usually lower). Faure et al., (1963) used biogenic lacustrine carbonates to directly estimate the mean Sr isotopic composition of the exposed rocks of the 2.5-2.7 b.y. Kenoran (Superior) Province of North America to be 0.721±0.005. Younger provinces gave correspondingly less radiogenic mean $^{87}Sr/^{86}Sr$. Gast (1960) had previously obtained similar values using a less direct technique. These studies suggest that sediments derived from large continental areas are unlikely to have mean $^{87}Sr/^{86}Sr$ of 0.730 or greater. Model ages for the three most radiogenic samples (7,8,12) calculated using 0.730 for the 'initial' $^{87}Sr/^{86}Sr$ are between 550 and 700 m.y.. These calculated values strongly suggest that these sedimentary rocks were deposited during Lower Paleozoic or Upper Precambrian time.

2.6 DISCUSSION

The results of the limited sampling reported here demonstrate that it is possible to distinguish between sedimentary units within a complex metamorphic terrain using isotope data. This is possible in this case because of the probable large differences in age or provenance, or both, between the units present.

The largely volcanogenic sediments of the late Early Cretaceous Alisitos formation had been shown previously to have Sr isotopic characteristics consistent with derivation from a synchronous igneous arc (Early and Silver, 1973). The present study, in combination with the earlier work of Early and Silver (1973) and Criscione et al., (1978), demonstrates that there is remarkable isotopic homogeneity within the bulk of the (apparently) prebatholithic rocks of much of the northern Peninsular

Ranges. This homogeneity is most simply interpreted as showing approximate contemporaneity (to within perhaps 100 m.y.), and similar source materials for all of these rocks. The data are consistent with, but do not prove, suggestions from scattered fossil localities that all of these graywacke-slate dominated sequences are of Mesozoic age.

Although these data limit the boundary between the relatively non-radiogenic (?Mesozoic) and the relatively radiogenic (?pre-Mesozoic) suites to within a few kilometers in places, the nature of this contact is completely unknown. The boundary could be a depositional contact or a fault of one of several types (strike-slip, normal or thrust).

2.6.1 Regional Implications

Models for the Mesozoic development of the western margin of the North American continent are currently in a state of flux. Several episodes of Cenozoic and Mesozoic disruption of the continental margin have been suggested by various authors. Latest Cenozoic truncation and translation by the Gulf of California - San Andreas rift-transform system is comparatively well understood (e.g., Hill and Dibblee, 1953; Crowell, 1962; Atwater, 1970), although uncertainty exists as to the role of a proposed "proto - San Andreas" (e.g., Nilsen, 1978; Hall, 1981). Total offset on the currently active strand of the San Andreas seems to be about 330 km of right-lateral motion (Crowell, 1981). Faults west of the main San Andreas system may add another 120 km of right-lateral motion, giving the 450 km of total offset across the plate margin inferred to have occurred since initiation of the current rift-transform system by Atwater and Molnar (1973).

Deciphering the effects of earlier displacements has proven difficult. Jones et al., (1982) and Howell et al., (1982a,b) suggest that the western margin of North America has been constructed from a collage of accreted terranes, some of which are inferred to have been translated in a right-lateral sense (northward) along the continental margin many thousands of kilometers. Silver and Anderson (1974, 1983), on the other hand, propose that the continental margin has been truncated and disrupted in Late Jurassic time, and cite evidence for major (1000+ km) left-lateral translation along the continental margin. Silver points out that the elucidation of such lateral displacements is complicated by the occurrence of considerable younger horizontal displacement involving transport distances of 100 km or more (Silver, 1982, 1983).

It is thus of interest to consider whether the sedimentary rock units (and their subjacent basement materials) of the Peninsular Ranges have plausible correlatives elsewhere along the continental margin of North America, or whether they are indeed truly exotic as has been suggested by Jones and Howell and their colleagues. The nature of possible basement materials and their relative positions is of fundamental importance in understanding the origins, histories, and inter-relationships of the various magmatic arcs that developed adjacent to this continental margin throughout Mesozoic time.

2.6.2 STRONTIUM ISOTOPE DATA FROM PRE-CENOZOIC SEDIMENTARY AND METASEDIMENTARY ROCKS OF WESTERN NORTH AMERICA

Isotope data offer potential for paleogeographic reconstruction in three areas - age information, provenance inference, and direct correlation. Although the isotopic and geochemical characteristics of the

plutonic rocks of western North America are among the best documented of any suite of rocks anywhere, there has been relatively little work published on the isotope systematics of the sedimentary and metasedimentary rocks of the same region.

Several studies contain isotope data pertinent to the present discussion. The work of Criscione et al., (1978) on shales from the Bedford Canyon Formation and the Santa Monica slates has been detailed above. A similar study by McJunkin et al., (1979) found, for fine-grained argillite deposited on pillow basalts of the Smartville ophiolite sequence of the northern Sierra foothills a Rb/Sr whole rock age of 152±3.6 m.y. and initial $^{87}Sr/^{86}Sr$ of 0.70932±0.00025. This age agrees well with zircon U-Pb dates (155-164 m.y.) on plagiogranites from the underlying ophiolitic suite (Bond et al., 1977; McJunkin et al., 1979; Xenophontos and Bond, 1978). The value obtained for the initial $^{87}Sr/^{86}Sr$ is considerably higher than estimates for contemporaneous sea-water (Burke et al., 1982)[≈ 0.7068], suggesting the presence of a continent-derived component in these argillites.

Peterman et al., (1967) studied Sr isotope systematics within parts of the Great Valley Sequence and the Franciscan Formation of central California. They reported inferred initial $^{87}Sr/^{86}Sr$ of 0.7045-0.7081 for samples from the Franciscan Formation, and initial $^{87}Sr/^{86}Sr$ of 0.7030-0.7043 for samples from the Great Valley Sequence that range in age from Early to Late Cretaceous. The data from the Great Valley Sequence indicate derivation with very little isotopic modification from the western-most rocks of the early to mid Mesozoic Sierra Nevada batholith (or its volcanic equivalents), or from similar rocks elsewhere along the

Mesozoic magmatic arc. The Franciscan Formation rocks, on the other hand, show evidence for either more interaction with sea-water Sr or a small component of older crustal material.

Several samples of pre-batholithic rock have been analysed as part of a Rb, Sr and Sr isotope study of the Sierra Nevada batholith (Kistler and Peterman, 1973). Two composite samples from the Upper Paleozoic or Early Mesozoic Calaveras sequence of the Sierran foothills (FD39, FD46) have initial Sr of ≈0.707-0.709. Neodymium data for these samples are interpreted as indicating the derivation of a major component from Precambrian continental sources (DePaolo, 1981). The apparent low initial $^{87}Sr/^{86}Sr$ thus suggests that alomost complete equilibration with sea-water strontium occurred during sedimentation or diagenesis. A muscovite quartzite from a roof pendant within the batholith (Le 143) is probably from the lower unit of the Shoo Fly Complex (Schweickert, 1981). It has relatively high $^{87}Sr/^{86}Sr$ for its $^{87}Rb/^{86}Sr$ (0.7497 and 4.035, respectively), consistent with the Lower Paleozoic age inferred for the lower Shoo Fly (e.g., Schweickert, 1981).

Samples of other rock types, including volcanic, volcanic composite, and highly metamorphosed varieties, were also analysed (Kistler and Peterman, 1973).

2.6.5 POSSIBLE CORRELATIVES OF THE NON-RADIOGENIC ("?MESOZOIC") GROUP

Relations within the older Mesozoic rocks of the Peninsular Ranges are not well known. Within the Santa Ana Mountains Triassic and Jurassic rocks of similar lithologies are tectonically interleaved in complex fashion (Criscione et al., 1978; T.E. Davis, personal communi-

cation, 1982). The package has been interpreted as an accretionary prism (Criscione et al., 1978) and perhaps represents the oceanward part of a forearc assemblage that has been disrupted by tectonic interleaving synchronous with deposition (during presumed Triassic and Jurassic subduction) or perhaps by later subduction or transform processes. If this interpretation is correct, it is not immediately clear as to where the arc that provided these supposed forearc sediments is now located.

East of the Santa Ana Mountains the metasedimentary rocks apparently form a less tectonically disrupted sequence, with increasing proportions of rocks interpreted as having more continental affinities (e.g., Schwarcz, 1969; Merriam, 1946). Amphibolites, quartzites and shale-graywacke units increase in abundance eastward. In the Julian area limestones (marbles) begin to be more important elements within the section. All of the lithological relations point to an eastern source for these sediments, with the eastern-most rocks indicating proximity to a nearby continental mass (e.g., Schwarcz, 1969).

The thick carbonate-schist-gneiss (limestone - volcaniclastic) sequence that is exposed at Windy Point in the northern San Jacinto Mountains could represent the most continentward part of this assemblage. If so, this argues for a contribution to this sedimentary pile from young igneous materials. Perhaps the relative contributions from different source terrains to this developing sedimentary pile varied as a function of time. Alternatively, the Windy Point rocks could be correlative with the metamorphosed argillite and tuffaceous argilllite, graywacke, conglomerate, chert, limestone, and basalt of the section described in the Sierra Pintas of northern Baja California that includes at least

a small late Paleozoic component (McEldowney, 1970).

Jones et al., (1976) correlate the Santa Monica slates and the Bedford Canyon Formation with the western and eastern metamorphic belts of the Sierran foothills, respectively. More recent workers have subdivided the eastern metamorphic belt of Jones and colleagues. Saleeby, for instance, recognizes a more westerly Calaveras sequence and a more easterly Kings sequence (Saleeby, 1981). The Calaveras was deposited in deeper water, and contains only a minor component of silicieous volcanic material compared to the Kings sequence. The relatively non-radiogenic suite defined here for the pre-batholithic rocks of the Peninsular Ranges has similar Sr isotopic properties to composite samples from the Calaveras Formation of the Sierran foothills (FD39, FD46) reported by Kistler and Peterman (1973). The term "Calaveras Formation" is used differently by different authors (e.g., Schwiekart, 1981; Saleeby, 1981). The Calaveras (in the sense of Saleeby, 1981) has yielded fossils of Permo-Carboniferous and Triassic age, although the Permo-Carboniferous limestones are interpreted as allochthonous blocks enclosed in a younger sedimentary matrix (Saleeby, 1981). The presence of blocks of older limestone in a younger clastic matrix is also a feature of the Bedford Canyon Formation (J. Criscione, personal communication, 1983). The paleontological and isotopic data are consistent with this proposed correlation of the Mesozoic assemblages of the Peninsular Ranges and the Calaveras Formation of the western Sierra Nevada.

Jones et al., (1976) pointed out significant lithological disparities between these apparently similar age rocks. These disparities apparently relate to comparison of the Peninsular Ranges rocks with the

siliceous-volcanic rich Kings sequence. Relations between the Calaveras and Kings sequences are not clear (Saleeby, 1981), although similarities between the western-most rocks of the Kings sequence and the eastern-most rocks of the Calaveras may be interpreted as showing that the two sequences were once gradational into each other (Saleeby, 1981).

The Kings sequence, a thick section of quartzite, argillite, limestone and volcanic and volcaniclastic rocks of Late Triassic through Medial Jurassic age (Saleeby, 1981) is more similar to the eastern-most portions of the shale-sandstone assemblage of the Peninsular Ranges. The Kings sequence could conceivably be the continentward extension of the Peninsular Ranges rocks offset in a left-lateral sense along the continental margin in post-Middle Jurassic time as implied by the model of Silver and Anderson (1983). If so, the Calaveras sequence would be the northward extension of the more westerly part of the non-radiogenic belt.

The close of the Middle Jurassic seems to mark a major change in the provenance of sedimentary materials deposited along this part of the continental margin. Sediments younger than Middle Jurassic (e.g., Santa Monica slates, Great Valley Sequence) tend to have low initial $^{87}Sr/^{86}Sr$, indicating increased contributions from primitive materials recently added to the continent. This is also a time of considerable tectonic complexity, and a time of transition from the Jurassic magmatic arc to the Cretaceous arc system (Fig. 2.3).

The isotope data currently available are thus seen to be consistent with correlations made from other information between the metasedimentary sequences of the Peninsular Ranges and those of the Sierra

Nevada. However, rocks of similar age and lithofacies could well have been deposited adjacent to any continental margin abutting the paleo-Pacific (or even elsewhere!), so that age and lithological correlation does not necessarily imply any geographical relationship. Isotope studies of sediment provenance might, in favourable circumstances, be able to demonstrate spatial relationship between similar age sedimentary sequences, or even relationship to a particular source area. It is not yet possible to do this for the Mesozoic sedimentary sequences of western North America using strontium isotope systematics.

2.7 CONCLUSIONS

The data presented here demonstrate that Sr isotopes can be used to make inferences regarding the age and provenance of metasedimentary rocks within a major batholithic terrain. In particular, Sr isotope data have been used to distinguish belts of apparently different age metasedimentary rocks within the Peninsular Ranges of southern California. The strontium isotope data allows the recognition of two groups of rocks that have disparate isotope properties. Approximate boundaries between these two suites can be delineated, even within rocks of high (upper amphibolite facies) metamorphic grade.

A third suite (that includes the late Lower Cretaceous Alisitos Formation) has been previously shown to have different Sr isotope properties to either of the suites delineated herein (Early and Silver, 1973), but is much more simply and satisfactorily differentiated using more traditional criteria such as paleontology and sedimentology.

There appears to be no systematic variation of Sr isotope prop-

erties with geographic position within the non-radiogenic belt. Samples collected specifically for this project included a variety of rock-types, but were generally from the finer-grained portions of the sequences. Estimated depositional $^{87}Sr/^{86}Sr$ for these samples falls within the range reported for contemporaneous sea-water Sr by Burke et al., (1982). It is impossible to infer whether the $^{87}Sr/^{86}Sr$ of the sediments is a provenance characteristic, or is the result of at least partial equilibration between the sedimentary pile and sea-water. This precludes use of these data for inference of sedimentary provenance for these rocks. Initial $^{87}Sr/^{86}Sr$ for the shales from the Bedford Canyon formation studied by Criscione et al., (1978) is more radiogenic than that estimated for the metamorphosed arenites and quartzites studied here. The Bedford Canyon formation data were interpreted by Criscione et al., (1978) as indicating derivation of this unit from an old igneous-metamorphic terrain. These data may also be interpreted as resulting from the incorporation of detrital micas (not necessarily particularly old) that failed to equilibrate with sea-water Sr into the finer-grained portions of the sedimentary pile.

Rocks from the quartz-rich sequences of the eastern batholith have distinctly more radiogenic Sr than the graywacke-rich sequences of the central and western batholith. Three samples of metasedimentary rock from east of the eastern Peninsular Ranges mylonite zone have Sr isotope properties consistent with a probable Ordovician age inferred from paleontologic data. Samples of schist, gneiss and quartzite from the San Jacinto Mountains have Sr isotope properties that imply the presence of a pre-Mesozoic (perhaps Lower Paleozoic or Precambrian) component within these metasedimentary sequences.

The available Sr isotope data from Mesozoic sedimentary rock sequences of western North America are permissive of deposition of these materials adjacent to the then existing continental margin. However, they cannot be used to disprove hypotheses that involve large components of either sinistral or dextral transport along this developing margin during or following deposition.

CHAPTER 3

GEOLOGY OF THE NORTH-WEST SAN JACINTO MOUNTAINS

PART 1: PREVIOUS WORK AND STRATIGRAPHY

3.1 INTRODUCTION

The following discussion of the geology of the San Jacinto Mountains is intended to introduce the major rock units, and to provide a context within which the subsequent detailed discussion of field, stratigraphic, structural, and petrographic relationships can be considered. Regional context has been provided in Chapters 1 and 2; this chapter (Ch. 3) presents geological and stratigraphic data pertinent to the present study, while Chapters 4, 5, and 6 respectively present detailed structural, petrographic, and mineral chemical data.

The north-western San Jacinto Mountains are underlain by a variety of metamorphic and igneous rocks of pre-Cretaceous and Cretaceous age, and by local veneers of clastic sedimentary rocks. These various units are differentiated on the geological map (Plate 1, end pocket). As the major aim of the present project was a study of the igneous rocks, only a cursory structural and stratigraphic examination of the various areas of exposure of metasedimentary rock was made. With the exception

---

[1] Sample locations are given relative to the 1000-meter Universal Transverse Mercator grid, zone 11, 1927 North American Datum, which is superimposed on the geological map (Plate 1) and which is available on all recent topographic maps issued by the United States Geological Survey. Appendix 3 is a description of the use of this grid system.

of the rocks exposed at Windy Point and vicinity (G.R. 349508)[1], the metasedimentary sequences are dominated by quartz-rich schists and gneisses. Lesser amounts of quartzite and metacarbonate are also present. The sequence at Windy Point contains plagioclase amphibolites, various calc-silicate rocks, and abundant metacarbonate. Metamorphic grade is consistently in the almandine-amphibolite sub-facies of regional metamorphism, and mineral assemblages suggest metamorphic temperatures of 600-650°C and pressures of 3.2-4.2 kb.. Present relief alone implies a variation of 0.7 kb, and peak temperature reached was probably quite variable, especially adjacent to large intrusive masses. Isotopic data from the sedimentary rocks presented above (Ch. 2, p.60) are consistent with the interpretation that at least some of the metamorphism relates to emplacement of the igneous rocks.

Field mapping has allowed the recognition of many (perhaps hundreds) of individual igneous intrusive units. Only the larger of these are shown on the geological map (Plate 1). Units were differentiated using a combination of lithological and structural features. A relative chronology of emplacement has been established. This allows the igneous rocks to be subdivided into two major groups - "early intrusives" and "major tonalites". "Early intrusives" are generally small, having dimensions ranging from the meter scale to a few kilometers, and cover the entire compositional range of the calc-alkaline rock suite (from olivine-bearing gabbro-norites to granodiorites and granites). These intrusions commonly show evidence for deformation and recrystallization, especially adjacent to contacts with large younger intrusive masses.

The "major tonalites" clearly post-date these small early

intrusions, and comprise the bulk of the igneous material of the San Jacinto Mountains. Three separate intrusive units were mapped in detail (Plate 1). The oldest major tonalite intrusion, called simply Unit I (Kt_1) is a large elongate body oriented north-west south-east, and is some 42x8 km in maximum lateral dimensions. It was intruded into pre-existing igneous and metasedimentary materials. Contacts are sharp, and there has been little visible interaction between the tonalite and the older rocks. Before solidification was complete Unit I was intruded by the second major tonalite unit, Unit II (Kt_2). This mass apparently had a large (10x10 km) funnel-shaped core from which a long dike-like apophysis extends some 25 km into the country rocks (including Unit I). Unit III (Kt_3) intrudes both Unit I and Unit II, and was probably emplaced before Unit II was completely solidified. It crops out over an approximately rectangular area of about 20x12 km, and appears funnel-shaped in three dimensions, the funnel opening upwards. Areas of roof-rock to all three intrusions are still extant, and the sides of the intrusions commonly dip inward. Considerable field evidence exists for multiple episodes of relative movement <u>within</u> each major intrusion (and also within several of the smaller early masses) and it appears very probable that each pluton was sequentially filled by many small increments of magma rising along a conduit or conduits and then being added to the expanding chamber.

Field relations allow for the determination of the relative timing of emplacement of the various intrusive units but can give little information on the absolute chronology. The evidence that suggests that Units II and III were at least in part emplaced into older intrusions that had not yet solidified implies that development of the entire igneous

construct could have been geologically quite rapid. Studies of U-Th-Pb isotope systems in multiple zircon fractions from five bodies covering the entire field-determined age sequence have been conducted by L.T. Silver. These data demonstrate unequivocally that the entire igneous complex crystallized within a very short period of time, at most some 2 m.y. The "early intrusives" are thus intimately related temporally as well as spatially to the larger (and better studied) "major tonalites". Because subtle geochemical and isotopic differences between these two groups become critical in developing a model for the genesis of the whole igneous complex it is important to stress that this subdivision into "early" and "major" intrusives is an arbitrary subdivision of a probable continuous sequence of intrusive activity.

3.2 PREVIOUS WORK

Much of the early geological investigation within the vicinity of the San Jacinto Mountains was stimulated by the occurrence of earthquakes, both within the immediate region and further afield. The earliest published study was of the effects of the San Jacinto earthquake of 1899. As part of the extensive investigation that followed the disastrous 1906 San Francisco temblor, Lawson et al. (1908) traced the San Jacinto fault from northwest of the town of San Jacinto southeastwards to Borrego Valley. They note that the 1899 temblor probably occurred on this fault. A large earthquake in 1918 stimulated further geological investigation of the San Jacinto fault system (Arnold, 1918; Rolfe and Strong, 1918; Townley, 1918).

Vertebrate fossils collected from Tertiary sediments that overlie both the pre-Cretaceous metamorphic rocks and the Cretaceous intrusive

rocks in the San Timoteo badlands and Bautista Canyon areas were described by Frick (1921). This paper contains a brief description of the struture and sedimentology of the often poorly consolidated terrestrial clastic units hosting the fossil material. The lowest unit, the Mount Eden Formation ("Eden beds" of Frick, 1921) crops out around San Jacinto Potrero (G.R. 060470) where it consists of pebbly sandstone and thin clay beds. It is of Hemphillian (Pliocene) age. Overlying the Mount Eden Formation are thick deposits of weakly indurated alluvial materials, the San Timoteo Formation. In the badlands east and southeast of Hemet (Plate 1) similar poorly consolidated sediments were named by Frick the Bautista Beds. Both the San Timoteo Formation and Bautista Beds yielded fossils diagnostic of Blancan (Plio-Pleistocene) age.

The first systematic geological mapping within the area was a reconnaissance study of the San Jacinto 30-minute (1:125,000) quadrangle (Fraser, 1931)[Fig. 3.1]. Fraser recognised and separated all of the major units defined by later workers. He also mapped and named many of the strands of the San Jacinto fault system for the first time. A detailed study of this fault system (Sharp, 1967) includes a large scale geological map that covers the southern-most portion of the area mapped during the present project (Fig. 3.1). Regional scale mapping by T.W. Dibblee in 1967-1968 (Dibblee, 1971; 1981a,b,c,d,e,f) covers the entire area of the San Jacinto Mountains (Fig. 3.1). Detailed reports by Brown (1968, 1980, 1981), Morton (1972) and Sydnor (1975) cover smaller, generally well-exposed portions of the area under current investigation. The work of Brown (1968, 1981) and Sydnor (1975) provides detail within the metasedimentary rocks, and has been used extensively in the preparation of the geological map (Plate 1). Morton et al. (1980) published

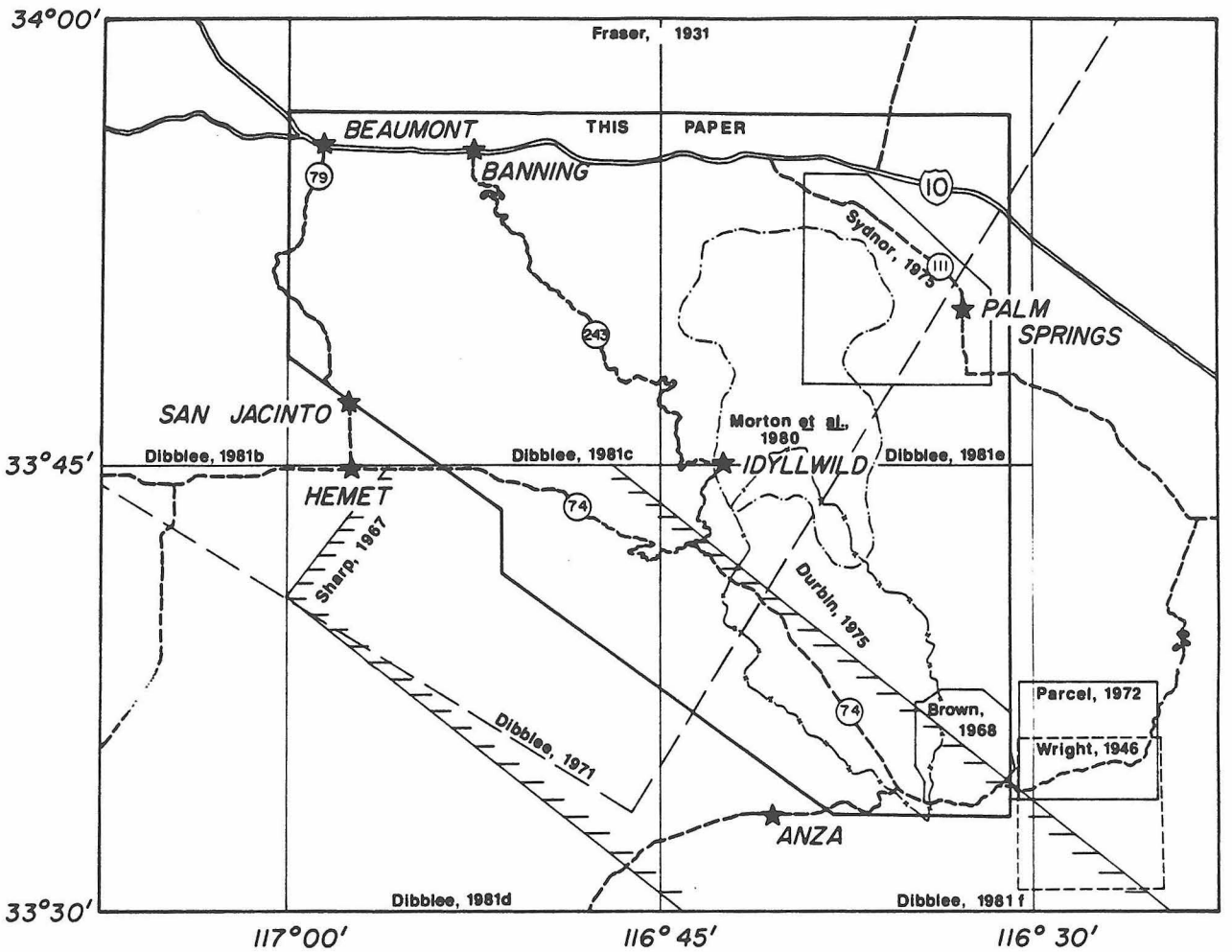

INDEX MAP TO GEOLOGICAL STUDIES IN THE SAN JACINTO MOUNTAINS

Figure 3.1. Previous geological studies in the San Jacinto Mountains.

a 1:62,500 scale geological map of that part of the study area within Mount San Jacinto State Park and adjoining National Forest Wilderness areas.

A recent publication of the South Coast Geological Society (Brown and Ruff, 1981) contains several short papers covering a variety of aspects of the geology of the San Jacinto Mountains. In addition to the papers by Dibblee and by Brown mentioned above other papers discuss seismic, hydrogeologic, economic geology and geophysical studies of selected areas. This volume also contains two short summaries of various aspects of the present study (Hill, 1981a,b).

3.3 ROCK UNITS

3.3.1 PRE-BATHOLITHIC ROCKS

The oldest rocks exposed in the San Jacinto Mountains are thick sequences of metasedimentary rocks that form the host rocks to the younger batholithic materials. Work on these metasedimentary rocks has been restricted largely to (1) delineation of outcrop extent, (2) a study of mineral assemblages in selected samples, and (3), a regional-scale study of Sr isotope properties (Ch. 2).

The distribution of metasedimentary rocks is shown on the geological map (Plate 1). Major areas of outcrop occur along the steep eastern scarp of the San Jacinto Mountains southward from Windy Point (G.R. 349508); astride the Desert Divide of the southern San Jacinto Mountains south from Red Tahquitz (G.R. 323352) to the Pines-to-Palms Highway; along the north-eastern and south-western flanks of Thomas Mountain (G.R. 295200); and in an extensive area north from Gilman Hot

Spring (G.R. 011436) almost to Banning (G.R. 115545), and thence eastwards along the northern range-front to Twin Pines Ranch (G.R. 193473). Isolated exposures occur east of Twin Pines Ranch at the northern-most extremities of ridges jutting into San Gorgonio Pass. No metasedimentary rocks are exposed within the majority of the main mountain mass.

The metasedimentary rocks show a dichotomy of lithologies. The majority of outcrops are of quartz-rich schists and gneisses, with lesser interbedded quartzite and metacarbonate rock. These rocks have been called the Desert Divide Group by Brown (1968, 1981) and are metamorphic rocks apparently derived from quartz-rich clastic sediments with interbedded carbonate units. The thick sequence of rocks exposed at Windy Point described by Fraser (1931) and Sydnor (1975), however, contains amphibolite and plagioclase amphibolite as well as schists, gneisses and marbles, and is lithologically distinct from the quartz-dominated sediments found elsewhere within the map area. These rocks apparently formed from a laterally variable sequence containing a considerable immature clastic component. These two units are described below.

3.3.2 WINDY POINT METAMORPHICS

Distribution

A roughly triangular area of metasedimentary rock is exposed on the steep eastern face of San Jacinto Mountain northwest of Palm Springs. The sequence crops out for about 7 km across strike in the Windy Point area, and extends southwards for over 10 km to Tahquitz Canyon. These rocks have been mapped by Sydnor (1975) who used the informal name "Windy Point metamorphics", from Windy Point where they

are best exposed. The section at Windy Point was estimated to be 1700 to 1800 meters thick (Sydnor, 1975); a similar stratigraphic thickness probably occurs east of Windy Point, but is buried beneath the fill of the Coachella Valley (Plate 1).

Lithology

Because of tectonic complexity no attempt has been made to date to measure a stratigraphic section within the "Windy Point metamorphics". Sydnor describes marbles, graphitic marbles, calcareous quartz schists, calc-silicate rocks (skarns), biotite quartzite, flaser gneiss, migmatite, pegmatite and a variety of schists (including biotite-plagioclase-quartz schist and muscovite-garnet-quartz schist) from this rock unit. Skarns contain calcite, grossularite, diopside, and tremolite, with lesser amounts of wollastonite, titanite, quartz, plagioclase and biotite. Titanite is locally abundant, and reaches 15% by volume in some rocks.

Several finer-grained schists from Windy Point were collected for a survey of Rb/Sr, $^{87}Sr/^{86}Sr$ systematics within metasedimentary rocks of the Peninsular Ranges (Ch. 2). Quartz, biotite, plagioclase and an opaque mineral are common to all samples (complete sample descriptions are given in Appendix 2). Sample (15) contains relatively quartz-rich and plagioclase-rich layers at the scale of a few millimeters. Plagioclase composition is bimodal; most is sodic labradorite (An_{50-55}; Michel-Levy method), with a lesser amount of sodic oligoclase (An_{35}). A few large grains of alkali feldspar are also present. This rock appears to have had a feldspathic volcaniclastic protolith. Sample (16) contains abundant brown amphibole (optically negative, high 2V; possibly an Fe^{3+}-rich hornblende) and diopside, as well as quartz, biotite, plagioclase

(An_{30-35}), calcite and minor apatite and opaques. The protolith must have contained substantial Fe, Mg, and Ca. The rock is now a plagioclase amphibolite. Samples (18) and (19) also contain brown amphibole (optically negative, $2V \approx 90^{o}$) but no pyroxene. They are also plagioclase amphibolites.

A striking characteristic of these plagioclase amphibolites and plagioclase-rich schists is the relative scarcity of zircon, especially of prominent zircon crystals enclosed within biotite. This is in contrast to the rocks of the Desert Divide Group described below, and also to the graywackes from elsewhere in the Peninsular Ranges collected for Rb/Sr analysis (Ch. 2).

Protolith

Sydnor (1975) considered that the protolith of these rocks was a sequence of interbedded limestones, quartz arenite and argillaceous sediments with local dolomitic limestone. The abundance of plagioclase, the calcic nature of some of this plagioclase (An_{35-55}), and the abundance of mafic minerals (especially hornblende) noted above suggest a substantial contribution from a relatively mafic igneous terrain, either as immature graywackes or as volcanogenic sediments. The relatively quartz-rich rocks imply contributions from a more mature source, while the thick carbonate lenses attest to biogenic activity. Overall, the diverse nature of the materials present suggests complex derivation.

Age

The age of the metasedimentary rocks of the Windy Point metamorphics is unknown. Isotopic and regional considerations discussed above

(Ch. 2) suggest that these rocks may be of Upper Paleozoic or of Mesozoic age. Until fossil material is recovered no more definite age assignment than 'pre-Late Cretaceous' can be given to these rocks.

3.3.3 DESERT DIVIDE GROUP

Distribution

Elsewhere within the San Jacinto Mountains the metamorphic wall rocks are comprised of thick sequences of quartz-dominated metasedimentary rocks. The thickest package is exposed on the Desert Divide of the southern San Jacinto Mountains south of Red Tahquitz (G.R. 323352) where they have been named the Desert Divide Group by Brown (1968, 1981). The maximum exposed thickness of the Desert Divide Group is 4300 m (Dibblee, 1981a) with an asymmetric distribution of lithologies suggesting that there has been no gross repetition of section (Brown, 1981). Grading within thick (1 m+) quartzite units (G.R. 416183) suggests that the sequence has not been overturned.

Quartz-rich schists and gneisses crop out over much of the eastern and southeastern part of the map area, from the vicinity of Red Tahquitz (G.R. 323352) south to the Pines-to-Palms Highway (at about G.R. 400134); in small screens on both the northern and southern slopes of Thomas Mountain (G.R. 295200); in an extensive area around Dellamont (G.R. 069424) and east of San Jacinto Potrero (G.R. 060470); and as small screens on the northern slopes of the range at least as far east as Twin Pines Ranch (G.R. 193473).

Lithology

Brown subdivided the Desert Divide Group into two units, the Bull Canyon Formation and the Ken Quartzite (Brown, 1968, 1980). The Ken Quartzite was thought to conformably overlie the Bull Canyon Formation, and both the lower contact of the Bull Canyon Formation and the upper contact of the Ken Quartzite are intrusive; accordingly, the full stratigraphic thickness and upper and lower relations of the Desert Divide Group are unknown.

The Bull Canyon Formation is described by Brown (1981) as a heterogeneous assemblage of interlayered gneiss, schist, quartzite, marble and calc-silicate hornfels. Four recurrent facies are recognized: marble, a sillimanite gneiss facies, a quartz gneiss facies, and a schist facies. The marble consists of almost pure crystalline calcite (Brown, 1968, 1980). The sillimanite gneiss facies is dominated by a foliated rock composed of reddish-brown biotite, sillimanite, orthoclase, quartz, red (almandine?) garnet, minor muscovite and uncommon cordierite. The quartz gneiss facies consists of coarsely crystalline quartz (90-100%) with minor sillimanite, biotite, orthoclase, muscovite, zircon, titanite and an opaque mineral. Rocks mapped by Brown (1968) as sillimanite gneiss facies occur stratigraphically above and below the quartz gneiss facies The schist facies is composed predominantly of quartz-biotite schist with interlayered quartz schist and quartzite. Thick quartzite layers increase in abundance eastwards (and up section) towards the base of the overlying Ken Quartzite, suggestive of a gradational boundary between the two units. A very thin, discontinuous layer of amphibolite forms the uppermost part of the schist facies and marks the contact with the

Ken Quartzite.

The Ken Quartzite is composed of about 750 m of coarse- and medium-grained crystalline quartzite, generally containing in excess of 95% quartz. Three marble lenses, the largest some 40 m thick, occur within the quartzite, as do minor layers or lenses of sillimanite gneiss and calc-silicate rock.

Similar rock types to those described by Brown (1968, 1981) comprise the other exposures mapped as Desert Divide Group. Small masses of coarsely crystalline marble surrounded by quartz-rich schists and gneisses are common. Relatively large marble lenses were mapped on the northern slope of Thomas Mountain (G.R. 310206), and east of San Jacinto Potrero (G.R. 082449). Much more extensive exposures of marble have been mapped by Dibblee (1981c) immediately to the west of the area mapped in the present study. Apparently stratigraphically below the section measured by Brown (1968) is some 2000 m of rock comparable to his schist and sillimanite gneiss facies. Much of the western slope of the Desert Divide of the southern San Jacinto Mountains is underlain by these rock types (Dibblee, 1981d,e; Plate 1).

Metamorphic Conditions

The grade of metamorphism everywhere appears to be at the almandine-amphibolite sub-facies of regional metamorphism. The uniformity of metamorphic grade throughout this area has been noted by Fraser (1931), Sharp (1967) and Brown (1968, 1981). Sharp (1967) describes small patches of hornblende-hornfels facies rock apparently in minor contact aureoles around some plutons. Mineral assemblages described from the metamorphic

rocks of the southern San Jacinto Mountains by Brown (1968, 1981) are listed in Table 3.1., along with assemblages identified in the present project. Of particular interest is the co-existence of cordierite and biotite, biotite and garnet, and, in one rock, apparently cordierite, biotite and garnet. At one studied locality sillimanite - K-feldspar gneisses are interleaved with muscovite - quartz bearing assemblages, implying significant differences in either rock chemistry or volatile content, or perhaps both. Two schist samples from a roof pendant east of San Jacinto Potrero have the assemblage muscovite+biotite+sillimanite+ minor quartz. The muscovite breakdown reaction

$$\text{Muscovite} + \text{quartz} = \text{sillimanite} + \text{K-feldspar} + \text{water}$$

appears to have been arrested in these rocks because of limitation of one of the reaction components, quartz.

Assimilation of pelitic metasedimentary material occurs at the margins of some plutons. Minerals formed in the contaminated 'tonalite' include garnet, Fe-rich biotite, and apparently allanite. The effects of such contamination are generally only visible for a few tens of meters from the country rock. It was considered that Fe/Mg distribution between coexisting garnet and biotite in these contaminated rocks might be used to give a <u>minimum</u> temperature estimate at the contact of such an intrusion; this would be a maximum estimate for the metamorphic conditions in the country rock that relate to the emplacement of that pluton. Table 3.2 lists typical mineral compositions from a sample of contaminated tonalite collected adjacent to the contact of a large sill-like body near Red Tahquitz (G.R. 329354). Table 3.3 lists the typical composition of minerals from two sedimentary rocks a few tens of meters from the contact.

TABLE 3.1

METAMORPHIC MINERAL ASSEMBLAGES, DESERT DIVIDE GROUP

Quartz+zircon

Quartz+K-feldspar+biotite+sillimanite

Quartz+K-feldspar+biotite+sillimanite muscovite

Quartz+biotite+cordierite±muscovite

Quartz+biotite+K-feldspar+sillimanite+ilmenite±plagioclase

Quartz+biotite+K-feldspar+sillimanite+garnet+cordierite+plagioclase

Plagioclase+K-feldspar+quartz±muscovite (veins)

TABLE 3.2

MICROPROBE ANALYSES OF SELECTED MINERALS FROM SAMPLE LTS 383

	GARNET		BIOTITE	
SiO_2	37.49	37.08	32.15	33.23
TiO_2			4.07	4.11
Al_2O_3	21.21	21.16	17.40	18.09
FeO	35.03	34.00	26.38	26.65
MnO	2.82	2.90	0.14	0.14
MgO	1.18	1.16	3.14	3.26
CaO	2.99	2.36		
K_2O			9.61	9.42
F			0.23	0.49
Cl			0.18	0.17
Total	100.73	98.70	93.30	95.42
	Formula Proportions = 8 cations		Formula Proportions = 7 cations	
Si	3.02	3.05	2.72	2.74
Ti			0.26	0.25
Al	2.02	2.05	1.74	1.76
Fe	2.36	2.34	1.87	1.84
Mn	0.19	0.20	0.01	0.01
Mg	0.14	0.14	0.40	0.40
Ca	0.26	0.21		
K			1.04	0.99
F			0.06	0.13
Cl			0.03	0.02

TABLE 3.3

MICROPROBE ANALYSES OF SELECTED MINERALS FROM SAMPLE LTS 308

	CORDIERITE		BIOTITE	
SiO_2	48.36	48.13	34.93	35.33
TiO_2	0.09	-	3.93	3.25
Al_2O_3	32.01	32.23	19.84	20.35
FeO	9.99	9.57	21.23	21.11
MnO	0.12	0.14	0.03	0.03
MgO	6.81	7.06	6.69	6.96
Na_2O	0.33	0.38	0.08	0.16
K_2O			10.23	10.01
F			-	0.12
Cl			-	-
Total	97.73	97.51	97.20	97.33
	Formula Proportions = 11 cations		Formula Proportions = 7 cations	
Si	5.04	5.02	2.74	2.75
Ti	-	-	0.23	0.19
Al	3.94	3.96	1.84	1.87
Fe	0.87	0.83	1.40	1.38
Mn	-	-	-	-
Mg	1.06	1.10	0.78	0.81
Na	0.07	0.08	-	-
K			1.03	0.99
F			-	0.03
Cl			-	-

These data and the formulation of Holdaway and Lee (1977) imply Fe/Mg equilibration between biotite and garnet took place at a temperature of 730 ± 10°C. This is well in excess of the maximum temperature for muscovite stability in a muscovite-quartz bearing assemblage, so indeed appears to be a maximum temperature estimate for the conditions related to emplacement of this intrusive mass. The two reactions

Muscovite + quartz = sillimanite + K-feldspar + water

Fe-biotite + sillimanite + quartz = Fe-cordierite + K-feldspar + water

are both dependent on X_{H_2O}, the fraction of water in the vapour phase. No carbon bearing minerals (such as graphite or calcite) were identified in these rocks, so it will be assumed that X_{H_2O} is approximately one. This has the effect of increasing the temperature estimated for the muscovite breakdown reaction, and decreasing the pressure estimated from Fe/Mg partitioning between biotite and cordierite. The estimated P,T conditions for equilibration of these assemblages are shown diagramatically on Figure 3.2. It is estimated that these metamorphic rocks, currently exposed at an elevation of 2560m, formed at temperatures of 620-660°C at total pressures of between 3.2 and 3.5 kilobars. This implies that metamorphic rocks at lower elevations formed at somewhat higher pressures (and probably temperatures), perhaps 690-730°C, 3.9-4.2 kb (assuming a density of 2.7 gm/cm^3 for the overlying metasedimentary rock and a geothermal gradient of 30°C/km). The assemblage biotite+garnet+cordierite(+quartz+plagioclase+K-feldspar) implies considerably higher temperature conditions (720-800°C, depending on X_{H_2O}) at these pressures (3.2-4.2 kb), and this is consistent with the presence of veins of apparent mobilisate (quartz+plagioclase+K-feldspar) in these

Figure 3.2. Pressure - temperature grid, showing inferred metamorphic conditions for San Jacinto rocks (square). Data from Holdaway and Lee, 1977 (biotite-cordierite; garnet-cordierite); Holdaway, 1971 (aluminosilicates); Kerrick, 1972 (muscovite breakdown) and Piwinskii (1968) and Boettcher and Wyllie (1968)[granite melting].

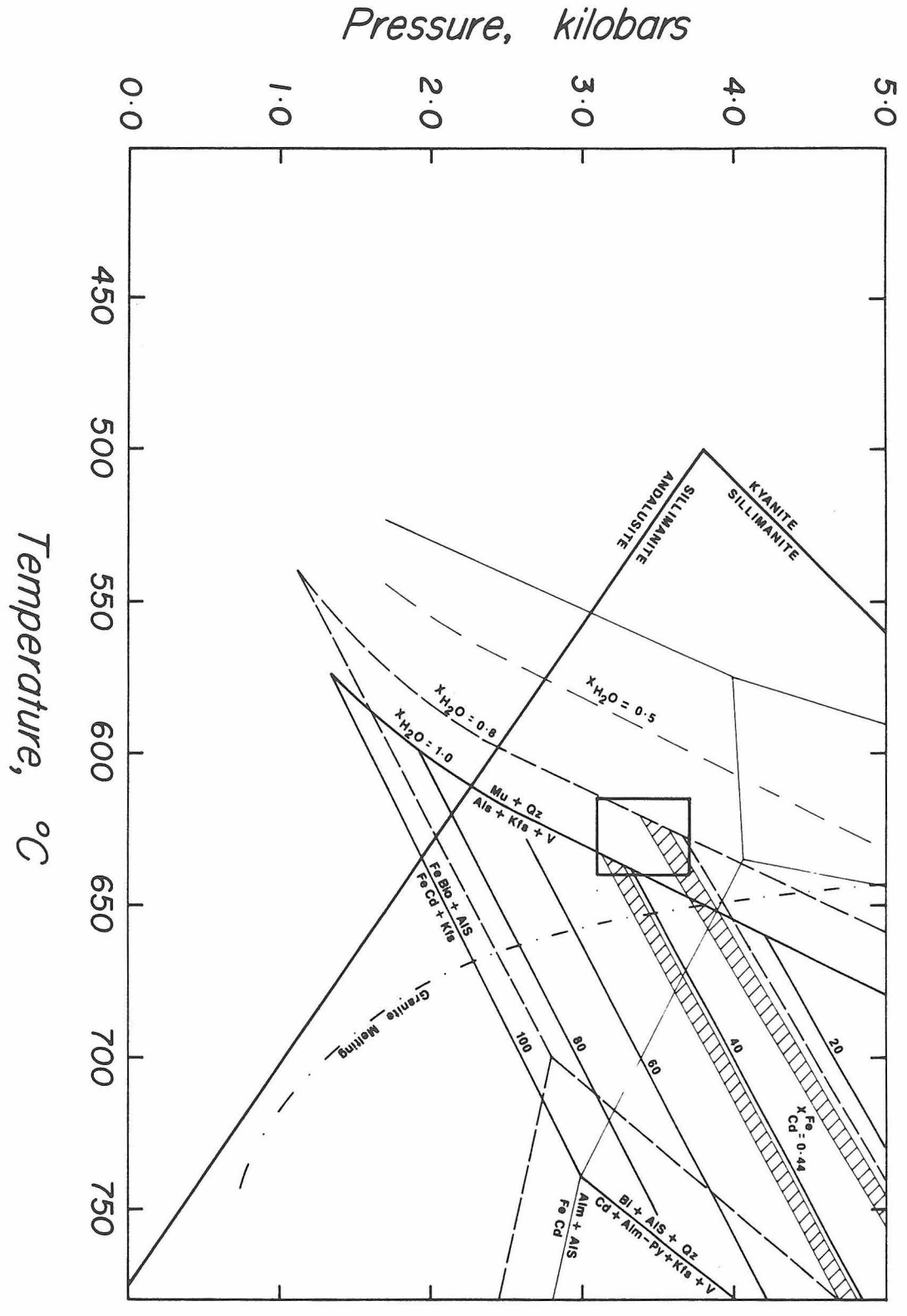
Pressure, kilobars
0·0
1·0
2·0
3·0
4·0
5·0
Temperature, °C
450
500
550
600
650
700
750
ANDALUSITE
SILLIMANITE
KYANITE
SILLIMANITE
$X_{H_2O} = 0.8$
$X_{H_2O} = 0.5$
$X_{H_2O} = 1.0$
Mu + Qz
Als + Kfs + V
Fe Bio + Als
Fe Cd + Kfs
Granite Melting
100
80
60
40
20
$X_{Cd}^{Fe} = 0.44$
Bi + Als + Qz
Cd + Alm - Py + Kfs + V
Alm + Als
Fe Cd

Figure 3.2

rocks.

Protolith

The Desert Divide Group consists of the metamorphosed equivalents of quartz-rich clastic sediments containing a considerable carbonate component. The apparently immense thickness of such quartz-rich rocks implies derivation from a nearby continental terrain.

Age

There are no rocks of known age within the Peninsular Ranges that appear similar to this section of quartz-rich sedimentary rocks. Lithologically similar rocks that crop out in the Jurupa Mountains some 50 km to the northwest of the San Jacinto Mountains (McEldowney, 1952) are also of unknown age.

Isotope data presented above (Ch. 2) are suggestive of an older (Early Paleozoic or Precambrian) rather than younger age for these rocks. However, the only definitive data available are that the rocks of the Desert Divide Group are intruded by 97 m.y. old plutons and are thus pre-Late Cretaceous in age.

3.3.4 RELATIONS BETWEEN THE WINDY POINT METAMORPHICS AND THE DESERT DIVIDE GROUP

The contact between the Windy Point Metamorphics and the Desert Divide Group has not been observed. It may be preserved in the small screens exposed on the steep western wall of Palm Canyon or in the exposures of metasedimentary rock north-west of Snow Creek. Assignment of some of the small exposures of metamorphic rock in these two areas has

been made somewhat arbitrarily.

3.4 BATHOLITHIC ROCKS

Various types of igneous rock that are collectively part of the Peninsular Ranges batholith of southern and Baja California crop out extensively in the San Jacinto Mountains. Individual masses range in composition from olivine gabbro to garnet-bearing granite; tonalite and low-K granodiorite dominate, however. Intrusions range in size from thin dikes and sills a few tens of centimeters in width to large plutons with lateral dimensions of tens of kilometers.

The igneous rocks have been somewhat arbitrarily subdivided into two groups on the basis of age relationships. Early intrusives tend to be small, with outcrop areas of a few square kilometers or less, and cover the complete compositional spectrum of the calc-alkaline rock suite. They are intruded by three large plutons of relatively homogeneous tonalite with outcrop areas measured in hundreds of square kilometers. These major tonalites are themselves intruded by several generations of volumetrically minor dikes and sills. Dikes of tonalite extending from these large plutons into the country rocks have not been differentiated, but in several areas form a significant proportion of the 'country rock' to their parent plutons. This is one indication of the close temporal as well as spatial relationship between the 'early intrusives' and 'major tonalites'.

3.4.1 EARLY INTRUSIVES

Only a few of the larger of the early intrusives have been studied in any detail. Contact relationships, and original extent are

often obscured by lack of outcrop, by removal by later intrusions, or both. Most masses are dike-like, with widths of a few tens of centimeters or less to a few bodies a few hundred meters or more in thickness. Lateral extent ranges from tens of meters to a few kilometers. The approximate outcrop area of several of the larger of the early intrusives is delineated on the geological map (Plate 1), as are several distinctive dikes or dike swarms. The lithology of these various units is briefly desribed below to give an indication of the range of igneous rock types present in the San Jacinto Mountains. The descriptions are ordered from the most mafic rock type to the most felsic. No age sequence is intended by this order.

Olivine Gabbro of Thomas Mountain

A mass of medium to coarse-grained olivine gabbro crops out on the southern ridge of Thomas Mountain (G.R. 345160). It is slightly more than one square kilometer in outcrop extent. This body is highly heterogeneous on the scale of tens of meters and includes anorthositic and hornblendic phases. It apparently intrudes the foliated biotite adamellite Thomas Mountain sill (Sharp, 1967).

Small masses of gabbroic rock outcrop in other areas within the San Jacinto Mountains. The largest are in Chino Canyon (at G.R. 355430), and have been mapped and described by Sydnor (1975). A small body of heterogeneous mafic rock crops out south of Fobes Ranch (at G.R. 350256) where it intrudes metamorphic and undifferentiated older igneous rocks. A gabbroic dike poorly exposed on brush covered slopes north of Quinn Flat (at G.R. 353222) may be an offshoot of this body. Three other masses of gabbro were mapped, and all lie along, and have been disrupted by,

contacts with larger tonalite plutons. One forms part of the southern wall to the quartz diorite of Lucky Deer Mine (G.R. 329198), a second lies along the southwestern contact of Unit II near Toolbox Spring (G.R. 313187), and the third is against the southwestern contact of Unit I on Rouse Hill (G.R. 211256).

Quartz Diorite of Lucky Deer Mine

Cropping out on the slopes of Thomas Mountain are many small poorly mapped bodies of intrusive rock ranging in composition from olivine gabbro to granite, aplite and pegmatite. One of the larger of these masses is poorly exposed on the northern slopes of Thomas Mountain north-east and southwest of Lucky Deer Mine (G.R. 330198). Fresh rock is exposed in roadcuts along the access road to the mine site. This intrusive is composed of fractured, relatively fine-grained plagioclase-rich tonalite or quartz diorite. Biotite flakes to 3 mm long are moulded around slightly larger (3-5 mm) white plagioclase tablets. Poorly formed hornblende crystals range in size downwards from about 3 mm, although a few large irregular prisms as much as 10 mm long are present. Small flecks of yellow-brown titanite, and larger (to 5 mm) rounded blebs of gray quartz are also visible in hand specimen.

This body is intrusive into a small gabbro mass and undifferentiated pegmatites and other igneous rocks along its southern margin. The northern boundary is the Thomas Mountain Fault. The intensity of fracturing increases northwards towards this structure. A similar rock crops out on the low hills north-west of the town of Thomas Mountain, on the opposite side of this fault.

Tonalite of Herkey Creek

Cropping out in the low hills at the north-western end of Garner Valley is a small body of distinctive biotite-hornblende-titanite tonalite. Although much of the original extent of this body is obscured by either Tertiary fanglomerates or by the Tertiary and Quaternary fill of Garner Valley extensive outcrops north of Herkey Creek campground (at G.R. 305272 and 309268) show a foliated tonalite with prominent hornblende prisms and biotite books to 10 mm set in a dense white matrix of plagioclase and quartz. The rock has a pronounced seriate porphyritic texture, and the idiomorphic forms of the biotite and hornblende are distinctive. Large flat surfaces of many hundreds of square meters in extent show that this rock is quite heterogeneous at all scales. Mineral banding is common, and features suggestive of current sorting of crystals within the magma chamber abound. These features are described in more detail in the section on magmatic structures (Ch. 4).

The tonalite of Herkey Creek is intruded by Unit I on its western margin. The northern margin is diffuse, the intrusion grading into a series of sub-parallel dikes striking about N20°W intrusive into older igneous rocks. The eastern margin is intrusive into similar heterogeneous older igneous materials.

A mass of similar rock crops out northwest and southeast of Angelus Hill (G.R. 136403). It too is intrusive into older igneous and metamorphic rocks, is in turn intruded by two of the major tonalites (Units I and III), and is locally quite heterogeneous. It forms the bulk of the screen of 'undifferentiated igneous' rock between Units I and III northwest from Indian Mountain (G.R. 195377) towards Poppet Creek

(G.R. 120425). Because of access problems the relationship of this unit to the granodiorite of Poppet Creek is not known.

Tonalite of Snow Creek

Many dikes and sills of predominantly mafic igneous rock crop out on the north face of San Jacinto Mountain, in the drainage of Snow Creek. This area has not been investigated in detail in this project. Thick dikes of commonly xenolith-rich foliated tonalite are interspersed with masses of more felsic tonalite or granodiorite, pegmatite and thin metasedimentary screens along the Pacific Crest Trail (G.R. 264467 to G.R. 282482). The mafic masses commonly have hornblende prisms and biotite books aligned in a foliation plane defined by the xenoliths. The common mafic rock is well exposed in the deeply excised gully west of the small township of Snow Creek (G.R. 283497), and on the slopes south of the town. It is a medium-grained biotite-hornblende-titanite tonalite, commonly with a marked imposed foliation. Biotite books and much fractured quartz lenses are commonly smeared into this foliation plane. Hornblende prisms are seldom more than about 5 mm long. In better preserved (less foliated) specimens biotite aggregates to 5 mm can be seen to often poikilitically enclose small (1-3 mm) plagioclase euhedra. Brown titanite is not as abundant as it is in many of the other tonalites. It is most apparent as large rhombohedral crystals to 4 mm in length.

The relationship of the various tonalite masses of this area, either to one another, or to other rock units, is poorly known. The xenolith-rich marginal phase of Major Tonalite Unit III clearly intrudes older foliated mafic tonalites in the steep gullies immediately west of the East Branch of Snow Creek (e.g., at G.R. 276449). Elsewhere the mafic

tonalites are cut by dikes of pegmatite and aplite. On the ridge southwest of Gorgonio (G.R. 277507) the mafic tonalites appear to intrude an earlier igneous complex containing abundant aplites and pegmatites as well as smaller masses of finer grained tonalite. Some of the tonalites exposed in the Snow Creek drainage could be northwesterly trending dikes emanating from the irregular northern margin of Major Tonalite Unit II. The prominent imposed foliation could result from stresses associated with emplacement of the large nearby Major Tonalite Unit III.

Granodiorite of Poppet Creek

Exposed along the course of Poppet Creek for about 2 km southwards from the southern-most part of the small township of Poppet Flat (from G.R. 123440 south) are outcrops of a distinctive foliated mafic granodiorite. Similar rock crops out for some 3.5 km to the northwest and for 2 km to the southeast of Poppet Creek.

The most striking feature of this rock in the field is the presence of a strong mineral foliation, and the biotite-hornblende ratio of about 1. The intensity of this mineral foliation contrasts markedly with that of the weakly foliated biotite tonalites which intrude this mass to the north and south. The intensity of this foliation decreases away from contacts with the large tonalite Units I and III, implying that it relates to emplacement of these later bodies. The unit shows geographically consistent variation from a K-feldspar rich mafic tonalite in the northern-most outcrops to a mafic-rich granodiorite and thence to a K-feldspar megacrystic granite in the more southerly outcrops.

Mapping suggests that the granodiorite of Poppet Creek is one of the oldest igneous units exposed in the San Jacinto Mountains. It has been intruded by two of the major tonalite units (I and III), and appears to have been intruded by another small tonalite body along its eastern margin. The intrusive nature of the contact with Unit I is well exposed on the ridge northwest of Forest Service Road 3S22 (e.g., at G.R. 109449), where lineated and foliated biotite-hornblende-titanite tonalite cuts the strongly foliated hornblende-biotite granodiorite of Poppet Creek. The contact appears to dip relatively shallowly northwards, and both the foliation and lineation within the younger unit parallel the contact. Small screens of quartzite occur irregularly along this contact; only the largest is shown on the geological map (Plate 1). Intensely foliated mafic granodiorite of the Poppet Creek mass is exposed along the road leading south from Poppet Flat (at G.R. 124441) adjacent to relatively unfoliated tonalite of Unit III, but the contact does not appear to be exposed. This contact was briefly exposed in a roadcut north of Poppet Creek (G.R. 122443) but has since been covered with scree. At the contact xenolith-bearing tonalite of Unit III cuts the foliation of the Poppet Creek at a shallow angle. Both xenoliths and a strong mineral lineation within the inferred younger tonalite were oriented parallel to this contact.

The original extent of the Poppet Creek body is thus unknown, but was probably once much larger. The unit grades from a K-feldspar rich tonalite at its northern-most outcrops to a K-feldspar rich granodiorite near the center of its outcrop area and then to a K-feldspar megacryst containing granite at its southern-most exposures. These observations suggest that only a fragment of an original concentrically

zoned pluton remains, the rest having been displaced (upwards?) by later intrusions (Unit I and Unit III).

Granodiorite of Apple Canyon

An elongate body of biotite granodiorite containing abundant large flesh-pink megacrysts of K-feldspar crops out southwards from Tahquitz Peak (G.R. 299348) to Apple Canyon (G.R. 318279) and the northern margin of Garner Vally (G.R. 325262) [Plate 1]. The outcrop pattern is that of a slightly S-shaped lens, some 10 km long and with a maximum width of a little over 1km. The rock shows a strong foliation defined by simply twinned aligned K-feldspar tablets 2-4 cm in maximum dimension. Thin biotite books, small hornblende prisms, and, where present, mafic xenoliths are also aligned in this foliation. Plagioclase shows a pronounced seriate-porphyritic texture, with individual crystals ranging down in size from 1 cm or more. Quartz occurs in large semi-equant masses to a maximum size of about 1 cm.

This body intrudes the apparently slightly older mixed igneous rocks that underlie much of the mountain slopes north of Garner Valley. Dikes of K-feldspar megacryst-bearing granodiorite occur for several kilometers north of Tahquitz Peak; these may be related to the main body of similar material further south. The northern limit of the megacryst-bearing dikes is about at the southern margin of Major Tonalite Unit II, suggesting that the latter unit (Unit II) may intrude the former (granodiorite dikes).

Granite dike, Little Thomas Mountain

Three dikes of coarse-grained granite have been mapped on and to the southeast of Little Thomas Mountain (G.R. 286208). The most extensive is up to about 50 m thick, and has been traced for 3.6 km along strike. The other two masses appear to be en echelon extensions of this main mass, offset sequentially about 500 m and 1000 m to the north.

The rock is coarse-grained, with anhedral to subhedral feldspars to 2 cm or more across. Irregular masses of gray quartz are of similar size. Smaller flakes of biotite (to 3 mm) are commonly surrounded by rusty haloes. All samples show evidence of alteration; as well as the haloes around biotite flakes, Fe-staining along fractures is common, and both feldspars are chalky-white in colour, and somewhat friable in hand specimen.

These dikes intrude older undifferentiated igneous rocks. They apparently do not intrude either of the nearby Major Tonalite units (I and II). This rock is very similar in appearance to the foliated biotite adamellite of the nearby Bautista Sill described by Sharp (1967).

Granite of Penrod Canyon

A body of biotite-garnet granite that crops out north of the southwestern end of Garner Valley has been called the Penrod Quartz Monzonite by Brown (1968, 1981). By the classification of plutonic rocks used in this study the rock is a granite (Streckeisen, 1973) with 30-40% quartz and 35-55% alkali feldspar. The rock is quite variable in composition, having various amounts of biotite and garnet as well as variable

quartz:alkali-feldspar:plagioclase ratios. Some samples have as much as 10% biotite, and little or no garnet; others have only a trace of biotite, but several percent of dark red garnet euhedra.

Subhedral masses of gray quartz to 5 mm are set in a dense chalk-white matrix of feldspar. Thin flakes of white-mica may be prominent along feldspar crystal faces. Much of the pluton shows some foliation, defined predominantly by alignment of thin biotite aggregates.

This pluton is an irregular mass some 4.5 km across and perhaps 9 km long. It has not been examined in detail in the current study. The eastern margin of this pluton is intrusive into the metasedimentary rocks of the Desert Divide Group; the contact is sharp. Reconnaissance of the northern margin in the vicinity of McGregor Flat (G.R. 384216) suggests that here the contact may be gradational, with an extensive hybrid zone in which sediments have been intruded by, and are reacting with, numerous masses of granite.

3.4.2 LATE TONALITES

Three major intrusive units composed dominantly of tonalite gradational to K-feldspar poor granodiorite underlie some 1000 km^2 of the northwestern San Jacinto Mountains. Although the three intrusive units can be differentiated easily using structural features, the rocks of all units are so similar in appearance that they will be described together.

The common rock of the main tonalites is medium-grained and is generally light grey in colour. The rock has a noticeable seriate-porphyritic texture, with the major minerals showing a range of grain size

from occasional crystals as large as 1.5 cm long completely gradational downwards to microscopic size. This feature is seen most prominently in the size distribution of hornblende, but in some rocks is also well displayed by plagioclase, biotite, quartz and sphene.

Biotite is the dominant mafic mineral, and is present both as well-formed books up to 5 mm in diameter and as irregular grains or masses of irregular grains of similar overall dimensions. Hornblende prisms are an ubiquitous feature of all but the most felsic granodiorites. The common rock shows an alignment of hornblende crystals of a range of sizes, from a maximum dimension of 1.5 cm down to tiny euhedral prisms a millimeter or less long.

White plagioclase commonly makes up slightly over one half of the rock. Individual crystals range in size from over 1 cm in length to microscopic size. Alignment of plagioclase tablets is discernible in hand specimen in some of the more mafic rocks.

Potassium feldspar varies in abundance inversely with the abundance of mafic minerals. In the more mafic rocks it occurs as thin films between other mineral grains. These films may be continuous over distances of several centimeters, giving conspicuous poikilitic plates enclosing all other minerals. In the more felsic tonalites K-feldspar occurs as anhedral grains to 5 mm or greater maximum dimension. These grains often contain abundant inclusions of other minerals.

Quartz comprises about one quarter of the average rock, and is present as large equant grains ("gum-drops") as well as smaller irregular grains. The "gum-drops" often have a purplish tint; some have hexagonal

sections. The maximum size of quartz grains increases from a few millimeters in the most mafic tonalites to perhaps 1.5 cm in the more felsic tonalites and mafic granodiorites. It then decreases again; in the most felsic granodiorites quartz again has maximum dimensions of a few millimeters. The large grains in the intermediate rocks are the best formed, and give particularly prominent "gum-drops" on slightly weathered surfaces. Quartz in the more mafic and in the more felsic rocks is usually more irregular in habit.

Honey-coloured titanite (sphene) is an ubiquitous constituent of these rocks. It commonly occurs as well-formed rhombohedra to 5 mm long. Occasional elongate prisms of allanite are seen in hand specimen. These may be as much as several millimeters long.

Discoidal mafic xenoliths are present throughout all units. They range in size from prominent masses a meter or more in length down to small dark patches a few centimeters or less in maximum dimension. Abundance varies widely, from areas where xenoliths dominate the rock (usually in the more mafic rocks closer to the mrgins of a unit) to places where there might be one or two xenoliths per 100 m^2. Areas of uncommonly high xenolith abundance tend to form linear or arcuate belts that can be mapped ("xenolith trains"). These features are described in more detail below.

Most variations on this basic theme are gradational and subtle, and largely relate to changes in the proportions of the minerals present. Hornblende abundance decreases from almost 10% (volume) in the most mafic rocks to rare or absent in the most felsic granodiorites. Biotite abundance falls similarly, from slightly less than 20% in mafic tonalites to

less than 5% in the most felsic rocks. Titanite abundance also decreases systematically with colour index, falling from a maximum of about 2.0% in some of the more mafic rocks to about 0.1% in felsic rocks. Plagioclase abundance remains comparatively constant at between 45-55 volume %. K-feldspar increases from 1-2% in mafic tonalites to around 15% in the (volumetrically minor) most mafic-poor rocks. Quartz comprises the balance of the rock, commonly some 20-30%. It is perhaps slightly more abundant in the felsic tonalites and K-feldspar poor granodiorites than in either more mafic or more felsic compositions.

Three variants on this common rock type appear to be related to proximity to the margins of plutons. Schlieren are commonly parallel or sub-parallel to the nearby pluton margin, and are often spatially associated with xenolith trains. Schlieren consist of concentrations of dark or light minerals, usually an alternating sequence of both. They are commonly not extensive, being only a few meters in length and a few tens of centimeters across. A few, however, are much more extensive, and can be traced for several tens of meters along strike, exposures permitting. The location of mapped schlieren is shown on Plate 2. A typical schlieren consists of hornblende prisms and titanite rhombohedra randomly aligned in a plane parallel to the schlieren margin(s). Biotite books may also be oriented in this plane. One boundary of a mafic schlieren is usually sharp, whilst the other is gradational into a felsic, relatively mafic-poor tonalite or granodiorite. The features of the shlieren seem to indicate an origin by flow sorting (Bhattacharji and Smith, 1964).

Fine-grained granodiorite with a pronounced foliation occurs along much of the northern margin of Unit III. The intensity of the

foliation, and the grain size both increase with increasing distance from the pluton margin. The grain size variations are interpreted as being related to crystal nucleation and growth rate differences near the roof or wall of the pluton, and the foliation appears related to shear imposed by later input of magma into the inflating magma chamber.

The most intriguing textural variation is the irregular development of a poikilitic-titanite facies that is commonly observed in marginal rocks of Units I and III. In this rock, aggregates of titanite are intergrown with plagioclase tablets and subhedral grains of quartz to give a distinct mottling to the rock. Individual titanite-plagioclase-quartz intergrowths may be as much as 3 cm across, and commonly have a core of a titanite aggregate or a centimeter-sized titanite poikiloblast surrounded by a ring of plagioclase and quartz. The margins of these felsic spots then grade into the usually mafic 'host' over a distance of a millimeter or so.

3.5 TERTIARY DEPOSITS

Overlying the older metasedimentary and igneous rocks with pronounced angular unconformity are sedimentary deposits of late Cenozoic age. These are largely terrestrial valley-fill sediments, and include extensive deposits of extremely poorly-sorted boulder conglomerates with lesser amounts of better-sorted and finer-grained materials. Elsewhere, outside the limits of the present study area, these units include possible lacustrine clays (e.g., Dibblee, 1981a). Dibblee (1981a) subdivides these Tertiary deposits into the Mount Eden Formation, the San Timoteo Formation and the Bautista Beds. All three units crop out in the study area. The brief description below is modified from Dibblee (1981a).

3.5.1 MOUNT EDEN FORMATION

Well-indurated red-beds exposed around the San Jacinto Potrero (G.R. 060470) were called the Eden beds by Frick (1921), and later redesignated the Mount Eden Formation (or Beds) by Fraser (1931). No type section has been designated. In the vicinity of the San Jacinto Potrero this formation consists of light red thick-bedded pebbly sandstone with minor clay interbeds. This sandstone grades southeastward into coarse red fanglomerate and a thick body of quartz diorite landslide breccia. These materials were apparently deposited on a surface of considerable relief that in places is being exhumed by the present erosional cycle.

The Mount Eden Formation has yielded vertebrate remains of Hemphillian age (Frick, 1921; Savage et al., 1954).

3.5.2 TERRESTRIAL SEDIMENTARY DEPOSITS

This unit, which includes the San Timoteo Formation and the Bautista Beds as well as various un-named deposits south of San Gorgonio Pass consists of weakly indurated deposits of light-gray to buff arkosic sandstone, pebble and boulder conglomerate (Fig. 3.3a,b), and interbedded light-reddish to light-gray silty claystone. In the western San Jacinto Mountains these rocks have been called the San Timoteo Formation. This unit is conformable upon the Mount Eden Formation, but to the east and north it laps onto the crystalline rocks.

In the badlands east and southeast of San Jacinto and Hemet the terrestrial sedimentary deposits have been called the Bautista Beds by Frick (1921), and this usage has been continued by more recent workers

Figure 3.3a. Tonalite clasts in terrestrial sedimentary deposits. Road cut on Pines-to-Palms Highway, G.R. 283269. Hammer is 90 cm long.

Figure 3.3b. Gneiss and schist clasts in terrestrial sedimentary deposit, near head of fan. Morris Ranch Road, G.R. 377227. Hammer is 90 cm long.

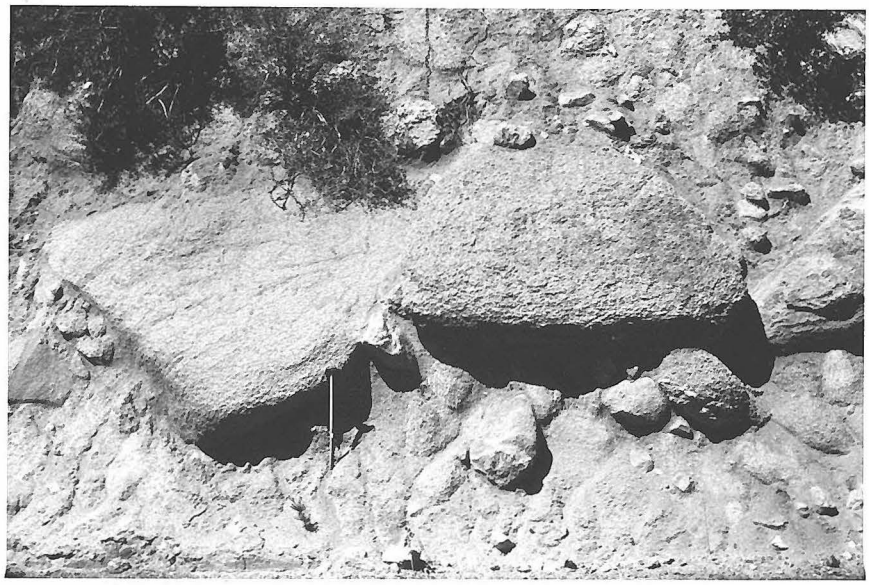

(e.g., Fraser, 1931; Sharp, 1967; Dibblee, 1981a). In this area the Bautista Beds are as much as 600 m thick (Dibblee, 1981a). Similar deposits crop out around, and presumably underlie much of Garner Valley, where gravity data are interpreted as indicating the presence of as much as 300 m of unconsolidated sediment overlying crystalline basement (Durbin, 1975). The deposits around Garner Valley retain much of their original alluvial fan form, and the materials grade upslope into less and less well sorted fanglomerates, and in some places, into what appears to be slope debris. Materials within each fan can be matched to source areas along either the Desert Divide of the southern San Jacinto Mountains or on the northern slopes of Thomas Mountain. Each fan thus has a distinctive clast population that relates to a specific source assemblage. The large fan extending northeastwards from Thomas Mountain village (G.R. 350190), for instance, contains a high proportion of clasts derived from the metamorphic rocks that crop out south and west of Pyramid Peak (G.R. 379265), while the fan exposed in the roadcuts near Keen Summit (G.R. 275272) contains relatively little metasedimentary materials, in keeping with the dominantly igneous materials of its source area.

Individual clasts within these fanglomerates can be quite large, to several meters in diameter (Fig. 3.3a,b).

Deposition of the various fans along the northern margin of Garner Valley appears to have been, at least in part, controlled by a structure that strikes southeastwards from east of the Garner Ranch (at G.R. 335245) to east of Pine Meadow (at G.R. 376180). Rapid thickening of fan deposits to the south of this line suggests that this was the location of a scarp during late Cenozoic time. No definite evidence for

a fault origin for this scarp was found during the present study.

The contact between the Bautista beds and the tonalites of the main mass of San Jacinto Mountain north of the San Jacinto Valley has been mapped as a fault (the Hot Springs fault) by Sharp (1967). In many places this is indeed the case, but in others boulder conglomerates can be seen to lie upon often deeply weathered tonalite. The thickness of the Tertiary deposits increases markedly across this fault, suggesting that it may have been active during, and in part controlled, deposition of the Bautista Beds.

The San Timoteo Formation in the San Timoteo Badlands west of the study area yielded vertebrate fossil remains diagnostic of Blancan (Plio-Pleistocene) age (Frick, 1921; Savage et al., 1954). Vertebrate remains of similar age (Blancan) have been recovered from the Bautista Beds (Frick, 1921; Savage et al., 1954; Morton and Gray, 1971).

Terrestrial sedimentary deposits similar to those described above are also found north of the divide between the San Jacinto and San Gorgonio rivers. A partially dissected fan is exposed in a canyon west of the village of Snow Creek. The existing remnant of this fan extends from an altitude of about 1150 m (3800') down to near the existing valley floor at about 500 m (1650'). The modern drainage is as much as 100 m below the upper surface of the old fan. A well-developed caliche horizon is present within the uppermost few meters of the old fan gravels. This uppermost surface projects to approximately the present level of the lowest point in San Gorgonio Pass (here at about 350 m), implying that either there has been little tectonic readjustment within the southernmost Pass since development of the fan or that sediment accumulation within

the Pass has kept pace with uplift of the San Jacinto Block since fan development.

Tertiary terrestrial deposits are also found in the drainage following the eastern trace of the Lawrence Fault (G.R. 147506), but have not been studied in more than a cursory fashion.

3.6 QUATERNARY DEPOSITS

3.6.1 POSSIBLE QUATERNARY GLACIAL DEPOSITS

The Santa Ana 1:250,000 geological sheet shows a small deposit of questioned glacial origin to the southeast of San Jacinto Peak (at G.R. 300409). This deposit has been desribed by Sharp, Allen and Meier (1957, p.93) thus:

> " A tongue of bouldery debris extends northeast into Round Valley from an amphitheater heading in the saddle south of San Jacinto Peak. This deposit terminates as a bulbous mass at about 9800 feet and shows evidence of two episodes of development, but it lacks the morainal loops and closed depressions so typical of glacial deposits on San Gorgonio Mountain. Still the general relations incline one to regard it as more likely of glacial origin than not."

This deposit is less than 700 m (2300') long; the elevation in the saddle referred to above (at G.R. 296409) is about 3175 m (10,400'). Although thick snow accumulated in this sheltered area is often amongst the last to melt in summer, the area over which snow accumulates is not particularly extensive, and seems incapable of supporting a true glacier. The overall form of the deposit suggests that it is more likely to have resulted from periglacial phenomena, perhaps as a rock glacier, than from a true glacier.

3.6.2 ACTIVE ALLUVIAL MATERIALS

These are abundant within the study area, particularly within the channels of the San Jacinto and San Gorgonio Rivers. These materials grade downwards in size from boulders a meter or more in diameter. Many slopes are mantled by more or less active colluvial blankets; these colluvial deposits are commonly gradational into alluvial deposits, and, particularly in areas where both alluvial and colluvial materials are derived by reworking of the Tertiary continental sediments may be difficult to differentiate precisely.

Similar relations almost certainly occurred during accumulation of the older alluvial materials. In many cases definite alluvial deposits on the headward part of fans grade into the colluvial materials of the slope mantle. This makes definition of the upper parts of the Tertiary alluvial materials quite difficult at times.

CHAPTER 4

GEOLOGY OF THE SAN JACINTO MOUNTAINS

PART 2: STRUCTURE

4.1 INTRODUCTION

Although the primary thrust of the current project was petrological and geochemical rather than structural, important data have been collected on two divergent aspects of the structural history of the San Jacinto Mountains. First, detailed reconnaissance within the major plutons has resulted in a considerable body of data on igneous structures within these bodies. Interpretation of these data allow a partial record of magma chamber inflation and solidification to be elucidated. Second, mapping of the inter-relationships of the various igneous bodies enables quantitative estimates of offset on several faults of the San Jacinto fault system to be determined. These faults are north of the area studied in detail by Sharp (1967), and add significantly to estimates of the total displacement across the entire system. Two major faults add 5.2 km to the 24 km of offset determined by Sharp (1967) across the combined San Jacinto and Thomas Mountain structures, giving a total best estimate of 29.0±1.1 km of right-lateral displacement for the entire system.

The relation of the rocks of the San Jacinto Mountains to rocks of similar age elsewhere in both the Peninsular Ranges and further afield (e.g., the Sierra Nevada) has been affected considerably by post-batholithic structures. The effects of these structures on placing the petrological, geochemical, and isotopic data obtained from the San Jacinto Mountains in regional context are significant. These structures are thus

described below, and some regional implications of each set of structures discussed.

4.1.1 STRUCTURAL SETTING

The San Jacinto Mountains are part of the "San Jacinto - Santa Rosa Mountains Block", a lens shaped area of high relief bounded to the north and east by the active extensional terrane of the Coachella Valley - Salton Depression and its westerly extension into San Gorgonio Pass, and to the south and west by the various stands of the active San Jacinto fault system (Fig. 4.1). The southern part of the study area is cut by numerous strands of this seismically active fault system; however, the main mass of the mountain appears to have been little disrupted by the current episode of tectonic activity, and is currently quiet seismically (Fig. 4.2).

San Jacinto Mountain forms the northern-most segment of the Peninsular Ranges, a west-tilted uplift with a steep eastern face that parallels the Gulf of California and its extension into the Imperial and Coachella Valleys. Maximum elevation is at San Jacinto Peak (3293 m). Relief to the immediate north and east of San Jacinto Peak is precipitous; the head of the Snow Creek fan, 6.0 km north of the peak is 2,700 m lower in elevation, and the city of Palm Springs, in the Coachella Valley 11.0 km east of the peak is at an elevation of about 150 m, some 3,150 m lower in elevation.

The cause of this tremendous relief is not known for certain. Allen (1957) proposed that a fault buried beneath the alluvial fill of the southern part of San Gorgonio Pass was responsible (south bounding

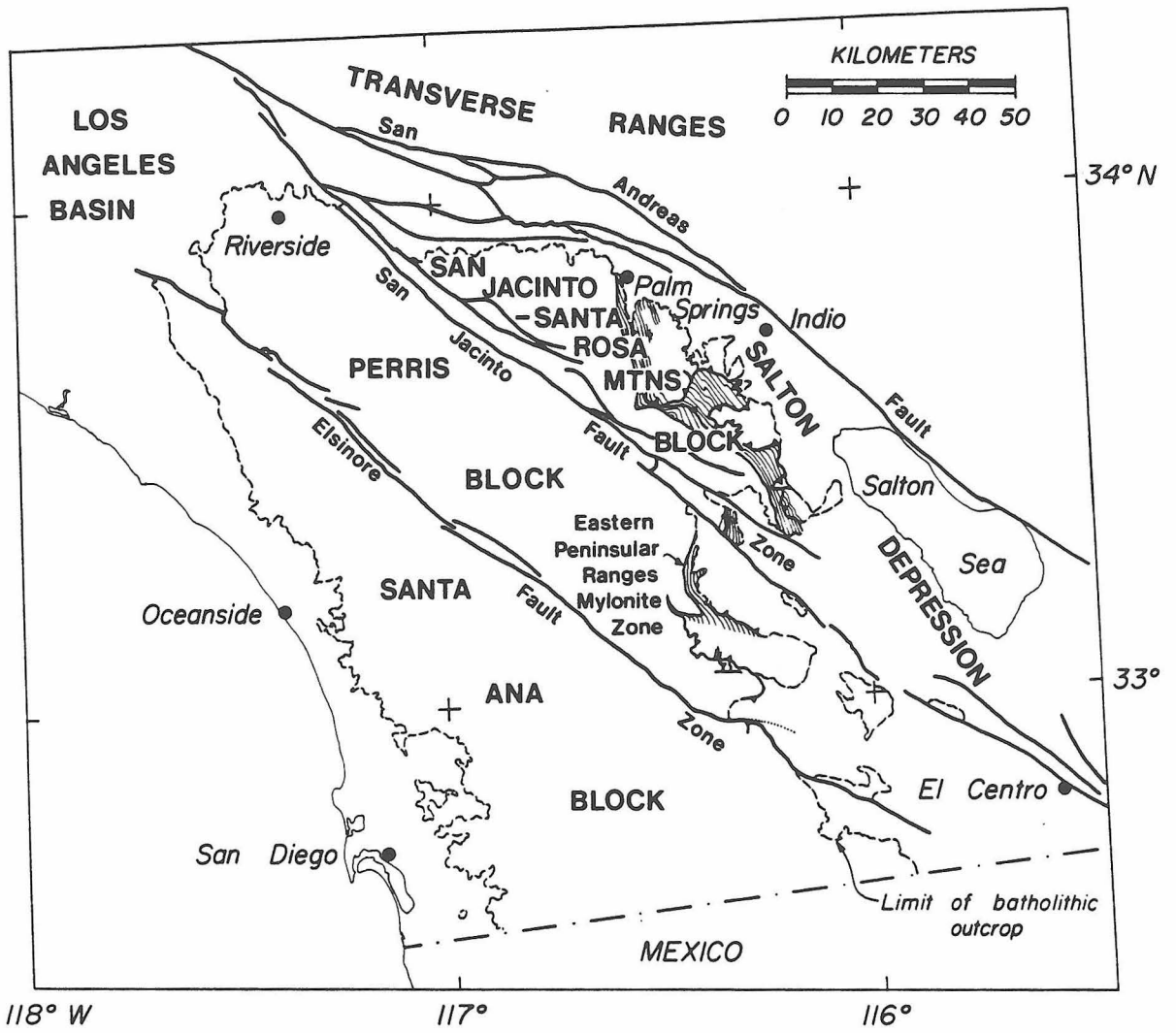

STRUCTURAL SETTING OF THE NORTHERN PENINSULAR RANGES, SOUTHERN CALIFORNIA

Figure 4.1. Structural setting of the San Jacinto Mountains at the northeastern margin of the Peninsular Ranges, southern California.

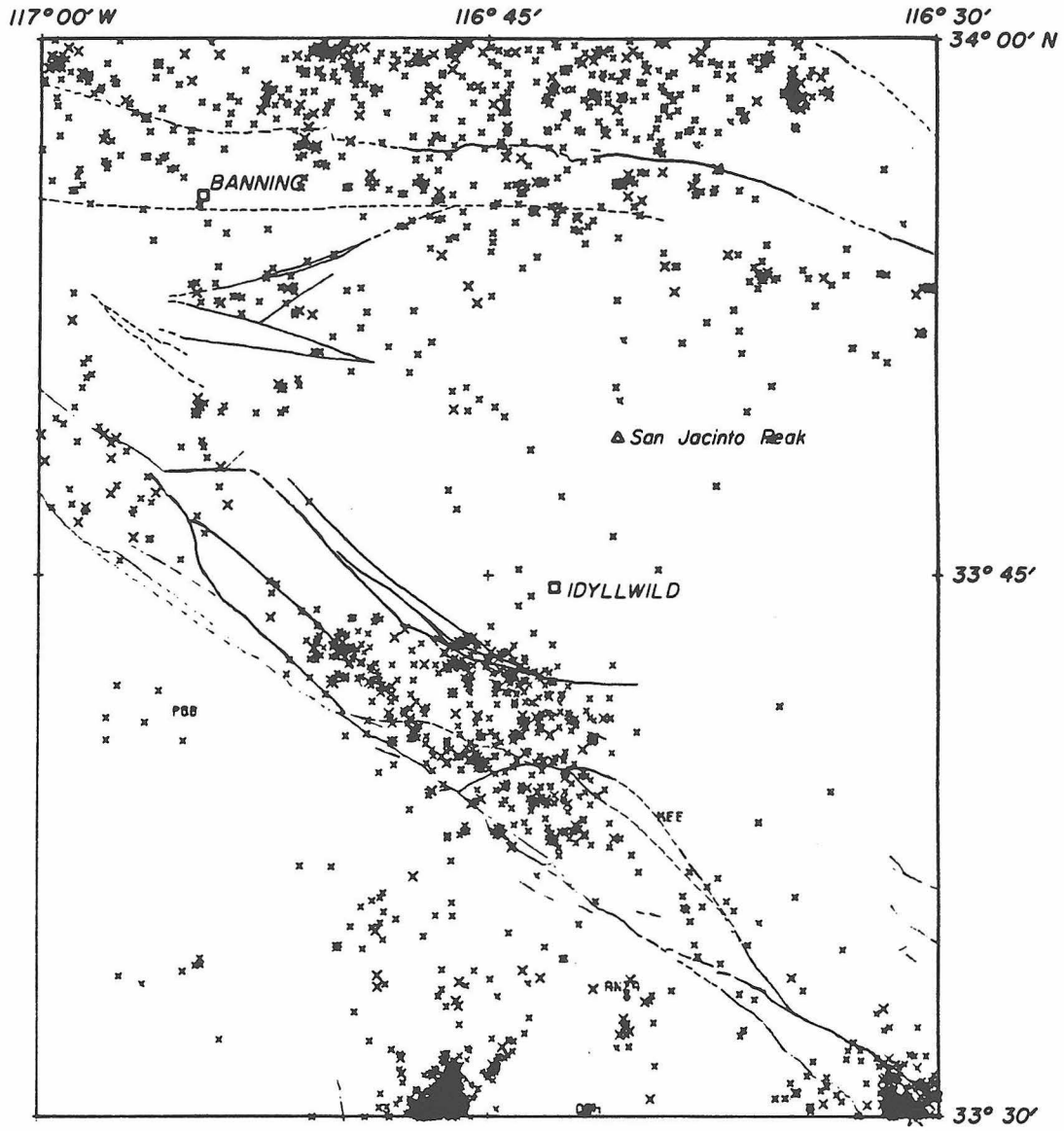

Figure 4.2. Located earthquake epicenters, San Jacinto Mountains and vicinity, southern California. Map courtesy of Chris Sanders, 1981 from SCARLET. Note lack of earthquake activity within the main mountain mass.

fault of Banning Pass). A well north of this proposed feature bottomed in sediments at a depth of 1,640 meters, giving some indication of the probable amount of vertical movement on this structure (Willingham, 1981). Interpretation of gravity data suggests a similar amount of basement offset (Willingham, 1981). Up is to the south. This is a minimum estimate of total vertical separation across this structure; the total amount of displacement in a vertical sense could be in excess of 4.5 km, the vertical separation between the inferred buried basement north of this presumed fault and the maximum elevation in the mountains to the south. If this feature is a fault, it does not appear to be currently active. The Lawrence Fault has an appropriate trend and apparent sense of motion (north side down) to be a splay from this presumed buried fault; if so, the age of latest movement on this part of the system might be given by the terrestrial sediments deposited in the valley cut along the Lawrence Fault southeast of Banning (Plate 1).

The San Jacinto fault system has been described in detail by Sharp (1967). He documented a total of 24 kilometers of right-lateral displacement across the main strands of this structure, and inferred that in addition there may have been 1.5 - 3 km of vertical displacement as well, with the south side up. The San Jacinto Valley, which may contain as much as 2400 m of late Tertiary sediment (e.g., Willingham, 1981) has been interpreted as a pullapart basin developed within an en echelon fault system (e.g., Crowell and Ramirez, 1979).

As briefly mentioned above, neither of these two major fault systems (south bounding fault of Banning Pass, San Jacinto fault) appear to have disrupted the main mass of San Jacinto Mountain.

4.2 YOUNG (POST-BATHOLITHIC) STRUCTURES

As briefly described above, the current structural setting of the San Jacinto Mountains is dominated by the younger features to the north, east, and southwest. The combined effects of these predominantly Neogene features has been to isolate the Cretaceous and pre-Cretaceous rocks of the San Jacinto Mountains from materials of equivalent ages that presumably once occurred to the north and east, but have been either removed by post-Cretaceous faulting or are buried beneath the alluvium of the Coachella Valley and San Gorgonio Pass. This disruption of the batholith complicates attempts at relating this area of the Peninsular Ranges to either similar age batholithic rocks to the north and east, or attempts at developing a coherent picture of the tectonic environment at the time of batholith development. In particular, the relationship of the batholith to the North American craton has been obscured by several distinct episodes of tectonic activity, involving large-scale translation on both steeply dipping (e.g., Hill and Dibblee, 1953) and shallow (e.g., Sharp, 1979; Silver, 1983) fault systems.

To the south the rocks of the San Jacinto Mountains have been offset from the bulk of the batholith along the various strands of the San Jacinto fault system (Sharp, 1967). The northern-most strands of this system are also responsible for minor disruption within the San Jacinto Mountains, and the effects of this disruption need to be allowed for in the discussion of both inter- and intra-plutonic variability within the San Jacinto Mountains. Mapped offsets of igneous contacts allow these effects to be quantified, allowing restoration of pluton configurations to their presumed original configurations.

The batholith has also been extensively disrupted by movement on the post-Cretaceous eastern Peninsular Ranges mylonite zone (Sharp, 1967, 1979). Some of the regional aspects of this structure have been described above (Ch. 2, p.37 and following). The mylonite zone skirts the eastern edge of the map area, and westward projection puts the base of the mylonite zone only a few kilometers above the highest exposed plutonic rocks. It is thus reasonable to expect that some effects of this major crustal feature may be apparent within the study area away from its immediate area of outcrop.

These various features are described below, with the younger, better known features first.

4.3.1 THE SAN JACINTO FAULT SYSTEM

The majority of faults mapped or inferred during the course of this study (Fig. 4.3) appear to be part of the San Jacinto fault system. This feature has been mapped and described in detail by Sharp (1967). Sharp (1981) estimates an average late Pleistocene through Holocene offset rate of 8 to 12 mm/yr (with a right-lateral sense of displacement) across this feature. Wherever a sense of offset could be determined it was right-lateral, and usually also down to the southwest. Exceptions are on the Hot Springs fault immediately west of Herkey Creek Campground (at G.R. 293261) where shattered tonalite is apparently thrust over Tertiary conglomerates (the fault-plane dips at approximately 60o to the southwest), and along the shallowly-dipping faults both west and east of Lake Hemet, which appear to be thrusts with the upper plates moving to the northwest. The apparent thrust relationship at the Herkey Creek locality probably developed by juxtaposition of dissimilar rocks along

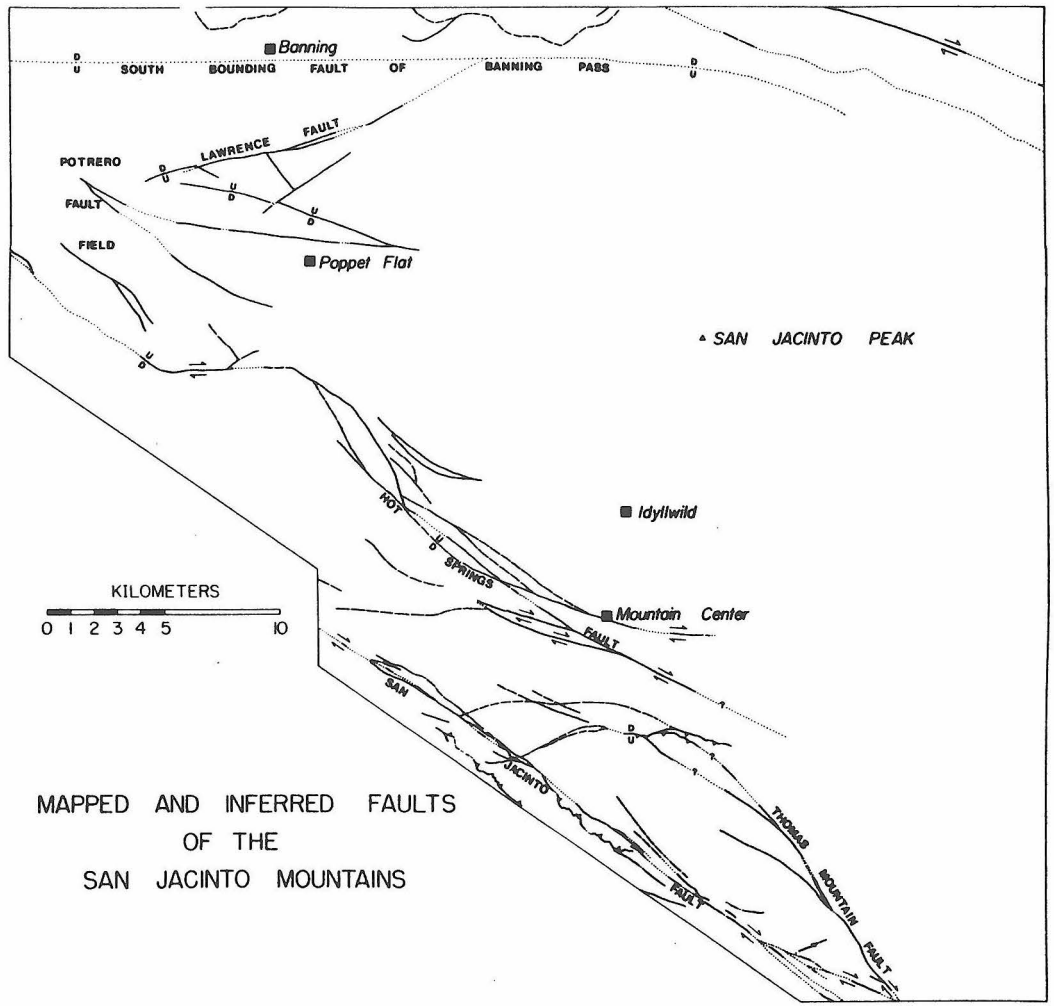

Figure 4.3. Mapped and inferred faults within the San Jacinto Mountains and immediate vicinity. From this study, Sharp (1967), and Rogers (1965).

a southwesterly-dipping strike-slip fault cutting an area with high relief (T.W. Dibblee, personal communication, 1981).

The area between the main strand of the San Jacinto fault and the Hot Springs fault is quite shattered. Numerous fractures and small faults were observed, but appear to have insignificant total offset. They may be marked by both slickensided surfaces and photo lineaments. Faults with measureable offsets have well developed crush or gouge zones where exposed (e.g. Hot Springs fault in roadcuts at G.R. 293261 and at G.R. 165345) and form prominent air-photo features as well as being marked by ground water barriers, terraces, and other features indicative of relatively recent activity.

San Jacinto Fault

This feature forms the southwestern boundary of the study area. It shows many features indicative of current activity (offset streams, closed depressions, shutter ridges, benches, a major sag pond) and has been described in detail by Sharp (1967), who demonstrated a total of about 23 km of displacement across this structure. The trace of this fault on the geological map (Plate 1) is largely taken from this study.

Hot Springs Fault

This structure runs parallel to the main strand of the San Jacinto fault system, but is offset to the north some 6 kilometers. It was first recognized by Fraser (1931), and various features of it have since been described by Sharp (1967) and Dibblee (1981a). Through much of the area it forms a series of anastomosing strands, many of which are buried beneath both the current alluvial fill of the San Jacinto River

and the older sedimentary deposits of the Bautista Beds. The contacts of Major Tonalite Unit II are offset 4.5±0.6 km across this structure (Plate 1.)

Thomas Mountain and related faults

The Thomas Mountain fault was first recognized by Fraser (1931). Sharp shows it as a northwest striking feature diverging from the San Jacinto fault south and east of the current study area and disappearing to the northwest under the Quaternary fill of Garner Valley. Towards its southeastern end within the area mapped in the present study this fault shows a well defined crush and shear zone across which are juxtaposed various meatasedimentary and igneous rocks. Partially eroded scarps within fan deposits along the northwestern projection of this trend mark the position of the fault for some distance north of these bedrock exposures. No certain evidence for the position of this fault has been observed north of a small knoll of heavily dissected fan gravels south of the Thomas Mountain road (at G.R. 308227). A contact within the crystalline rocks further to the north occurs on trend with the fault up to this point, and has been assumed to represent the northwestern extension of this structure. The actual nature of this contact is not known.

A variably oriented zone of gouge that dips more or less shallowly to the south is well exposed in roadcuts leading to the south (left) abutment of the flood spillway of Hemet Reservoir. The canyon extending to the west, away from the spillway wall is cut into sheared and crushed tonalite. This fault has been previously mapped by Sharp (1967). To the west of the immediate vicinity of the dam the trace of

the fault is mostly beneath the alluvium of the San Jacinto River valley. However, at G.R. 253245 a fault contact between sheared tonalite and indurated alluvial materials is exposed in the south bank of the river, and a prominent photo lineament curves gradually towards the San Jacinto fault from this point (Plate 1). To the east of the spillway wall this fault again separates older alluvial materials from sheared tonalite, then disappears under the recent alluvium around Lake Hemet. A break of slope within the fan gravels suggests that this fault may curve around to have a more southeasterly striking surface trace, as shown on the geological map (Plate 1). This break in slope coincides with an inflection in the gravity profile across northwestern Garner Valley (Durbin, 1975).

The observed relations of the faults exposed within the canyon of the San Jacinto River suggest that they are thrust faults, and that the southeastern section of Thomas Mountain forms a relatively coherent block moving in a northwesterly direction over the underlying tonalites north of the canyon. The most recent activity on the Thomas Mountain fault, which parallels the inferred direction movement of this Thomas Mountain block, could thus represent a tear within, or perhaps the northeastern margin of the upper plate. There is no evidence either for or against the suggestion of Sharp (1967) that the Thomas Mountain fault continues northwestward beneath the fill of Garner Valley to meet the Hot Springs fault north of Lake Hemet.

Sharp determined an offset of 1.3 km across the Thomas Mountain fault to the south of the area considered here. Very general constraints on offset allowed across the assumed northwestward thrust extension of this structure are consistent with this estimate. Fault plane solutions

for micro-earthquakes having epicenters beneath the northern part of Thomas Mountain have been interpreted as showing contemporary thrusting consistent with the geometry described or inferred above (J. Pechmann, personal communication, 1983).

Gravity data have been interpreted as indicating as much as a 300 m vertical component on this fault, up to the south (Durbin, 1975); however, other interpretations of the gravity data are possible.

Un-named Faults

A northwest - southeast striking fault passes through the small village of Mountain Center (G.R. 255293). Prominent vegetated benches on the steep slope to the north and west of Dry Creek (at and around G.R. 235302) appear to mark several parallel splays of this fault. To the east of Mountain Center, in Johnson Valley, this fault offsets the western contact of Major Tonalite Unit II 0.7±0.3 km in a right-lateral sense (Plate 1).

Many other faults occur within the igneous rocks to the north of the Hot Springs fault (Plate 1). The relatively monotonous nature of the igneous rocks, and the apparently small offsets across these structure preclude accurate estimates of total displacements. The stepped bench topography of much of this area, relations within the fanglomerates, and regional considerations all suggest that at least part of the movement on these structures is down to the south.

Total Displacement Across the San Jacinto Fault System

Sharp (1967) used offsets of contacts or packages of distinctive rock types within the crystalline basement to determine the total displacement across the San Jacinto fault system. Similar features mapped as part of the study of the igneous rocks of the San Jacinto Mountains can be used to estimate displacement on several faults not considered by Sharp, largely because they were at or beyond the limits of his map area. Estimated displacements across the Hot Springs fault and the fault through Mountain Center have been noted above. These estimates are tabulated below (Table 4.1), along with estimates of displacement on the San Jacinto and Thomas Mountain faults (Sharp, 1967).

Table 4.1

ESTIMATED DISPLACEMENTS ACROSS INDIVIDUAL STRANDS OF THE SAN JACINTO FAULT SYSTEM

Fault	Displacement (Kilometers)
San Jacinto	22.5 ± 0.2
Thomas Mountain	1.3
Hot Springs	4.5 ± 0.6
Mountain Center	0.7 ± 0.3
Total, San Jacinto fault system	29.0 ± 1.1

This is slightly greater than the total displacement of about 24 km estimated by Sharp (1967) using offset of the Santa Rosa mylonite zone and offset of a sequence of rocks from southern Thomas Mountain to Bautista Creek. However, the sinuous nature of the mylonite zone and

its generally shallow dip allow some latitude in displacement estimates made using this feature. The estimate of 29 km total displacement arrived at above compares well with that of Bartholomew (1970), made from a combination of his mapping, gravity data, and reinterpretation of Sharp's data. Bartholomew also concluded that there was little evidence for a significant component of vertical displacement across the fault zone, and this appears consistent with observed metamorphic mineral assemblages on Thomas and Cahuilla Mountains, which imply similar conditions of metamorphism for the metasedimentary sequences of these two areas.

The best available estimate of total displacement across the entire San Jacinto fault system is thus 29 kilometers of right-lateral motion, with little or no vertical component.

Timing of Motion

The various strands of the San Jacinto fault system appear to have largely controlled deposition of the late Tertiary terrestrial sediments. Dating of the sediments should thus allow an estimate of the initiation and duration of faulting in this area. The Mount Eden Formation has been assigned to the Hemphillian (middle Pliocene) on the basis of both vertebrate (Frick, 1921; Savage et al., 1954) and plant (Axelrod, 1950) remains. Vertebrate remains from the San Timoteo Formation are Blancan (late Pliocene), while those from the Bautista Beds apparently include both Blancan and Irvingtonian (earlier Pleistocene) forms (Frick, 1921; Savage et al., 1954). Sharp (1981) correlates an ash bed within the Bautista Beds northwest of Anza with the Bishop Tuff, radiometrically dated at 0.73 m.y. (Dalrymple, 1980). Correlation of the North American faunal stages with the radiometric time scale has

been reviewed by Berggren and Van Couvering (1974). The base of the Irvingtonian is put at 1.45±0.05 m.y.; that of the Blancan is at 3.7±0.1 m.y.. Sedimentation thus began before about 4 million years ago, and continued through until at least 700,000 years ago. Considerable local relief apparently was not developed until the end of Mount Eden time, suggesting that this may have been about the beginning of initiation of a through-going fault system. If faulting has continued at a constant rate since then (probably unlikely), this implies an average offset rate of 7 mm/yr (over 4.0 m.y.). This compares with the average offset rate of between 8 and 12 mm/yr estimated by Sharp (1981) for the last 0.73 m.y.. The agreement between the two estimates implies that strain accumulation across the San Jacinto fault may have continued at an approximately constant rate since initiation of the through-going fault system perhaps 4 million years ago.

Development of Garner Valley as a Pull-Apart Basin

Garner Valley is a small elongate basin about 25 km long and up to 3 km across that in places contains in excess of 300 m of late Tertiary sediments (Durbin, 1975). An additional thickness of late Tertiary sediment (perhaps 100 m) has been removed by recent erosion. Interpretation of gravity and well data show that the maximum thickness of terrestrial sediments is along the southwestern edge of the valley, adjacent to the trace of the Thomas Mountain fault (Durbin, 1975). The Thomas Mountain fault is a relatively young structure, and may postdate development of the sediment-filled trough of Garner Valley. It apparently offsets the Buck Ridge fault 1.3 km in a right-lateral sense (Sharp, 1967), implying that all motion on the Buck Ridge fault had been accomm-

odated by the time of initiation of the younger (Thomas Mountain) structure. The bottom of the valley shallows toward the northeast, so that the eroded remnants of fans along this edge of the valley are resting on the crystalline basement (Fig. 4.4). The greatest thicknesses of alluvium are at a point beneath the large fan coming off the northern face of Thomas Mountain.

The Hot Springs fault, with 4.5 km of measured displacement immediately to the west, apparently dies out under the alluvial fill at the northern end of Garner Valley. A search in the exposed crystalline rocks on the eastward projection of the trend of the fault failed to find any evidence for a significant structure cutting these rocks. Mapping of units within the Desert Divide Group (Brown, 1968, 1981) confirms the absence of a through-going structure to the east of Garner Valley. The Buck Ridge fault at the southern end of Garner Valley (Fig. 4.4) is parallel to the Hot Springs fault, and has had about 5.5 km of right-lateral displacement across it (Sharp, 1967). This is very similar to the combined displacement across the Hot Springs and Mountain Center faults (5.2±0.9 km) estimated above. The geometry of this system suggests that Garner Valley developed as a pull-apart basin between the Hot Springs and Buck Ridge faults. The asymmetric geometry of the valley itself suggests that the depression is most simply explained as an erosional feature in the upper plate above a very shallowly dipping normal fault (Fig. 4.5). This appears to be the only simple model for the origin of this feature that can satisfy both the available geometric and geological constraints.

Figure 4.4. Simplified geological map of Garner Valley and vicinity, showing offset of Major Tonalite Unit II on Hot Springs fault. Compiled from Plate 1, and Sharp (1967).

MAP SYMBOLS

Qal	=	Quaternary alluvium
Kt_3	=	Major tonalite Unit III
Kt_2	=	Major tonalite Unit II
Kt_1	=	Major tonalite Unit I
Unpatterned	=	undifferentiated igneous and metamorphic rocks
Patterned	=	Late Tertiary terrestrial sediments

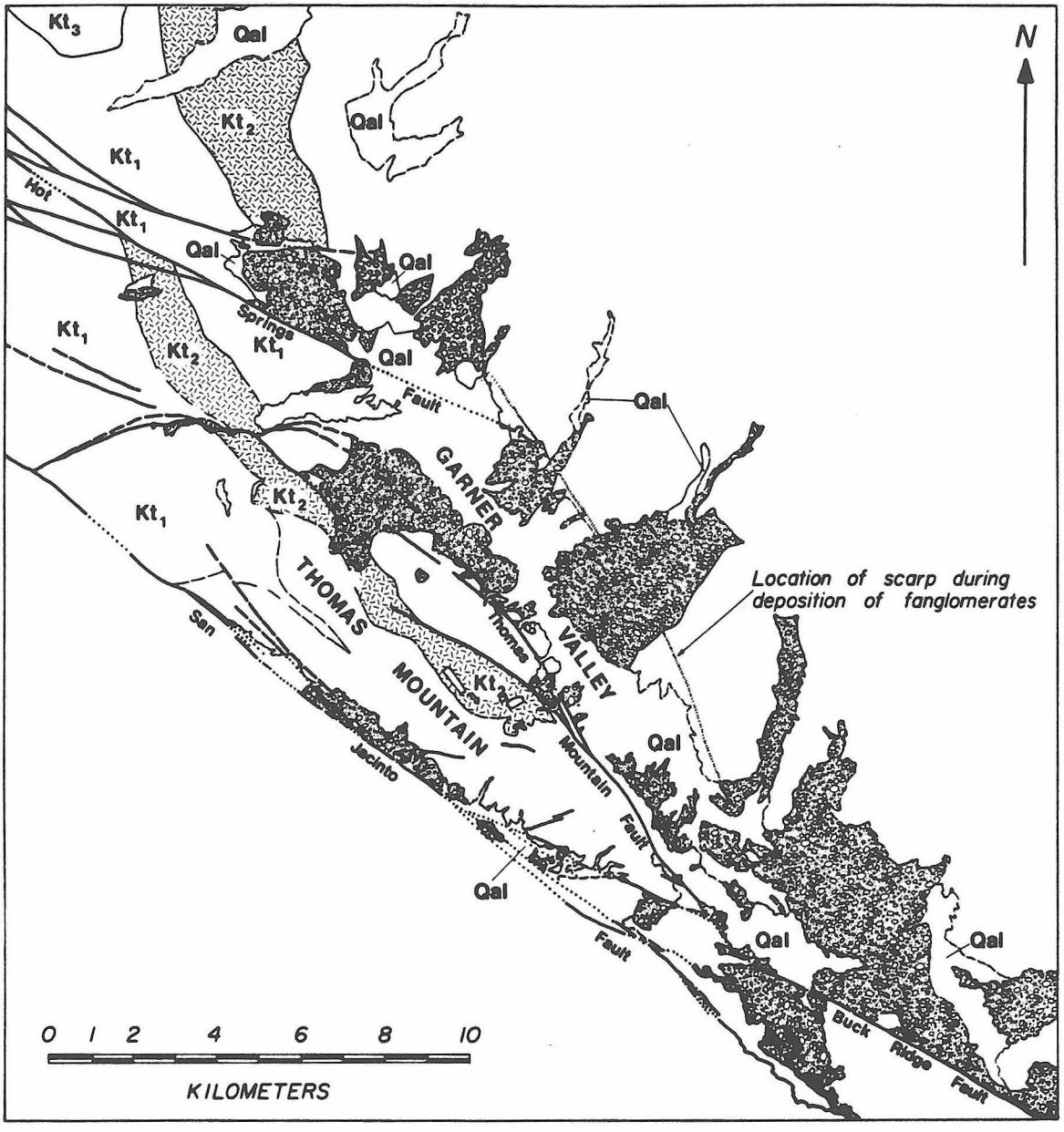
Kt3
Qal
Kt2
Kt1
Hot
Springs
Fault
GARNER
VALLEY
THOMAS
MOUNTAIN
San
Jacinto
Thomas
Mountain
Fault
Location of scarp during deposition of fanglomerates
N
0 1 2 4 6 8 10
KILOMETERS
Buck
Ridge
Fault

Figure 4.5. Schematic illustration of model for development of Garner Valley as a pull-apart basin.

Stage 1

Initiation of right-lateral motion on parallel, en echelon Hot Springs and Buck Ridge faults, and development of a low angle slip surface between these two faults.

Stage 2

Right-lateral motion on Hot Springs and Buck Ridge faults, and accompanying movement of upper plate down and to the southeast on low angle structure. Movement is accompanied by substantial shattering of the trailing edge of the upper plate.

Stage 3

Accelerated erosion of shattered rocks of the trailing edge of the upper plate, accompanied and followed by deposition of terrestrial sediments derived from both the northeast (ancestral divide of the southern San Jacinto Mountains) and the southwest (ancestral Thomas Mountain).

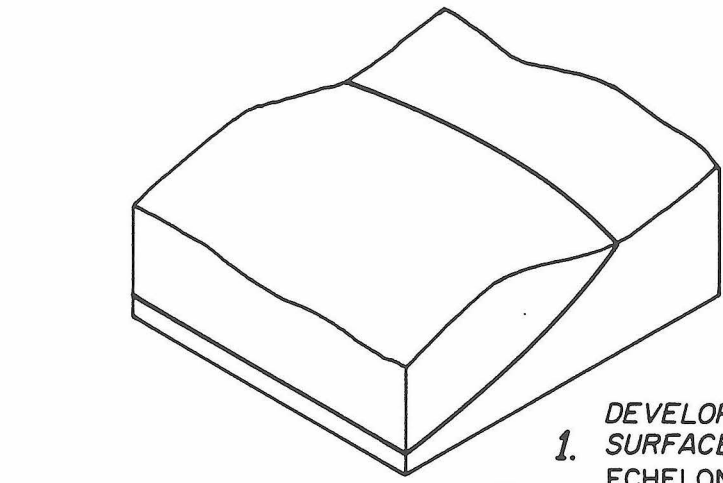

1. DEVELOPMENT OF DETACHMENT SURFACE BETWEEN TWO EN ECHELON RIGHT-LATERAL FAULTS

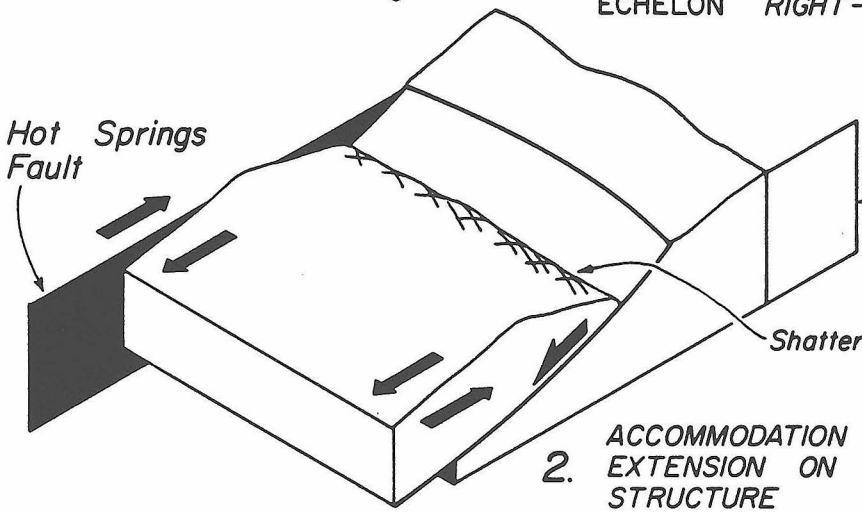

2. ACCOMMODATION OF UPPER CRUSTAL EXTENSION ON DETACHMENT STRUCTURE

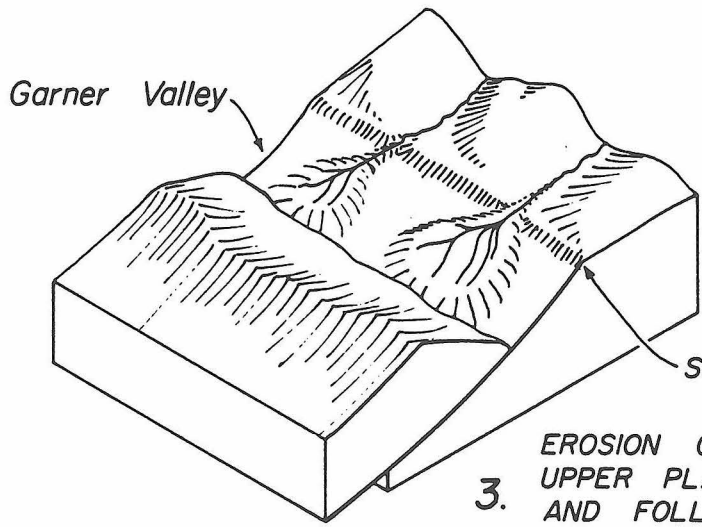

3. EROSION OF TRAILING EDGE OF UPPER PLATE CONCURRENT WITH, AND FOLLOWED BY, DEPOSITION OF TERRESTRIAL SEDIMENTS

DEVELOPMENT OF GARNER VALLEY (SCHEMATIC)

4.2.2 LAWRENCE FAULT

The Lawrence fault cuts metasedimentary and igneous rocks south of Banning (Fig. 4.3). It was named and first mapped by Fraser (1931). East of the Lawrence adit of the San Jacinto tunnel of the Colorado Aqueduct the Lawrence fault bifurcates. At the point where this fault system crosses the Banning - Idyllwild road the slice between the two strands consists of crushed and shattered metaseimentary rock. Accentuated erosion in this crush zone has resulted in the development of prominent linear drainages that flow respectively westward and eastward from a point near Mount Edna. Terrestrial sediments accumulated in the east-flowing drainage apparently post-date latest movement on this structure.

The Lawrence fault was crossed by the Lawrence adit of the San Jacinto tunnel, and Henderson (1939) describes the Lawrence fault as a minor local feature.

The Lawrence fault in part juxtaposes metasedimentary and igneous rocks from the roof zone above Major Tonalite Unit III (to the north) against tonalites of Unit III (to the south). The sense of movement is thus down to the north. No estimate of horizontal offset can be made with the data available; it is probably small.

This structure could be a splay of the South Bounding fault of Banning Pass. The sense of movement (up to the south) is similar, and the Lawrence fault must either intersect or merge with the south bounding fault beneath the alluvium of San Gorgonio Pass only a short distance from its last outcrop within the crystalline rocks. Like the south

bounding fault it appears to pre-date deposition of terrestrial sediments in valleys along the north face of the mountain.

4.2.3 SOUTH BOUNDING FAULT OF BANNING PASS

Various authors have speculated as to the origin of the tremendous relief along the northern range front of the San Jacinto Mountains. Allen (1957) suggested that the San Jacinto Mountains had been uplifted along a fault buried beneath the alluvial fill of southern San Gorgonio (Banning) Pass. Interpretation of gravity data (Willingham, 1981) suggests that this proposed structure exists, and has a minimum of 1.6 km vertical displacement across it. Larger scale considerations suggest that total vertical offset may be in excess of 4.5 km; this is the vertical separation between the top of exposed basement in the San Jacinto Mountains, and the top of buried basement beneath the valley fill to the north of the geophysically located structure.

No evidence for faults related to this structure, with the possible exception of the Lawrence fault, has been found within the study area. A partially dissected steeply-sloping alluvial fan in a canyon to the west of Snow Creek grades to the approximate level of the current pass. This implies that either there has been no offset since deposition of this fan, or that sedimentation within the pass has balanced tectonic activity. The latter appears less likely, so it is suggested that movement on the south bounding fault of Banning Pass pre-dates deposition of terrestrial sediments along the northern range front.

4.2.4 POTRERO FAULT FIELD

A series of approximately northwest trending faults in the northwestern corner of the study area has been termed the Potrero Fault filed by Henderson (1939). These faults have associated spring lines, topographic benches, and, where exposed, may show well-developed gouge zones. Considerable shattering of rock is associated with these faults; the shattered zone is often of considerably greater extent north of the fault (Henderson, 1939). Most of these faults dip towards the northeast. The sense and amount of offset on these faults is unknown; it appears small.

4.3 A PRE-TERTIARY RECONSTRUCTION OF THE SAN JACINTO MOUNTAINS

Figure 4.6 presents a pre-faulting reconstruction of the area mapped in this project. It shows the inferred original disposition of the various intrusive units described above. This reconstruction restores the offsets on the Hot Springs, Mountain Center and Thomas Mountain faults (Table 4.1). It also assumes the model for development of Garner Valley as a pull-apart basin. This reconstructed pre-faulting (palinspastic) base is used for the presentation of geographical variation in geochemical, petrological and isotopic data obtained for the intrusive rocks.

4.4 EASTERN PENINSULAR RANGES MYLONITE ZONE

The existence of a mylonite zone of considerable regional extent within the eastern-most Peninsular Ranges was first reported by Lockwood (1961). This structure, called the eastern Peninsular Ranges mylonite zone by Sharp (1979) has been traced southwards from near Palm Springs almost to the international border with Mexico (Sharp, 1979)[Fig.

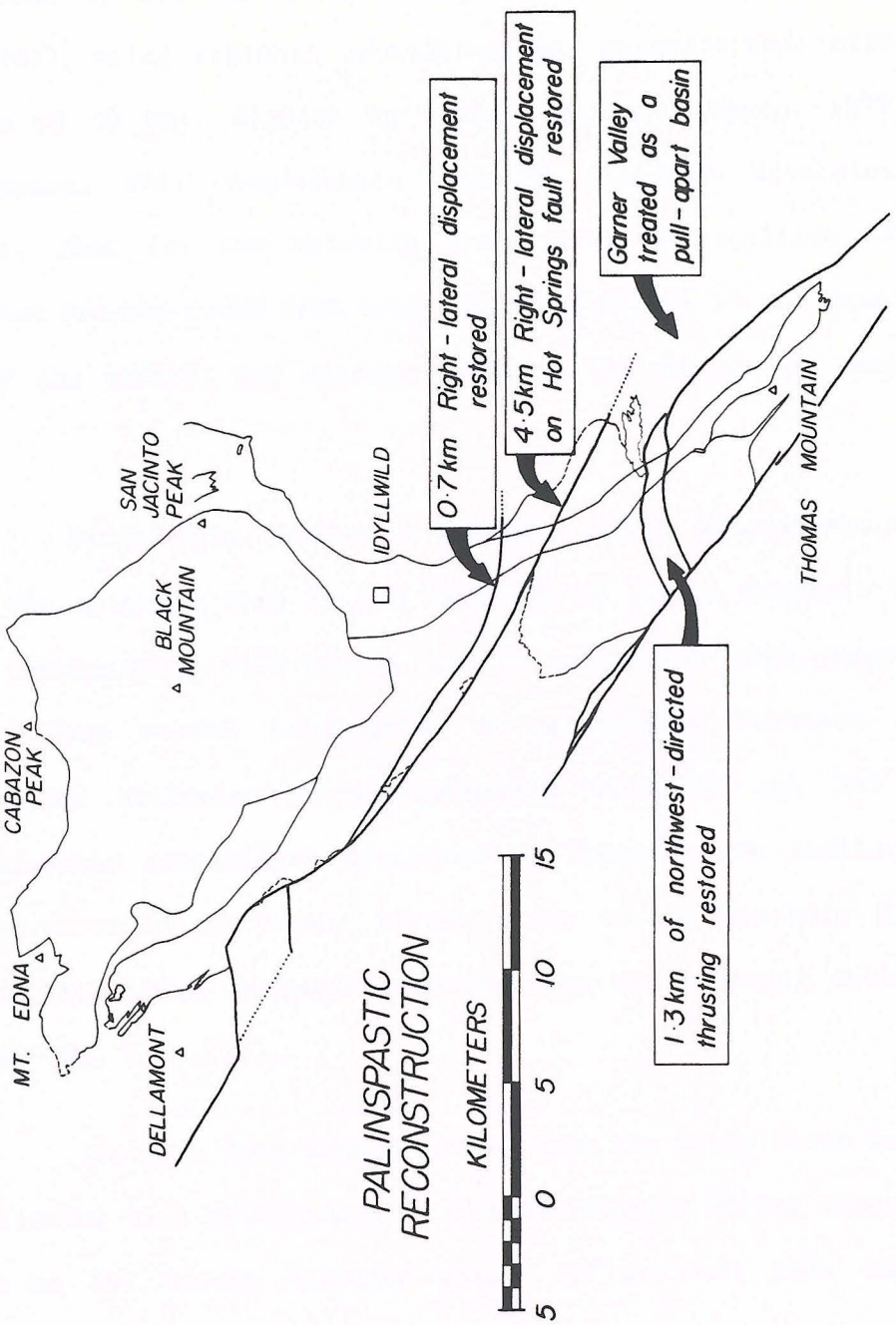

Figure 4.6. Palinspastic reconstruction of the San Jacinto Mountains prior to Tertiary faulting.

4.7]. Sharp used geometric constraints to show that a minimum of 11 km of displacement had occurred on the northern-most section of the mylonite zone, termed by him the northern Santa Rosa Mountains thrust. Silver (1982, 1983), using regional considerations, suggests that offset may be in excess of 50 km. Studies by various authors (Sharp, 1979; Parcel, 1981; Simpson, 1983) demonstrate that the transport direction is east over west, that is, the mylonite zone marks the position of a major thrust that brought rocks from some unknown distance to the east or northeast over the central and western parts of the Peninsular Ranges batholith.

Petrofabric studies by Theodore (1970) demonstrate that movement on the mylonite zone in the vicinity of Coyote Mountain took place at high temperatures (580-660oC), and at relatively high pressures (3.4-7.0 kb). More recent calibration of metamorphic reaction conditions changes these estimates to approximately 600-700oC and 3-5 kilobars. The metamorphic assemblages described by Theodore are similar to those described above in the Desert Divide Group of the southern San Jacinto Mountains, for which comparable temperature and pressure estimates have been made (Ch. 3, p.103).

Isotopic data from a schist from the Windy Point metamorphics are consistent with development of the schistosity having occurred during movement on the nearby mylonite zone. If correct, this implies that metamorphic conditions prevailing here during development of the mylonite were similar to those prevailing further to the south. The mylonite zone thus appears to have been a deep-seated structure, as argued by Theodore (1970). F.K. Miller (quoted in Sharp, 1979) has interpreted K-Ar data as

Figure 4.7. Eastern Peninsular Ranges mylonite zone (Sharp, 1979).

Thin wavy lines show foliation trends within the mylonite zone. Thick lines show cross-cutting thrusts, which may be of more than one generation (Sharp, 1979; E.G. Frost, personal communication, 1983).

The western boundary of this map in the area of the San Jacinto Mountains coincides approximately with the eastern boundary of the current study area.

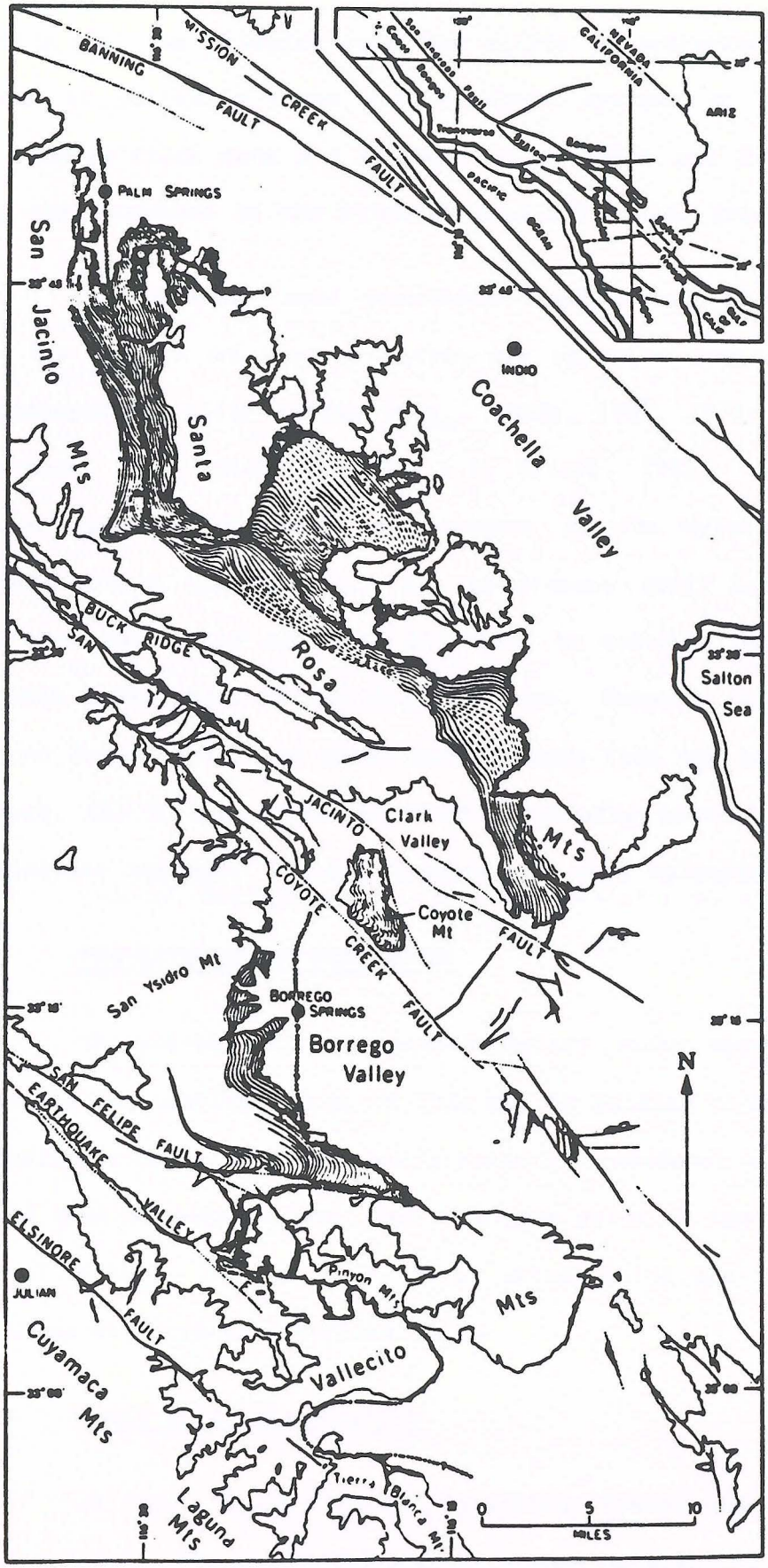
BANNING FAULT
MISSION CREEK FAULT
PALM SPRINGS
San Jacinto Mts
Santa Rosa
INDIO
Coachella Valley
BUCK RIDGE
SAN JACINTO
Clark Valley
Salton Sea
Coyote Mt
COYOTE CREEK FAULT
San Ysidro Mt
BORREGO SPRINGS
Borrego Valley
SAN FELIPE EARTHQUAKE VALLEY FAULT
ELSINORE FAULT
JULIAN
Cuyamaca Mts
Pinyon Mts
Vallecito
Laguna Mts
Tierra Blanca Mt
N
0 5 10
MILES

indicating that the mylonite zone was active at approximately 70 m.y., and reset or partially reset K-Ar isotopic systems at or about this time. Fission track data are interpreted by Dokka and Frost (1976) as showing that movement on the mylonite zone had ceased prior to 62 m.y..

The mylonite zone post-dates emplacement of the plutonic rocks. The margins of plutons within the mylonite zone commonly show well-developed mylonitic fabric (e.g., Sharp, 1967, 1979; Brown, 1968, 1981; Sydnor, 1975; Dibblee, 1981a,e,f; Parcel, 1981). No geological effects certainly attributable to movement on the mylonite zone have been found within the main part of the present study area. The main plutons have apparently not been disrupted by tectonic activity synchronous with development of the mylonite zone. However, both K-Ar (Armstrong and Suppe, 1972) and Rb-Sr mineral data from the major tonalites (this work, Ch. 9) may be interpreted as showing partial resetting of the respective isotopic systems synchronous with mylonite development.

4.5 PRE-BATHOLITHIC STRUCTURES

The pre-batholithic metasedimentary rocks show evidence of considerable deformation. Some of this may be related to emplacement of the batholithic rocks, some apparently relates to movement on the mylonite zone, and some appears to have been developed prior to igneous activity. Structural features of the Windy Point metamorphics and of the Desert Divide Group are briefly described below.

4.5.1 WINDY POINT METAMORPHICS

All rocks show a strong foliation; Sydnor did not recognise original bedding. The dominant foliation trends parallel to the border of

the nearby pluton. Mylonites are present locally, and the development of the prominent foliation probably relates to movement on the eastern Peninsular Ranges mylonite zone (Sydnor, 1975; Sharp, 1979). Lineations within this foliation plane measured by Sydnor suggest movement along northwest-southeast slip-lines. The asymmetric distribution of attitudes of lithological layering measured by Sydnor (1975) [generally, easterly dips are shallower than westerly dips] is consistent with development of much of the observed layering during transport of the upper (eastern) rocks over the western rocks. Deformation associated with movement on the mylonite zone was apparently sufficiently intense and widespread to have so far masked any pre-mylonite structure within these rocks except for intrusive relations with dikes and sills related to the large nearby plutons.

4.5.2 DESERT DIVIDE GROUP

Much of the outcrop of the Desert Divide Group is sufficiently distant from either the mylonite zone or the margins of large plutons to be apparently free of structural effects related to these features. Within the large area of exposure along the Desert Divide of the southern San Jacinto Mountains the rocks of the Desert Divide Group dip monotonously to the east with relatively shallow dips (Brown, 1968, 1981; Dibblee, 1981a,e,f). Intense deformation within marble lenses suggests the presence of similar deformation within the Desert Divide Group as a whole.

Elsewhere structures within the metasedimentary rocks correlated with the Desert Divide Group appear to be dominated by those related to emplacement of nearby plutons.

4.6 IGNEOUS STRUCTURES

Structures related to the igneous rocks can be considered in two more or less distinct categories - those external to the plutons, or otherwise intimately related to emplacement of the plutons, and those completely internal to a pluton which largely result from processes acting remote from the outer contacts of the plutons.

4.6.1 EXTERNAL AND CONTACT-RELATED STRUCTURES

A general observation is that contacts between the igneous rocks and both their metasedimentary and igneous wall-rocks are sharp, and cut pre-existing structures at a high angle. A strong imposed foliation parallel to the contact is usually present in wall-rocks and may be apparent as much as several kilometres from the contacts of the three major tonalite intrusions. The orientation of imposed foliations varies throughout the area (Fig. 4.8), and apparently relates, at least in part, to emplacement of the major tonalites.

Where well exposed the outermost rocks of individual intrusions show a range of internal structural features. The northern contact of Unit III is well exposed in several road-cuts (e.g., at G.R. 135495 and 183472). Here the contact with metasedimentary wall-rocks varies from sharp to gradational over several hundred meters. In exposures where the contact is sharp (Fig. 4.9a) the outermost rocks of the tonalite are relatively fine-grained, felsic, and are strongly foliated. This foliation parallels the nearby contact. Bedding within the metasedimentary sequences also approximately parallels the contact. However, individual quartzite units are still visible, and show only minor boudinage or other

Figure 4.8. Observed attitudes of imposed foliations within metasedimentary and igneous rocks excepting the major tonalite units, and observed attitudes of bedding within metasedimentary rocks. Palinspastic base.

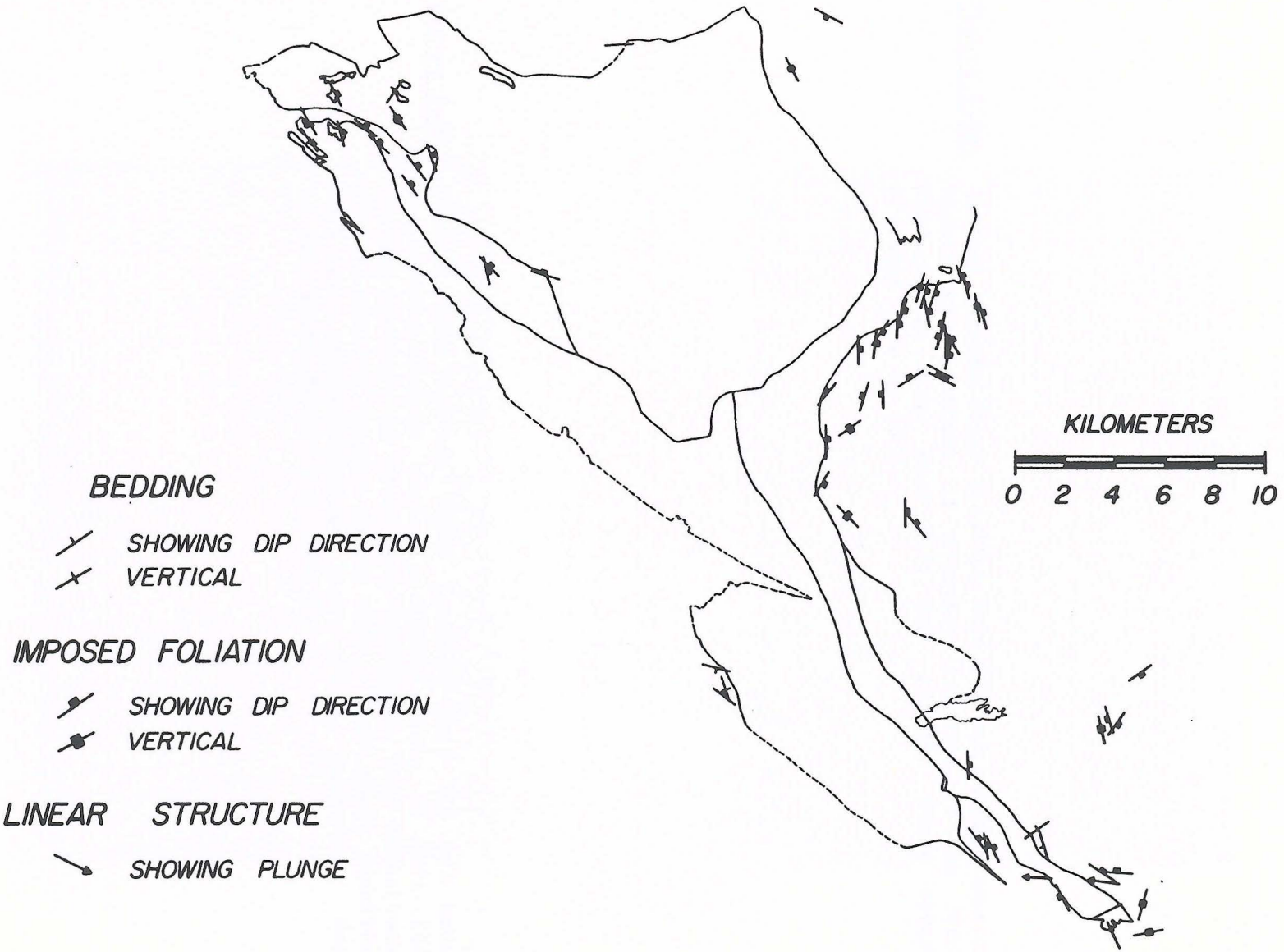
KILOMETERS
0 2 4 6 8 10
BEDDING
SHOWING DIP DIRECTION
VERTICAL
IMPOSED FOLIATION
SHOWING DIP DIRECTION
VERTICAL
LINEAR STRUCTURE
SHOWING PLUNGE

Figure 4.9a. Contact between Major Tonalite Unit III and metasedimentary host rocks. Contact is arrowed; tonalite to the left. Road cut on State Road 243, G.R. 135495. Photo covers of about 15 m by 10 m.

Figure 4.9b. Contact zone between Major Tonalite Unit III and metasedimentary country rocks, northern margin of Unit III. Contact consists of mixed zone similar to that illustrated that is several hundred meters wide. Light gray, tonalite; dark gray, metasedimentary rock; white, pegmatite. Road to Twin Pines Ranch, G.R. 183472.

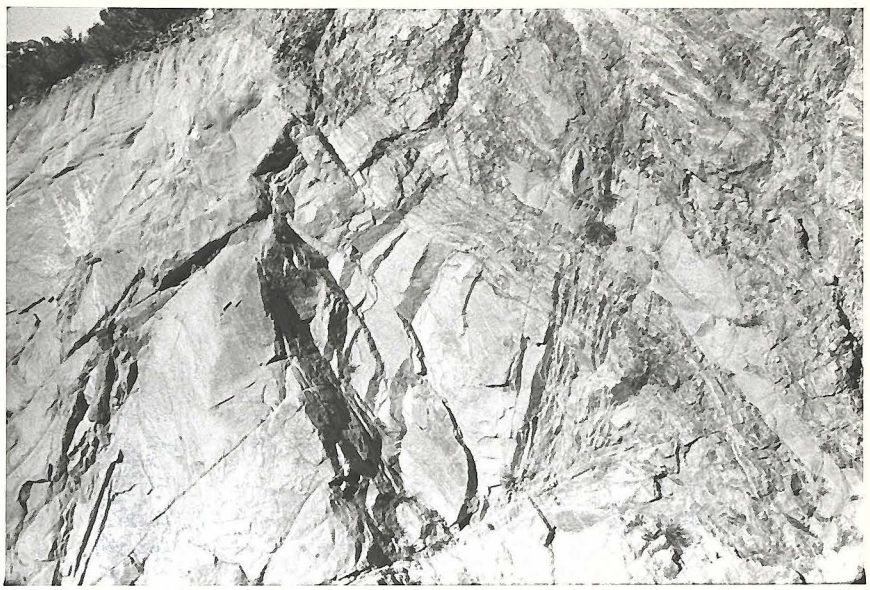

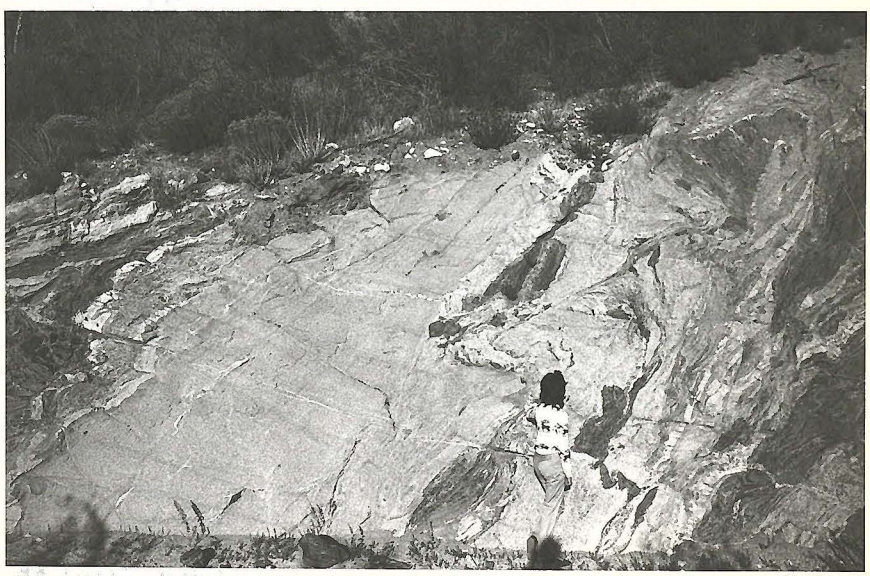

Figure 4.10. Geologic map of the northwestern contact of Unit I.

SYMBOLS

Qal	=	Quaternary alluvium
Tco	=	Terrestrial sedimentary rocks
Kt_3	=	Major tonalite Unit III
Kt^1	=	Major tonalite Unit I
pKu	=	Undifferentiated igneous and metasedimentary rocks
pKm	=	Pre- Late Cretaceous metasedimentary rocks (m = marble)

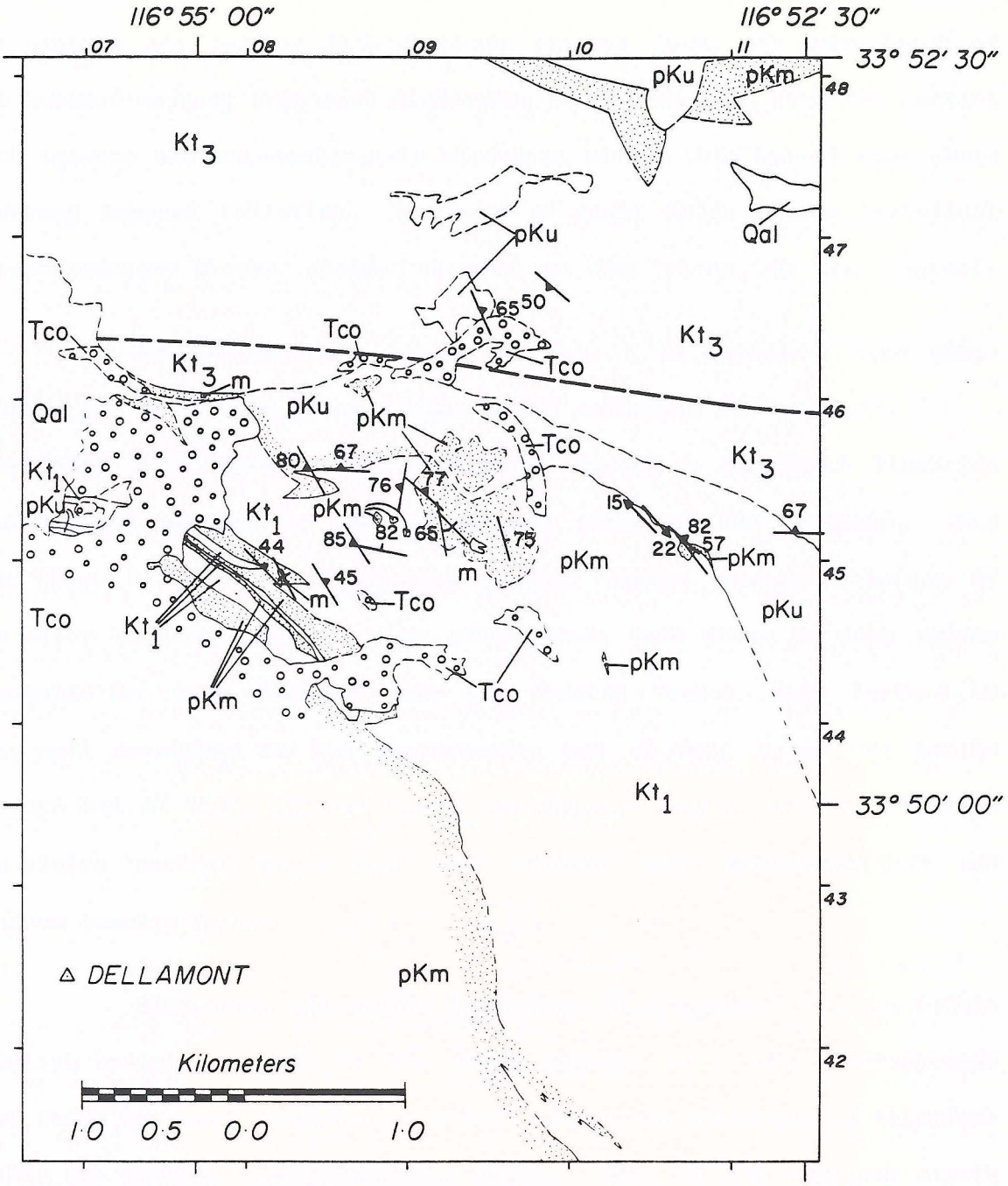
116° 55′ 00″
116° 52′ 30″
33° 52′ 30″
33° 50′ 00″
07
08
09
10
11
48
47
46
45
44
43
42
Kt3
pKu
pKm
Qal
Tco
m
Kt1
65
50
80
67
76
77
82
85
44
45
75
15
22
57
△ DELLAMONT
Kilometers
1·0
0·5
0·0
1·0

deformation. Elsewhere along this northern contact igneous and metasedimentary rocks alternate over a distance of as much as several hundred meters (Fig. 4.9b). Sedimentary screens elongate parallel to the contact are cut by heterogeneous igneous rock; the importance of the metasedimentary component diminishes northwards away from the contact Both igneous and metasedimentary materials within this hybrid zone share a strong imposed foliation. The axes of tight folds within individual metasedimentary blocks plunge steeply in the plane of the contact.

The northwestern margin of Unit I is intrusive into metasedimentary rocks containing a significant carbonate and quartzite component. Both marbles and quartzites exhibit a prominent lineation that plunges steeply in the approximate plane of the contacts. This area (Fig. 4.10) also illustrates another common contact relation of the major tonalite units - they often grade into dikes or dike swarms traceable for some distance into the country rocks. This feature is also well developed at the southeastern end of Unit I, at the southeastern end of Unit II, and along the eastern margin of Unit II where the pluton narrows to a sill that invades both metasedimentary and igneous country rocks.

Elsewhere, the common occurrence of a strong foliation within xenolith trains adjacent to the outer contact of a unit demonstrates that there has been considerable strain across the solid-liquid interface within the growing and solidifying pluton. Much of the relative strain between the inflating pluton and its wall rocks has been apparently accommodated <u>within</u> the outermost part of the pluton.

Contact relations of early intrusives

Most of the early intrusives are small, and have dike-like or sill-like form. Contacts either with metasedimentary or igneous host rocks are generally sharp (Fig. 4.11a). Exceptions occur, however (e.g., the northern margin of the granite of Penrod Canyon). Hybrid rocks, apparently formed through physical mixing at different scales, are common throughout the early intrusives. Such mixed rocks are spectacularly exposed in the walls of Chino Canyon (Fig. 4.11b), where they have been studied in detail by Sydnor (1975). Boundaries between the different lithologies present in these mixed rocks are commonly still sharp (Fig. 4.11b).

The smaller bodies commonly have finer grain-size than do either the larger early intrusives or the major tonalites. They also commonly show a pronounced imposed foliation parallel or subparallel with the closest contact. This imposed foliation is interpreted as resulting from stresses applied to already crystalline marginal materials by continued flow of magma into or through the volume represented by the exposed dike or sill.

Relatively few dikes or sills (bodies with thicknesses or widths of less than about 100 m) distant from the major tonalites have the composition of the major tonalites. Such bodies are generally a little more felsic than the common rock of the major intrusives. Dikes and sills with similar compositions to those of the major tonalites are generally spatially associated with one of the major intrusive units, and can often be followed to the outer contact of the nearby major tonalite intrusive.

CONTACT RELATIONS WITHIN EARLY INTRUSIVES

Figure 4.11a. Sill of felsic tonalite cutting metasedimentary rocks north of major tonalite Unit III. Roadcut on State Road 243, G.R. 121510.

Figure 4.11b. "Hybrid" or "mixed" zone, south wall of Chino Canyon, showing multiple episodes of diking, and apparent physical disaggregation of earlier materials during later intrusion.

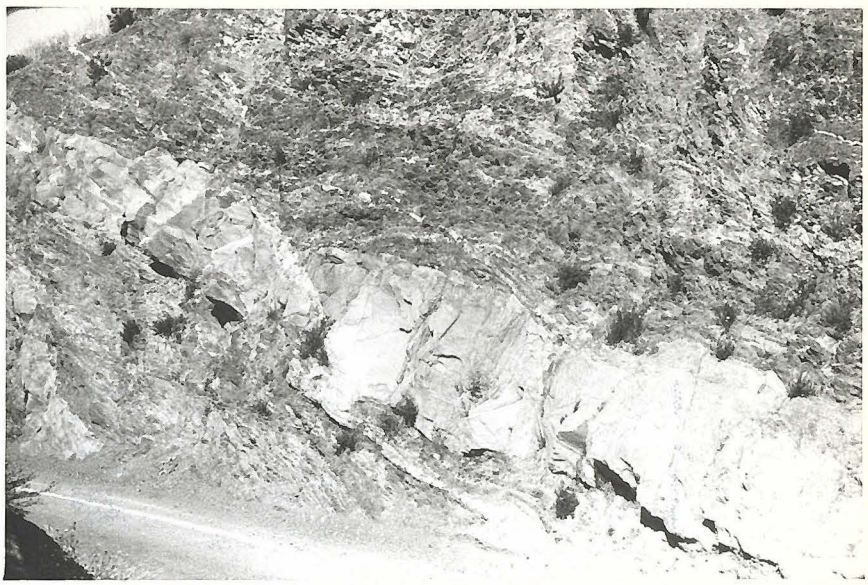

4.6.2 INTERNAL STRUCTURES

Igneous foliations and lineations

Orientation of minerals (most prominently hornblende and biotite) to define a planar foliation is common throughout the various igneous masses of the San Jacinto Mountains. Alignment of the long axes of prismatic or tabular crystals within this foliation may give an igneous lineation as well. In some mafic rocks devoid of a foliation a strong lineation may be developed. Measured foliations and lineations are shown on Fig. 4.12 and on Plate 2.

The foliation is commonly best defined by alignment of hornblende and biotite prisms within the foliation plane (Fig. 4.13). The long axis of hornblende prisms (and, less commonly, plagioclase tablets) may be oriented within this plane to give a lineation, but this is not common as the development of foliation alone. The intensity of development of foliation is roughly proportional colour index; in the most mafic rocks a foliation (and often a related lineation) is strongly developed, while in the more felsic rocks from all units planar and linear structures are commonly absent. Part of the central part of Unit III is comprised of relatively featureless felsic tonalite and low-K granodiorite apparently lacking any preferred mineral orientation.

In thin section the foliation shows as an alignment of hornblende prisms, as elongation of biotite grains, and by a rough alignment of plagioclase tablets. Except for rocks from a narrow zone adjacent to the contact of Unit III there is no evidence in thin section for cataclasis of mineral grain boundaries. Grain boundaries

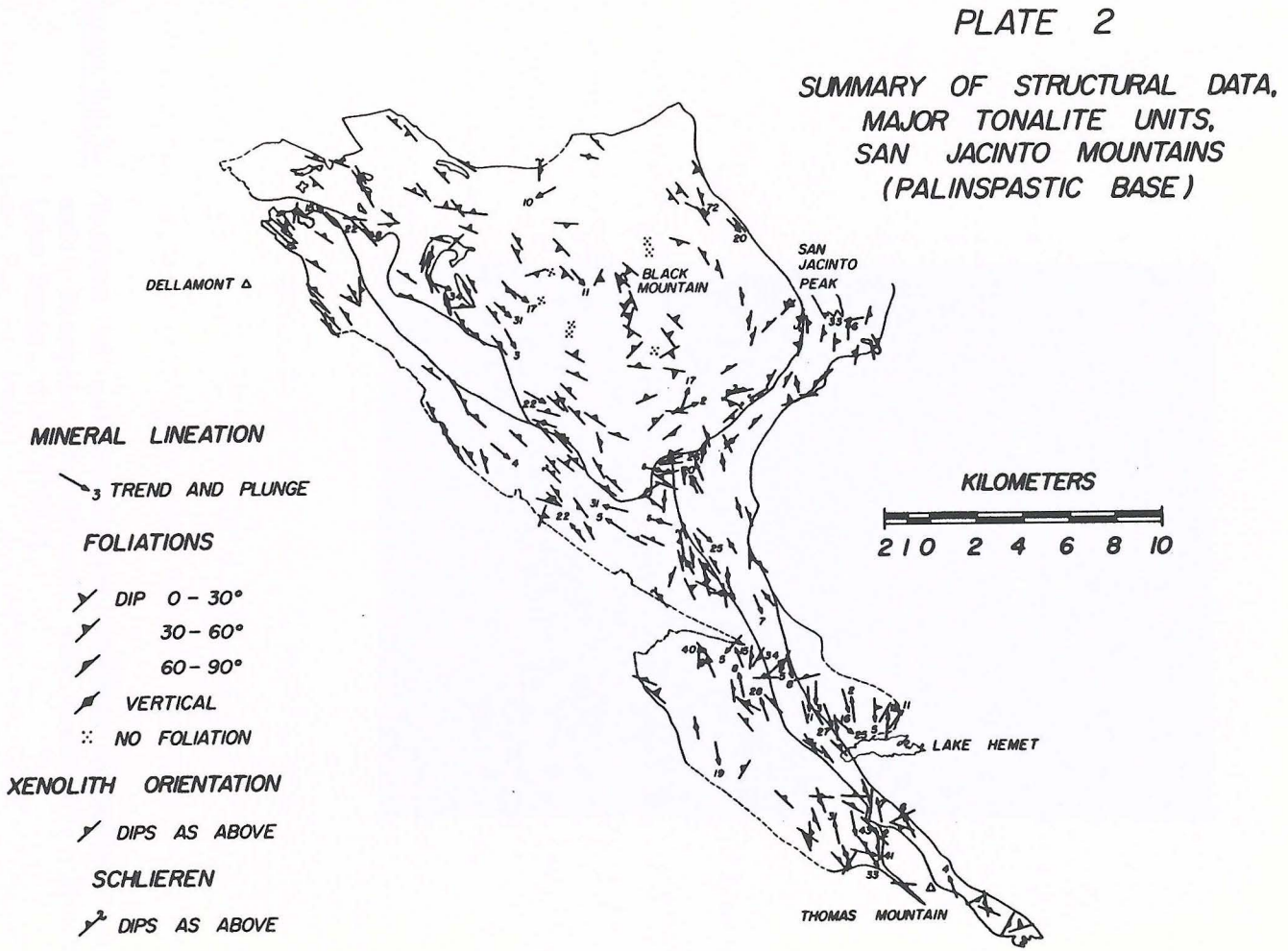

Figure 4.12. Summary of structural data (mineral foliations and lineations, schlieren, xenolith orientation) for the major tonalite units.

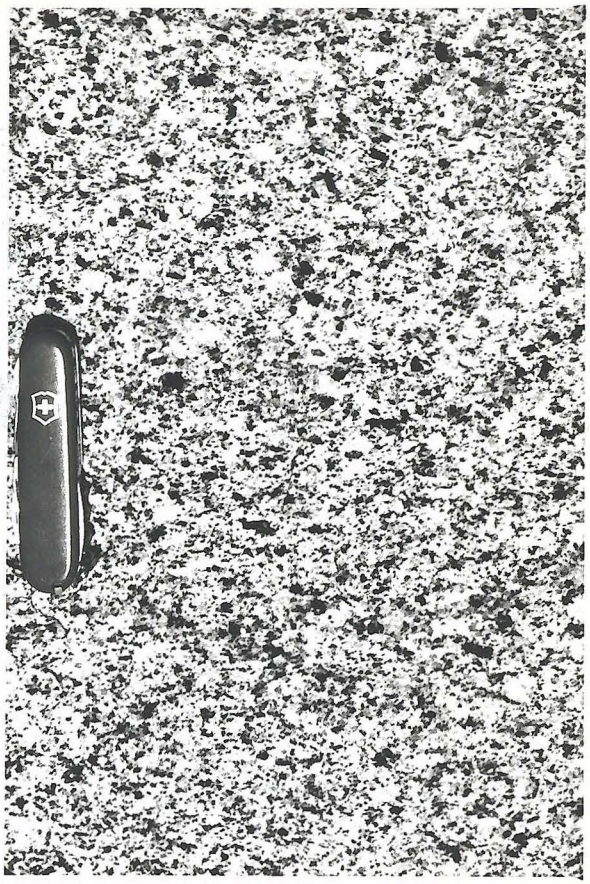

Figure 4.13. Texture of mafic tonalite showing prominent alignment of mafic minerals (hornblende and biotite). North shore of Lake Hemet, G.R. 274251.

retain their presumed igneous features, and minerals show little or no evidence for imposed strain after crystallization. Poikilitic titanite-plagioclase-quartz ellipsoids (which are more fully described below, Ch. 5) in the more mafic rocks of Unit I commonly are oriented in the foliation plane, and show no evidence for imposed strain in their constituent minerals.

These relationships are interpreted as showing that the foliations and lineations observed in these rocks result from magmatic processes.

Schlieren and other mineral layering

Mineral banding defined by relative concentration of particular mineral phases (most commonly hornblende, biotite, and plagioclase) is common throughout the igneous rocks of the San Jacinto Mountains. Schlieren is a non-genetic term used to describe streaky, wisplike or non-stratiform concentrations of light or dark minerals. Figure 4.14a illustrates typical schlieren from a mafic tonalite. Individual schlieren are usually from a centimeter or two, to 20 centimeters wide, and from a few tens of centimeters to a few tens of meters long. Most are defined by a relative abundance of dark minerals, but felsic schlieren are also present (Fig. 4.14a). Margins are usually diffuse, and the minerals compositionally identical to those of the homogeneous host rock.

Layering is used to describe rhythmic variation in the concentration of minerals bounded by at least one relatively abrupt (usually planar) face. A typical example is illustrated in Fig. 4.14b. The dark layers have high concentrations of hornblende and biotite, and

SCHLIEREN AND MINERAL BANDING

Figure 4.14a. Typical schlieren in mafic tonalite. Note relatively abrupt upper margin and diffuse lower margin to the mafic schlieren in the center of the photograph. Two felsic schlieren are arrowed. Broken blocks beside Pines-to-Palms Highway, near Keenwild Forest Service Station (G.R. 261298).

Figure 4.14b. Mineral banding in low-K granodiorite. Pacific Crest Trail, G.R. 271376. Pluton margin is to the right.

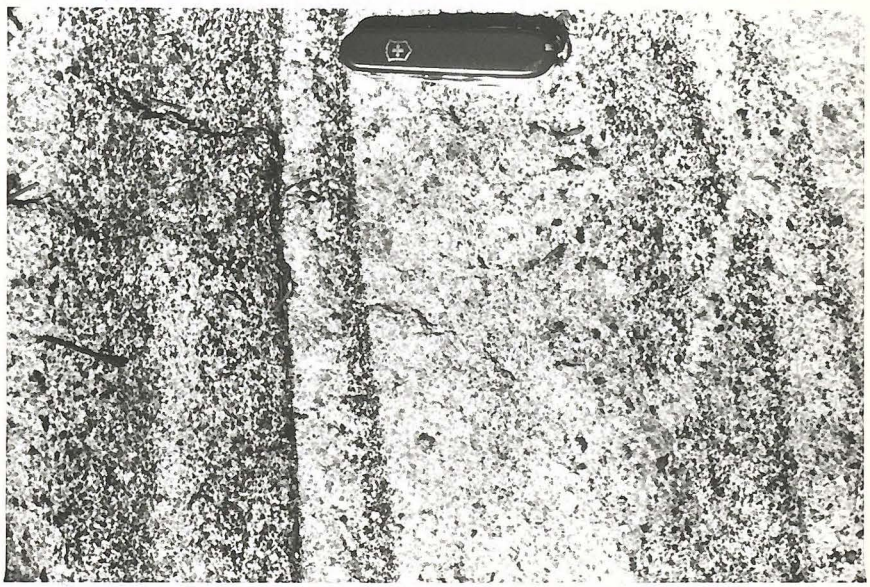

MINERAL LAYERING

Figure 4.15a. Mineral layering within tonalite of Herkey Creek. Similar features occur within the major tonalite units. Pluton contact is to the top of the photograph. The prominent mineral layering is interpreted as resulting from flow alignment by currents within the magma chamber paralleling the pluton wall. G.R. 309268.

Figure 4.15b. Mineral layering and possible scour features within mafic tonalite. Pluton contact is to the top of the photograph. Locality as for Fig. 4.15a.

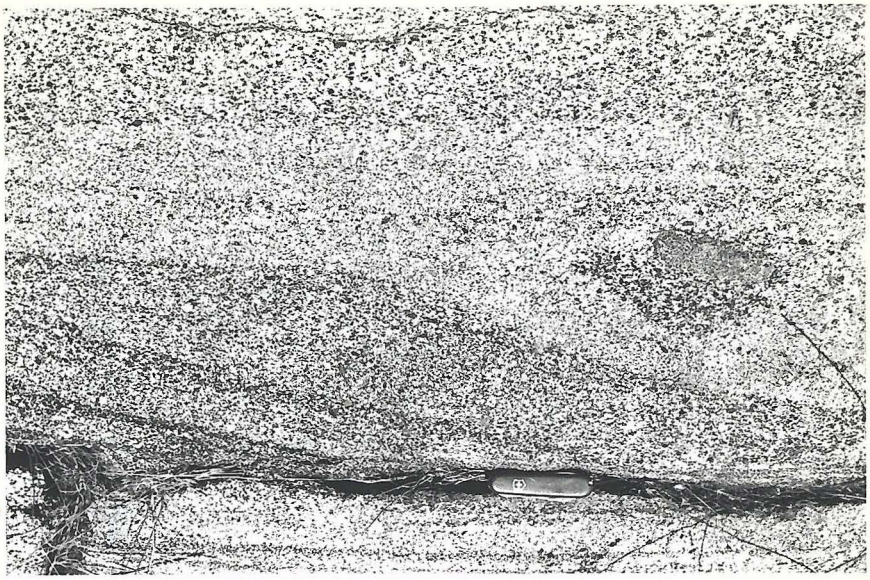

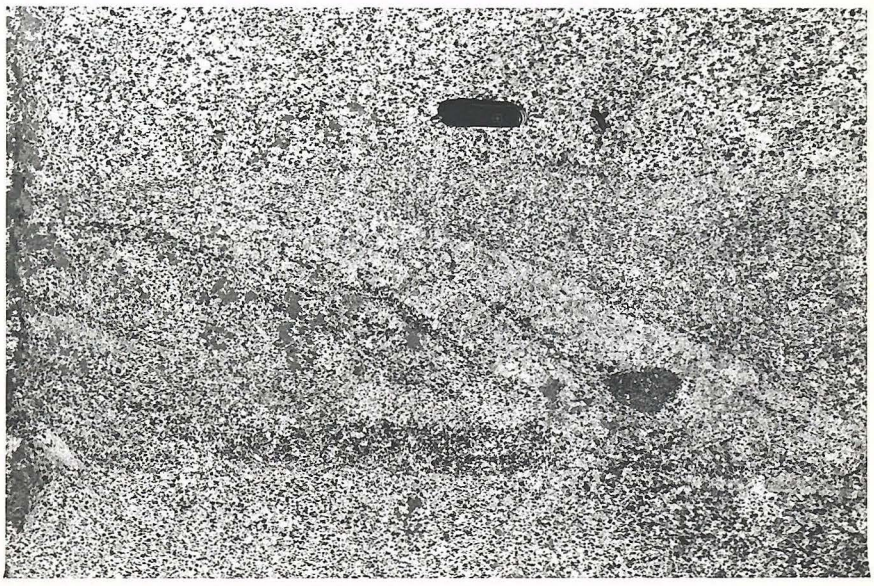

often titanite; light layers are dominantly composed of plagioclase and quartz, with subordinate K-feldspar. Occasional layers are continuous for over one hundred meters; most, however, are a few tens of centimeters to a few meters in length.

Groups of layers commonly exhibit features suggestive of the action of current activity adjacent to the wall of the cooling magma chamber. Figures 4.15a and 4.15b illustrate features most simply interpreted as showing the action of sedimentary-like processes - erosion and flow sorting - within the crystallizing magma chamber. If this interpretation is correct, it implies that movement of silicate liquid relative to the crystalline or quasi-crystalline chamber walls was sufficiently rapid to allow erosion of the wall, and for flow differentiation or sorting to occur.

All features described above are found in both early intrusives and in major tonalites. Sclieren and mineral layering are particularly prominent adjacent to the mixed zones described above. Fig. 4.16 shows mineral banding prominently developed within a thin sill cutting pegmatites in a mixed zone in the roof rocks to Unit II.

Xenoliths

Dark ellipsoidal xenoliths are common throughout the three major tonalites, and also are present in the more mafic of the smaller earlier intrusions. They range in size from ellipsoids with long axes of a meter or more downwards to small dark spots of centimeter size. Xenolith abundance varies considerably, from over 50% of the rock in some xenolith trains to a few isolated xenoliths scattered over a several

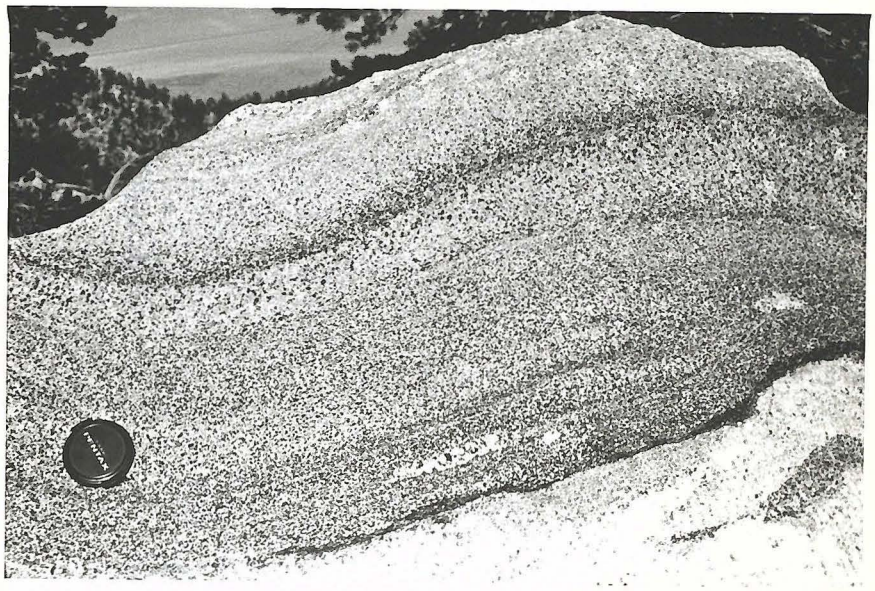

Figure 4.16. Mineral layering within a thin dike cutting pegmatite, early intrusives east of Cornell Peak (G.R. 315414). Up is to top of photograph.

hundred square meter exposure.

Xenoliths are commonly oriented in the foliation plane defined by the dark minerals or by schlieren, although in a few areas the dominant foliation and xenolith orientation are at an angle. Linearly extensive concentrations of xenoliths are common, and are called xenolith trains. The most extensively developed forms the outermost part of the eastern margin of Unit III, and has been traced continuously for over 27 km with the exception of a 4 km interval across the steep northern face of San Jacinto Mountain. Both the margins of, and foliations within this xenolith-rich zone generally dip inward, away from the contact, although dips are locally variable. The maximum true thickness of this feature is where where it crops out in the headwaters of Strawberry Creek, south of Marion Mountain (at G.R. 288383), where it is about 200 m thick.

Figures 4.17a and 4.17b illustrate relationships within a major xenolith train. Figure 4.17a, a view along strike of part of a major train, shows the strong foliation common within the most xenolith-rich parts of such a train. Also apparent is the veining of individual elongate xenolith masses by host tonalite and a sense that the whole has been arrested in the act of being broken into smaller blocks. This is better illustrated in Figure 4.17b, a view normal to the foliation plane. The irregular, often wispy outlines of individual mafic blocks obvious here are common features within the xenolith trains of these plutons. Pegmatoidal veins or patches with centimeter-sized hornblende, biotite, plagioclase and titanite euhedra in a quartzo-feldspathic matrix are more common in the matrix, but may cut the mafic material as well.

Figure 4.17a. View along a xenolith train. Note evidence for plastic deformation, high density of mafic xenoliths (dark), and strong foliation. Pacific Crest Trail west of Strawberry Cienaga (G.R. 277379).

Figure 4.17b. View normal to the foliation plane within a major xenolith train. Same outcrop as above. Note veining by lighter (tonalitic) material.

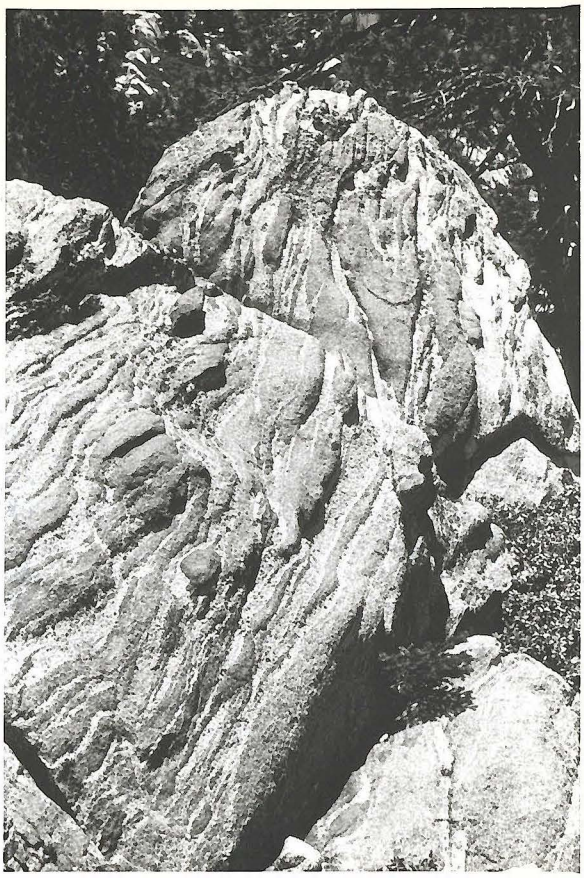

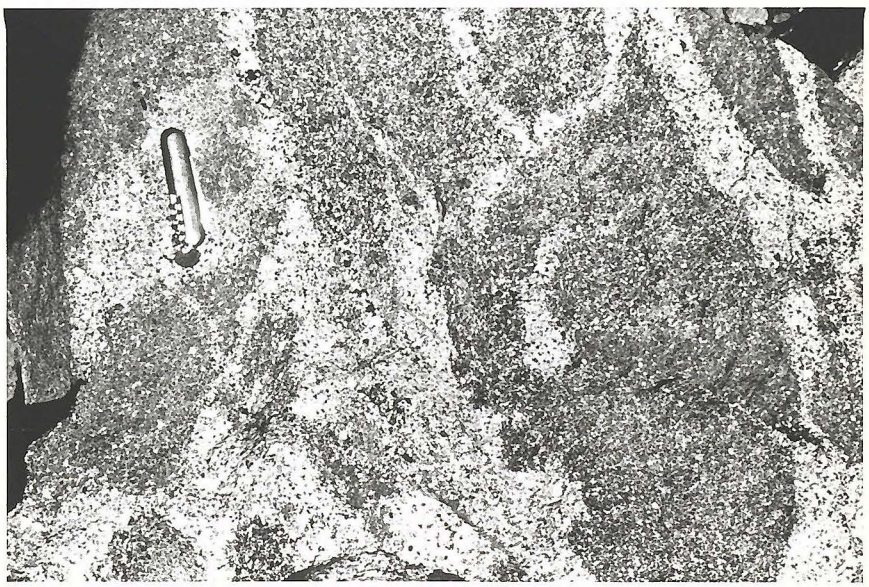

Dikes and sills intruding the major tonalite plutons

Several varieties of dikes intrude the tonalite of the large plutons. Many show evidence of interaction between dike and host suggesting relative synchroneity of emplacement. Field relations suggest a genetic link between one group of dikes and the xenolith trains. Accordingly, dikes intrusive into the major tonalites are described below preparatory to a discussion of the evidence for the relationship between this group of dikes and the xenolith trains.

Five types of dikes (and sills) intrusive into the late tonalites were observed. In approximate order of abundance they are

1. Mafic dikes of dioritic or mafic tonalite composition
2. Aplites
3. Pegmatites,
4. Tabular bodies of mafic tonalite composition containing abundant aligned plagioclase tablets,
5. Dikes of K-feldspar megacrystic granodiorite spatially associated with the irregular bodies of similar rock south-east of Poppet Flat.

Mafic dikes

Variously oriented tabular bodies of dark gray fine-grained to porphyroblastic rock are present throughout the area. They vary in size from narrow bodies a few tens of centimeters or less in width that extend across an outcrop for a few tens of meters to large masses several tens of meters in width that can be followed along strike for several kilometers. Contacts with host tonalite are usually sharp, although there

is often considerable veining of the dike-rock by the tonalitic host, or by more felsic liquids apparently derived from the tonalitic host. This veining is apparent at all scales, from apophyses of felsic material that extend a few millimeters in from the dike contact to masses of tonalite so extensive that the dike appears to be in the process of being broken into an assortment of randomly oriented dark blocks. In many places xenolith swarms appear to have formed from such disaggregation of mafic dikes.

In other outcrops dikes, sills or apophyses therefrom have margins that appear to indicate shearing of the dike material into a tonalitic or granodioritic host (Fig. 4.18).

Hand specimens of mafic dikes commonly show a fine-grained gray rock with abundant spots of white plagioclase porphyroblasts. These plagioclase porphyroblasts may have a long dimension of several millimeters, and commonly show strong orientation parallel to the walls of the dike.

In thin section aligned plagioclase crystals comprise about half the rock. Anhedral quartz grains are comprised of domains having undulose extinction oriented parallel to the plane defined by plagioclase alignment. Anhedral to subhedral biotite and hornblende also show alignment in this plane. Anhedral titanite is also present. The consistent orientation of minerals within the dikes is interpreted as a flow feature imposed as the dike was emplaced. Some relative movement in the same direction apparently continued after crystallization was largely complete, as evidenced by the strain features in the quartz grains.

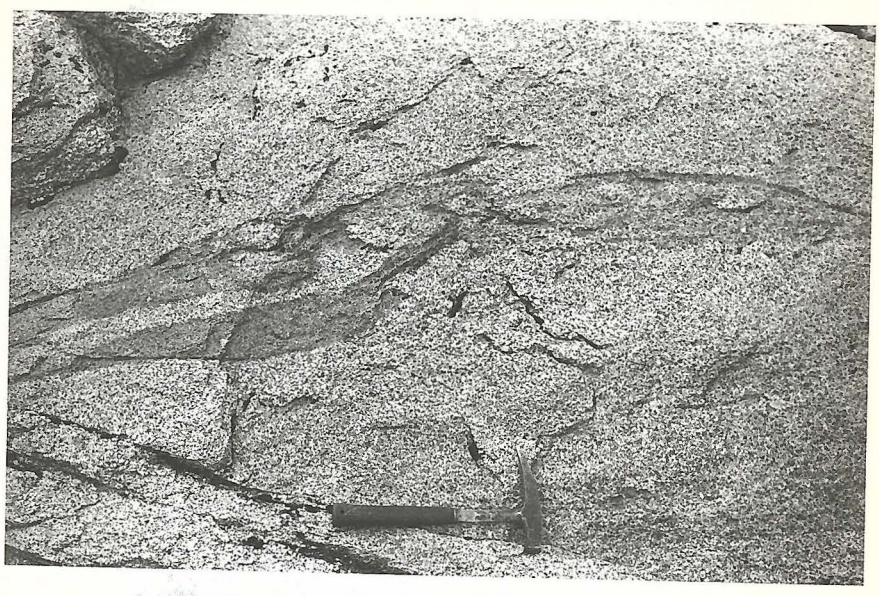

Figure 4.18. Mafic dike intruding low-K granodiorite, Black Mountain Road. This dike can be followed for several tens of meters; the photograph shows one of its extremities where it is apparently being sheared into the surrounding granodiorite. G.R. 232417.

Aplites

Masses of pink or red stained aplite are found throughout the San Jacinto Mountains. These bodies are usually of small dimensions (widths of centimeters to meters, lengths of tens to hundreds of meters), and appear to be most abundant in the area along the contact between Units II and III. Here they cut the tonalites of both Units II and III, as well as the large xenolith train of the outer-most part of Unit III. No consistent orientation of aplites was observed.

Pegmatites

Pegmatite dikes and sills occur throughout the major tonalites. They are usually of small dimension - a few centimeters to a few meters in width, and up to a few hundreds of meters in length. Quartz, plagioclase and K-feldspar crystals to several centimeters in length comprise most of these rocks; biotite, white mica and allanite are common accessory phases.

Feldspar-rich mafic tonalites

A peculiar mafic tonalite containing prominent well-formed plagioclase tablets appears in certain exposures to cut the more common tonalite of the major intrusions. It has been observed in the outermost parts of Units II and III, and in one of the small early intrusions (tonalite of Herkey Creek). In places this rock does not appear to be in dikes, but rather represents accumulations of plagioclase tablets that grade into more normal tonalites over a distance of tens of centimeters or more. This rock (or one texturally very like it) appears to form the outermost part of Unit II in the area north and south of Keenwild

(G.R. 262295), where the plagioclase tablets are aligned parallel to the contact. Figure 4.19 shows an outcrop of an apparent dike into the tonalite of Herkey Creek. The margins of the dike are parallel to the foliation plane within the host tonalite. Cross-cutting scallops of lighter material show the effects of relative movement across the 'dike' contacts.

The origin and inter-relationship of these various features having large (10 mm) aligned plagioclase tablets is not understood.

K-feldspar granodiorite dikes

These dikes are spatially related to small irregular masses of distinctive K-feldspar bearing granodiorite intruding Unit III south of Poppet Flat. Like the larger masses they are intrusive into the host tonalites. Their origin is uncertain.

RELATIONSHIP OF MAFIC DIKES AND XENOLITHS

In many locations within the San Jacinto Mountains dikes and xenoliths are seen to be intimately related. Figure 4.20 shows a syn-plutonic dike being veined by the host tonalite, and Figure 4.21a shows a situation where the breaking up of a large dike is more advanced. Figure 4.21b shows the inferred final stage of the process of disintegration of such a plutonic dike to yield a xenolith train of disaggregated irregular blocks more or less randomly oriented in a tonalite matrix. Figure 4.22 shows diagramatically the inferred development of a xenolith train from a dike. Compton (1962, p.291) suggested a similar origin for inclusion swarms in tonalite near French Lake, Sierra Nevada, California.

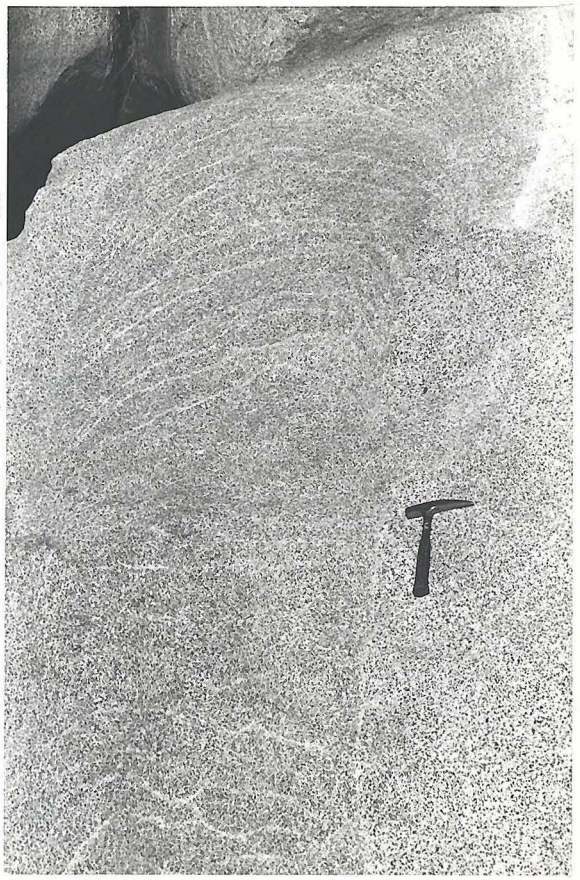

Figure 4.19. Photograph of a plagioclase-rich "dike" cutting mafic tonalite, tonalite of Herkey Creek. View is looking down onto a flat rock surface. The slightly darker gray "dike" contains abundant plagoclase tablets aligned parallel to the contacts. The contact shows some shearing over a distance of a few centimeters. The leucocratic scallops are interpreted as filling cracks formed within the still moving dike material towards the end of crystallization. About 50 m west of Apple Canyon road, G.R. 309268.

Figure 4.20. Synplutonic dike intruding xenolith-rich tonalite of Unit III. Hammer is 90 cm long. Red Hill Truck Trail southwest of Pine Cove (G.R. 220337).

Figure 4.21a. Intermediate stage in disaggregation of a mafic dike. Ridge immediately west of the West Fork of Snow Creek (G.R. 276449). Hat is about 30 cm across.

Figure 4.21b. Inferred final stage of dike disaggregation to give a xenolith train. Note irregular shapes of individual xenoliths. Indian Mountain Truck Trail (G.R. 200375).

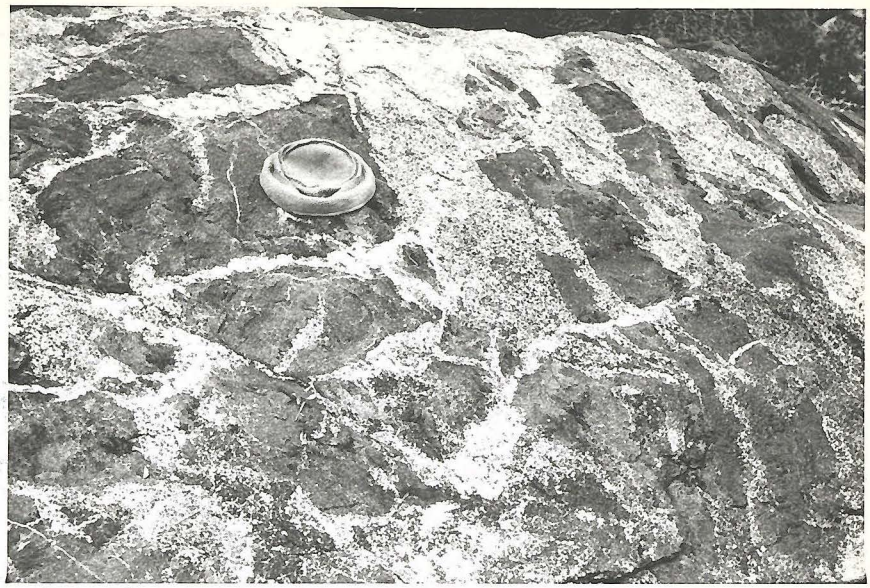

Figure 4.22. Diagramatic illustration of inferred relationship between mafic dikes and xenolith trains.

(a) Wall of crystallizing magma chamber, showing solidified material to right and silicate liquid containing suspended crystals (magma) to left.

(b) Propagation of crack across solid-magma interface, followed by movement of mafic liquid into crack. Magma adjacent to interface behaves brittlely at the time-scale of crack propagation.

(c) Flow of liquid through dike, with inferred addition of new liquid to liquid already in the magma chamber.

(d) Mixing of new added liquid with old liquid, probably accompanied by considerable precipitation of plagioclase and hornblende (because of temperature differences between dike liquid and magma chamber). Partly solidified dike is veined by tonalitic liquids from the magma chamber.

(e) Re-establishment of currents within the magma chamber that redistribute material (hybrid liquid, suspended crystals, and disaggregated dike-rock) parallel to the pluton walls.

(f) Repeat of cycle.

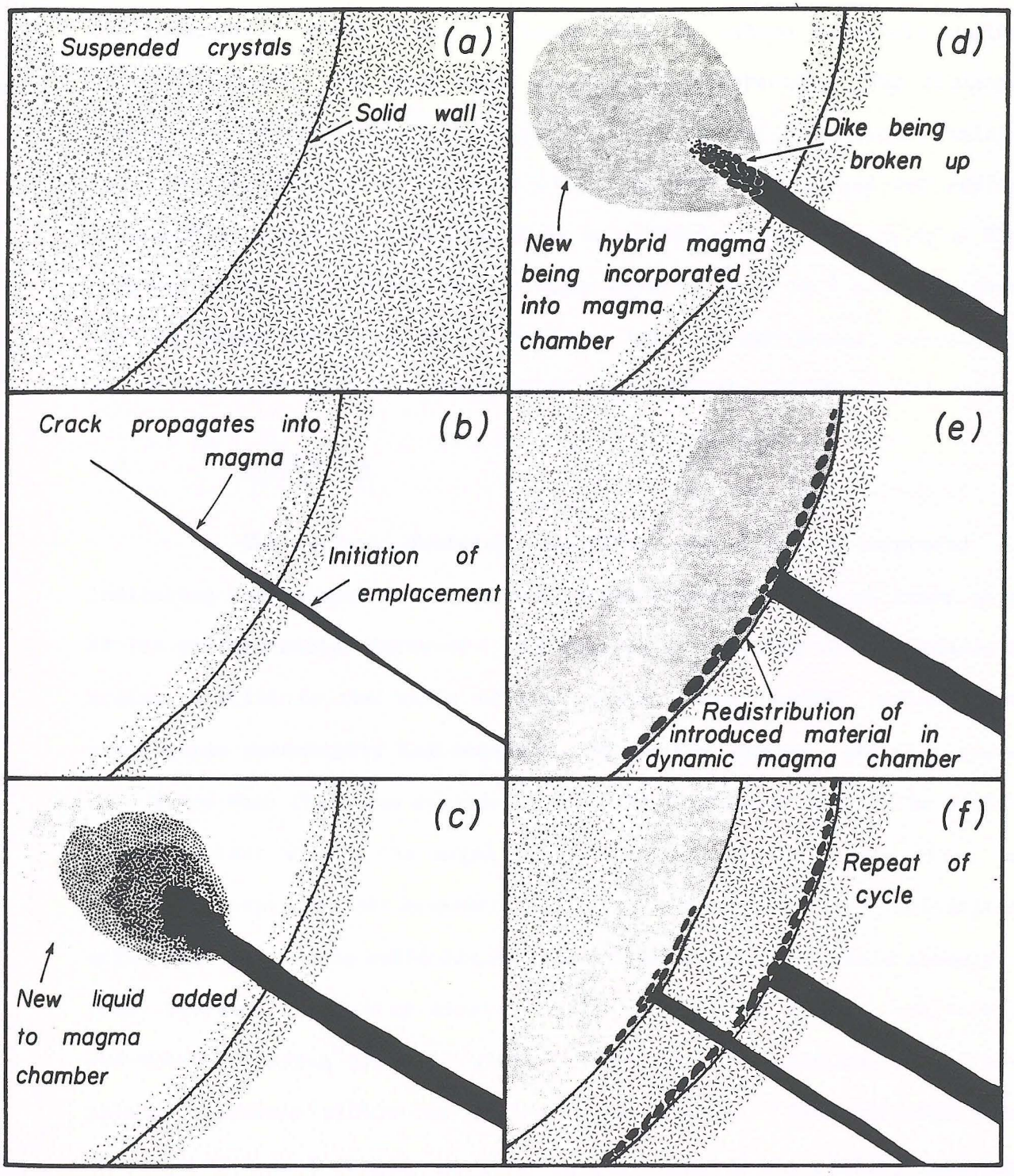
Suspended crystals
(a)
Solid wall
(d)
Dike being broken up
New hybrid magma being incorporated into magma chamber
Crack propagates into magma
(b)
Initiation of emplacement
(e)
Redistribution of introduced material in dynamic magma chamber
(c)
New liquid added to magma chamber
(f)
Repeat of cycle

The apparent intrusion of dike material into incompletely solidified silicate liquid implies that this silicate liquid must have had substantial yield strength, being able to behave brittlely during dike emplacement, and then more plastically afterwards. The distance that dikes penetrated into the liquid (away from the solid-liquid interface) is unknown, but potentially offers an efficient method for adding substantial volumes of new liquid to an inflating chamber. A dike 3 m wide and 1 km long could, with a flow rate of only 10^{-3} m/sec deliver 10^{-1} km^3 magma per year. Such a delivery rate, if continuous, could fill one of the major tonalite chambers in approximately 10,000-20,000 years.

4.8 DISCUSSION

The various features described above are interpreted as indicating the presence of a dynamic magma chamber during at least part of its solidification interval. The disruption of dikes to form xenolith trains parallel to the walls of the crystallizing chamber implies that new liquids potentially had access to this magma chamber, and that there were times when there was considerable relative movement across the solid-liquid contact within the magma chamber. The presence of the dikes is further interpreted as demonstrating that the incompletely solidified magma adjacent to the solid-liquid contact had substantial yield strength. Other features, including mineral foliations and lineations, schlieren, and mineral banding are most simply interpreted as resulting from flow-related processes within the cooling magma chamber. This inferred flow seems to have been largely parallel to the walls of the pluton, implying that measurement of flow-related features can be used to follow the progressive development of the plutons as they solidified.

GEOMETRIC RELATIONS OF FOLIATIONS AND LINEATIONS WITHIN INDIVIDUAL INTRUSIVES

Unit I

Unit I (Kt_1) is elongate north-west south-east, and so are foliations and lineations within the intrusion (Plate 2). Most measured foliation planes dip between 50 and 80 degrees to the northeast. The only major exception to this is adjacent to the western contact with Unit II, where for up to 1 km from the contact the dominant foliation within Unit I is oriented about N30°W, paralleling the contact with the younger Unit II. Rocks within this marginal zone commonly show evidence for two foliations (Fig. 4.23), one paralleling the nearby contact and the other, usually weaker oriented parallel to the foliation distant from this disturbed zone. Within this disturbed zone xenoliths commonly are aligned parallel to the main foliation (N45°W) although the dominant mineral alignment in the same rock may be the apparently later, more northerly oriented (N30°W) plane.

Unit II

The irregular outcrop pattern of this unit is mirrored by the orientation of both foliations and lineations within it (Plate 2). The roof to this pluton is still extant in several places; on and around Cornell Peak (G.R. 313413), on the Hidden Lake Divide (G.R. 327399) and south and east of Toolbox Spring (G.R. 316191). In these areas the orientation of foliations is scattered, and dips are generally shallow. Elsewhere both foliations and lineations are approximately parallel to the nearest mapped contact. This appears true even where the contact is

Figure 4.23a. Double foliation within Unit I tonalite adjacent to contact with Unit II. West of Pines-to-Palms Highway, G.R. 255307.

Figure 4.23b. Sketch from photograph showing orientation of long axis of mafic mineral grains.

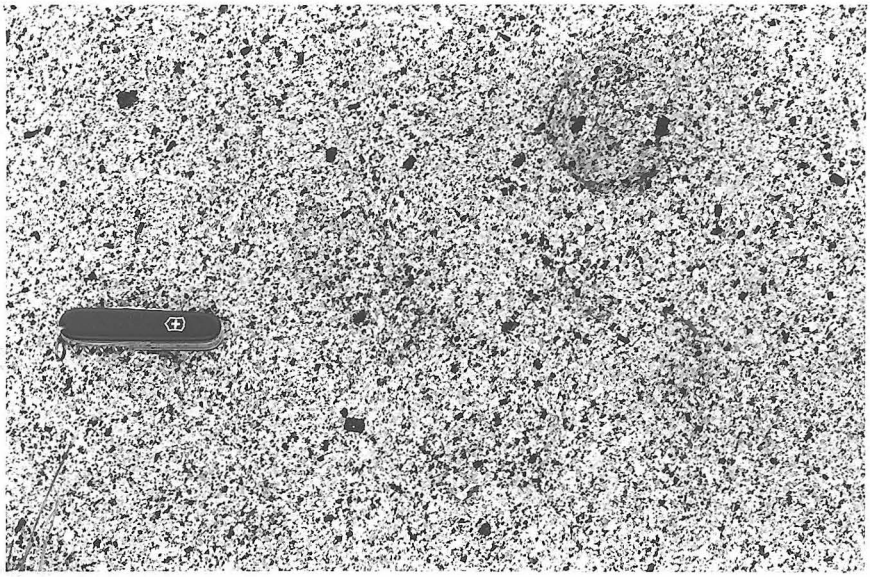

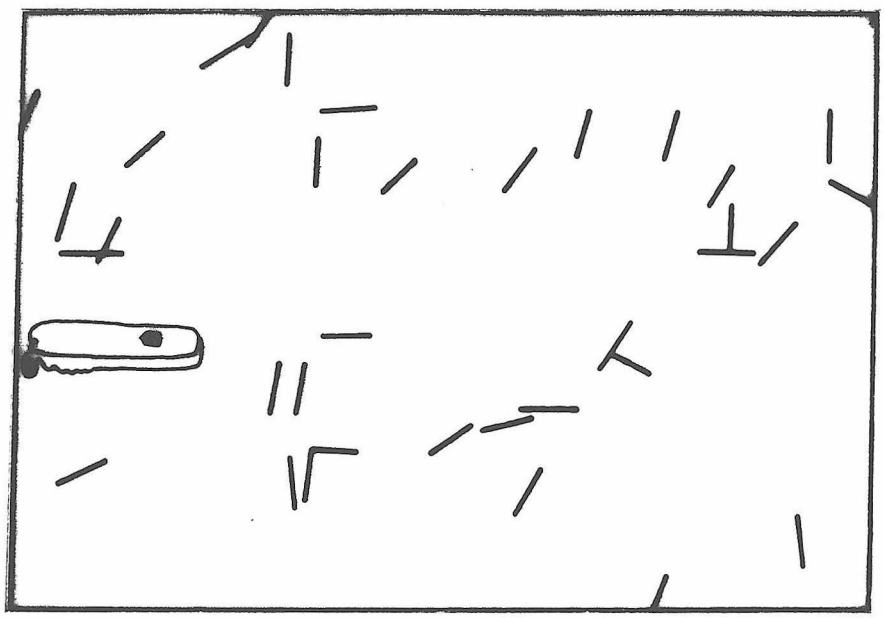

with the later Unit III [along the northwestern contact from Pine Cove (G.R. 244359) to near San Jacinto Peak (G.R. 301414)]. There is no petrographic evidence for significant deformation after crystallization, so this orientation of the plane of foliation parallel to the contact of the younger intrusive is interpreted as resulting from emplacement of Unit III before Unit II was completely solidified.

Unit III

This, the latest and most complete of the three major tonalite intrusives, is best considered in two parts. Throughout much of the eastern portion of this pluton foliations and lineations are arranged more or less concentrically around a point near Black Mountain (G.R. 224424). The plane of the foliation generally shallows inwards from dips of 60-70° around the contact to 15-30° in the central part of the pluton. Much of the western portion of the pluton appears to be relatively close to the original roof zone; roof pendants are extant in several places. A relatively extensive area northeast of the township of Poppet Creek is underlain by an heterogeneous mixture of igneous rocks. Lithologies present include tonalite of Unit III, foliated coarse-grained mafic tonalite, and flat-lying pegmatite sheets (Fig. 4.24). This area is inferred to be the roof zone of Unit III.

Within these areas that are inferred to be close to the original roof of this pluton the orientation of the plane of foliation within Unit III tonalites is much more variable than it is in the more deeply exhumed rocks further east. This variability apparently relates to an original irregular upper contact (roof) to this pluton. Similar irregular and generally shallowly dipping foliation planes are apparent high on Black

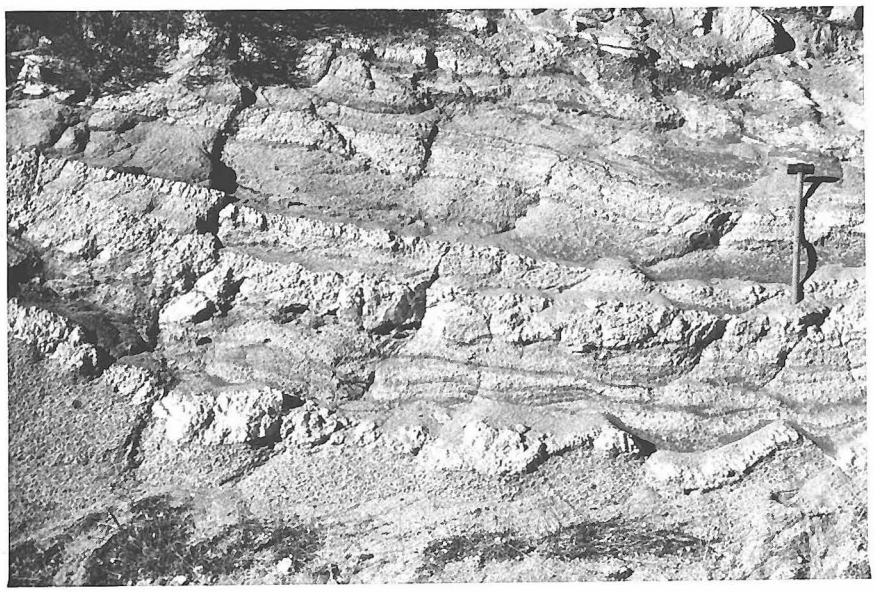

Figure 4.24. Flat-lying pegmatite sheets within roof-zone of Unit III. The apparent rhythmic nature of these features may indicate rhythmic volatile build-up, pegmatite crystallization and volatile loss.

Mountain, and around the summit of San Jacinto Peak, suggesting proximity to the roof in these two areas.

The field observations can be combined to develop a three-dimensional picture of Unit III (Plate 1, reproduced also as Fig. 4.25). Along much of the northern margin the contact dips outward away from the pluton. This is the area where roof pendants and inferred roof-zone rocks are present; this contact is thus interpreted as a steeply north-dipping roof. This upper contact flattens eastward, until it dips shallowly beneath metasedimentary and igneous host rocks on the ridge west of Snow Creek. From here eastward the mapped contact dips inwards, first shallowly and then progressively more steeply until dips of 70-80° to the south are found across the steep northern face of San Jacinto Mountain. Thus, on the ridge west of Snow Creek both upper and lower contacts are present, and the pluton thins into a sill intruding the country rocks.

South of San Jacinto Peak the contact dips consistently inwards, first to the west and then to the north and northeast. The three-dimensional form of the pluton thus approximates that of an upward-opening funnel.

The orientation of foliation planes mirrors this external contact, suggesting that the pluton crystallized inwards more or less symmetrically. Foliations shallow inwards, and are generally also shallow and variable in the vicinity of mapped roof rocks. The presence of variably oriented shallowly dipping foliation on and around San Jacinto Peak and Black Mountain are interpreted as resulting from the proximity to the roof of these two topographically high locations. Thus much of the exposed part of Unit III is probably not far (more than a kilometer or so)

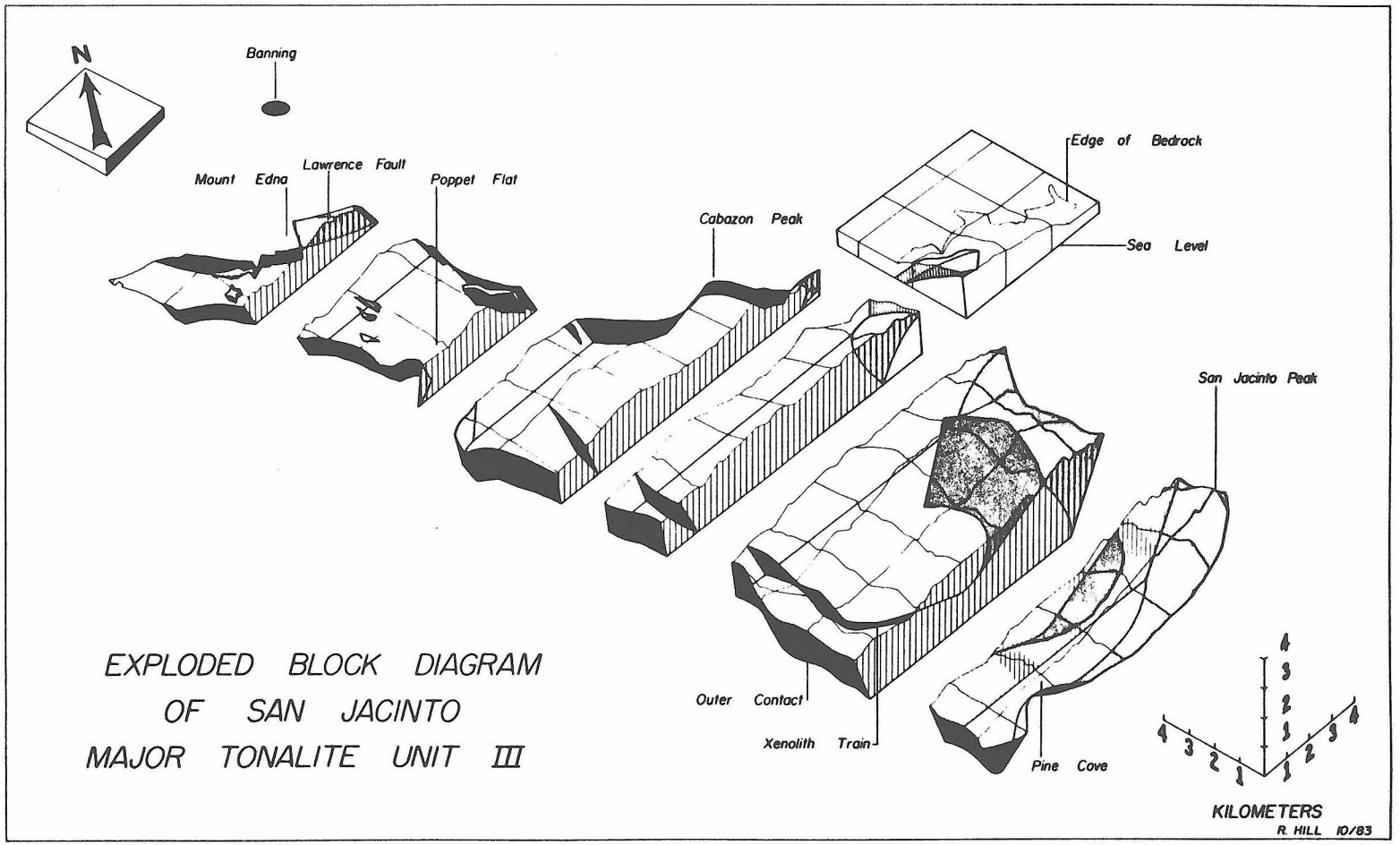

Figure 4.25. Exploded block diagram showing three-dimensional form of Unit III. North-dipping contacts are black; south- and west-dipping contacts are in gray. Contacts projected to sea level.

from an original, relatively flat-lying but irregular pluton ceiling.

CHAPTER 5

GEOLOGY OF THE SAN JACINTO MOUNTAINS

PART 3: PETROGRAPHY OF IGNEOUS ROCKS

5.1 INTRODUCTION

This chapter presents petrographic data on the characteristic lithologies of the three major tonalites, and on several of the smaller igneous bodies that are exposed within the San Jacinto Mountains. It is intended that these descriptions and discussions convey general mineral, modal, textural and paragenetic information on the mineral assemblages of the various rock units. No attempt at a comprehensive description of all analysed samples is made here. Although the smaller bodies cover the compositional range gabbro through granite, detailed consideration of the various gabbro bodies is beyond the scope of the present project. The three major tonalites encompass a limited compositional ranges (from tonalite to low-K granodiorite). These variations may show systematic geographic patterns (this is particularly the case for Unit III), and are documented below.

5.2 EARLY INTRUSIVES

5.2.1 QUARTZ DIORITE OF LUCKY DEER MINE

This intrusive is composed of relatively fine-grained plagioclase-rich quartz diorite (Table 5.1; Fig. 5.1). White plagioclase tablets range downwards in size from 3-5 mm. Biotite and hornblende have similar maximum dimensions. Smaller masses of yellow-brown titanite,

TABLE 5.1

MODAL DATA FOR QUARTZ DIORITE OF LUCKY DEER MINE

LTS 381

Quartz	15.0
K-feldspar	0.5
Plagioclase	67.1
Biotite	10.5
Hornblende	5.3
Titanite	0.6
Apatite	tr
Zircon	tr
Opaques	0.4
Epidote	tr
Chlorite	0.6
White mica	0.1
Total	101.1
Colour Index	17.4 ± 0.9

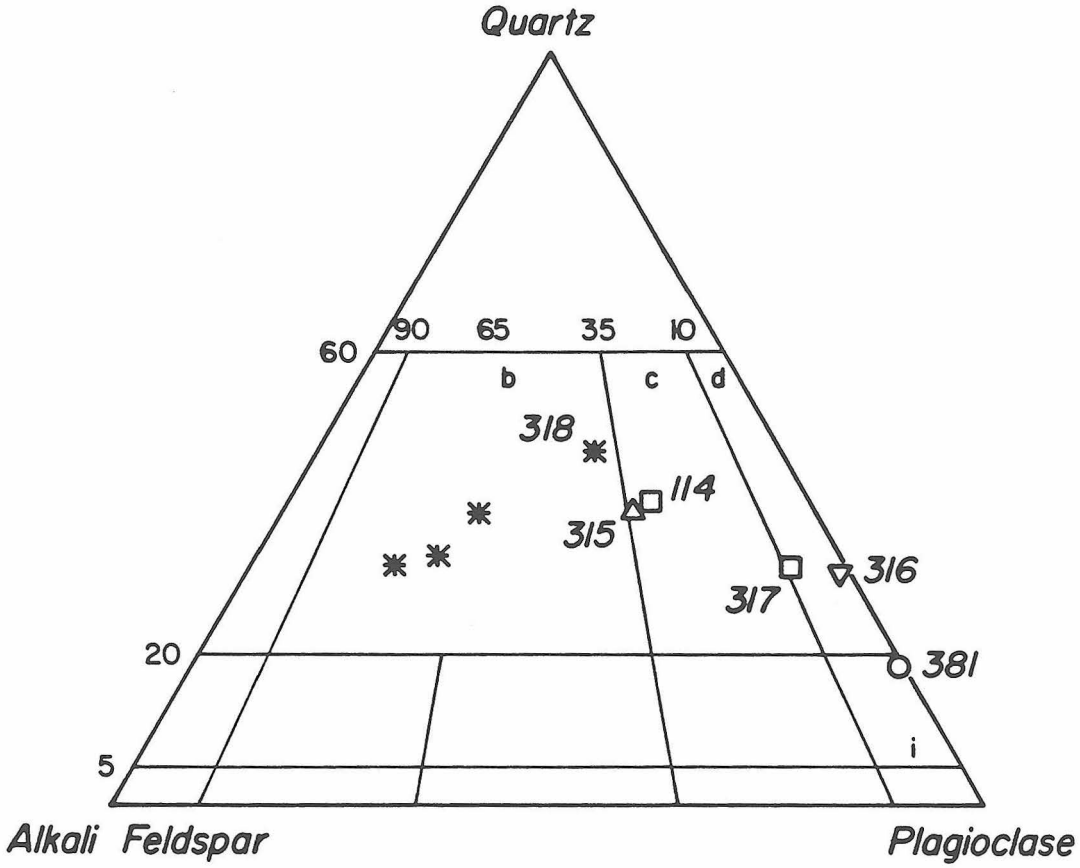

Figure 5.1. Classification of early intrusives (after Streckeisen, 1973).

and relatively large rounded blebs of gray quartz (to 5 mm) are also visible in hand specimen.

In thin section ragged biotite, subhedral hornblende and anhedral quartz are interstitial to, or are moulded around, large subhedral plagioclase tablets. Most titanite is interstitial to this plagioclase framework; some also appears to be replacing biotite during chloritization of that mineral. Plagioclase is strongly zoned, with many oscillations (>10) superimposed on a normal zonation from a calcic center (labradorite) to a sodic rim (oligoclase).

5.2.2 TONALITE OF HERKEY CREEK

In hand specimen the tonalite of Herkey Creek is distinguished by the presence of large well-formed hornblende prisms and biotite books in a dense white matrix of plagioclase and quartz. Some quartz is present as prominent large (5 mm) 'gumdrops', approximately equant, somewhat rounded grains. Both amphibole and biotite show a prominent seriate-porphyritic size distribution, with the larger crystals being as much as 1 cm across. The mafic minerals commonly define a foliation plane. Titanite is present in both irregular aggregates and as euhedral grains.

Except for a relative paucity of titanite, this rock has very similar mineral proportions (Table 5.2) to the major tonalites. The quite different textures may result from different crystallization or nucleation rates; they do not appear to reflect any significant compositional differences.

In thin section the seriate-porphyritic size distribution of aligned plagioclase tablets is striking. Euhedral plagioclase crystals

TABLE 5.2

MODAL DATA FOR TONALITE OF HERKEY CREEK

LTS 316

Quartz	24.5
K-feldspar	0.8
Plagioclase	54.3
Biotite	12.9
Hornblende	6.1
Titanite	0.2
Apatite	0.2
Zircon	tr
Allanite	0.2
Opaques	0.3
Epidote	0.1
Chlorite	0.3
White mica	tr
Total	99.9
Colour Index	20.1 ± 1.0

(An_{40-35}) are poikilitically enclosed by both biotite and quartz. Plagioclase contains abundant inclusions of apatite, an equant opaque mineral (most probably ilmenite), and small hornblende prisms. Hornblende prisms often include small plagioclase tablets. Quartz is also present in large equant rounded grains, as euhedral prisms, and as irregular space-filling masses between other minerals. Biotite is also present as irregular grains; hornblende is yellow-brown to dark blue-green, subhedral to euhedral, and contains ilmenite inclusions. It commonly occurs in both aggregrates of several small equant grains to 0.5 mm in size and as larger individual grains to several millimeters across. Large prisms of zoned reddish-brown to light brownish-yellow allanite have thin epidote sheaths and appear to have grown simultaneously with plagioclase. Titanite is commonly anhedral, filling spaces between other grains. K-feldspar occurs as stringers. Apatite, ilmenite and zircon are the accessory phases. Biotite shows minor replacement by chlorite, epidote and titanite.

The first phases to crystal were apparently plagioclase and hornblende, perhaps followed quickly by quartz. Because quartz commonly does not include other minerals, even where it must have been crystallizing for a substantial period of time before the appearance of another phase (e.g., K-feldsapr), it is difficult to place the first appearance of quartz in paragenetic sequence. The common occurrence of large, equant quartz crystals implies that quartz was able to grow for some time without physical interference from other mineral phases. Quartz is thus interpreted to have been an important early-appearing phase in this rock. Quartz and plagioclase probably continued to crystallize throughout much of the history of the rock. The other minerals are interpreted to have appeared in the sequence allanite, followed by biotite, titanite, and

last, K-feldspar.

5.2.3 TONALITE OF SNOW CREEK

This rock is a foliated, medium-grained biotite-hornblende-titanite tonalite. Hornblende prisms are seldom more than 5 mm long. Biotite aggregrates to 5 mm long often poikilitically enclose small (1-3 mm) plagioclase euhedra. In thin section small randomly oriented subhedral to euhedral plagioclase tablets comprise approximately half of the rock. Large quartz grains (to 2 mm across) commonly show either pronounced undulose extinction and recrystallization of margins, or complete recrystallization to give a mosaic of tiny interlocking sub-grains. Green-brown to yellow-brown hornblende prisms may contain small rounded opaque inclusions. Ragged biotite flakes are grouped into aggregrates; biotite is commonly partly intergrown with otherwise euhedral titanite. Titanite also occurs in well-formed rhombs. K-feldspar occurs as stringers between other grains.

5.2.4 TONALITES AND GRANODIORITES NORTHEAST OF TAHQUITZ PEAK

North and east of Tahquitz Peak many small masses of diverse igneous rock crop out. The most common is a foliated tonalite; also present are granodiorites and minor amounts of pegmatite and aplite.

The common tonalite shows a pronounced foliation defined by elongation of mafic mineral aggregrates and quartz lenses. Biotite and hornblende occur in conspicuous aggregrates of a number of small grains; this, and a lack of large titanite crystals enable these rocks to be easily distinguished from other tonalites within the study area. Garnet appears as a phase in some of these tonalites adjacent to masses of meta-

sedimentary rocks. Blocks of metasediment can be seen at all stages of incorporation into the intruding tonalite, and the development of garnet is related to these contamination processes.

In thin section the rock has a hypidiomorphic granular texture. Subhedral plagioclase has a marked seriate-porphyritic grain-size distribution. Hornblende occurs in brown-green to brownish-yellow prisms commonly found among aggregrates that also include irregular red-brown to chocolate-brown biotite flakes. Biotite includes abundant small apatite prisms; rounded ilmenite grains and apatite prisms are also found as inclusions within hornblende. Quartz occurs as both large grains with pronounced undulose extinction, and as space-filling masses between the other minerals. The latter commonly are recrystallized into many small sub-grains.

Euhedral to subhedral allanite is a common accessory, apparently especially close to contacts with metasedimentary rocks. Within a few tens of meters of contacts with metasedimentary country rocks large poikiloblastic garnets appear. The garnets are reddish-purple in thin section. Hornblende and garnet are not found together.

5.2.5 GRANODIOROTE OF POPPET CREEK

This pluton shows considerable variability in mineral proportions. Table 5.3 lists modal analyses of a hornblende-rich tonalite and a granodiorite from this body (see also Fig. 5.1). The more mafic rocks are generally found along the northern margin of this body, while along the southern margin (an intrusive contact with the younger Unit I) granodiorite with K-feldspar megacrysts predominates. Mafic rocks are also

TABLE 5.3

MODAL DATA FROM THE GRANODIORITE OF POPPET CREEK

	LTS 317	LTS 114
Quartz	23.0	32.3
K-feldspar	4.7	14.9
Plagioclase	45.8	34.0
Biotite	12.0	8.7
Hornblende	13.0	8.6
Titanite	0.4	0.4
Apatite	tr	0.1
Zircon	tr	tr
Allanite	tr	0.1
Opaques	0.1	tr
Orthopyroxene	-	tr
Epidote	0.8	0.6
Chlorite	tr	0.2
White mica	-	tr
Calcite	-	tr
Total	99.8	99.9
Colour Index	26.3 ± 0.8	18.6 ± 0.8

generally strongly foliated.

In the tonalites and more mafic granodiorites biotite and hornblende in approximately equal proportions comprise some 30% (volume) of the rock. Hornblende prisms to 10 mm and biotite aggregates of similar size appear to have been rotated into the foliation plane by granulation and recrystallization. Large (to 15 mm long) elongate lenticular much fractured quartz grains or aggregates have a slight purplish tint. Both the quartz and white plagioclase tablets to 5mm long are elongate in the foliation plane. K-feldspar is present as large poikilitic crystals to several centimeters across, and as smaller discrete grains. Occasional crystals of dark brown titanite and brownish allanite are also apparent in hand specimen. The hornblende:biotite ratio remains approximately constant throughout the tonalites and granodiorites (at about 1). The the imposed foliation is still a striking feature in the granodiorites. In the granodiorites the grain-size of the felsic minerals increases. Poikilitic K-feldspar grains give way to irregular grains which in turn give way to discrete subhedral to euhedral crystals as the rock becomes more felsic.

In thin section simply twinned hornblende subhedra, pleochroic from brown to blue-green, range in size from a few tenths to over ten millimeters in length. Along with aggregates of golden to dark brown biotite flakes they define a strong mineral foliation. Biotite shows some undulose extinction and kinking of grains, but in general shows only minor evidence of brittle deformation.

Plagioclase tablets form an interlocking matrix; grain boundaries against both quartz and other plagioclase crystals are commonly scalloped, suggesting growth from a trapped interstitial liquid. There is a weak preferred alignment of plagioclase crystals in the plane defined by the mafic mineral foliation. The bulk of the plagioclase is of sodic andesine to calcic oligoclase composition (An_{25-40}). Uncommon moth-eaten within large oscillatory-zoned plagioclase crystals appear to be quite calcic (calcic bytownite or anorthite). These cores are mantled by a clear intermediate plagioclase, which is then in turn overgrown by the bulk of the crystal which zones normally from intermediate labradorite to calcic oligoclase, but with many (>10) oscillatory interuptions to this overall trend. Cores within the more felsic rocks are commonly almost completely replaced by networks of optically continuous epidote. Bent plagioclase twin lamellae attests to post-crystallization deformation of this mineral.

Quartz commonly shows pronounced undulose extinction or apparent incipient recrystallization into elongate domains. This suggests that much of the imposed stress has been accommodated by plastic flow within the large quartz grains and aggregates. Individual grains are anhedral, and often occur in aggregates of several interlocking optically distinct quartz crystals.

K-feldspar occurs as large irregular crystals that poikilitically enclose all other mineral phases, as smaller anhedral crystals, and, in the more felsic rocks, as simply-twinned subhedral tablets of centimeter size. Microperthite stringlets are commonly developed. Myrmekitic intergrowths of plagioclase and quartz are common at plagioclase - K-

feldspar boundaries.

Accessory phases include titanite, apatite, allanite, zircon, epidote, opaque minerals, and rare orthopyroxene cores within hornblende. Titanite occurs as both large (to 3 mm) discrete rhombs, and as small subhedral grains associated and apparently intergrown with hornblende - biotite aggregates. Many of the titanite rhombs are aligned in the foliation plane defined by the other mafic minerals. Such grains completed most, if not all, of their growth unrestricted by impingement against the faces of competing minerals. Relatively large (to 0.3 mm) irregular opaque grains and stubby apatite crystals are common inclusions within euhedral titanite. Small apatite prisms are also common inclusions within hornblende, biotite and plagioclase. Yellow-brown to dark red-brown pleochroic allanite prisms are invariably at least partially sheathed by very slightly pleochroic (in yellows and greens) epidote. This epidote sheath appears to replace both hornblende and biotite where they are adjacent to an allanite grain.

Optically similar epidote occurs as anastomosing masses replacing plagioclase (usually calcic cores), hornblende and biotite. Sparse equant opaque grains are most commonly found as inclusions within hornblende, and are less commonly found in titanite and plagioclase. Zircon euhedra commonly are surrounded by prominent pleochroic haloes developed in both biotite and hornblende.

Orthopyroxene was found within a large (5 mm) composite hornblende grain. Although the overall form of this hornblende grain is of a single well formed prism, it is composed of at least four optically distinct subgrains. Three of these sub-grains are replacing slightly

pleochroic (pink to green) hypersthene (optically negative, 2V ≈ 60°). This is the only pyroxene noted after examination of over 200 thin sections from a wide variety of igneous rock types except for that in the small bodies of two-pyroxene gabbro that are scattered throughout the San Jacinto Mountains.

Alteration includes replacement of plagioclase, hornblende and biotite by epidote, chloritization of biotite, and minor clouding and development of small flakes of uncoloured mica within plagioclase. As the bulk of the epidote obviously replaces either hornblende or biotite (with relatively small amounts replacing plagioclase cores), and as chlorite replaces biotite, both epidote and chlorite are included in the determination of colour index (Table 5.3).

Petrographic Peculiarities of the Granodiorite of Poppet Creek

This small pluton exhibits several characteristics which distinguish it from other studied igneous rocks from the San Jacinto Mountains. On the basis of field relations it is among the oldest; it has a high hornblende/biotite ratio (approximately 1:1, compared to the more common 1:4 to 1:10); and it contains hypersthene cores within hornblende and calcic plagioclase cores within large plagioclase tablets. The relatively K-feldspar rich mafic rocks (colour index > 20) and the occurrence of titanite euhedra aligned in an apparent flow foliation are also unusual. Apatite is noticeably less abundant in this unit than in any other igneous unit studied, and the plagioclase abundance is relatively low at a given colour index. These mineralogical peculiarites (low titanite, apatite and plagioclase; abundant K-feldspar) are reflections of the rock chemistry (Ch. 7), and appear to reflect primary differences between the liquid

composition that gave this intrusion and the liquids that generated most of the surrounding plutons.

Orthopyroxene and calcic plagioclase may have been the first minerals to crystallize, followed by an opaque mineral, apatite, titanite, more sodic plagioclase and hornblende, and then by allanite, biotite, and quartz, and much later by K-feldspar.

An alternate explanation is that the orthopyroxene and calcic plagioclase present in this rock is xenocrystal, and indicates assimilation of pre-existing mafic material.

5.2.6 PORPHYRITIC GRANODIORITE OF APPLE CANYON

This small body is distinguished by the presence of abundant large (to several centimeters) flesh-pink simply twinned K-feldspar phenocrysts that are oriented to give a prominent foliation. Biotite books and plagioclase tablets (the latter to 1 cm in length) are also aligned in this foliation plane. Uncommon hornblende prisms are seldom more than 5 mm in length. Table 5.4 presents modal data for a single sample of granodiorite from this body.

In thin section subhedral simply twinned orthoclase crystals show considerable microperthite. Plagioclase tablets are also subhedral, and show some alignment in the plane defined by the K-feldspar. Large quartz aggregrates (to a few centimeters) are anhedral, may consist of several individual grains, and show strongly undulose extinction. Subhedral to anhedral yellow-brown to dark chocolate-brown biotite often forms selvedges around plagioclase tablets. Blue-green to brownish-yellow amphiboles are usually subhedral, and commonly show some replacement by

TABLE 5.4

MODAL DATA FOR GRANODIORITE OF APPLE CANYON

LTS 315

Quartz	34.6
K-feldspar	18.7
Plagioclase	36.4
Biotite	8.3
Hornblende	1.6
Titanite	tr
Apatite	tr
Zircon	tr
Allanite	tr
Epidote	0.2
White Mica	0.2
Total	100.0
Colour Index	10.1 ± 0.7

epidote. Epidote is also present as a sheath on reddish-brown allanite. Accessory phases include apatite and zircon. Minor amounts of white-mica and calcite appear to be alteration products of K-feldspar and plagioclase, respectively.

5.2.7 GRANITE DIKE FROM LITTLE THOMAS MOUNTAIN

Several dikes of coarse-grained granite cut both earlier igneous rocks and metasedimentary country rocks around Little Thomas Mountain. These dikes are composed of the most felsic igneous rocks studied that do not show evidence of either considerable post-crystallization alteration or interaction with enclosing metasedimentary rocks.

In thin section the rock has a hypidiomorphic granular texture. Plagioclase, K-feldspar and quartz are present in approximately equal amounts. Subhedral plagioclase shows weak normal zoning. Large subhedral to anhedral microperthite crystals and anhedral quartz, along with plagioclase, form almost all of the rock. Small irregular biotite crystals fill spaces between the other minerals. Some myrmekite is present. Apatite and zircon are the accessory minerals.

5.2.8 GRANITE OF PENROD CANYON

This body of medium-grained, equigranular biotite-garnet granite was named the Penrod Quartz Monzonite after Penrod Canyon by Brown (1968). The rock is a granite by the I.U.G.S. classification (Streckeisen, 1973), and is here re-named the granite of Penrod Canyon. The rock contains small amounts of dark biotite, and may contain dark red garnets which often show well-developed dodecahedral form. Modal analyses of four

TABLE 5.5

MODAL DATA FOR GRANITE OF PENROD CANYON

	LTS 318	85 [1]	19	271
Quartz	44.7	35	32	30
K-feldspar	20.1	35	45	49
Plagioclase	30.5	20	20	15
Biotite	2.1	9	tr	4
Garnet	1.4	tr	1	2
Fibrolite	0.6	-	-	-
White mica	0.6	0.5	1.0	tr
Total	100.0	100	99	100
Colour Index	3.5 ± 0.6			

[1] Data from Brown (1981).

Figure 5.2. Photomicrograph of granite of Penrod Canyon. Photograph is 3 mm across.

G = Garnet

S = Sillimanite needles replacing biotite

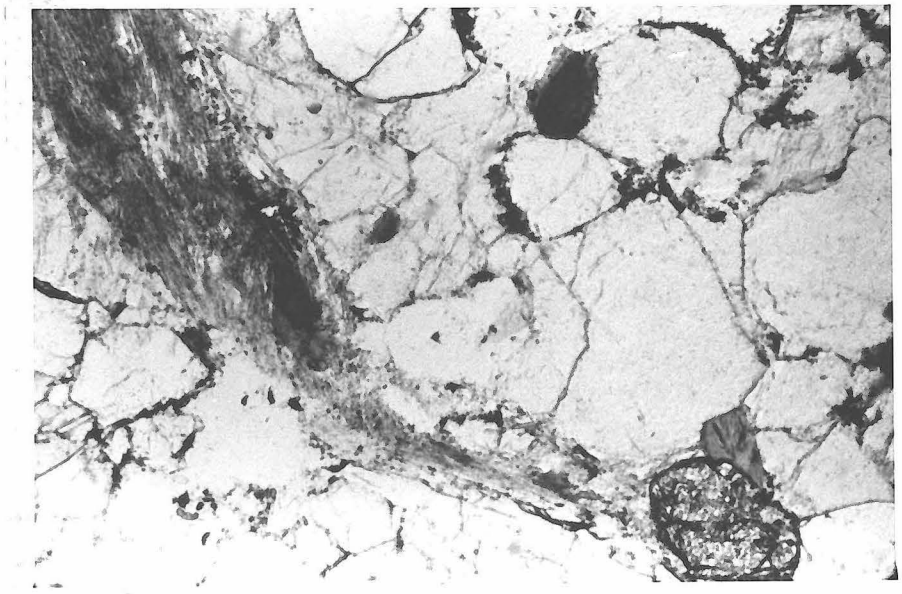

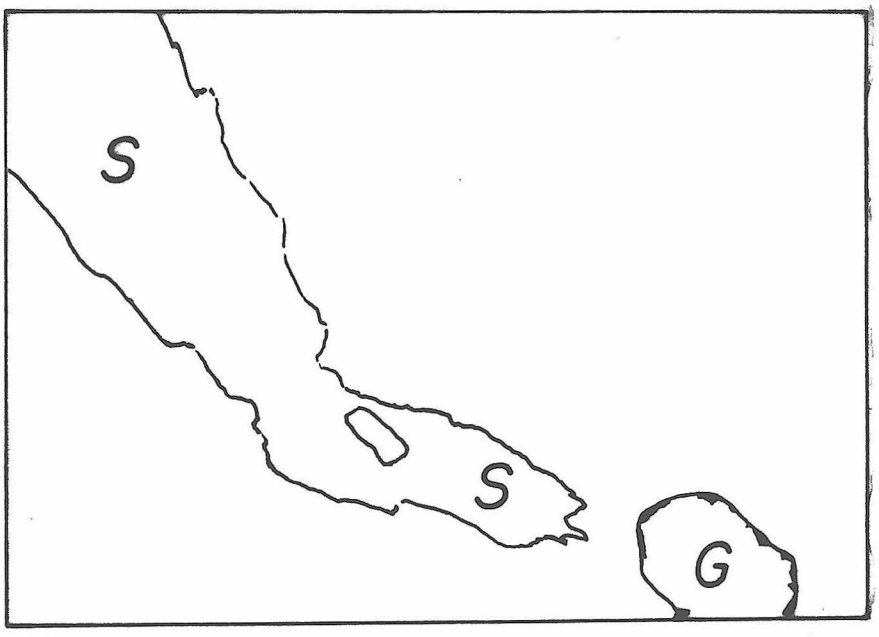
S
S
G

samples of the granite of Penrod Canyon are presented in Table 5.5. Brown (1968, 1981) noted that this pluton showed variable composition, and this is seen in the data of Table 5.5. The more marginal rocks tend to be more quartz-rich, and may contain tourmaline (Brown, 1968, 1981).

In thin section the rock is seen to have a hypidiomorphic-granular texture. Small rounded to subequant plagioclase crystals (to 0.8 mm) are randomly oriented in a matrix of rounded quartz grains (to 5 mm) and anhedral microperthitic K-feldspar (to 3 mm). Small biotite flakes (to about 0.4 mm, but commonly much smaller) are often aligned along the edges of large quartz or feldspar grains. This alignment is consistent, and gives a weak foliation to the rock. Small rounded purplish-pink garnets may show prominent growth zones. Biotite has been partly replaced by sheafs of tiny sillimanite needles ('fibrolite')[Fig. 5.2]. Very thin white-mica flakes are present in cracks in K-feldspar.

Much of this pluton shows evidence of post-crystallization alteration. Iron-staining and a cata clastic foliation are commonly observed in hand specimen; white-mica veins and feldspar alteration are common in thin sections. The replacement of biotite by sillimanite, and apparent annealing textures (120° inter-grain angles, recrystallization of the margins of large grains) suggest that alteration took place at relatively high temperatures. A system of quartz veins, some auriferous, cuts this pluton and is radially symmetrical about its approximate center (Unruh and Ruff, 1981). Alteration and recrystallization may have been synchronous.

5.3 MAJOR TONALITES

The rocks of the three major tonalites show similar compositional variations. All range from mafic tonalites with >15% biotite and >5% hornblende and only minor K-feldspar to granodiorites with <10% biotite, trace amounts of hornblende, and 8-10% K-feldspar. Although this total compositional range is small compared to that of some other large, well-studied plutons of the Sierra Nevada batholith (e.g., Tuolumne Meadows: Bateman and Chappell, 1979; Mount Givens: Bateman and Nokleberg, 1978), within Unit III it is geographically regular in a manner analogous to that described for these other large systems. That is, the outer, more marginal rocks tend to be more mafic than the inner, more felsic ones. This difference in the compositional range of large zoned plutons from the two batholiths (Peninsular Ranges and Sierra Nevada) may reflect differences in the tectonic environments in which the batholithic rocks evolved, or it may simply be a response to crystallization at different levels within the crust.

Complete modal data for selected rocks from the three major tonalites are presented in Table 5.6. These data are plotted on the Quartz-Plagioclase-Alkali Feldspar diagram (Fig. 5.3). These samples cover a relatively restricted field, from tonalite to low-K granodiorite. The limited nature of this compositional variation is shown by Figure 5.4, which shows photographs of a mafic tonalite and a felsic low-K granodiorite from Unit I. These two rocks cover the entire compositional range of the major tonalites.

Partial modal data for a larger sample of rocks from the major intrusive units are collected in Appendix 4. These data are used to

TABLE 5.6

MODAL DATA FOR MAJOR TONALITES

	SAMPLE NUMBER				
	LTS 147	LTS 287	LTS 221	LTS 152	LTS 212
Quartz	28.1	21.9	22.5	28.8	29.4
K-feldspar	1.5	5.1	1.5	7.9	8.4
Plagioclase	51.6	57.0	53.2	49.1	52.6
Biotite	13.2	11.7	15.4	12.2	8.4
Hornblende	4.0	2.0	6.6	0.5	0.3
Titanite	1.2	1.3	0.7	1.0	0.2
Apatite	0.1	0.4	0.1	0.3	0.1
Zircon	0.1	tr	0.1	tr	tr
Opaques	tr	0.1	tr	0.1	tr
Epidote	tr	0.7	0.1	tr	0.5
Chlorite	tr	tr	tr	tr	tr
White mica	0.3	n.d.	tr	tr	0.2
Total	100.1	100.2	100.2	99.9	100.1
Colour Index	20.3 ± 1.2	15.9 ± 1.0	23.4 ± 1.1	13.8 ± 0.9	10.7 ± 0.8

LTS 147 Mafic tonalite, Unit I
LTS 287 Mafic tonalite, Unit II
LTS 221 Mafic tonalite, Unit III
LTS 152 Tonalite, Unit III
LTS 212 Low-K granodiorite, Unit III

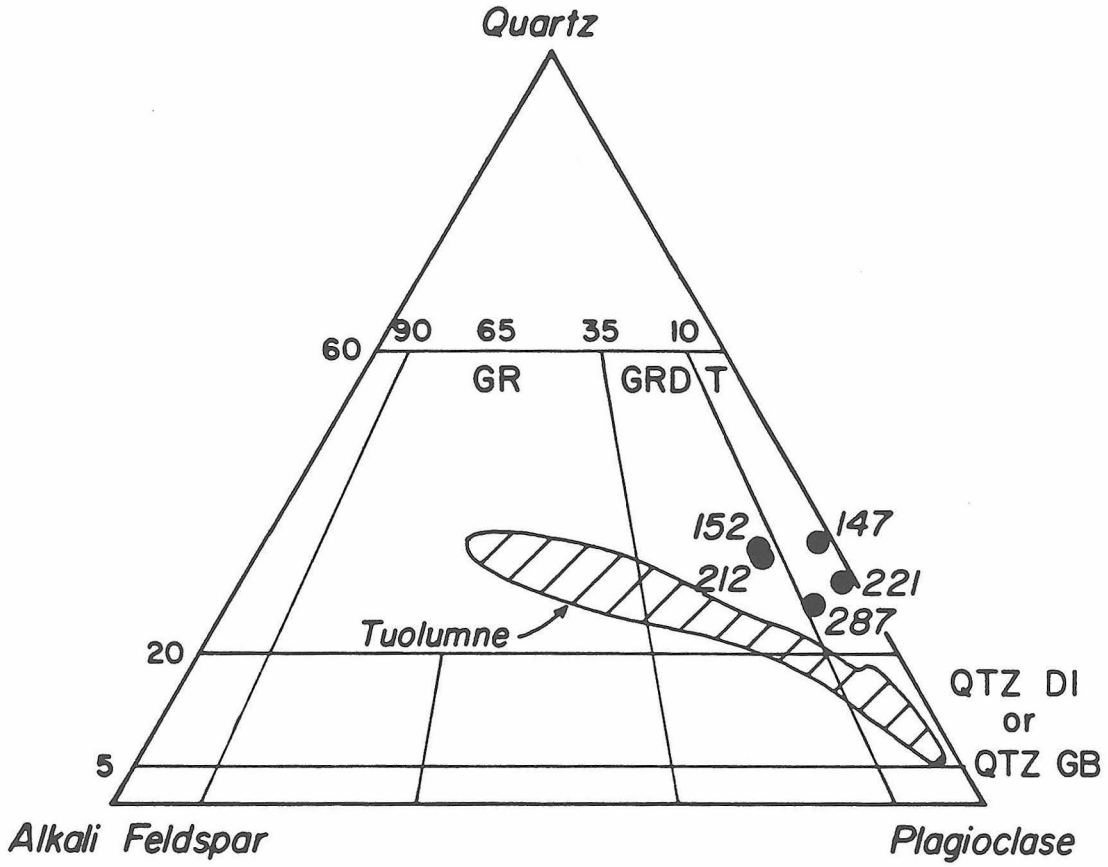

GR → GRANITE
GRD → GRANODIORITE
T → TONALITE
QTZ DI → QUARTZ DIORITE (Plag < An_{50})
QTZ GB → QUARTZ GABBRO (Plag > An_{50})

Figure 5.3. Classification of five representative major tonalite samples (after Streckeisen, 1973). Field for Tuolumne Intrusive complex from Bateman and Chappell (1979).

VARIATION WITHIN MAJOR TONALITES

Figure 5.4a. Photograph of mafic tonalite, showing aligned mafic minerals and poikilitic titanite within ovoid bleached spots. This rock is typical of the poikilitic-titanite facies of Unit I, and is one of the more mafic tonalites from Unit I. Old Control Road, G.R. 192325. Approximately life size.

Figure 5.4b. Photograph of granodiorite. Note lower Colour Index and relatively isotropic nature compared to the foliated tonalite above. Sample LTS 322, Old Control Road, G.R. 211329. Approximately life size.

These two photographs illustrate the complete range of rock types found within the major tonalite units.

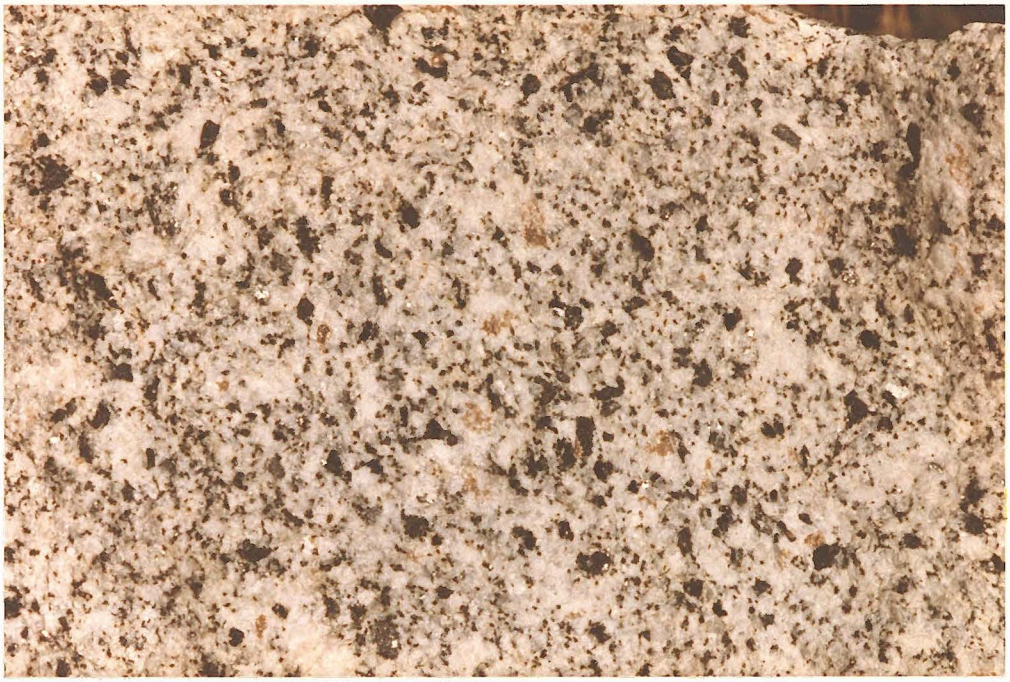

quantify the geographic variation in the composition of the three tonalite units. In general, the more mafic rocks of Unit I and Unit II tend to be more marginal, but the pattern is complex and the limited available data do not allow for adequate resolution of the nature of any variation. The situation is quite different for Unit III, however, where the available data can be contoured to show a pattern of regularly decreasing mafic mineral content away from the pluton margins (Fig. 5.5). Titanite also shows a similar pattern of decreasing abundance away from the outer contact. Unit III is, on the whole, slightly less mafic than is either Unit I or Unit II.

Throughout all three plutons the common rock type is a medium-grained tonalite. Plagioclase comprises approximately 50% of all rocks, quartz about 25%, and K-feldspar and the mafic minerals the rest. The rock has a seriate-porphyritic texture, with the major minerals ranging down in size from maximum dimensions of 10-15 mm. Because of the similar nature of the rocks from all three units, they are described together below.

In thin section the average rock is seen to be hypidiomorphic-granular, with a seriate-porphyritic grain-size distribution. Plagioclase tablets may show up to 10 oscillatory zones superimposed upon an overall normal zonation from an intermediate andesine center to an oligoclase-andesine rim (An_{40-30}). Apatite prisms are ubiquitous inclusions within plagioclase. Occasional small crystals of hornblende may be found arranged along a prominent growth-zone within a large plagioclase tablet.

Quartz occurs as anhedral aggregates of sutured sub-grains, commonly showing pronounced undulatory extinction. Often these quartz

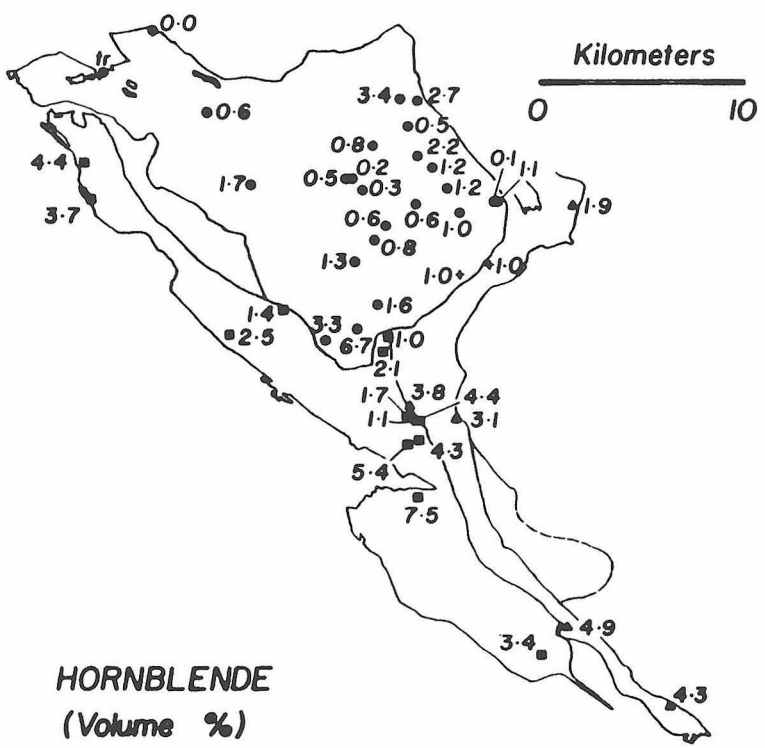

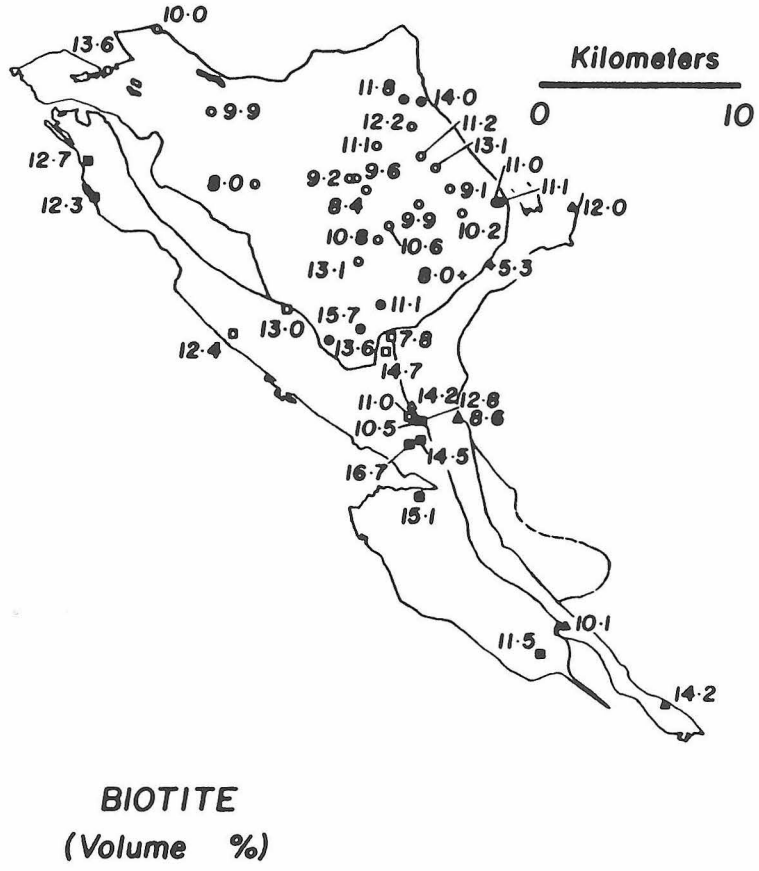

Figure 5.5. Hornblende and biotite abundances, major tonalites.

mosaics will have a large subequant central grain surrounded by smaller presumably later anhedral overgrowths.

Simply twinned subhedral to euhedral hornblende is pleochroic from a light yellowish-brown to slightly bluish dark greenish-brown or dark bluish-green. Inclusions in hornblende are common, and include equant ilmenite grains, small stubby apatite prisms, rounded grains of complexly twinned plagioclase, small euhedral zircons, and large irregular masses of quartz and biotite. Hornblende is commonly intergrown with titanite (Fig. 5.6), plagioclase, and other hornblende grains. Intergrowth with quartz is also present. There is some replacement of hornblende by a clear epidote.

Biotite occurs as well-formed prisms (books) and as irregular grains. It is pleochroic from yellow-brown to dark chocolate-brown. Zircon and apatite crystals are ubiqitous inclusions. Biotite often occurs in aggregates with hornblende and titanite, as well as in discrete grains scattered throughout the rock. Where allanite is present it is usually associated with biotite aggregates.

Titanite occurs as characteristic sphenoidal euhedra. It is slightly pleochroic in pink. Irregular ilmenite inclusions are common, and titanite is commonly intergrown with hornblende.

Potassium feldspar shows the widest range of textural relation ships of any mineral present. In mafic rocks it occurs as large poikilitic crystals enclosing all other minerals (Fig. 5.7). As it becomes more abundant in the more felsic rocks the number and size of inclusions decrease until in the most felsic rocks K-feldspar occurs as large (to

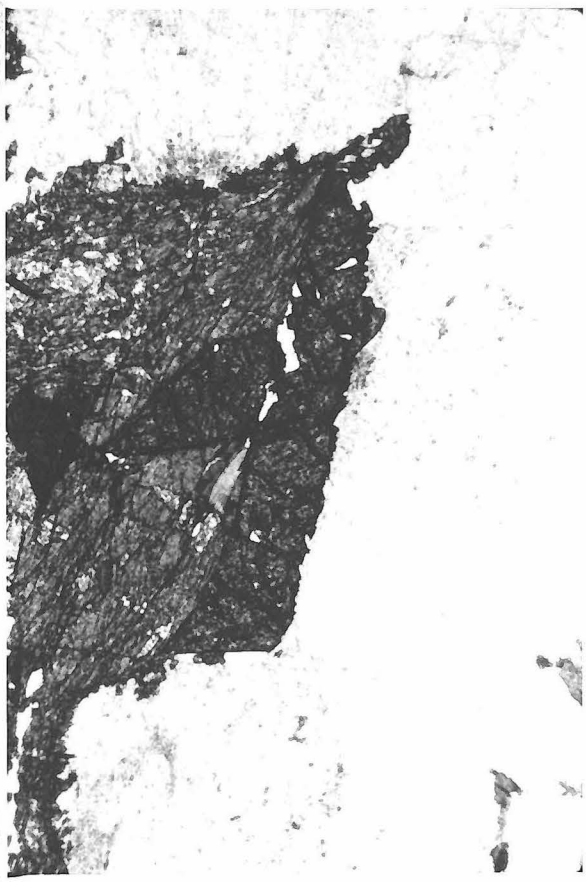

Figure 5.6. Photomicrograph of intergrown hornblende and titanite in sample LTS 360. Photomicrograph is 3 mm across.

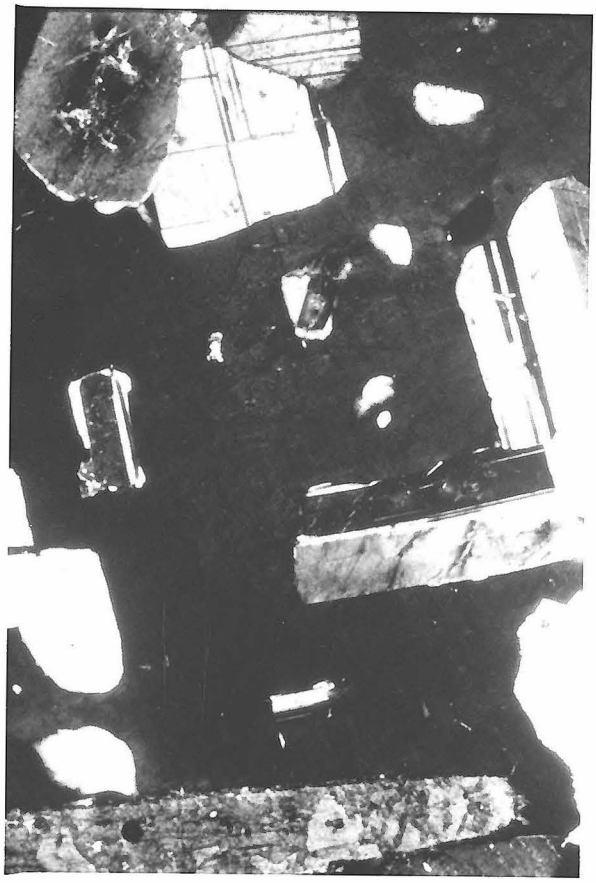

Figure 5.7. Photomicrograph of euhedral plagioclase (striped), equant quartz and euhedral allanite (gray, at bottom) within part of a large poikilitic K-feldspar crystal (black). Sample LTS 217, a tonalite from Unit I. Side of photomicrograph is 3 mm long.

10 mm) discrete anhedral grains intergrown with other minerals and relatively free of inclusions. Microperthite is common, and extinction is usually highly patchy. Compositional data (Ch. 6) suggest crystallization as orthoclase, with later subsolidus unmixing.

Accesory minerals are apatite, zircon, ilmenite and allanite. The allanite is pleochroic from light yellowish-brown to dark red-brown. It occurs as elongate prisms to 0.5x5 mm, and is usually sheathed by an irregular growth of clear epidote (Fig. 5.8a). Prominent growth zones are common (Fig. 5.8b), and uncommon inclusions are probably ilmenite. Where allanite is immediately adjacent to biotite anomalous pleochroism within the latter mineral suggests that considerable radiation damage has accumulated within the biotite structure.

Most thin section show a few tenths of a percent of secondary minerals. These include chlorite replacing biotite, epidote replacing hornblende, the development of very fine-grained cloudy material within feldspars (sericite?) and occasional flakes of white mica or small masses of carbonate within plagioclase.

5.3.1 TITANITE DISTRIBUTION AND TEXTURAL RELATIONS

Honey-coloured titanite is a minor but prominent phase in most rocks of the major tonalitic units, varying in abundance from trace amounts in some of the more felsic rocks to almost 2% (by volume) in some of the more mafic tonalites. Contrasting textural associations of titanite are observed, and there are consistent variations in the mode of occurrence of titanite between the different intrusive units. Titanite is thus the only mineral phase that has been observed to have consist-

Figure 5.8a. Photomicrograph of epidote-sheathed allanite crystal. Epidote gray with prominent cleavage; allanite dark gray with prominent growth zones. Also present: plagioclase (hexagonal grain within epidote), K-feldspar (much of the surrounding white material), and biotite. Sample LTS 289, a mafic tonalite from Unit II. Base of photomicrograph is 3.25 mm across.

Figure 5.8b. Photomicrograph of large growth-zoned allanite crystal. Sample LTS 145, a felsic tonalite from Unit III. Base of photomicrograph is 3.25 mm across.

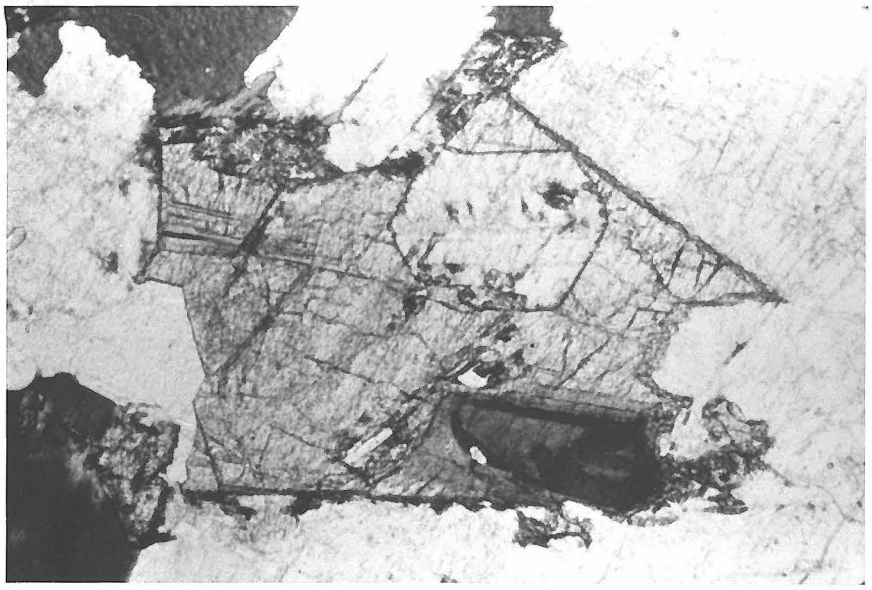

ently different relationships in different of the large intrusive units.

Single grains commonly occur in all sizes from microscopic to about 5 mm in longest dimension. Occasional euhedra within coarse-grained schlieren may reach 10 mm or more in size. Titanite in these rocks shows two distinctive forms of occurrence. In some, generally more mafic rocks titanite occurs as large (to 10 mm or more) poikilitic masses enclosing equant quartz and plagioclase crystals, and commonly surrounded by a leucocratic halo of quartz and plagioclase that may be as much as 3 cm in diameter. In other rocks titanite occurs as sphenoidal euhedra. The two strikingly different textural relationships appear to be completely intergradational. The poikilitic titanite texture is best developed in marginal rocks. In the best-developed examples of this poikilitic-titanite facies titanite that is crystallographically continuous for 10 mm or more poikilitically encloses small plagioclase tablets and equant quartz grains (Fig. 5.9a). The texture is reminiscent of the poikilitic K-feldspar plates except that titanite is the host phase and plagioclase and quartz the included phases rather than the plagioclase, hornblende, biotite and titanite found within the K-feldspar poikloblasts. These titanite-plagioclase-quartz intergrowths form ellipsoidal structures up to two or three centimeters in diameter. These ellipsoids are flattened in the plane of the mineral foliation, and have their long axis aligned parallel to a mineral lineation where one is present.

This texture is particularly prominent within Unit I on the north slope of Baldy Mountain (G.R. 265273), and again in the outcrops along the steep face of the San Jacinto River valley north of the San Jacinto fault (G.R. 193330 and westward).

Figure 5.9a shows the core of a small titanite-plagioclase-quartz ellipsoid. Features present here suggest that the titanite competed for space with both quartz and plagioclase as it grew, but did not compate for space with K-feldspar. Titanite growth appears to have been restricted by impingement against the faces of previously crystallized plagioclase tablets.

Figure 5.9b shows a space-filling titanite that has had its form controlled by impingement on the faces of large plagioclase tablets. Plagioclase appears to have largely finished crystallization before the bulk of the titanite had been formed.

The alignment of the ellipsoidal structures in the plane of the mineral foliation implies that both the ellipsoids and discrete hornblende and plagioclase tablets were able to be oriented by some process, presumably flow within the magma chamber.

Commonly, with increasing distance from the intrusive contact (and related increase in felsic component) the margins of the ellipsoids become more diffuse and the titanite steadily adopts a more euhedral form. The best developed sphenoidal forms characteristically occur when small titanite crystals occur adjacent to, or are enclosed within, the margins of biotite flakes, or where titanite euhedra are enveloped within K-feldspar poikiloblasts (Fig. 5.10a).

Ilmenite is the most common phase included within titanite. It commonly occurs as irregular or skeletal grains (Fig. 5.10b). This relationship may result from a reaction producing titanite at the expense of pre-existing ilmenite.

Figure 5.9a. Photomicrograph of poikilitic titanite from the center of a titanite-plagioclase-quartz ellipsoid. Titanite (light, prominent cleavage) surrounds plagioclase euhedra. Dark mass at top of photomicrograph is quartz. Sample LTS 324, a mafic tonalite from Unit I. Base of photomicrograph is 3.25 mm across.

Figure 5.9b. Photomicrograph showing space-filling titanite. Anhedral titanite (dark) and plagioclase (striped), with a small mass of irregular quartz (white) intergrown with the titanite near the right margin of the photomicrograph. Sample LTS 316, idiomorphic-biotite - hornblende - tonalite of Herkey Creek.

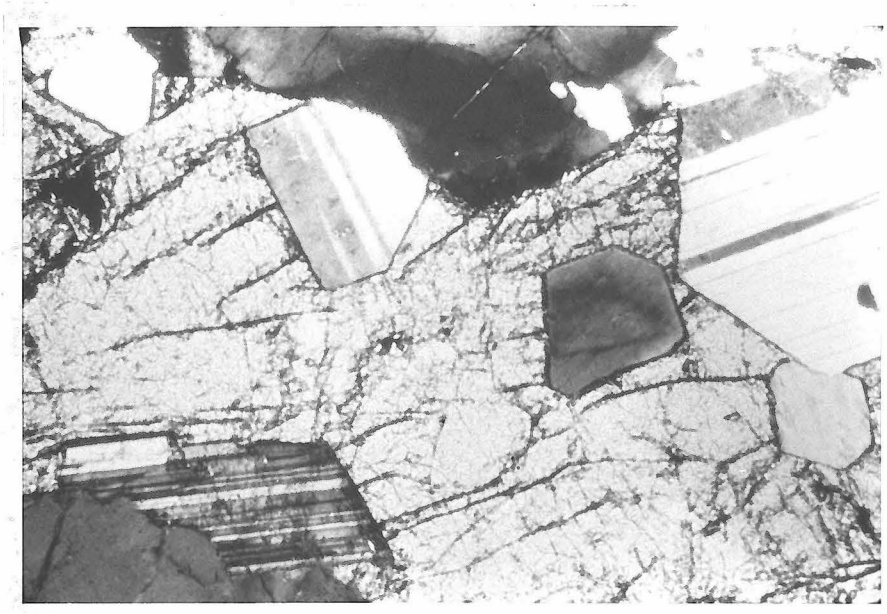

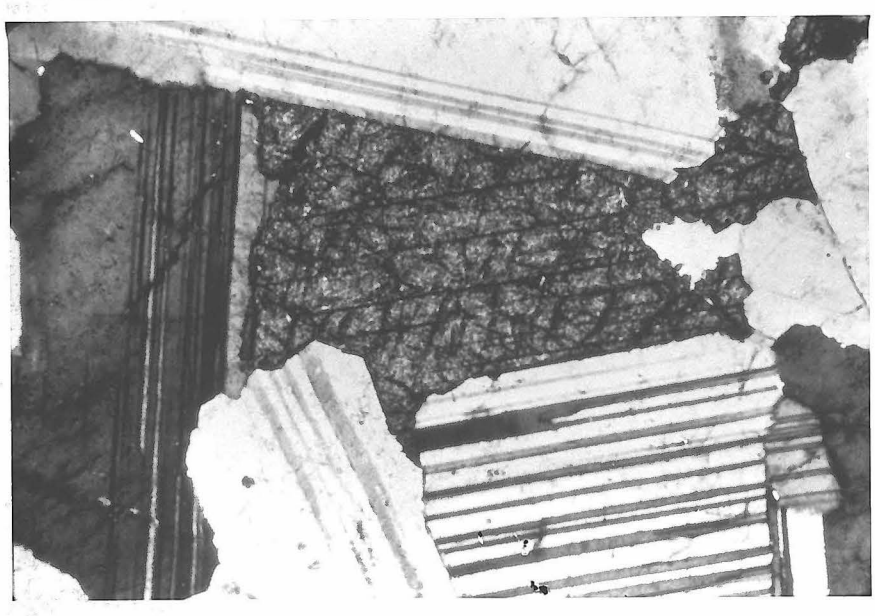

Figure 5.10a. Photomicrograph of euhedral titanite (diamond-shaped) within a large K-feldspar poikiloblast. Sample LTS 288, a granodiorite from Unit II. Base of photomicrograph is 3.25 mm across.

Figure 5.10b. Photomicrograph of ilmenite inclusions (black) within large intergrown titanite euhedra (dark gray). Sample LTS 152, a tonalite from Unit III. Base of photomicrograph is 3.25 mm across.

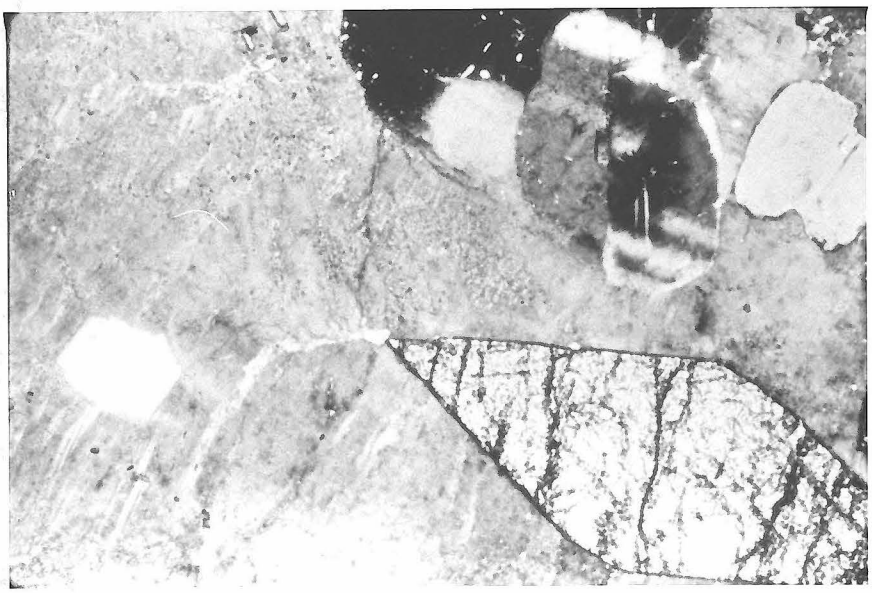

The complete range of titanite textural relations is present within all three well-studied major tonalite units. Variations occur in the relative importance of each type from unit to unit. Within Unit I, most mafic marginal rocks show well developed ellipsoidal structures, and euhedral titanite does not begin to become common for some kilometers away from pluton margins. Even then it occurs most commonly in either the more felsic rocks or as titanite euhedra poikilitically enclosed by K-feldspar.

In Unit II ellipsoidal structures, though present in the most marginal rocks, are in general not well developed and tend to be small (diameter 1 cm or less). Titanite in the more mafic rocks of Unit II is usually present as irregular "space-filling" grains, with some titanite crystal faces developed, and some moulding around earlier grains (Fig. 5.9b). Within a few hundred meters of the pluton margins euhedral titanite is common, and, as in Unit I, often occurs spatially associated with biotite or as well-formed crystals within K-feldspar poikiloblasts.

Within Unit III ellipsoidal structures are only well-developed within the relatively felsic tonalites immediately below the pluton roof south of Banning (G.R. 130491). Here prominent titanite-plagioclase-quartz spheres occur within slightly foliated relatively fine-grained felsic tonalite adjacent to both metasedimentary and igneous wall-rocks. Elsewhere within this unit, even within the most mafic tonalites adjacent to pluton contacts, titanite invariably occurs as euhedral crystals. These may be aligned in a foliation plane defined by hornblende prisms and plagioclase tablets, and the perfect crystal form of the titanite in this association implies that it crystallized from the melt early along with the plagioclase and hornblende.

The observations detailed above suggest a consistent variation in titanite paragenesis as crystallization progressed within each unit, and that the factor(s) controlling titanite precipitation differed for the first solids to crystallize from each succeeding intrusive unit. Euhedral titanite is not common in Unit I until the central, more felsic rocks crystallized; within Unit II it appears very soon after crystallization commenced, and it was one of the first minerals to appear throughout most of Unit III.

It is not clear why titanite shows such a range of parageneses. Chemical data presented below (Ch. 7) show that Unit III (in which titanite is an early appearing phase) has lower Ti at a given SiO_2 than does either Unit I or Unit II. The difference is not great, however, and it is difficult to understand why titanite should appear earlier in the relatively Ti-poor rock. The controlling factor may be f_{O_2}; it is difficult to evaluate the effect of such a parameter in these rocks with the data available.

Titanite was probably not an important phase within the liquids which ultimately crystallized to give the observed rocks prior to the arrival of these liquids in the magma chambers; i.e., titanite was probably not present in the plumbing system through which liquids were transported to the magma chamber. Once the liquids reached the various magma chambers, titanite began to appear as a discrete phase, but with different paragenetic relations in each. Within Unit III began to crystallise early, along with ilmenite, plagioclase and hornblende. It must be considered in any fractional crystallization process developed to explain variations within this unit. The role of titanite in the two

earlier intrusive units is more difficult to evaluate from textural evidence. It could have been an important early crystallizing phase during much of the solidification of Unit II; it was probably not an important early phase in Unit I.

Gromet and Silver (1983) demonstrate that accessory phases, particularly titanite and allanite, are the likely major hosts for the REE within the tonalites of the Peninsular Ranges batholith. They argue that early separation of these phases will produce distinctive REE behaviour patterns which have not been observed within the batholithic samples studied to date (Gromet, 1979), implying that any crystal fractionation scheme invoked to explain batholithic REE behaviour cannot involve simply the observed crystallizing phases in their observed proportions.

The observations on titanite paragenesis in the major tonalites detailed above imply that the effects of titanite separation on REE behaviour are limited to those during solidification of a high-level magma chamber. As the importance of fractional crystallization (either by gravity settling or by lateral accretion) appears relatively limited within these rocks, rock REE distributions will be largely the product of original liquid endowments. This point has been argued persuasively by Gromet and Silver (1983) for the batholith as a whole.

5.3.2 MINERAL PARAGENESES WITHIN THE MAJOR TONALITES

The observed mineral relations described above suggest that hornblende was the first mineral to begin crystallization, followed by plagioclase, biotite and quartz, and K-feldspar in that order. The common occurrence of several included phases in the margins of minerals that

began crystallization early in the paragenetic sequence (such as inclusions or intergrowths of plagoclase, biotite, quartz and titanite within hornblende) are interpreted as indicating that once a phase had begun to crystallize it remained as a crystallizing phase for an extended period. Within Units I and II titanite did not begin to precipitate until relatively late in the history of the rocks; within Unit III it apparently did appear relatively early in the crystallization sequence. Ilmenite, which is commonly found as inclusions within titanite, apparently was an early crystallizing phase, perhaps crystallizing with hornblende and plagioclase early in the petrogenetic sequence. The common occurrence of allanite as large prisms within K-feldspar poikiloblasts and the relative lack of allanite in other textural relationships is interpreted as showing that allanite was relatively late in the paragenetic sequence.

It is difficult to place quartz in the paragenetic sequence; the reasons have been discussed above. The ubiquitous large (10 mm) equant quartz crystals, which may show evidence of hexagonal bipyramidal form, apparently crystallized free from interference from other grains. Quartz is not found as inclusions within the central parts of either plagioclase or hornblende crystals, suggesting that it did not begin to crystallize until these faces had been precipitating for some time.

5.3.3 XENOLITHS AND DIKE-ROCKS

Both mafic xenoliths and mafic dikes are common throughout the three major tonalites, and field relations have been interpreted as showing a genetic link between the two (Ch. 4). If this interpretation is correct, it implies that both dikes and xenoliths may be samples of the more mafic liquids introduced into the inflating magma chambers.

The mineral parageneses of these rocks may thus give an indication of the relative importance of the various crystallizing phases prior to introduction of these liquids into the magma chamber.

The dikes and xenoliths contain the same minerals as the tonalites, but in quite different proportions and with different mineral-mineral relations. Modal analyses of a typical dike and a typical mafic xenolith are presented in Table 5.7. As with the tonalites, both dike and xenolith are dominated by plagioclase (67 and 49%, respectively). The high plagioclase abundance of the dike may reflect plagioclase enrichment in this particular sample, perhaps by flow differentiation. The xenolith contains considerably more hornblende (18%) and quartz (23%) compared with the dike (5% and 9%, respectively). The dike is much more biotite-rich than the xenolith. The xenolith is a tonalite and the dike a quartz diorite by the Streckeisen (1973) classification.

In thin section, the xenoliths show relatively large (to a few millimeters) euhedral to subhedral plagioclase tablets, smaller euhedral to subhedral hornblende prisms and large rounded equant quartz grains forming an interlocking framework filled in by smaller and less well formed plagioclase, hornblende and quartz crystals, along with irregular biotite and anhedral titanite (Fig. 5.11). Some plagioclase tablets contain rounded cores (Fig. 5.11), suggesting a complex crystallization history. The bulk of the plagioclase has a composition a little more calcic than that of the host tonalites (An_{45-40} compared with An_{40-35}). Hornblende, plagioclase and quartz appear to have been the important early crystallizing phases.

TABLE 5.7

MODAL DATA FOR A MAFIC XENOLITH AND A MAFIC DIKE

	Mafic xenolith (Tonalite) [1] LTS 377	Mafic dike (Quartz diorite) LTS 214
Quartz	22.6	9.1
K-feldspar	0.4	tr
Plagioclase	48.8	67.2
Biotite	8.1	17.0
Hornblende	18.1	5.3
Titanite	1.6	0.5
Apatite	0.2	0.3
Zircon	tr	tr
Opaques	tr	tr
Allanite	0.2	0.1
Epidote	tr	0.5
Chlorite	tr	tr
Total	100.0	100.0
Colour Index	28.0 ± 2.5	23.4 ± 1.9

[1] Classification after Streckeisen (1973).

PHOTOMICROGRAPHS OF A TYPICAL MAFIC XENOLITH

Figure 5.11a. Photomicrograph of a tonalitic xenolith showing large core within a euhedral plagioclase crystal (center-left), smaller plagioclase tablets, subhedral to euhedral hornblende, equant quartz, and anhedral to subhedral bitotite. Sample LTS 378 (crossed nicols). Photomicrograph is 3.25 mm across base.

Figure 5.11b. Field of view as above, plane polarized light.

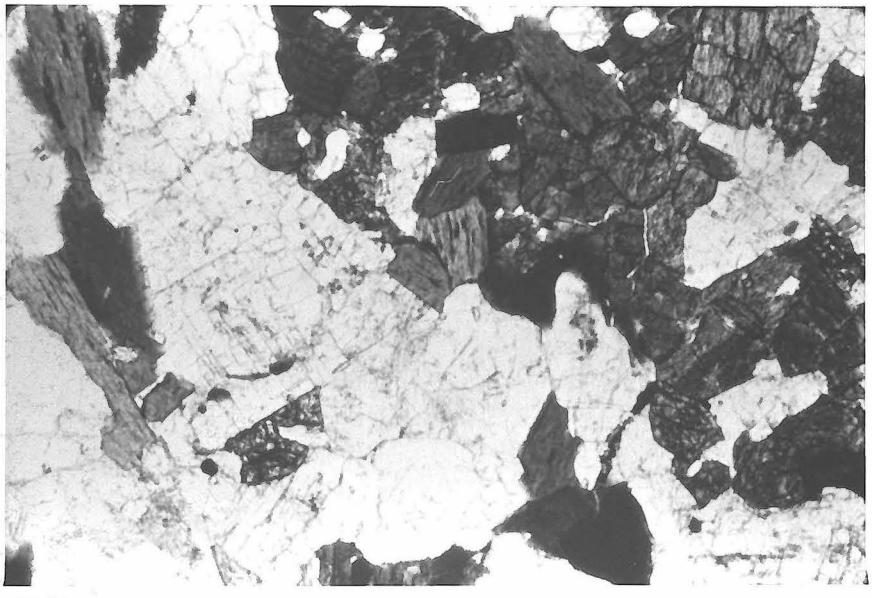

PHOTOMICROGRAPHS OF A MAFIC (QUARTZ DIORITE) DIKE

Figure 5.12a. Photomicrograph illustrating alignment of plagioclase tablets (striped), quartz with strong undulatory extinction (shades of gray), biotite and hornblende. Sample LTS 214. Crossed nicols. Photomicrograph is 3.25 mm across base.

Figure 5.12b. Field of view as above, plane polarized light.

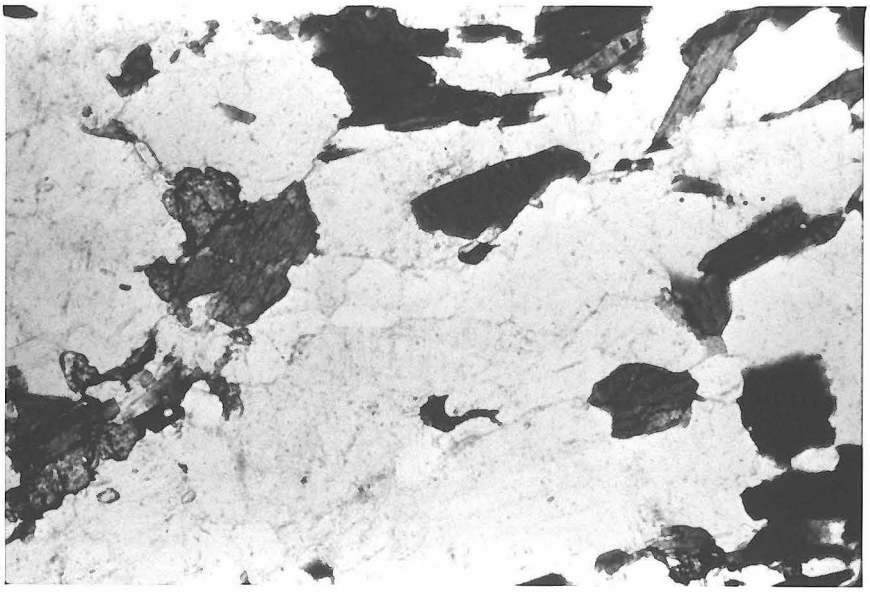

If crystallization of this material largely took place after injection into the tonalitic liquid of the magma chamber, the presence of well-formed relatively large crystals of hornblende, plagioclase and quartz suggests that these crystals were already present in suspension, implying crystallization prior to reaching the level of the observed magma chamber.

The mafic dike again shows large subhedral plagioclase tablets, large quartz grains, and subhedral to euhhedral hornblende, but also contains well-formed crystals of biotite (Fig. 5.12). All minerals show alignment within a prominent foliation plane; the quartz crystals also show considerable evidence for strain approximately in this plane after crystallization had finished. This may result from stresses related to emplacement of the dike. Biotite was apparently an important early crystallizing phase in this rock along with hornblende, plagioclase and quartz. Again titanite is present as an apparently late space-filling phase.

The early appearing phases in the tonalites are also hornblende, plagioclase and quartz. The apparent efficiency of sorting by flow action within the magma chamber (to give mineral layering and schlieren) is interpreted as indicating the presence of relatively crystal-free liquids within the upper crustal magma chambers. Plagioclase and hornblende are commonly the dominant phases involved in such mineral seggregations, implying that they were the only phases present. These features, in combination with the petrographic observations presented above are interpreted as indicating that plagioclase and hornblende (and perhaps ilmenite) were liquidus phases at the time of injection of liquids into the upper crustal

magma chambers. Quartz may have been; if not, it almost certainly appeared as a significant phase within a short time of injection of the liquids into the chamber.

The petrographic evidence from the xenoliths in particular appears to support the inference from the mafic tonalites that hornblende and plagioclase were the early crystallizing (probable liquidus) phases when liquids were introduced into the magma chambers. The evidence from the xenoliths suggests that quartz may have been a liquidus phase also. Biotite probably was not, and titanite and K-feldspar almost certainly were not crystallizing phases from at least the more mafic liquids prior to introduction into the cooling magma chambers.

The inferred paragenetic sequence can be used, in conjunction with experimental data, to place broad constraints on the temperature and water content of the silicate liquids at the time that they were added to the growing magma chambers. For instance, Eggler (1972) concluded that calc-alkaline andesites must, in general, contain <3 wt.% H_2O in order to explain the common occurrence of plagioclase phenocrysts in these rocks. The presence of hornblende apparently requires at least 3.0 wt.% H^2O in the liquid phase (not bulk magma) from which it crystallises (Burnham, 1979).

Wyllie (1977) presents a schematic $T\text{-}X_{H_2O}$ diagram for tonalite at 10 kb. The tonalite used in the experimental studies is broadly comparable to the tonalites from the San Jacinto Mountains, except that quartz is generally more abundant and K-feldspar less abundant in the latter rocks. For the major tonalites hornblende and plagioclase appeared first, followed by quartz and biotite. Hornblende, plagioclase and

perhaps quartz were liquidus phases at the time of introduction of liquids (plus suspended crystals) into the magma chambers. At 10 kb this implies this paragenetic sequence implies a water content of approximately 2.5-3.0 wt.%, and a temperature of at least 820°C for the composition discussed by Wyllie (1977). A temperature of 1,000°C or more is needed before this composition becomes fully liquid. The relatively steep dP/dT slope of the mineral-out boundaries (e.g., Wyllie, 1977, p.56) suggests that these estimates would not be changed markedly as pressure dropped from 10 to 4 kb. The temperatures estimated from these data are minimum values; other factors (different compositions, % crystallinity) suggest that the actual temperature of materials being added to the San Jacinto magma chambers was probably at least 900-1,000°C, and may have well have been somewhat higher. Water content appears to have been around 3 wt.%. Experimental data on rocks with the composition of the San Jacinto tonalites would be needed to arrive at better estimates for these parameters.

5.4 SUMMARY

1. The relatively homogeneous major tonalites span a much more limited compositional and petrographic range than do the early intrusives.

2. All except the most felsic plutons contain plagioclase, quartz, biotite, hornblende, K-feldspar, titanite, allanite, and an opaque mineral, most probably ilmenite. In the most felsic rocks hornblende, titanite and probably allanite are not found.

3. Mineralogy within the three major tonalites is monotonous. Rocks from all three units consist of approximately 50% plagioclase, 25% quartz, and varying amounts of the other minerals. Biotite abundance

varies from 17 to 8.4% in the common rocks (and to as little as 5% in minor felsic differentiates), hornblende varies from 8 to 0%, and titanite varies from about 2 to 0%. As biotite, hornblende and titanite abundance decreases, K-feldspar increases, from about 1% in the most mafic rocks to 8-10% in the low-K granodiorites.

4. Within Unit III these changes in mineral abundances vary systematically; the marginal rocks are more mafic, and the central rocks more felsic.

5. Xenoliths and mafic dikes of tonalite and quartz diorite composition contain the same minerals as do the tonalite plutons, but in different proportions. Hornblende, plagioclase and perhaps quartz are interpreted to have been liquidus phases at the time of injection of these liquids into the cooling magma chambers. Biotite and titanite apparently were not.

6. Titanite is the only phase that has consistently different textural relations from unit to unit. Within Unit I it appears to be a relatively late-crystallizing phase throughout much of the pluton; in Unit II it is a late-crystallizing phase in the marginal tonalites but then becomes a liquidus phase (joining hornblende, plagioclase, quartz and biotite) for the bulk of the crystallization of this unit. In Unit III titanite appears to have been a liquidus phase throughout the crystallization history.

7. Orthopyroxene (probably hypersthene) being replaced by hornblende were found in a single thin section from the granodiorite of Poppet Creek. With the exception of samples from the small gabbro masses, this was the only pyroxene observed in nearly 200 thin sections. This rock also includes other evidence of a complex crystallization history.

In particular, large plagioclase tablets often contain distinct calcic (An_{80}-An_{90}) cores mantled by more sodic (An_{40}-An_{25}) rims, and relatively large, irregular opaque grains, probably ilmenite, are common inclusions within titanite rhombs.

8. Available experimental data imply that the liquids were emplaced into the magma chambers at temperatures of at least 900°C. The apparently small proportion of suspended crystals within these liquids at the time of injection are consistent with much higher temperature estimates, perhaps 1,000-1,100°C.

CHAPTER 6

MINERAL CHEMISTRY

6.1 INTRODUCTION

The composition of a mineral phase precipitating from a silicate melt is some function of the composition of that melt and of prevailing physical conditions (e.g. pressure, temperature, presence or absence of a vapour phase). Ideally, if the compositions of an entire suite of co-existing minerals are known it should be possible to calculate the physical and chemical parameters that prevailed during crystallization of that mineral suite. This commonly requires the presence of exchange equilibria involving cation distribution between two or more phases, and experimental calibration of such equilibria. When these conditions are met considerable information can be obtained on intensive parameters prevailing during crystallization of silicate liquids (e.g., Barker et al., 1975; Wones, 1980; Wyborn et al., 1981).

The relatively simple mineralogy of the San Jacinto rocks precludes detailed calculation of the physico-chemical conditions prevailing during crystallization. For much of the crystallization history plagioclase, hornblende, biotite, titanite, ilmenite and quartz were the precipitating phases. K-feldspar, a relatively sodic plagioclase and quartz were also precipitated from trapped liquid, along with minor amounts of the mafic phases. Cation exchange between these various phases, particularly those reactions involving hornblende (essentially all) are complex, and to date remain largely uncalibrated.

However, growth of a mineral from a melt implies an approach to chemical equilibrium between the melt and the growing crystal. Determination of the chemistry of a phase as a function of the extent of crystallization of that melt should allow for the recognition of changes in the composition of the melt, as well as the recognition of gross changes in external parameters such as temperature and pressure. Accordingly, electron microprobe data have been obtained for the various mineral phases from 10 selected rocks covering the compositional range of the major tonalites. These data demonstrate a surprising lack of variation in the composition of the major mineral phases precipitating from these liquids as solidification progressed. This is in sharp contrast to data obtained for plutonic complexes in, for instance, the Sierra Nevada batholith (e.g., Mt. Givens Granodiorite, Bateman and Nokleberg, 1978; Tuolumne Intrusive Complex, Bateman and Chappell, 1979). For instance, for comparable variation in SiO_2 content, plagioclase ranges from about An_{52} to An_{12} in Mt. Givens (Bateman and Nokleberg, 1978), from An_{42} to An_9 in the Tuolumne Intrusive complex (Bateman and Chappell, 1979) and from An_{44} to to An_{25} in San Jacinto (this work). This is the total observed range in plagioclase composition for the three intrusions; the mean composition of plagioclase as a function of progressive solidification shows a much smaller change (from perhaps An_{40} to An_{30} in San Jacinto, for example). This implies remarkable constancy of either liquid composition, or of external parameters (pressure, temperature), or both during the crystallization of this magma.

This chapter presents the mineral chemical data obtained for rocks from the San Jacinto intrusive complex. Because of the striking similarity of all rocks from the three major tonalite units in terms of

their petrography, mineral chemistry, and rock chemistry (Ch. 7), the following data are organized by mineral species rather than by rock unit. The paragenesis of each mineral is an important parameter in the interpretation of these and other data; detailed description of the textural relationships of each mineral is thus included with the chemical data.

The colour index of these rocks varies from about 30 to 5 or less. Rock chemistry varies accordingly. Within Unit III mineral proportions vary systematically away from the walls of the intrusion (Ch. 5). Although the total variations in either mineral abundance or in rock chemistry are small compared to those found in other well-studied zoned calc-alkaline intrusive complexes (e.g., Tuolumne Intrusive complex (Bateman and Chappell, 1979); Mount Givens Granodiorite (Bateman and Nokleberg, 1978)), the sense of the variations present in the San Jacinto rocks (particularly within Unit III) mirrors those of the Sierran rocks, suggesting a similar genesis.

6.2 MINERAL COMPOSITIONS AND TEXTURAL RELATIONS

6.2.1 PLAGIOCLASE

Plagioclase is the dominant mineral of the tonalites, comprising some 50% (volume) of the whole complex. Over 200 determinations of plagioclase composition were made with the electron microprobe, and selected analyses are presented in Table 6.1. The total range of analysed plagioclase compositions from tonalites and granodiorites is from An_{44} to An_{25}. Slightly more calcic compositions (to An_{47}) were found in a mafic xenolith. Plagioclase within a single rock commonly has a range in An

Figure 6.1. Histograms of plagioclase composition for 11 rocks and 2 xenoliths. Numbers in brackets underneath sample numbers are rock SiO_2 content (wt.%). LTS 292 is a low-K granodiorite; samples LTS 291 and 216 are mafic xenoliths. Xenolith samples LTS 291 and 216 are from host tonalite LTS 290 and 215, respectively. LTS 216 probably represents part of an early-crystallizing mafic phase, or a schlieren reincorporated into the tonalitic liquid.

Note slight decrease in mean Anorthite content (from An_{35-36} to An_{30}) as SiO_2 increases.

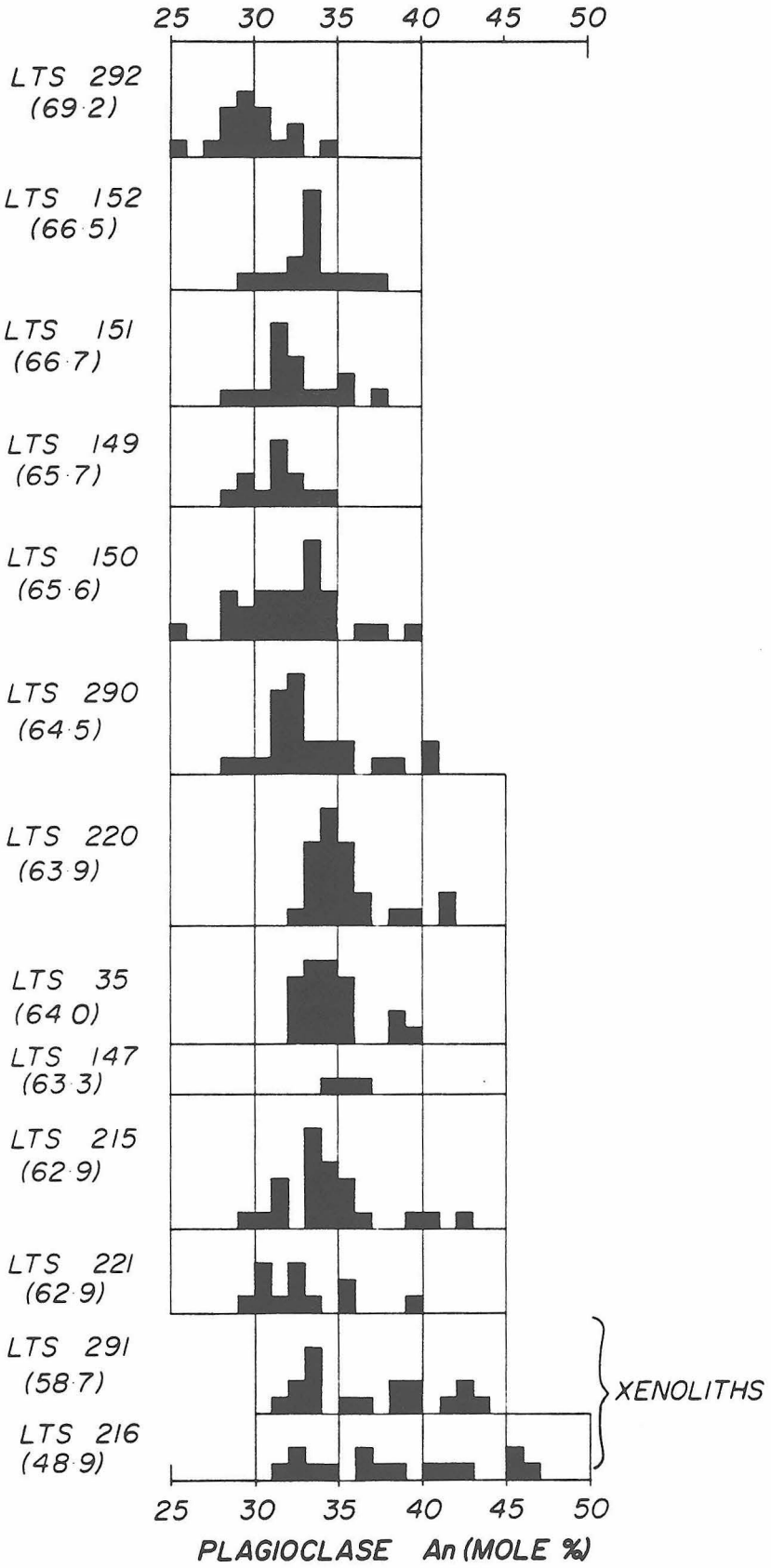
25 30 35 40 45 50
LTS 292 (69·2)
LTS 152 (66·5)
LTS 151 (66·7)
LTS 149 (65·7)
LTS 150 (65·6)
LTS 290 (64·5)
LTS 220 (63·9)
LTS 35 (64·0)
LTS 147 (63·3)
LTS 215 (62·9)
LTS 221 (62·9)
LTS 291 (58·7)
LTS 216 (48·9)
XENOLITHS
25 30 35 40 45 50
PLAGIOCLASE An (MOLE %)

TABLE 6.1.

CALTECH MICROPROBE LABORATORY

ELECTRON MICROPROBE ANALYSES OF FELDSPARS IN SAMPLES LTS 290,291 AND 292

$(Na,K)AlSi_3O_8 - CaAl_2Si_2O_8$

WEIGHT PERCENT OF OXIDES

	LTS 291 Mafic xenolith		LTS 290 Mafic tonalite		LTS 290 Mafic tonalite			LTS 292 Low-K granodiorite		
	Plag core	Plag rim	Plag core	Plag rim	Plag core	Plag rim	K-fs	Plag core	Plag rim	K-fs
SiO_2	56.13	59.64	57.54	58.95	57.05	59.22	63.96	59.54	60.98	64.07
Al_2O_3	26.71	24.93	26.26	25.08	26.19	24.65	18.80	25.44	24.52	18.71
FeO	0.08	0.07	0.12	0.03	0.06	0.03	BDL	0.08	0.07	0.07
CaO	9.67	7.09	8.50	6.66	8.89	6.93	0.02	6.06	6.84	0.10
Na_2O	7.18	7.17	7.34	9.04	7.57	8.94	1.16	8.04	7.79	1.41
K_2O	0.17	0.17	0.24	0.18	0.22	0.13	14.81	0.26	0.17	14.15
BaO	0.06	0.06	NDL	0.07	NDL	0.11	1.25	NDL	0.06	1.27
AB	56.8	66.1	60.2	70.4	59.9	69.5	10.6	69.5	66.7	13.1
AN	42.3	32.4	38.5	28.7	38.9	29.8	0.1	29.0	32.4	0.5
OR	0.9	1.5	1.3	0.9	1.2	0.7	89.3	1.5	0.9	86.4
T_K[1]					760			820		

[1] Two-feldspar equilibration temperature (in Kelvins) calculated using the formulation of Haselton et al., (1983).

content of 10 to 12 mole%. Figure 6.1 graphically illustrates the plagioclase compositional data. Here a series of histograms of plagioclase composition are arranged by (rock) SiO_2 content. Ordering by decreasing colour index would give a similar diagram. There is some tendency for the more SiO_2-rich rocks to have a slightly more sodic mean plagioclase composition. Because of an attempt to analyse the most sodic and most calcic plagioclase in each rock the data are biased towards analyses of extreme compositions. Even so, a simple mean of all the analyses obtained for a single rock should give a reasonable estimate (probably erring on the sodic side) of that rock's bulk plagioclase composition. The mean plagioclase An content thus obtained falls from about An_{35} in the most mafic rocks to around An_{30} in the most felsic rock analysed. The mean An content of plagioclase from the two xenoliths analysed is perhaps a little higher (by a few mole % An) than in either their host tonalites or in the most mafic rocks analysed.

In fact, this method of estimating mean plagioclase composition errs slightly in favour of the more sodic compositions. Mass balance using the observed mineral abundances, and rock and mineral chemical data (for phases other than plagioclase) gives a range of mean plagioclase composition that falls from about An_{40} in the most mafic tonalites to An_{30} in the low-K granodiorites.

Plagioclases from the three major tonalite plutons have been analysed. Within the somewhat limited sampling there is no discernible difference between the composition of the plagioclase contained within the different intrusive units.

Figure 6.2. Composition of analyzed plagioclases and K-feldspars on the Anorthite-albite-K-feldspar triangular diagram. Tie-lines join analyses from abutting plagioclase (rim) and K-feldspar.

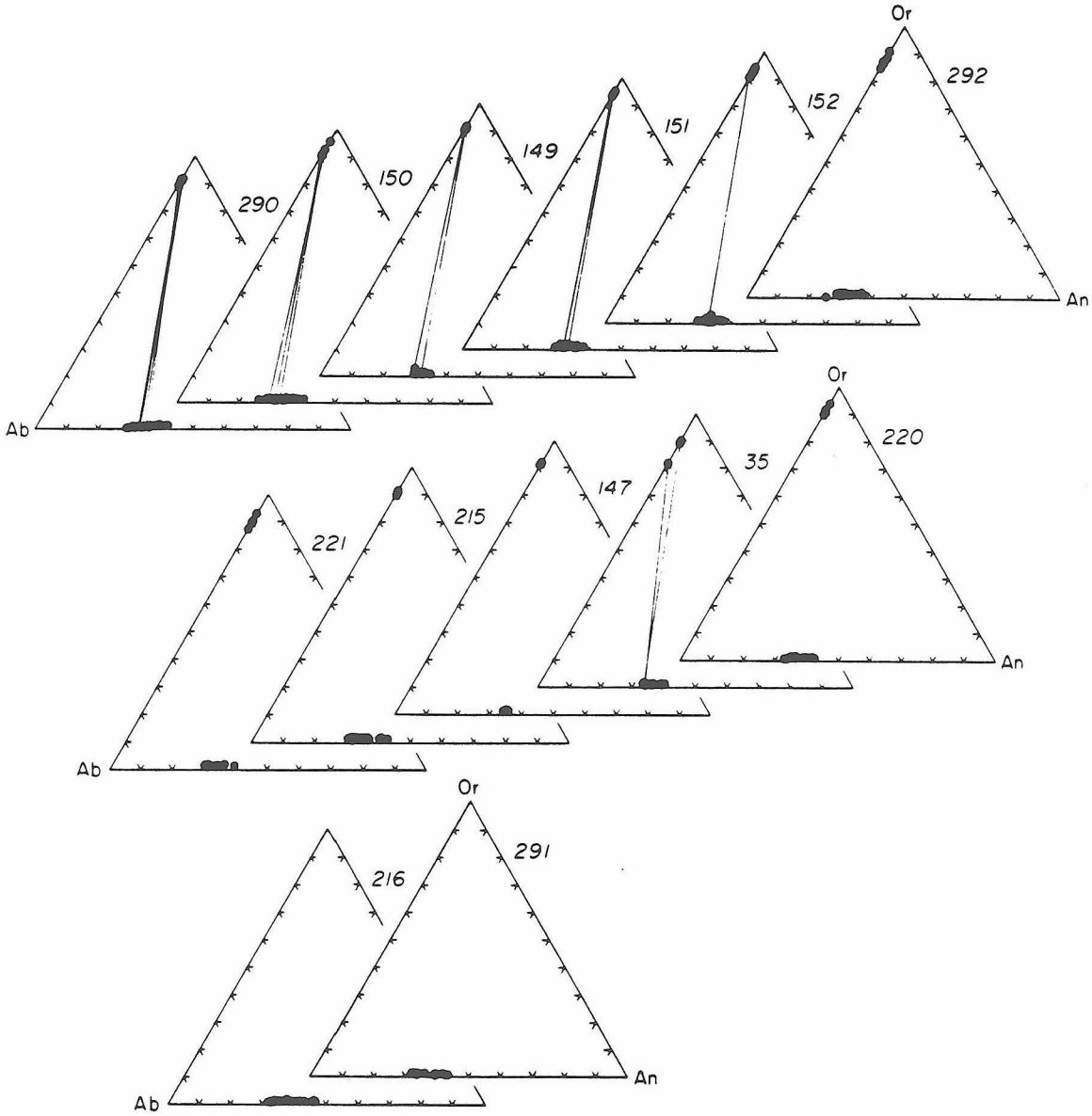
Or
292
152
151
149
150
290
An
Ab
Or
220
35
147
215
221
An
Ab
Or
291
216
An
Ab

Orthoclase contents (Or) of plagioclases are commonly in the range $Or_{0.5}$ to $Or_{1.5}$, with a few grains having up to 3 mole % Or. These data are shown graphically on Fig. 6.2, the Or-Ab-An feldspar triangle.

6.2.2 K-FELDSPAR

Alkali feldspar is a minor phase in most of these rocks. Within the major tonalites it comprises from about 1 to 10 volume percent of the rock. Analyses of typical K-feldspars co-existing with sodic plagioclase are listed in Table 6.1. Orthoclase contents are commonly between 85 and 95 mole percent. Two-feldspar equilibration temperatures calculated using the formulation of Haselton et al. (1983) are listed in Table 6.1. The low values obtained ($\approx 400^{o}C$) are interpreted to indicate continued sub-solidus re-equilibration during a prolonged thermal history. Feldspars from a small body of mafic tonalite that crops out north of the major tonalite units contains feldspars that imply slightly higher equilibration temperatures (Table 6.2). These higher values perhaps reflect slightly more rapid decay of the thermal anomaly around this much less extensive body.

All analysed K-fedspars show considerable Ba contents (between 0.9 and 1.3 wt.% BaO). This implies crystallization of K-feldspar from a liquid having approximately 1,000 to 1,600 ppm Ba (Long, 1978), presumably a relatively Ba-rich fractionated liquid late in the crystallization history of each rock. The small range of K-feldspar Ba/K ratios suggests that the composition of the liquid from which these feldspars crystallized was approximately constant from place to place throughout the large plutons.

TABLE 6.2

CALTECH MICROPROBE LABORATORY

ELECTRON MICROPROBE ANALYSES OF FELDSPAR IN SAMPLE LTS 35

$(Na,K)AlSi_3O_8$ - $CaAl_2Si_2O_8$

WEIGHT PERCENT OF OXIDES

	Plag rim	K-fs	Plag core	Plag rim	K-fs
SiO_2	59.35	64.48	57.62	59.44	64.50
Al_2O_3	25.43	18.32	26.48	25.28	18.93
FeO	BDL	0.16	0.10	0.03	0.17
CaO	7.23	BDL	8.54	7.10	BDL
Na_2O	7.80	2.02	7.03	7.93	2.61
K_2O	0.18	13.52	0.19	0.22	12.91
BaO	BDL	1.16	0.04	BDL	0.88
AB	65.5	18.5	59.2	66.1	23.5
AN	33.5	0.0	39.8	32.7	76.5
OR	1.0	81.5	1.0	1.2	0.0
T_K[1]	940		1030		

[1] Two-feldspar equilibration temperature (in Kelvins) calculated using the formulation of Haselton et al. (1983)

6.2.3 BIOTITE

The dominant mafic mineral in all rocks is biotite. Representative analyses are listed in Table 6.3. The composition of biotite, like that of plagioclase, varies little throughout the major plutons. Ti, Al, Mn and Na contents remain approximately constant, both within a single sample, and between different samples. The parameter Mg/(Mg + Fe)[atomic] does vary, from 0.44 to 0.36. It tends to be slightly higher in the more mafic rocks (Fig. 6.3). The lack of an accommodating charge balance relationship, such as sympathetic variation in Ti or Al, suggests that the ratio $Fe^{3+}/(Fe^{2+} + Fe^{3+})$ remains relatively constant throughout these biotites.

These biotites have a substantial F content, some 1,500 to 6,000 ppm. This implies a rock F content of perhaps 200-500 ppm. Similarly, the biotite data suggest rock Cl contents of 20-50 ppm.

6.2.4 HORNBLENDE

The possibilities for substitution within the amphibole structure are enormous. Routine microprobe analysis is not capable of differentiating ferrous and ferric iron (Fe^{2+} and Fe^{3+}), nor of analysing for hydroxyl (OH^-). Thus, any recalculation of the microprobe analysis of a hornblende into a structural formula is model dependent. Tables 6.4 and 6.5 list typical hornblende compositions as determined by the electron microprobe. Three different models are used for calculating a structural formula from each analysis. They are all based on the generalized amphibole structural formula

TABLE 6.3

CALTECH MICROPROBE LABORATORY

ELECTRON MICROPROBE ANALYSES OF BIOTITES IN SAMPLES LTS 215,292
$(K,Na,Ca)_1\ (Mg,Fe^{2+},Fe^{3+},Ti,Mn,Al^{VI})_3\ (Si,Al^{IV})_4\ O_{10}\ (OH,F,Cl)_2$

WEIGHT PERCENT OF OXIDES

	LTS 215 Mafic tonalite		LTS 292 Low-K granodiorite	
SiO_2	35.59	36.26	36.29	35.93
TiO_2	3.45	3.21	2.45	3.12
Al_2O_3	15.00	15.55	16.15	15.51
FeO	21.31	21.87	22.92	22.45
MnO	0.26	0.33	0.36	0.40
MgO	9.07	8.92	8.27	7.21
CaO	BDL	BDL	BDL	BDL
Na_2O	0.08	0.11	0.05	0.09
K_2O	10.40	9.78	9.79	10.19
F	0.14	0.59	0.50	0.18
Cl	0.05	0.05	0.02	0.03
Total	95.28	96.41	96.58	95.03

NUMBER OF CATATOMS NORMALIZED TO 7.0

Si	2.849	2.856	2.855	2.910
Ti	0.208	0.190	0.145	0.190
Al	1.416	1.444	1.498	1.481
Fe	1.427	1.441	1.508	1.521
Mn	0.018	0.022	0.024	0.027
Mg	1.083	1.047	0.970	0.871
Na	0.012	0.017	0.008	0.014
K	1.062	0.983	0.983	1.053
F	0.035	0.147	0.124	0.046
Cl	0.007	0.007	0.003	0.004
Al^{IV}	1.151	1.144	1.145	1.090
Al^{VI}	0.265	0.300	0.353	0.391
Mg/(Mg+Fe)	0.431	0.421	0.391	0.364

Figure 6.3. Histograms of $Mg/(Mg + Fe^{2+} + Mn)$ for analyzed mafic minerals. Figures in brackets under sample numbers give rock SiO_2 contents (wt.%). 292 is a low-K granodiorite; 216 and 291 are mafic xenoliths from tonalites 215 and 290, respectively. All other samples are tonalites.

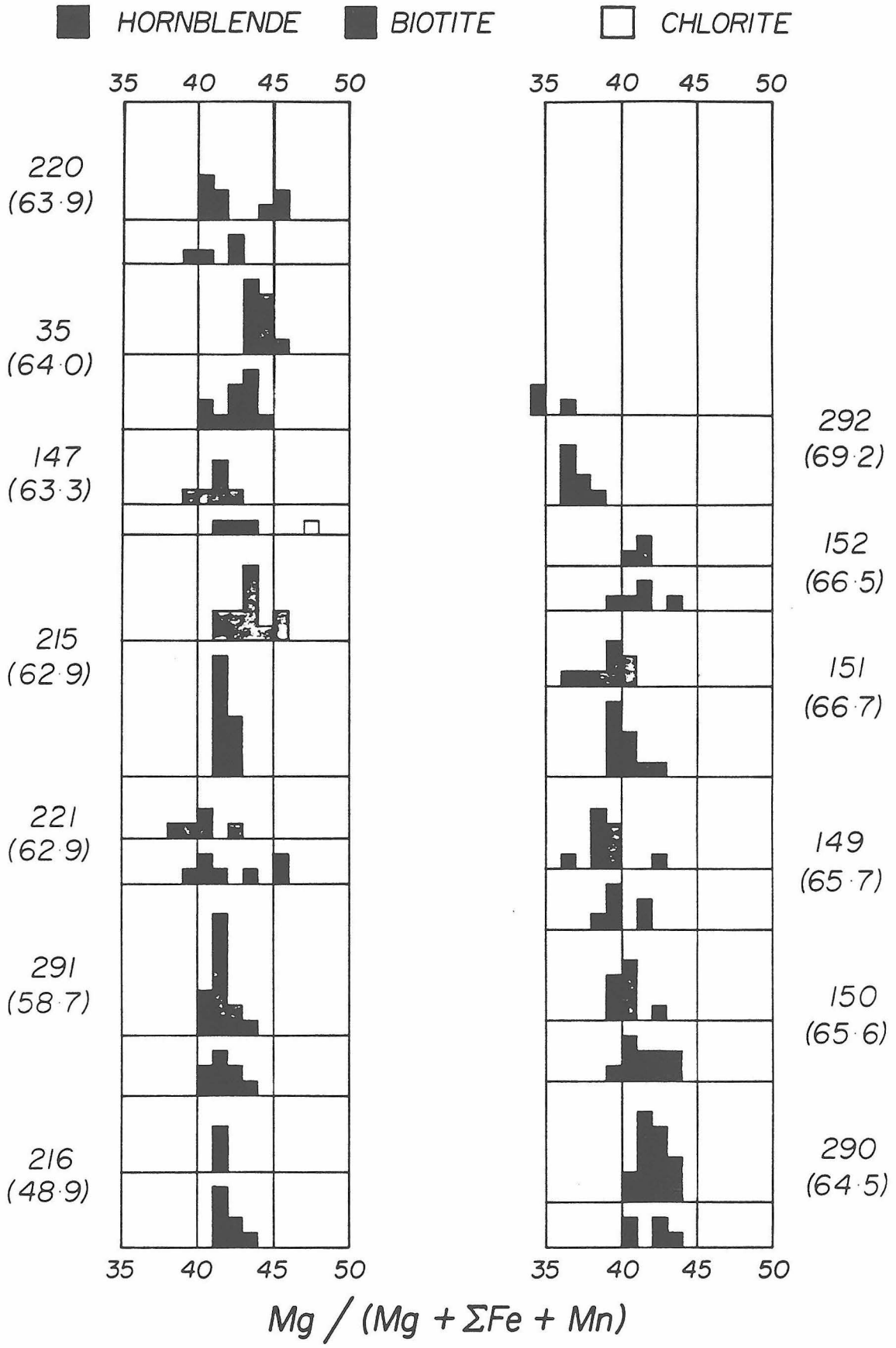
HORNBLENDE
BIOTITE
CHLORITE
35 40 45 50
220 (63·9)
35 (64·0)
147 (63·3)
215 (62·9)
221 (62·9)
291 (58·7)
216 (48·9)
292 (69·2)
152 (66·5)
151 (66·7)
149 (65·7)
150 (65·6)
290 (64·5)
Mg / (Mg + ΣFe + Mn)

$$A_{0-1}\ X_2\ Y_5\ Z_8\ O_{22}\ (OH)_2$$

where

A = Na, K

X [the M_4 site] = Na, Ca, Fe^{2+}, Mg, Mn

Y [M_1,M_2,M_3 sites] = Mg, Fe^{2+}, Fe^{3+}, Mn, Cr^{3+}, Al^{VI}, Ti^{4+}

Z [tetrahedral site] = Al^{VI}, Si

(OH) can be variously substituted for by halogens (F, Cl), or, in oxy-hornblendes, by O^{2-}.

The three normalizations used are:-

1. Cations - (Na + K) = 15 (assumes Na in M_4 = 0)
2. Cations - (K) = 15 (assumes Na in A = 0)
3. Cations - (Ca + Na + K) = 13 (assumes Fe,Mg,Mn in M_4 = 0)

The various normalizations assign an Fe^{2+}/Fe^{3+} by balancing cationic charges. In amphiboles from metamorphic environments it is often possible to differentiate between these various normalization schemes because it is impossible to obtain the necessary charge balance with some site occupancies (Laird, 1978). This is not the case for the majority of the San Jacinto analyses, where all three normalizations commonly result in correct charge balance (compare the calculated values for the parameters Al^{IV}NaM4 and A+2TiOC3 listed in Tables 6.4 and 6.5).

Co-existing hornblende and biotite from the Sierra Nevada batholith have similar $Fe^{3+}/(Fe^{2+}+ Fe^{3+})$ (Dodge and Ross, 1971). The similarity of the tonalites and granodiorites of the Sierra Nevada batholith to those of the present study, and the lack of correlation between amphibole and rock chemistry shown by the Sierran samples suggest that this relationship may hold for the San Jacinto rocks as well. If this is the

CALTECH MICROPROBE LABORATORY

ELECTRON MICROPROBE ANALYSES OF AMPHIBOLE IN SAMPLE LTS 215

$A\ X_2\ Y_5\ Z_8\ O_{22}\ (OH,F,Cl)_2$ [A=Na,K,Vacancy; X=Ca,Na,K,Mn; Y=Mg,Fe^{2+},Fe^{3+},Al^{VI},Ti,Mn,Cr; Z=Si,Al

	1.	2.	3.	4.
SiO_2	46.02	45.32	43.99	43.91
TiO_2	1.15	1.26	1.60	1.33
Al_2O_3	8.19	8.52	9.76	9.37
Cr_2O_3	BDL	NDL	NDL	0.06
FeO	19.36	19.30	20.09	19.99
MnO	0.44	0.46	0.41	0.42
MgO	9.21	9.16	8.25	8.74
CaO	10.30	10.96	11.90	10.56
Na_2O	1.11	1.20	1.32	1.33
K_2O	1.09	1.00	1.29	1.29
F	0.12	0.22	BDL	BDL
Cl	0.05	0.07	0.11	0.06
Total	96.98	97.39	98.72	97.05

(1) TOTAL CATIONS - (NA+K) = 15; (2) TOTAL CATIONS - K = 15; (3) TOTAL CATIONS - (NA+K+CA) = 13

	(1)	(2)	(3)	(1)	(2)	(3)	(1)	(2)	(3)	(1)	(2)	(3)
Si	7.053	6.901	6.889	6.917	6.757	6.809	6.670	6.502	6.636	6.760	6.586	6.629
Ti	0.133	0.130	0.130	0.145	0.141	0.142	0.183	0.178	0.182	0.154	0.150	0.151
Al	1.480	1.448	1.446	1.533	1.498	1.509	1.745	1.701	1.736	1.701	1.657	1.668
Cr	0.000	0.000	0.000	0.004	0.004	0.004	0.002	0.002	0.002	0.007	0.007	0.007
Fe	2.482	2.429	2.424	2.464	2.407	2.426	2.548	2.484	2.535	2.575	2.508	2.524
Mn	0.057	0.056	0.056	0.059	0.058	0.059	0.053	0.051	0.052	0.055	0.053	0.054
Mg	2.104	2.059	2.056	2.085	2.036	2.052	1.865	1.818	1.856	2.006	1.954	1.967
Ca	1.691	1.655	1.652	1.793	1.751	1.764	1.933	1.885	1.924	1.742	1.697	1.708
Na	0.330	0.323	0.322	0.355	0.347	0.350	0.388	0.378	0.386	0.397	0.387	0.389
K	0.213	0.209	0.208	0.195	0.190	0.192	0.250	0.243	0.248	0.253	0.247	0.248
F	0.058	0.057	0.057	0.106	0.104	0.105	0.000	0.000	0.000	0.000	0.000	0.000
Cl	0.013	0.013	0.013	0.018	0.018	0.018	0.028	0.028	0.028	0.016	0.015	0.015
OX	3.090	3.023	3.018	2.656	2.595	2.615	1.300	1.267	1.293	3.034	2.956	2.975
Fe^{3+}		0.605	0.683		0.858	0.515		1.072	0.144		1.004	0.712
Fe^{2+}	2.482	1.824	1.742	2.464	1.549	1.911	2.548	1.412	2.392	2.575	1.504	1.813
Al^{IV}	0.947	1.099	1.111	1.083	1.243	1.191	1.330	1.498	1.364	1.240	1.414	1.371
Al^{VI}	0.533	0.349	0.335	0.451	0.255	0.318	0.415	0.203	0.373	0.461	0.243	0.296
Na M4		0.323	0.322		0.347	0.236		0.378	0.076		0.387	0.292
A Na+K	0.543		0.183	0.550		0.306	0.638		0.558	0.650		0.346
Al^{IV}NaM4	0.947	1.422	1.433	1.083	1.590	1.427	1.330	1.876	1.440	1.240	1.801	1.663
A+2TiOC3	1.341	1.422	1.484	1.294	1.590	1.427	1.421	1.876	1.440	1.427	1.801	1.663
Na+K		0.532			0.537	0.542		0.621	0.634		0.634	0.637
Al^{VI}TiFe^{3+}		1.084			1.254	0.975		1.453	0.699		1.397	1.159
$Mg/Mg+Fe^{2+}$	0.433	0.557	0.513	0.452	0.559	0.510	0.418	0.554	0.432	0.433	0.557	0.513
Mg/Mg+ Fe	0.453	0.453	0.453	0.452	0.452	0.452	0.418	0.418	0.418	0.433	0.433	0.433
Fe^{3+}/ Fe		0.400			0.356	0.212		0.432	0.057		0.400	0.282

CALTECH MICROPROBE LABORATORY

ELECTRON MICROPROBE ANALYSES OF AMPHIBOLES FROM SAMPLE LTS 292

$A\ X_2\ Y_5\ Z_8\ O_{22}\ (OH,F,CL)_2$ [A=Na,K,Vacancy; X=Ca,Na,K,Mn; Y=Mg,Fe,Al,Ti,Mn,Cr; Z=Si,Al]

	1.	2.	3.
SiO_2	43.07	41.16	42.69
TiO_2	1.12	1.10	1.15
Al_2O_3	9.19	9.98	9.85
Cr_2O_3	0.05	0.03	BDL
FeO	21.94	22.65	22.71
MnO	0.59	0.57	0.56
MgO	7.31	6.96	6.93
CaO	11.52	11.55	11.57
Na_2O	1.24	1.32	1.23
K_2O	1.18	1.34	1.32
F	0.16	0.09	0.76
Cl	0.03	0.03	0.05
Total	97.33	96.74	98.49

(1) TOTAL CATIONS - (NA+K) = 15; (2) TOTAL CATIONS - K = 15; (3) TOTAL CATIONS - (NA+K+CA) = 13

	(1)	(2)	(3)	(1)	(2)	(3)	(1)	(2)	(3)
Si	6.668	6.507	6.623	6.434	6.267	6.402	6.576	6.41[9]	6.531
Ti	0.130	0.127	0.130	0.129	0.126	0.129	0.133	0.130	0.132
Al	1.678	1.637	1.666	1.839	1.792	1.830	1.789	1.746	1.777
Cr	0.006	0.006	0.006	0.004	0.004	0.004	0.000	0.000	0.000
Fe	2.842	2.773	2.822	2.962	2.885	2.947	2.927	2.857	2.906
Mn	0.077	0.076	0.077	0.075	0.074	0.075	0.073	0.071	0.073
Mg	1.687	1.647	1.676	1.622	1.580	1.614	1.592	1.554	1.581
Ca	1.911	1.865	1.898	1.935	1.884	1.925	1.910	1.864	1.897
Na	0.372	0.363	0.370	0.400	0.390	0.398	0.367	0.359	0.365
K	0.233	0.227	0.232	0.267	0.260	0.266	0.259	0.253	0.258
F	0.078	0.076	0.078	0.045	0.043	0.044	0.370	0.362	0.368
Cl	0.008	0.008	0.008	0.013	0.013	0.013	0.008	0.008	0.008
OX	2.762	2.695	2.744	3.405	3.316	3.388	1.553	1.516	1.543
Fe^{3+}	0.113	1.225	0.425	0.363	1.549	0.592	0.165	1.261	0.480
Fe^{2+}	2.728	1.548	2.397	2.598	1.336	2.355	2.762	1.596	2.426
Al^{IV}	1.332	1.493	1.377	1.566	1.733	1.598	1.424	1.581	1.469
Al^{VI}	0.346	0.144	0.289	0.273	0.058	0.232	0.365	0.165	0.308
Na M4		0.363	0.102		0.359	0.103		0.390	0.075
A Na+K	0.605		0.499	0.627		0.519	0.667		0.589
Al^{IV}Na M4	1.332	1.857	1.479	1.424	1.940	1.572	1.566	2.123	1.674
A+2Ti-OC3	1.332	1.857	1.479	1.424	1.940	1.572	1.566	2.123	1.674
Na+K	0.605	0.590	0.602	0.667	0.650	0.664	0.626	0.612	0.623
$Al^{VI}Fe^{3+}$Ti	0.589	1.496	0.844	0.765	1.733	0.953	0.663	1.556	0.920
$Mg/Mg+Fe^{2+}$	0.376	0.504	0.404	0.360	0.482	0.388	0.378	0.529	0.399
$Mg/Mg+\Sigma Fe$	0.366	0.366	0.366	0.348	0.348	0.348	0.347	0.347	0.347
$Fe^{3+}/\Sigma Fe$	0.040	0.442	0.151	0.056	0.441	0.165	0.123	0.537	0.201

case, the measured $Fe^{3+}/(Fe^{2+}+ Fe^{3+})$ for the rock must, by mass balance, approximate the $Fe^{3+}/(Fe^{2+}+ Fe^{3+})$ of both the hornblende and the biotite within that rock. This ratio falls in the range 0.03 to 0.41 for the San Jacinto rocks, with most samples having an $Fe^{3+}/(Fe^{2+}+ Fe^{3+})$ of 0.16 to 0.34. Accordingly, $Fe^{3+}/(Fe^{2+}+ Fe^{3+})$ of the amphiboles must be about 0.2 to 0.3.

On Figure 6.4 are plotted calculated $Fe^{3+}/(Fe^{2+}+ Fe^{3+})$ ratios for the amphiboles from two rocks as derived for the different normalization schemes. These two rocks - a mafic tonalite (LTS 290) and an included xenolith (LTS 291) - have quite different measured $Fe^{3+}/(Fe^{2+}+ Fe^{3+})$ of 0.22 and 0.33, respectively. For the tonalite it is often impossible to balance charges successfully if normalization 1 is used, implying that this model for the amphibole structural formula (no Na in M4) is not valid in this case. As expected from the rock $Fe^{3+}/(Fe^{2+}+ Fe^{3+})$, calculated $Fe^{3+}/(Fe^{2+}+ Fe^{3+})$ appears to be somewhat higher for amphiboles from the xenolith than the tonalite. These data are interpreted as showing that none of the ideal ordered structural assignments apply for these amphiboles, and that in the true structural formulae there is substantial sodium in the A site and (Fe^{2+},Mg,Mn) in the M4 site. The presence of some sodium in the M4 site is not excluded by these data.

These data also suggest that the amphiboles from the xenolith either contain more Fe^{3+} (compared to total Fe) than do the amphiboles from the tonalite, or contain more Na in the A site and less (Fe^{2+},Mg,Mn) in the M4 site than their tonalitic counterparts.

Figure 6.4. Histograms of $Fe^{3+}/(Fe^{2+} + Fe^{3+})$ for amphiboles from samples 290 and 291 showing effects of different amphibole structural formula calculations. Inverted triangles give $Fe^{3+}/(Fe^{2+} + Fe^{3+})$ of the host rock. Both rock 291 and its included hornblendes are more Fe^{3+}-rich than rock 290 or its included hornblendes.

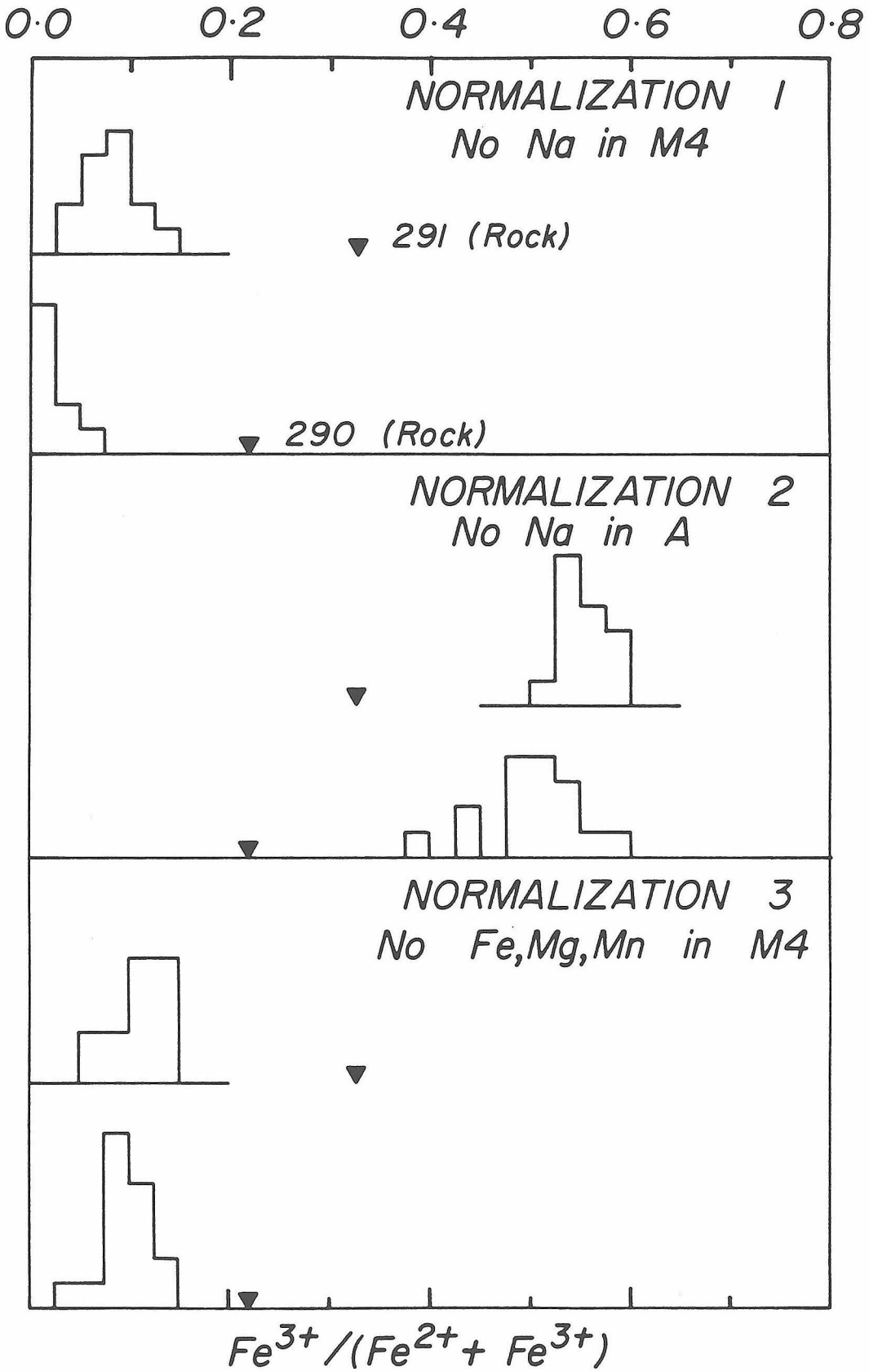
0·0
0·2
0·4
0·6
0·8
NORMALIZATION 1
No Na in M4
291 (Rock)
290 (Rock)
NORMALIZATION 2
No Na in A
NORMALIZATION 3
No Fe,Mg,Mn in M4
Fe3+/(Fe2+ + Fe3+)

Figure 6.5a. (Left) Al^{IV} versus (Na + K) for selected amphiboles from the San Jacinto Mountains, showing effects of different normalization schemes. Field for hornblendes from the Sierra Nevada batholith from Dodge et al., 1968

Figure 6.5b. (Right) Al^{IV} versus ($Al^{VI} + Fe^{3+} + Ti$). As above. "Probable San Jacinto field" combines all available amphibole data obtained in this study.

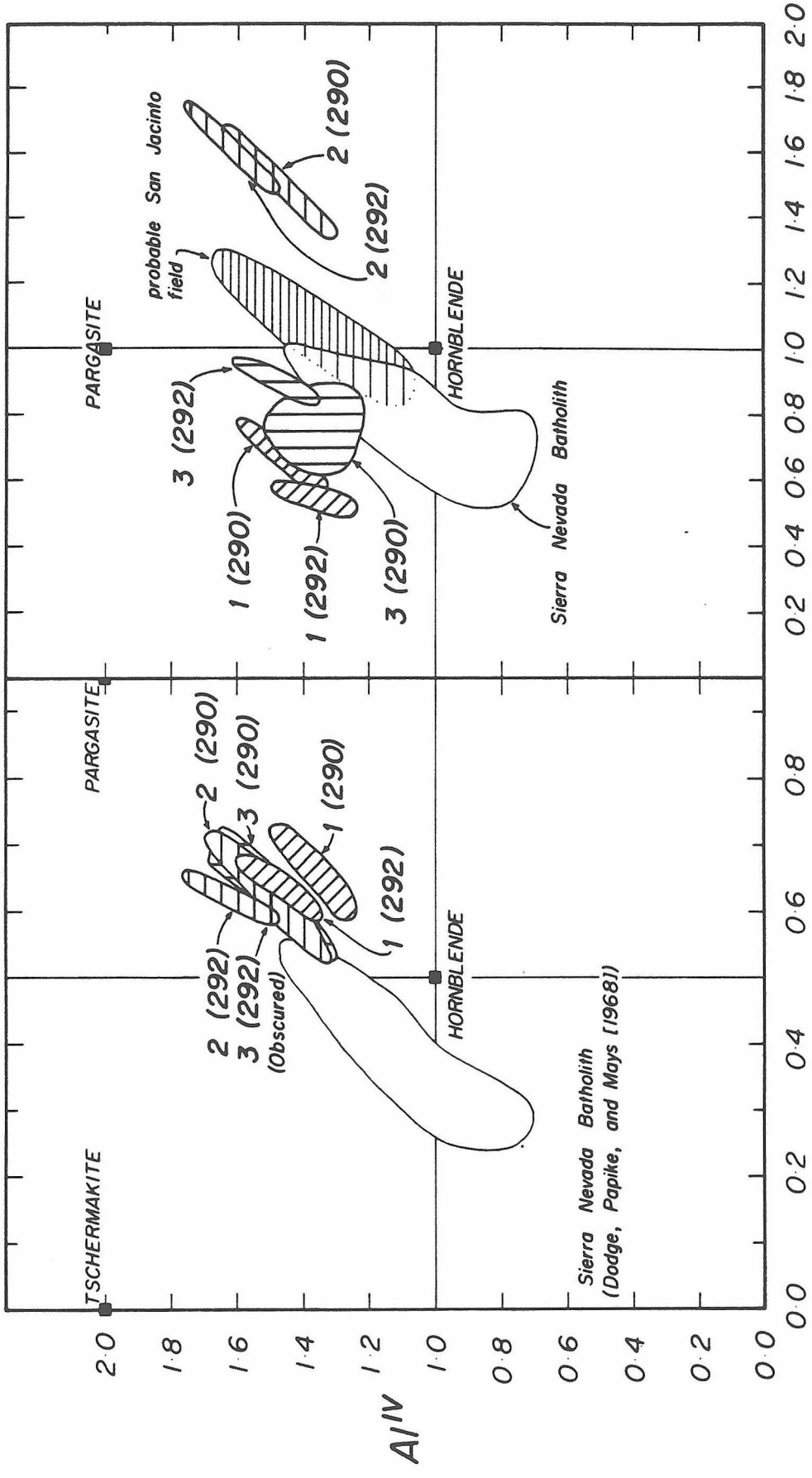
TSCHERMAKITE
PARGASITE
HORNBLENDE
PARGASITE
HORNBLENDE
Sierra Nevada Batholith
(Dodge, Papike, and Mays [1968])
2 (292)
3 (292)
(Obscured)
2 (290)
3 (290)
1 (290)
1 (292)
probable San Jacinto field
3 (292)
1 (290)
1 (292)
3 (290)
2 (292)
2 (290)
Sierra Nevada Batholith
Al^{IV}
$Al^{VI} + Fe^{3+} + Ti$
$Na + K$
0·0
0·2
0·4
0·6
0·8
1·0
1·2
1·4
1·6
1·8
2·0

Values of $Fe^{3+}/(Fe^{2+}+ Fe^{3+})$ of between 0.2 and 0.3 are intermediate between the $Fe^{3+}/(Fe^{2+}+ Fe^{3+})$ calculated from the microprobe analyses by normalizations 2 and 3 [no Na in the A site, and no (Fe,Mn,Mg) in the M4 site, respectively], implying that the actual cation site occupancies are intermediate between those assumed in the structural calculations. The effects of the different normalizations are compared on Figure 6.5.

Whatever the actual structural formulae, it is apparent that the major variation in the amphiboles from these rocks is the result of a coupled substitution involving Fe^{3+} in the octahedral site and Al^{3+} in the tetrahedral site. The sum Fe^{3+} + Ti + Al^{VI} probably varies from ≈0.7 to 1.3, with the bulk of this variation being in Fe^{3+} differences. Tetrahedrally co-ordinated aluminium (Al^{IV}) varies accordingly from about 1.1 to 1.7 cations per 24(O,OH).

If it is assumed that the actual structural assignments for these amphiboles are intermediate in site occupancy between Models 2 and 3 it is possible to make some estimate of variations in amphibole chemistry from rock to rock. Figure 6.5b compares the Al distribution [between tetrahedral (IV) and octahedral (VI) sites] for amphiboles from a tonalite and a granodiorite from Unit III. Sample LTS 290 is tonalite from near the northern margin of this pluton, and sample LTS 292 is a granodiorite from the relatively felsic core of the body. The variations within amphiboles from a single rock are more significant than the variations between rocks. Regardless of the normalization used, it is obvious that there are real variations within the chemistry of these amphiboles. Tetrahedrally co-ordinated Al varies by 0.4 formula units [per 24(O,OH)],

and there are corresponding changes in Na + K and in Al^{VI} + Ti + Fe^{3+}. There is some suggestion that the amphiboles in the more felsic rocks are more aluminous, with higher Al^{IV} and correspondingly higher Fe^{3+} (for charge balance); alternatively, the more felsic rocks might be considered to be more Fe^{3+} rich, with the increase in Al^{IV} the result of charge balance. Variations in Al^{VI} are smaller, and do not appear systematic.

Also shown on Fig. 6.5 is a probable field for the actual structural formulae of San Jacinto amphiboles estimated by comparison of model and rock $Fe^{3+}/(Fe^{2+} + Fe^{3+})$. This field is, of course, only an approximation, but is useful for comparative purposes. The San Jacinto amphiboles are hornblendes with considerable hastingsite component, and some tschermaks component in the most Al- and Fe^{3+}-rich samples. Total Al [per 24(O,OH)] varies from about 1.2 to 1.8 formula units.

The hornblendes from the San Jacinto Mountains are noticeably more aluminous and have higher octahedral (Al + Ti + Fe^{3+}) and higher (Na + K) than do the hornblendes from the Sierra Nevada batholith analysed by Dodge et al. (1968). This is consistent with suggestions (e.g., Dodge et al., 1968; de Albuquerque, 1975; Helz, 1979) that the amount of Al in hornblendes from calcalkaline rocks is a function of the temperature of formation, with the more aluminous hornblendes in general forming at higher temperatures. Dodge et al. (1968) suggest that some of their relatively low-Al hornblendes have equilibrated to lower temperature compositions during a later metamorphic event. A higher temperature of equilibration for the San Jacinto hornblendes (as compared to the Sierra Nevada batholith) is consistent with the different rock compositions

involved, the Sierra Nevada rocks being in particular more potassic than the K-poor San Jacinto ones.

Variation in the parameter Mg/(Mg + Σ Fe + Mn)[Mg number] is independent of normalization, but does not accurately reflect amphibole chemistry because it neglects changes in $Fe^{3+}/(Fe^{2+}+ Fe^{3+})$. Figure 6.6 summarizes the measured variation in Mg number (assuming all Fe is present as Fe^{2+}) for the analysed hornblendes. The Mg number thus calculated varies from 0.46 to 0.34. In the more mafic rocks the Mg number is between about 0.41 and 0.44; it falls to less than 0.4 in the intermediate rocks, and to around 0.35 in the most felsic rocks. Part of this variation could result from systematic variation of Fe^{3+} within these amphiboles, causing the variation in Mg/(Mg + Fe^{2+} + Mn) to be over-estimated where all the Fe is attributed to Fe^{2+}. A similar situation would arise if any fixed $Fe^{3+}/(Fe^{2+} + Fe^{3+})$ is used in the calculation, rather than the value of zero assumed above.

6.2.5 TITANITE (SPHENE)

A study of the rare earth element (REE) distribution between the various mineral phases of a granodiorite from the northern Peninsular Ranges batholith demonstrates that the two minor phases sphene and allanite together account for the bulk of the REE [in the studied rock (Gromet and Silver, 1983)]. A similar situation is likely to prevail for the rocks studied here; accordingly, an understanding of titanite and allanite paragenesis is critical to the interpretation of REE data obtained in the course of the present study. Titanite occurrence is probably very sensitive to variation in f_{O2} (e.g., Helz, 1973) as well as to other intensive chemical parameters such as the activity of silica, titanium

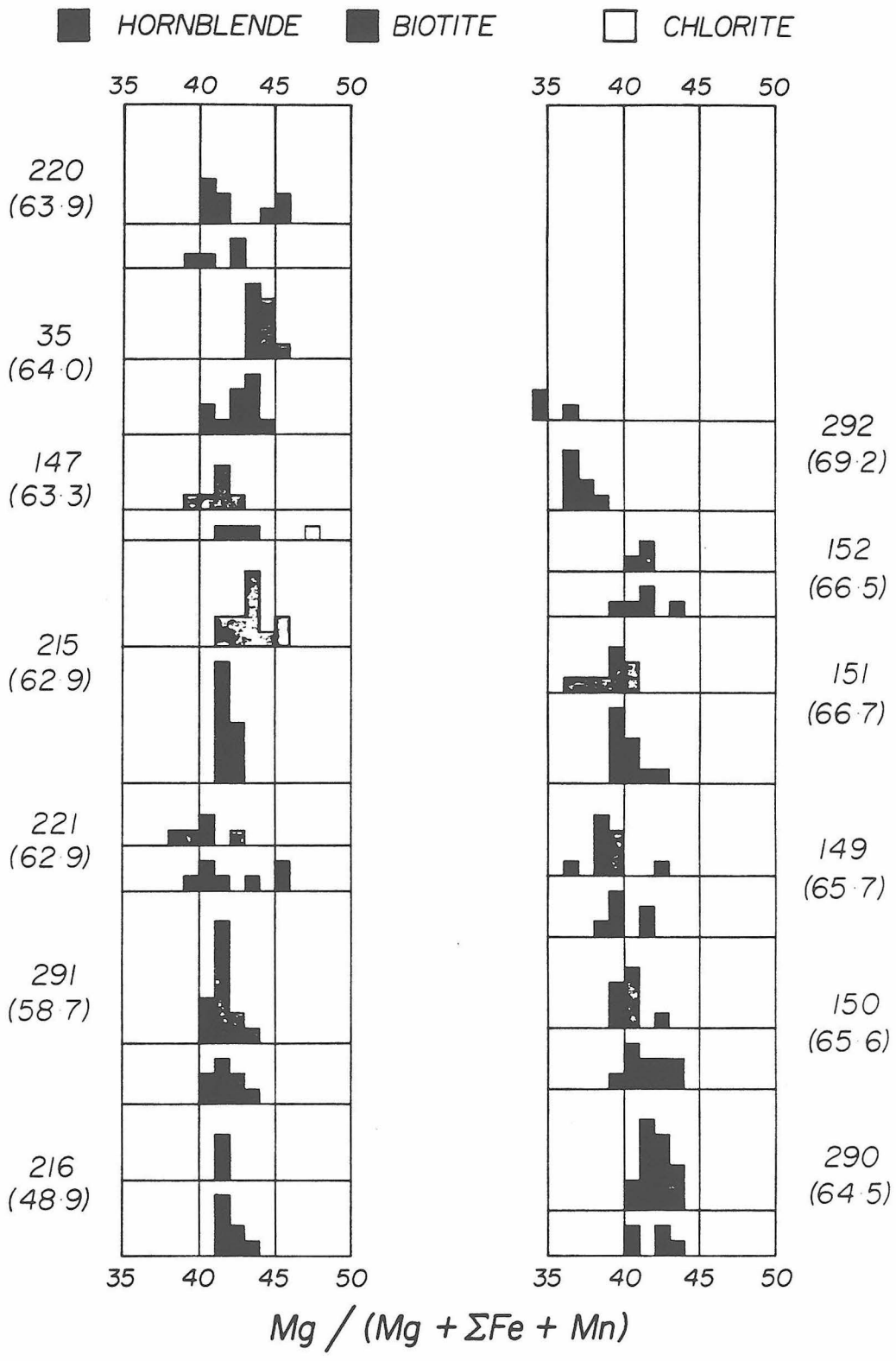

Figure 6.6. Mg/(Mg + ΣFe + Mn) for analysed hornblendes, biotites, and a single chlorite.

and calcium. Data on the behaviour of titanite during progressive solidification may thus hold information on the redox state of the magma from which it crystallized.

Table 6.6 lists typical analyses of titanites from the major tonalites, and a single analysis of titanite from the tonalite of Snow Creek (sample LTS 35). These analyses show considerable substitution of Al and Fe for Ti, up to 0.1 formula units. Some titanites, especially those from the more felsic rocks (e.g., LTS 292) show considerable F substitution for OH, again up to a maximum of about 0.1 formula unit. There appears to be no correlation between the two substitutions. The extent of these substitutions is shown on Figure 6.7. Sample LTS 292 is a low-K granodiorite from the center of Unit III; titanites from this sample have considerably higher fluorine contents than do titanites from the other rocks. There appear to be no chemical (and thus structural formulae) differences between titanites from the three major tonalite units.

6.2.6 ILMENITE

Opaque minerals are not common within the major tonalites; they comprise perhaps 0.02% by volume of the average rock (19 out of a total of over 85,000 counted points in thin sections from the three major tonalites were opaque minerals). Ilmenite was the only opaque mineral identified. The more mafic rocks contain slightly more opaque mineral than the more felsic rocks; the variation is from about 0.04 to <0.01% (by volume).

TABLE 6.6

CALTECH MICROPROBE LAB.

ELECTRON MICROPROBE ANALYSES OF TITANITE (SPHENE)

$CaTi[SiO_4](O,OH,F)$

WEIGHT PERCENT OF OXIDES

Sample:	810a	737a	737b	737c	738a	738b
SiO_2	30.18	30.22	30.02	30.92	30.57	30.49
TiO_2	36.50	36.33	36.31	36.43	36.23	35.84
Al_2O_3	1.78	1.27	1.03	1.33	1.69	2.09
FeO	0.70	0.82	0.77	0.89	1.16	1.33
MnO	0.04	0.17	0.08	0.16	0.07	0.06
MgO	n.d.	n.d.	n.d.	n.d.	n.d.	n.d.
CaO	28.56	28.28	28.64	29.47	28.57	28.63
Ce_2O_3	n.d.	0.29	0.04	n.d.	n.d.	n.d.
F	0.01	0.18	0.38	0.48	0.90	1.02
Total	97.77	97.51	97.11	99.48	98.81	99.03

NUMBER OF CATATOMS NORMALIZED TO 3.0

Ca	1.009	1.006	1.023	1.026	1.004	1.003
Ce	-	0.004	-	-	-	-
Ti	0.906	0.908	0.911	0.890	0.894	0.882
Al	0.069	0.050	0.040	0.051	0.065	0.081
Mg	-	-	-	-	-	-
Mn	0.001	0.005	0.002	0.004	0.002	0.002
Fe	0.019	0.023	0.021	0.024	0.032	0.036
Si	0.995	1.005	1.001	1.004	1.003	0.997
F	0.001	0.019	0.040	0.054	0.093	0.105

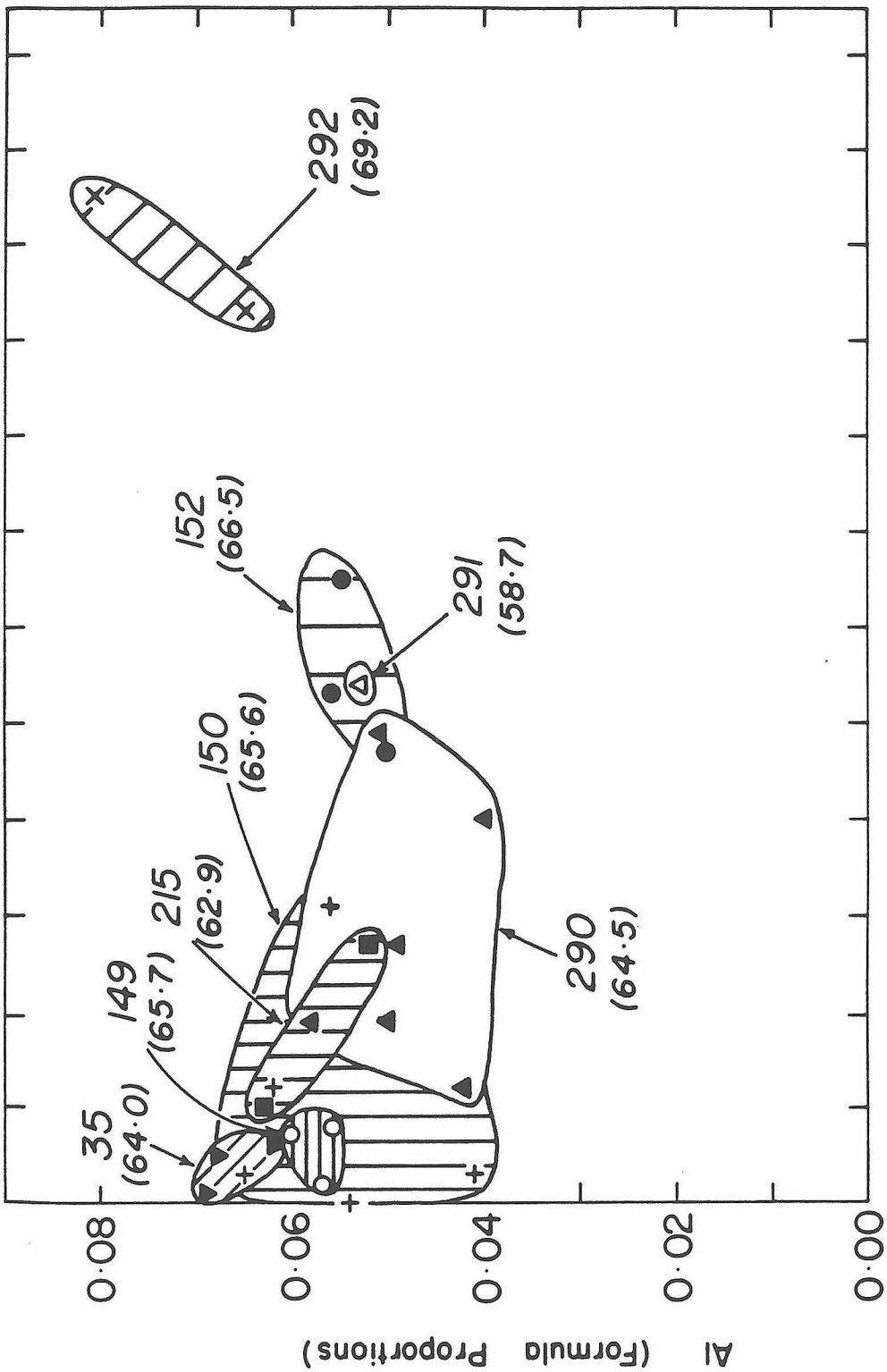

Figure 6.7. Structural Al versus F (formula proportions) for analysed titanites.

Ilmenite occurs most commonly as small equant inclusions within hornblende, biotite or titanite, and as more ragged irregular grains within titanite. Individual grains are seldom larger than 0.1 mm; most are much smaller. The remnants of probable large (millimeter-size) skeletal grains are rarely found within titanite; it appears that titanite has commonly either replaced or nucleated upon earlier ilmenite, or both. There does not appear to be any reaction between either hornblende or biotite and included ilmenite. Rarely ilmenite grains are included within other minerals.

In reflected light single grains of ilmenite appear homogeneous, lacking obvious exsolution textures.

This apparent homogeneity is seen in the analytical data. Thirteen microprobe analyses of ilmenite from four rocks are presented in Table 6.7. There is little variation in the composition of these analysed grains. Compositions range from $Il_{91}Py_8Hm_1$ to $Il_{88}Py_7Hm_5$; much of this apparent variation is not analytically significant. These data are plotted in the $(Mn,Fe)O-TiO_2-(Fe_2O_3)/2$ (Fig 6.8) and $(Mg,Mn)TiO_3-FeTiO_3-Fe^{2+}Fe^{3+}O_3$ (Fig. 6.9) triangular diagrams. Ilmenites from the most Mn-poor rock (Ch. 7) have the lowest pyrophanite contents; otherwise, there is no simple relationship between ilmenite composition and rock chemistry.

The presence of only one opaque oxide precludes the use of the magnetite-ilmenite geothermometer (Buddington and Lindsley, 1964) in any rigorous fashion on these rocks.

TABLE 6.7

CALTECH MICROPROBE LAB.

ELECTRON MICROPROBE ANALYSES OF ILMENITE - HAEMATITE

$Fe^{2+}TiO_3 - Fe^{2+}Fe^{3+}O_3$

WEIGHT PERCENT OF OXIDES

728e	728f	728g	732a	732b	737a	737b	724a	724b	728a	728b	728c	728d
0.07	0.06	0.12	0.20	0.16	0.06	0.11	0.14	0.10	0.05	0.10	0.08	0.07
50.97	50.91	51.24	50.52	52.35	50.62	49.81	49.10	49.17	51.71	51.59	51.76	50.74
n.d.	n.d.	n.d.	n.d.	n.d.	n.d.	n.d.	n.d.	n.d.	n.d.	n.d.	n.d.	n.d.
0.07	n.d.	n.d.	0.04	n.d.	n.d.	n.d.	0.02	n.d.	n.d.	0.04	n.d.	0.08
0.12	0.10	n.d.	0.06	n.d.	n.d.	0.04	0.03	0.16	0.01	n.d.	0.06	0.06
2.99	2.89	3.19	3.87	3.58	3.44	3.22	2.38	2.49	3.34	3.59	3.34	3.04
45.24	45.64	45.21	43.60	44.17	45.61	46.43	45.41	44.56	45.37	44.47	44.65	45.64
n.d.	n.d.	n.d.	0.02	0.08	n.d.	n.d.	0.05	0.07	n.d.	n.d.	n.d.	n.d.
n.d.	n.d.	n.d.	0.01	n.d.	n.d.	n.d.	0.02	n.d.	n.d.	n.d.	n.d.	n.d.
n.d.	n.d.	n.d.	0.18	0.03	n.d.	0.05	n.d.	n.d.	0.02	0.03	n.d.	n.d.
99.46	99.60	99.76	98.50	100.42	99.88	99.76	97.15	96.55	100.50	99.82	99.89	99.63
		NUMBER OF CATATOMS NORMALIZED TO 2.0						NUMBER OF CATATOMS NORMALIZED TO 2.0				
0.002	0.002	0.003	0.005	0.004	0.002	0.003	0.004	0.003	0.001	0.003	0.002	0.002
0.970	0.968	0.974	0.972	0.989	0.959	0.944	0.957	0.964	0.975	0.980	0.982	0.965
-	-	-	-	-	-	-	-	-	-	-	-	-
0.001	-	-	0.004	-	-	0.004	-	-	-	0.001	-	0.002
0.005	0.004	-	0.002	0.002	0.006	0.004	0.001	0.006	-	-	0.002	0.002
0.064	0.062	0.068	0.084	0.076	0.073	0.069	0.052	0.055	0.071	0.077	0.071	0.065
0.958	0.965	0.955	0.932	0.928	0.961	0.979	0.984	0.971	0.952	0.939	0.942	0.965
-	-	-	-	0.001	-	-	0.001	0.001	-	-	-	-
-	-	-	-	-	-	-	-	-	-	-	-	-
-	-	-	0.004	0.001	-	0.001	-	-	-	0.001	-	-
								MOLAR PERCENT				
0.453	0.377	-	0.230	0.188	0.563	0.377	0.116	0.623	0.037	-	0.226	0.226
6.422	6.193	6.837	8.424	7.637	7.344	6.891	5.239	5.507	7.102	7.695	7.145	6.520
90.327	90.303	90.672	88.995	91.333	88.053	87.378	90.611	90.439	90.487	90.500	90.954	89.878
2.798	3.127	2.491	2.351	0.843	4.037	5.355	4.034	3.431	2.374	1.804	1.675	3.376
3.486	3.337	3.461	4.378	3.929	4.035	3.733	2.733	3.119	3.612	3.883	3.717	3.431
45.804	45.869	45.908	45.027	45.860	44.934	44.891	46.238	46.009	45.787	45.662	45.861	45.710
1.419	1.588	1.261	1.190	0.423	2.061	2.751	2.058	1.746	1.201	0.910	0.844	1.717
49.291	49.206	49.369	49.405	49.788	48.969	48.624	48.971	49.127	49.399	49.545	49.578	49.141

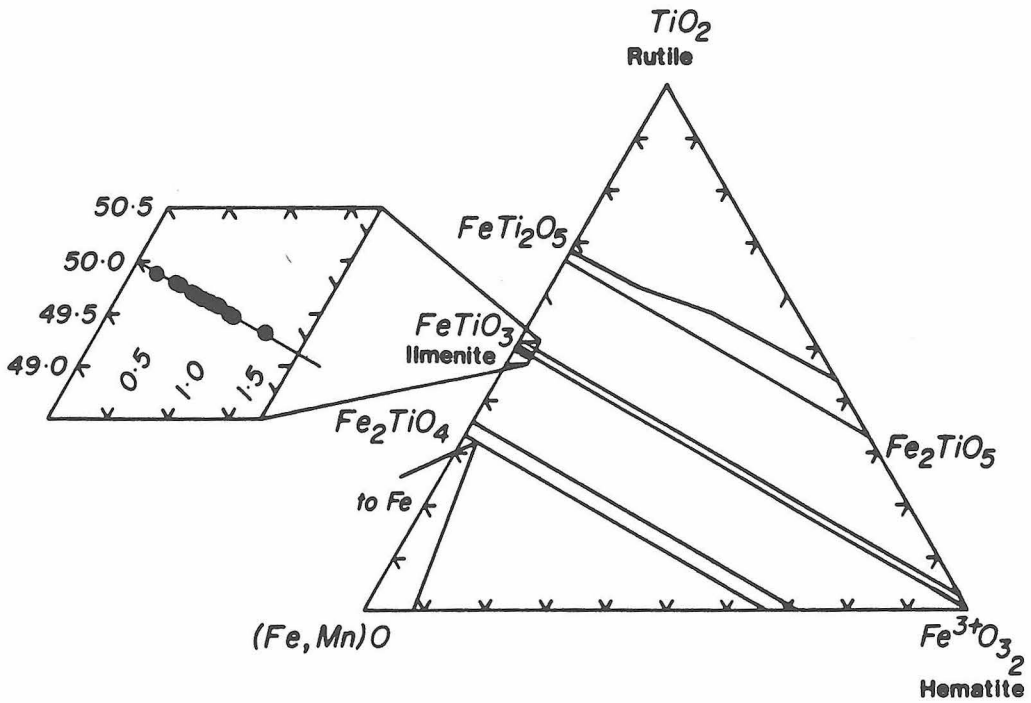

Figure 6.8. Ilmenite analyses plotted in the TiO_2-(Fe,Mn)O-$1/2Fe_2O_3$ triangle. Inset shows expanded scale.

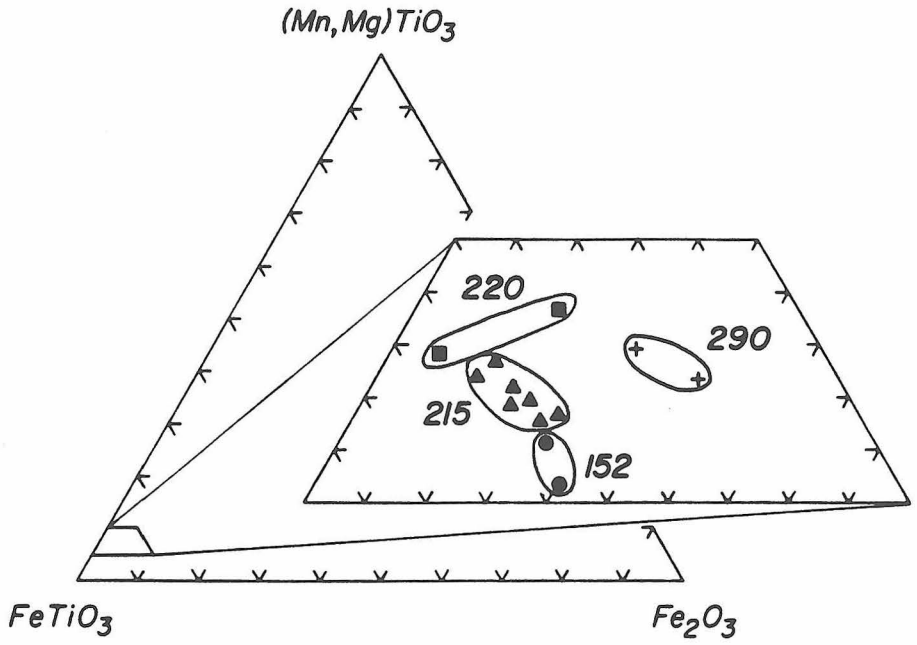

Figure 6.9. Ilmenite analyses plotted in the (Mn,Mg)TiO_3-$FeTiO_3$-Fe_2O_3 triangle. Inset shows expanded scale.

6.2.7 APATITE

Stubby apatite crystals to about 0.1 mm long are ubiquitous throughout the major tonalites. Mean abundance is about 0.15 vol.%; abundance varies from ≈0.3 vol.% in some of the more mafic tonalites to 0.1% or less in the most felsic rocks. Apatite is found as inclusions within all of the major mineral phases present: plagioclase, quartz, hornblende, biotite, K-feldspar and titanite. It is also rarely found surrounded by, or sharing crystal faces and apparently co-crystallizing with, ilmenite. Apatite comes early in the paragenesis of these rocks.

Seven analyses of apatite from four rocks are presented in Table 6.8. All analyses are of fluor-apatites; some have greater than the stoichiometric amount of fluorine for a fluor-apatite [$Ca_5(PO_4)_3F$], perhaps indicating the presence of a substantial carbonate-apatite component. Similar non-stoichiometry of apatites from the Lucerne pluton has been noted by Wones (1980), who suggested that it may result from subsolidus exchange of (F,OH) between apatite and other minerals, notably biotite during prolonged cooling or a later thermal event. Whatever the cause of this effect, it unfortunately precludes use of the apatite-biotite geothermometer (Carmichael and Stormer, 1971; Ludington, 1978) on the San Jacinto rocks.

These apatites may contain rare earth elements (REE) at the levels of a few hundred to perhaps a thousand parts per million (ppm). Routine microprobe determination of the REE at low abundance levels is problematical. The values reported here (Table 6.8) could be in error by as much as an order of magnitude (too high), or even be analytical artefacts caused by incorrect allowance for interference from other

TABLE 6.8

CALTECH MICROPROBE LAB.

ELECTRON MICROPROBE ANALYSES OF APATITE

$Ca_5 (PO_4,CO_3,OH)_3 (F,OH)$

WEIGHT PERCENT OF OXIDES

Sample:	715	723	728-1	728-2	728-3	728-4	737
SiO_2	0.24	0.15	0.28	0.18	0.17	0.20	0.24
Al_2O_3	n.d.	n.d.	n.d.	n.d.	n.d.	n.d.	n.d.
FeO	0.02	0.12	0.09	0.09	0.08	0.05	0.38
MgO	n.d.	n.d.	n.d.	n.d.	n.d.	n.d.	n.d.
CaO	52.40	55.63	56.57	57.16	56.35	56.32	58.41
Y_2O_3	n.d.	0.03	n.d.	0.02	0.06	n.d.	0.07
La_2O_3	0.05	0.05	0.06	0.07	0.01	0.10	0.06
Ce_2O_3	n.d.	0.23	0.28	0.17	0.33	0.37	0.26
Nd_2O_3	n.d.	0.14	0.22	0.23	0.14	n.d.	0.30
Na_2O	n.d.	n.d.	0.01	n.d.	n.d.	n.d.	n.d.
P_2O_5	41.27	41.74	41.55	40.77	40.58	40.17	40.80
F	4.75	5.80	4.10	3.59	4.31	4.74	3.78
Cl	0.05	0.02	0.05	0.03	0.03	0.03	n.d.
Total	96.77	101.51	101.47	100.79	100.24	99.98	102.71

NUMBER OF CATATOMS NORMALIZED TO 8.0

Ca	4.916	5.001	5.032	5.093	5.075	5.094	5.112
Si	0.021	0.013	0.023	0.015	0.014	0.017	0.020
Al	-	-	-	-	-	-	-
Fe	0.001	0.008	0.006	0.006	0.006	0.004	0.026
Mg	-	-	-	-	-	-	-
Na	-	-	0.002	-	-	-	-
Y	-	0.002	-	0.001	0.003	-	0.003
La	0.002	0.001	0.002	0.002	-	0.003	0.002
Ce	-	0.007	0.009	0.005	0.010	0.011	0.008
Nd	-	0.004	0.007	0.007	0.004	-	0.009
P	3.060	2.964	2.920	2.871	2.888	2.871	2.822
F	1.316	1.539	1.077	0.944	1.146	1.266	0.977
Cl	0.007	0.003	0.007	0.004	0.004	0.004	-

elements (J.A. Woodhead, personal communication, 1983). The apatite analyses may thus be indicating the presence of REE at about the detection limit of the microprobe in its normal operating mode; no importance should be attached to the reported values.

6.2.8 ALLANITE-EPIDOTE

Pleochroic allanite prisms as much as several millimeters in length are an uncommon but apparently ubiquitous component of the major tonalites. Average abundance is about 0.02 vol.%, and appears not to vary significantly from mafic to felsic rock types. It is notably more common in many of the earlier intrusives, however, where it may be as much as ten times more abundant than in the later major tonalites.

Table 6.9 presents analyses of epidotes from three rocks. Although Th is not determined, the low REE contents and high totals suggest that these analyses are of epidote rather than allanite. Much of the iron is apparently present as Fe^{3+}; in all analyses, the sum of Al and inferred Fe^{3+} is approximately 3.0. The three analyzed points are of either the outer parts of allanite grains, or of distinct epidote sheaths surrounding an allanite prism.

6.3 CONCLUSIONS

1. Plagioclase composition within these rocks (the major tonalites) is surprisingly constant. The total observed range in rocks is An_{44} to An_{25}; analyses from xenoliths extend this observed range to An_{47}. The range of mean plagioclase compositions estimated for each rock is even smaller, from perhaps An_{40} to An_{30}. This implies that relatively constant physico-chemical conditions prevailed throughout crystallization.

TABLE 6.9

CALTECH MICROPROBE LAB.

ELECTRON MICROPROBE ANALYSES OF ALLANITE EPIDOTE

$(Ca,REE,Th,Fe^{2+},Mn)_2\ (Al,Fe^{3+},Fe^{2+},Mn,Ti)_3\ Si_3\ O_{12}\ (O,OH,F)$

WEIGHT PERCENT OF OXIDES

Sample:	715	723	810
SiO_2	36.74	37.96	38.53
TiO_2	0.13	0.20	0.11
Al_2O_3	24.56	23.92	25.83
FeO	9.67	11.76	10.13
MnO	0.34	0.69	0.18
MgO	n.d.	0.02	0.01
CaO	20.89	22.32	22.76
Y_2O_3	n.d.	n.d.	n.d.
La_2O_3	n.d.	n.d.	n.d.
Ce_2O_3	0.16	n.d.	0.35
Nd_2O_3	n.d.	n.d.	n.d.
F	0.28	0.02	0.02
Total	92.65	96.89	97.46

NUMBER OF CATATOMS NORMALIZED TO 8.0

Ca	1.853	1.900	1.918
Y	-	-	-
La	-	-	-
Ce	0.005	-	0.010
Nd	-	-	-
Fe^{2+}	0.100	0.083	0.040
Al	2.398	2.241	2.354
Fe	0.570	0.699	0.627
Ti	0.008	0.012	0.006
Mn	0.024	0.046	0.012
Mg	-	0.002	0.001
Si	3.042	3.016	3.031
F	0.073	0.004	0.005

2. Calculated feldspar equilibration temperatures are low (≈ 400°C), suggesting considerable sub-solidus re-equilibration.

3. Biotites show a relatively limited range of composition. Mg/(Mg + Fe) varies from 0.44 to 0.36; Ti, Al, Mn and Na contents remain approximately constant.

4. Hornblendes also show a limited range of chemistry. Mg/(Mg + Fe) falls from 0.46 in the most mafic rocks analyzed to 0.34 in the most felsic. Part of this variation may be accommodated by systematic variation of $Fe^{3+}/(Fe^{2+} + Fe^{3+})$, so that the actual variation in $Mg/(Mg + Fe^{2+})$ may be even less than this. Within the limitations of the available data it appears that Al^{IV} varies by about 0.4 formula units, with corresponding changes in (Na+K), Al^{VI}, Ti and Fe^{3+}. Total Na+K varies from approximately 0.50 to 0.65 formula units; Ti varies from 0.12 to 0.18.

Given the wide range of substitutions possible (and common) within the amphibole structure, these data are interpreted as indicating a relatively constant physico-chemical environment throughout hornblende crystallization. The relatively aluminous nature of the San Jacinto hornblendes suggests crystallization at relatively high temperatures (cf. Sierra Nevada batholith).

5. Data from other minerals (titanite, allanite-epidote, ilmenite, apatite) show considerable chemical homogeneity within these accessory phases. The presence of only one opaque mineral (ilmenite), and apparent excess F in the apatite preclude use of the magnetite-ilmenite and biotite-apatite geothermometers for these rocks.

6. There is no systematic variation in titanite chemistry with textural relations. Titanites from a low-K granodiorite are more F-rich (as are biotite and hornblende) than those from tonalites.

CHAPTER 7

GEOCHEMISTRY

7.1 INTRODUCTION

The chemical composition of an igneous rock is a complex function of the chemistry of the source and the conditions under which partial fusion was accomplished, probably followed by extensive modification by processes operating during magma collection and transport, and during crystallization. Even so, study of the chemistry of granitic rocks has had tremendous influence on the development of current theories of granite (in the broadest sense) genesis (e.g., Larsen, 1948; Presnall and Bateman, 1973; Chappell and White, 1974; White and Chappell, 1977; Compston and Chappell, 1979; Collins et al., 1982). For example, Chappell and White (1974) demonstrated that the contrasting chemical characteristics of two major granitoid groups exposed in south-eastern Australia reflected source composition variations more or less directly. Granodiorites and tonalites interpreted to have been derived from a largely metasedimentary source have the geochemical characteritics [low Na/(Na + K), high Al/(Na + K + Ca), low $Fe^{3+}/(Fe^{2+} + Fe^{3+})$] expected for such rocks; in contrast, granodiorites and tonalites derived from a dominantly igneous protolith have the geochemical characteritics expected for these materials.

In western North America, the majority of rocks from the Cretaceous portion of the Sierra Nevada batholith are K-rich and Ca-poor relative to those from the Peninsular Ranges (e.g., Larsen, 1948; Bateman and Dodge, 1970; Presnall and Bateman, 1973; Silver et al., 1979). This systematic difference has been related to regional-scale variation in

the source regions from which the two batholiths were derived (e.g., Taylor and Silver, 1978). Because of suggestions that the igneous rocks of the San Jacinto - Santa Rosa Mountains block had chemical characteristics intermediate between those of the main Peninsular Ranges and Sierra Nevada batholiths (Baird et al., 1974a,b; Taylor and Silver, 1978), geochemical characterization of the San Jacinto igneous rocks was an important aim of this study.

7.2 ANALYTICAL PROCEDURES

A total of one hundred and four igneous rocks (including 6 xenoliths) and 11 metasedimentary rock samples from the San Jacinto Mountains have been analysed for 11 major and 19 trace cations, and for S, H_2O^+, H_2O^- and CO_2 by Dr. B.W. Chappell in his laboratory at the Australian National University, Canberra. In addition, REE data for two samples have been provided by 8 REE elements by Dr. L.P. Gromet at Brown University.

Approximately 500 gm of rock chips randomly selected from a larger sample were powdered in a tungsten-carbide lined Spex "Shatterbox". An aliquot of this powder was then analysed by the methods of Norrish and Hutton (1969) and Norrish and Chappell (1977). Major and minor elements (Si, Ti, Al, Fe, Mg, Mn, Ca, K, S, and P) were determined by X-ray fluorescence spectrometry of glass discs fused with lithium borate and doped with a La_2O_3 absorber (Norrish and Hutton, 1969). Hygroscopic water (H_2O^-) was determined by weight loss on heating at 110°C for two hours. H_2O^+ and CO_2 were determined by firing samples at 1200°C for 30 minutes in a stream of dry nitrogen followed by collection on P_2O_5 and "carbosorb" respectively. Ferrous iron was determined by titration of a

boric-sulphuric-phosphoric acid buffered solution with potassium dichromate following sample digestion in warm $HF-H_2SO_4$ in a closed Pt crucible. Na was determined by flame photometry of an acidic solution using a Li internal standard.

The trace elements (Ba, Rb, Sr, Pb, Th, U, Zr, Nb, Y, La, Ce, Nd, Sc, V, Cr, Mn, Ni, Cu, Zn and Ga) were determined by XRF spectrometry on pressed powder pellets (Norrish and Chappell, 1977) using directly measured absorption coefficients for the heavier elements. Corrections are made for non-linear backgrounds and inter-element interferences. Limits of detection for each element are as outlined by Norrish and Chappell (1977) and precision for most elements is estimated to be better than ± 5%. Duplicate analyses of one tonalite (LTS 152) are listed in Table 7.1. All components determined by XRF spectrometry agree to better than ± 5% except the trace elements La, Ce, and Nd. For most elements agreement is at the ± 2% level or better. Determination of Fe^{3+} and H_2O^+ is not as precise. Agreement of Na_2O, determined by flame photom etry, is excellent.

The REE determinations are by standard isotope dilution and mass spectrometry techniques. Details are given in Gromet (1979), except that sample dissolution was by $HF-HClO_4$ attack in a teflon bomb (Krogh, 1973). Values are believed accurate to ± 2%.

Most of the samples for which Rb and Sr concentrations were determined by XRF spectrometry have also had Rb and Sr determined by isotope disolution mass spectrometry (Ch. 9). Agreement for Sr is excellent, usually to better than ± 2%. Rb is not quite as good. Results obtained by the two techniques are compared in Appendix 5.

TABLE 7.1

COMPARISON OF DUPLICATE ANALYSES OF LTS 152

	1.	2.
SiO_2	66.08	66.95
TiO_2	0.69	0.71
Al_2O_3	16.73	16.35
Fe_2O_3	0.48	0.73
FeO	2.75	2.59
MnO	0.05	0.05
MgO	1.24	1.12
CaO	4.31	4.35
Na_2O	4.12	4.01
K_2O	2.06	1.99
P_2O_5	0.17	0.18
S	<0.02	<0.02
H_2O+	0.61	0.54
H_2O-	0.06	0.08
CO_2	0.10	0.12
rest	0.23	0.23
O=S		
Total	99.68	100.00
Ba	855	820
Rb	72	71
Sr	558	546
Pb	9.5	
Th	9.2	
U	2.2	
Zr	162	157
Nb	8.5	9.0
Y	9	10
La	19	24
Ce	41	52
Nd	14	18
Sc	6	
V	48	52
Cr	17	19
Mn	405	390
Ni	4.0	4.5
Cu	<0.5	<0.5
Zn	93	91
Ga	22.2	22.0

Comparison of Isotope Dilution and X-Ray Fluorescence Spectrometry

	Rb	Sr
XRF	71.5 ± 0.5	552 ± 6
I.D.	72.6	542.6

7.3 ANALYTICAL RESULTS

Chemical data are listed in Tables 7.2 through 7.15. The total range in SiO_2 for analysed igneous rocks from the San Jacinto Mountains is 45.1 to 73.7 weight percent and demonstrates the wide variation present in the rocks of this small area. Figure 7.1, a Harker diagram for K_2O, illustrates much of the observed range of chemistry for the San Jacinto rocks. The classification of volcanic rocks used is one modified somewhat from McKenzie and Chappell (1972) by Gill (1981). It is shown here for comparative purposes only; it cannot be proved that most of the San Jacinto rocks give liquid compositions. Unlike volcanic rocks, where it is often reasonable to assume that an analysis gives a liquid composition, the analyses of the San Jacinto rocks (and of plutonic rocks in general) are probably not of liquid compositions, but of solids crystallizing from an evolving liquid of generally unknown composition. Petrological considerations, particularly the consistent (though small) normal zoning of plagioclase feldspar, suggest that the liquid co-existing with any of the San Jacinto samples is probably in general more Si, Na and K rich than the (analysed) solid; the disparity, however, is probably not large enough to alter the general comparison between these plutonic rocks and calc-alkaline volcanic suites. Silver and Chappell (unpublished data) find that there is an almost complete chemical coherence between spatially related plutonic and volcanic suites from elsewhere in the batholith, supporting the use of plutonic-volcanic comparisons for these rocks (L.T. Silver, personal communication, 1983).

The more mafic rocks of the major tonalites approximate the composition of High-Si andesites.

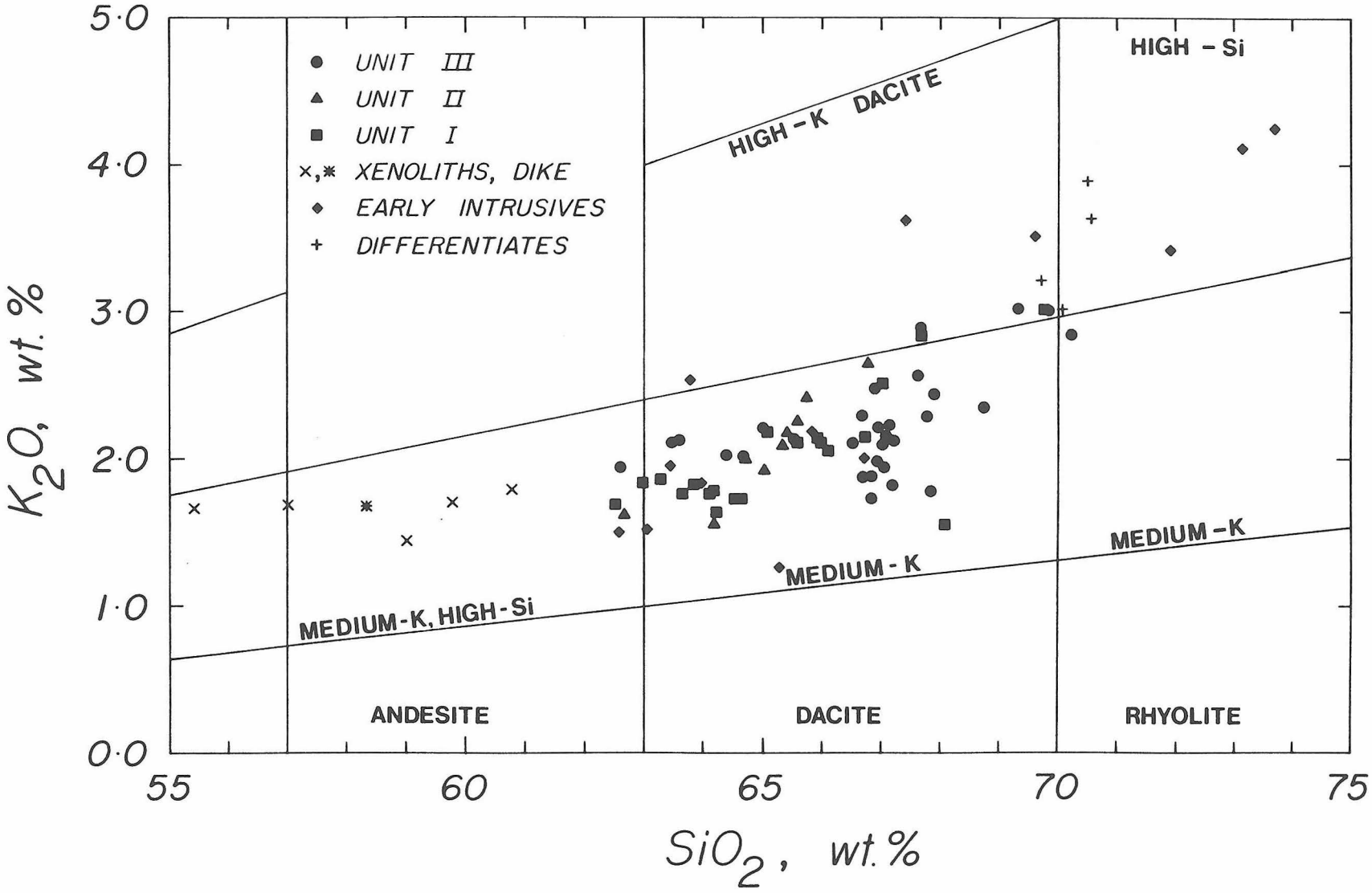

Figure 7.1. Harker diagram for K_2O. Andesite classification from Gill (1981).

TABLE 7.2

ANALYTICAL DATA FOR MAJOR TONALITE UNIT I

	LTS323	LTS215	LTS147	LTS319	LTS330	LTS220	LTS362	LTS325	LTS372	LTS324	LTS219
SiO_2	62.53	62.91	63.27	63.65	63.83	63.93	64.10	64.21	64.57	64.63	65.05
TiO_2	0.95	1.01	0.95	0.90	0.95	1.03	0.84	0.81	0.72	0.87	0.83
Al_2O_3	17.07	16.75	16.76	17.16	16.72	16.60	16.56	17.33	17.09	17.15	16.10
Fe_2O_3	1.55	0.89	0.90	0.86	1.33	0.85	1.32	0.62	0.31	0.63	1.32
FeO	3.11	3.76	3.59	3.29	2.98	3.23	2.87	3.25	3.06	2.91	2.67
MnO	0.07	0.07	0.06	0.06	0.07	0.06	0.06	0.07	0.06	0.06	0.06
MgO	1.79	1.84	1.74	1.63	1.64	1.59	1.53	1.58	1.39	1.44	1.43
CaO	5.46	5.51	5.27	5.40	5.29	5.40	5.04	5.18	5.05	5.23	4.62
Na_2O	3.85	3.72	3.83	3.91	3.77	3.82	3.79	4.08	4.19	3.99	3.76
K_2O	1.70	1.84	1.86	1.76	1.83	1.79	1.77	1.64	1.73	1.73	2.20
P_2O_5	0.23	0.24	0.22	0.21	0.22	0.22	0.20	0.21	0.19	0.20	0.20
S	<0.02	<0.02	<0.02	<0.02	<0.02	<0.02	<0.02	<0.02	<0.02	<0.02	<0.02
H_2O+	0.95	0.87	0.90	0.80	0.85	0.69	0.95	0.76	0.79	0.74	0.79
H_2O-	0.21	0.11	0.11	0.11	0.22	0.09	0.15	0.11	0.10	0.12	0.19
CO_2	0.10	0.10	0.21	0.09	0.05	0.05	0.12	0.10	0.27	0.17	0.34
rest	0.23	0.24	0.24	0.24	0.22	0.24	0.24	0.22	0.21	0.24	0.23
O=S											
Total	99.80	99.86	99.91	100.07	99.97	99.59	99.54	100.17	99.73	100.11	99.79
Ba	770	755	695	865	735	725	990	735	720	915	765
Rb	56	60	63	53	63	58	53	49	48	46	64
Sr	585	574	600	595	580	616	539	575	582	615	523
Pb	8	9	8	9	9	12	8	9	11	9	13
Th	6.2	8.2	10.4	5.6	4.4	10.0	13.0	9.5	8.0	10.0	10.6
U	1.8	1.6	1.8	1.2	1.6	2.2		2.2		1.4	2.4
Zr	191	189	200	177	196	187	166	134	150	152	199
Nb	9.5	11.5	10.5	10.0	11.5	13.5	13.0	9.5	8.0	10.0	12.5
Y	13	15	15	13	14	17	25	13	14	13	17
La	23	25	33	19	18	25	28	21	23	19	23
Ce	49	55	74	43	42	59	37	45	31	46	58
Nd		22	28			25					23
Sc	9	9	9	7	8	8	8	9	8	8	8
V	48	76	58	41	44	68	41	53	44	41	59
Cr	11	19	24	14	15	14	8	14	10	15	16
Mn	560	505	470	500	530	445	495	545	465	460	450
Ni	2	7	8	3	2	3	<1	1	<1	3	5
Cu	1	7	8	<1	2	1	<1	<1	<1	1	<1
Zn	118	109	114	106	106	101	106	107	98	98	104
Ga	22.8	22.8	23.0	22.4	22.0	22.6	21.2	21.8	21.6	21.4	22.8

TABLE 7.2 (CONTINUED)

ANALYTICAL DATA FOR MAJOR TONALITE UNIT I

	LTS150	LTS300	LTS299	LTS217	LTS321	LTS301	LTS361	LTS363	LTS218	LTS298	LTS322
SiO_2	65.57	65.66	65.69	66.11	66.11	66.56	67.67	68.07	69.44	69.56	70.06
TiO_2	0.72	0.74	0.75	0.68	0.66	0.66	0.61	0.56	0.49	0.46	0.49
Al_2O_3	16.70	16.57	16.43	15.65	16.57	16.28	15.44	15.72	14.93	15.28	15.22
Fe_2O_3	1.14	0.93	0.86	1.08	0.68	0.85	1.41	1.23	0.72	0.71	0.58
FeO	2.43	2.64	2.75	2.20	2.79	2.37	1.78	1.64	1.72	1.57	1.76
MnO	0.05	0.06	0.06	0.05	0.06	0.06	0.05	0.04	0.03	0.04	0.04
MgO	1.20	1.30	1.27	1.13	1.25	1.21	1.08	1.01	0.85	0.77	0.81
CaO	4.66	4.55	4.48	4.16	4.48	4.26	3.69	4.25	3.32	3.51	3.34
Na_2O	3.95	3.86	3.95	3.70	3.93	4.00	3.50	3.82	3.38	3.53	3.62
K_2O	2.12	2.16	2.14	2.48	2.15	2.17	2.84	1.56	3.25	3.01	3.06
P_2O_5	0.18	0.18	0.18	0.16	0.18	0.17	0.14	0.12	0.11	0.11	0.11
S	<0.02	<0.02	<0.02	<0.02	<0.02	<0.02	<0.02	<0.02	<0.02	<0.02	<0.02
H_2O+	0.75	0.92	0.62	0.77	0.64	0.68	0.84	0.87	0.63	0.46	0.51
H_2O-	0.05	0.13	0.15	0.17	0.11	0.07	0.19	0.16	0.13	0.16	0.07
CO_2	0.10	0.08	0.15	0.18	0.08	0.13	0.13	0.10	0.33	0.15	0.12
rest	0.22	0.23	0.20	0.26	0.21	0.19	0.24	0.20	0.31	0.31	0.22
O=S											
Total	99.84	100.01	99.68	98.78	99.90	99.66	99.61	99.35	99.64	99.63	100.01
Ba	740	805	585	1050	715	515	1065	730	1640	1685	970
Rb	69	80	68	92	78	78	94	48.5	89	74	91
Sr	560	560	503	503	550	505	493	552	513	521	426
Pb	9	12	10	13	12	12	14	8	15	11	15
Th	5.6	11.2	11.4	11.0	11.4	13.8			10.6	9.0	10.8
U	1.4	2.8	1.8	2.0	1.8	2.1			1.6	1.6	1.8
Zr	157	178	189	183	165	178	149	137	146	122	138
Nb	7.5	10.0	10.5	11.0	7.0	10.0	7.5	5.0	8.0	7.5	9.0
Y	10	13	16	14	7	12	8	4	8	7	13
La	18	21	27	23	31	23	34	52	23	20	19
Ce	38	47	62	56	59	49	34	55	48	41	40
Nd	7	18	23	21		17			14	11	
Sc	7	7	6	6	6	6	4	3	4	5	5
V	51	44	44	48	34	42	28	25	35	26	21
Cr	11	8	11	23	13	14	13	10	14	12	8
Mn	390	455	500	370	430	480	380	300	265	290	335
Ni	5	2	3	6	2	4	<1	<1	4	2	<1
Cu	1	3	2	1	<1	3	<1	5	1	9	<1
Zn	92	101	106	92	96	94	90	76	68	60	62
Ga	22.0	22.0	22.2	21.6	21.8	21.8	20.0	19.4	18.8	18.2	18.4

TABLE 7.3

ANALYTICAL DATA FOR TWO MAFIC XENOLITHS FROM MAJOR TONALITE UNIT I

	LTS216	LTS320
SiO_2	48.89	55.42
TiO_2	1.98	1.24
Al_2O_3	19.46	16.10
Fe_2O_3	2.04	1.48
FeO	7.32	7.05
MnO	0.13	0.16
MgO	3.56	4.29
CaO	6.80	7.58
Na_2O	4.13	3.21
K_2O	2.91	1.65
P_2O_5	0.44	0.22
S	<0.02	0.02
H_2O+	1.38	1.16
H_2O-	0.17	0.11
CO_2	0.12	0.15
rest	0.33	0.25
O=S		0.01
Total	99.66	100.18
Ba	1095	745
Rb	111	45
Sr	582	491
Pb	9	6
Th	3.0	0.2
U	1.0	<0.2
Zr	339	150
Nb	17.0	9.5
Y	26	24
La	16	12
Ce	40	41
Nd	26	
Sc	21	20
V	148	125
Cr	8	110
Mn	1015	1215
Ni	8	11
Cu	32	2
Zn	213	202
Ga	28.6	22.8

TABLE 7.4

ANALYTICAL DATA FOR MAJOR TONALITE UNIT II

	LTS148	LTS287	LTS329	LTS289	LTS368	LTS328	LTS326	LTS149	LTS327	LTS288
SiO_2	62.66	63.79	64.18	64.90	65.01	65.35	65.58	65.74	66.79	70.46
TiO_2	0.95	0.85	0.83	0.88	0.81	0.73	0.82	0.72	0.66	0.41
Al_2O_3	17.11	15.87	17.10	15.98	16.53	16.28	16.31	16.58	15.83	14.02
Fe_2O_3	0.88	0.80	0.64	0.96	0.85	1.40	0.76	0.64	0.54	0.70
FeO	3.73	3.13	3.20	3.12	2.79	2.73	3.05	2.87	3.17	1.18
MnO	0.06	0.06	0.06	0.08	0.06	0.07	0.06	0.05	0.07	0.03
MgO	2.12	1.52	1.58	1.59	1.33	1.32	1.38	1.29	1.16	0.69
CaO	5.52	4.67	5.24	4.81	4.85	4.55	4.61	4.48	4.01	3.05
Na_2O	3.87	3.81	4.00	3.59	4.03	3.79	3.75	3.91	3.06	3.23
K_2O	1.62	1.98	1.55	2.17	1.92	2.09	2.26	2.41	2.65	3.89
P_2O_5	0.22	0.19	0.20	0.21	0.19	0.18	0.18	0.18	0.16	0.09
S	<0.02	<0.02	<0.02	<0.02	<0.02	<0.02	<0.02	<0.02	<0.02	<0.02
H_2O+	0.71	1.03	0.82	0.93	0.79	0.87	0.75	0.60	0.65	0.53
H_2O-	0.03	0.14	0.13	0.13	0.15	0.21	0.14	0.08	0.08	0.21
CO_2	0.09	0.32	0.18	0.14	0.06	0.10	0.15	0.15	0.15	0.13
rest	0.25	0.23	0.22	0.24	0.23	0.20	0.24	0.22	0.21	0.37
O=S										
Total	99.82	98.39	100.01	99.73	99.60	99.87	100.04	99.92	99.99	99.79
Ba	930	750	760	830	780	695	940	815	846	2235
Rb	49	72	48	71	62	79	89	83	83	95
Sr	622	502	600	517	571	468	525	452	405	505
Pb	6	11	8	11	10	11	13	10	14	19
Th	5.4	11.8	6.0	11.4		9.2	11.4	9.8	8.4	9.4
U	0.8	2.8	1.2	2.4		2.0	3.6	2.4	2.2	1.6
Zr	178	180	174	180	185	174	180	186	179	107
Nb	12.5	14.0	8.0	13.0	11.0	10.5	10.5	10.0	9.5	8.5
Y	16	19	10	22	16	18	17	19	26	10
La	15	28	22	29	42	24	27	22	16	20
Ce	38	62	43	63	47	50	59	50	43	46
Nd	18	25		26				20		13
Sc	9	8	8	8	7	8	6	6	7	4
V	64	62	43	52	35	33	33	45	30	33
Cr	16	19	13	19	8	11	9	16	10	9
Mn	450	490	495	590	455	465	460	420	580	250
Ni	6	6	2	6	<1	2	1	5	<1	3
Cu	3	2	<1	2	<1	<1	<1	2	1	<1
Zn	110	107	108	102	99	100	98	85	85	55
Ga	23.4	23.0	22.0	21.2	21.8	20.6	20.8	21.2	19.4	17.4

TABLE 7.5

ANALYTICAL DATA FOR MAJOR TONALITE UNIT III

	LTS221	LTS376	LTS360	LTS290	LTS374	LTS369	LTS152	LTS335	LTS331	LTS151	LTS146
SiO_2	62.91	63.47	63.60	64.50	64.68	64.99	66.47	66.53	66.67	66.72	66.79
TiO_2	0.86	0.81	0.80	0.77	0.77	0.73	0.70	0.62	0.63	0.63	0.59
Al_2O_3	16.17	16.97	16.95	16.96	16.74	16.45	16.55	16.59	16.55	16.68	16.77
Fe_2O_3	1.37	0.71	0.81	0.85	0.65	0.94	0.52	0.90	0.60	0.56	0.74
FeO	3.45	3.17	3.27	2.88	3.06	2.76	2.67	2.27	2.56	2.62	2.41
MnO	0.07	0.06	0.06	0.07	0.06	0.06	0.05	0.05	0.06	0.05	0.05
MgO	2.05	1.48	1.44	1.44	1.43	1.42	1.22	1.13	1.13	1.12	1.07
CaO	5.40	5.00	4.89	4.82	4.84	4.18	4.32	4.35	4.19	4.37	4.17
Na_2O	3.48	4.00	3.96	4.03	3.98	3.81	4.07	4.04	3.99	4.23	4.07
K_2O	1.97	2.11	2.13	2.04	2.01	2.21	2.02	2.11	2.30	1.88	2.23
P_2O_5	0.16	0.20	0.20	0.19	0.20	0.20	0.17	0.16	0.17	0.16	0.16
S	<0.02	<0.02	<0.02	<0.02	<0.02	<0.02	<0.02	<0.02	<0.02	<0.02	<0.02
H_2O+	0.96	0.77	0.81	0.89	0.75	1.16	0.58	0.68	0.63	0.66	0.70
H_2O-	0.24	0.13	0.09	0.11	0.10	0.37	0.07	0.12	0.10	0.04	0.05
CO_2	0.16	0.14	0.09	0.19	0.07	0.12	0.11	0.07	0.11	0.08	0.08
rest	0.19	0.21	0.22	0.22	0.19	0.21	0.23	0.24	0.23	0.19	0.25
O=S											
Total	99.44	99.23	99.32	99.96	99.53	99.61	99.72	99.86	99.92	99.99	100.13
Ba	570	605	700	700	505	710	838	930	880	500	1025
Rb	80	78	75	82	83	90	72	64	67	72	67
Sr	432	566	575	579	518	501	552	570	545	547	550
Pb	12	11	12	12	12	11	11	11	11	8	9
Th	17.2			10.6			10.6	7.2	5.6	9.6	8.8
U	4.8			2.4			2.5	1.6	1.2	1.8	1.8
Zr	124	195	186	180	184	176	160	168	165	170	165
Nb	9.0	9.5	11.5	10.0	9.5	8.5	9.3	8.3	9.0	9.0	9.0
Y	13	11	21	11	14	12	10	13	13	14	14
La	23	40	26	23	51	39	22	21	21	22	20
Ce	44	38	31	49	51	35	47	43	45	48	46
Nd	14			17			16			18	16
Sc	8	8	8	7	7	7	6	6	6	6	5
V	83	41	42	51	40	37	50	28	29	42	36
Cr	12	10	10	13	9	9	18	12	12	10	10
Mn	580	500	500	540	480	475	398	420	430	380	355
Ni	6	<1	<1	3	<1	<1	5	<1	1	4	3
Cu	<1	2	<1	2	1	1	<1	<1	<1	<1	1
Zn	97	99	101	97	89	93	92	91	93	87	87
Ga	20.8	23.2	23.6	23.0	22.0	22.0	22.1	21.4	21.6	22.0	2.18

TABLE 7.5 (CONTINUED)

ANALYTICAL DATA FOR MAJOR TONALITE UNIT III

	LTS373	LTS370	LTS222	LTS371	LTS337	LTS336	LTS334	LTS333	LTS359	LTS375	LTS332
SiO_2	66.83	66.91	66.92	66.96	67.02	67.06	67.07	67.14	67.17	67.24	67.63
TiO_2	0.54	0.57	0.62	0.61	0.68	0.56	0.59	0.67	0.60	0.53	0.58
Al_2O_3	16.51	16.37	16.26	15.99	16.46	16.52	16.22	16.08	16.15	16.13	16.17
Fe_2O_3	0.32	0.85	1.32	0.60	0.59	0.50	0.58	0.69	0.55	0.58	0.64
FeO	2.47	2.16	1.97	2.41	2.49	2.41	2.81	2.66	2.58	2.38	2.26
MnO	0.05	0.05	0.05	0.05	0.06	0.05	0.05	0.06	0.05	0.05	0.05
MgO	0.97	1.01	1.11	1.12	1.10	1.06	1.19	1.22	1.10	1.03	1.04
CaO	4.20	3.96	4.26	4.20	4.29	4.28	4.12	4.15	4.13	4.18	3.92
Na_2O	4.04	4.06	4.17	3.98	4.02	4.01	3.89	3.87	3.95	3.89	3.90
K_2O	1.89	2.48	1.75	2.22	2.10	1.95	2.16	2.24	1.82	2.13	2.57
P_2O_5	0.15	0.15	0.17	0.15	0.16	0.16	0.17	0.16	0.15	0.13	0.14
S	<0.02	<0.02	<0.02	<0.02	<0.02	<0.02	<0.02	<0.02	<0.02	<0.02	<0.02
H_2O+	0.69	0.77	0.76	0.66	0.63	0.68	0.69	0.62	0.74	0.67	0.65
H_2O-	0.08	0.11	0.18	0.08	0.08	0.12	0.11	0.09	0.10	0.13	0.06
CO_2	0.14	0.11	0.22	0.13	0.03	0.17	0.15	0.07	0.11	0.10	0.11
rest	0.21	0.25	0.19	0.25	0.23	0.22	0.24	0.25	0.20	0.18	0.24
O=S											
Total	99.08	99.81	99.95	99.41	99.94	99.75	100.04	99.97	99.40	99.35	99.96
Ba	660	1085	435	1055	945	845	995	1060	680	600	1040
Rb	77	76	76	63	66	66	68	69	61	80	85
Sr	564	551	537	542	555	595	545	535	549	488	510
Pb	12	13	10	10	11	12	10	11	10	13	15
Th			11.2		6.6	6.0	8.4	7.0			8.2
U			1.6		2.4	1.4	1.2	1.6			1.8
Zr	186	174	174	171	159	158	161	175	1589	129	154
Nb	8.5	9.0	9.5	9.5	11.5	6.5	7.0	10.0	10.0	6.5	9.0
Y	12	11	12	15	23	8	6	15	13	7	12
La	38	44	23	44	16	14	28	20	40	37	19
Ce	42	46	52	49	40	32	54	44	42	39	42
Nd			18								
Sc	6	5	5	5	6	6	6	6	5	6	5
V	18	26	45	30	28	26	30	31	28	28	27
Cr	8	7	13	11	11	10	12	12	9	9	9
Mn	385	395	375	405	435	375	425	440	375	405	400
Ni	<1	<1	3	<1	1	<1	<1	1	<1	<1	<1
Cu	<1	<1	<1	<1	<1	<1	<1	<1	<1	<1	<1
Zn	94	92	97	88	91	90	95	95	96	75	84
Ga	21.8	21.2	22.8	20.4	20.8	20.4	20.8	20.8	22.2	19.8	20.8

TABLE 7.5 (CONTINUED)

ANALYTICAL DATA FOR MAJOR TONALITE UNIT III

	LTS366	LTS367	LTS145	LTS292	LTS365	LTS212	LTS358
SiO_2	67.68	67.79	67.90	69.16	69.83	70.11	70.57
TiO_2	0.52	0.56	0.56	0.44	0.40	0.45	0.40
Al_2O_3	15.99	15.63	15.41	15.51	14.95	15.02	14.79
Fe_2O_3	0.70	0.64	0.68	0.70	0.54	0.57	0.44
FeO	2.16	2.36	2.23	1.84	1.81	1.91	1.50
MnO	0.06	0.05	0.05	0.04	0.04	0.04	0.03
MgO	0.89	0.98	1.94	0.78	0.69	0.76	0.71
CaO	3.54	3.80	3.75	3.20	2.98	3.08	2.98
Na_2O	4.01	4.03	3.83	3.78	3.70	3.71	3.15
K_2O	2.90	2.29	2.44	3.05	3.04	2.86	3.64
P_2O_5	0.13	0.15	0.13	0.11	0.10	0.11	0.09
S	<0.02	<0.02	<0.02	<0.02	<0.02	<0.02	<0.02
H_2O+	0.64	0.76	0.74	0.76	0.64	0.64	0.63
H_2O-	0.09	0.16	0.04	0.09	0.08	0.10	0.13
CO_2	0.09	0.05	0.17	0.19	0.14	0.12	0.12
rest	0.24	0.22	0.25	0.27	0.24	0.27	0.31
O=S							
Total	99.64	99.47	100.12	99.92	99.18	99.75	99.49
Ba	1005	805	1130	1325	1125	1280	1805
Rb	98	73	69	79	78	82	80
Sr	469	487	520	505	443	479	518
Pb	14	10	10	13	13	13	14
Th			9.0	10.8		14.0	
U			1.4	1.4		1.4	
Zr	172	191	151	178	170	172	122
Nb	9.0	10.5	7.5	7.5	7.5	8.5	6.5
Y	11	16	12	8	8	8	6
La	49	48	20	22	51	26	35
Ce	52	51	45	48	56	57	33
Nd			15	15		18	
Sc	5	5	6	4	4	4	3
V	22	26	38	22	14	31	16
Cr	5	9	12	9	11	15	9
Mn	430	415	370	340	335	300	235
Ni	<1	<1	4	2	<1	5	<1
Cu	3	<1	1	<1	<1	<1	<1
Zn	86	94	82	83	78	68	45
Ga	20.8	20.6	20.2	19.8	19.2	19.8	16.6

TABLE 7.6

ANALYTICAL DATA FOR TWO MARGINAL (POSSIBLY ALTERED) SAMPLES FROM UNIT III

	LTS213	LTS297
SiO_2	67.65	68.65
TiO_2	0.53	0.51
Al_2O_3	16.45	15.70
Fe_2O_3	0.50	0.64
FeO	2.31	2.22
MnO	0.04	0.05
MgO	0.94	0.81
CaO	4.11	3.65
Na_2O	4.14	3.79
K_2O	1.80	2.36
P_2O_5	0.15	0.13
S	<0.02	<0.02
H_2O+	0.68	0.64
H_2O-	0.08	0.12
CO_2	0.18	0.23
rest	0.21	0.23
O=S		
Total	99.77	99.73
Ba	630	820
Rb	86	96
Sr	556	480
Pb	14	16
Th	12.0	16.0
U	4.8	4.2
Zr	183	243
Nb	10.0	9.5
Y	10	10
La	24	30
Ce	55	69
Nd	19	22
Sc	5	4
V	33	19
Cr	14	11
Mn	305	375
Ni	3	1
Cu	<1	<1
Zn	91	74
Ga	22.4	20.2

TABLE 7.7

ANALYTICAL DATA FOR FOUR MAFIC XENOLITHS FROM UNIT III

	LTS379	LTS291	LTS377	LTS378
SiO_2	57.02	58.70	59.77	60.79
TiO_2	1.45	1.41	1.26	1.18
Al_2O_3	16.55	17.18	17.38	17.01
Fe_2O_3	1.66	1.95	1.06	1.38
FeO	5.53	3.79	4.21	3.87
MnO	0.14	0.12	0.09	0.08
MgO	3.13	2.21	2.16	2.24
CaO	6.80	6.82	6.19	5.87
Na_2O	3.76	4.08	4.03	3.77
K_2O	1.69	1.45	1.71	1.79
P_2O_5	0.31	0.37	0.31	0.27
S	<0.02	<0.02	0.02	<0.02
H_2O+	1.12	0.98	1.01	1.08
H_2O-	0.11	0.19	0.14	0.20
CO_2	0.05	0.12	0.07	0.02
rest	0.20	0.21	0.26	0.26
O=S			0.01	
Total	99.52	99.58	99.66	99.81
Ba	390	375	795	820
Rb	78	64	65	69
Sr	482	590	672	652
Pb	9	11	8	7
Th		3.4		
U		0.8		
Zr	223	277	250	240
Nb	11.5	14.0	11.0	9.5
Y	19	22	16	14
La	35	11	43	54
Ce	30	32	48	50
Nd		21		
Sc	12	13	10	9
V	99	69	57	60
Cr	46	29	19	20
Mn	1060	915	660	600
Ni	6	7	1	2
Cu	14	14	11	10
Zn	173	136	127	127
Ga	22.8	23.8	23.8	23.2

TABLE 7.8

ANALYTICAL DATA FOR A MAFIC DIKE INTRUSIVE INTO UNIT III

	LTS214
SiO_2	58.36
TiO_2	1.31
Al_2O_3	18.29
Fe_2O_3	1.70
FeO	3.96
MnO	0.06
MgO	1.80
CaO	6.41
Na_2O	3.99
K_2O	1.65
P_2O_5	0.35
S	<0.02
H_2O+	0.93
H_2O-	0.26
CO_2	0.15
rest	0.33
O=S	
Total	99.55
Ba	1095
Rb	44.5
Sr	790
Pb	7
Th	7.2
U	0.4
Zr	390
Nb	14.5
Y	18
La	33
Ce	77
Nd	31
Sc	8
V	61
Cr	11
Mn	495
Ni	6
Cu	1
Zn	159
Ga	26.8

TABLE 7.9

ANALYTICAL DATA FOR THE TONALITE OF SNOW CREEK

	LTS302	LTS035
SiO_2	63.21	63.98
TiO_2	0.96	0.97
Al_2O_3	16.68	17.02
Fe_2O_3	1.58	0.84
FeO	2.67	3.66
MnO	0.07	0.06
MgO	1.61	1.66
CaO	5.14	5.27
Na_2O	3.74	3.81
K_2O	1.95	1.84
P_2O_5	0.21	0.24
S	<0.02	<0.02
H_2O+	1.26	0.70
H_2O-	0.25	0.04
CO_2	0.20	0.01
rest	0.27	0.24
O=S		
Total	99.80	100.84
Ba	940	830
Rb	61	50
Sr	630	603
Pb	11	11
Th	11.6	6.6
U	2.4	1.6
Zr	186	162
Nb	13.5	11.0
Y	28	20
La	33	25
Ce	82	58
Nd	38	24
Sc	8	8
V	55	57
Cr	12	10
Mn	520	455
Ni	4	4
Cu	2	2
Zn	109	93
Ga	22.0	21.4

TABLE 7.10

ANALYTICAL DATA FOR THE GRANODIORITE OF POPPET CREEK

	LTS317	LTS114
SiO_2	63.77	67.42
TiO_2	0.75	0.52
Al_2O_3	15.81	15.05
Fe_2O_3	0.81	0.87
FeO	4.07	2.80
MnO	0.08	0.07
MgO	2.39	1.60
CaO	5.17	3.71
Na_2O	3.07	3.09
K_2O	2.53	3.62
P_2O_5	0.12	0.09
S	<0.02	<0.02
H_2O+	0.89	0.72
H_2O-	0.16	0.14
CO_2	0.13	0.18
rest	0.20	0.20
O=S		
Total	99.95	100.08
Ba	775	805
Rb	98	137
Sr	284	232
Pb	11	18
Th	12.2	19.4
U	2.0	2.2
Zr	169	166
Nb	9.0	10.0
Y	25	20
La	21	
Ce	51	61
Nd		19
Sc	14	9
V	76	56
Cr	34	26
Mn	640	560
Ni	6	5
Cu	5	2
Zn	78	72
Ga	17.6	17.4

TABLE 7.11

ANALYTICAL DATA FOR SAMPLES FROM FIVE EARLY INTRUSIVES

	LTS381	LTS316	LTS211	LTS315	LTS382
SiO_2	62.59	53.04	68.91	69.61	73.12
TiO_2	0.85	0.82	0.44	0.40	0.24
Al_2O_3	17.43	17.64	15.12	15.07	13.52
Fe_2O_3	0.49	0.73	0.76	0.54	0.56
FeO	3.60	3.56	1.59	2.44	1.61
MnO	0.06	0.07	0.03	0.06	0.04
MgO	1.65	1.60	0.71	0.87	0.37
CaO	5.58	5.72	3.50	3.05	1.90
Na_2O	3.98	3.81	3.96	3.44	3.26
K_2O	1.50	1.56	1.78	3.52	4.12
P_2O_5	0.21	0.21	0.11	0.07	0.05
S	<0.02	<0.02	<0.02	<0.02	0.02
H_2O+	0.89	0.75	0.62	0.58	0.49
H_2O-	0.09	0.09	0.21	0.12	0.12
CO_2	0.20	0.11	0.06	0.14	0.19
rest	0.21	0.20	0.21	0.20	0.17
O=S					0.01
Total	99.33	99.92	98.01	100.11	99.77
Ba	690	680	660	940	885
Rb	46	51	71	113	92
Sr	627	545	535	227	142
Pb	7	9	10	13	10
Th		3.2	12.6	15.6	
U		1.2	3.4	1.4	
Zr	158	149	218	143	142
Nb	9.0	7.5	9.0	8.0	8.0
Y	12	11	11	13	13
La	23	10	29	29	38
Ce	26	25	65	56	51
Nd			22		
Sc	9	7	4	6	5
V	47	41	28	27	9
Cr	12	9	11	11	7
Mn	495	545	255	465	340
Ni	<1	1	4	<1	<1
Cu	<1	3	<1	<1	<1
Zn	106	102	69	61	43
Ga	22.0	22.0	21.6	16.6	15.8

TABLE 7.12

ANALYTICAL DATA FOR TWO SAMPLES FROM THE GRANITE OF PENROD CANYON

	LTS364	LTS318
SiO_2	71.92	73.70
TiO_2	0.19	0.09
Al_2O_3	14.94	14.61
Fe_2O_3	0.39	0.23
FeO	1.36	0.86
MnO	0.05	0.03
MgO	0.35	0.16
CaO	1.66	1.23
Na_2O	4.16	3.99
K_2O	3.42	4.25
P_2O_5	0.05	0.04
S	<0.02	<0.02
H_2O+	0.54	0.28
H_2O-	0.08	0.09
CO_2	0.15	0.09
rest	0.15	0.11
O=S		
Total	99.41	99.76
Ba	720	445
Rb	130	165
Sr	145	79
Pb	21	25
Th		6.8
U		1.6
Zr	107	71
Nb	12.0	11.5
Y	13	13
La	26	11
Ce	26	22
Nd		
Sc	4	3
V	2	<1
Cr	6	5
Mn	390	255
Ni	<1	<1
Cu	2	<1
Zn	66	52
Ga	17.4	18.0

TABLE 7.13

ANALYTICAL DATA FOR SAMPLES FROM EAST AND NORTHEAST OF TAHQUITZ ROCK

	RELATIVELY UNCONTAMINATED				DIFFERENTIATES		CONTAMINATED		
	LTS314	LTS293	LTS380	LTS311	LTS294	SCB744	LTS271	LTS383	LTS384
SiO_2	65.86	66.70	67.89	68.91	59.91	78.53	65.95	68.20	68.83
TiO_2	0.71	0.61	0.41	0.44	0.84	0.10	0.39	0.34	0.30
Al_2O_3	16.20	16.04	15.47	16.32	16.48	11.84	17.24	16.34	15.93
Fe_2O_3	0.73	0.59	0.63	0.35	1.07	0.18	0.60	0.96	0.61
FeO	3.28	3.33	3.43	2.66	5.99	0.56	3.59	3.06	2.97
MnO	0.07	0.08	0.09	0.05	0.18	0.02	0.03	0.17	0.13
MgO	1.27	1.21	0.39	0.55	1.80	0.14	0.29	0.29	0.21
CaO	4.43	3.54	3.35	3.44	3.92	1.64	3.57	3.05	3.02
Na_2O	3.82	4.35	4.42	4.87	3.77	3.07	4.66	4.50	4.30
K_2O	2.18	2.01	2.02	1.39	4.14	3.28	2.00	1.72	2.30
P_2O_5	0.10	0.12	0.11	0.04	0.20	0.03	0.08	0.05	0.06
S	<0.02	<0.02	<0.02	<0.02	<0.02	<0.02	<0.02	<0.02	<0.02
H_2O+	0.75	0.75	0.60	0.49	0.93	0.30	0.60	0.49	0.51
H_2O-	0.10	0.09	0.10	0.12	0.10	0.06	0.11	0.06	0.11
CO_2	0.19	0.16	0.06	0.18	0.21	0.06	0.10	0.08	0.18
rest	0.21	0.15	0.50	0.22	0.28	0.15	0.46	0.29	0.43
O=S									
Total	99.97	99.73	99.47	100.03	99.82	99.96	99.67	99.60	99.89
Ba	720	410	3135	785	1200	855	2490	1290	2545
Rb	81	108	38	52	151	83	76	55	62
Sr	465	267	314	288	249	193	321	248	282
Pb	11	11	8	9	16	16		15	9
Th	7.0	13.2		6.6	9.4	7.2	7.2		
U	1.8	1.8		1.0	1.2	1.2	2.2		
Zr	186	126	439	366	224	61	489	444	377
Nb	10.5	11.5	10.5	12.0	19.0	5.5	19.0	13.5	14.5
Y	16	12	22	9	60	8	21	54	30
La	18	21	89	39	17	8	71	99	112
Ce	34	46	91	80	48	18	163	104	118
Nd		15			24	6	58		
Sc	8	5	11	14	17	1	34	15	18
V	33	45	4	4	69	5	17	<1	<1
Cr	11	11	9	11	16	7	13	9	9
Mn	545	625	680	365	1360	125	235	1340	1045
Ni	1	4	<1	<1	4	<1	5	<1	<1
Cu	1	1	2	<1	1	5	1	<1	<1
Zn	98	103	94	109	164	18	123	68	91
Ga	20.8	21.0	20.2	23.4	23.8	17.8	23.6	21.0	19.8

TABLE 7.14

ANALYTICAL DATA FOR METASEDIMENTARY ROCKS, DESERT DIVIDE GROUP

	LTS308	LTS309	LTS310	LTS313	LTS312	LTS389
SiO_2	56.22	89.33	89.80	54.07	54.60	91.48
TiO_2	1.06	0.32	0.32	1.03	1.13	0.38
Al_2O_3	20.98	6.09	4.77	24.11	23.53	3.79
Fe_2O_3	2.17	0.26	0.34	1.76	1.73	0.09
FeO	5.38	1.19	0.94	7.13	6.59	1.00
MnO	0.07	0.02	0.02	0.07	0.07	0.01
MgO	2.37	0.42	0.36	2.81	2.51	0.28
CaO	0.22	0.86	0.54	0.49	0.46	0.74
Na_2O	1.33	1.58	1.25	1.44	1.57	0.91
K_2O	5.10	0.77	0.55	4.67	5.25	0.43
P_2O_5	0.08	0.01	0.02	0.09	0.10	0.01
S	0.95	<0.02	<0.02	<0.02	<0.02	<0.02
H_2O+	1.79	0.50	0.47	1.43	1.51	0.27
H_2O-	0.70	0.13	0.09	0.32	0.38	0.06
CO_2	2.02	0.14	0.12	0.19	0.21	0.06
rest	0.27	0.12	0.09	0.27	0.30	0.11
O=S	0.47					
Total	100.24	99.74	99.68	99.88	99.94	99.62
Ba	870	380	175	975	1175	140
Rb	129	34	27	183	193	19
Sr	114	78	59	119	121	60
Pb	37	7	5	6	9	5
Th	20.5	2.0	8.2	26.0	24.5	
U	3.6	3.2	2.8	3.8	4.2	
Zr	244	338	302	244	278	477
Nb	20.0	9.0	8.5	23.0	28.0	7.5
Y	46	4	8	26	43	9
La	51	5	15	55	59	36
Ce	114	14	33	118	121	53
Nd						
Sc	19	6	5	18	20	4
V	134	18	18	106	97	13
Cr	116	35	31	147	128	29
Mn	505	150	145	560	520	105
Ni	52	2	1	60	63	1
Cu	43	4	3	<1	2	<1
Zn	144	31	25	100	83	17
Ga	27.8	7.4	5.6	30.8	31.2	4.2

TABLE 7.15

ANALYTICAL DATA FOR METASEDIMENTARY ROCKS, WINDY POINT METAMORPHICS

	LTS386	LTS388	LTS385	LTS387
SiO_2	45.20	51.95	63.98	67.20
TiO_2	2.81	1.41	0.88	0.73
Al_2O_3	13.17	17.93	12.88	13.30
Fe_2O_3	1.21	2.25	3.25	1.64
FeO	8.34	6.60	2.05	3.25
MnO	0.14	0.19	0.08	0.05
MgO	8.85	4.30	3.21	2.16
CaO	11.96	7.35	2.38	5.03
Na_2O	1.58	2.39	1.90	0.52
K_2O	3.37	2.33	3.90	1.79
P_2O_5	0.53	0.24	0.19	0.18
S	<0.02	<0.02	0.03	0.28
H_2O+	1.55	1.68	1.52	1.56
H_2O-	0.19	0.39	0.41	0.50
CO_2	0.53	0.09	3.59	2.61
rest	0.29	0.26	0.52	0.33
O=S			0.01	0.14
Total	99.72	99.36	100.76	100.99
Ba	665	920	3140	1525
Rb	149	67	156	80
Sr	364	530	169	386
Pb	8	8	14	8
Th				
U				
Zr	198	141	207	171
Nb	61	8.5	15.5	17.0
Y	27	23	17	17
La	76	22	43	43
Ce	67	30	51	47
Nd				
Sc	24	20	18	17
V	187	155	189	136
Cr	162	15	128	101
Mn	1070	1475	635	425
Cu	141	21	39	49
Ni	8	9	42	46
Zn	150	136	189	119
Ga	18.8	20.8	17.4	16.8

7.3.1 MAJOR TONALITES

Major and minor elements

The three major tonalite units are chemically similar. SiO_2 in all three units varies from about 62.5 to 70.6 wt.%. Relationships between major elements are remarkably systematic. Figure 7.2 show Harker diagrams for selected major elements. Ti, Al, Fe, Mn, Mg, Ca and P all decrease linearly with increasing SiO_2. The trend for Mg, however, shows a break in slope at about 66-67 wt.% SiO_2. Na increases slightly with increasing SiO_2, then falls rapidly in the most felsic rocks. K shows considerable scatter, but with an approximate trend to increasing K as SiO_2 increases (Fig. 7.2).

Although all three units show a virtual overlap in chemical composition (but see below), the bulk composition of Unit III is both more felsic and more homogeneous than that of the other two units. Nearly 60% of the analyses of rocks from this unit (and probably a comparable or larger area of outcrop) show an extremely restricted range in SiO_2 of 66.5-68.0 wt.%. Only a relatively small proportion of the rocks sampled from the other two units (30%) have more than 66.5 % SiO_2, consistent with field observations that they are generally a little more mafic than Unit III. This is shown graphically on Figure 7.3. An SiO_2 value of 65.5 divides Units I and III into a relatively mafic and a more felsic group, and also appears to divide the rocks into two groups with some differences in trace element characteristics. An SiO_2 value of 65.5 is thus used to somewhat arbitrarily subdivide these samples into "mafic tonalites" and "normal tonalites".

Figure 7.2. Harker diagrams for selected major elements, major tonalite units. All data from Tables 7.2 - 7.8, except LTS 216.

Squares	-	Unit I
Triangles	-	Unit II
Circles	-	Unit III
Plus signs	-	Felsic differentiates
Crosses	-	Mafic xenoliths
Asterisk	-	Mafic dike intruding Unit III

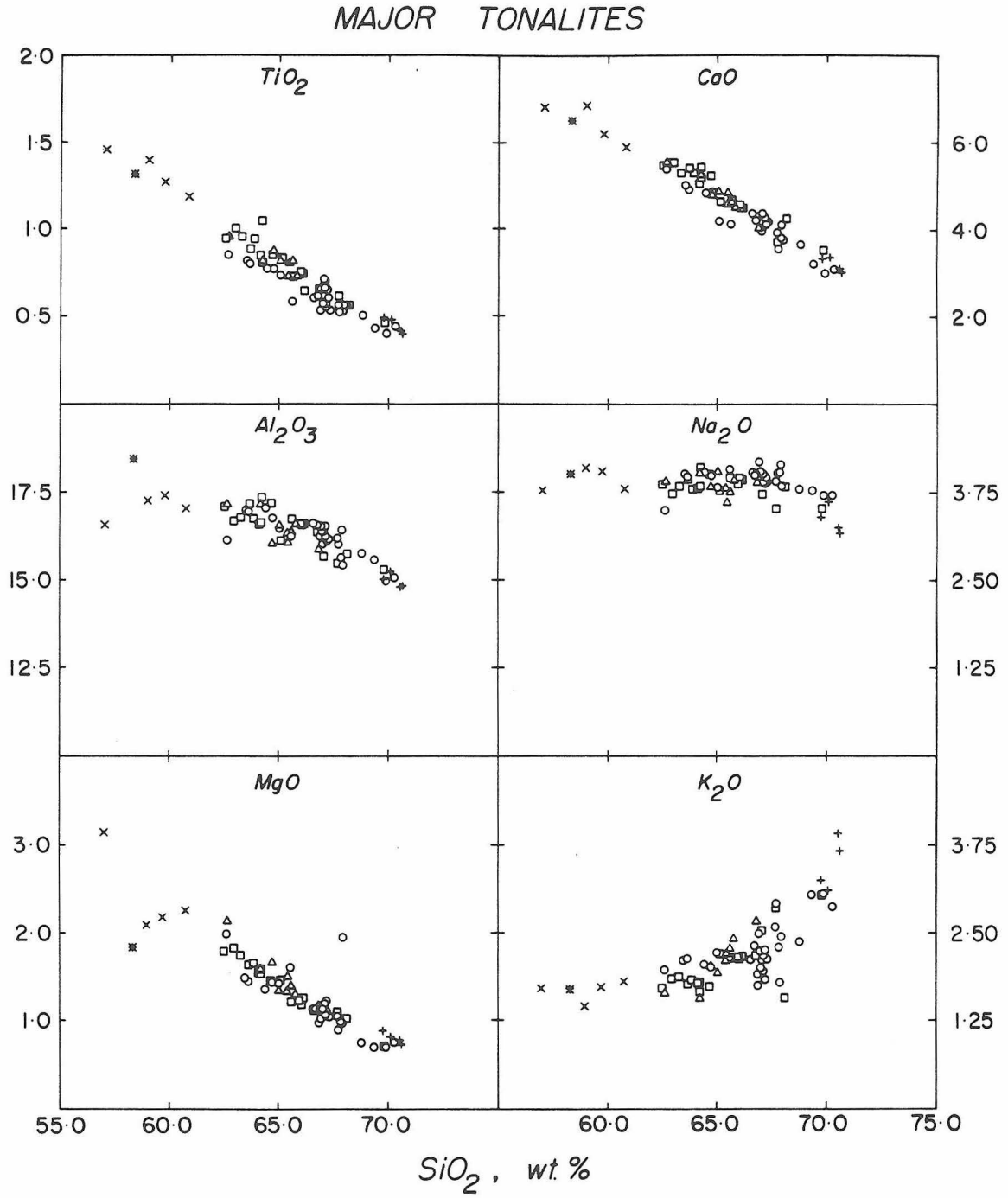
MAJOR TONALITES
TiO2
CaO
Al2O3
Na2O
MgO
K2O
2·0
1·5
1·0
0·5
6·0
4·0
2·0
17·5
15·0
12·5
3·75
2·50
1·25
3·0
2·0
1·0
3·75
2·50
1·25
55·0
60·0
65·0
70·0
60·0
65·0
70·0
75·0
SiO2, wt %

Figure 7.2

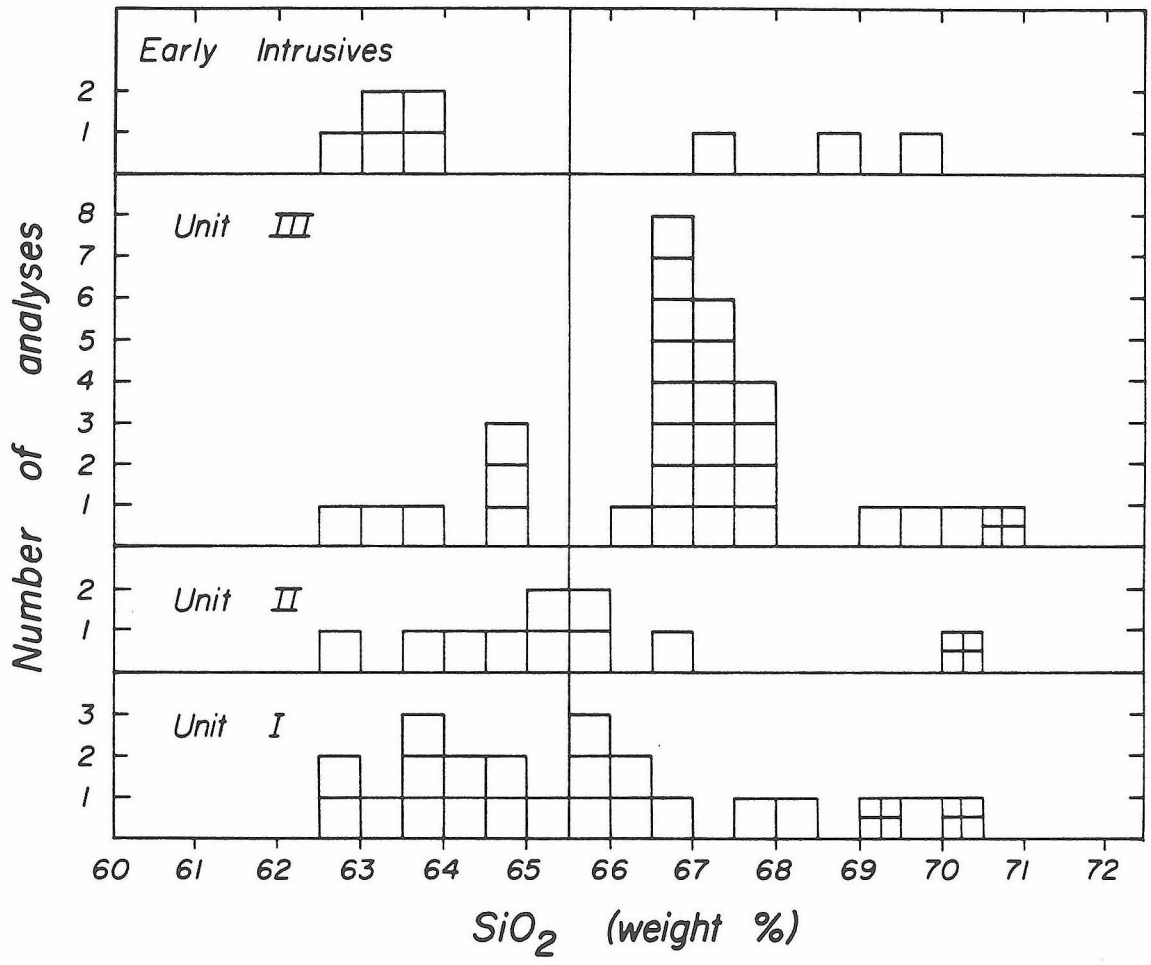

Figure 7.3. Histogram showing distribution of SiO_2 abundance, by unit.

In general, the three units show a near complete overlap in the ranges of their chemical compositions. There are, however, a few exceptions. Rocks from Unit III generally have slightly less TiO_2 and more Al_2O_3 and Na_2O for a given SiO_2 content than do rocks from Units I and II (Fig. 7.2); rocks from Unit III also show a much wider variation in K_2O content at a given SiO_2 than do rocks from the other two units. Some rocks from a restricted area of Unit III (the "Pine Cove salient" - samples 221, 374, 375, 376) have higher Mg, and lower Ti, Al, Ca, Na, and P at a particular SiO_2 than do other samples from this unit.

H_2O^+ correlates negatively with SiO_2, as would be predicted from the decreasing abundance of hydrous phases as the rocks become more felsic. Values fall from around 1.0 wt.% in the most mafic rocks to 0.5-0.6 wt.% in the most felsic. Burnham (1979) estimates that a minimum of 3.0 wt.% H_2O in the liquid is needed before amphibole will crystallize. As amphibole is a stable phase in all of these rocks, it is implied that a considerable amount of water has been lost from the system during crystallization. Although F and Cl abundances were not determined for these samples, mineral chemical data (Ch. 6) and mineral abundances imply approximate F contents of 0.3 to 0.05 wt.%, and very approximate Cl contents of 70 to 20 ppm. Both fluorine and chlorine abundances are inferred to fall sharply in the more felsic rocks, and the F and Cl contents of minerals (biotite and hornblende) in the most mafic rocks are very approximately 5 and 2 times (respectively) those of minerals in the most felsic rocks (Ch. 6, Tables 6.3 and 6.4).

These mineral data suggest that F and Cl abundances were lower in the more SiO_2-rich melts, implying either substantial loss of a halo-

gen-bearing liquid (such as an aqueous fluid), or by removal of F and Cl from the melt through incorporation in mineral phases (hornblende, biotite, apatite, titanite).

Trace elements

Trace element correlations with SiO_2 show much more complex variation patterns than do the more abundant components (Figs. 7.4-7.6).

- Ba, Rb, Pb, and Th show a general tendency to increase with SiO_2;
- Sr, Zr decrease slightly, while
- Sc, V, Cr, Zn, and Ga show a pronounced linear decrease with increasing SiO_2.
- U, Nb, Y, La, Ce, Nd, Ni, Cu show no systematic variation with changing SiO_2.

These variations are similar to those observed in many other calc-alkaline rock suites (e.g., Bateman and Chappell, 1979; Gill, 1981).

Trace element abundance patterns are often discussed in terms of geochemically similar behaviour and this approach has considerable value in mafic and intermediate rock types (e.g., Gill, 1981). However, in more felsic rocks elements that show geochemical coherence in more mafic compositions may show considerable fractionation because of the appearance of incompatible-containing phases such as biotite, K-feldspar, apatite, zircon, titanite and allanite. Biotite, for instance, is capable of considerable fractionation of K from Rb; K-feldspar can efficiently separate Ba from Sr, and if zircon is a precipitating phase Zr need not increase in late-stage liquids. Accordingly, the trace element data will be discussed below in terms of the mineral phases likely to be

Figures 7.4 - 7.6. Harker diagrams for selected trace elements.

Squares	-	Unit I
Triangles	-	Unit II
Circles	-	Unit III
Plus signs	-	Felsic differentiates
Crosses	-	Mafic xenoliths
Asterisk	-	Mafic dike intruding Unit III

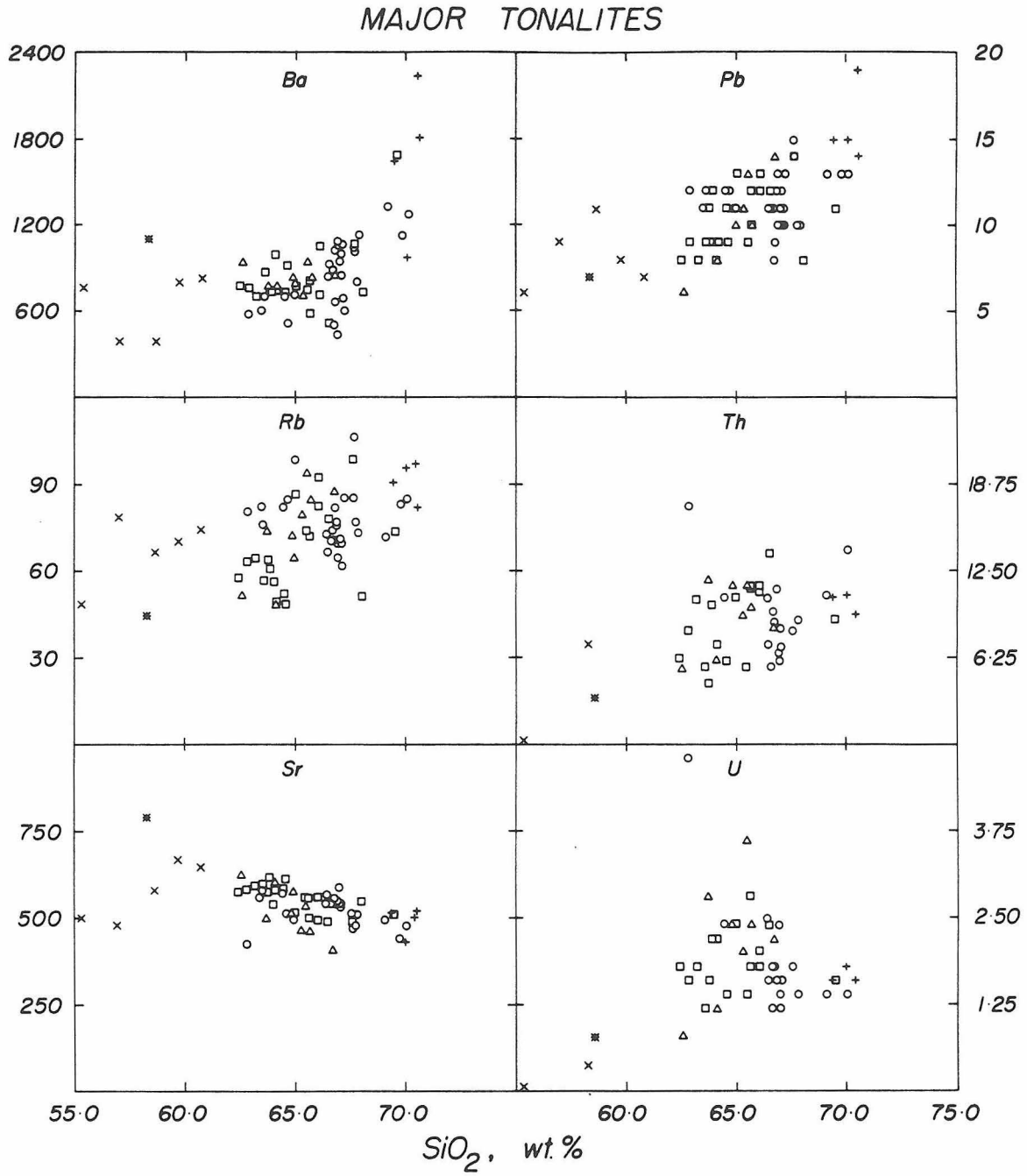
MAJOR TONALITES
Ba
Pb
Rb
Th
Sr
U
2400
1800
1200
600
20
15
10
5
90
60
30
18·75
12·50
6·25
750
500
250
3·75
2·50
1·25
55·0
60·0
65·0
70·0
75·0
SiO2, wt.%

Figure 7.4.

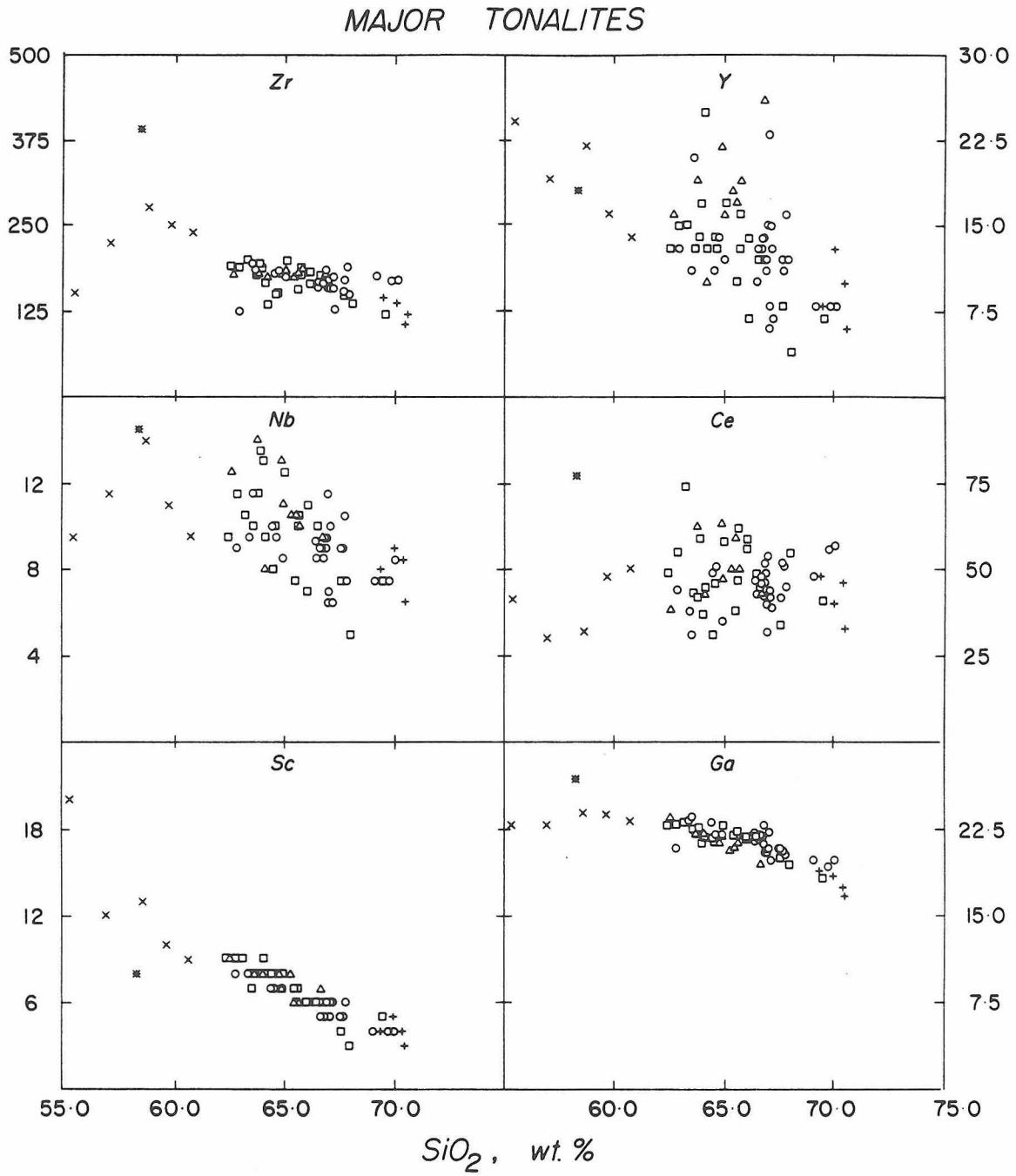
MAJOR TONALITES
Zr
Y
Nb
Ce
Sc
Ga
500
375
250
125
30·0
22·5
15·0
7·5
12
8
4
75
50
25
18
12
6
22·5
15·0
7·5
55·0
60·0
65·0
70·0
60·0
65·0
70·0
75·0
SiO2, wt. %

Figure 7.5.

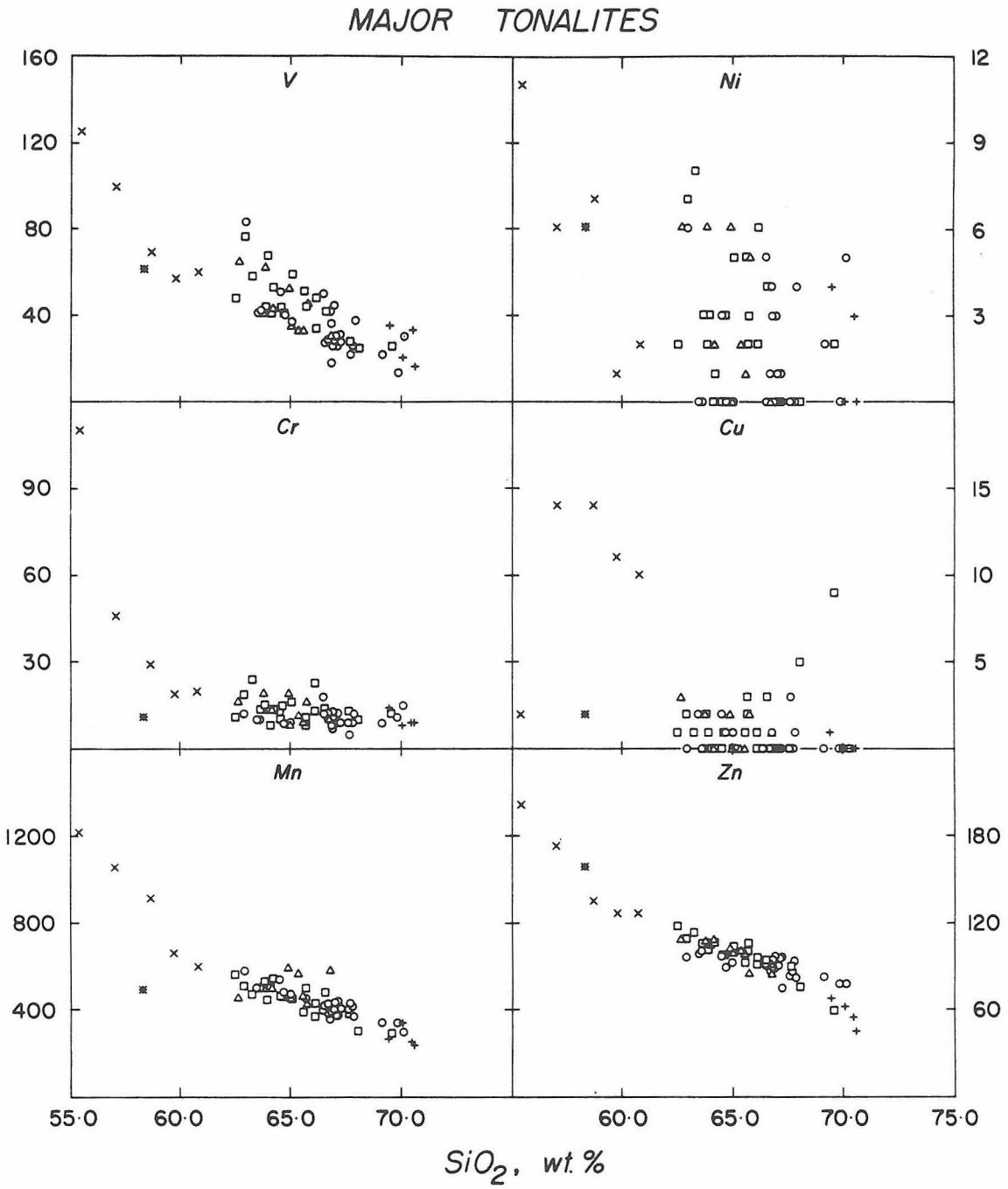
MAJOR TONALITES
V
Ni
Cr
Cu
Mn
Zn
160
120
80
40
12
9
6
3
90
60
30
15
10
5
1200
800
400
180
120
60
55·0
60·0
65·0
70·0
60·0
65·0
70·0
75·0
SiO2, wt.%

Figure 7.6.

important in controlling the behaviour of the various species.

Felsic "differentiates"

As well as samples collected to be representative of the rock at a particular locality, four samples were collected that are considerably more felsic than the typical surrounding rock. Three of these samples (LTS 218, 288, 358) are from areas where schlieren are prominently developed, and field relations suggested that the more felsic rocks were the products of crystal-liquid separation at a relatively small (tens to hundreds of metres) scale. The fourth sample (LTS 322) is from large mass of felsic rock (perhaps 50x1000 m) near the center of Unit III. Although representative of the rock at the local scale (hundreds to a thousand meters), this sample is considerably more felsic than the bulk of this unit. Again, it appeared that crystal fractionation might be a viable mechanism for generating these centrally located more felsic rocks (cf. Bateman and Chappell, 1979) and these samples were collected in part to test this hypothesis.

These 4 samples are differentiated on the various element-element diagrams. There is an apparent complete gradation between these most felsic end-member compositions and the more typical tonalites in the field. Relatively felsic rocks are probably over-represented in terms of relative abundances (although the central region of Unit III is relatively felsic), and this is reflected in an apparent high-SiO_2 group on the Harker diagrams (Figs. 7.2, 7.4-7.6).

The geochemical effects of these processes are best seen in the behaviour of K and related elements (Rb and Ba). These four samples have,

Figure 7.7. K_2O versus Rb, Ba, TiO_2 and Zr.

Open symbols	-	"mafic" tonalites (SiO_2 < 65.5 wt.%)
Closed symbols	-	"normal" tonalites
Squares	-	Unit I
Triangles	-	Unit II
Circles	-	Unit III
Plus signs	-	Felsic differentiates
Crosses	-	Mafic xenoliths
Asterisks	-	Mafic dike intruding Unit III

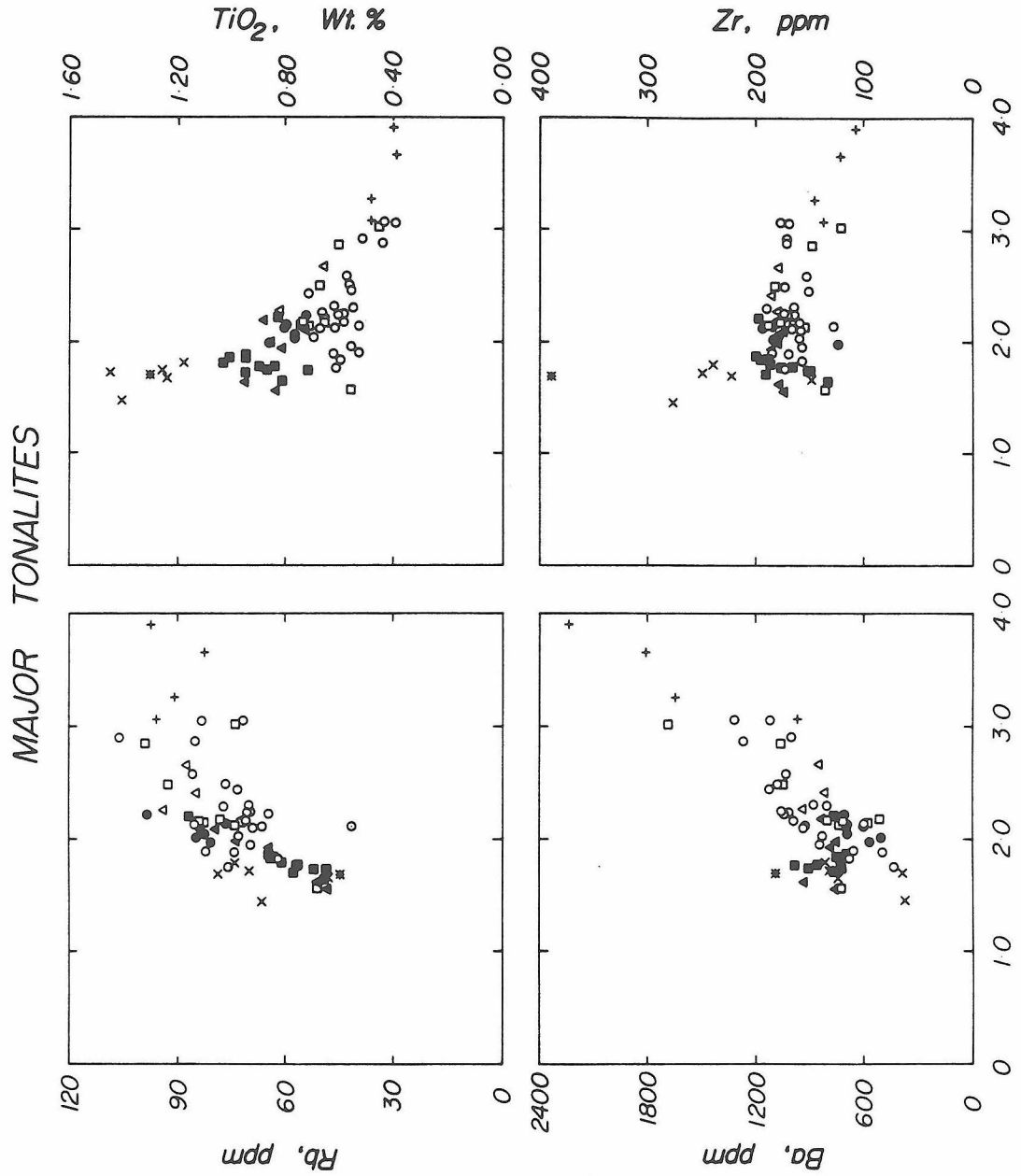

Figure 7.7

as expected from their mineralogy, high SiO_2 and K_2O. They also have high Ba [Ba increases linearly with K (Fig. 7.7)], and K/Rb increases dramatically in the more K-rich rocks. This is the expected behaviour where biotite is an important crystallizing phase, as it is in these rocks. The linear covariation of K and Ba, with Ba increasing about 3 times more rapidly than K argues that Ba is being relatively efficiently excluded from the minerals of the more mafic rocks. This behaviour is consistent with precipitation of the assemblage plagioclase + hornblende + biotite + quartz + titanite leaving a liquid enriched in SiO_2 and Ba, and, to a lesser extent, K.

The geochemistry of these samples is thus consistent with them having crystallized from evolved liquids formed by removal of the observed mineral phases from a less evolved earlier liquid, that is, they are the end products of fractional crystallization processes acting within the solidifying magma chamber. They thus potentially allow the recognition of the effects of this process in less extreme cases.

Ca, Na, and Sr - Elements associated with feldspars

Plagioclase feldspar comprises about 55 ± 3 wt.% of most rocks. It is the dominant site for Na in all rocks, and is also the major site for Ca. Mass balance shows that even for the most mafic rocks at least 75% of the calcium is contained in plagioclase with the rest largely distributed between hornblende and titanite (Table 7.19). Only minor amounts of Ca are contained in other minerals (epidote, allanite, apatite, K-feldspar). Titanite contains about twice as much Ca as a similar amount (wt. fraction) of hornblende. The Ca/(Ca + Na) for the rock therefore gives an approximate upper limit for the mean Ca/(Ca + Na) of the plagioclase.

TABLE 7.16.

CALCIUM APPORTIONMENT AMONG PHASES

Assumed Mineral Compositions

	Plag.	Hblde	Biotite	Titanite	Apatite
SiO_2	57.55	44.81	32.21	31.25	
TiO_2		1.22	3.10	37.37	
Al_2O_3	26.46	8.17	15.23	1.60	
Fe_2O_3		6.57	7.45	0.77	
FeO		13.80	15.63		
MnO		0.42	0.33	0.21	
MgO		9.29	9.75		
CaO	9.00	11.81		27.80	52.40
Na_2O	6.80	1.11	0.04		
K_2O	0.19	0.86	9.81		
P_2O_5					41.27
F		0.22	2.57		4.75
Cl		0.04	0.06		0.05
Total	100.00	98.30	99.20	99.00	96.77
Density	2.67	3.3	3.0	3.5	3.15

Rock Values

	LTS147 wt.%	LTS221 wt.%	LTS212 wt.%
Plag.	50.3	51.3	52.0
Quartz	27.3	21.6	29.1
Hblde	4.8	7.9	0.4
K-fs	1.4	1.4	8.1
Biotite	14.6	16.8	9.4
Titanite	1.5	0.9	0.3
Access.	0.1	0.1	0.9
CaO (wt.%)	5.27	5.40	3.08
Na_2O (wt.%)	3.83	3.48	3.71
Ca/(Ca + Na)	0.432	0.462	0.314

Calculated Plagioclase

CaO	4.35	4.28	2.81
Na_2O	3.78	3.39	3.70
Ca/(Ca + Na)	0.389	0.411	0.295
Ca/(Ca + Na) [normative]	0.416	0.435	0.317
Ca/(Ca + Na) [microprobe]	0.354	0.328	0.298
Ca in plag.	83%	79%	91%

This limits the mean anorthite content of plagioclase in the most mafic rocks to a composition more sodic than An_{44}. If a requisite amount of Ca and Na are then apportioned to hornblende and titanite, a model mean plagioclase content can be calculated (Table 7.19). Sample LTS 221 is from the "Pine Cove salient", and has lower Na_2O than rocks with comparable SiO_2 from elsewhere in the major tonalites. Even so, it has a relatively sodic model plagioclase composition of An_{41}. Sample LTS 147 is representative of the most mafic rocks from the major tonalites, and has a model composition of An_{39}; sample LTS 212 is one of the most felsic rocks analyzed, and has a model plagioclase composition of An_{30}. Table 7.19 also lists the simple mean of the plagioclase microprobe analyses for each rock. As discussed above (Ch. 6) the microprobe determinations are biased in favour of the extremes of composition, and a simple mean of all determinations probably over-represents the proportion of relatively sodic "rim" compositions, particularly in the more mafic rocks. It is concluded that the mean plagioclase composition of the most mafic (highest Ca/(Ca + Na), lowest SiO_2) rocks from each unit is $An_{40 \pm 1}$, and that the most calcic plagioclase in these rocks is only a few mole % more calcic (An_{43}, Fig. 6.1).

The rock chemistry thus confirms the indications from the mineral chemical data that the plagioclase composition remains remarkably constant throughout all of these rocks. The total (microprobe) observed range is from An_{43} to An_{25}, compared to the range of An_{41} to An_{30} calculated from mass balance considerations. These data imply that the bulk of the plagioclase within each rock also has an extremely restricted compositional range. The composition of plagioclase is extremely sensitive to physico-chemical conditions prevailing during crystallization

(e.g., Bowen, 1913; Johannes, 1978), so that the restricted range of compositions found for the San Jacinto rocks implies both remarkably constant physical (particularly T) and chemical [particularly Ca/(Ca + Na) and X_{H_2O}] conditions during crystallization of these huge volumes of silicate liquid. These data argue strongly against the operation of closed-system fractional crystallization processes being important during solidification of the major tonalite plutons. They do not restrict more complex models involving fractional crystallization within an open system.

Alternately, these data could be interpreted as demonstrating that post-crystallization equilibration, perhaps with the remaining liquid, has been extraordinarily efficient.

The partitioning of trace elements between different crystal phases, and between crystallizing phases and melt may also be a very sensitive indicator of the stability of both physical and chemical conditions during progressive crystallization or partial fusion. Figure 7.8 shows the covariance of Sr and Ca in the San Jacinto rocks. Except for the most felsic samples, the data from each unit define an approximately linear array with positive slope. The behaviour of Sr (relative to Ca) differs from unit to unit, but appears reasonably consistent within each unit. Data from the mafic tonalites define a relatively tight linear field over which Sr decreases from 620 to 460 ppm as CaO decreases from 5.5 to 4.5 wt.%. The normal tonalites tend to have higher Sr at a given CaO than the mafic tonalites. Significantly, the most mafic rocks from each unit have very similar Sr (600 $\pm$ 20 ppm) and Ca (5.4 0.2 wt.%), as well as similar SiO_2 and Ca/(Ca + Na). This implies that the plagioclase in these rocks also has similar Sr content, again suggestive that at least

Figure 7.8. Sr - Ca for major tonalites.

Filled symbols	-	"Mafic" tonalites
Open symbols	-	"Normal" tonalites
Squares	-	Unit I
Triangles	-	Unit II
Circles	-	Unit III
Plus signs	-	Felsic differentiates
Crosses	-	Mafic xenoliths
Asterisk	-	Mafic dike intruding Unit III

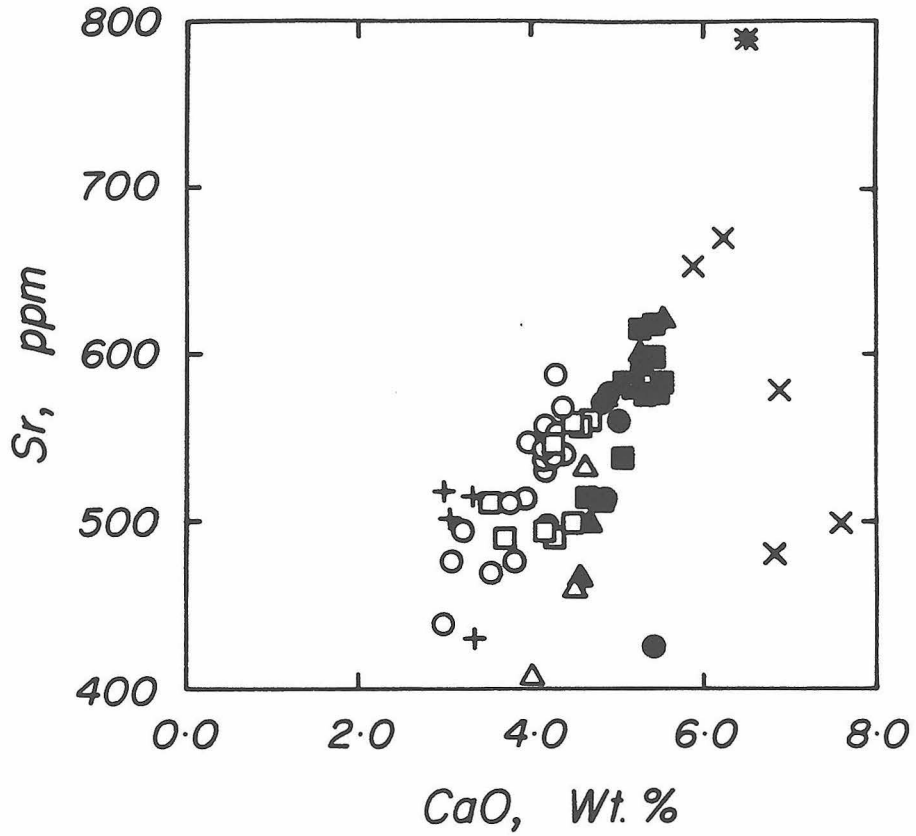

Figure 7.8

the most mafic rocks from each unit crystallized from liquids of near identical composition at remarkably similar temperature and X_{H_2O}. The trend shown by the mafic tonalite group appears to differ significantly from the trend for in-situ fractionation defined by the four felsic differentiates, perhaps implying that the features apparent in the geochemistry of the mafic rocks were already present when the liquids from which they crystallized were injected into the evolving magma chamber. This further implies variation in the composition of liquids injected into magma chamber.

Biotite - K, Rb and Ba

Biotite is the most important site for both K and Rb in almost all rocks. For a typical mafic tonalite (LTS 147) ≈93% of the Rb and ≈77% of the K is accounted for by the biotite (Table 7.20). Plagioclase can account for almost all of the remainder of the Rb (≈ 7%), with only minor amounts in other minerals (hornblende, K-feldspar). K is distributed between biotite (77%), K-feldspar (13%), plagioclase (7%) and hornblende (3%). The mass fraction of K-feldspar estimated after first apportioning the appropriate amount of K to the other minerals is 0.017, which agrees well with the visually determined estimate of 0.014 (Table 5.7). For LTS 152, a more felsic tonalite, K is distributed between biotite (67%), K-feldspar (23%), plagioclase (6%) and hornblende (4%). The mass fraction of K-feldspar calculated by mass balance (≈ 0.03) is significantly less than the visual estimate (0.072), reflecting the irregular distribution of large poikolitic plates of K-feldspar in this rock. Rb is distributed between biotite (92%), plagioclase (3%) and K-feldspar (5%), with only minor amounts in other minerals.

TABLE 7.17.

APPORTIONMENT OF K AND RB BETWEEN MINERAL PHASES

	LTS147	LTS152
	Rock	
K_2O (wt.%)	1.86	2.02
Rb (ppm)	64.4	72.6
	Biotite	
K_2O (wt.%)	9.8	9.8
Rb (ppm)	410	490
	Plagioclase	
K_2O (wt.%)	0.2	0.2
Rb (ppm)	5.2	2.7

	Percent K in mineral phase	
Biotite	77	67
Plagioclase	7	6
Hornblende	3	4
Other	13	23
	Calculated Mass Fraction K-feldspar	
	0.017	0.030
	K-feldspar Mass Fraction from Visual Determination	
	0.014	0.072

	Percent Rb in mineral phase	
Biotite	93	92
Plagioclase	7	3
Other	-	5

Figure 7.9a. Biotite versus Rb content, major tonalites

Squares	-	Unit I
Triangles	-	Unit II
Circles	-	Unit III
Plus signs	-	Felsic differentiates
Crosses	-	Mafic xenoliths

Figure 7.9b. Biotite versus K_2O content, major tonalites. Symbols as above.

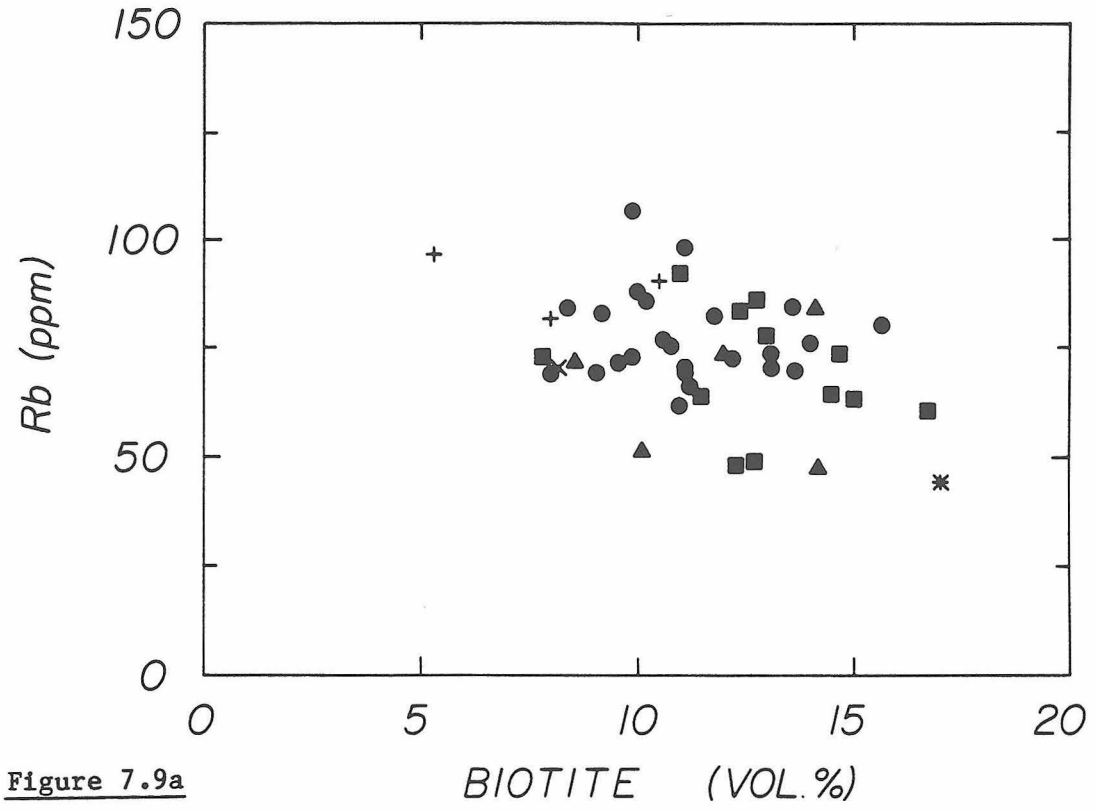

Figure 7.9a

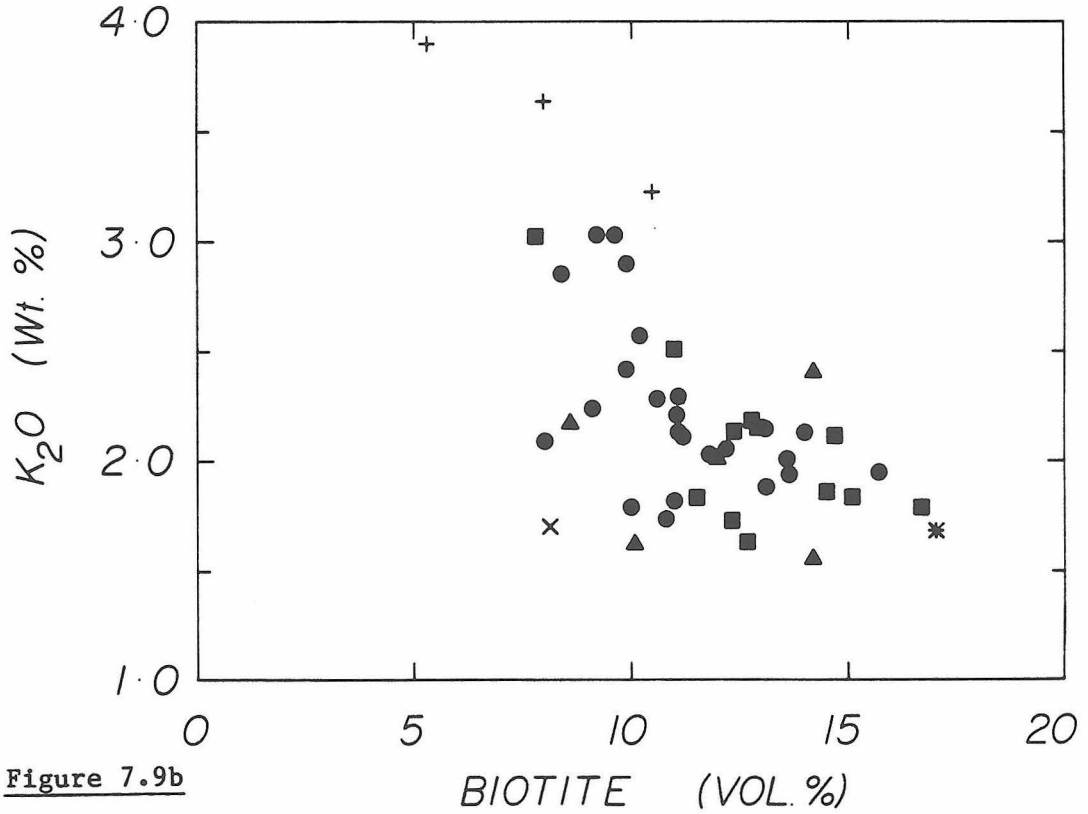

Figure 7.9b

Figure 7.10. K/Rb versus K_2O for major tonalites.

Filled symbols	-	"Mafic" tonalites
Open symbols	-	"Normal" tonalites
Squares	-	Unit I
Triangles	-	Unit II
Circles	-	Unit III
Plus signs	-	Felsic differentiates
Crosses	-	Mafic xenoliths
Asterisk	-	Mafic dike intruding Unit III

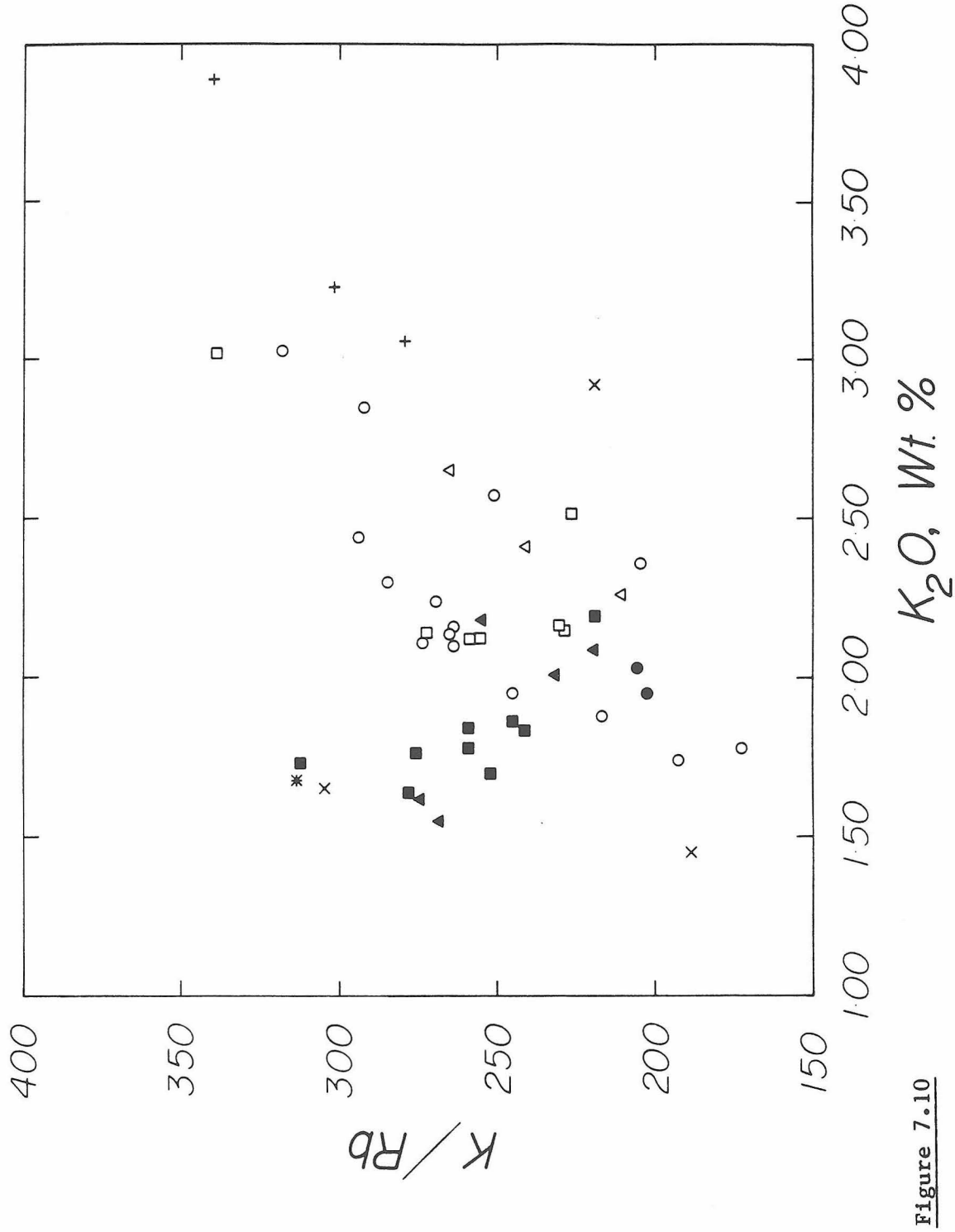

Figure 7.10

If these rocks are in part accumulates, then there should be a systematic relationship between the abundance of that mineral and the concentration of an element strongly partitioned into that mineral. Such might be expected to be the case for biotite, K and Rb. Figure 7.9 shows that both K and Rb tend to decrease in the most biotite-rich rocks, implying that biotite accumulation is not responsible for the observed K and Rb behaviour. Figure 7.10 shows K/Rb as a function of K abundance. Biotite addition should lower K/Rb and increase K; biotite removal would leave a residual liquid with increased K/Rb and either increased or decreased K depending on the proportion of biotite removed. For rocks from Units I and II with $> \approx 2.2$ wt.% K_2O and for all rocks from Unit III biotite removal leaving a liquid with increased K/Rb and K_2O is indicated. For rocks from Units I and II more mafic than this K/Rb increases rapidly as K decreases. This behaviour cannot be explained by high-level processes involving the observed mineralogy, and is interpreted as indicating that the more mafic rocks crystallized from liquids that had acquired these K/Rb characteristics prior to injection into the San Jacinto magma chambers.

It thus appears that the more mafic rocks (that is, the majority of Units I and II, and, perhaps, the outer third of Unit III) may have inherited much of their geochemical signature from the liquids from which they crystallized. The volumetrically less significant felsic tonalites and low-K granodiorites of Units I and II, and perhaps the majority of the rocks of the more felsic Unit III are interpreted as showing the effects of a high-level overprint involving fractional crystallization of the observed mineral assemblage. Although the appearance of mineral phases is apparently in the order plagioclase + hornblende, followed by

quartz, biotite and titanite, these five minerals probably crystallized simultaneously through much of the crystallization interval of these rocks. Precipitation of these phases will tend to decrease the Ca/(Ca + Na) and Mg/(Mg + Fe) of the remaining liquid, consistent with the decrease in these parameters observed in both the four felsic differentiate samples, and with their general decrease in the more central, more felsic liquids. Precipitation of 15-20% (weight) biotite will have the effect of buffering the K content of liquids in equilibrium with the most mafic solids. As the importance of biotite decrease, this will no longer be the case, and K of residual liquids will begin to increase.

The higher Rb content of the analysed biotite from LTS 152 relative to that from LTS 147 is consistent with the former having been precipitated from a more Rb-rich liquid. This suggests that Rb may also increase in residual liquids, though not at the same rate as does K.

The lack of a relationship between biotite and K abundance described above is interpreted as indicating that the decrease in K/Rb with increasing K apparent for the more mafic rocks is not the result of a process involving biotite. The correlation of K and Rb is shown on Figure 7.7. This diagram shows that K increases rapidly while Rb increases only slowly in the more felsic rocks, so that although the four felsic differentiates have twice as much K as the most mafic rocks, they do not have proportionately more Rb. Figure 7.11 combines the available K, Rb and K/Rb information for both rocks and minerals. The inset shows the K-Rb relations of the mafic tonalites. These are the samples for which K/Rb decreases as K increases; the slope of the linear array defined by these data is not consistent with either biotite addition or removal,

Figure 7.11. Rb versus K_2O showing available mineral chemical data. Inset shows data for the "mafic" tonalites, mafic xenoliths, and a mafic dike, as well as a histogram of observed K_2O content in hornblendes.

For inset,

Squares	-	Unit I
Triangles	-	Unit II
Circles	-	Unit III
Crosses	-	Mafic xenoliths
Asterisk	-	Mafic dike intruding Unit III

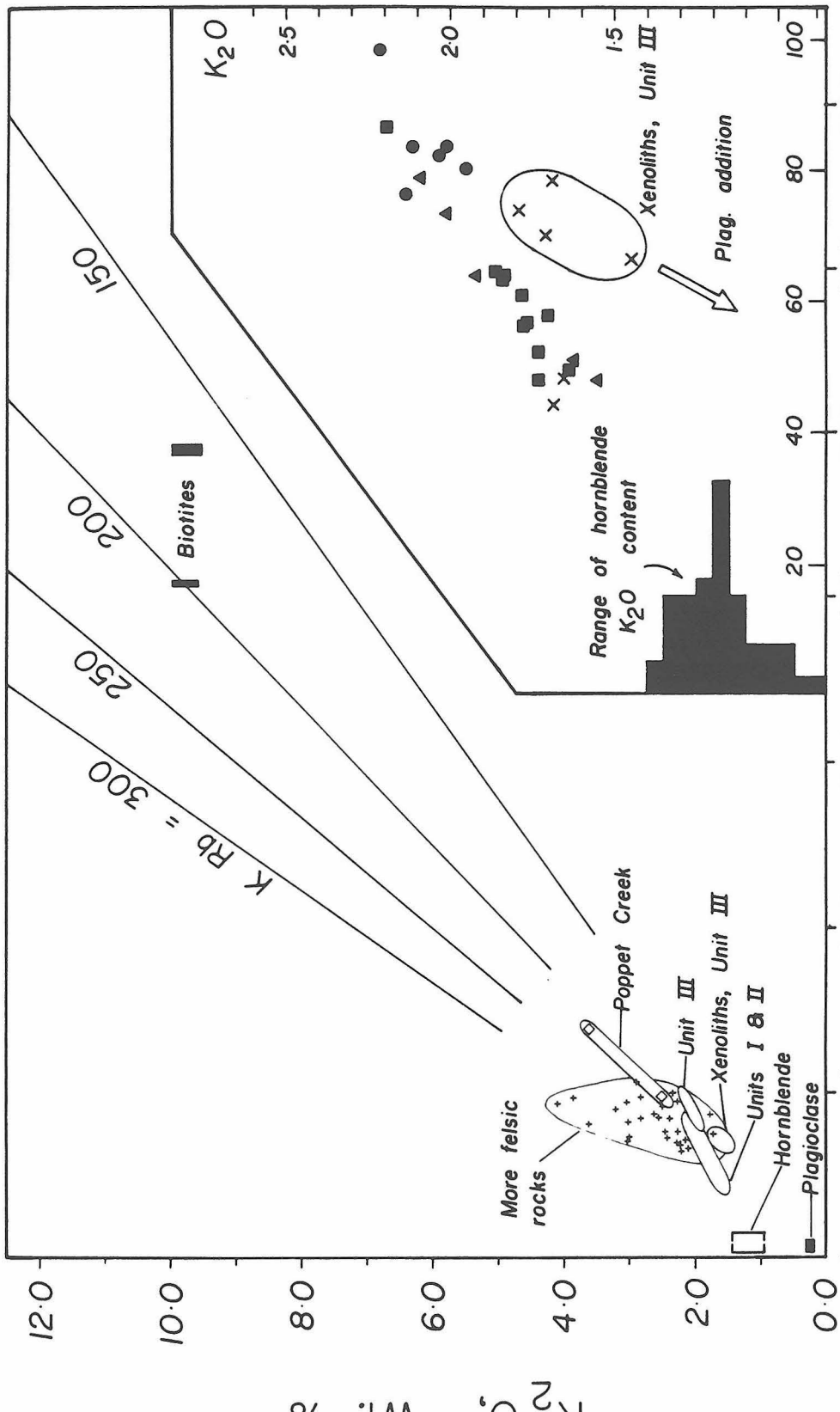
K_2O, Wt. %
Rb, ppm
K Rb = 300
250
200
150
Biotites
K_2O
Range of hornblende K_2O content
Xenoliths, Unit III
Plag. addition
Poppet Creek
Unit III
Xenoliths, Unit III
Units I & II
Hornblende
Plagioclase
More felsic rocks

Figure 7.11

but appears to implicate another mineral phase, possibly hornblende. Xenoliths from Unit III fall on a trend suggesting either plagioclase addition or derivation from a residual liquid from which plagioclase has been removed. This trend (away from the origin) is also the expected path for liquids from which phases containing only minor amounts of both K and Rb have been removed. Such phases could include orthopyroxene, olivine, quartz, opaque minerals and garnet. For the normal tonalites (plotted on the main part of the diagram) removal of a combination of plagioclase and biotite yields liquid trajectories with steeper slopes, consistent with the observed K-Rb relations. Note that removal of a solid containing 15-20% biotite leads to an increase in K in the remaining liquid, but will yield at most only a slight increase in Rb and may give a residual liquid with decreased Rb.

It is difficult to reconcile the apparent hornblende control of K-Rb relations in the mafic rocks with the relative unimportance of hornblende as a crystallizing phase (compared with plagioclase, quartz and biotite) in the magma chamber. This suggests that at least some of the geochemical features of these rocks are inherited from liquids that had obtained these characteristics prior to emplacement into these high-level magma chambers, consistent with the interpretation of Ca-Sr data from these rocks.

If the chemistry of the dikes and xenoliths approximates that of liquids introduced into these magma chambers as is argued above from field evidence, then there appear to have been at least two distinct groups of liquids involved, one having geochemical features indicative of hornblende control of K-Rb fractionation, and another having geochemical features suggestive of plagioclase or plagioclase + biotite

control. The latter group could also have inherited its K-Rb relations from processes involving other low-K, low-Rb phases (such as garnet or olivine) but this is impossible to evaluate here. The first group (those apparently having hornblende removal features) falls in the field defined by the most mafic rocks, suggesting that these rocks might approximate liquid compositions.

It has been argued above that the analysed rocks from the major tonalite units can be divided into two main groups. A group comprised predominantly (but not exclusively) of the more mafic tonalites (arbitrarily defined as having <65.5 wt.% SiO_2) appears to have more or less directly inherited the geochemical signature(s) of the liquids that were being injected into the inflating magma chambers. The second group, consisting of the more felsic "normal" tonalites, appears to reflect an overprint from high-level processes. The volumetrically minor rocks sampled by the four felsic differentiates show the most extreme effects of this high-level process, inferred to involve some fractional removal of earlier crystallizing phases (hornblende, plagioclase, biotite, quartz, and titanite) to leave a geochemically evolving residual liquid.

It is suggested that hornblende may be an important phase in yielding the K-Rb characteristics of the liquids from which the more mafic rocks crystallized. It further appears that these liquids had obtained these geochemical signatures <u>before</u> their injection into these high-level magma chambers. However, the available data do not allow differentiation between several plausible processes that are capable of producing these effects. For instance, although the data appear to implicate hornblende-liquid separation, it is not possible to distinguish between hornblende residual from a partial fusion event, and hornblende

separation following precipitation from its host liquid.

The model developed for the origin of the K-Rb features of the more felsic rocks [that they crystallized from evolved liquids from which plagioclase + biotite (+ hornblende + quartz + titanite)] had been removed by earlier precipitation is the model of Bateman and Chappell (1979); early precipitation of higher temperature phases leaves an evolving liquid enriched in components that do not enter these early formed precipitates. However, a significant number of the analysed San Jacinto rocks have K-Rb and Ca-Sr characteristics that apparently resulted from processes that were operating before the liquids from which these rocks crystallized were injected into the magma chamber. Specifically, features of these rocks are most consistent with hornblende control of K-Rb relations in their parent liquids. Two xenolith/dike analyses have similar properties. A second group of xenoliths has features indicative of control of K-Rb relations by a different mineral assemblage, perhaps involving plagioclase + biotite. The role of phases containing only minor amounts of both K and Rb in the evolution of the K-Rb patterns is impossible to evaluate.

Elements that tend to mimic K geochemically show similar behaviour. U, like K, is excluded by most major early-crystallizing phases. Figure 7.12 shows the behaviour of U compared to that of K (and K-Rb). In the mafic tonalites both K and U increase slowly together. In the more felsic rocks, K increases rapidly while U remains relatively constant at 1.2 to 2.4 ppm. The groupings differentiated by their K-Rb characteristics are also recognised on the K-U diagram. The three samples that apparently extend the mafic trend to high U (>2.8 ppm) also fall on the mafic trend for K-Rb, suggesting that this apparent extension to high K, Rb, and U is real. The K-U data are consistent with the

Figure 7.12a. K_2O versus Rb, major tonalites.

Filled symbols	-	"Mafic" tonalites
Open symbols	-	"Normal" tonalites
Squares	-	Unit I
Triangles	-	Unit II
Circles	-	Unit III
Plus signs	-	Felsic differentiates
Crosses	-	Mafic xenoliths
Asterisk	-	Mafic dike intruding Unit III

Figure 7.12b. K_2O versus U, major tonalites. Symbols as above.

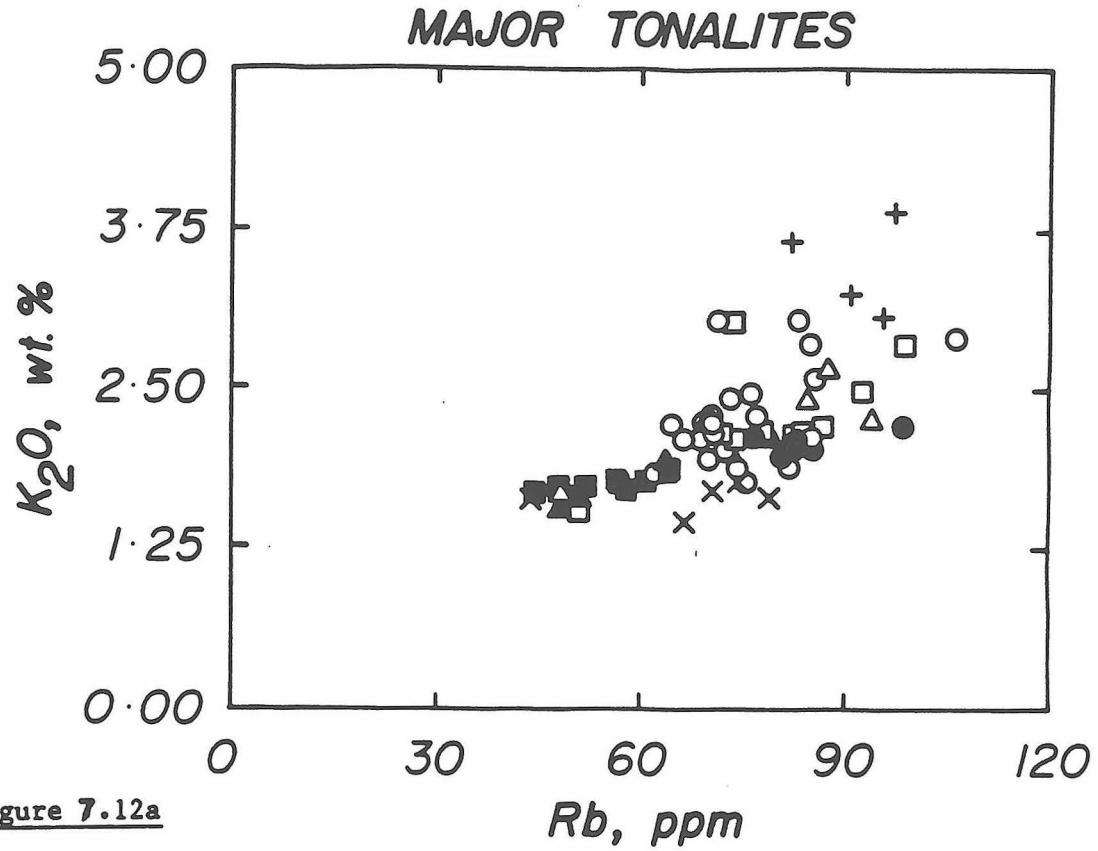

Figure 7.12a

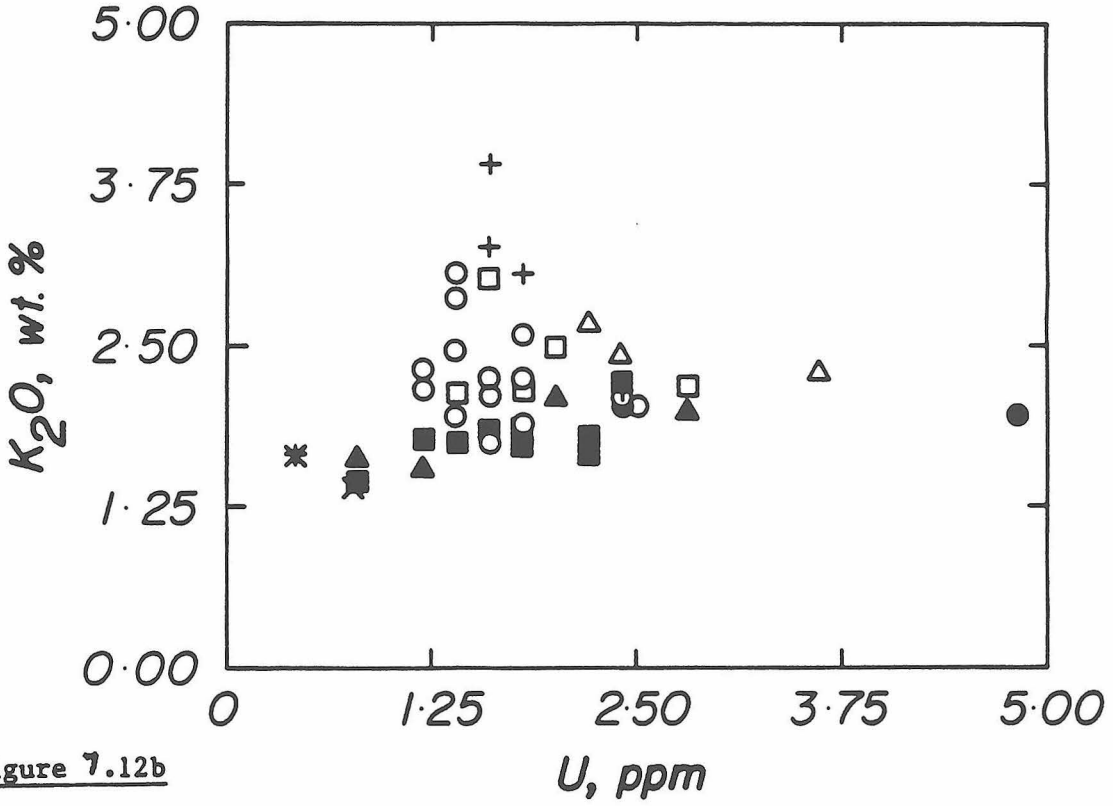

Figure 7.12b

suggestion made above that the geochemistry of the mafic rocks is controlled by different processes to those pertaining to the more felsic rocks. The rapid increase in K combined with no change in U (for the felsic rocks) is consistent with the presence of phases such as sphene, allanite and zircon that can substitute significant amounts of U in their structure, with the amount actually incorporated being largely controlled by the abundance of U in the liquid from which a particular crystal precipitates.

The covariation of U and Th (Figure 7.13) suggests that Th abundance is also controlled by two separate stages of behaviour, although it is likely that the mineral buffering Th abundance in residual liquids (most likely allanite) is not the major site for U as well.

Covariance of Ba and K (Figure 7.7) is most simply explained as showing that K and Ba are excluded from the bulk solid assemblage crystallizing at any stage, with Ba consistently excluded more efficiently than is K. Ba abundance increases about three times more rapidly than does K abundance, and Ba abundance overall increase by a factor of ten. Such behaviour is compatible with control of K and Ba abundance by crystal fractionation, but requires very special conditions for it to result from partial fusion processes. This does not rule out a partial fusion origin for this correlation, especially if the relative proportions of residual phases vary systematically with changing source composition.

Elements controlled by a polymineralic assemblage - Ti, V

Most elements will have their geochemical behaviour (during <u>any</u> geochemical process, including partial fusion, fractional crystallization or even weathering) controlled by more than one mineral phase. In the San

Figure 7.13. U versus Th, major tonalites.

Filled symbols	-	"Mafic" tonalites
Open symbols	-	"Normal" tonalites
Squares	-	Unit I
Triangles	-	Unit II
Circles	-	Unit III
Plus signs	-	Felsic differentiates
Crosses	-	Mafic xenolith
Asterisk	-	Mafic dike intruding Unit III

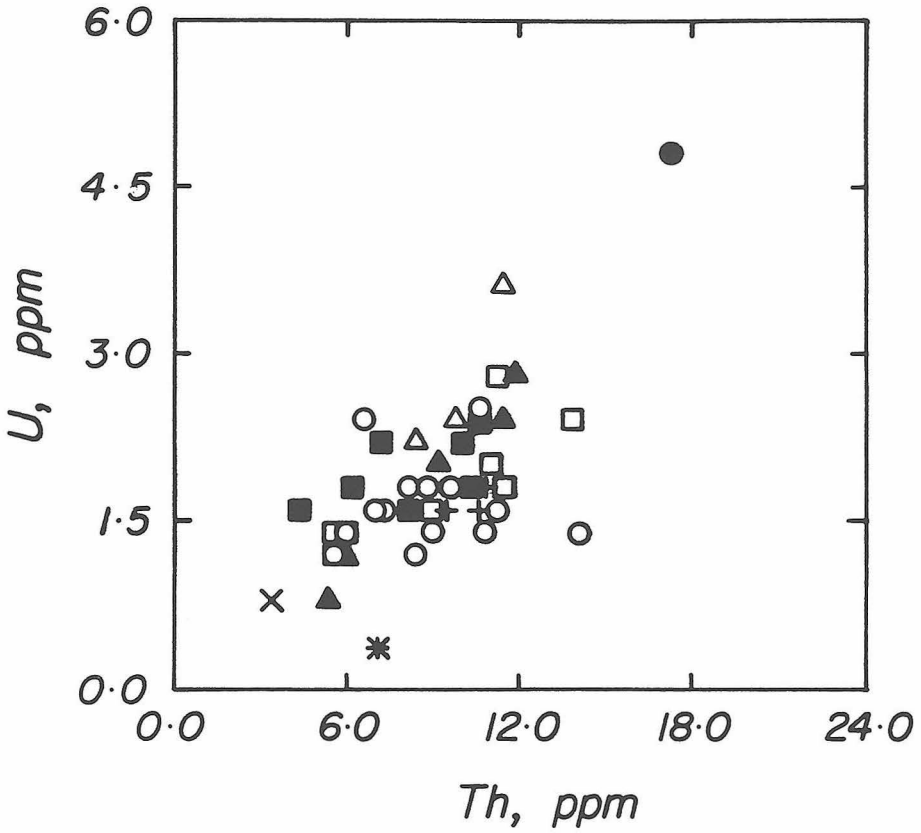

Figure 7.13

Jacinto rocks Ti, for instance, is proportioned approximately equally between titanite and biotite, with minor amounts in hornblende and ilmenite. If these were early crystallizing phases, it would be expected that any residual liquid resulting from their precipitation would be depleted in Ti. Their presence as residual phases during partial fusion would have similar effects. Alternatively, if the observed compositional trends result from progressive fusion in the absence of an important Ti phase then Ti would be expected to be most abundant in the first-formed and presumably most felsic melts, and less abundant in later melts. Suggested phases include titanchondrodite $[(Mg,Fe^{2+},Ti)_5(SiO_4)_2(F,OH)_2]$, titanclinohumite $[(Mg,Fe^{2+},Ti)_9(SiO_4)_4(F,OH)_2]$ and titanphlogopite $[K_2(Mg,Fe^{2+},Ti)_6(Si_6Al_2O_{20})(OH,F)_4]$ as well as ilmenite $[FeTiO_3]$ and perovskite $[(Ca,Na,Fe^{2+},REE)(Ti,Nb)O_3]$. The potential role of the first three of these phases has been considered by T.H. Green (1980) and Gill (1981), among others, and they conclude that they are unlikely to be sufficiently abundant to be important in controlling Ti behaviour in calc-alkaline rocks. Both ilmenite and perovskite are common phases in kimberlites, attesting to their presence at mantle pressures. Again, the role of these minerals in controlling Ti behaviour in calc-alkaline rocks is not well understood.

Figure 7.7 shows the covariation of Ti and K. As was the case for K and Rb, and K and U, relations within the more felsic rocks are consistent with removal of the observed mineral assemblage (plagioclase + biotite + quartz + hornblende + titanite) yielding a liquid enriched in K and slightly depleted in Ti. A higher proportion of a low-Ti phases (quartz or plagioclase) is indicated for Unit III. A mixture of plagioclase ($\pm$ quartz), biotite and titanite can give the same effect as hornblende removal, so it is not possible to uniquely identify the precip-

itating phase(s) from the Ti-K data alone.

Pearce and Norry (1979) suggested that comparison of relationships between Ti, Zr, Y and Nb may be used to discriminate between conflicting petrogenetic hypotheses, and to allow determination of the relative importance of various fractionating phases in the fractional crystallization case. In particular, all four elements are partitioned strongly into hornblende and biotite compared to other likely major phases; this should make discrimination of processes involving either of these two minerals relatively straightforward. Unfortunately, it is usually not possible to discriminate between the effects of hornblende versus biotite controlled behaviour for these four elements.

The abundance of zircon (very approximately 0.05 %) is sufficient to account for the bulk of the Zr present in these rocks. Precipitation of zircon throughout the crystallization sequence is able to explain the decreased Zr abundance in the more felsic rocks.

Behaviour of the other elements considered by Pearce and Norry (Nb, Y) are complex, and are not consistent with the action of a single simple process. Y abundance during fractional crystallization within the magma chamber is likely to be controlled by precipitation of minor phases such as titanite, allanite and zircon (Gromet and Silver, 1983); even modest changes in the relative abundances of these phases from sample to sample will yield complex patterns of behaviour.

Rare Earth Element Behaviour

REE analyses for two rocks are presented in Table 7.21 (L.P. Gromet, written communication, 1983). The features of these REE patterns are those described by Gromet (1979) as characteristic of tonalites and

TABLE 7.18.

ANALYTICAL DATA FOR RARE EARTH ELEMENTS

(L.P. GROMET, WRITTEN COMMUNICATION, 1983)

	LTS 152		LTS 147		CHONDRITIC* VALUES
	ppm	x chondrites	ppm	x chondrites	ppm
Ce	55.5	87.0	88.3	138.4	0.6379
Nd	24.7	52.1	37.1	78.3	0.4738
Sm	4.05	26.3	6.53	42.4	0.1540
Eu	0.995	17.1	1.53	26.4	0.05802
Gd	2.92	14.3	4.90	24.0	0.2043
Dy	1.96	7.71	3.18	12.5	0.2541
Er	0.928	5.59	1.45	8.73	0.1660
Yb	0.686	4.16	1.16	7.03	0.1651

* Evensen, N.M., Hamilton, P.J., and O'Nions, R.K., 1978, Rare-earth abundances in chondritic meteorites: Geochemica et Cosmochimica Acta 42, 1199-1212

low-K granodiorites from the eastern portion of the batholith, namely pronounced LREE enrichment coupled with HREE depletion. The REE abundance levels of LTS 152 are almost identical to those measured by Gromet in a similar felsic tonalite from the Cahuilla Valley pluton immediately south of the San Jacinto fault zone (Gromet, 1979). This is further indication of the strong chemical coherence of the rocks from the San Jacinto Mountains with rocks from elsewhere in the batholith (L.P Gromet, written communication 1983). These data are shown on the familiar REE diagram normalized to the chondritic average of Evensen et al., 1978 (Fig. 7.14).

Figure 7.15 shows Ce/Y versus Ce for the less accurate XRF data. There is a considerable spread of Ce values, from ≈30 to ≈75 ppm, and in Ce/Y ratio, from ≈1.5 to ≈8.5. Although agreement between the two methods is not good for absolute abundance levels, comparison of chondrite normalized Ce/Y (XRF) and Ce/Yb (ID) ratios suggests that there is considerable internal consistency within the XRF data. At a given Ce content the more SiO_2-rich rocks tend to have higher Ce/Y, i.e., more highly fractionated REE patterns. This fractionation results from both Ce increase and Y decrease, with the latter in general being more important.

The data for the mafic tonalites from Units I and III form diffuse linear arrays, with Ce/Y for Unit I increasing from 2 (at 30 ppm Ce) to 5 (at 75 ppm Ce). The xenolith and dike analyses fall within or slightly to the low Ce/Y side of the fields defined by their host units.

These data are consistent with the interpretation that the more SiO_2-rich "fractionated" rocks crystallized from liquids which had had REE-containing minerals removed previously. Removal of titanite will deplete HREE more efficiently than LREE (Gromet and Silver, 1983), and this is consistent with the increase in Ce/Y at relatively constant Ce.

Figure 7.14. Rare Earth Element (REE) patterns for two rocks from the major tonalite units, normalized to the chondritic average of Evensen et al., 1978. Sample LTS 147 is a mafic tonalite from Unit I; Sample LTS 152 is a tonalite from Unit III. Data from L.P. Gromet, written communication, 1983.

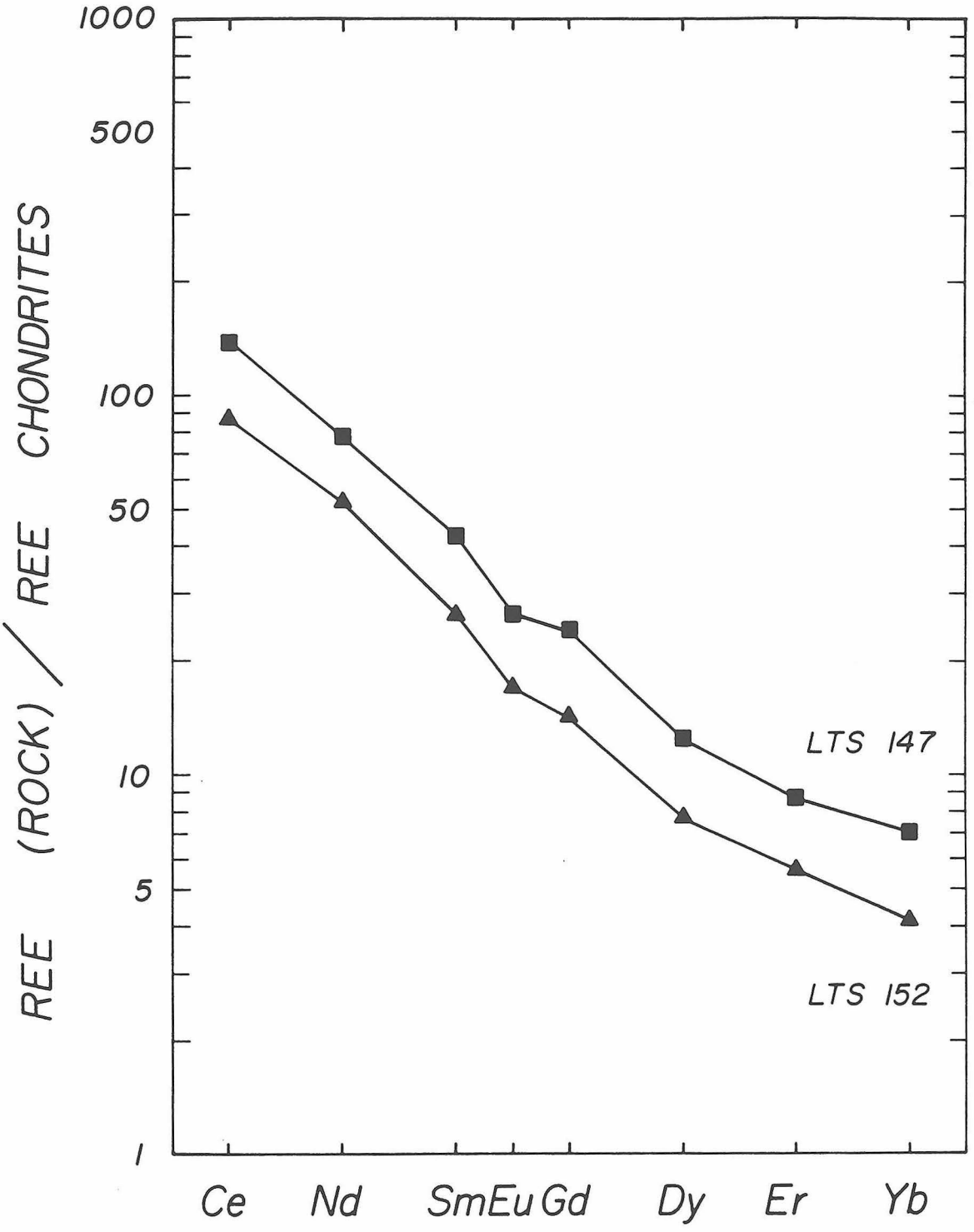
1000
500
100
50
10
5
1
REE (ROCK) / REE CHONDRITES
LTS 147
LTS 152
Ce
Nd
SmEu
Gd
Dy
Er
Yb

Figure 4.14

Figure 7.15. Ce/Y versus Ce for major tonalites.

Filled symbols	-	"Mafic" tonalites
Open symbols	-	"Normal" tonalites
Squares	-	Unit I
Triangles	-	Unit II
Circles	-	Unit III
Plus signs	-	Felsic differentiates
Crosses	-	Mafic xenoliths
Asterisk	-	Mafic dike intruding Unit III

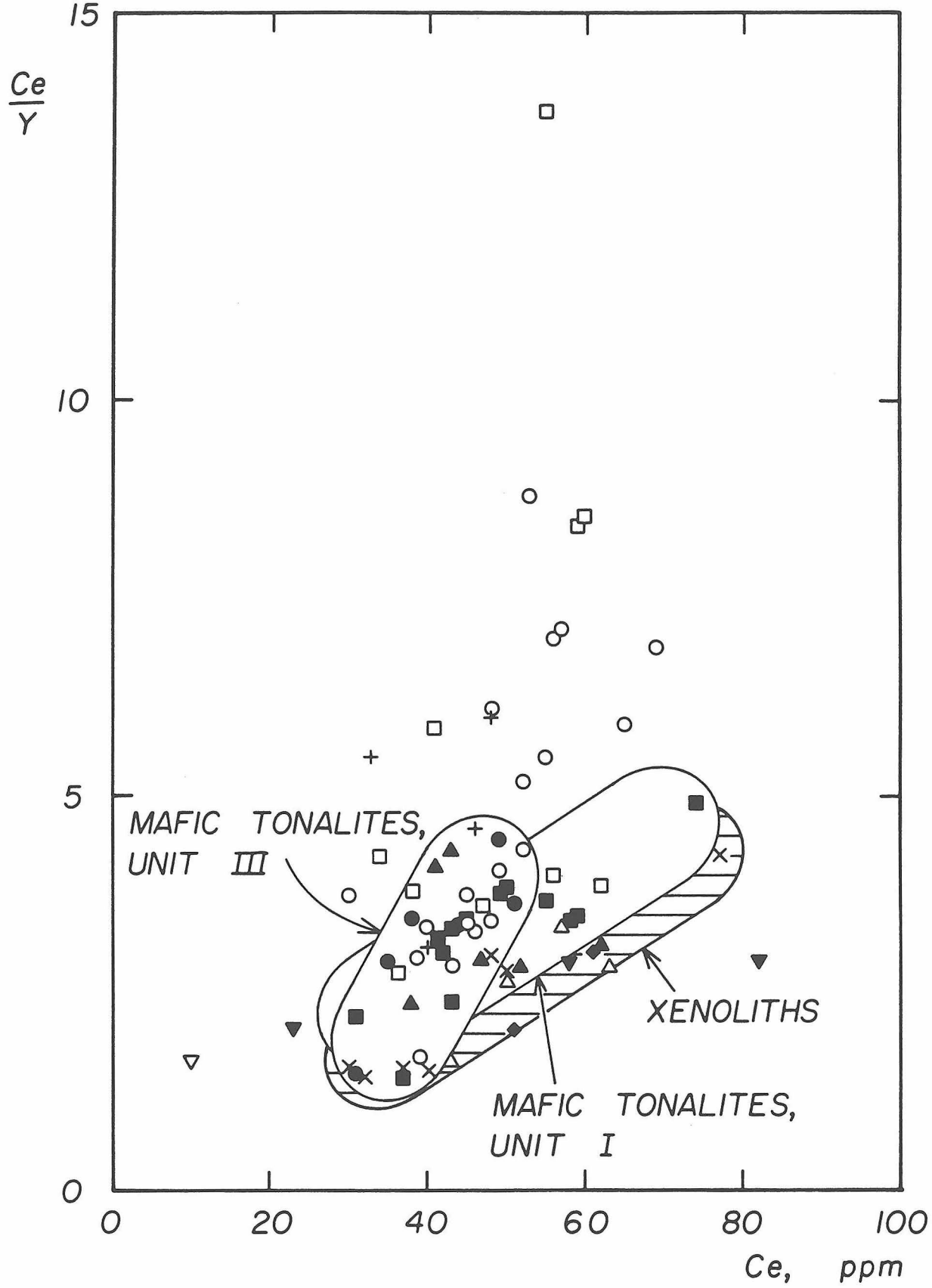
15
Ce/Y
10
5
0
MAFIC TONALITES, UNIT III
XENOLITHS
MAFIC TONALITES, UNIT I
0
20
40
60
80
100
Ce, ppm

Figure 7.15

The considerable scatter evident in the data for the more felsic rocks could result from removal of accessory phases in even slightly different proportions. This feature of REE fractionation where behaviour is controlled by minor phases has been predicted by Gromet and Silver (1983).

The trend shown by the mafic rocks - Ce/Y and Ce increase together - is consistent with the removal, either during fractional crystallization or by being left as residue in the source, of garnet, clinopyroxene, or amphibole. Gromet (1979) has argued that the complete REE data are most consistent with garnet control, and the data of Table 7.21 are consistent with this conclusion. This is further evidence that many of the geochemical characteristics of the mafic tonalites were derived with apparently little modification from the liquids from which they crystallized.

7.4 EARLY INTRUSIVES

The early intrusives show a much wider range of chemistry than do the major tonalites. However, with some exceptions, the gross geochemical features of the major tonalites are shared by the smaller earlier bodies. The small tonalite masses tend to have lower Ti, Fe, Mg and K at a given SiO_2, and marginally higher Ca and Al. Trace element abundances follow major element patterns - Rb, Pb, V and Cr tend to be lower as well in these rocks. The granodiorite of Poppet Creek is distinctive because of its high K (and Rb, Pb, and Th), but also has higher Mg, Fe, V and Cr, and lower Al, Na, P and Ga at a given SiO_2 than all other rocks. The K-feldspar megacryst bearing granodiorite of Apple Canyon, and a felsic dike from Thomas Mountain have, in general, the chemical characteristics of the more felsic of the major tonalites, as do samples from the Penrod Quartz Monzonite with the exception of lower Ca and higher Na.

The granodiorite of Poppet Creek is the sole analysed intrusive which differs significantly in its general chemical relations from the major tonalites. This body is much less plagioclase-rich than the other tonalites and low-K granodiorites, has an unusually high hornblende: biotite ratio of ≈1, and contains significant K-feldspar even in the most mafic rocks. This pluton also has lower Ce/Y at a given Ce than almost any other rock, implying that it has a much less fractionated REE pattern. These chemical differences could result from a different source composition, from a different residual mineralogy, from different fractionating phases during ascent from the zone of partial fusion, or from some combination of these factors.

7.5 SAMPLES FROM NORTH AND EAST OF TAHQUITZ PEAK, AND THE ROLE OF SEDIMENT CONTAMINATION

Cropping out on the high plateau of the southern San Jacinto Mountains north from Red Tahquitz are numerous small bodies of tonalite and granodiorite. Schlieren are common and locally abundant, and comb structure is present within these heterogeneous rocks. Irregular masses of iron-rich garnet are common adjacent ot contacts with enclosing metasedimentary rocks, and small garnets are observed for some distance from sediment/intrusive contacts, suggesting that sediment contamination may be more or less important in many of these rocks. Analyses of these samples are listed in Table 7.13. Only two rocks appear to be representative of "uncontaminated" undifferentiated materials on the basis of field criteria, and even these show considerable evidence for recrystallization. These two samples have geochemical characteristics similar to the other rocks from the San Jacinto Mountains. Five samples show effects of sediment contamination, and are characterized by extremely low Mg/(Mg +

Fe^{2+}), low Ti, variable Al, and high Ba, Zr, and REE. The contamination process is unlikely to involve simple mixing of sediment with a tonalitic melt (e.g., Bowen, 1928; Taylor, 1979), and no attempt has been made to model the complex sequence of processes likely to have been operating. Nevertheless, the high REE abundances in particular seem to reflect the high REE contents of the incorporated sediments (Table 7.14). Three geochemical features appear characteristic of sediment incorporation - low $Mg/(Mg + Fe^{2+})$ and extremely high Zr (>350 ppm) and REE (Ce>150x chondrites) abundances. These features are not seen in any rocks for which there is no a priori evidence for sediment incorporation. The most likely site for Zr in both the sedimentary and in the igneous rocks is zircon; the high Zr of the contaminated rocks thus implies substantial contamination by zircon from the sedimentary rocks. If these sedimentary rocks are old as is suggested by Sr isotope data (Ch. 2) then U-Th-Pb studies of zircon separates would be extremely sensitive to only small amounts of sediment contamination.

7.6 SUMMARY

All analysed uncontaminated igneous rocks from the San Jacinto Mountains share strikingly similar geochemical characteristics with the exception of the granodiorite of Poppet Creek. Rocks obviously contaminated by sediment incorporation have distinctive chemical characteristics which readily enable their distinction from all other rocks. These characteristics do not appear important in any other rocks with the possible exception of the samples from the Penrod Quartz Monzonite. The geochemistry of all other rocks is thus assumed to be of igneous derivation.

The major tonalites can be subdivided into three groupings on the basis of SiO_2 content, and certain trace element characteristics. "Mafic" tonalites have characteristics which suggest derivation from a liquid which had hornblende either as an important residual or fractionating phase. Volumetrically minor "felsic differentiates", selected using field criteria, have geochemical features consistent with derivation by crystal separation from liquids approximately represented by the composition of the mafic tonalites. "Normal" tonalites (and low-K granodiorites) have features intermediate between the other two groups, and could represent either products of lesser amounts of fractionation, different degrees of partial fusion, derviation from a source of different composition, or mixtures of more and less fractionated end-members (represented by the mafic tonalites and the felsic differentiates).

Five mafic xenoliths and a single dike have geochemical characteristics consistent with those of their host tonalites, but are somewhat more mafic, spanning the SiO_2 range 55.4-60.8 wt.% (cf., mafic tonalites 62.5-65.5). They have geochemical characteristics that strongly imply consanguineity, and may represent samples of liquids containing various amounts of suspended crystals (particularly plagioclase and hornblende) that were chilled upon introduction into the crystallizing magma chamber. If the similarities between the xenoliths and the mafic tonalites result from similar processes, then the xenolith compositions may imply that the tonalites had more mafic precursors, and that the "liquid line of descent" from ≈55 to 65 wt.% SiO_2 was controlled by processes in which hornblende removal and perhaps plagioclase addition were important factors.

CHAPTER 8

OXYGEN ISOTOPE RESULTS

8.1 INTRODUCTION

The processes that affect the oxygen isotopic composition of rocks differ fundamentally from those that affect other isotope tracers (Sr, Pb, and Nd) commonly used in igneous petrology. Variations in the isotopic composition of oxygen result from the mass dependence of the molecular vibrational frequencies of different isotopic species. Variations in the isotopic composition of the other elements listed above are the result of variable enhancement of the relative abundance of particular radiogenic isotopic species by radioactive decay processes, not by mass-dependent chemical or physical fractionation. The isotopic composition of oxygen thus reflects the effects of different geological processes than those that affect the isotopic composition of one of these heavier elements (Sr, Pb, Nd).

Oxygen has three naturally occurring isotopes, ^{16}O, ^{17}O, and ^{18}O. Ordinarily, only the $^{18}O/^{16}O$ ratio is measured and it is assumed that variations in ^{17}O abundance can be simply related to variations in ^{16}O and ^{18}O. Except in a few meteorites (e.g., Clayton et al., 1973) this indeed appears to be the case.

The $^{18}O/^{16}O$ variations in a given system are strongly temperature dependent as well as being process dependent. For a given reaction, the fractionation of $^{18}O/^{16}O$ is greatest at low temperatures and typically decreases (as $1/T^2$) with increasing temperature. At very high temp-

temperatures fractionations should become negligible (e.g. Urey, 1947; Bigeleison and Mayer, 1947).

Measured $^{18}O/^{16}O$ ratios of samples are usually reported in terms of the fractional difference (in parts per thousand, per mil) from the $^{18}O/^{16}O$ of a standard material, generally Standard Mean Ocean (SMOW)[Craig, 1961).

$$\delta^{18}O_{sample}, \text{ per mil} = \frac{\left(\frac{^{18}O}{^{16}O}\right)_{sample} - \left(\frac{^{18}O}{^{16}O}\right)_{standard}}{\left(\frac{^{18}O}{^{16}O}\right)_{standard}} \times 1000$$

A sample with a $\delta^{18}O$ value of +10 per mil is thus enriched in ^{18}O (or is greater in $^{18}O/^{16}O$ ratio) by 10% , relative to the standard. Negative δ values imply depletion by that amount relative to the standard. The range of terrestrial δ values (relative to SMOW) is from about -60 to + 40 per mil (e.g., Taylor, 1968).

8.2 RESULTS

8.2.1 ANALYTICAL PROCEDURES

The procedures used in the present study for oxygen isotope analysis follow closely those of Taylor and Epstein (1962a), with the exception that pure F_2 gas, not a mixture of HF and F_2 is used for the sample attack. Six analyses of the Rose Quartz intra-laboratory standard gave 8.44 ± 0.05 (2σ). An aliquot of Rose Quartz Standard was run with each five samples, and was used to monitor and correct for day to day variations in the behaviour of the spectrometer, as discussed by Taylor and Epstein (1962a).

A 20-30 mg aliquot taken from the same powders used for chemical and strontium isotope analyses was used for the oxygen isotopic determination. The data obtained for the Rose Quartz Standard suggest that analyses are reproducible to ± 0.05 per mil.

Oxygen isotope results obtained for 34 igneous and 4 metasedimentary rocks from the northwestern San Jacinto Mountains are listed in Table 8.1. Also included in this table are data for three rocks analysed previously for $\delta^{18}O$ (Taylor and Silver, 1978). Figure 8.1 shows the location of samples and the measured $\delta^{18}O$ obtained for each sample. Figure 8.2 is a histogram showing the data for the rocks analysed. Two features of these data deserve comment. Samples adjacent to pluton contacts with metasedimentary wall rocks have higher $\delta^{18}O$ values than samples distant from such contacts, and these samples are distinguished in Table 8.1. The majority of the reported data are from a single large (20x12 km) tonalitic pluton (Unit III). When rocks from adjacent to the pluton margin which show petrographic evidence for interaction with the wall-rocks (generally, samples from within 300 m of contacts with metasedimentary wall-rocks) are removed from consideration, eighty percent (15 of 18) of the remaining samples from Unit III have a restricted range of $\delta^{18}O$ values (from 10.07 to 10.36). There are insufficient data from the other units to allow generalizations about their $\delta^{18}O$ variations; however, the total range of measured whole-rock $\delta^{18}O$ values in plutonic rocks from the northwesern San Jacinto Mountains is only +9.0 to +10.6 (excluding samples affected by interaction with metamorphic country rock, and one olivine gabbro sample with $\delta^{18}O$ = +7.8).

8.3 DISCUSSION

Before the primary $\delta^{18}O$ variations in igneous rocks of the San Jacinto Mountains can be discussed, it is necessary to evaluate the role of secondary processes that can potentially modify the $\delta^{18}O$ of a rock subsequent to crystallization. By primary is meant the $\delta^{18}O$ characteristics of the rock (and thus its contained minerals) at the time of crystallization.

8.3.1 METAMORPHIC EFFECTS

Many workers have shown that the emplacement of a body of hot magma into relatively permeable, water-saturated country rocks commonly initiates the development of a hydrothermal circulation system in response to the superimposed lateral thermal gradient (e.g., Taylor, 1971, 1974, 1977; Forester and Taylor, 1977; Cathles, 1977; Norton and Knight, 1977). As the magma cools and crystallizes these hydrothermal systems collapse into and alter the recently solidified igneous rocks. The amount of interchange between the igneous rock and the hydrothermal fluid is a complex function of the permeability of the affected rocks, the water/rock ratio of the system, and the chemical and isotopic differences between the rock and the fluid. This model and these factors are well illustrated by detailed studies of the Skaergaard intrusion and its superimposed hydrothermal system (Taylor and Forester, 1979; Norton and Taylor, 1979).

Turi and Taylor (1971) studied the effects of a possible hydrothermal system initiated by the Domenigoni Valley Granodiorite, a stock emplaced into ^{18}O-rich metamorphic rocks near the northern end of the Peninsular Ranges batholith. The effects of exchange between the relatively light oxygen of the pluton ($+7.4\pm0.2$) and the relatively ^{18}O-rich meta-

TABLE 8.1.

OXTGEN ISOTOPIC DATA

SAMPLE NO.		COLOUR INDEX (VOLUME %)	$\delta^{18}O$, permil
	IGNEOUS COUNTRY ROCKS		
Granodiorite of Poppet Creek			
LTS 114	Fol. bi-hb granodiorite [1]	18.6 ± 1.0 [2]	9.53*
317	Fol. bi-hb granodiorite	27.6 ± 1.1	9.25
Tonalite of Snow Creek			
LTS 35	Fol. bi-hb-tn tonalite	20.9 ± 1.2	10.18*
Tonalite of Lucky Deer Mine			
LTS 381	Fine-grained bi-hb tonalite (a)	17.4 ± 0.9	10.12
Penrod 'Quartz Monzonite'			
LTS 318	Fol. gar-(sill) granite (a)	3.5 ± 0.6	11.90
SCB 794	Altered gar-(sill) granite (a)	8.4 ± 0.6	14.26
SCB 794Q	Auriferous quartz vein		14.60
Gabbro of Thomas Mountain			
LTS 27	Olivine gabbro	56.4 ± 2.7	7.82*
Un-named sill south of Banning			
LTS 211	Fol. bi tonalite (a)	10.6 ± 1.0	11.50
	METAMORPHIC COUNTRY ROCKS		
SCB # 747A	Qtz+bi+cd+il+K-fs+sill gneiss		13.51
747B	Qtz+bi+cd+mu gneiss		13.15
747C	Qtz+bi+cd+mu gneiss		13.23
779A	Qtz+bi+sill+K-fs+gar+cd gneiss		11.54
	MAJOR TONALITIC UNITS		
Unit I			
LTS 219	Bi-hb-tn tonalite	20.3 ± 1.2	9.76*
298	Bi-hb-tn low-K granodiorite	9.5 ± 0.8	10.43
324	Bi-hb-tn tonalite (a)	17.2 ± 0.8	10.34
325	Bi-hb-tn tonalite	19.5 ± 0.9	10.17
363	Bi-hb-tn tonalite	16.8 ± 0.9	10.14

TABLE 8.1 (CONTINUED)

Unit II			
LTS 329	Bi-hb-tn tonalite	20.7 ± 1.2	9.72
Unit III			
LTS 145	Bi-hb-tn low-K granodiorite	11.0 ± 0.7	10.28
146	Bi-hb-tn low-K granodiorite	13.3 ± 0.9	10.36
151	Bi-hb-tn tonalite	15.3 ± 0.9	10.07
152	Bi-hb-tn tonalite	13.8 ± 0.9	10.13
212	Bi-hb-tn low-K granodiorite	9.2 ± 1.0	10.35
213	Bi-tn low-K granodiorite (a)	10.5 ± 0.9	10.97
221	Bi-hb-tn tonalite	23.4 ± 1.1	8.99
290	Bi-hb-tn tonalite	16.6 ± 1.0	9.63
292	Bi-hb-tn low-K granodiorite	10.7 ± 0.8	10.57
331	Bi-hb-tn tonalite	13.3 ± 0.8	10.07
332	Bi-hb-tn tonalite	15.6 ± 0.8	10.22
333	Bi-hb-tn tonalite	11.9 ± 0.7	10.17
334	Bi-hb-tn tonalite (b)	15.7 ± 0.9	10.43
335	Bi-hb-tn tonalite	15.3 ± 0.8	10.15
336	Bi-hb-tn tonalite (a)	14.3 ± 0.8	10.51
337	Bi-hb-tn tonalite	10.3 ± 0.7	10.24
358	Bi-hb-tn low-K granodiorite	9.5 ± 0.7	10.06
359	Bi-hb-tn tonalite	12.4 ± 0.6	10.14
360	Bi-hb-tn tonalite (a)	18.7 ± 0.9	10.46
365	Bi-hb-tn tonalite (a)	10.7 ± 0.7	10.93
366	Bi low-K granodiorite	10.8 ± 0.7	10.20
367	Bi-hb-tn low-K granodiorite	11.9 ± 0.7	10.26
369	Bi low-k granodiorite	13.7 ± 0.8	10.03

---

1 Abbreviations used: Bi = Biotite; Hb = Hornblende; Tn = Titanite
Fol = Foliated

2 Quoted error in the Colour Index is 1σ from counting statistics

* Taylor and Silver (1978)

(a) Sample from within 300m of contact with metasedimentary wall-rock.
(b) Sample with petrographic evidence for substantial sub-solidus alteration

Figure 8.1. Location of analysed samples, San Jacinto mountains, southern California.

Squares	-	Unit I
Tringles	-	Unit II
Circles	-	Unit III
Plus signs	-	Felsic differentiates
Diamonds	-	Early intrusives
Asterisks	-	Measedimentary rock samples

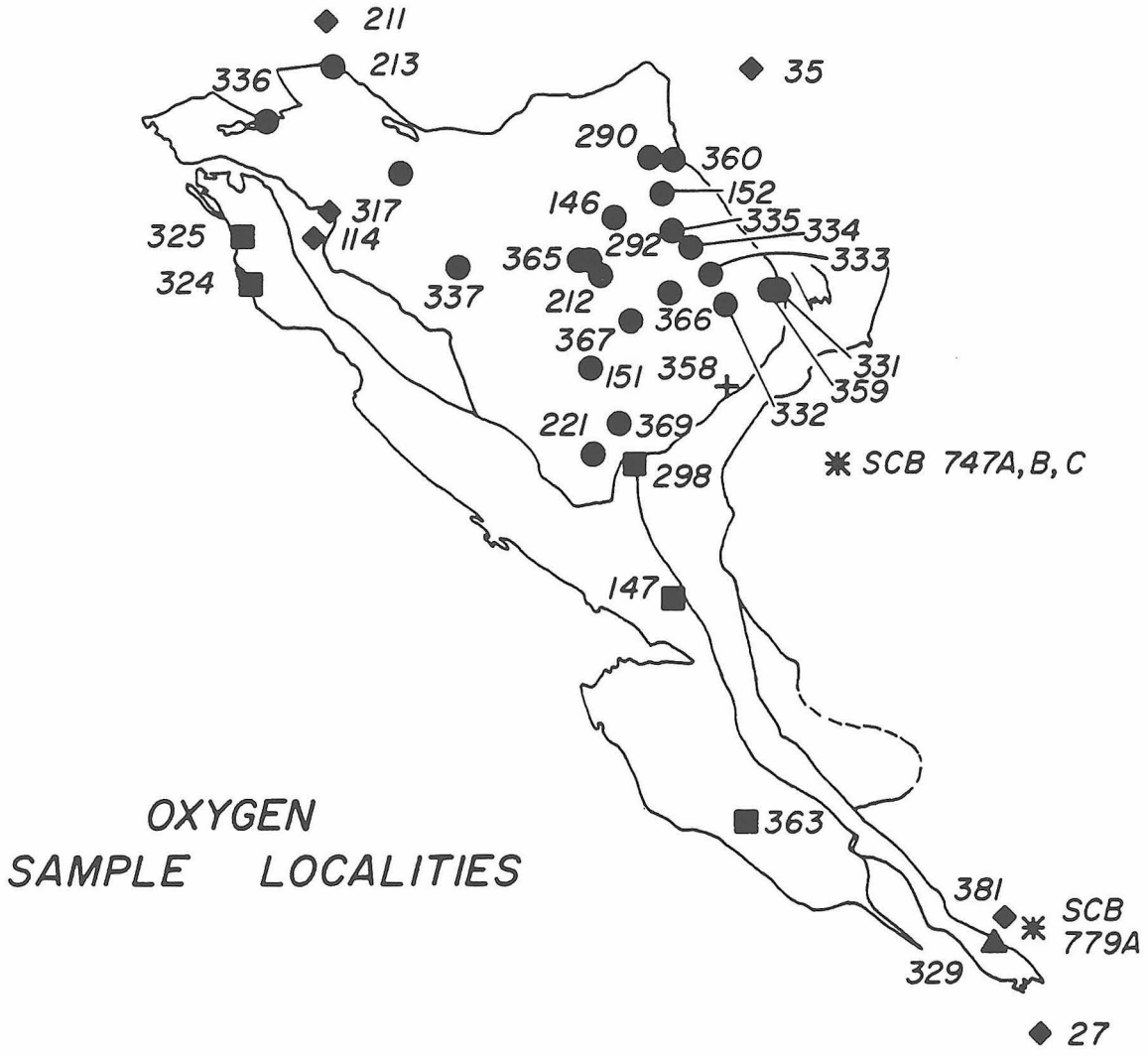
211
213
336
35
290
360
152
146
335
334
292
333
317
114
325
324
365
337
212
366
367
151
358
331
359
332
221
369
298
SCB 747A, B, C
147
363
381
SCB
779A
329
27
OXYGEN
SAMPLE LOCALITIES

Figure 8.1

Figure 8.2. Histogram of observed $\delta^{18}O$ values showing distribution by rock unit.

Filled squares	-	"Mafic" tonalites (<65.5 wt.% SiO_2)
Open squares	-	"Normal" tonalites (>65.5 wt.% SiO_2)
Plus signs	-	Felsic differentiates
Circles	-	Samples from within 300m of exposed or inferred metasedimentary wall-rocks
S	-	Metasedimentary rocks (quartz-rich gneisses) from the Desert Divide Group
Q	-	Quartz (+ minor feldspar) vein cutting granite of Penrod Canyon at Hemet Belle Gold Mine

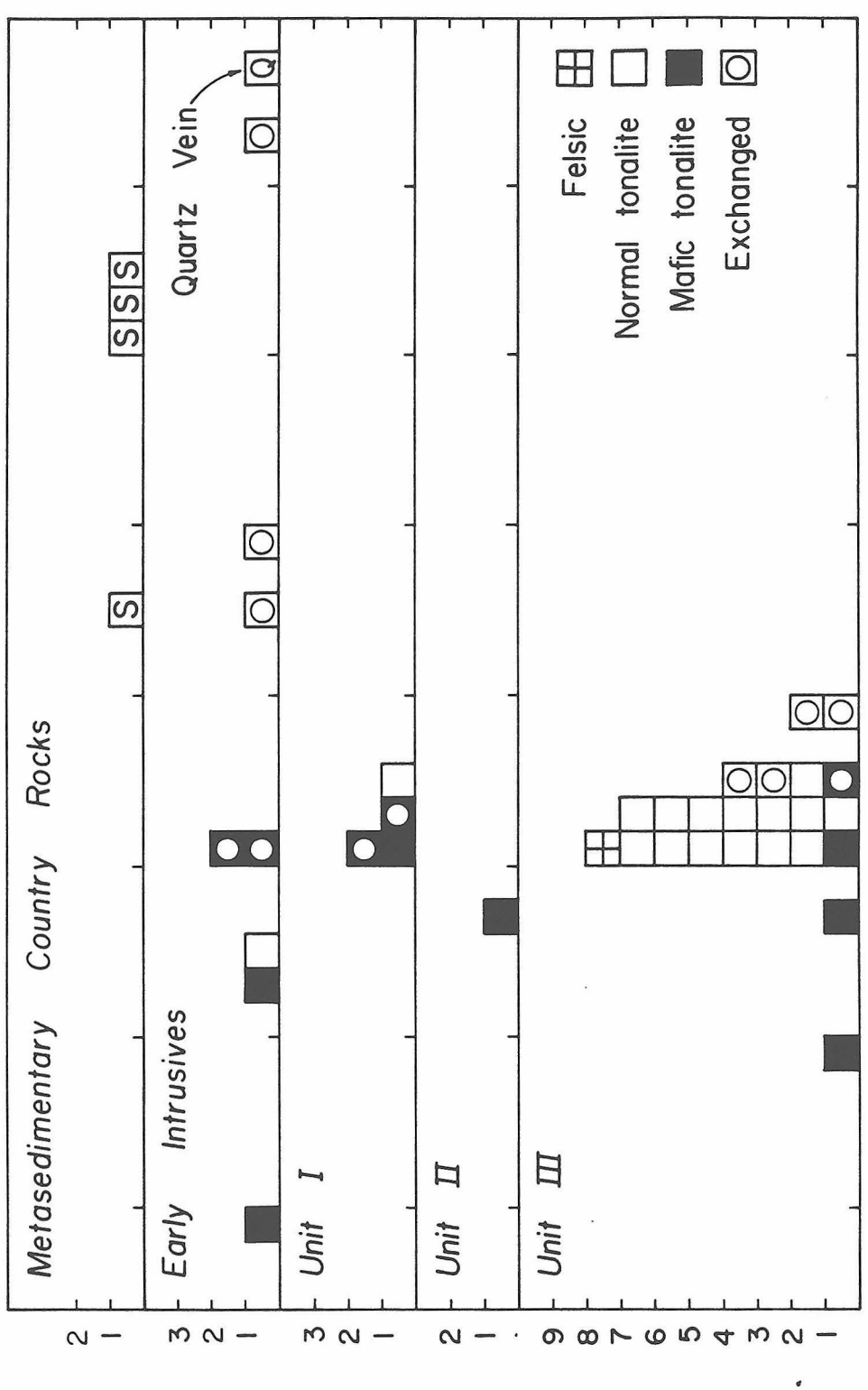
Metasedimentary Country Rocks
Early Intrusives
Quartz Vein
Unit I
Unit II
Unit III
Felsic
Normal tonalite
Mafic tonalite
Exchanged
Number of analyses
δ18O, ‰

Figure 8.2

morphic metamorphic pore fluids derived from the country rock are detectable for some distance inward from the pluton margin. The isotopic composition of these fluids was buffered by the large oxygen reservoir of the surrounding, isotopically heavy (+20) cordierite and sillimanite schists. This study demonstrated that a hydrothermal system with its oxygen isotopic composition buffered by the oxygen of the wall-rocks can be induced by a pluton, and that the effects of this hydrothermal system can be seen in the oxygen isotopic composition of the rocks of the outer part of the pluton. However, the possibility that some of the ^{18}O-enrichment in the margins of this pluton took place during the magmatic stage by assimilation and/or exchange between silicate melt and wall-rock must also be considered.

Many of the intrusive bodies of the San Jacinto Mountains also appear to have interacted with their wall rocks in the same fashion as did the Domenigoni Valley Granodiorite. Metamorphic assemblages in the country rocks include sillimanite+K-feldspar+quartz+cordierite+biotite ±garnet± plagioclase as well as muscovite+quartz+sillimanite(fibrolite)+biotite and muscovite+quartz+biotite+cordierite+ilmenite. These assemblages imply metamorphic temperatures of 600-650°C at total pressures of 3.2-4.2 kb (Ch. 3). It has been argued above that these metamorphic conditions are related to intrusion of the igneous rocks (Ch. 3). At such temperatures the isotopic fractionations between minerals and water are small (Friedman and O'Neil, 1977). This is shown on Figure 8.3, modified from Friedman and O'Neil (1977). Measured $\delta^{18}O$ values in the metamorphic country rocks range from 11.5 to 13.5. These data imply that any fluids present (perhaps largely metamorphic water derived from dehydration reactions during progressive regional metamorphism) would have $\delta^{18}O$ values of approximately

Figure 8.3. Graph illustrating selected plagioclase(An_{60})-mineral, and and plagioclase(An_{60})-water oxygen isotope fractionation as a function of temperature (in degrees Celsius). Modified from Friedman and O'Neil (1977) by addition of plagioclase-water fractionation from Bottinga and Javoy (1973).

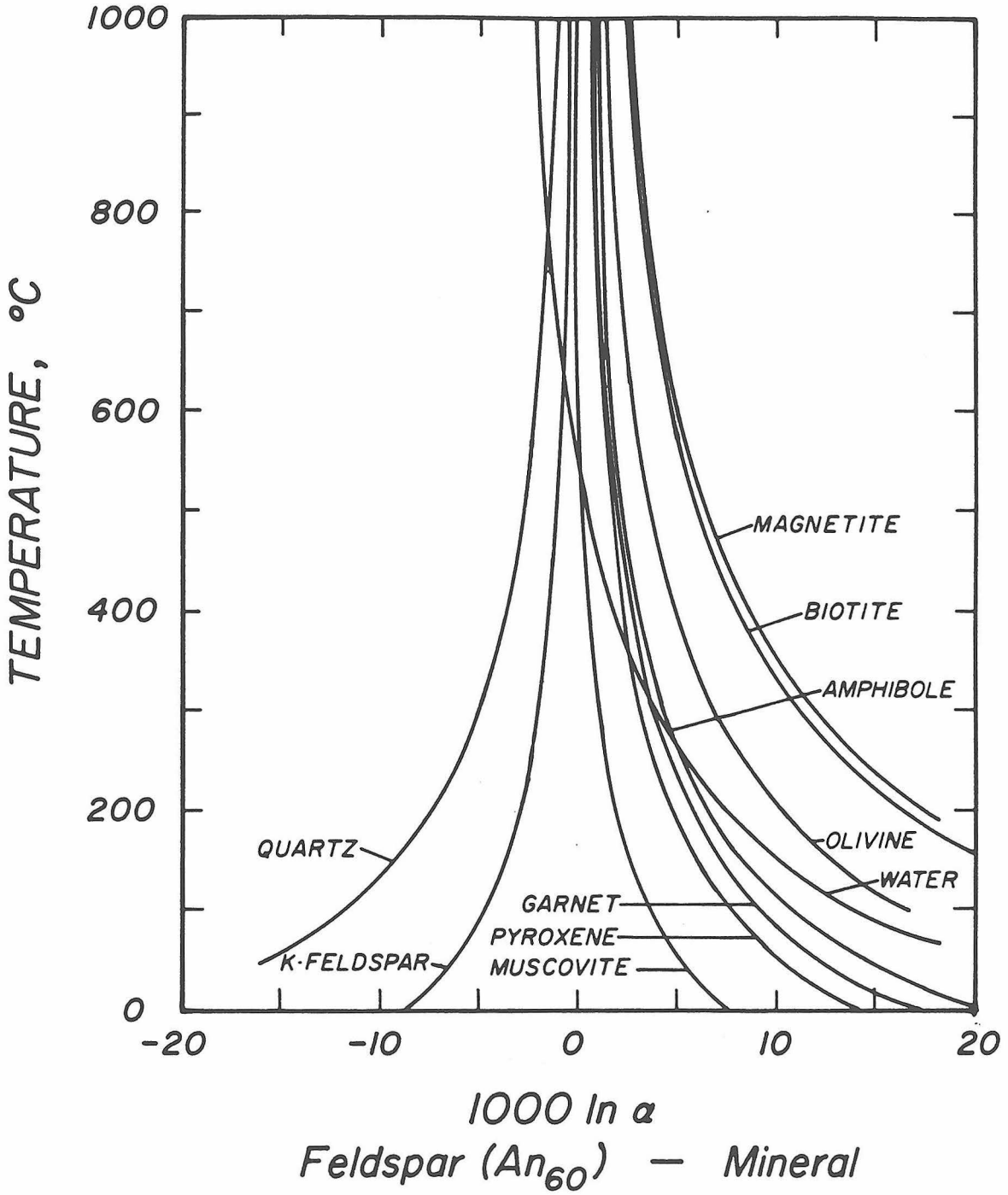
1000
800
600
400
200
0
TEMPERATURE, °C
-20
-10
0
10
20
1000 ln α
Feldspar (An60) — Mineral
MAGNETITE
BIOTITE
AMPHIBOLE
OLIVINE
WATER
GARNET
PYROXENE
MUSCOVITE
QUARTZ
K-FELDSPAR

Figure 8.3

+10.5 to +13.5. A small pluton of foliated garnet-bearing granite intrusive into metasedimentary rocks north of Garner Valley (the granite of Penrod Canyon) has $\delta^{18}O$ = +11.9. A system of auriferous quartz veins is centered upon and cuts this pluton (Ruff and Unruh, 1979), and areas of alteration are spatially associated with this vein system. A sample of the altered granite has $\delta^{18}O$ = +14.3, and a quartz (+ minor feldspar) vein has $\delta^{18}O$ = +14.6. At 500-600°C this vein would have been in equilibrium with water with a $\delta^{18}O$ value of +11.2 to +14.1 (Shiro and Sakai, 1972). This is approximately the isotopic composition of water that would have been in equilibrium with the enclosing metasedimentary rocks, suggesting that this pluton initiated a hydrothermal system, the water in which was buffered by the surrounding metasedimentary rocks. The "unaltered" rock has thin white-mica selvedges developed on fractures cutting K-feldspar crystals, and also contains felted masses of sillimanite (fibrolite). These combined data are consistent with deposition of the vein quartz from a hydrothermal fluid in isotopic equilibrium with the surrounding metamorphic rocks, and with the apparent high $\delta^{18}O$ of the pluton being the result of exchange with these hydrothermal fluids.

Similar exchange effects might be expected in the multitude of small intrusions that preceded emplacement of the main tonalitic units, but few isotope data have been collected to ascertain whether this is indeed the case. If so, and the few data obtained are suggestive that it is, then the effects of exchange may be complicated somewhat by the sequential imposition of hydrothermal systems set up by each new intrusive. For example, masses of tonalite adjacent to the upper (and northern) contact of Unit III that crop out along St. Rte. 243 south of Banning are mineralogically and texturally quite similar to the nearby rocks of

Unit III; however, an analysed sample (LTS 211) has elevated $\delta^{18}O$ (+11.5) and high initial $^{87}Sr/^{86}Sr$ (0.7080). These data are interpreted as resulting from exchange of both oxygen and strontium with circulating fluids during interaction with an imposed hydrothermal system, or possibly with local assimilation and exchange between the silicate melt and the country rocks. However, given the limited data set available, there is no way to exclude the possibility that these effects result from a much more extensive circulative system related to later emplacement of the adjacent and much larger Unit III.

Samples obtained adjacent to the contacts of the major plutons with metasedimentary wall rocks commonly have elevated $\delta^{18}O$ values when compared to those of samples more interior to that intrusive unit. These marginal samples commonly show textural evidence for post-crystallization reaction with an aqueous fluid. Substantial chloritization of biotite, the development of turbidity in feldspar, and the replacement of hornblende and more calcic feldspar by epidote are common only in rocks adjacent to mapped or projected pluton contacts. Accordingly, samples from within 300 m of mapped or projected pluton/metasedimentary rock contacts are differentiated in Table 8.1. In contrast, samples adjacent to contacts with older igneous bodies do not show any systematic variation in $^{18}O/^{16}O$, and generally also show less evidence for sub-solidus alteration.

These observations are interpreted as showing that there was interaction between the igneous rocks and their metasedimentary host rocks, but that this interaction was not extensive and only affected the marginal rocks of the larger intrusives.

8.3.2 PRIMARY IGNEOUS $^{18}O/^{16}O$

If the exchange effects described above are deleted from further consideration, the total range in primary $\delta^{18}O$ values observed for igneous rocks from the San Jacinto Mountains is from +9.0 to +10.6, with the exception of a sample of rare olivine gabbro which has $\delta^{18}O$ = +7.8. The bulk of the analyses show a very restricted variation in $\delta^{18}O$ of +10.0 to +10.4. Rocks with $\delta^{18}O$ values of less than 10.0 tend to be noticeably more mafic, while those with $\delta^{18}O$ of 10.3 or greater tend to be more felsic. This systematic variation of $\delta^{18}O$ with composition is particularly striking for Unit III. Figure 8.4 shows the geographic distribution of $\delta^{18}O$ in unaltered samples from this pluton. Marginal samples tend to have lower and more variable $\delta^{18}O$ than do samples more interior to this unit. Within the better studied eastern part of this pluton $\delta^{18}O$ values increase systematically inwards, from +10.0 or less in the marginal tonalites to as high as +10.5 in the central granodiorites. This concentric variation of $\delta^{18}O$ mirrors the petrological and geochemical variations described above (e.g., mineral abundance, Ch. 5; mineral chemistry, Ch. 6). The covariation of $\delta^{18}O$ and petrological parameters is well shown on Figure 8.5, a plot of measured $\delta^{18}O$ versus Colour Index. The majority of the samples from Unit III apparently show a slight increase in $\delta^{18}O$ (from +10.05 to +10.35) as Colour Index falls from 15.5 to 9.0. The other samples from Unit III, and the few samples from the other units, show a much wider range in both $\delta^{18}O$ and Colour Index. Before the origin of these correlations can be considered, it is necessary to provide context in which these observations can be discussed.

Figure 8.4. Geographic distribution of measured $\delta^{18}O$ values, Unit III.

Filled symbols - "Mafic" tonalites (<65.5 wt.% SiO_2)
Open symbols - "Normal" tonalites
Plus signs - Felsic differentiate

Brackets indicate samples from within 300 m of exposed or inferred metasedimentary country rocks that have not been used in the contouring.

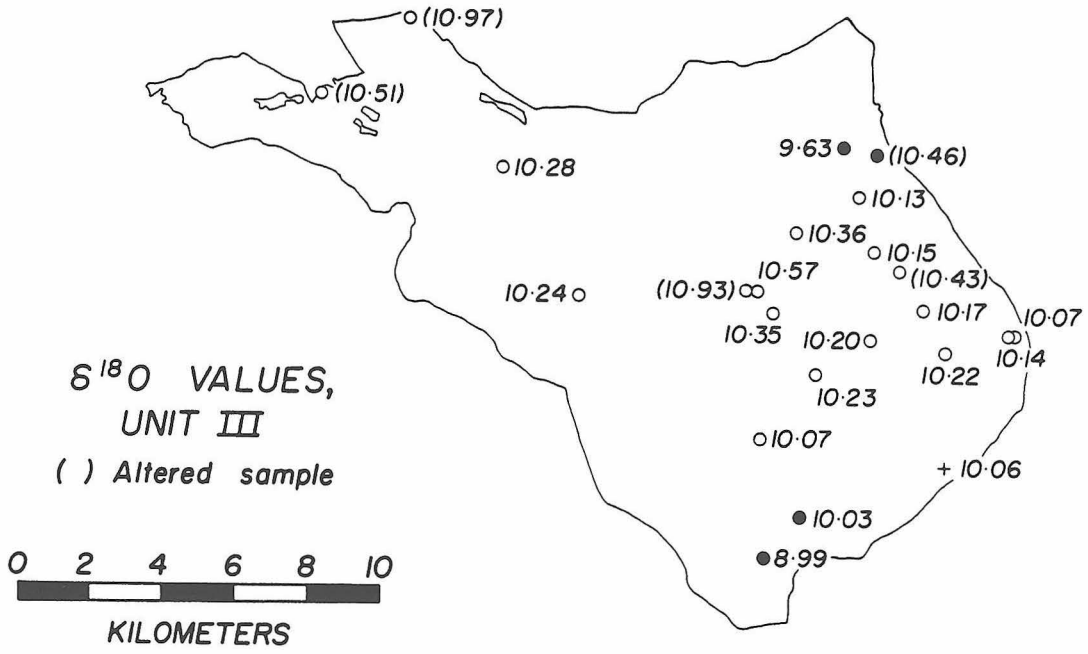
(10·97)
(10·51)
10·28
9·63
(10·46)
10·13
10·36
10·15
10·57
(10·43)
10·24
(10·93)
10·17
10·07
10·35
10·20
10·14
10·22
10·23
10·07
+ 10·06
10·03
8·99
δ18O VALUES,
UNIT III
( ) Altered sample
0 2 4 6 8 10
KILOMETERS

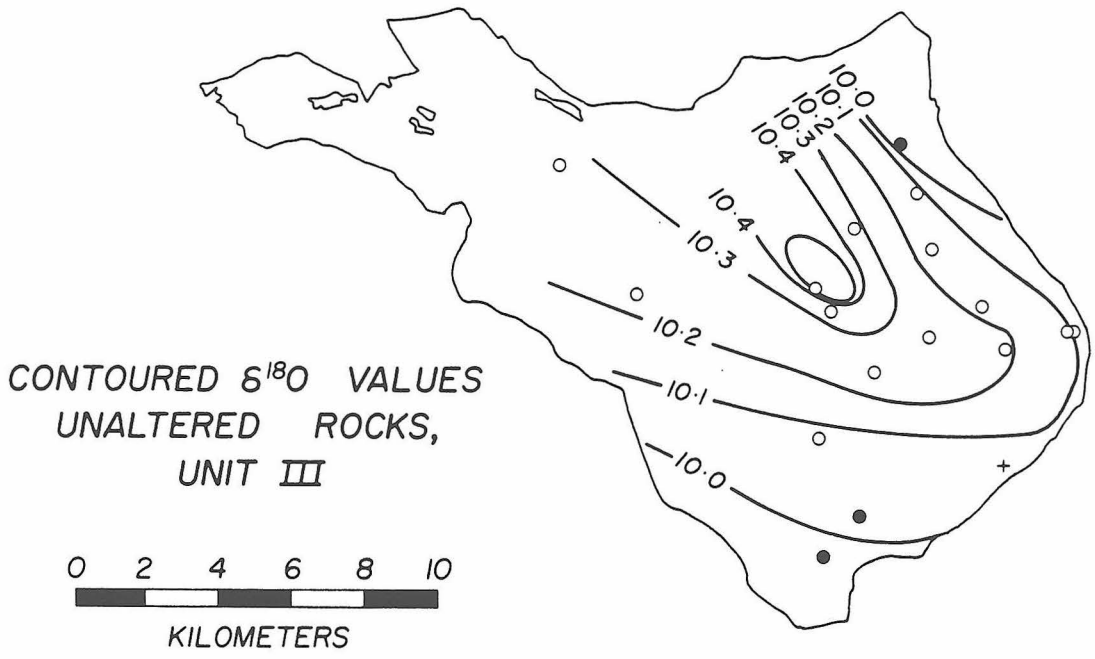
10·0
10·1
10·2
10·3
10·4
10·4
10·3
10·2
10·1
10·0
CONTOURED δ18O VALUES
UNALTERED ROCKS,
UNIT III
0 2 4 6 8 10
KILOMETERS

Figure 8.4

Figure 8.5. Graph showing correlation between Colour Index (volume %) and measured $\delta^{18}O$ for tonalites and low-K granodiorites from the north-western San Jacinto Mountains.

Filled symbols	-	"Mafic" tonalites
Open symbols	-	"Normal" tonalites
Squares	-	Unit I
Triangles	-	Unit II
Circles	-	Unit III
Plus sign	-	Felsic differentiate
Diamonds	-	Granodiorite of Poppet Creek
Inverted triangles	-	Early intrusives

Samples from within 300m of metasedimentary wall-rocks and samples for which there is petrographic evidence for substantial subsolidus alteration enclosed in brackets.

Range of $\delta^{18}O$ values obtained for metasedimentary rocks samples shown by horizontal bar.

Fields for samples from the central part of Unit III which show regular geographic variation of $\delta^{18}O$ values, and for two samples from close to the inferred roof of this pluton are shown.

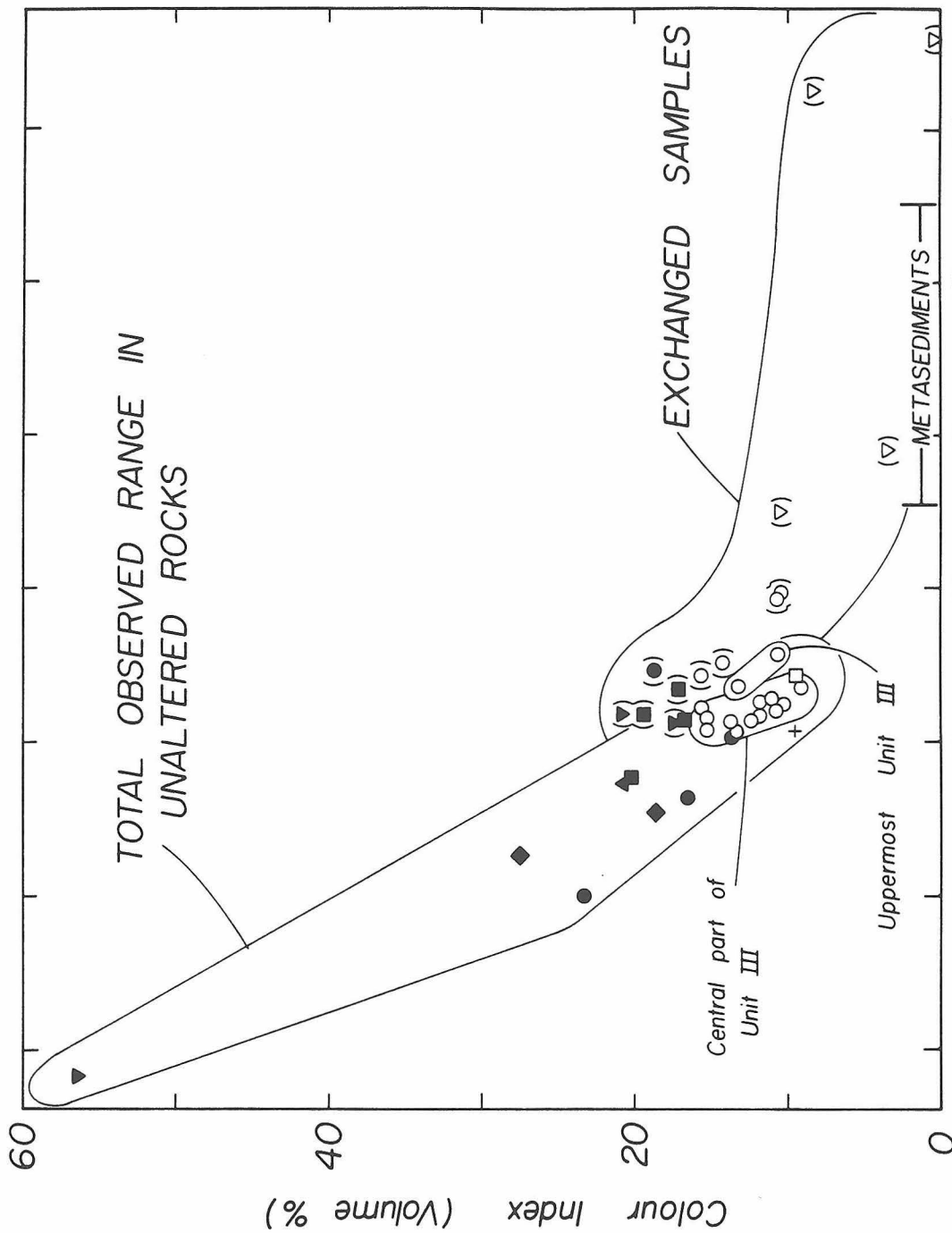
TOTAL OBSERVED RANGE IN UNALTERED ROCKS
EXCHANGED SAMPLES
METASEDIMENTS
Central part of Unit III
Uppermost Unit III
Colour Index (Volume %)
δ 18O, permil
0
20
40
60
8
9
10
11
12
13
14

Figure 8.5

8.4 ORIGIN OF THE $\delta^{18}O$ CHARACTERISTICS OF THE SAN JACINTO ROCKS

8.4.1 $^{18}O/^{16}O$ VARIATIONS IN IGNEOUS ROCKS

Variation in the $^{18}O/^{16}O$ of igneous rocks has been extensively studied by H.P. Taylor, Jr., and his co-workers (e.g., see review papers by Taylor (1974, 1977, 1978). Figure 8.6 (from Taylor, 1974) is a compilation of $^{18}O/^{16}O$ data from a wide variety of igneous rock types from many localities. The total range of values reported is some 25 per mil, from about -10 to +15. Many igneous rocks do not maintain their original magmatic oxygen isotopic composition, but interact extensively with hydrothermal fluids near the surface of the earth. Interactions involving low $\delta^{18}O$ fluids derived from meteoric waters are common in continental environments, and account for much of the scatter to low $\delta^{18}O$ values apparent on Fig. 8.6 (e.g., Taylor, 1971, 1974, 1983; Taylor and Forester, 1971, 1979). Interaction with ^{18}O-rich metamorphic waters has also been documented (e.g., Turi and Taylor, 1971), and this tends to increase the $\delta^{18}O$ values in the border zones of many granitic plutons.

In general, unaltered basalts and gabbros have $\delta^{18}O$ values between +5.5 and +6.5, whilst granodiorites and granites are more likely to have $\delta^{18}O$ values of +8 to +10 or more (e.g., Taylor and Epstein, 1962a, b; Taylor, 1978; O'Neil and Chappell, 1977). However, as originally pointed out by Taylor and Epstein (1962b, p.682), this generalization breaks down in detail.

Figure 8.6. Observed $\delta^{18}O$ values of igneous rocks and minerals from a a wide variety of localities (Taylor, 1974). Note generally consistent difference between whole rock $\delta^{18}O$ values for basalts and gabbros (+ 5.5—+7.5) and plutonic granites, granodiorites and tonalites (+7.0—+13). Observed range for unexchanged plutonic rocks from the Peninsular Ranges batholith is +6 to +13 per mil (Taylor and Silver, 1978).

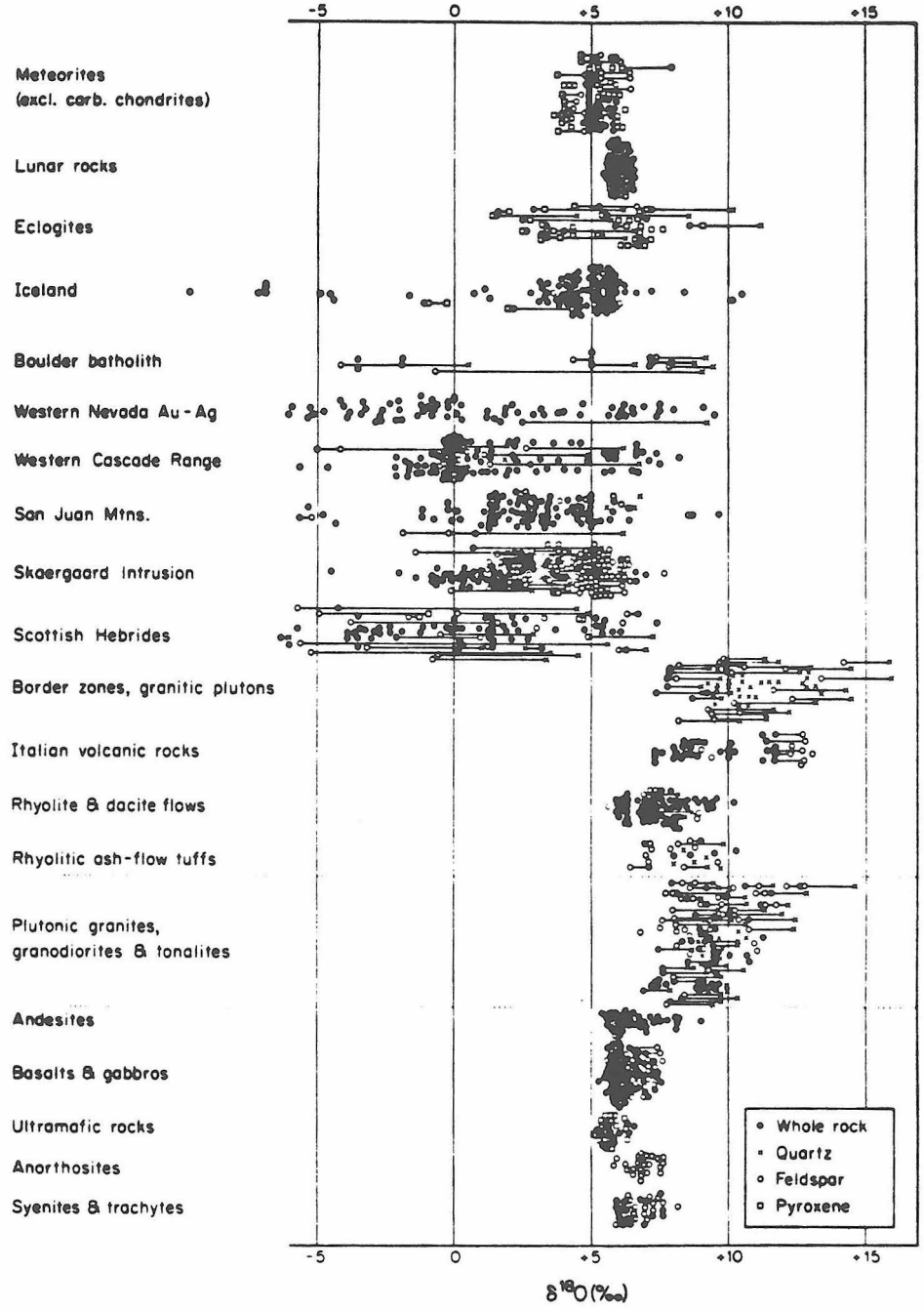

δO^{18}-values of igneous rocks and minerals from a variety of localities.

Figure 8.6

8.4.2 CAUSES OF PRIMARY $^{18}O/^{16}O$ VARIATION IN IGNEOUS ROCKS

There appear to be three major plausible explanations for the variation in $^{18}O/^{16}O$ found for igneous rocks. These are

1. Fractionation processes, either within a crystallizing magma chamber or conduit system, or during partial fusion;
2. Derivation from source regions with pre-existing variations in $^{18}O/^{16}O$; and
3. Assimilation of, or exchange with wall rocks surrounding either the conduits or the magma chamber.

These processes are not, of course, mutually exclusive, and there could be a complete and complex gradation from one extreme to the other.

Fractionation Processes

The liquid portion of a magma can be expected to continuously change composition (both chemical and isotopic) as it crystallizes because in general the solid precipitated at any instant will differ in composition from the coexisting liquid. The early formed crystals tend to be more mafic and lower in SiO_2, and are also usually relatively enriched in ^{16}O compared to ^{18}O (e.g., Taylor and Epstein, 1962a; Friedman and O'Neil, 1977). Residual liquids accordingly tend toward both increased $\delta^{18}O$ values and higher SiO_2 as crystallization proceeds. The simplest case of such a process is fractional distillation (Rayleigh, 1896), where the instantaneous solid precipitated is isolated from further interaction with the remaining liquid. Isolation may result from physical transport of the precipitated solids, by armouring of the precipitated

Figure 8.7. Diagram showing relationship between $\delta^{18}O$ and percent solidified for a simple Rayleigh distillation model. See text for further discussion. Initial $\delta^{18}O$ value of liquid = +6.00. Values of $\Delta = \delta_{\text{liquid}} - \delta_{\text{solid}}$ shown on respective curves.

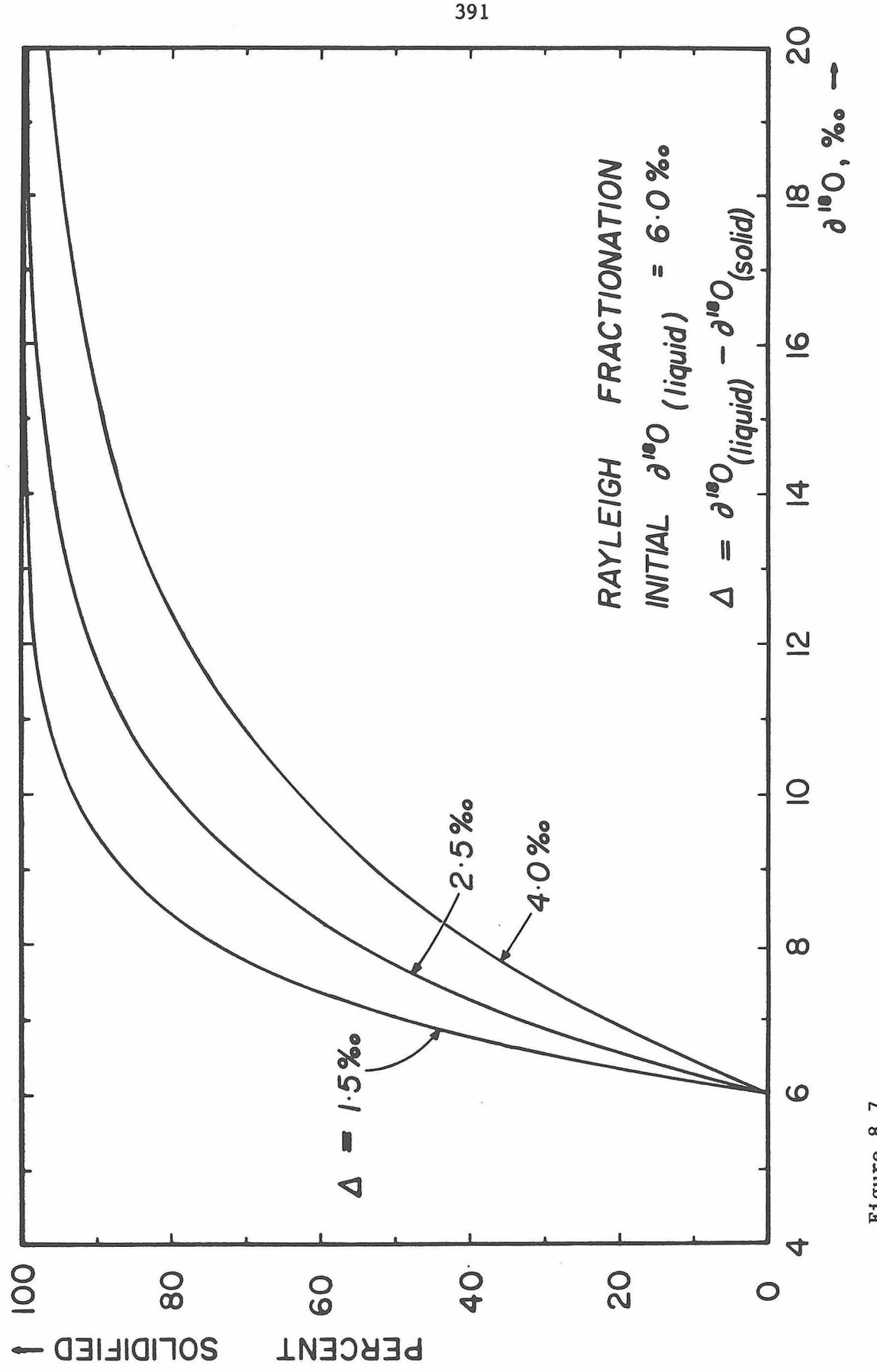
RAYLEIGH FRACTIONATION
INITIAL $\delta^{18}O_{(liquid)}$ = 6·0‰
$\Delta = \delta^{18}O_{(liquid)} - \delta^{18}O_{(solid)}$
Δ = 1·5‰
2·5‰
4·0‰
PERCENT SOLIDIFIED →
0
20
40
60
80
100
4
6
8
10
12
14
16
18
20
$\delta^{18}O$, ‰ →

Figure 8.7

grains, or may result from the slow rate of solid-liquid exchange processes. The application of this process to oxygen isotope fractionation within a cooling silicate liquid was discussed by Taylor and Epstein (1962b), and they show that it is unlikely that large volumes of material with substantially modified $\delta^{18}O$ (by more than a few per mil) can be produced in this manner. Figure 8.7 illustrates graphically the magnitude of variation obtainable by fractional crystallization. If $\delta^{18}O$(liquid)-$\delta^{18}O$(solid)[Δ] is small(<1.5 per mil) the bulk of the system shows little variation in $\delta^{18}O$; the last 20% of the liquid to solidify, however, may show substantial variation in $\delta^{18}O$. Matsuhisa et al., (1973) estimate Δ of 0.3-0.5 per mil for tholeiitic and ≈1.0 per mil for calc-alkaline rock series in Japan, suggesting that Δ in natural systems is not likely to be large. This conclusion has been supported by other studies of natural systems, and it appears that the maximum whole rock $\delta^{18}O$ variation resulting purely from fractional crystallization in nature is less than 1.5 per mil (Taylor and Silver, 1978; Matsuhisa, 1979; Muehlenbachs and Byerly, 1982; Chivas et al., 1982).

The effects of fractionation during partial fusion have been considered in detail by Kyser et al., (1982). Using both empirically (Kyser et al., 1981) and experimentally (Muehlenbachs and Kushiro, 1974) determined estimates of the fractionation between silicate liquids and co-existing minerals, they concluded that for temperatures in the range 1100 to 1300°C and with reasonable variations in the conditions under which melting occurred variation of $\delta^{18}O$ within the derivative liquids of perhaps a few tenths per mil could result. This conclusion holds for the three models of melt production considered (fractional fusion, equilibrium fusion and disequilibrium fusion). At such high temperatures

garnet, clinopyroxene and orthopyroxene have almost identical equilibrium $\delta^{18}O$ (i.e., $\Delta_{cpx-opx} \approx 0$), so that variation of the relative proportions of these phases in the residue will have no effect on the $\delta^{18}O$ of the liquid (Kyser et al., 1982). Varying the relative amounts of olivine and these three minerals could, depending on the temperature of fusion, change the $\delta^{18}O$ of resultant melts by a maximum of about 1.0 per mil. This would, however, require an unlikely change from an olivine-free to an olivine-only residue.

The second process that could yield considerable variation in the $^{18}O/^{16}O$ of igneous rocks is the presence of pre-existing variation in the source volumes from which the rocks are generated. Most mafic and ultramafic rocks appear to be derived from a large reservoir with essentially homogeneous $^{18}O/^{16}O$, presumed to be the mantle (e.g., Taylor, 1968). Kyser et al., (1982) report the presence of small variations in the mean $\delta^{18}O$ values of unaltered basaltic rocks from different environments. The $\delta^{18}O$ values of Hawaiian tholeiites are $+5.4\pm0.4$, those of MOR basalts are $+5.7\pm0.5$, and those of alkali basalts are $+6.2\pm0.5$. Potassic lavas have $\delta^{18}O$ values of 7.5 ± 1.5, and appear confined to continental environments. Kyser et al., (1982) concluded that these small differences result from variations in the $\delta^{18}O$ values of the respective source volumes accumulated from previous melting events. The relatively high $\delta^{18}O$ values of the potassic continental lavas are suggested to derive from subcontinental lithosphere which has become isotopically heavy after extraction of several previous volumes of melt, or through introduction of sedimentary ^{18}O-rich material. The total range of $\delta^{18}O$ values obtainable in liquids derived from oceanic mantle thus appears to be from +5.0 to +6.7; liquids derived from subcontinental mantle for which there is no evidence

for prior sedimentary injection may have slightly higher $\delta^{18}O$ values (7.0-7.5). These variations are suggested to largely reflect $\delta^{18}O$ heterogeneity within the mantle rather than to result from fractionation processes during partial fusion (Kyser et al., 1982).

Gregory and Taylor (in preparation) re-interpret the data of Kyser et al., (1981, 1982) as showing evidence for (oxygen) isotopic disequilibrium between the constituent minerals from many mantle-derived mafic nodules. They suggest that this apparent disequilibrium results from partial exchange with a metasomatizing fluid within the mantle, and they estimate that this fluid may have $\delta^{18}O$ values as high as +7.5. This still appears to limit the $\delta^{18}O$ values of mantle-derived melts to about +8 or less.

In contrast, more felsic rocks appear to be generated from much more variable source volumes. Rocks more felsic than basalt are volumetrically unimportant in all but the continental and island arc environments, where the $\delta^{18}O$ range of possible source materials is much greater than that thought to be present in the mantle. Continental rocks span the $\delta^{18}O$ range from +40 (authigenic silica in accreted sediments) through carbonates (+30), clastic sedimentary rocks (commonly +10 to +20), and igneous rocks derived from unmodified mantle (+5 to +7) to hydrothermally altered rocks of various types with $\delta^{18}O$ values of 0 or lower (e.g., Taylor, 1968). Both island arc and continental rocks could also be derived directly from the mantle with no interaction with older continental crustal material.

It thus appears that primary $\delta^{18}O$ values for unexchanged igneous rocks of about +5.0 or less cannot result from normal fractionation

processes, and must be related to original source properties. On the other hand, $\delta^{18}O$ values greater than +6 may result from either fractionation processes or from source variation, or from some combination of these two processes such as combined assimilation-fractional crystallization (e.g., Taylor, 1980; DePaolo, 1981).

8.4.3 $^{18}O/^{16}O$ VARIATIONS IN THE PENINSULAR RANGES BATHOLITH

An extensive body of data on the oxygen isotopic composition of both rocks and minerals is now available for the Peninsular Ranges batholith of southern California and northern Baja California. Taylor and Epstein (1962a,b) presented the first total-rock and mineral data from this batholith for six samples of igneous rock, and a further series of analyses of four metasedimentary rocks and selected minerals. This work showed the existence of variation in the $\delta^{18}O$ value obtained for different plutons, and also provided much data on the distribution of $\delta^{8}O$ among different mineral phases.

Taylor and Silver (1978) and Silver et al., (1979) summarize their large body of data for rocks from the northern 500 km of the batholith. This study showed that

1. The majority of the rocks had apparently retained their original $\delta^{18}O$.
2. The variation of $\delta^{18}O$ was geographically controlled and is largely independent of rock type,
3. The range of primary $\delta^{18}O$ values increased from about +6.0 near the coast to +12.0 or greater inland.
4. A longitudinal $\delta^{18}O$ 'step', or regional discontinuity separated the batholith into an eastern and a western portion. This step

is reflected as a paucity of $\delta^{18}O$ values between +8.5 and +9.0.

These data are shown graphically on Figures 8.8 and 8.9. Figure 8.8 is a histogram showing the distribution of $\delta^{18}O$ values as a function of rock type. Important points are (1) the bimodal subdivision into a western relatively low-$\delta^{18}O$ batholith ($\delta^{18}O < 8.5$) and an eastern relatcvely high-$\delta^{18}O$ batholith (with $\delta^{18}O > 9.0$), and (2) the uniformity of $\delta^{18}O$ values for all igneous rock types from gabbro to quartz monzonite and granodiorite on the west side of the $\delta^{18}O$ step. Figure 6.9 shows the geographic distribution of $\delta^{18}O$ in rocks from the northern Peninsular Ranges batholith. Since the publication of Taylor and Silver's paper it has been recognised that there has been considerable tectonic telescoping within the northeastern margin of the batholith, notably across the eastern Peninsular Ranges mylonite zone (Sharp, 1979; Silver, 1982, 1983). Figure 6.10 is based on Figure 1 of Taylor and Silver (1978), but the rocks of the upper and lower plates have been contoured separately. Some 30 km of right-lateral displacement across the San Jacinto fault zone (Sharp, 1967; Ch. 4) have been restored as well. This re-analysis strengthens considerably the consistent west-to-east pattern of $\delta^{18}O$ variation shown by Taylor and Silver (1978).

Early and Silver (1973) had previously reported on calculated initial strontium isotope data for many of the samples for which oxygen isotope data were presented. Taylor and Silver (1978) showed that a general linear correlation existed between $\delta^{18}O$ and initial $^{87}Sr/^{86}Sr$ (Sr_i). In general, rocks with less radiogenic initial strontium had lower $\delta^{18}O$ values than did rocks with more radiogenic initial strontium

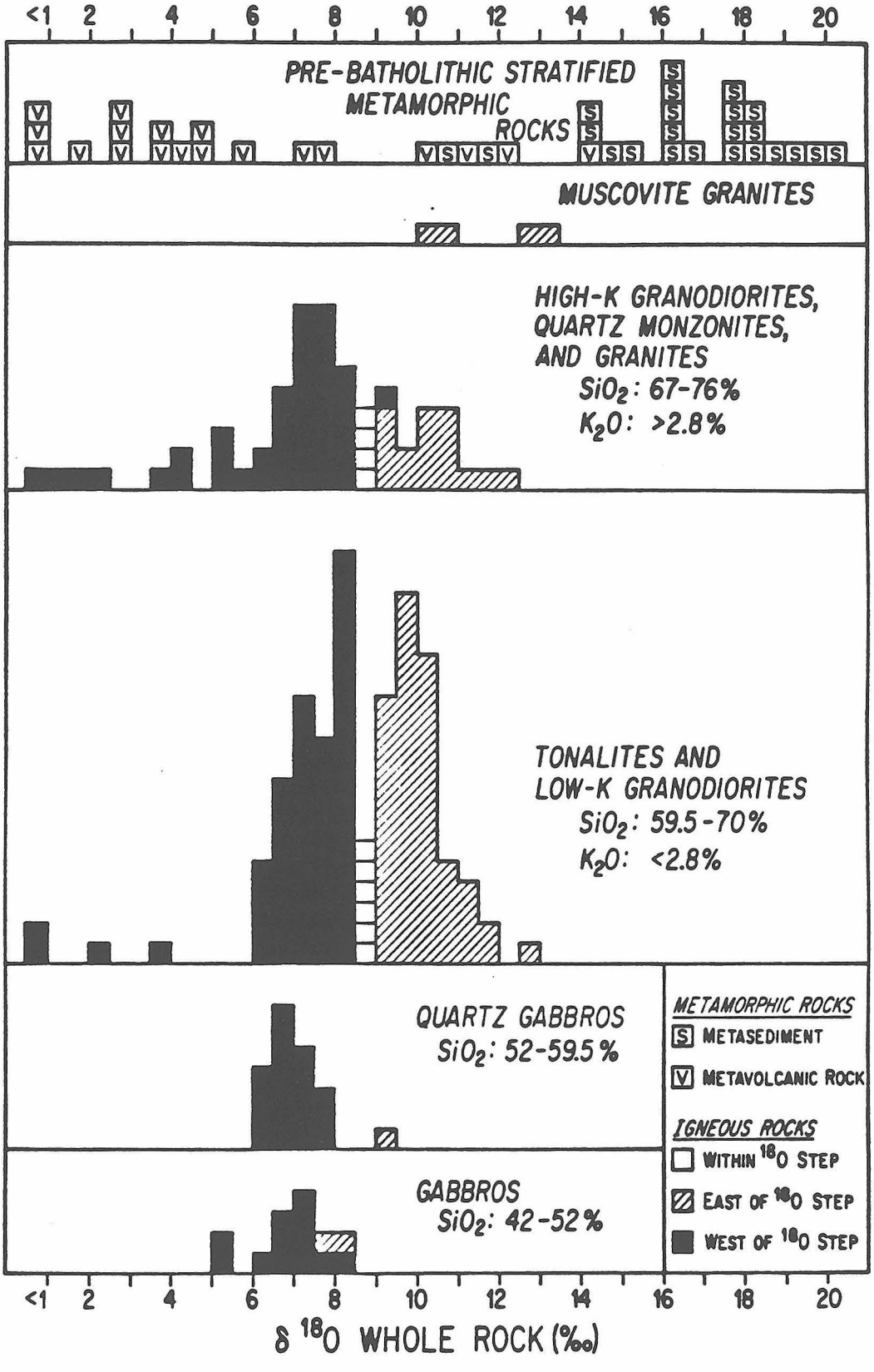

Figure 8.8. Histogram of $\delta^{18}O$ values for rocks from the northern Peninsular Ranges batholith. From Silver et al., 1979.

Figure 8.9. Contoured $\delta^{18}O$ values for the northern Peninsular Ranges. From Taylor and Silver, 1978.

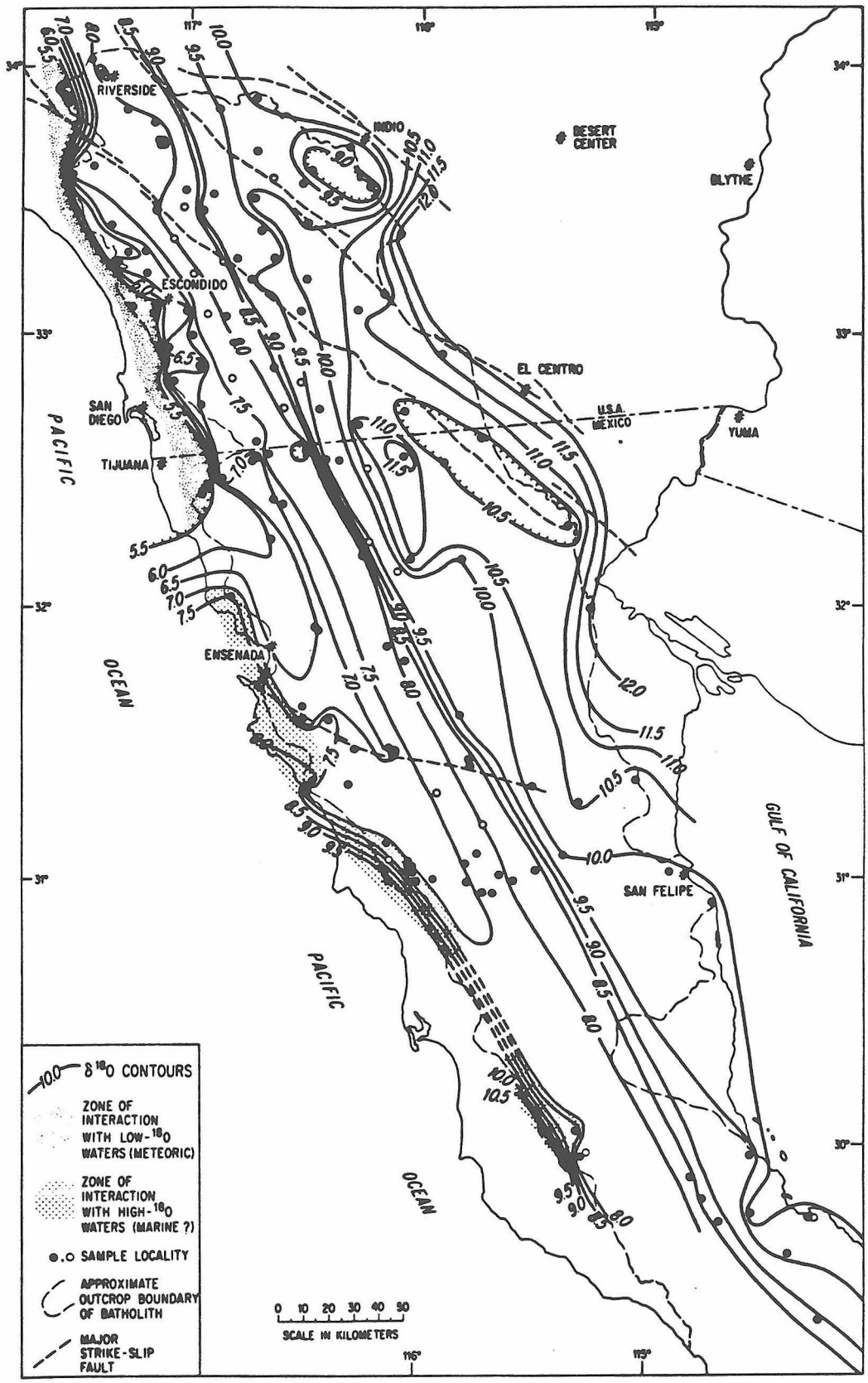
RIVERSIDE
INDIO
DESERT CENTER
BLYTHE
ESCONDIDO
EL CENTRO
SAN DIEGO
U.S.A.
MEXICO
YUMA
TIJUANA
PACIFIC
OCEAN
ENSENADA
SAN FELIPE
GULF OF CALIFORNIA
117°
116°
115°
34°
33°
32°
31°
30°
δ 18O CONTOURS
ZONE OF INTERACTION WITH LOW-18O WATERS (METEORIC)
ZONE OF INTERACTION WITH HIGH-18O WATERS (MARINE ?)
SAMPLE LOCALITY
APPROXIMATE OUTCROP BOUNDARY OF BATHOLITH
MAJOR STRIKE-SLIP FAULT
0 10 20 30 40 50
SCALE IN KILOMETERS

Figure 8.9

Figure 8.10. Contours of $\delta^{18}O$ values for the northern Peninsular Ranges batholith, modified from Taylor and Silver (1978) by treating data from west (below) and east (above) the eastern Peninsular Ranges mylonite zone separately. See text for further explanation. Eastern Peninsular Ranges mylonite zone from Sharp, 1979; restoration of offset on San Jacinto fault zone after Sharp (1967), and this study (Ch. 4).

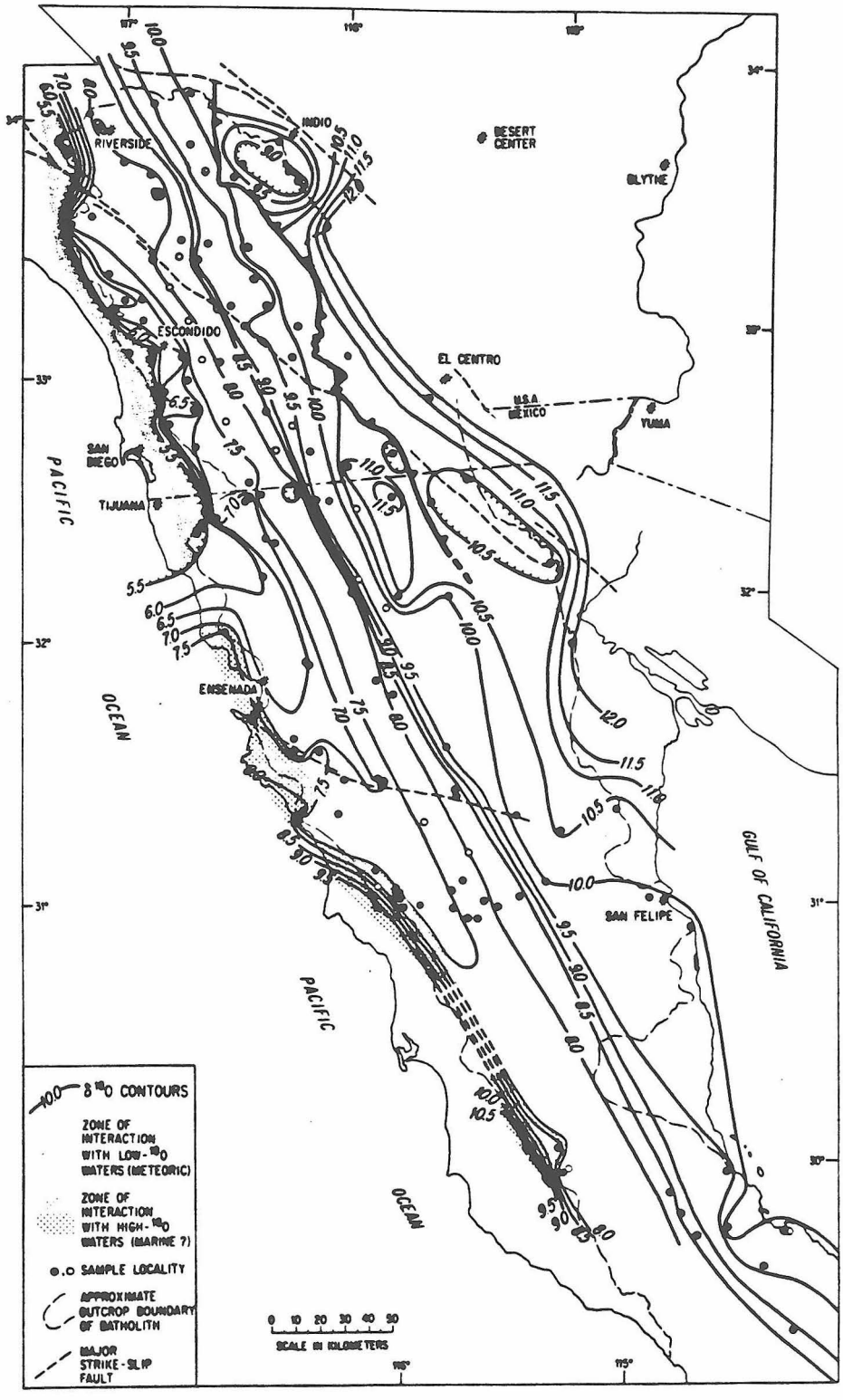
RIVERSIDE
INDIO
DESERT CENTER
BLYTHE
ESCONDIDO
EL CENTRO
U.S.A.
MEXICO
YUMA
SAN DIEGO
TIJUANA
ENSENADA
SAN FELIPE
PACIFIC
OCEAN
GULF OF CALIFORNIA
δ 18O CONTOURS
ZONE OF INTERACTION WITH LOW-18O WATERS (METEORIC)
ZONE OF INTERACTION WITH HIGH-18O WATERS (MARINE ?)
SAMPLE LOCALITY
APPROXIMATE OUTCROP BOUNDARY OF BATHOLITH
MAJOR STRIKE-SLIP FAULT
0 10 20 30 40 50
SCALE IN KILOMETERS

Figure 8.10

Figure 8.11. Diagram showing correlation of Initial $^{87}Sr/^{86}Sr$ and $\delta^{18}O$ for the northern Peninsular Ranges batholith. From Taylor and Silver, 1978.

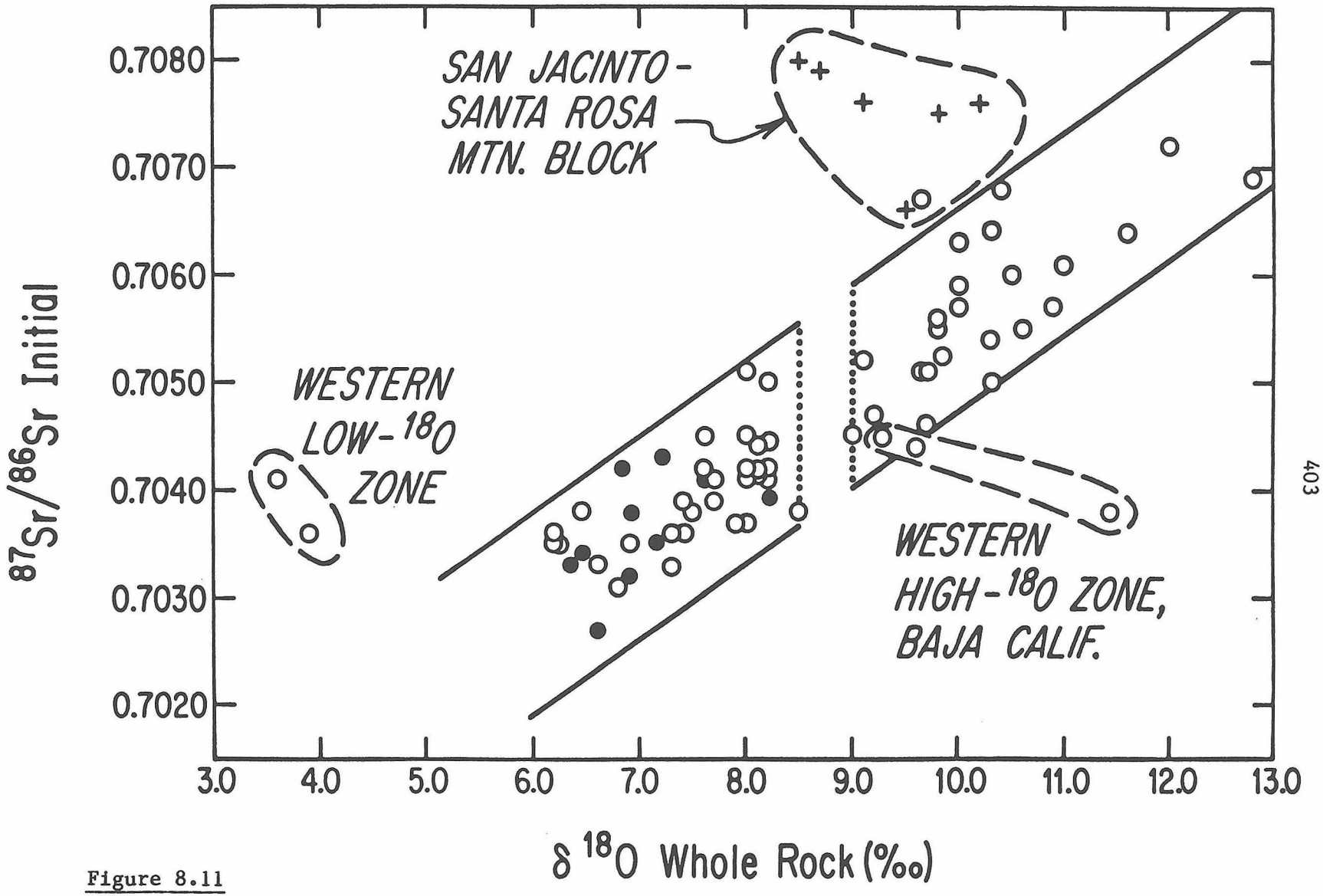
SAN JACINTO-
SANTA ROSA
MTN. BLOCK
WESTERN
LOW-18O
ZONE
WESTERN
HIGH-18O ZONE,
BAJA CALIF.
0.7080
0.7070
0.7060
0.7050
0.7040
0.7030
0.7020
87Sr/86Sr Initial
3.0
4.0
5.0
6.0
7.0
8.0
9.0
10.0
11.0
12.0
13.0
δ 18O Whole Rock (‰)

Figure 8.11

(Fig. 8.11). Rocks from the San Jacinto - Santa Rosa Mountains block fall off the trend and define a separate field at higher Sr_i and lower $\delta^{18}O$ than do those from the rest of the batholith. It was suggested that this was the result of the incorporation of material derived from older cratonic basement or associated lithosphere into these rocks. Many of these samples are from the upper plate, and may in fact have been emplaced into older cratonic basement or its cover (L.T. Silver, personal communication, 1982). However, samples from the north-western San Jacinto Mountains are from the lower plate and still deviate from the trend defined by Sr_i-$\delta^{18}O$ for the bulk of the batholith. This is the geographic area of interest in the present study.

8.4.4 $\delta^{18}O$ IN THE SAN JACINTO ROCKS

We now return to consideration of the origin of the patterns of $\Delta^{18}O$ distribution within the igneous rocks of the San Jacinto Mountains. Extrapolation of the batholithic trends reported by Taylor and Silver (1978) and Silver *et al.*, (1979) suggest that on the basis of regional considerations alone a variation in $\delta^{18}O$ values from about +9.5 to +10.5 might be expected. This is indeed the case, with the total observed variation in the common igneous rocks being from +9.0 to +10.6. The negative correlation with Colour Index (Fig. 8.5), and the striking homogeneity of the bulk of the analyzed samples are not expected from the regional observations, however, and the origin of these phenomena needs to be considered in more detail.

Several processes could account for the correlation of $\delta^{18}O$ and rock chemistry. These include:

1. Simple mass balance considerations. If all minerals crys-

tallized from a reservoir of constant oxygen isotopic composition, and different rocks contained differing proportions of these minerals, a correlation between Colour Index and $\delta^{18}O$ could result. The more felsic rocks have greater proportions of minerals that tend to concentrate $\delta^{18}O$ (quartz, K-feldspar) while the biotite, hornblende and titanite of the more mafic rocks tend to exclude ^{18}O.

2. Progressive sampling of a fractionating system, with later crystallized solids precipitating from liquids with steadily increasing $\delta^{18}O$.

3. Assimilation of $\delta^{18}O$-rich metasedimentary wall rocks with concomitant fractional crystallization.

4. A systematic change in source conditions so that liquids produced at different times had different $\delta^{18}O$. This could plausibly result from changes in the source volumes partially melted at different times, or by derivation of the more felsic (and isotopically heavier) magmas at lower temperatures, where isotope fractionations are greater. Also included in the broad heading of changing source conditions could be changes in the degree of partial melting, or changes in the residual mineralogy during progressive melting.

Model (4) is difficult to evaluate without considerable data from other independent geochemical systems. However, the work of Kyser et al., (1982) suggests that the plausible variation in $\delta^{18}O$ that could be produced by varying source conditions (P, T, amount of fusion, small variation in residual mineralogy) is small, perhaps a few tenths per mil. For fractional fusion at 1100°C (leaving a residue with constant proportions of olivine 60%, pyroxenes + garnet 40%), variation in F (the percent fusion) from 20 to 50 changes $\delta^{18}O$ of the liquid by about 0.3 per

mil. Variation in many other geochemical parameters (e.g., trace element abundances) would be much larger, and such large variations are not seen, suggesting that this simple model is not the major cause of the variation in $\delta^{18}O$. Major changes in the proportions of the phases involved in partial fusion would require substantial variation in the composition of the presumed mantle source away from a normal mantle composition. If this is the case, prior modification of the mantle composition could also involve modification of its oxygen isotopic composition, and the small variations expected from melting processes might be indistinguishable from other processes.

Strontium isotope data to be presented below (Ch. 9) seem to rule out (3) as being important. $\delta^{18}O$ data from co-existing minerals are needed to quantitatively evaluate (1) and (2). Although such measurements were not made in the present study, either experimentally or empirically determined mineral fractionations can be used to evaluate the likely magnitude of these processes. Although its mineral paragenesis is not identical to those of the San Jacinto rocks, the Bonsall tonalite sample studied by Taylor and Epstein (1962a,b) has sufficiently similar chemistry and mineralogy (Larsen, 1948) for their data to give an estimate of the likely mineral-mineral fractionations present in the San Jacinto rocks. These are listed in Table 8.2. The measured fractionations compare favourably with experimentally determined values for temperatures of 700-800°C (Fig. 8.3), implying that there has been relatively little post-crystallization modification of these isotopic systems.

Data on titanite and K-feldspar $\delta^{18}O$ were not obtained for the Bonsall tonalite sample. However, data obtained for these minerals from

TABLE 8.2.

MINERAL-MINERAL FRACTIONATIONS FOR THE BONSALL TONALITE (TAYLOR AND EPSTEIN, 1962a)

Mineral Pair	Fractionation, permil
Plagioclase-Quartz	-1.8
Plagioclase-K feldspar	-0.7
Plagioclase-Titanite	+0.8
Plagioclase-Hornblende	+1.6
Plagioclase-Apatite	+1.8
Plagioclase-Epidote	+2.3
Plagioclase-Biotite	+3.1

other rocks analysed by Taylor and Epstein (1962a) can be used to estimate the relevant fractionations for these minerals relative to the values reported for the Bonsall tonalite.

These data can be used to estimate the variation in $\delta^{18}O$ to be expected from simple variation of mineral proportions, assuming crystallization from a reservoir with constant $\delta^{18}O$. A variation in Colour Index of from 25 to 10 should result in a variation in $\delta^{18}O$ of about 0.5 per mil. Because variation in Colour Index is a complex function of the changing proportions of several different phases, a range in $\delta^{18}O$ is expected for a particular value of Colour Index. If plagioclase is assumed to have a $\delta^{18}O$ value of 10.1, use of the Δ values of Table 8.2 and the modal data presented in Ch. 5 gives a $\delta^{18}O$ value of 9.85 ± 0.25 at a Colour Index of 25, and $\delta^{18}O$ of 10.35 ± 0.25 at a Colour Index of 10. This calculated mass balance trajectory is shown on Figure 8.12; the majority of the rocks of Unit III could have solidified from an homogeneous oxygen reservoir with a $\delta^{18}O$ value of approximately +10.2. Data from other intrusions can be interpreted similarly. The two samples from the granodiorite of Poppet Creek have almost exactly the variation in $\delta^{18}O$ predicted from their respective modes by this simple model; this is also the case for two of the samples from Unit I, one a mafic tonalite and the other a granodiorite.

Although these effects can explain the relatively small variations in $\delta^{18}O$ shown by many of the more felsic samples, they cannot explain the relatively large variations in $\delta^{18}O$ shown by the remaining, generally more mafic samples, nor do they explain the puzzling corollary that the bulk of Unit III apparently crystallized from a homogeneous (at

Figure 8.12. Colour Index (volume %) versus measured $\delta^{18}O$ for unaltered, unexchanged rocks from the San Jacinto Mountains. "Calculated mass balance trajectory" is locus of field obtained if ^{18}O is distributed among rocks according to observed mineral abundances using the mineral-mineral fractionation data from the Bonsall tonalite (Taylor and Epstein, 1962a) and assuming $\delta^{18}O_{plag}$= +10.05% . The variation in $\delta^{18}O$ observed in the two samples from the Granodiorite of Poppet Creek can be explained solely by the observed differences in mineral proportions, as can the variations exhibited by most of the more felsic rocks from Unit III ("Central part of Unit III"). Two other samples from Unit III are from adjacent to the inferred position of the roof of this intrusion, but show no petrographic evidence for interaction with an aqueous fluid. These two samples have higher $\delta^{18}O$ for a given value value of Colour Index, and are differentiated as 'Uppermost Unit III'. Mafic samples from all units show a wide range in measured $\delta^{18}O$ values, of +9.0 to +10.1.

Filled symbols - "Mafic" tonalites (<65.5 wt.% SiO_2)
Open symbols - "Normal" tonalites

Squares - Unit I
Circles - Unit III
Plus sign - Felsic differentiate
Diamonds - Granodiorite of Poppet Creek

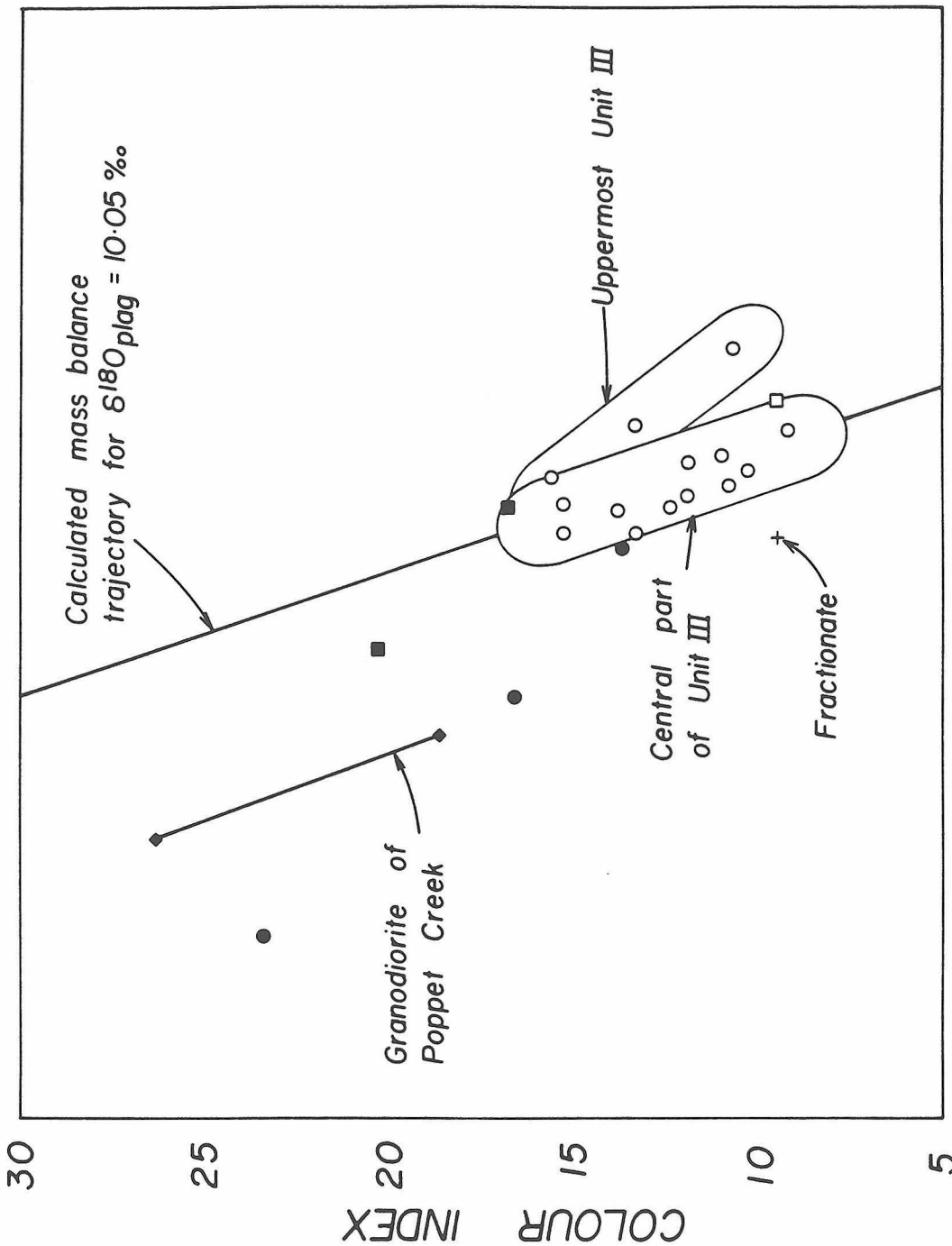
Calculated mass balance trajectory for $\delta^{18}O_{plag}$ = 10·05 ‰
Uppermost Unit III
Central part of Unit III
Fractionate
Granodiorite of Poppet Creek
COLOUR INDEX
30
25
20
15
10
5
9·0
10·0
11·0
$\delta^{18}O$, permil

Figure 8.12

least for oxygen) reservoir.

Available data are not adequate to analyse rigorously the expected effects of fractional crystallization on the $^{18}O/^{16}O$ properties of these rocks. The most complete data are available for Unit III, and the following discussion relates to that intrusive unit. The similarity of many features of Unit III to comparable features of the other large tonalitic bodies suggests that interpretations made using data from Unit III probably are more widely applicable. Unit III is a large (20x12 km) intrusive unit, funnel-shaped in three dimensions, that is gradational from marginal tonalite to central low-K granodiorite. Work by Muehlenbachs and Kushiro (1974) and Kyser et al., (1982) suggests that plagioclase in these rocks will have approximately the same $\delta^{18}O$ as does the liquid (to within a few tenths per mil). If the mineral-mineral fractionations of the Bonsall tonalite are applicable, $\Delta_{\text{solid-liquid}}$ for these rocks is small (-0.5 in the most mafic rocks to perhaps +0.1 in the more felsic central granodiorites). Colour Index and thus the magnitude of Δ decrease rapidly inwards away from the contact; as crystallization proceeds the effectiveness of any fractional crystallization process in modifying $\delta^{18}O$ thus decreases rapidly. Calculation shows that a simple fractional crystallization model using observed mineral proportions and the mineral-mineral fractionation data of Taylor and Epstein (1962a) results in an increase in $\delta^{18}O$ of perhaps 0.3 per mil after crystallization is 90% complete. Most of this variation will result from crystallization of the more mafic marginal rocks; over the bulk of the intrusion, the oxygen isotopic composition will remain approximately constant, as Δ is expected to be approximately zero.

These calculations argue strongly that the observed oxygen isotope variations are not the result of fractional crystallization processes acting within the magma chamber. Even if such a process were operative, the mineralogy of likely crystalline products appears to be incapable of more than very minor modification of the oxygen isotopic composition of residual liquids. The data presented here cannot be used to argue either for or against such processes being important prior to emplacement of these magmas into the exposed crustal chambers.

These model calculations imply that the relatively large variations in $\delta^{18}O$ observed in the more mafic rocks did not result from high-level processes, but rather already existed when the liquids from which these rocks crystallized were introduced into the magma chamber. This original variation appears to extend from a $\delta^{18}O$ value of perhaps +10.5 down to values of at least as low as +9.0. The correspondence of these values with those predicted from regional considerations to be likely in these rocks strongly argues that this larger range results from processes similar to those that produced the batholith-scale variation. Taylor and Silver (1978) and Silver et al., (1979) argue that this batholith-scale variation reflects a regular west-to-east change in the properties of the source materials from which the batholith was generated. Such an interpretation does not explain the correlation of $\delta^{18}O$ with mineralogy seen in the San Jacinto rocks (Fig. 8.5), but it does appear to be the most plausible explanation for the total observed variation in $\delta^{18}O$ within the study area.

8.5 CONCLUSIONS

1. Oxygen isotope data have been obtained for samples of igneous and metasedimentary rocks from the northwestern San Jacinto Mountains. These data are approximately in agreement with the conclusions of Taylor and Silver (1978) that $\delta^{18}O$ values of common igneous rocks from this portion of the Peninsular Ranges batholith range from +9.5 to +10.2.

2. When all rock types are considered, primary $\delta^{18}O$ variation is at least from +7.8 to +10.6. The extreme high and low values, however, are from unusually mafic or felsic rock types, respectively. The vast majority of samples have a narrow range of $\delta^{18}O$ values, from +10.0 to +10.4, and cover the compositional range tonalite to low-K granodiorite.

3. Four samples of metasedimentary rock have $\delta^{18}O$ values of +11.5 to +13.5. These values are lighter than values reported in Silver et al., (1979) for the common metasedimentary wall rocks to the batholith. In particular, the $\delta^{18}O$ of high-grade metamorphic country rocks around the nearby Domenigoni Valley pluton are +18 to +20 (Turi and Taylor, 1971). These data clearly indicate variations in sedimentary protolith within the batholith.

4. The emplacement of the various intrusive bodies stimulated the development of hydrothermal cells. The high $\delta^{18}O$ values of the fluids involved in these cells were buffered by the metasedimentary wall-rocks. The oxygen isotope system is very susceptible to such hydrothermal exchange effects, and thus provides a very sensitive indicator to the action of such phenomena.

5. The effects of these hydrothermal systems are pronounced within the smaller, older intrusives but are limited to the margins of the large late tonalitic bodies.

6. Primary $\delta^{18}O$ values within Unit III increase inwards, from +10.0 in the marginal tonalites to+ 10.4 or more in the central low-K granodiorites. Model calculations suggest that much of this variation can be explained simply by varying the proportion of minerals in these rocks. If correct, this implies that the bulk of Unit III crystallized from a liquid of approximately constant oxygen isotopic composition. Consideration of a plausible fractional crystallization scheme for Unit III suggests that this process is not capable of producing more than a very minor increase in $\delta^{18}O$ as crystallization proceeds.

7. Substantial variations in the $\delta^{18}O$ values of the more mafic rocks appear to reflect original variations in the oxygen isotope properties of the source materials from which these rocks were derived. The range of values observed (+9.0 to +10.5) is compatible with the regional pattern of $\delta^{18}O$ variation reported for the batholith by Taylor and Silver (1978) and Silver et al., (1979). This implies similar source compositions for the San Jacinto rocks and for the bulk of the batholith to the south and southwest.

8. The only large reservoir of oxygen recognized to date with such high $\delta^{18}O$ values is that of rocks that have been affected by low temperature chemical processes at or near the Earth's surface. These include sedimentary rocks, particulary those containing authigenic or biogenic minerals such as clays and silica, and the hydrothermally altered upper parts of the oceanic crust (e.g., Gregory and Taylor, 1981). The oxygen isotope data presented above strongly implicate such materials as being important in the genesis of the San Jacinto igneous rocks. Taylor and Silver (1978) suggest that such a component is necessary to explain the oxygen isotopic properties of rocks from the eastern part of the

batholith in general.

9. There is an apparent conflict between the observation that the San Jacinto rocks were derived from an isotopically heterogeneous (at least for oxygen) source and the striking uniformity of oxygen isotopic composition observed for the bulk of Unit III that implies that an efficient homogenization process somehow (and somewhere) acts to remove the isotopic differences present in these apparently initially heterogeneous materials before crystallization is complete. Such a process could presumably be active prior to or during melting, during transport, or within the crystallizing magma chamber itself. The oxygen isotope data in isolation do not enable constraints to be placed on the nature of this hypothesized process.

CHAPTER 9

STRONTIUM ISOTOPE RESULTS

9.1 INTRODUCTION

A principal aim of this study was to identify and delineate variations in the calculated initial isotopic composition of strontium (Sr_i) and oxygen within several individual intrusive units, and to attempt explain the origin of such variations. Sampling was therefore conducted with several goals in mind. Samples were collected, where possible, to provide geographic coverage; to provide a representative suite of the major rock types of the plutons; and, in a few cases, to provide an internal check of the method adopted for determining Sr_i. A number of samples were collected immediately adjacent to metamorphic country rocks to determine if contamination effects resulting from intrusion - wall-rock interactions were detectable.

Strontium isotope data for five igneous rock samples from the San Jacinto mountains (Early and Silver, 1973; Kistler et al., 1973; L.T. Silver, unpublished data) available at the beginning of the present study showed that a considerable variation in Sr_i ($\approx$0.7060-0.7075) existed within the Late Cretaceous intrusives of this relatively small area. The geological mapping presented above (Ch. 3; Plate 1) shows that these five samples are from different intrusive masses. However, these data both defined the approximate range of values of Sr_i found within this limited area, and also demonstrated that the general nature of Sr_i variation within the San Jacinto Mountains was similar to that found for rest of the Peninsular Ranges batholith (Early and Silver, 1973; Silver and Early,

1977; Silver et al., 1979). These workers had shown that, for the northern 600 km of the batholith, Sr_i in rocks unaffected by hydrothermal systems increased systematically eastwards, from values as low as 0.703 in some of the western-most batholithic rocks to values of 0.708 in the desert ranges of the northeastern batholith (Fig. 9.1). Another distinctive feature of these data is the systematic west-to-east change in the behaviour of Rb and Sr within similar rock types (especially within tonalites and low-K granodiorites)[Silver and Early, 1977; Silver et al., 1979]. Rb and Sr show strong covariation within elongate zones (domains) that parallel the long axis of the batholith. The slopes of the linear arrays defined by this (negative) covariation decrease systematically from west to east, so that for a given Rb content the more easterly rocks have much higher Sr abundances. The range of Rb content does not vary much from domain to domain; Sr content does, however, increasing from <100 ppm in western rocks to 700 ppm or more in some of the eastern tonalites (L.T. Silver, unpublished data).

9.1.1 SAMPLING PROCEDURES

Access to fresh unaltered rock for samples generally was not a problem. Lower elevations within the study area are well served by roads, whilst at higher elevation a network of hiking trails provides ready access to most places. Considerable blasting has been used in the construction of both roads and trails. Samples have been collected from such blasted material where possible. Exceptions are in the large "bowl" northwest of Black Mountain, and in the low hilly country north and northwest of Indian Mountain through to Poppet Creek (Plate 1). Both of these areas have undergone deep weathering, probably during Pliocene time, and

Figure 9.1. Regional variation of initial Sr isotopic composition (Sr_i) in plutonic rocks of the northern Peninsular Ranges batholith, southern California and northern Baja California (from Early and Silver, 1973, and Silver and Gromet, unpublished data). Location of the San Jacinto Mountains study area is shown.

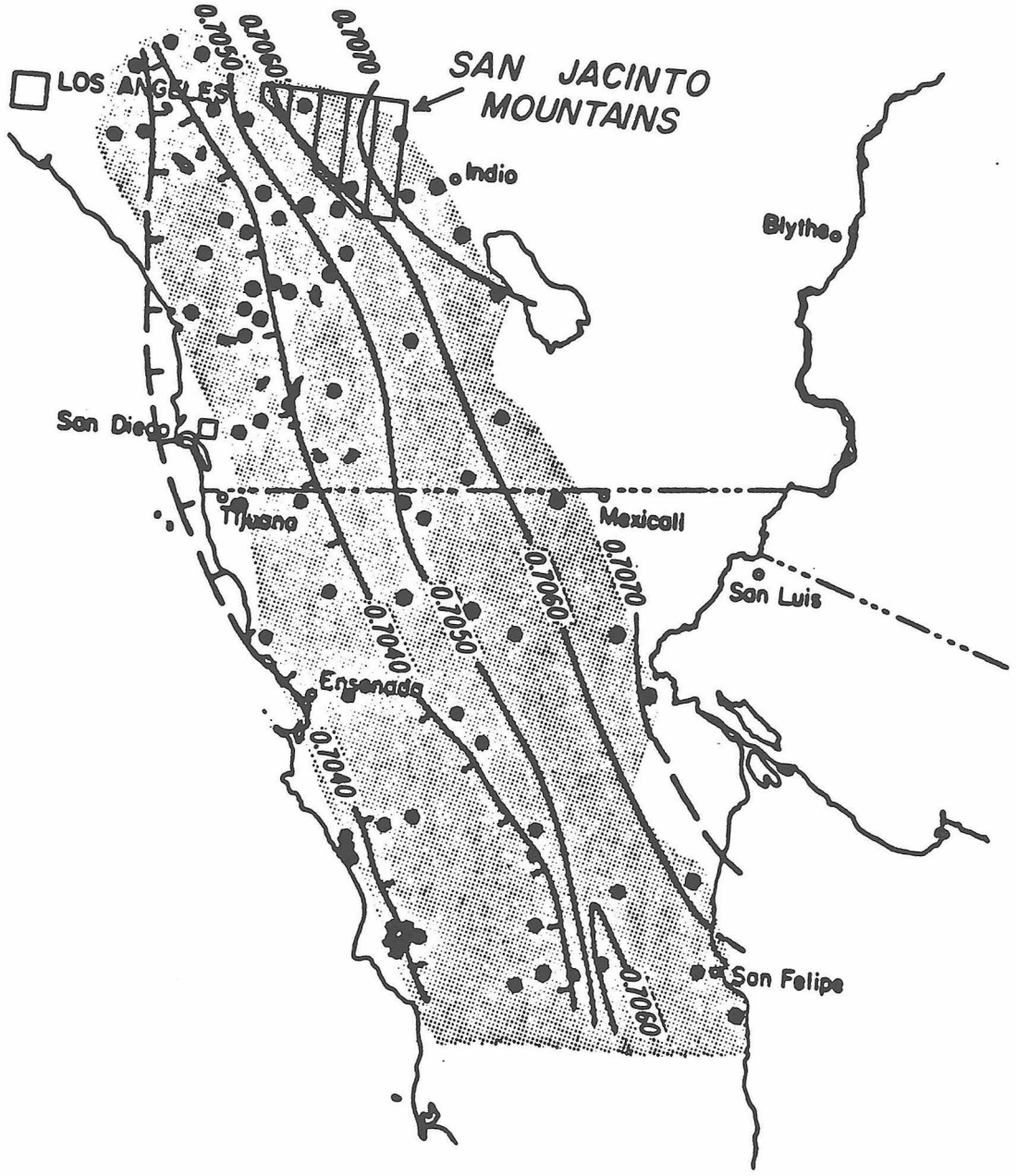
LOS ANGELES
SAN JACINTO MOUNTAINS
Indio
Blythe
San Diego
Tijuana
Mexicali
San Luis
Ensenada
San Felipe
0.7050
0.7060
0.7070
0.7040

Figure 9.1

have not been dissected by Quaternary erosion.

From 1kg to 10kg of fresh rock was collected at each site. Approximately 500gm of randomly selected chips were ground to a fine powder in a tungsten-carbide - lined Spex "Shatterbox". For the majority of samples, a 50 - 100 gm aliquot was then ground for an additional 12 minutes. This extra grinding step was necessitated by requirements of the XRF analytical procedure, not by the isotope dilution analysis (Appendix 4). 50-80 mg of this fine powder was then utilised in the Rb-Sr analysis, and a separate 25-30 mg was taken for the oxygen isotopic determination. Rb and Sr concentrations and Sr isotopic composition were were measured by standard isotope dilution and mass spectrometry procedures. These are detailed in Appendix 1. Within-run precision on the strontium isotopic composition was usually better than $\pm$ 0.00006 (2 $s.e._{mean}$). The precision of a Rb/Sr determination is estimated as being $\pm$1%. Experimental accuracy and precision are reviewed in Appendix 1. All $^{87}Sr/^{86}Sr$ data have been normalised to a value of 0.70800 for the MIT (Eimer and Armend) $SrCO_3$ standard.

Sr_i has been calculated utilising the U-Pb age of 97$\pm$1 m.y. obtained from U-Pb isotope studies of zircons from five separate rock samples by L.T. Silver (cited in Hill et al., 1982).

9.2 STRONTIUM ISOTOPIC RESULTS

Rb and Sr concentrations, $^{87}Rb/^{86}Sr$, measured $^{87}Sr/^{86}Sr$, and calculated initial $^{87}Sr/^{86}Sr$ for 76 representative igneous rock samples and 6 xenolith samples from the north-western San Jacinto Mountains are presented in Table 9.1. Locations of analysed samples are shown on the

TABLE 9.1.

IGNEOUS COUNTRY ROCKS

Sample Number	Rock type	Measured Rb	Measured Sr	Measured $^{87}Rb/^{86}Sr$	Measured $^{87}Sr/^{86}Sr$	Calculated $^{87}Sr/^{86}Sr$, at 97 m.y.
	North-western San Jacinto Mountains					
Tonalite of Lamb Canyon						
LTS 153	Bi-hb-tn ton.	35.4	676.1	0.151	0.70593 ± 6	0.70572
Granodiorite of Poppet Creek						
LTS 114	Fol. bi-hb grd.					
LTS 317	Fol. bi-hb grd.	98.1	283.5	1.002	0.70787 ± 4	0.70649
Un-named sill south of Banning						
LTS 211	Fol. bi ton.	68.8	519.4	0.383	0.70857 ± 4	0.70804
	Northern San Jacinto Mountains					
Tonalite of Snow Creek						
LTS 35	Fol. bi-hb-tn ton.	57.9	602.9	0.278	0.70804 ± 8	0.70765
LTS 302	Fol. bi-hb-tn ton.	61.8	612.0	0.292	0.70828 ± 6	0.70788
	Thomas Mountain					
Tonalite of Lucky Deer Mine						
LTS 381	Bi-hb ton.	49.7	632.7	0.227	0.70644 ± 6	0.70612
Un-named dike, Thomas Mountain						
LTS 382	Fol. granite dike	93.7	138.6	1.956	0.70840 ± 4	0.70570
Olivine gabbro of Thomas Mountain						
LTS 27	Calcic gabbro					
	Garner Valley and Desert Divide					
Granodiorite of Apple Canyon						
LTS 315	K-fs megacrystic grd.	119.7	227.2	1.525	0.70872 ± 6	0.70662
Tonalite of Herkey Creek						
LTS 316	Bi-hb-tn ton.	53.0	538.2	0.285	0.70673 ± 8	0.70634

TABLE 9.1. (CONTINUED)

Penrod 'Quartz Monzonite'						
LTS 318	Fol. bi-gar-(sill) gr.	171.0	78.3	6.328	0.72050 ± 10	0.71177
High plateau of San Jacinto Mountain south-east of San Jacinto Peak						
Un-named igneous rocks from north-east of Idyllwild						
LTS 293	Bi ton.	107.7	266.8	1.168	0.70850 ± 9	0.70689
LTS 314	Fol. bi-hb ton.	80.0	461.7	0.501	0.70746 ± 4	0.70677
MAJOR TONALITIC UNITS						
Unit 1						
LTS 147	Bi-hb-tn ton.	64.4	594.9	0.313	0.70804 ± 8	0.70760
LTS 150	Bi-hb-tn ton.	73.8	559.8	0.381	0.70754 ± 4	0.70701
LTS 215	Bi-hb-tn ton.	63.1	581.6	0.314	0.70782 ± 11	0.70739
LTS 216	Mafic xenolith	118.8	578.4	0.595	0.70818 ± 7	0.70736
LTS 217	Bi-hb-tn ton.	92.4	495.4	0.540	0.70803 ± 5	0.70728
LTS 218	Bi-hb-tn low-K grd.	90.4	513.5	0.509	0.70801 ± 3	0.70730
LTS 219	Bi-hb-tn ton.	86.5	513.5	0.488	0.70793 ± 3	0.70726
LTS 220	Bi-hb-tn ton.	60.8	617.6	0.285	0.70778 ± 6	0.70738
LTS 298	Bi-hb-tn low-K grd.	73.5	510.5	0.417	0.70755 ± 7	0.70698
LTS 299	Bi-hb-tn ton.	71.9	499.5	0.417	0.70769 ± 8	0.70712
LTS 300	Bi-hb-tn ton.	83.6	558.2	0.434	0.70757 ± 8	0.70697
LTS 301	Bi-hb-tn ton.	78.0	491.9	0.459	0.70778 ± 7	0.70715
LTS 319	Bi-hb-tn ton.	56.5	598.7	0.273	0.70744 ± 5	0.70706
LTS 320	Mafic xenolith	48.0	498.5	0.279	0.70748 ± 6	0.70709
LTS 321	Bi-hb-tn ton.	82.5	560.2	0.426	0.70758 ± 8	0.70699
LTS 322	Bi grd.	95.3	429.8	0.642	0.70777 ± 10	0.70688
LTS 323	Bi-hb-tn ton.	57.7	575.9	0.290	0.70732 ± 4	0.70692
LTS 324	Bi-hb-tn ton.	48.3	615.4	0.227	0.70654 ± 5	0.70623
LTS 325	Bi-hb-tn ton.	49.0	580.1	0.244	0.70654 ± 3	0.70620
LTS 330	Bi-hb-tn ton.	63.9	575.7	0.321	0.70789 ± 3	0.70744
LTS 361	Bi-hb-tn ton.	98.5	490.2	0.581	0.70786 ± 3	0.70706
LTS 362	Bi-hb-tn ton.	56.2	538.9	0.302	0.70715 ± 4	0.70673
LTS 363	Bi-hb-tn ton.	51.0	546.9	0.270	0.70718 ± 6	0.70681
LTS 372	Bi-hb-tn ton.	52.0	583.7	0.258	0.70640 ± 6	0.70605
Unit II						
LTS 148	Bi-hb-tn ton.	50.9	620.1	0.237	0.70737 ± 6	0.70704
LTS 149	Bi-hb-tn ton.	84.3	459.8	0.531	0.70762 ± 8	0.70696
LTS 287	Bi-hb-tn ton.	73.3	489.2	0.426	0.70776 ± 6	0.70717
LTS 288	Bi-hb-tn grd.	96.8	500.9	0.559	0.70778 ± 5	0.70701
LTS 289	Bi-hb-tn ton.	71.5	510.2	0.405	0.70796 ± 8	0.70740
LTS 326	Bi-hb-tn ton.	93.7	533.0	0.509	0.70814 ± 4	0.70744
LTS 327	Bi-hb-tn ton.	87.3	406.9	0.621	0.70815 ± 3	0.70729
LTS 328	Bi-hb-tn ton.	78.9	463.8	0.492	0.70788 ± 4	0.70720
LTS 329	Bi-hb-tn ton.	47.9	599.6	0.231	0.70635 ± 4	0.70604
LTS 368	Bi-hb-tn ton.	63.9	573.3	0.323	0.70744 ± 4	0.70700

TABLE 9.1. (CONTINUED)

Unit III						
LTS 145	Bi-hb-tn ton.	73.1	510.6	0.414	0.70717 ± 8	0.70660
LTS 146	Bi-hb-tn ton.	70.4	541.8	0.376	0.70734 ± 6	0.70682
LTS 151	Bi-hb-tn ton.	74.1	540.3	0.397	0.70729 ± 6	0.70674
LTS 152	Bi-hb-tn ton.	72.6	542.6	0.387	0.70721 ± 5	0.70668
LTS 212	Bi-hb-tn grd.	84.8	477.2	0.514	0.70760 ± 5	0.70689
LTS 213	Bi-tn grd.	87.4	551.3	0.459	0.70696 ± 7	0.70633
LTS 221	Bi-hb-tn ton.	80.4	425.8	0.546	0.70797 ± 6	0.70721
LTS 222	Bi-hb ton.	75.4	538.5	0.405	0.70717 ± 11	0.70661
LTS 290	Bi-hb-tn ton.	82.3	571.4	0.417	0.70753 ± 4	0.70696
LTS 291	Mafic xenolith	66.2	580.2	0.330	0.70740 ± 4	0.70695
LTS 292	Bi-hb-tn grd.	71.5	494.2	0.419	0.70785 ± 5	0.70727
LTS 297	Fol. fine gr. bi grd	100.2	479.5	0.605	0.70808 ± 4	0.70725
LTS 331	Bi-hb-tn ton.	70.3	539.6	0.377	0.70700 ± 4	0.70648
LTS 332	Bi-hb-tn ton.	85.4	514.2	0.481	0.70758 ± 4	0.70692
LTS 333	Bi-hb-tn ton.	69.3	529.9	0.379	0.70740 ± 3	0.70688
LTS 334	Bi-hb-tn ton.	70.9	543.9	0.377	0.70733 ± 4	0.70681
LTS 335	Bi-hb-tn ton.	66.4	568.3	0.338	0.70702 ± 3	0.70656
LTS 336	Bi-hb-tn ton.	69.7	588.4	0.342	0.70631 ± 5	0.70583
LTS 337	Bi-hb-tn ton.	68.9	552.1	0.361	0.70709 ± 5	0.70660
LTS 358	Bi-hb-tn low-K grd.	81.6	517.4	0.457	0.70775 ± 4	0.70713
LTS 359	Bi-hb-tn ton.	61.8	543.0	0.329	0.70733 ± 4	0.70687
LTS 360	Bi-hb-tn ton.	76.3	576.9	0.383	0.70747 ± 4	0.70694
LTS 365	Bi-hb-tn ton.	82.9	438.8	0.546	0.70779 ± 5	0.70704
LTS 366	Bi-hb-tn low-K grd.	106.1	470.2	0.653	0.70757 ± 3	0.70667
LTS 367	Bi-hb-tn low-K grd.	76.9	478.2	0.465	0.70738 ± 4	0.70674
LTS 369	Bi-hb-tn ton.	98.3	497.4	0.572	0.70758 ± 3	0.70679
LTS 370	Bi-hb-tn ton.	76.3	547.1	0.403	0.70720 ± 5	0.70664
LTS 371	Bi-hb-tn ton.	64.6	538.9	0.348	0.70729 ± 6	0.70681
LTS 373	Bi-hb-tn ton.	81.8	556.4	0.425	0.70659 ± 2	0.70601
LTS 374	Bi-hb-tn ton.	84.7	513.4	0.478	0.70772 ± 4	0.70706
LTS 375	Bi-hb-tn ton.	85.1	486.8	0.506	0.70779 ± 3	0.70709
LTS 376	Bi-hb-tn ton.	82.8	561.0	0.427	0.70728 ± 6	0.70669
LTS 377	Mafic xenolith	70.0	670.6	0.302	0.70761 ± 4	0.70719
LTS 378	Mafic xenolith	73.9	651.7	0.328	0.70771 ± 5	0.70726
LTS 379	Mafic xenolith	78.5	481.7	0.471	0.70744 ± 5	0.70679
Mafic dike intrusive into Unit III						
LTS 214	Mafic dike	44.0	786.9	0.162	0.70861 ± 4	0.70839

geological map (Plate 1). The location of samples from the three major tonalitic intrusions are shown on a pre-faulting map of the area (Fig. 9.2). In addition, garnet bearing tonalites, granodiorites and granites that crop out around Red Tahquitz and along the Desert Divide of the southern San Jacinto Mountains are the products of contamination by metasedimentary country rocks (Ch. 3). Samples of these hybrid rocks were analysed to examine the effects of high-level incorporation of metasedimentary material into tonalitic magma. Analytical data for 5 such rocks are presented in Table 9.2.

Analysed samples of rocks from the early intrusives span the compositional range mafic tonalite-granite. Sr_i for apparently unexchanged samples varies from 0.7057 to 0.7078. Two samples analysed previously (an olivine gabbro and a K-feldspar rich tonalite) also have Sr_i within these limits (L.T. Silver, unpublished data). Samples of tonalite and low-K granodiorite from the large intrusive units show similar ranges of Sr_i. Within Unit I, Sr_i varies from 0.7060 to 0.7077; within Unit II the range is from 0.7058 to 0.7074, and for Unit III it is from 0.7058 to 0.7073. Figure 9.3 shows histograms of Sr_i for each rock unit.

9.3 DISCUSSION

A principal aim of this study was to document variations in primary Sr_i if possible. By primary Sr_i is meant the $^{87}Sr/^{86}Sr$ of a particular sample at the time of crystallization. Because various processes are capable of modifying the Rb, Sr and $^{87}Sr/^{86}Sr$ of a rock subsequent to crystallization the possible effects of such processes are examined prior to discussion of inferred primary Sr_i.

TABLE 9.2.

CONTAMINATED ROCKS, RED TAHQUITZ AREA

		measured				Calculated
		Rb	Sr	$^{87}Rb/^{86}Sr$	$^{87}Sr/^{86}Sr$	Sr_i at 97 m.y.
LTS 271	Gar bearing bi-all ton.	77.1	322.2	0.692	0.70814 ± 5	0.70718
LTS 311	Fol. bi-hb-all ton.	54.5	286.5	0.550	0.71265 ± 3	0.71189
LTS 380	Fol. bi-hb-all ton.	39.5	311.5	0.367	0.70806 ± 3	0.70756
LTS 383	Gar bearing bi-all ton.	56.0	254.4	0.637	0.70984 ± 3	0.70896
LTS 384	Gar bearing bi-all ton.	63.1	279.7	0.652	0.70801 ± 7	0.70711

Abbreviations used:
Gar = garnet; bi = biotite; all = allanite; Fol. = foliated

Figure 9.2. Location of analysed samples, major tonalite units, San Jacinto Mountians. Base is pre-faulting reconstruction showing inferred original distribution of major plutonic units.

Filled symbols - "Mafic" tonalites
Open symbols - "Normal" tonalites

Squares - Unit I
Triangles - Unit II
Circles - Unit III
Plus signs - Felsic differentiates

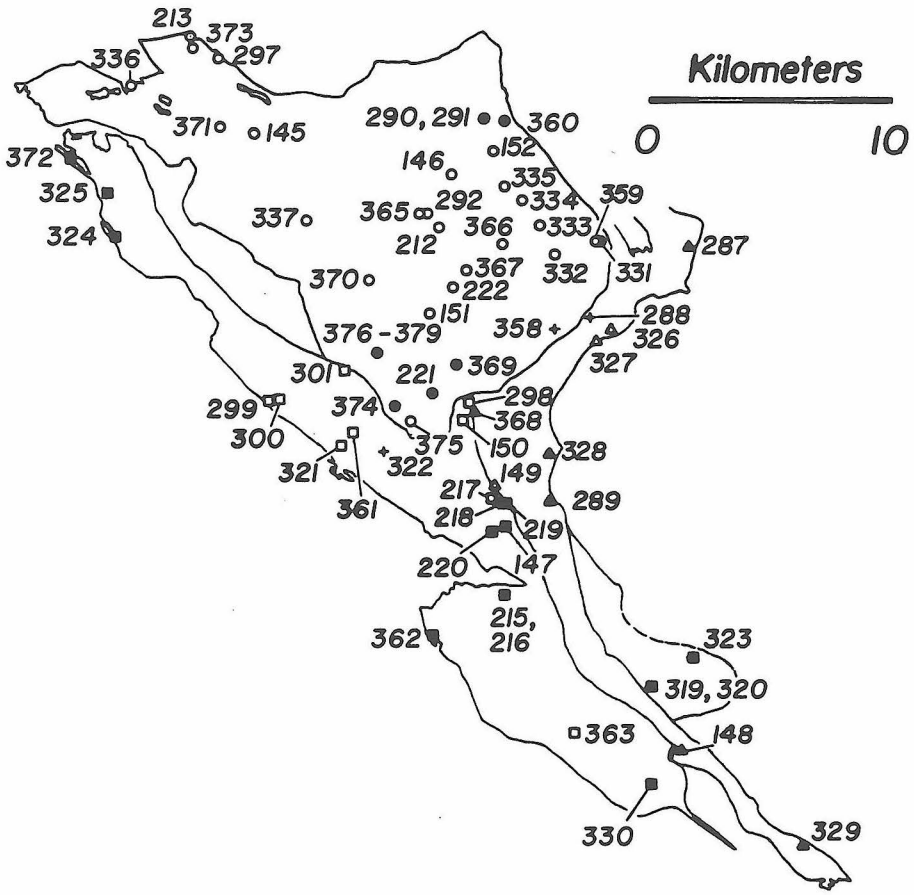

MAJOR TONALITES
Sample Localities

Figure 9.2

Figure 9.3. Histogram of Sr_i by intrusive unit, north-western San Jacinto Mountains.

Filled squares	-	"Mafic" tonalites
Open squares	-	"Normal" tonalites
Plus signs	-	Felsic differentiates
Crosses	-	Mafic xenoliths
Asterisk	-	Mafic dike intruding Unit III
Circles	-	Sample from within 300 m of meta-sedimentary wall-rocks

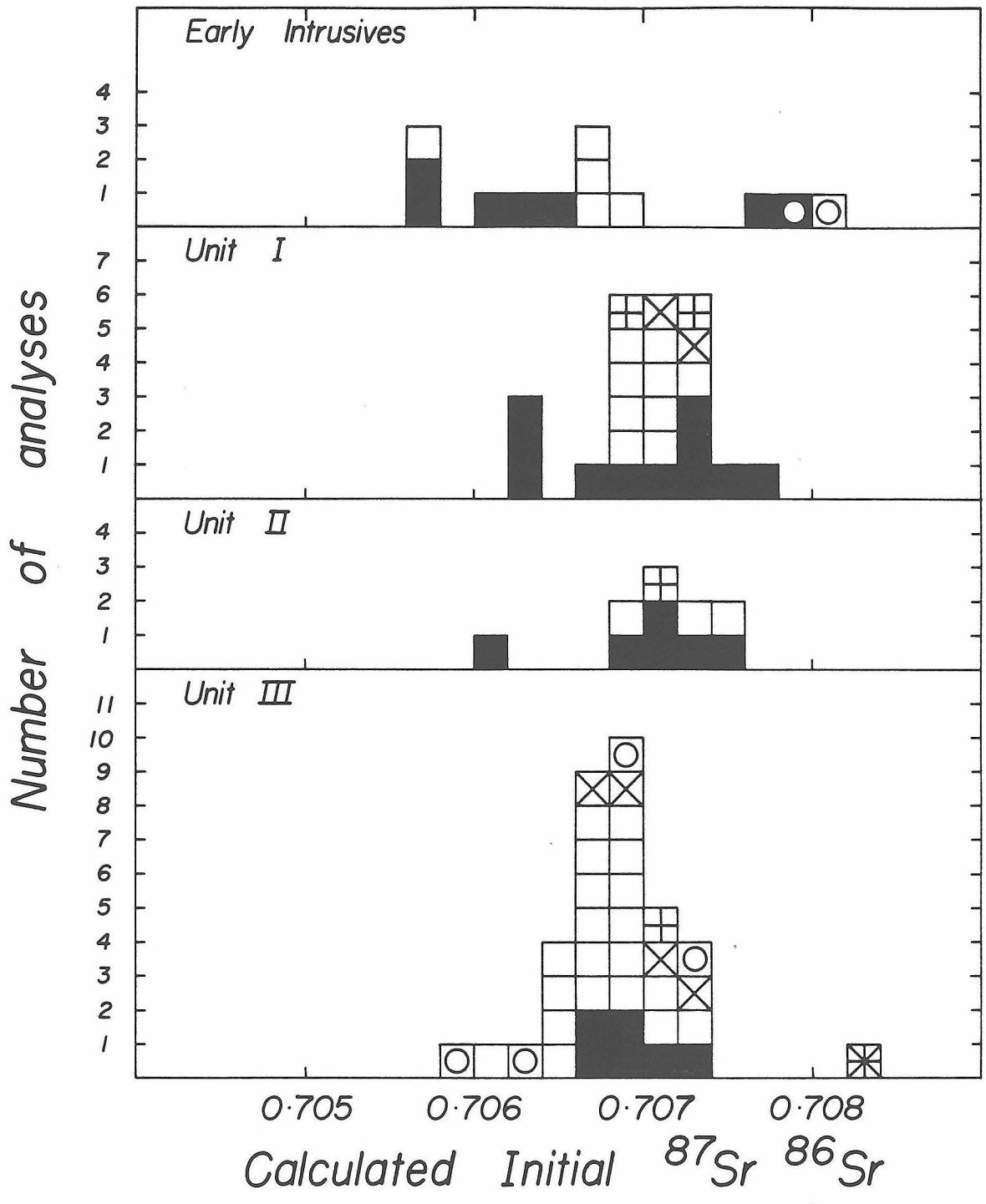
Early Intrusives
Unit I
Unit II
Unit III
Number of analyses
0·705
0·706
0·707
0·708
Calculated Initial ^{87}Sr ^{86}Sr

Figure 9.3

9.3.1. INTRUSIVE - WALL-ROCK INTERACTION

Several samples of igneous rock were collected adjacent to outcrops of metasedimentary country rock. Textural features peculiar to such marginal facies (Ch. 5) suggest that there has been some interaction between the igneous rocks and their metamorphosed sedimentary host materials. This interaction is likely to include incorporation of wall-rock materials into the igneous body by various processes, and/or chemical exchange involving a hydrothermal fluid. It is possible to alter the strontium and oxygen isotopic composition of an affected sample without seriously affecting its chemical composition. The contrast between the oxygen isotopic composition of the igneous rocks and the interacting hydrothermal fluids, in combination with the similar abundances of oxygen in both components, make oxygen isotope systematics particularly sensitive indicators of exchange for these systems (Ch. 8). Although the contrast between the strontium isotopic composition of the igneous and the metasedimentary rocks at the time of emplacement is much more marked than that for the oxygen system, if exchange was affected via a fluid medium, then the probable low strontium concentration of any such fluid compared to the strontium concentration of the igneous rocks may make the strontium system less sensitive to pluton - wall-rock interactions than the oxygen system.

Oxygen isotope data from several samples of tonalite and low-K granodiorite adjacent to contacts with metasedimentary rocks are interpreted as showing evidence for minor exchange between the oxygen of the igneous rocks and a circulating hydrothermal fluid buffered by the oxygen reservoir of the metasedimentary wall-rocks (Ch. 8). Strontium exchange

effects cannot be distinguished with certainty for many of these samples, probably because of either small water - rock ratios or low Sr concentrations in the exchanging fluids. Immediately adjacent to metasedimentary wall-rocks (within 100 m or so) Sr exchange effects appear to be discernible for at least two samples from the northwestern marginal zone of Unit III (213, 297) that show textural features interpreted as indicative of proximity to wall rocks. A sample of dike rock intrusive into metasedimentary roof rocks (211) in this area has similar textural features and is similarly interpreted as having acquired radiogenic strontium during interaction with these host materials. These three samples are the only samples from the major tonalitic units for which persuasive a priori evidence for interaction with the host rocks exists. The possibility of interactive exchange influencing the isotopic characteristics of several other samples (336,371,35,302) adjacent to the roof or walls of the plutons is predicated on interpretation of the oxygen isotopic data. It is suggested that for these samples any effects on the strontium isotope system are small. These samples are distinguished on the figures illustrating various aspects of the strontium isotope data.

Five samples of "contaminated" igneous rock show substantial increase in calculated Sr_i (Table 9.2). Values of Sr_i for these samples range from 0.708 to 0.713 compared to an inferred uncontaminated value of 0.7068 or less. These data imply that even in situations where field evidence suggests that several percent (bulk) contamination may have occurred the effects on the Sr isotopic composition may be relatively minor. Clearly, however, in the more extreme cases, it is a major effect. Calculation of the amount of contamination experienced by each sample is heavily dependent on the values chosen for the $^{87}Sr/^{86}Sr$ and Sr concen-

Figure 9.4. Histograms of Rb and Sr contents, arranged by intrusive unit.

Filled squares	-	"Mafic" tonalites
Open squares	-	"Normal" tonalites
Plus signs	-	Felsic differentiates
Crosses	-	Mafic xenoliths
Asterisk	-	Mafic dike intruding Unit III

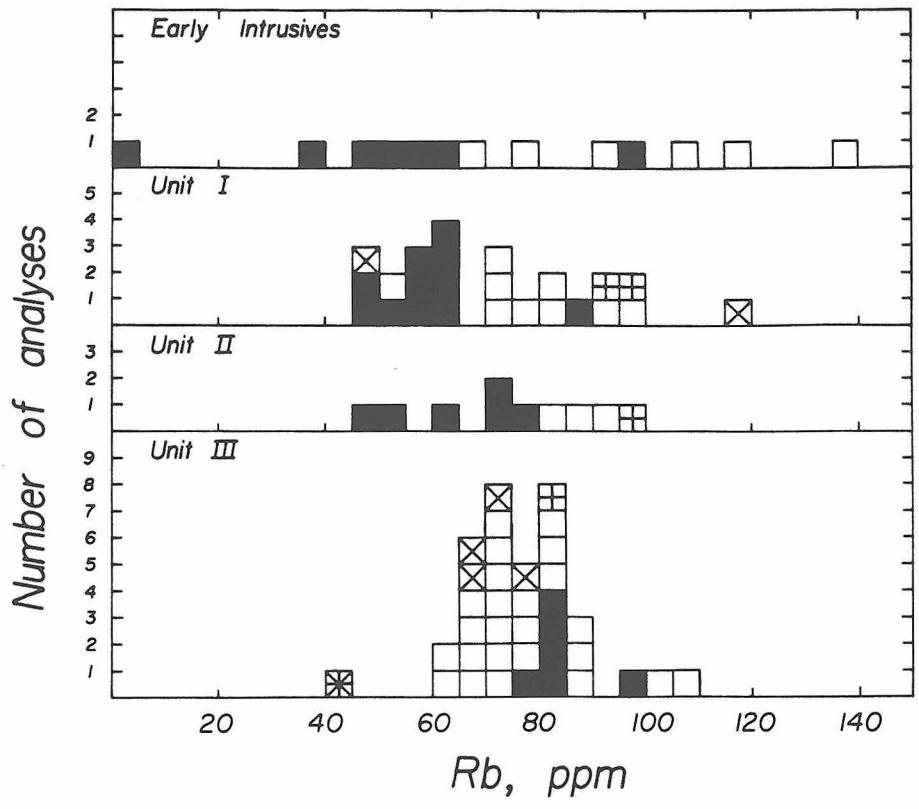
Early Intrusives
Unit I
Unit II
Unit III
Number of analyses
20
40
60
80
100
120
140
Rb, ppm

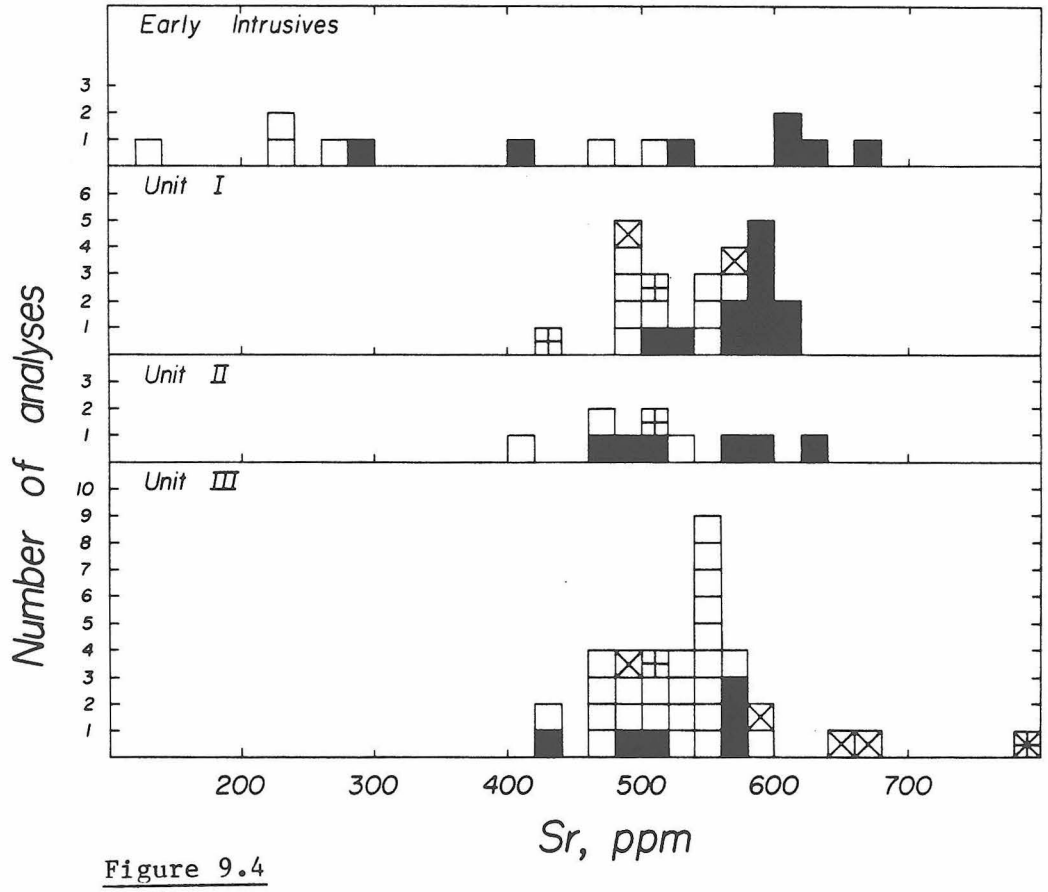
Early Intrusives
Unit I
Unit II
Unit III
Number of analyses
200
300
400
500
600
700
Sr, ppm

Figure 9.4

tration of the contaminant. The metasedimentary wall-rocks that are being incorporated at the margins of plutons show considerable range in $^{87}Sr/^{86}Sr$ (Table 2.1), making estimation of this parameter difficult.

Although considerably more felsic than the samples listed in Table 9.2, a sample from the granite of Penrod Canyon (LTS 318) shows both petrographic and oxygen isotopic evidence for considerable interaction with the host metasedimentary rocks. The oxygen isotope data presented earlier suggests that this interaction may have taken place with a circulating hydrothermal fluid largely buffered in composition by the properties of these metasedimentary rocks. The apparently high Sr_i calculated for this pluton (Table 9.1) is thus interpreted as resulting from post-crystallization exchange processes.

Overall, it thus appears that either incorporation of, or exchange with Sr from the wall rocks hosting these plutons can be attributed to only a few samples, was a relatively minor effect, and was largely restricted to those rocks for which there is other evidence for the action of such processes. It is concluded that for the vast majority of the analysed samples, pluton - wall-rock interactions are of negligible importance.

9.3.2 RB AND SR CONCENTRATIONS, AND RB-SR COVARIATION

The ranges of Rb and Sr concentrations are presented diagrammatically on Figure 9.4. The chemically more diverse early intrusives shows a wider range of values for Rb and Sr concentrations than do the more homogeneous large tonalites. The three large tonalitic units show less variation in their Rb and Sr abundances, consistent with their

relatively homogeneous nature.

There is a general correlation of trace element characteristics with rock type; tonalites and closely related low-K granodiorite contain from 400 to 700 ppm Sr, and between 35 and 100 ppm Rb; granodiorites (all from small individual intrusions) have lower Sr contents (200-300 ppm) and higher Rb (95-120 ppm). Rocks interpreted from field relations to be slightly more felsic differentiates from the main tonalites tend to have higher Rb contents and lower Sr contents than adjacent tonalite.

The Rb and Sr concentration data for the major tonalites are shown plotted on the location map (Fig. 9.5). Figure 9.6 shows the variation of Sr concentration within Unit III in more detail. Contours of equal Sr concentration emphasize the consistent geographic variation of this parameter within this unit. With few exceptions, Sr concentration decreases inwards, away from the pluton walls. There appears to be no correlation between Sr concentration and either elevation or inferred distance below the roof of the pluton, nor is any such geographic regularity apparent in either the Rb or Sr data for the other units. A notable exception to the regular concentric pattern of Sr concentration in Unit III is an area immediately west of Pine Cove (Plate 1; Samples LTS 221,374,375,376: Fig. 9.3). In this area, called the "Pine Cove salient" quite mafic tonalites, some containing aligned subhedral to euhedral plagioclase laths, show consistently lower Sr concentrations.

The concentrations of Rb in the three major tonalite units do not appear to show the systematic variation with position shown by the Sr concentration data for Unit III (Fig. 9.5).

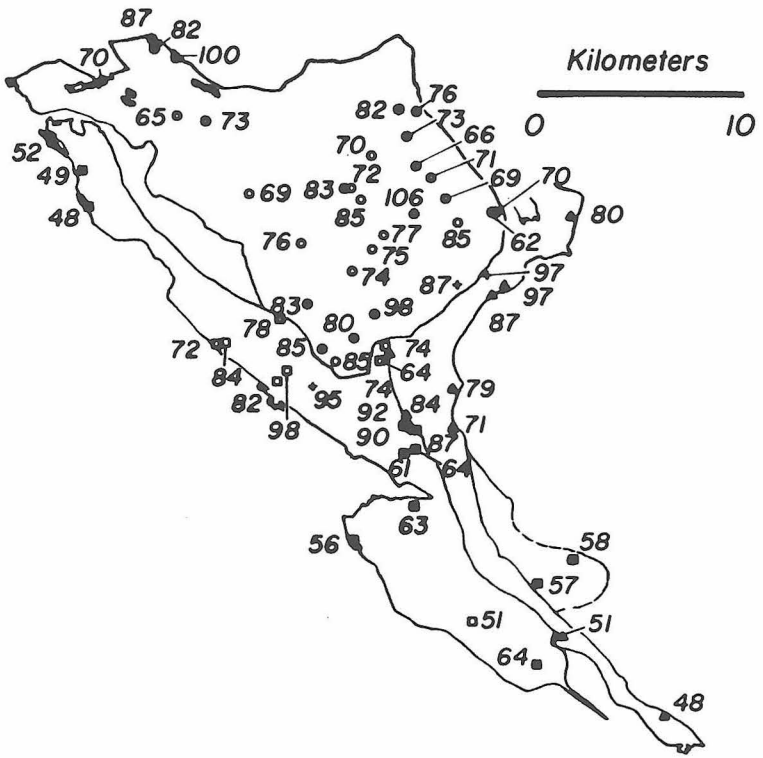

MAJOR TONALITES

Rb, ppm

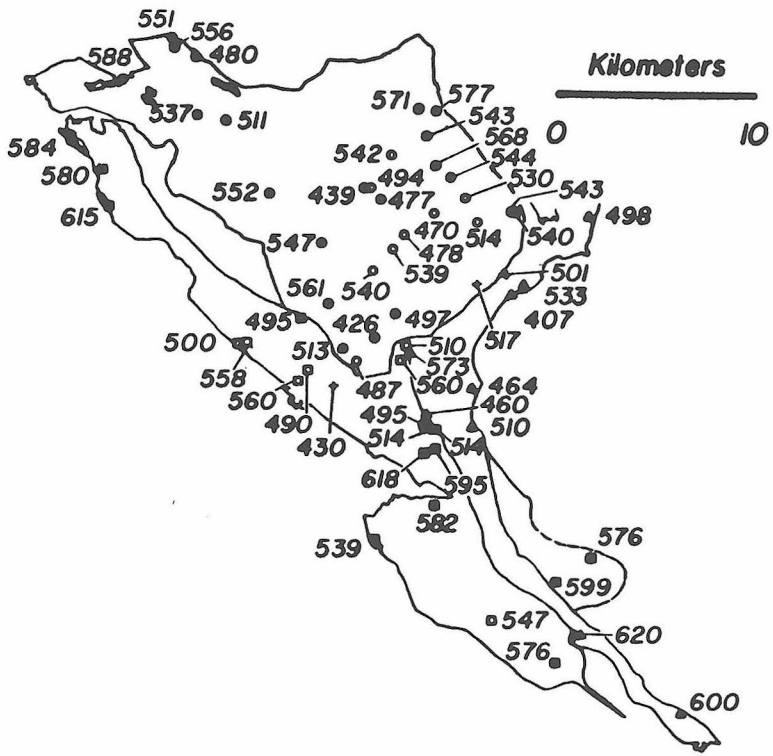

MAJOR TONALITES

Sr, ppm

Figure 9.5. Geographic distribution of Rb and Sr concentrations, major tonalites. Palinspastic base.

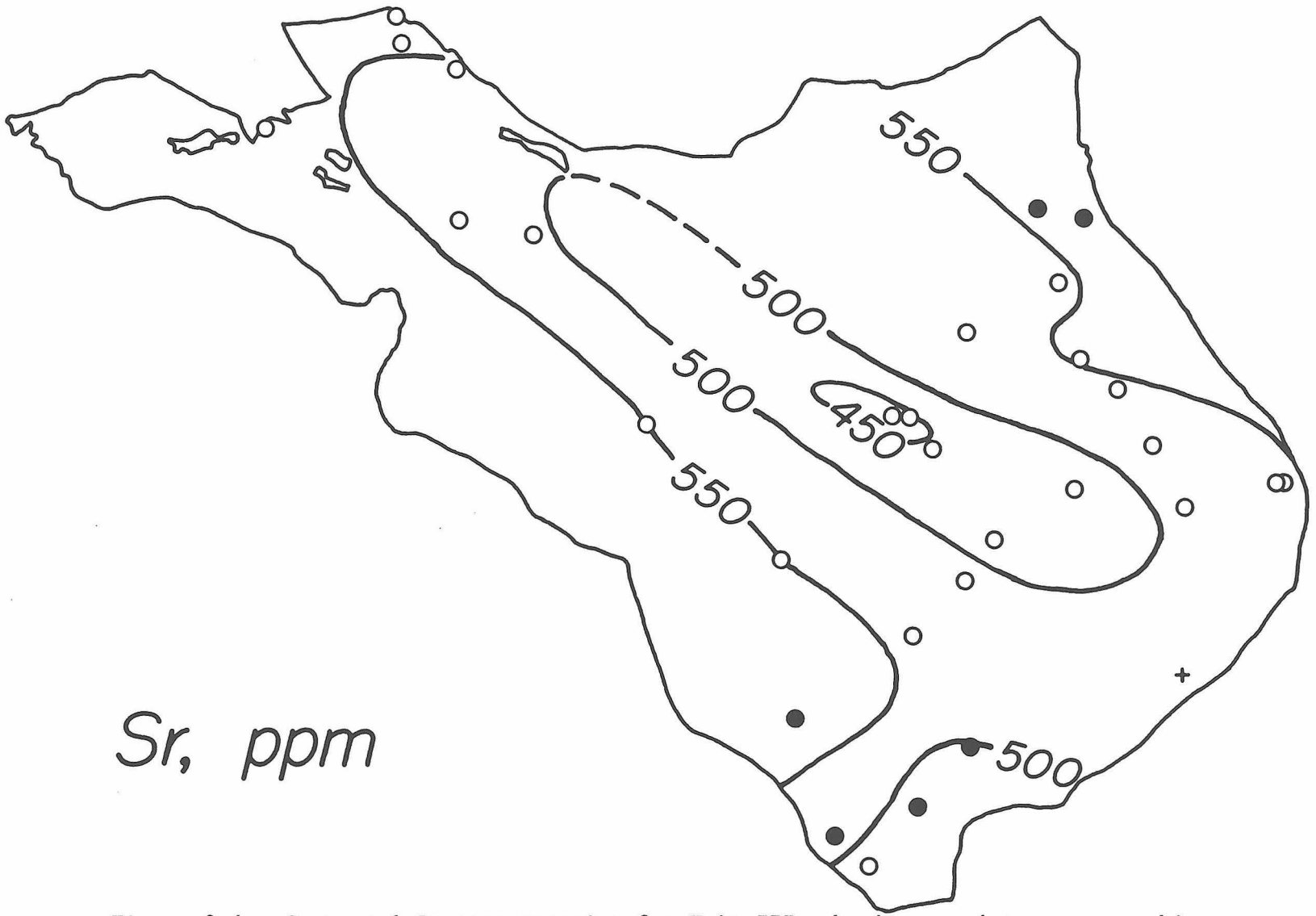

Figure 9.6. Contoured Sr concentration for Unit III, showing consistent geographic variation in this parameter.

Figure 9.7. Rb versus Sr, all data from the San Jacinto Mountains.

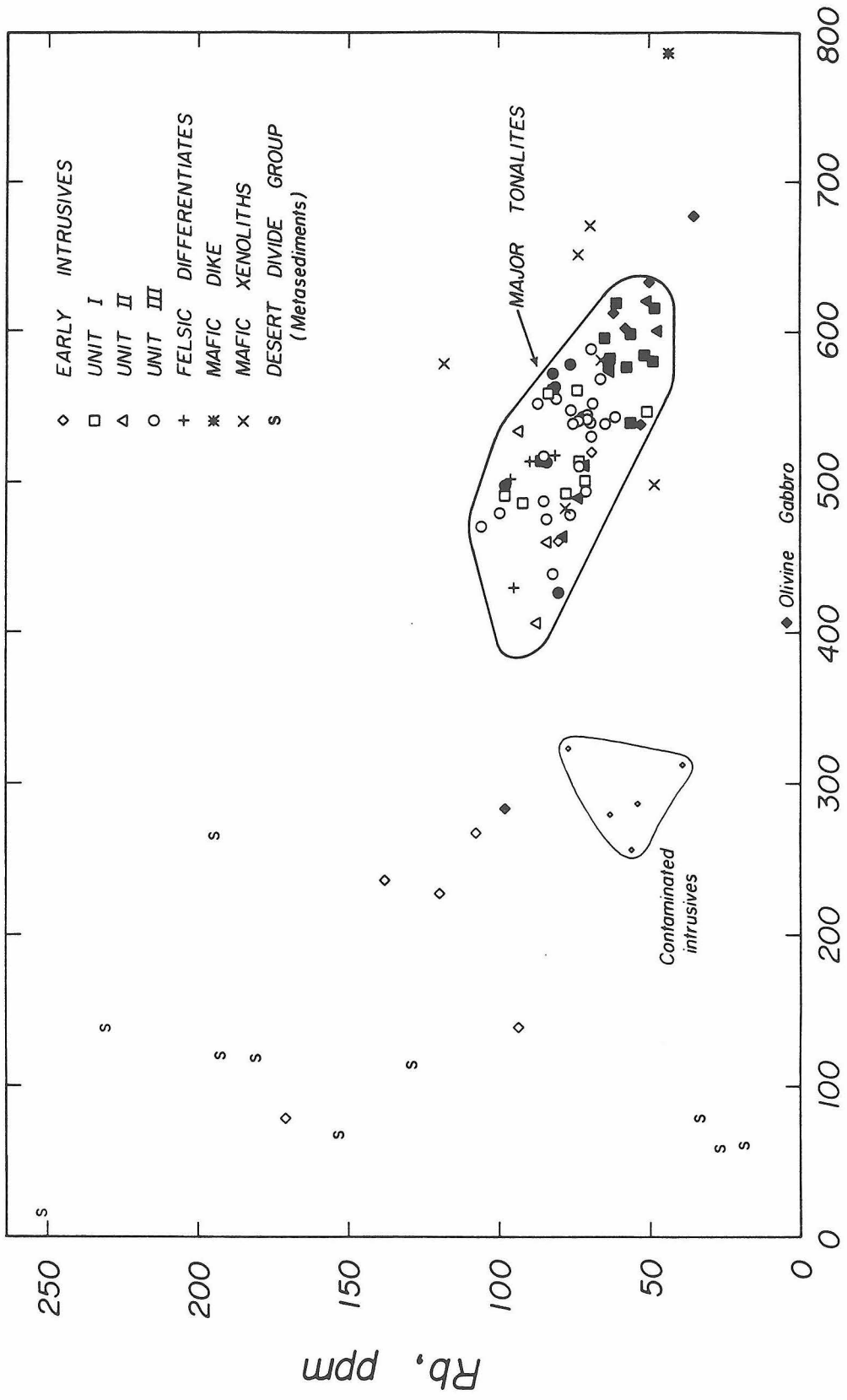
EARLY INTRUSIVES
UNIT I
UNIT II
UNIT III
FELSIC DIFFERENTIATES
MAFIC DIKE
MAFIC XENOLITHS
DESERT DIVIDE GROUP
(Metasedimenis)
MAJOR TONALITES
Olivine Gabbro
Contaminated intrusives
Rb, ppm
Sr, ppm
0
50
100
150
200
250
0
100
200
300
400
500
600
700
800

Figure 9.7

Figure 9.8. Rb-Sr diagram for Unit I, showing Rb-Sr sub-zones.

Filled symbols	-	Tonalites and granodiorites
Open symbols	-	Mafic xenoliths
Crosses	-	Southwestern sub-zone
Triangles	-	Central sub-zone
Squares	-	Northeastern sub-zone
Plus signs	-	Felsic differentiates
Circle	-	Low-K granodiorite

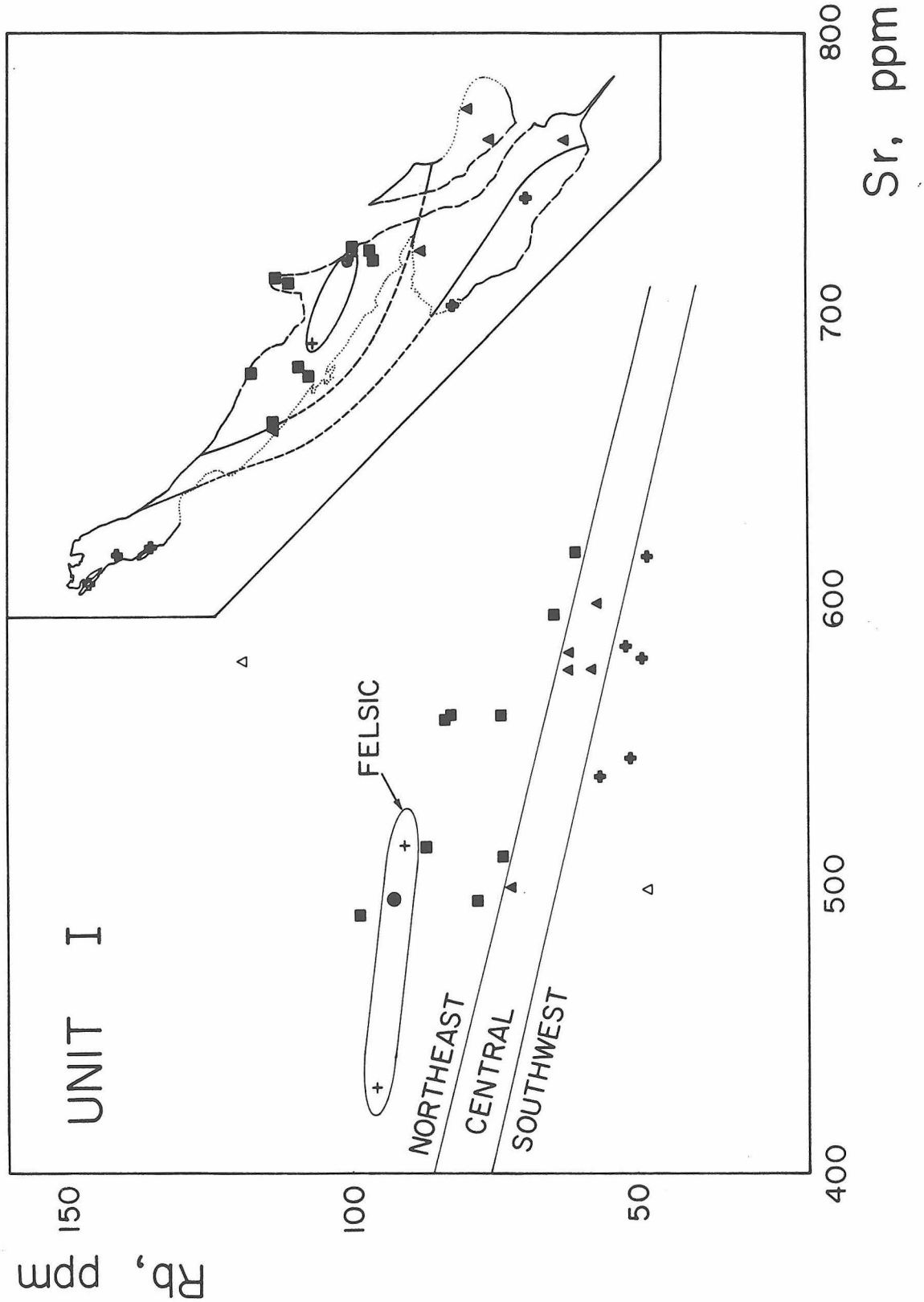
UNIT I
FELSIC
NORTHEAST
CENTRAL
SOUTHWEST
Rb, ppm
150
100
50
Sr, ppm
400
500
600
700
800

Figure 9.8

Figure 9.9. Rb-Sr diagram for Unit II.

Triangles - Tonalites and granodiorites
Plus sign - Felsic differentiate
Circle - Low-K granodiorite

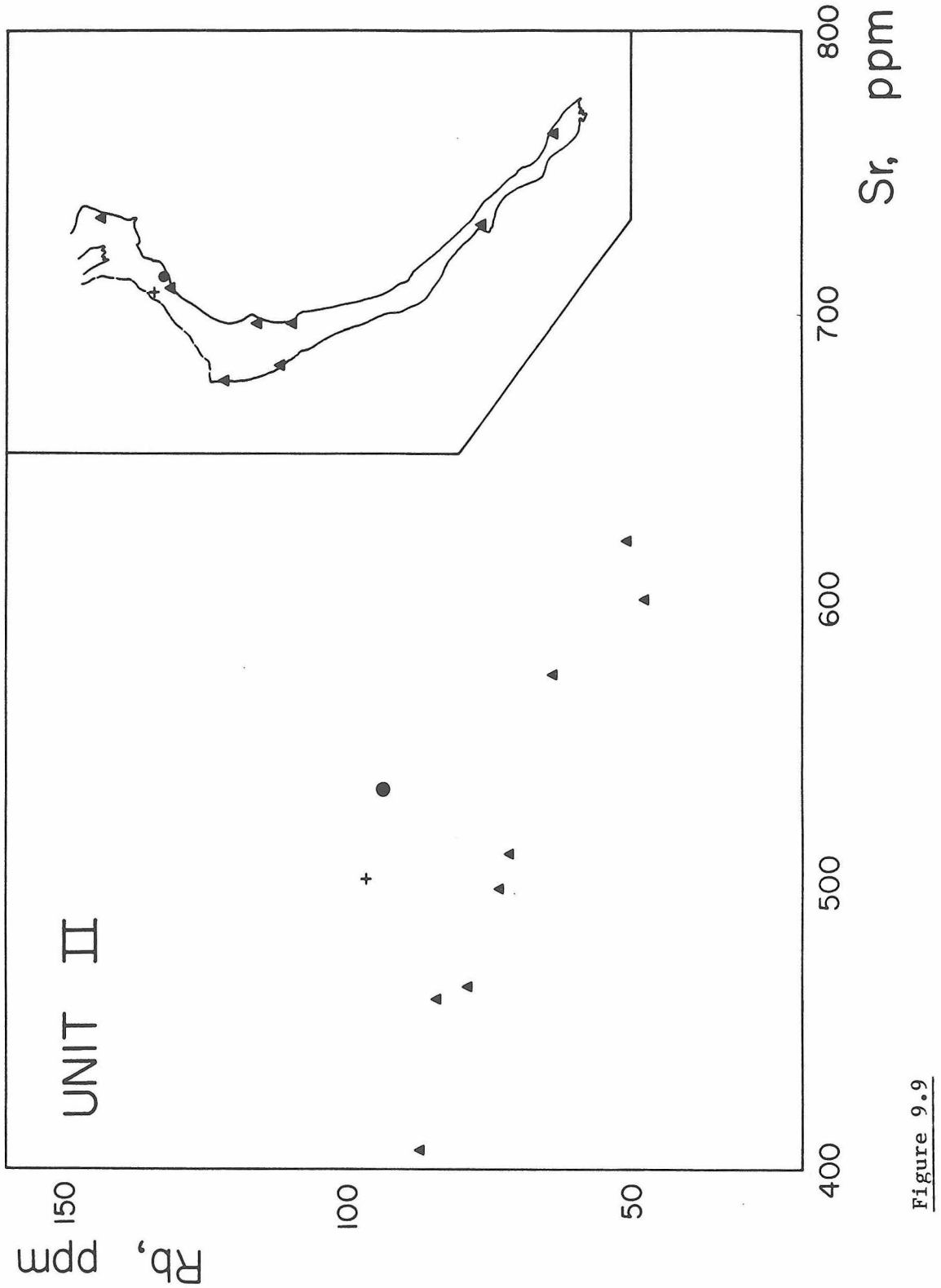

Figure 9.9

Figure 9.10. Rb-Sr diagram for Unit III, showing Rb-Sr sub-zones.

Filled symbols	-	Tonalites and low-K granodiorites
Open symbols	-	Mafic xenoliths
Plus sign	-	Felsic differentiate
Circles	-	Low-K granodiorites
Stars	-	Pine Cove salient
Half-filled squares	-	Central top
Squares	-	Intermediate level
Triangles	-	Central pluton distant from margin
Crosses	-	Northern margin

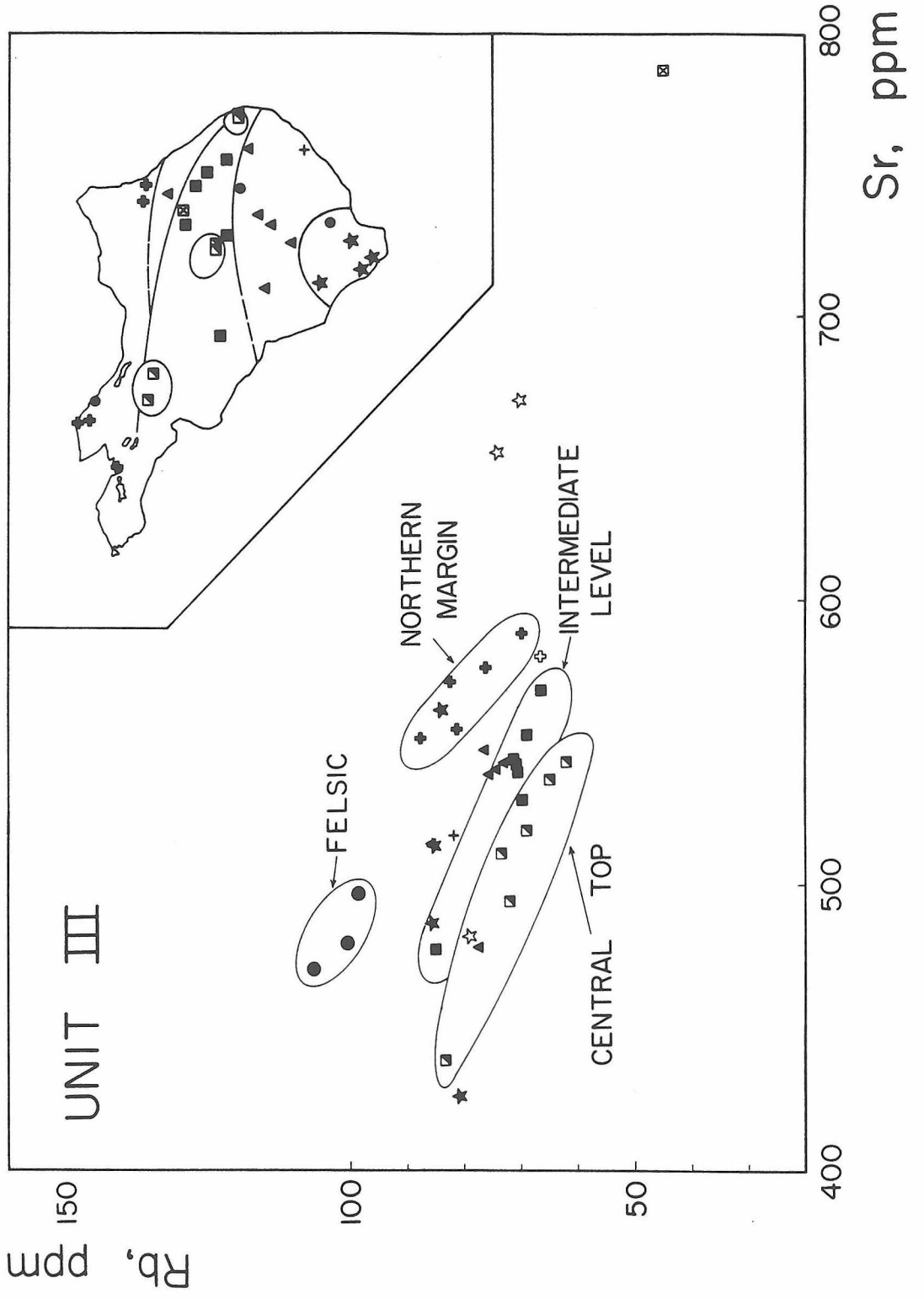
UNIT III
FELSIC
NORTHERN MARGIN
INTERMEDIATE LEVEL
CENTRAL TOP
Rb, ppm
150
100
50
400
500
600
700
800
Sr, ppm

Figure 9.10

Silver and Early (1977) used Rb and Sr concentration data to delineate 12 - 15 domains within the northern 600km of the Peninsular Ranges batholith. Each domain, comprised of many individual plutons and covering a diverse range of rock types was characterized by a particular linear covariation of Rb and Sr concentrations and a distinct set of Sr isotopic systematics. Rb-Sr concentration relations for igneous rocks from the San Jacinto Mountains are illustrated by Figs. 9.7-9.10. Figure 9.7 is a summary of all data from the area, whilst Figs. 9.8-9.10 show the data for the individual major tonalitic intrusive units (Units I, II and III, respectively) separately.

Several points are worth noting about the data displayed on Fig. 9.7. For the common igneous rock types there is a marked covariation between Rb and Sr, as has been found for the rest of the batholith (Silver and Early, 1977). Within the large tonalitic plutons there is considerable order to this covariation. Data from Unit I, the oldest of the major tonalite units is shown on Figure 9.8. Unit I is an elongate body some 35km long by 12km wide that apparently dips steeply to the northeast. Samples from the southwestern margin of this body have, in general, less Rb at a given Sr concentration than do samples from the center of the body. These in turn are Rb-poor relative to samples from the northeastern margin of this unit. Two samples that were collected because they are more leucocratic than surrounding tonalites are separated into a "felsic" group. These two samples, along with a third felsic tonalite with similar Rb-Sr characteristics, fall within the geographic confines of the northeastern sub-zone of Unit I, and tend to have more Rb and less Sr than the more common mafic tonalites (Color Index >15, SiO_2 <65.5 wt.%) that dominate the lithology of the unit. The gross pattern of northeastward

increase in the concentration of Rb at a particular Sr abundance mirrors the trend for the batholith as a whole as reported by Silver and Early (1973), and suggests that it is possible for the pronounced geographically related trends in trace element abundances characteristic of the batholith to be also reflected within a single intrusive unit.

Insufficient data exist for Unit II to be able to make the generalizations that can be made for Units I and III. The data points form a relatively tight linear array, with the only outliers being samples of relatively leucocratic rocks. These felsic samples are relatively Rb-rich and Sr-poor relative to associated tonalites.

Unit III is a large (20 x 12 km) funnel-shaped intrusion, the roof rocks to which are exposed in the Mount Edna - Cabazon Peak area south of Banning. They are inferred to have once been present within a relatively short distance above the highest present exposures of tonalite along the Black Mountain - Fuller Ridge - San Jacinto Peak physiographic spine that that forms the drainage divide between the Whitewater and San Jacinto Rivers (Plate 1). Within Unit III, distance from the known or inferred position of the roof rocks appears to be important in the pattern of correlated Rb-Sr behaviour. Rocks inferred to be closest to this roof zone have lower Rb (at a particular Sr concentration) than do rocks consecutively farther away (Fig. 9.10). Three other groups are distinguished on this diagram; a group of four samples from the "Pine Cove salient" that has relatively high and constant Rb (80-85 ppm) for a wide range in Sr concentration (425-560 ppm); a high Rb group from the northern margin of the pluton; and three samples that are more leucocratic than the majority of the surrounding tonalites. As is the case for Unit I there again

appears to be some reflection of the general batholithic trend to increased Rb northeastwards, but here with substantial vertical modification. Note also that the most mafic rock analysed from this unit (221), a tonalite from the 'Pine Cove Salient', has the lowest Sr concentration, and that only one data point from Unit III falls within the south-western sub-zone of Unit I, again consistent with the general batholithic trend.

If only samples distant from either the roof or walls of the pluton are considered (triangles and filled squares on Fig. 9.10) the Rb-Sr covariation becomes quite strong. This central group includes a relatively high proportion of relatively felsic rocks (Colour Index <12), and also includes the samples that show regular geographic variation in $\delta^{18}O$ values. These samples are all "normal" tonalites in the geochemical subdivision noted above (Ch. 7), and it appears probable that all of these geochemical features may be related. Within this relatively extensive area there does not appear to be more than a very general reflection of the batholith pattern (unlike that seen in either the more marginal, generally more mafic rocks from this unit, or for Unit I), suggesting that these correlated features do not relate to the regular west-to-east source variations observed for the batholith as a whole, but to some other feature or process.

These combined data for the three major tonalite units in conjunction with the observations presented for the batholith as a whole by Silver and Early (1977) strongly imply that the dominant direction of magma transport into these relatively high-level plutons is vertical, and that horizontal transport both prior to and after injection into the exposed upper crustal reservoirs is limited, although the pattern observed

for the central part of Unit III does not rule out horizontal transport at the scale of a few meters within this large magma chamber.

If the Rb-Sr domains reflect source characteristics, as argued by Silver and Early (1977) and Silver et al., (1979) then it appears that geographic variation within this source may be directly reflected in geographically consistent geochemical variation within a single pluton derived from this source. Although this phenomenon has been reported previously (Roddick, 1974; Roddick and Compston, 1977), the regional-scale picture available for the present study simplifies interpretation considerably. An important corollary of the observation that regional-scale geochemical variation can be found reflected in a single intrusive unit is that liquid homogenization processes within that intrusive unit cannot be particularly efficient. Either the length scale for convection must be small compared to the scale of the pluton (and convection, if occurring, is broken up into a number of independent cells), or the time scale for convection is large in comparison to the rate at which the pluton solidifies.

9.4 OBSERVATIONS ON INITIAL STRONTIUM ISOTOPIC COMPOSITION

The calculated initial strontium isotope ratio for each sample at the assumed time of crystallization (Sr_i) is listed in Tables 9.1 and 9.2. The range in Sr_i thus obtained for the various igneous intrusive units (the early intrusives and the late tonalites) is shown graphically on Figure 9.3.

Before considering the origin of this apparent variability of Sr_i processes that may affect the calculation of Sr_i must be considered.

9.4.1 POSSIBLE SOURCES OF ERROR IN CALCULATION OF SR_i

The calculation of the strontium isotopic composition for a particular sample (of any igneous rock unit) requires knowledge of the age, and precise determination of $^{87}Rb/^{86}Sr$ and $^{87}Sr/^{86}Sr$ for that sample at zero time (today). If these two ratios are known, it is possible to calculate the $^{87}Sr/^{86}Sr$ of the sample at any given time using the equation

$$(^{87}Sr/^{86}Sr)_m = (^{87}Sr/^{86}Sr)_t + (^{87}Rb/^{86}Sr)[\exp(\lambda t) - 1]$$

where the subscripts m and t refer to measured (t = 0) and time t ≠ 0, respectively, and λ, the constant for ^{87}Rb decay is taken to be 1.42×10^{-11} yr^{-1} (Steiger and Jaeger, 1977).

This calculation assumes that there has been closed system behaviour of both Rb and Sr since t, that is, there has been no movement of either rubidium or strontium into or out of the sample since the time for which $^{87}Sr/^{86}Sr$ is to be calculated. If t is the age of crystallization of an igneous body the inferred $^{87}Sr/^{86}Sr$ is usually called the "initial strontium ratio" (Sr_i) for the sample. The age of crystallization can either be determined independently (usually by other isotope systems), or by determining $^{87}Rb/^{86}Sr$ and $^{87}Sr/^{86}Sr$ for a suite of rocks or minerals inferred to have had identical $^{87}Sr/^{86}Sr$ at the time of essentially simultaneous rock or mineral formulation. The age equations thus obtained for the suite of samples can be solved simultaneously to give values for both the age and Sr_i. It is again assumed that there has been closed system behaviour of Rb and Sr for each analyzed sample. However, two extra assumptions are now needed - that all samples have identical age and had identical $^{87}Sr/^{86}Sr$ at this age.

If all the conditions of these assumptions are met, the errors in the determination of an Sr_i become solely analytical. If Sr_i is determined using an independently determined age then the error in Sr_i is directly related to the value of $^{87}Rb/^{86}Sr$ used in the calculation, and the uncertainty in the age determination. Larger values of these parameters thus introduce larger errors into the determination of Sr_i. For example, for a 100 m.y. old rock, a 1% error in the determination of $^{87}Rb/^{86}Sr$ leads to errors of approximately 2 parts in 10^6, 2 parts in 10^5 and 2 parts in 10^4 for $^{87}Rb/^{86}Sr$ values of 0.1, 1.0, and 10.0, respectively. A 1% error in the age determination results in the propagation of similarly sized uncertainties in Sr_i to those obtained for a 1% error in $^{87}Rb/^{86}Sr$.

Several factors combine to make this suite of rocks nearly ideal for the study of small variations in Sr_i, at least in analytical terms. The Neogene uplift and dissection, combined with the need for blasting in road and trail construction have made it relatively easy to collect "fresh" rock - rock apparently unaffected by surface weathering processes. This suggests that there might not have been open system behaviour of either Rb or Sr during the recent (surficial) history of the rock. A leaching study on a quartz + feldspar concentrate from one sample (Table 9.3) confirms that there is little or no loosely held strontium on the surfaces of quartz or feldspar, and, by inference, throughout the rock.

K-Ar, Rb-Sr and U-Th-Pb isotope data on mineral separates from these rocks (Armstrong and Suppe, 1972; this work; L.T. Silver, personal communication, 1979) may be interpreted as defining an extended but simple

TABLE 9.3.

RB, SR, AND $^{87}SR/^{8}$ SR DATA FOR MINERALS

	Rb, ppm	Sr, ppm	$^{87}Rb/^{86}Sr$	$^{87}Sr/^{86}Sr$
		LTS 147		
Rock	64.4	594.9	0.313	0.70805 ± 2
Biotite	406.3	9.31	128.3	0.87670 ± 31
		LTS 152		
Rock	72.6	542.6	0.387	0.70721 ± 2
Biotite	492.3	7.08	206.3	0.96401 ± 42
Plag + quartz				
Leach	0.113	0.568	0.578	0.70695 ± 3
Residue	2.65	546.4	0.014	0.70691 ± 2

decay of the thermal anomaly associated with the plutons. There is some suggestion from the regional-scale work of Krummenacher and his co-workers (Krummenacher et al., 1973; Silver et al., 1979), and from work in the nearby mylonite zones by Dokka and Frost (1976) that either the decay was terminated abruptly by tectonic activity at or around 60 m.y. ago, or there was complete to partial resetting of many isotope systems at this time, some 40 m.y. after crystallization of the igneous rocks. Alternately, the mineral data could be reflecting partial to complete resetting of the various isotopic systems in response to a thermal event related to Early Tertiary overthrusting (Sharp, 1979; Silver, 1982, 1983).

Whatever the cause of disturbance of the isotopic systems, the relatively minor development of hydrous secondary alteration phases (such as sericitisation of feldspar or chloritization of biotite) implies that the amount of aqueous fluid present was small during any possible post-crystallization thermal event.

The limited Rb-Sr mineral data presented in Table 9.3 demonstrate that, although the various mineral systems were apparently open to Rb and Sr for some time after crystallization, there appears to be little or no labile Rb or Sr currently present within these rocks. These data are shown on the isochron diagram (Fig. 9.11). The isotopic composition of Sr in both leachate and residue fractions of a plagioclase concentrate from LTS 152 are identical and significantly more radiogenic than expected for isotopic equilibrium with the biotite separate from this rock. There are several possible reasons for this discrepancy. Preparation of the biotite separate discriminated against altered or

Figure 9.11. Isochron diagram for mineral data from two rocks. Inset shows relations between plagioclase + quartz concentrate and total rock data.

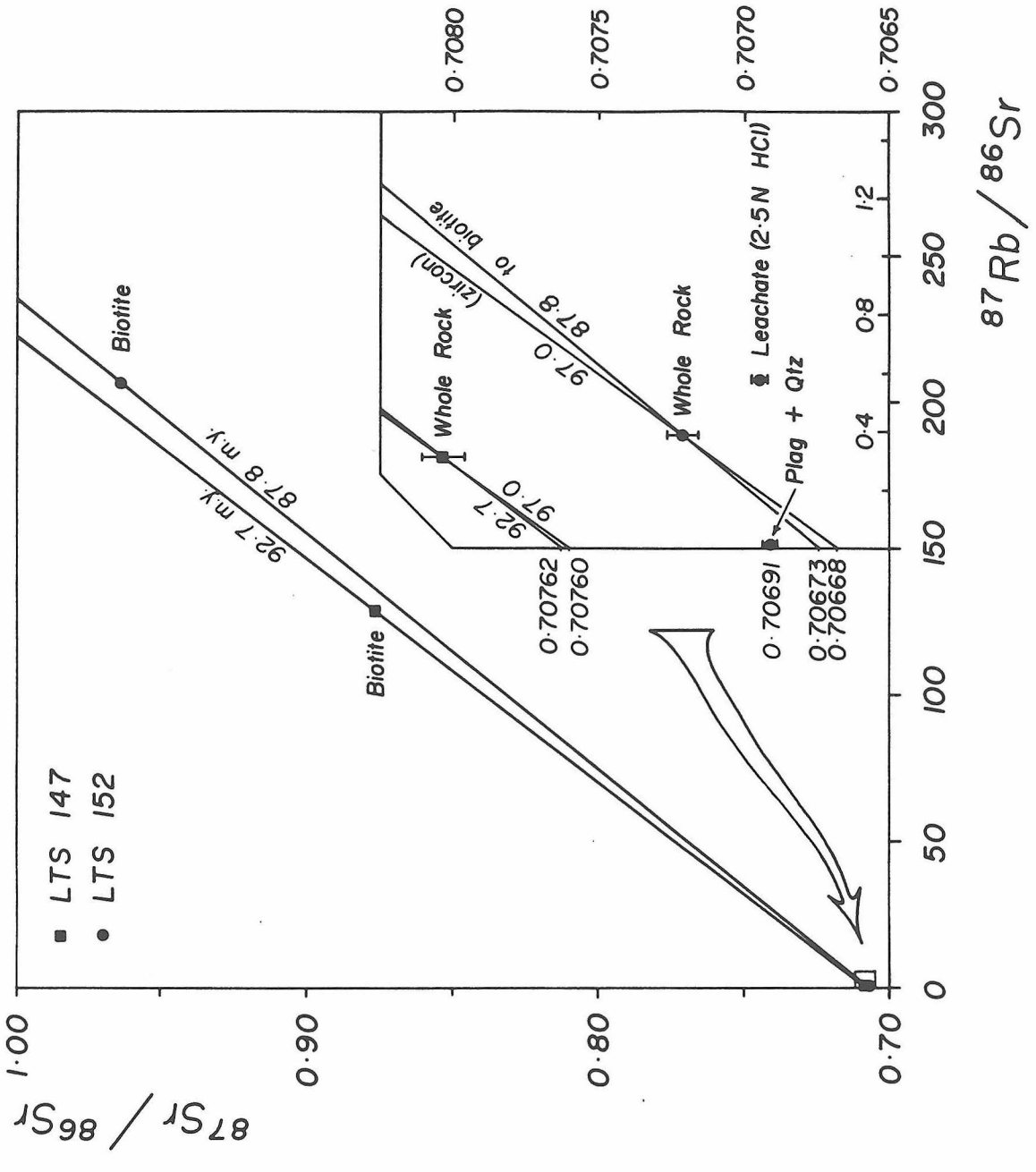
87Sr / 86Sr
87Rb / 86Sr
LTS 147
LTS 152
92·7 m.y.
87·8 m.y.
Biotite
Biotite
0·70762
0·70760
0·70691
0·70673
0·70668
Whole Rock
(zircon)
92·7
97·0
Whole Rock
to biotite
87·8
97·0
Leachate (2·5 N HCl)
Plag + Qtz

Figure 9.11

chloritized material; leakage of radiogenic Sr during chloritization followed by incorporation into plagioclase may explane at least some of the apparent ^{87}Sr excess in the plagioclase concentrate. An apparent "age" calculated from the plagioclase concentrate - total rock pair is approximately 55 m.y., and gives some indication of the maximum relative proportion of the radiogenic Sr developed in <u>situ</u> (in the last 97 m.y.) may be involved in exchange processes.

Preparation of a non-representative plagioclase sample could also yield an apparent ^{87}Sr excess in the analysed material. This is in fact suggested by the low Sr concentration of this plagioclase + quartz separate. Visual examination suggests that quartz comprises at most one third of the analysed material. This implies a maximum Sr concentration of about 900 ppm in the plagioclase, apparently insufficient to balance the rock concentration (540 ppm) unless another major Sr-rich phase is present. The low Sr concentration implied by these data is consistent with the plagioclase separate being relatively dominated by low-Sr, presumably low-Na rim material that could have incorporated substantial radiogenic Sr by sub-solidus processes.

Although these data show that there has been considerable exchange of radiogenic strontium between the various mineral phases of these rocks subsequent to crystallization they are interpreted as showing that radiogenic Sr lost from phases (apparently mostly from biotite) has been incorporated in other phases, dominantly plagioclase. Even if all of the excess radiogenic Sr in the plagioclase has been incorporated from an external source, the effect is still relatively small compared to the total range seen in the calculated Sr_i.

Three samples having a range of composition were collected from a restricted area along S.R. 243 south of Idyllwild (LTS 217,218, 219). With a range in color index from 13.2 to 18.1 it was expected that a range in $^{87}Rb/^{86}Sr$ would be encountered as well, allowing a check on whether calculated Sr_i was independent of Rb/Sr. Although a smaller range in $^{87}Rb/^{86}Sr$ than expected is present (0.488 - 0.540) the initial ratios calculated assuming a 97 m.y. age (0.70728 ± 5; 0.70730 ± 3; 0.70726 ± 3) agree within analytical uncertainties. These data are interpreted as arguing for closed system behaviour of Rb and Sr at the scale of the samples (approximately a liter).

The most crucial factors involved in the minimisation of errors in the calculation of Sr_i for these rocks is the combination of their young age, low Rb/Sr ratio, and their inferred closed system behaviour. For a typical rock, with $^{87}Rb/^{86}Sr = 0.4$, a 5% error in the measurement of this parameter contributes an error of less than ± 0.00003 to the calculated initial ratio. A 5% error in the age determination would contribute a similar but systematic error in the calculated Sr_i. The dominant uncertainty in Sr_i is thus, for most samples, the within and between run mass spectrometric uncertainty, which is generally better than ±0.00006 (8 parts parts in 10^5).

Although there is evidence for movement of radiogenic Sr at the mineral-grain scale, there does not appear to have been extensive mobility of Sr at the scale of a typical sample (a few kilograms).

Figure 9.12. Calculated Sr_i for igneous rocks from the San Jacinto Mountains, palinspastic base. Only the last three significant figures of a five-decimal-place value are shown for clarity (i.e., 678 = 0.70678)

Values in brackets are from mafic xenoliths.

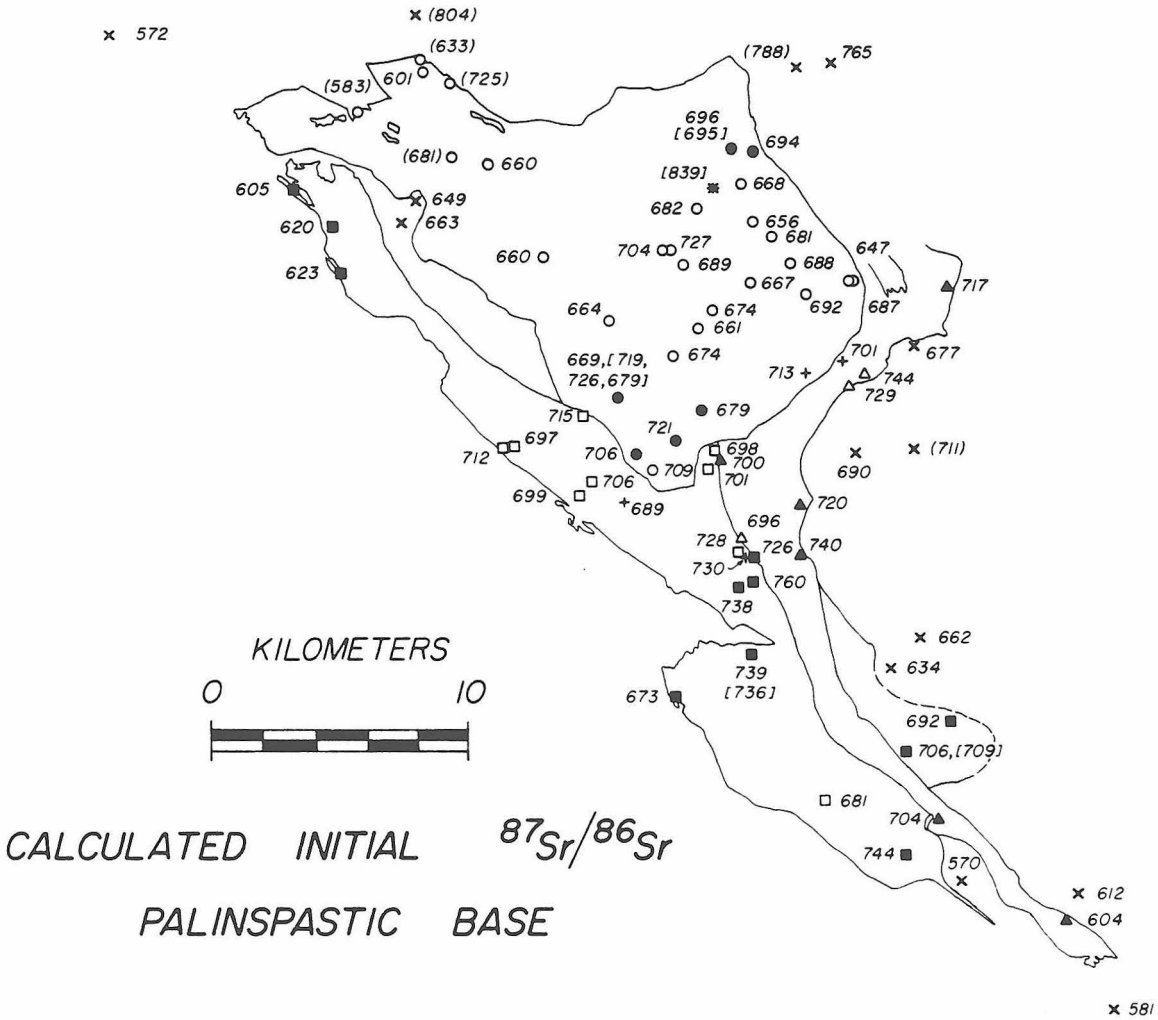
× 572
× (804)
(633)
(583)
601
(725)
(788)
765
696
[695]
694
(681)
660
[839]
668
605
649
663
682
656
620
681
704
727
647
660
689
688
623
667
717
664
674
692
687
661
701
677
669,[719,
726,679]
674
713
744
729
715
679
721
697
712
706
698
700
709
701
690
(711)
706
699
689
720
696
728
726
740
730
760
738
662
634
739
[736]
673
692
706,[709]
681
704
744
570
612
604
581
KILOMETERS
0
10
CALCULATED INITIAL 87Sr/86Sr
PALINSPASTIC BASE

Figure 9.12

Figure 9.13. Contoured Sr_i (at 97 m.y.) for early intrusives from the San Jacinto Mountains. Palinspastic base. Only the data indicated are used in the contouring. Note consistent northeastward increase in Sr_i for these compositionally diverse samples.

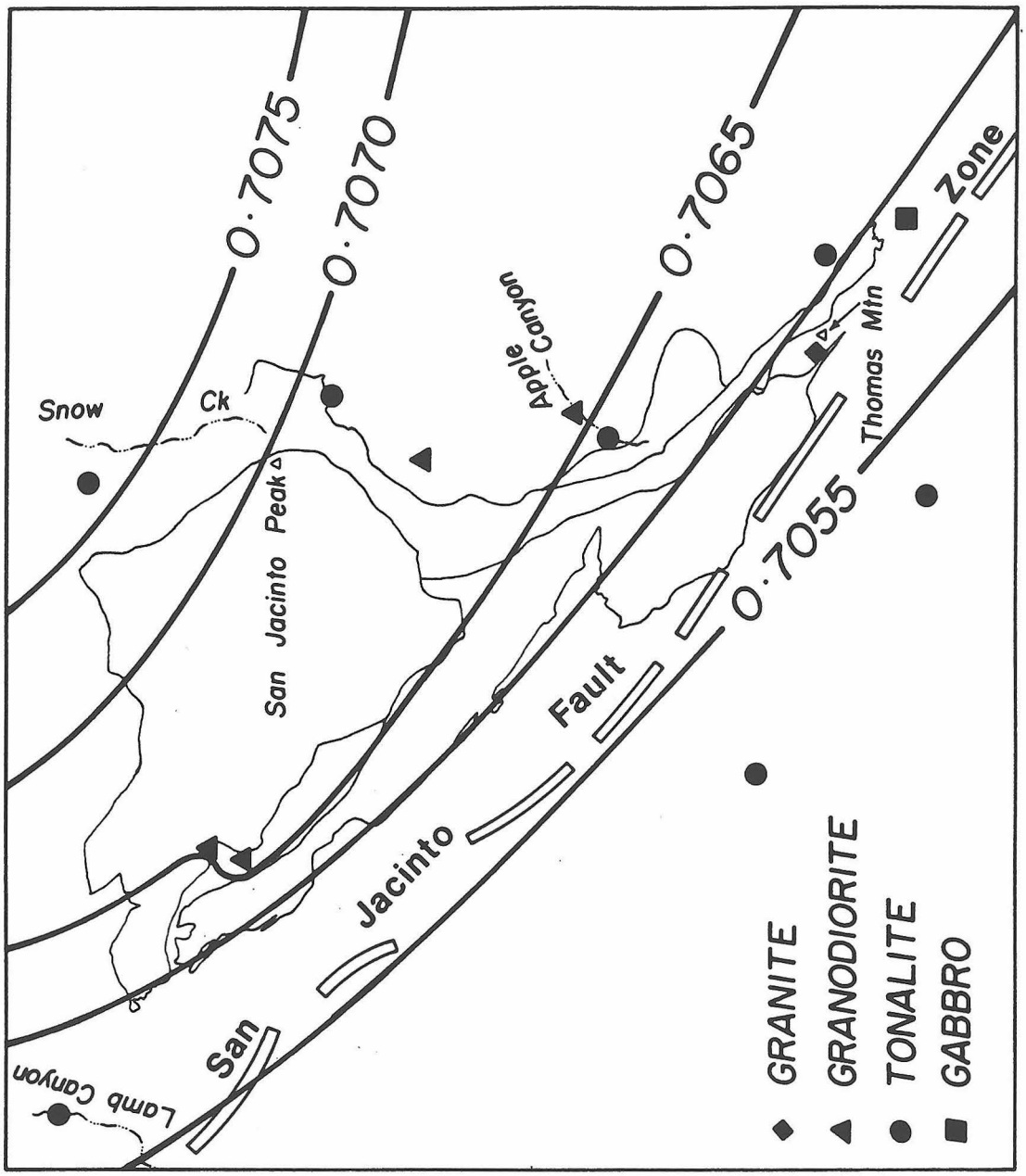
0.7075
0.7070
0.7065
0.7055
Snow
Ck
San Jacinto Peak
Apple Canyon
Thomas Mtn
Zone
Fault
Jacinto
San
Lamb Canyon
GRANITE
GRANODIORITE
TONALITE
GABBRO

Figure 9.13

Figure 9.14. Contoured Sr_i for Unit I, palinspastic base. Only the last two significant figures of a four-decimal-place figure are shown for clarity.

Filled symbols - "Mafic" tonalites
Open symbols - "Normal" tonalites'
Plus sign - Felsic differentiates

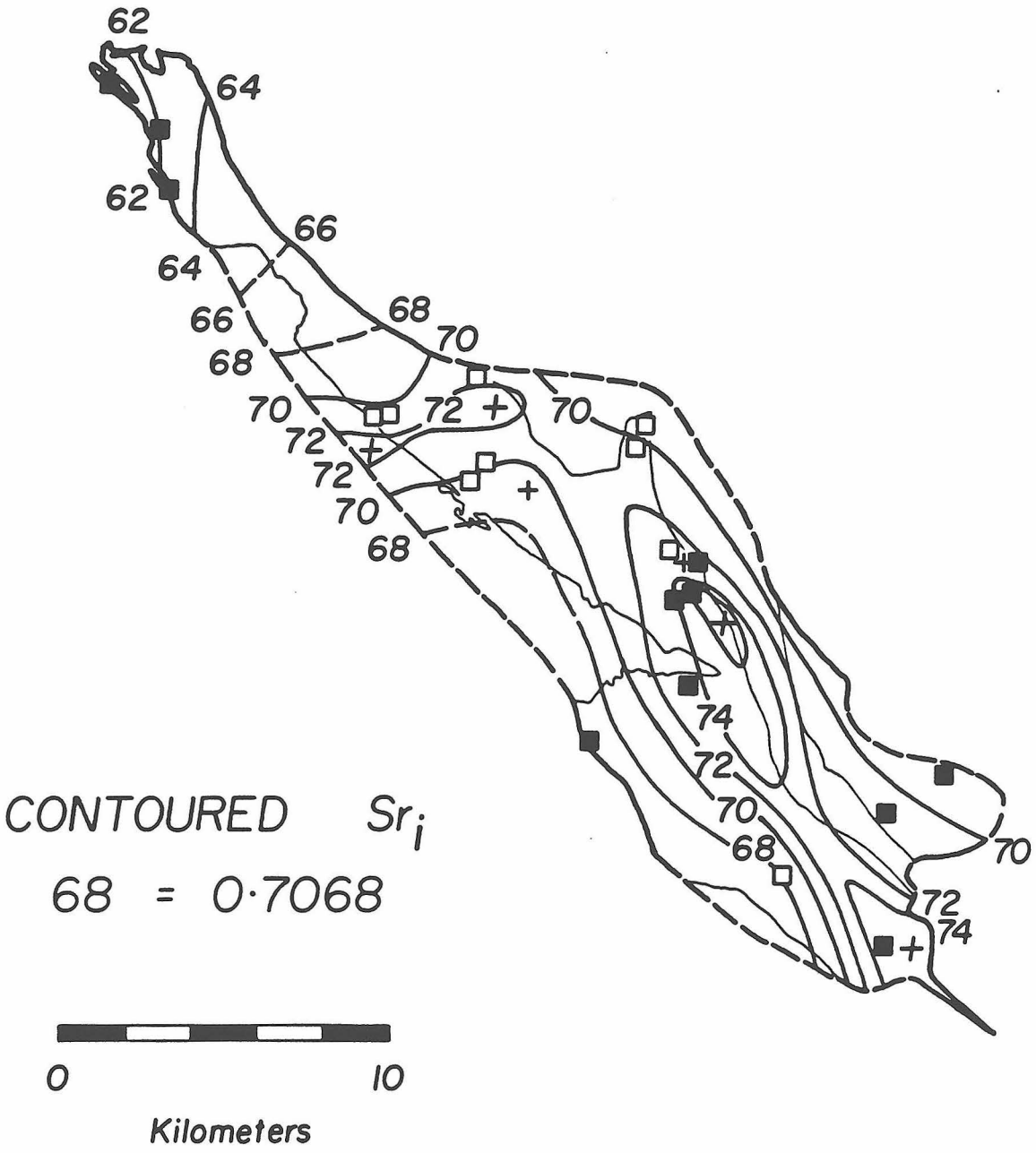
62
64
62
66
64
68
66
70
68
70
72
72
70
68
70
72
74
72
70
68
70
72
74
CONTOURED Sr$_i$
68 = 0·7068
0
10
Kilometers

Figure 9.14

Figure 9.15. Contoured Sr_i for Unit II, palinspastic base. Only the last two digits of a four-decimal-place value are shown for clarity.

Filled symbols - "Mafic" tonalites
Open symbols - "Normal" tonalites
Plus sign - Felsic differentiate

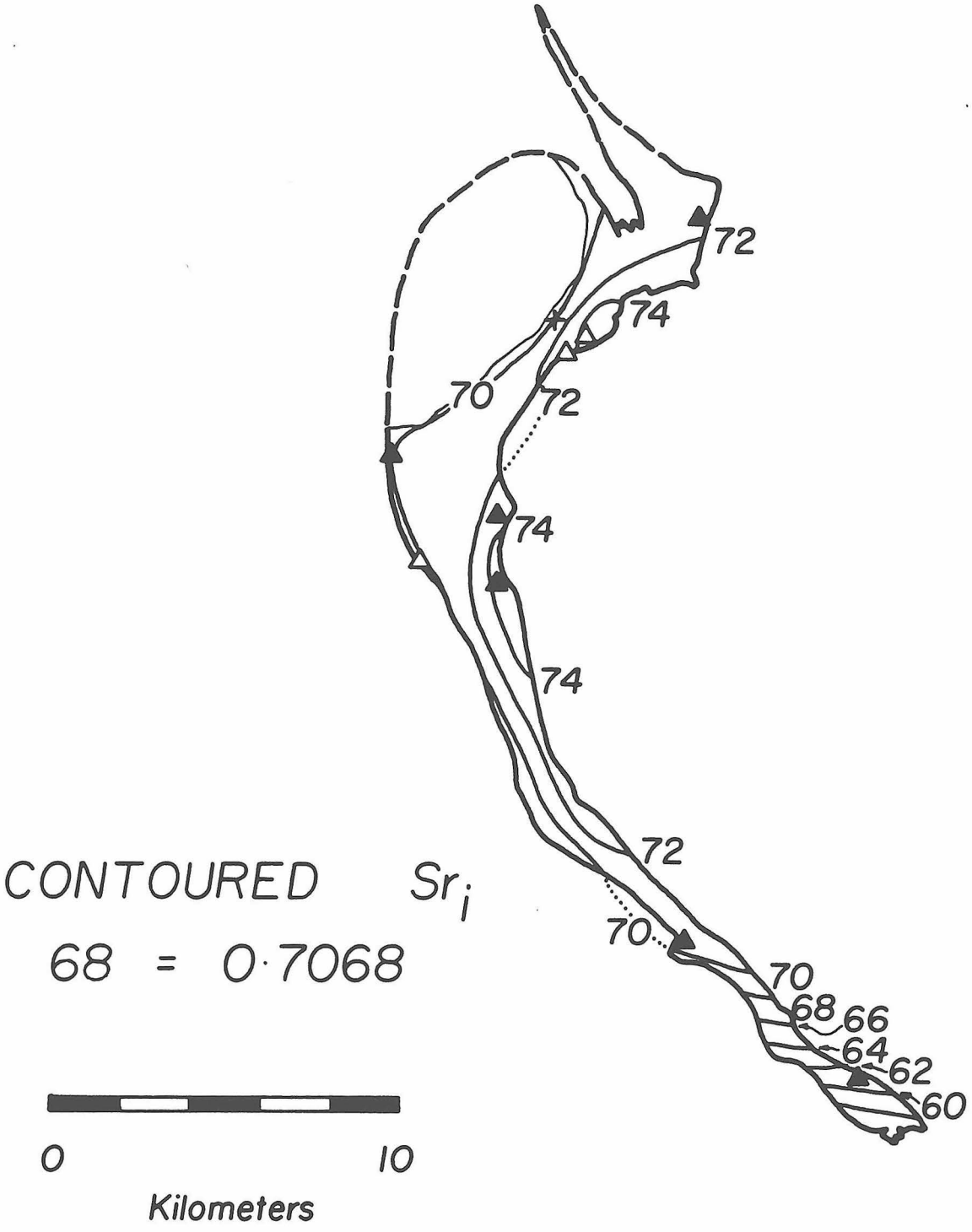
72
74
70
72
74
74
72
70
70
68
66
64
62
60
CONTOURED Sr_i
68 = 0·7068
0
10
Kilometers

Figure 9.15

Figure 9.16. Contoured Sr_i for Unit III, palinspastic base. Only the last two significant figures of a four-decimal-place value are shown for clarity.

Filled symbols - "Mafic" tonalites
Open symbols - "Normal" tonalites
Plus sign - Felsic differentiate

58
60
62
64
66
68
68
66
70
CONTOURED Sr_i
68 = 0·7068
0
10
Kilometers

Figure 9.16

9.4.2 GEOGRAPHICAL VARIATION OF SR_i

The geographic distribution of calculated Sr_i for all analysed igneous rock samples excepting the granite of Penrod Canyon and the contaminated samples from Red Tahquitz are shown on Figure 9.12.

A more detailed analysis of Sr_i as a function of geographical location is shown on figures 9.13, 9.14, 9.15, and 9.16 for the early intrusives, Unit I, Unit II, and Unit III, respectively. It is clear that there are significant variations in Sr_i within the igneous rocks of the northwest San Jacinto Mountains, and that these variations are strongly correlated with position.

Data for uncontaminated igneous country rocks are plotted on Figure 9.13. Most of these bodies are of small size; the largest have dimensions of a few kilometers. The consistent north-eastward increase in Sr_i displayed by these samples is striking, and is entirely consistent with the pattern demonstrated for the rest of the batholith by other workers (Early and Silver, 1973; Silver *et al.*, 1975; Silver and Early, 1977; L.T. Silver, unpublished data). These samples range over almost the entire compositional field of igneous rocks - from olivine gabbro to true granite. Over this entire compositional range it appears that Sr_i of these samples is determined solely by position.

Figure 9.14 shows the geographical distribution of Sr_i within Unit I, the oldest of the main tonalitic bodies. Although sample coverage is somewhat limited, it is clear that this unit contains rocks with substantially different Sr_i (0.7060 to 0.7076), and that this variation is not completely random. Rather, a ridge of high values in the central -

southeastern portion of the pluton gives way to lower values in all directions. Highs along this ridge are spaced 10 - 12 km apart.

Unit III shows the most complex pattern of geographical distribution of Sr_i. The western portion of the pluton shows an apparent regular increase in Sr_i northeastwards. This regular variation is replaced in the central and eastern part of the pluton by a pattern of highs and lows that is apparently related to geographic position only, and is not obviously influenced by elevation, rock type, or distance from contacts. Samples with similar Sr_i come from a wide range of elevations (over 900 m), whilst adjacent samples at comparable elevations may have quite different Sr_i. Samples from the "Pine Cove salient" form group with (perhaps anomalously) higher Sr_i than might be expected from extrapolation of trends from outside this area.

The lack of covariation of Sr_i with any other measured petrological, geochemical or isotopic parameter, or with geography, is best illustrated by data from Unit III (Fig. 9.17) where the geographic regularity of other parameters is so striking, but appears also to be a feature of all other igneous rock units of the San Jacinto Mountains. This implies that, for this region, there must be significant decoupling of the processes responsible for Sr isotopic properties from those responsible for these other petrologic characteristics. This is in sharp contrast to correlations observed in other parts of the batholith (L.T. Silver, personal communication, 1983).

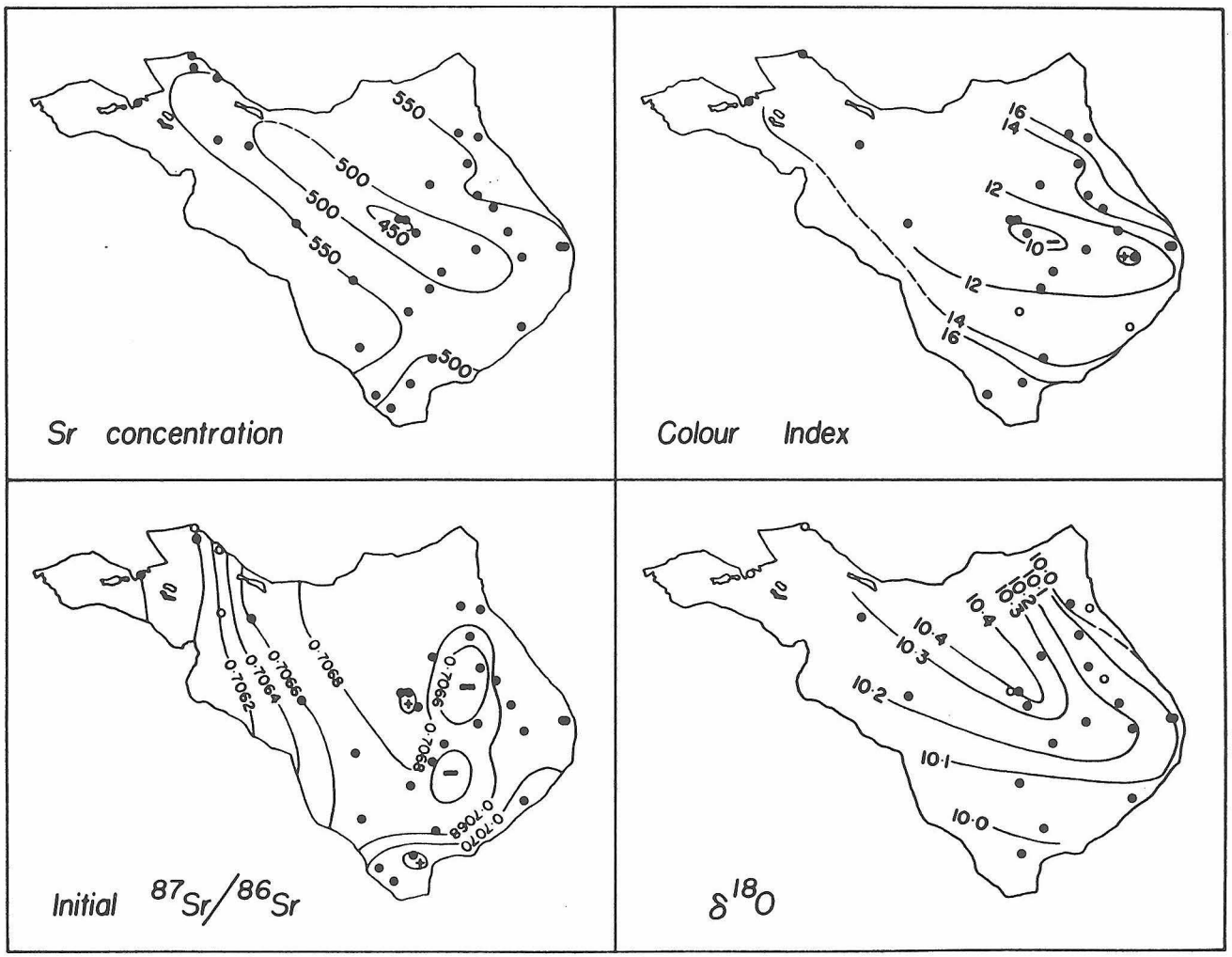

Figure 9.17. Geographic variation in Sr concentration (ppm), Sr_i, Colour Index (vol.%), and $\phi^{18}O$ (per mil) for Unit III.

9.4.3 RELATION OF INITIAL $^{87}SR/^{86}SR$ TO $^{87}RB/^{86}SR$ AND SR CONCENTRATION

The variation (or lack thereof) of Sr_i with Sr concentration may hold information regarding the origin of variation in one or both parameters. Figure 9.18 summarizes the available Sr concentration - Sr composition data from the major tonalites. Figures 9.19, 9.20 and 9.21 show the Sr_i-Sr concentration data for Units I, II and III, respectively. Grouping of the data by the sub-zones defined on the pattern of Rb-Sr covariation (Figs. 9.8-9.10) is also shown. No obvious correlation of Sr concentration with Sr_i is apparent. In the discussion of the Rb-Sr data for Unit III it was noted that a central group of samples showed particulary consistent covariation. The inner-most rocks from this pluton are differentiated on Figure 9.21 as "pluton remote from contacts". These samples are all probably more than a kilometer from the nearest contact, almost always the pluton roof, and show a relatively restricted range in Sr_i (from 0.7066 to 0.7068) compared to the much larger range (0.7058 to 0.7073) shown by samples from closer to the pluton walls.

Figure 9.22 shows the $^{87}Sr/^{86}Sr$ and $^{87}Rb/^{86}Sr$ data for the major tonalites plotted on the isochron diagram. A reference isochron for 97 m.y. is shown. The data for Unit I are grouped by Rb-Sr subzone. Felsic samples, as expected, have higher $^{87}Rb/^{86}Sr$ than the predominant tonalites. There does appear to be a weak overall tendency for samples with higher $^{87}Rb/^{86}Sr$ to have higher $^{86}Sr/^{87}Sr$. This effect is much larger than could be expected from the accumulation of radiogenic Sr since the time of crystallization alone given the observed Rb and Sr abundances.

Figure 9.18. Calculated Sr_i versus Sr concentration, major tonalites.

Filled symbols	-	Tonalites and granodiorites
Open symbols	-	Mafic xenoliths
Plus signs	-	Felsic differentiates
Squares	-	Unit I
Triangles	-	Unit II
Circles	-	Unit III

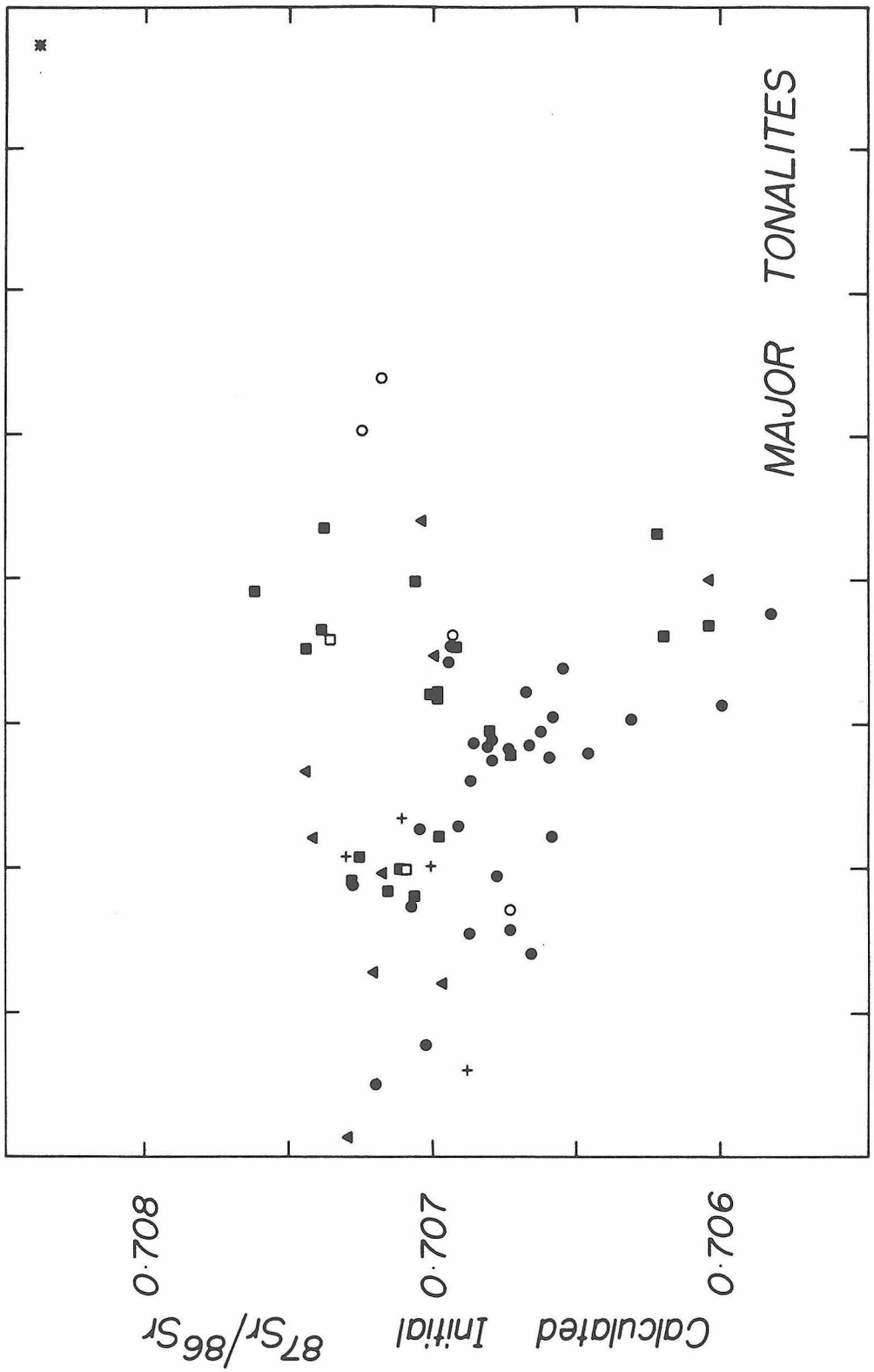
MAJOR TONALITES
Calculated Initial $^{87}Sr/^{86}Sr$
0·708
0·707
0·706
450
550
650
750
Sr, ppm

Figure 9.18

Figure 9.19. Calculated Sr_i versus Sr concentration, Unit I. Rb-Sr subzones from Fig. 9.8.

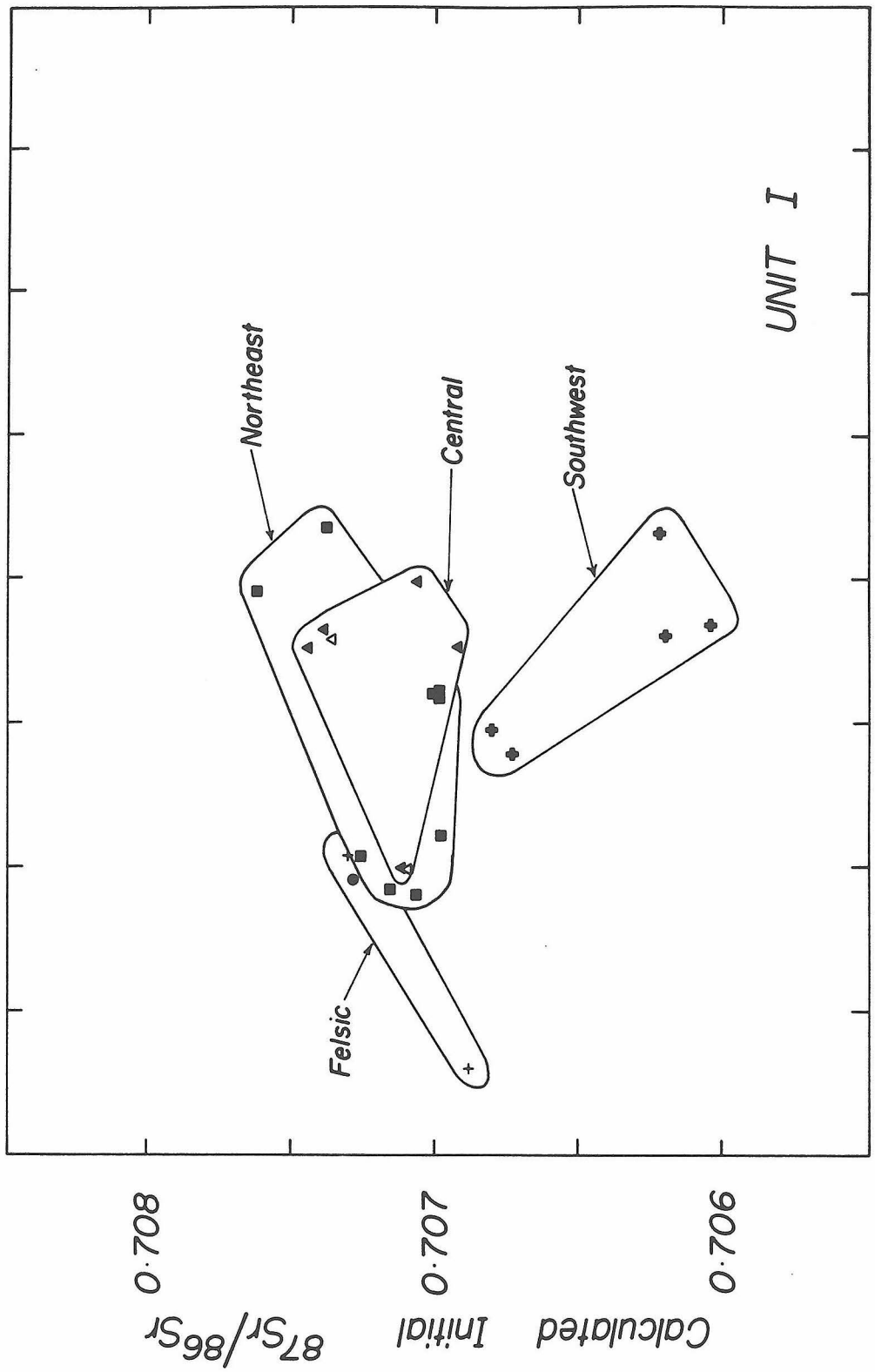
Calculated Initial $^{87}Sr/^{86}Sr$
0·708
0·707
0·706
450
550
650
750
Sr, ppm
UNIT I
Northeast
Central
Southwest
Felsic

Figure 9.19

Figure 9.20. Calculated Sr_i versus Sr concentration, Unit II.

Triangles - Tonalites
Plus sign - Felsic differentiate
Circle - Low-K granodiorite

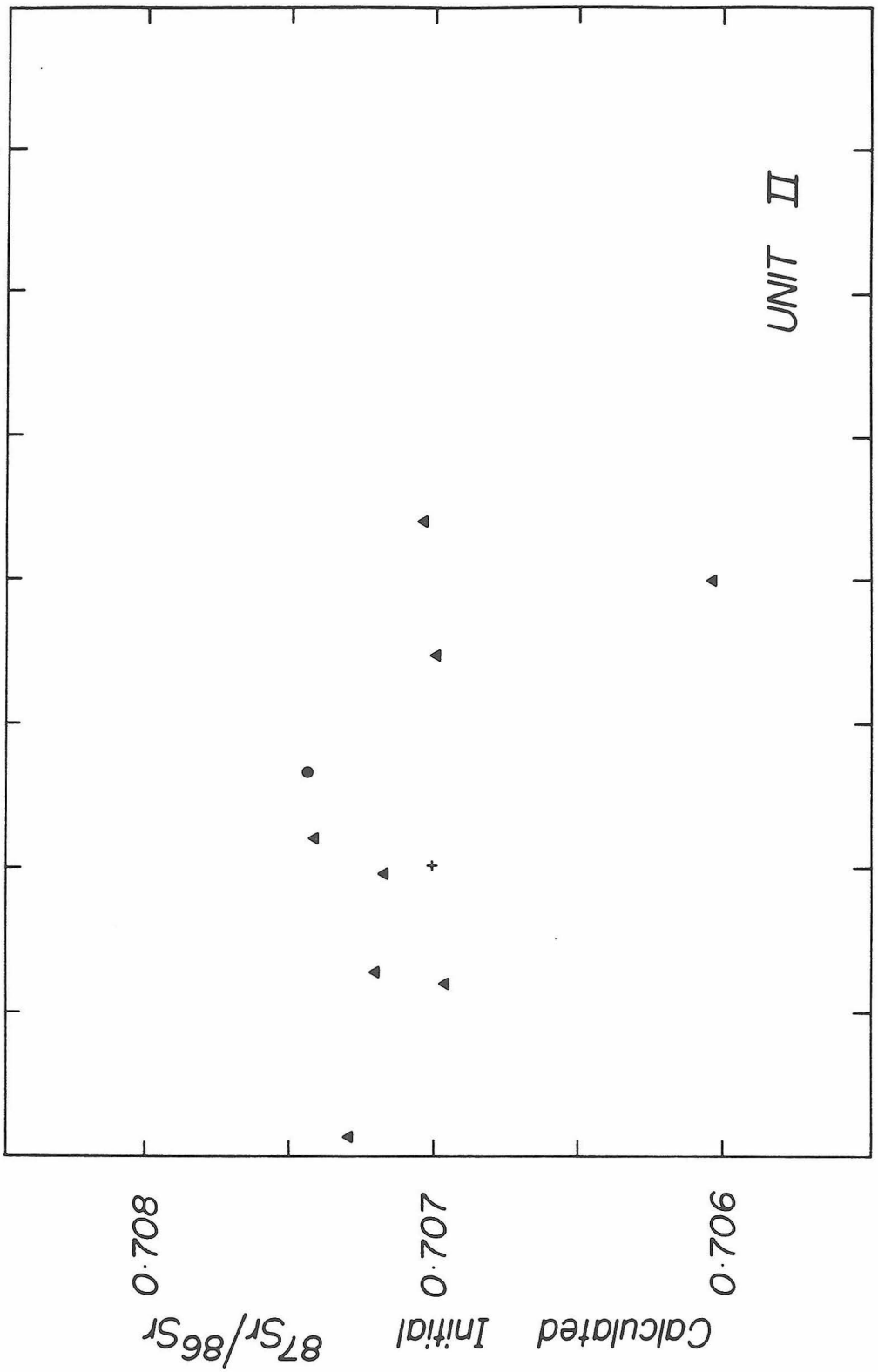
UNIT II
Sr, ppm
450
550
650
750
0·706
0·707
0·708
Calculated Initial 87Sr/86Sr

Figure 9.20

Figure 9.21. Calculated Sr_i versus Sr concentration, Unit III. Rb-Sr sub-zones from Fig. 9.10.

Field for central part of pluton remote from contacts (including roof) is shown.

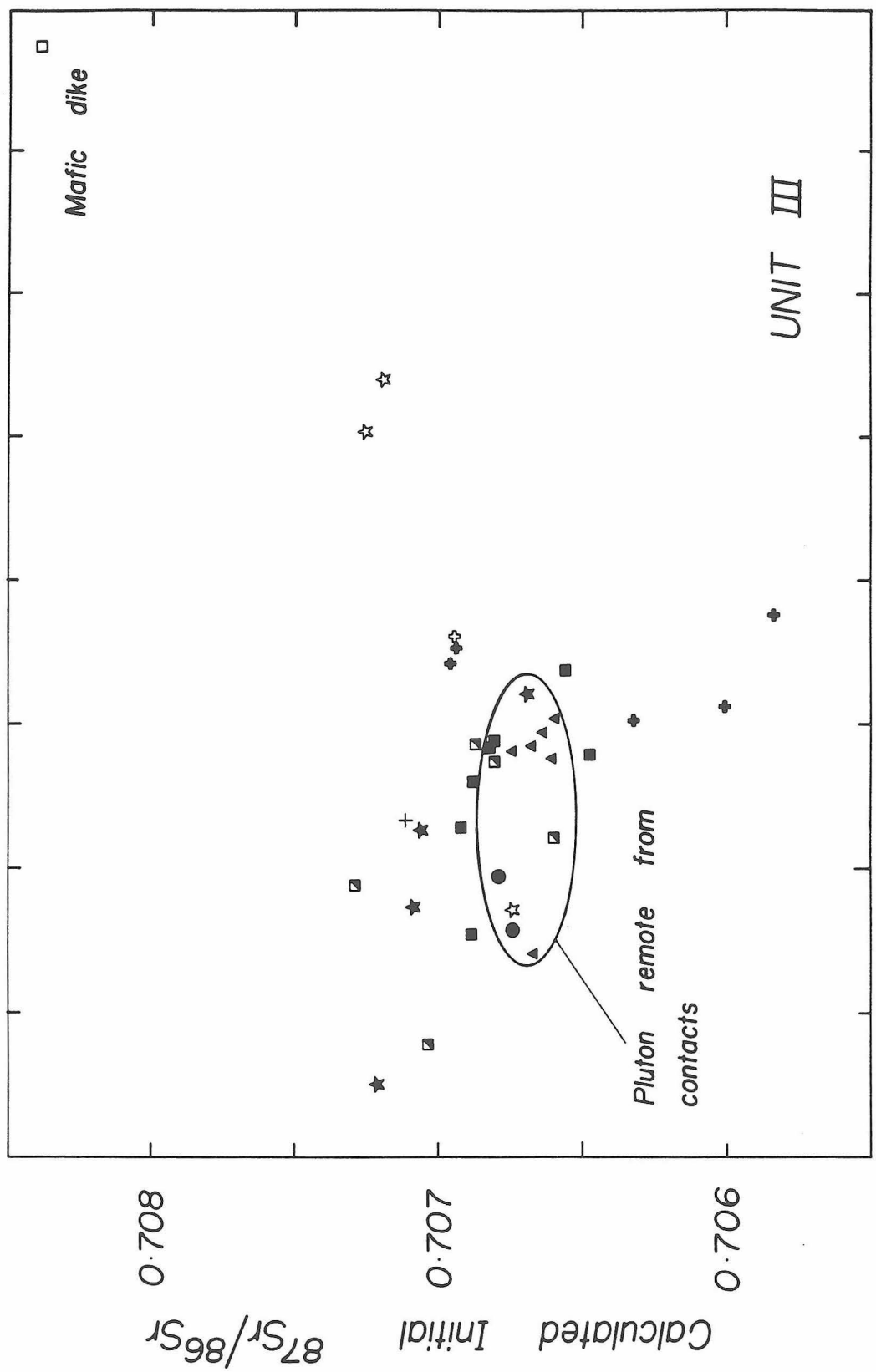
Mafic dike
UNIT III
Pluton remote from contacts
Sr, ppm
450
550
650
750
0·706
0·707
0·708
Calculated Initial 87Sr/86Sr

Figure 9.21

Figure 9.22. Isochron diagrams for samples from the San Jacinto Mountains.

Filled symbols	-	"Mafic" tonalites
Open symbols	-	"Normal" tonalites
Plus signs	-	Felsic differentiates
Crosses	-	Mafic xenoliths
Asterisk	-	Mafic dike intruding Unit III
Squares	-	Unit I
Triangles	-	Unit II
Circles	-	Unit III

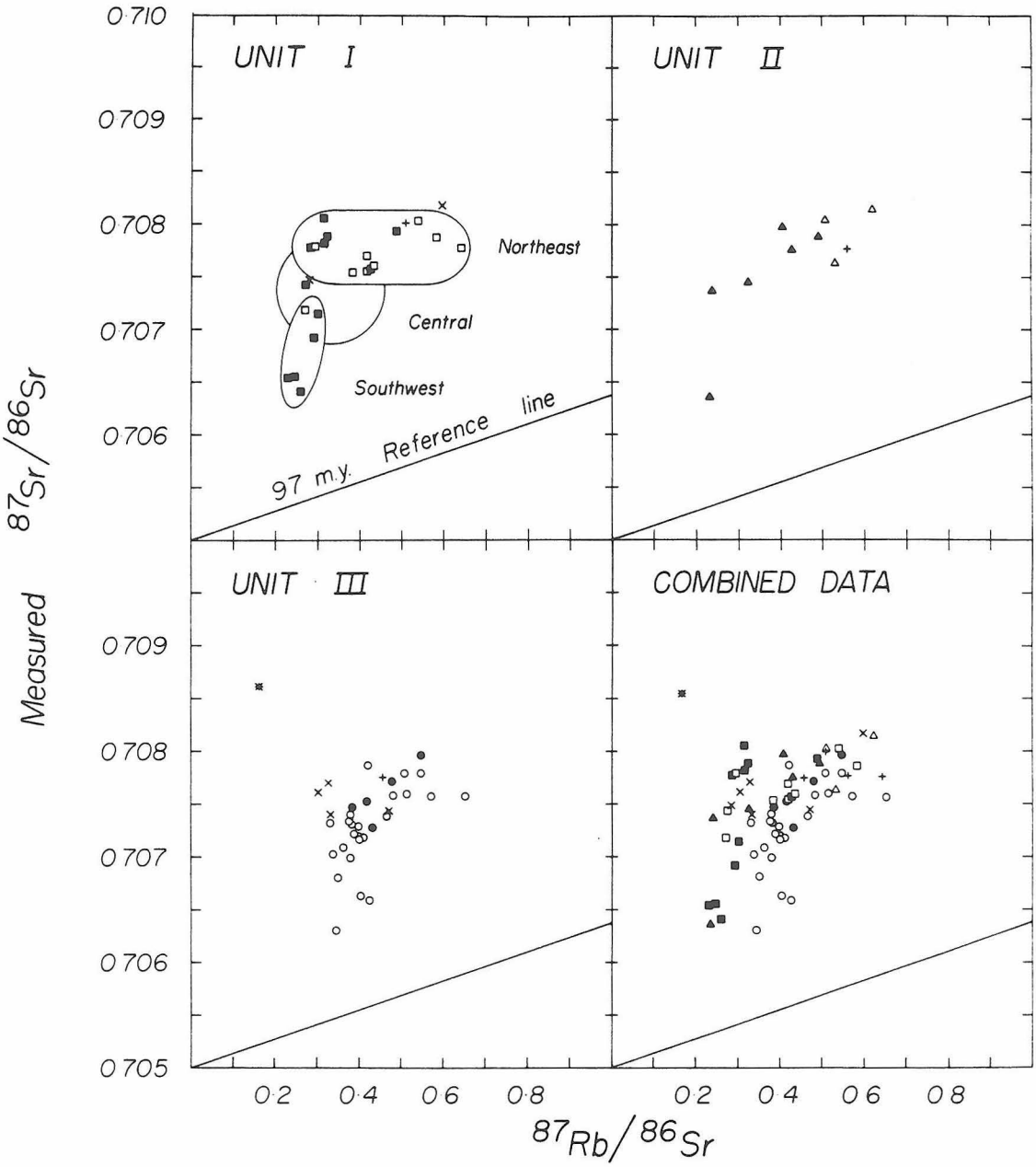
UNIT I
UNIT II
UNIT III
COMBINED DATA
Northeast
Central
Southwest
97 m.y. Reference line
0.710
0.709
0.708
0.707
0.706
0.705
0.2
0.4
0.6
0.8
Measured $^{87}Sr/^{86}Sr$
$^{87}Rb/^{86}Sr$

Figure 9.22

A brief digression from this systematic development is offered. It is obvious from inspection of Figure 9.22 that use of the total rock method of Rb-Sr dating for these rocks would be fraught with difficulties. One of the fundamental assumptions needed for application of this technique - that the system had homogeneous $^{87}Sr/^{86}Sr$ at the time of crystallization - is not valid. As the isotopic systems evolve, however, the amount of radiogenic strontium accumulated from in situ ^{87}Rb decay becomes large compared to the small $^{87}Sr/^{86}Sr$ variations initially present, and the error introduced by these initial variations becomes progressively less significant. Table 9.4 lists 'ages' calculated for each unit 903 m.y. in the future. The deviation from the true age (1,000 m.y.) is now of order 10% or less, still significant but much less of a problem than is the case today.

9.5 COMPARISON OF RB, SR AND $^{87}SR/^{86}SR$ DATA FROM THE SAN JACINTO MOUNTAINS WITH DATA FROM THE REST OF THE PENINSULAR RANGES BATHOLITH

A major determining factor in the selection of the San Jacinto Mountains as the site for the detailed study reported here was the availability of a large body of data on regional relationships within the Peninsular Ranges batholith (e.g., Early and Silver, 1973; Silver et al., 1979; Taylor and Silver, 1978; L.T. Silver, unpublished data). Comparison of inter-relationships within these data (e.g., Taylor and Silver, 1978), and comparison with published data from the Sierra Nevada batholith to the north (e.g., Silver, 1982, 1983) suggested that batholithic rocks of the San Jacinto Mountains had some characteristics transitional between those of the bulk of the Peninsular Ranges batholith to the south and

TABLE 9.4.

REGRESSION ANALYSIS OF RB/SR AND SR ISOTOPIC DATA

			M.S.W.D.
	UNIT III		
1	214 ± 109	0.70604 0.00067	35.4
2	1,158 ± 107	0.70577 ± 0.00064	13.3
	UNIT II		
1	222 ± 126	0.70628 ± 0.00080	48.8
2	1,154 ± 137	0.70609 ± 0.00078	24.6
	UNIT I		
1	197 ± 99	0.70645 ± 0.00055	58.8
2	1,163 ± 120	0.70611 ± 0.00061	29.9

1. Data regressed to give standard isochron age (slope) and intercept. Actual age (zircon U-Pb) is 97 ± 1 m.y.

2. Data "aged" for 903 m.y., then regressed. Actual age should be 1,000 m.y.

the Sierra Nevada batholith to the north.

Within the Peninsular Ranges batholith Sr_i increases systematically towards the east-northeast (Early and Silver, 1973; Silver et al., 1979; L.T. Silver, unpublished data). With the exception of a single sample from a pluton with a complex post-emplacement history no plutonic rock from the nothernmost Peninsular Ranges west of the mylonite zone has yielded an Sr_i value >0.706 except for the rocks of the San Jacinto Mountains described above (Early and Silver, 1973; Hill and Silver, unpublished data). Rocks from above (and east of) the mylonite zone commonly have Sr_i values of 0.706 or higher (Hill and Silver, unpublished data). The mylonite zone is the locus of considerable telescoping within the batholith (Silver, 1983), bringing generally more radiogenic rocks westward over the generally less radiogenic rocks of the central and western peninsula. Various geochemical characteristics (higher K, traces of inherited zircon) of these upper plate rocks have been interpreted as evidence for involvement of pre-existing cratonic material in magma genesis (Taylor and Silver, 1978), and the details of the origin of this presumably more continentward portion of the batholith are beyond the scope of the present study. It is important to note, however, that although the igneous rocks of the San Jacinto Mountains share at least some of the isotopic properties of these upper plate rocks, they are not in general more K-rich than are tonalites from elsewhere in the central or western batholith, nor do they show inheritance in their zircon populations. These observations appear to limit drastically the amount of involvement of old chemically evolved crustal material (such as intermediate or felsic igneous rocks, or most sediments) in the petrogenesis of the San Jacinto plutons.

Elsewhere along the North American continental margin tectonic significance has been attached to particular features of patterns of Sr_i. Kistler and Peterman (1973) noted the close correspondence between the nature of the country rock and Sr_i in the plutons of the Sierra Nevada batholith, and concluded that the line $Sr_i = 0.706$ apparently reflected the boundary between miogeoclinal and eugeoclinal deposition through the late Precambrian and Paleozoic, and, by inference the western edge of the North American craton. The line $Sr_i = 0.704$ marks the easternmost boundary of exposures of ultramafic rocks since interpreted as ophiolitic fragments emplaced along a major crustal boundary or suture (e.g., Saleeby, 1979), implying that igneous rocks with $0.704<Sr_i<0.706$ were emplaced through relatively young continental crust, and those with $Sr_i<0.704$ were emplaced through largely oceanic materials. East of the $Sr_i = 0.706$ line the pattern is more complex, with significant reversals of the apparent trend to generally higher Sr_i continentward. The distance between the $Sr_i = 0.704$ and $Sr_i = 0.706$ contours is small (at most a few tens of kilometers), implying that the area underlain by relatively young continental crust was quite narrow. Interpretation of the tectonic evolution of the Sierran foothills has changed significantly since the publication of Kistler and Peterman's paper, with more recent workers suggesting that the foothills may be the site of major tectonic disruption both prior to and during the development of this multi-generation batholith (e.g., Silver and Anderson, 1974, 1983; Saleeby, 1981; Schweikert, 1981). Given this apparently complex evolution, caution must be exercised in interpreting the isotope data from the Sierra Nevada batholith.

The orderly eastward increase in Sr_i within the Peninsular Ranges batholith from "oceanic" values of 0.704 or less to "continental"

Figure 9.23. Sr_i versus δ^1 O, San Jacinto Mountains. Ticks against symbols indicate probable increase in observed $\delta^{18}O$ because of minor exchange with adjacent wall rocks. Stippled field for "Main Peninsular Ranges Batholith" from Taylor and Silver, 1978.

Total observed ranges of inferred primary Sr_i and $\delta^{18}O$ shown by arrows.

Filled symbols	-	"Mafic" tonalites
Open symbols	-	"Normal" tonalites
Squares	-	Unit I
Triangle	-	Unit II
Circles	-	Unit III
Diamonds	-	Granodiorite of Poppet Creek
Plus sign	-	Felsic differentiate

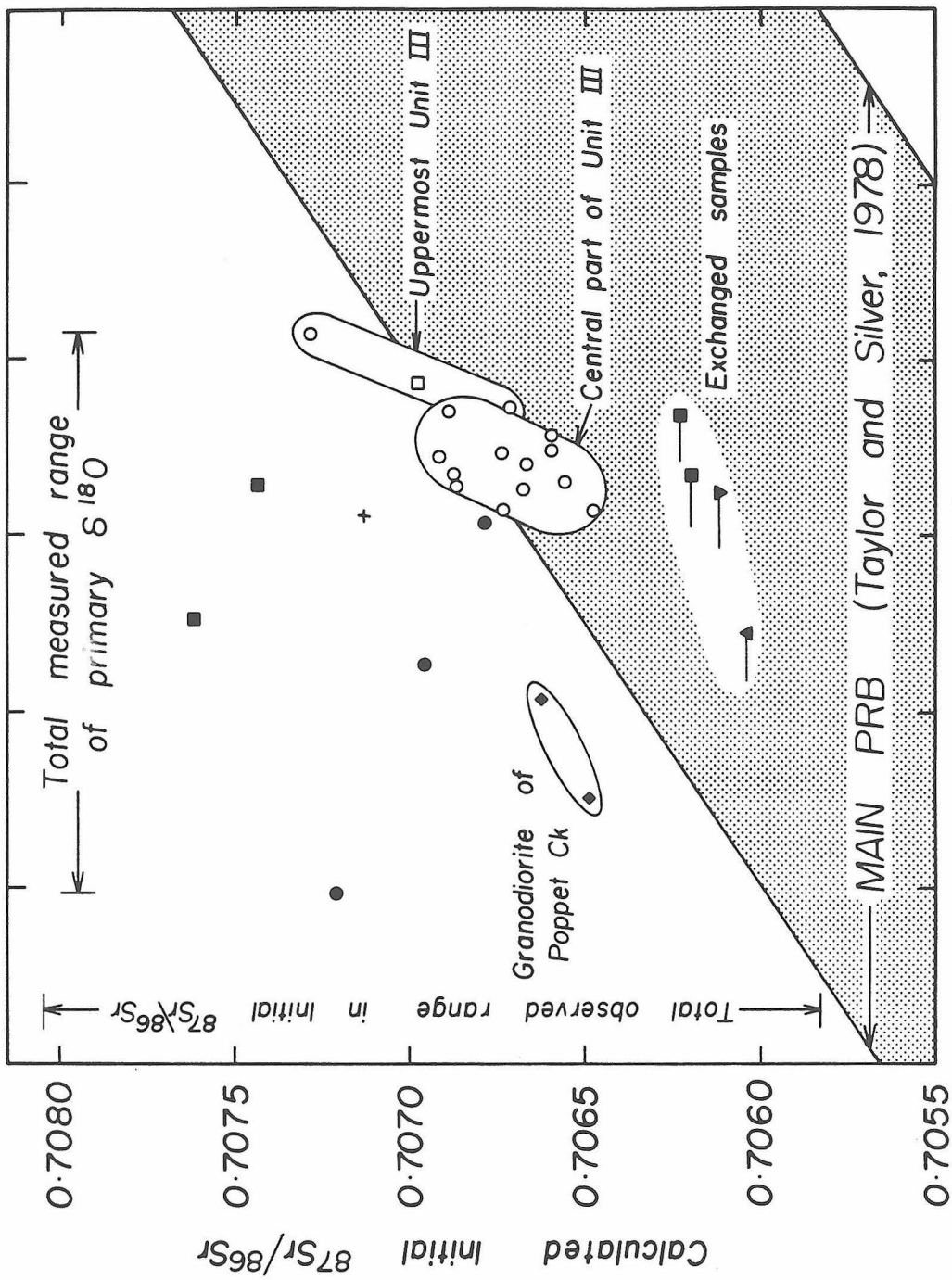
Calculated Initial $^{87}Sr/^{86}Sr$
0·7080
0·7075
0·7070
0·7065
0·7060
0·7055
Total observed range in initial $^{87}Sr/^{86}Sr$
Total measured range of primary $\delta^{18}O$
Granodiorite of Poppet Ck
MAIN PRB (Taylor and Silver, 1978)
Uppermost Unit III
Central part of Unit III
Exchanged samples
9·0
10·0
11·0
$\delta^{18}O$, permil

Figure 9.23

Figure 9.24. Sr_i versus $\delta^{18}O$, Peninsular Ranges batholith. From Taylor and Silver, 1978.

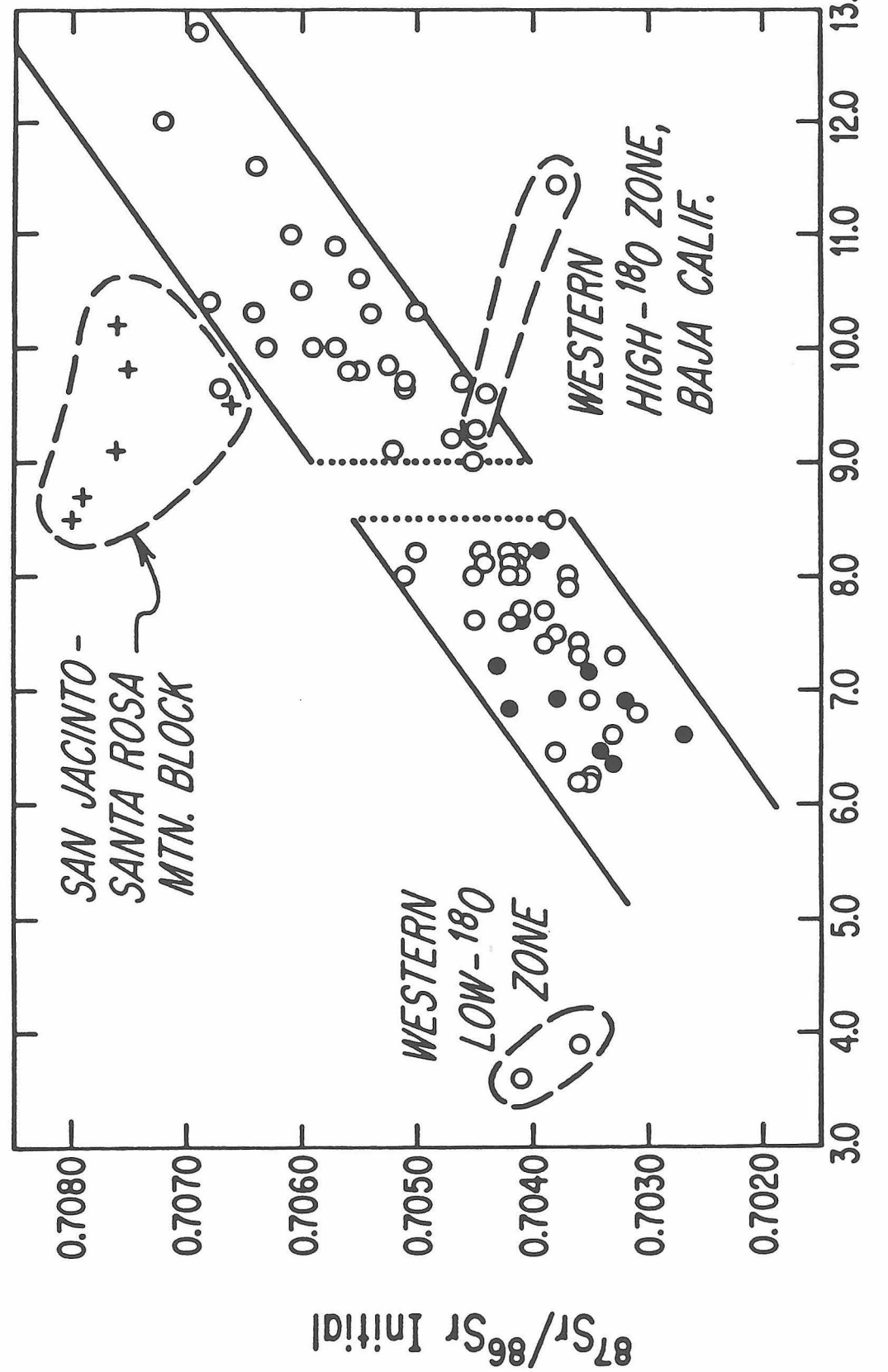
SAN JACINTO-
SANTA ROSA
MTN. BLOCK
WESTERN
LOW-18O
ZONE
WESTERN
HIGH-18O ZONE,
BAJA CALIF.
87Sr/86Sr Initial
δ 18O Whole Rock (‰)
0.7080
0.7070
0.7060
0.7050
0.7040
0.7030
0.7020
3.0
4.0
5.0
6.0
7.0
8.0
9.0
10.0
11.0
12.0
13.0

Figure 9.24

Figure 9.25. Sr_i versus $\delta^{18}O$ for the Peninsular Ranges batholith (from Taylor and Silver, 1978) and the San Jacinto Mountains (this work, Taylor and Silver, 1978). Field for Upper Plate Rocks inferred from Taylor and Silver, 1978, and Silver et al., 1979.

Primary values for rocks from the San Jacinto Mountains largely overlap the field of the Upper Plate Rocks. The majority of the San Jacinto data fall slightly to the low-$\delta^{18}O$, high-Sr_i side of the main batholith trend.

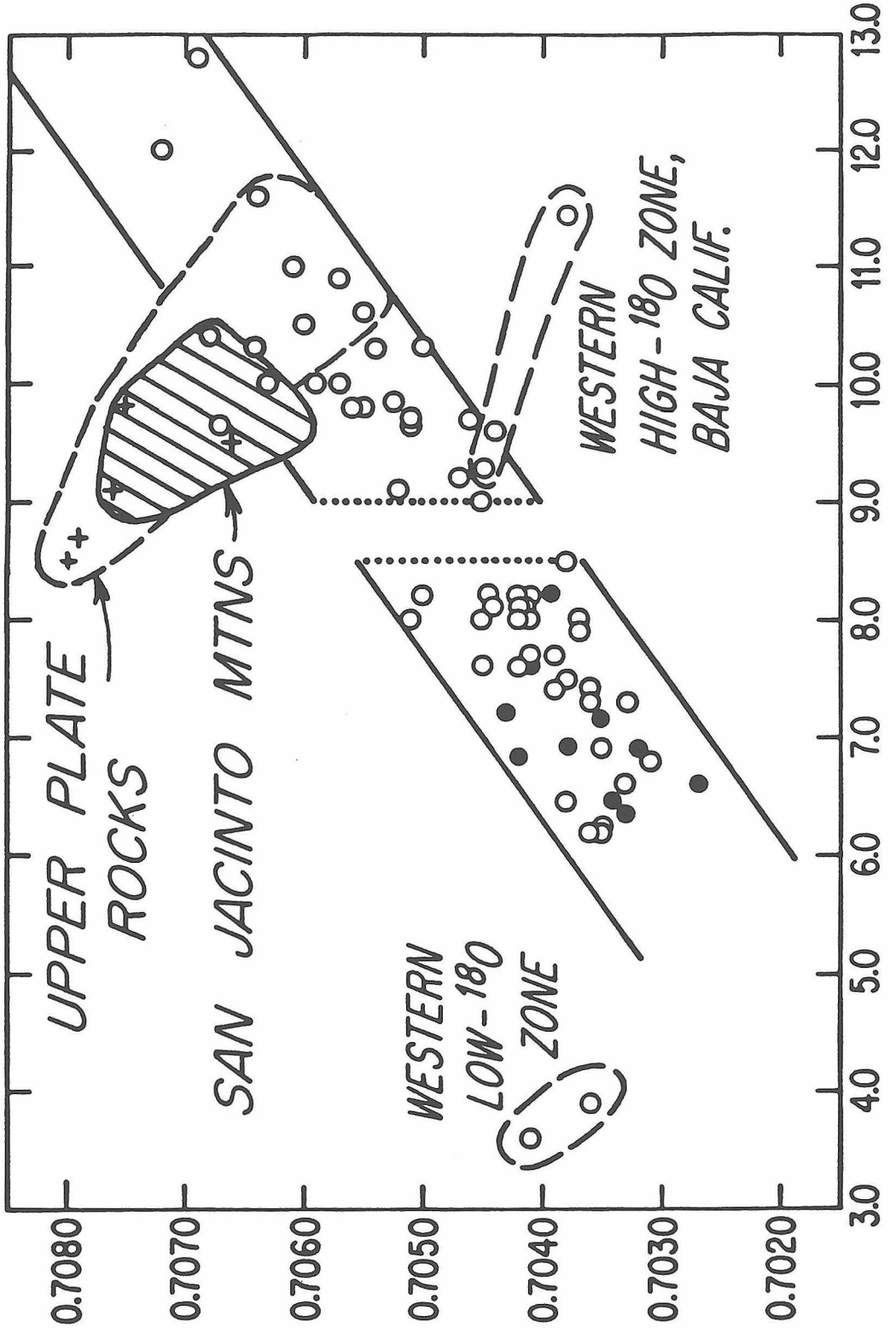
UPPER PLATE ROCKS
SAN JACINTO MTNS
WESTERN LOW-18O ZONE
WESTERN HIGH-18O ZONE, BAJA CALIF.
87Sr/86Sr Initial
δ 18O Whole Rock (‰)
0.7080
0.7070
0.7060
0.7050
0.7040
0.7030
0.7020
3.0
4.0
5.0
6.0
7.0
8.0
9.0
10.0
11.0
12.0
13.0

Figure 9.25

values of 0.706 or higher occurs over a distance of some 70 km northeasterly from the coast to the southwestern San Jacinto Mountains, and apparently over even greater distances further south where the mylonite zone disrupts this pattern. These data imply either a continual gradational source, or consistent variation in the relative importance of two or more sources over an immense area.

Figure 9.23 shows the observed covariation in Sr_i and δ^1 O for rocks from the San Jacinto Mountains. Most of the samples are from Unit III, and show a relatively limited range in both $\delta^{18}O$ values (10.1-10.4) and Sr_i (0.7065-0.7070). These samples have isotopic properties that partially overlap those reported for igneous rocks elsewhere in the batholith west of the mylonite zone (Taylor and Silver, 1978; Silver et al., 1979)[Fig. 9.24]. Samples from other plutons (granodiorite of Poppet Creek, Major Tonalite Units I and II) as well as more mafic rocks from Unit III extend the field for the San Jacinto rocks considerably, so that it substantially overlaps the field defined for rocks from the "San Jacinto - Santa Rosa Mountains Block" by Taylor and Silver (1978). This is shown on Figure 9.25, except that the "San Jacinto - Santa Rosa Mountains Block" of Taylor and Silver is not recognized as such, but has been largely replaced by a field for samples from above (east of) the mylonite zone. The data from the San Jacinto Mountains presented here largely overlap the field thus defined for upper plate rocks, suggesting that the component that is dragging both data groups to the low-$\delta^{18}O$ side of the batholith array is important within both suites. If this material had $\delta^{18}O$ values typical of mafic igneous rocks (+5.5 to +6.5), then it is implied that as much as 50% of the oxygen in some of the upper plate rocks and a minimum of 25% of the oxygen in the most extreme San Jacinto

sample (LTS 221; $\delta^{18}O$ = +9.0) may have come from this component. If significant fractionation (of oxygen) occurred during the genesis of these rocks, estimates of the importance of this anomalous component would increase. For the bulk of the San Jacinto rocks, however, this "continental" component was apparently far less important, contributing less than 10% of the oxygen of the analyzed rocks. The inferred low $\delta^{18}O$, the lack of inherited zircon, and the apparent lack of major and trace element geochemical features correlative with the inferred importance of this component in determining the isotopic composition of the San Jacinto rocks are interpreted as indicating that this component was otherwise grossly similar chemically to the other component(s) contributing to the characteristics of the batholithic rocks. A possible source for such material is older sub-continental lithosphere that is slightly enriched in ^{87}Sr and depleted in ^{143}Nd relative to normal mantle because of a small long term enrichment in Rb relative to Sr, and depletion in Sm relative to Nd, respectively. Unlike situations to the east, where Silver (personal communication) has interpreted the geochemical and geological data as indicating transport of plutons through, and undergoing significant interaction with, the cratonic lithosphere and its superjacent sedimentary sequences, there appears to be little identifiable involvement of upper crustal-type materials in the development of the San Jacinto rocks.

By older crustal lithosphere is meant relatively mafic material currently resident in either the lower crust or upper mantle that attained its present character at or about the time of development of the superjacent continental crust, or rocks relatively little modified from such materials. This material may not have the geochemical signature typical

of upper crustal rocks, such as high K, Si, Rb relative to Sr, and Nd relative to Sm.

The geographic complexity of the isotopic patterns described above, whilst indicating the apparent involvement of such crustal lithosphere do not necessarily indicate "crustal contamination". Similar geographic complexity of isotope variation is not known from elsewhere in the peninsular batholith, although similar detailed studies of individual plutons are well advanced (Silver, Hill, and others, unpublished data). This implies that the boundary between these two different regions of differing Sr_i behaviour (which is approximately coincident with the San Jacinto Fault zone) is a fundamental and long-lived geologic feature, perhaps the extreme south-western limit of the North American craton. This boundary is approximately coincident with the Sr_i = 0.706 contour; however, the important characteristic is believed to be the change in behaviour in the geographic distribution of Sr_i, not in the absolute value of this parameter.

9.6 CONCLUSIONS

1. Rb and Sr concentration, and $^{87}Sr/^{86}Sr$ data have been obtained for igneous rocks from the north-western San Jacinto Mountains. These data confirm the conclusion from earlier more regional scale studies that Sr_i for these rocks varies from approximately 0.7060 to 0.7075 (Evernden and Kistler, 1970; Early and Silver, 1973). Negative covariation of Rb with Sr is similar to that reported from elsewhere in the Peninsular Ranges batholith by Silver and Early (1977).

2. Interaction of the plutonic rocks with metasedimentary country rocks, either by assimilation or via exchange with a hydrothermal

fluid appears to be limited to a narrow marginal zone where there is other evidence (field relations, petrographic features) for the action of such processes. Except for these limited volumes of material, the Rb, Sr and $^{87}Sr/^{86}Sr$ characteristics of the San Jacinto rocks appear to reflect original magmatic properties.

3. Although individual mineral systems appear to have been slightly open to particularly ^{87}Sr movement for some time after crystallization ceased, these data are interpreted as showing that ^{87}Sr leaving one phase (in particular, biotite) was incorporated within another phase (plagioclase). It thus appears that the rock, at the scale of a typical sample (500 gm), has approximated a closed system since crystallization.

4. In general rocks with higher Rb content have lower Sr contents, and vice versa. Rb-Sr covariation is consistent with the pattern described for the whole batholith by Early and Silver (1977). However, the detailed scale of the sampling reported above demonstrates that the batholith-scale variations reported by Silver and Early (1973) can also be found within individual intrusive units. This implies that original source variations in geochemical parameters can be transported considerable distances without efficient homogenization. This in turn implies that the magma collection and transport processes, as well as processes acting within the magma chamber (such as convection) may in combination be incapable of completely homogenizing original heterogeneities within the original liquids. This further suggests that either the length scale of convection, if present, is small relative to the size of the magma chamber (giving a number of individual convective cells), or that the time scale of convection is long compared to the time taken for magma to crystallize. The latter case could include the situation where high

yield strength of the silicate liquid substantially retards or even prohibits convective overturn, or the case of a dynamic magma chamber where new batches of heterogeneous liquid are being intermittently introduced into the crystallizing chamber.

5. Substantial variation in Sr_i exists within each major intrusive unit. These isotopic variations are apparently unrelated to any other petrological or isotopic parameter for which data are available, but are geographically consistent. These data reinforce the conclusions from evaluation of the Rb-Sr data that homogenization processes acting during melt collection, transport and crystallization were incapable of completely homogenizing an originally heterogeneous liquid.

6. The geographic variation of Sr_i within the igneous rocks of the San Jacinto Mountains differs fundamentally from that observed elsewhere in the batholith, suggesting that an important geologic structure separates the two areas. The coincidence of this boundary inferred from Sr_i characteristics of igneous rocks with both the appearance of "anomalous" oxygen isotopic compositions within these rocks, and a major change in the nature of the pre-batholithic metasedimentary rocks lends further support to this inference. The combined geological, petrological and isotopic data appear most simply explained if this boundary is the southwesterly limit of the North American craton.

7. On the Sr_i-$\delta^{18}O$ diagram the bulk of the San Jacinto rocks fall within or just to the low $\delta^{18}O$ side of the main Peninsular Ranges batholith array defined by Silver and Taylor (1978). The entire data set appears to require the involvement of at least three distinct components in the genesis of these rocks. Two of these components are common to the main part of the batholith remote from inferred continental inter-

action, and the geochemical and isotopic requirements of the third [major and trace element chemistry grossly similar to that of the other source component(s), low $\delta^{18}O$, only moderately increased $^{87}Sr/^{86}Sr$ ($\approx$0.708 or slightly higher), no inheritable zircon] are most consistent with old slightly enriched (in Rb relative to Sr) mafic material. These requirements appear to be most simply met by old subcontinental lithosphere. This third component may contribute 25% or more (on an atom basis) of the most effected San Jacinto rocks; however, the bulk of the igneous materials present in the San Jacinto Mountains appear to have been derived from the same source materials as was the bulk of the batholith remote from this inferred "continental" component.

CHAPTER 10

SUMMARY OF DATA FROM THE SAN JACINTO MOUNTAINS AND ADJOINING REGION IMPORTANT IN CONSTRAINING BATHOLITHIC DEVELOPMENT

10.1 INTRODUCTION

Data obtained for the igneous rocks of the San Jacinto Mountains in the present study allow many important constraints to be placed on the genesis of these rocks. These data are even more powerful when considered in terms of the regional framework developed by Silver and his co-workers. It is the purpose of this chapter to briefly summarize the important observations presented above that will be used to develop, first, a model of the processes acting during inflation and crystallization of the exposed magma chambers, and second a model for the origin and evolution of the liquids parental to the studied rocks. The chapter immediately following (Ch. 11) discusses the potential role of magma chamber processes in modifying the composition of liquids from the time they were injected into the various high level chambers until the time they crystallized. The final chapter (Ch. 12) considers chemical and isotopic regularities, the origin of which cannot be simply explained by high-level processes, and develops a model that appears compatible with data obtained in the course of the present study, with the regional-scale observations of L.T. Silver and his co-workers, and with more general constraints on the origin of continental margin generally calc-alkaline igneous rocks.

It is important to remember the unique tectonic setting of the San Jacinto Mountains with respect to the rest of the Peninsular

Ranges batholith. The additional complexities potentially added by the inferred presence of old basement mean that caution should be exercised in extending conclusions drawn from the data obtained in this study to the rest of the batholith, and to calc-alkaline rocks in general.

10.1.1 GEOLOGICAL AND PETROGRAPHIC OBSERVATIONS

1. A large proportion of the area studied is underlain by igneous rocks that appear to have developed within a very restricted interval of time. Abundant compositionally heterogeneous early intrusives are intruded by three large plutons (outcropping over about 1000 km^2) of dominantly tonalitic composition. Field data are interpreted as demonstrating that the second and third of these masses to be emplaced were intruded before the immediately prior body was completely crystalline. Interpretation of zircon U-Pb isotopic data obtained by L.T. Silver extends this near synchroneity of emplacement to the small early intrusives as well. Zircons from five separate intrusive bodies (two small early intrusions, and each of the later major tonalites) are analytically indistinguishable, and imply crystallization of all bodies within a narrow time interval 97 ± 1 m.y. ago.

2. The near synchroneity of emplacement of these intrusive masses implies that an enormous volume of igneous material was added to this portion of the upper crust within a very short time. The available relief allows a minimum thickness of igneous material of 3 km to be measured for one body. Regional and geophysical considerations suggest that as much as one half of the thickness of the crust of this area may have been formed at this time. This suggests that perhaps 2×10^4 km^3 of new material was added to the crust within at most a few million years.

The bulk composition of the exposed part of this material is tonalitic, with a mean composition of approximately 50% (weight) plagioclase (An_{35}), 25% quartz, 15% biotite, 6% K-feldspar, 3% hornblende and 1% titanite.

This implies the availability of a large Ca-, Al- and Si-rich relatively K-poor source.

3. Although almost the entire compositional range of the calc-alkaline rock suite is represented in the area, the vast majority of the exposed igneous rock has a restricted compositional range, from mafic tonalite to K-poor granodiorite.

4. As well as having relatively homogeneous bulk chemistry, the common rock types also show an extemely limited range of mineral composition. Within the major tonalites mean plagioclase composition varies from about An_{40} to An_{30} in rocks ranging in composition from mafic tonalite to K-poor granodiorite. Other minerals show similar restricted compositional ranges. These observations suggest effective buffering of the physico-chemical conditions prevailing throughout crystallization of these large bodies.

5. The large tonalitic plutons contain abundant dark ellipsoidal xenoliths, at least some of which are demonstrably derived from the break-up of synplutonic dikes. A combination of geological, petrological and chemical evidence may be interpreted as showing that the majority of (but not all) xenoliths within these plutons had a similar origin. This implies that 1) liquids were being added to the various magma chambers while they were solidifying, and 2) that the partly crystalline liquids adjacent to the advancing pluton walls had considerable

yield strength, as they were able to fracture in a brittle manner to accommodate dike emplacement.

6. Dispersion of xenoliths away from their inferred source dikes into elongate xenolith trains that commonly parallel the pluton wall implies movement within the liquid parallel to the chamber wall.

7. Schlieren, mineral banding and apparent scour structure and cross-bedding also imply relative movement both between liquid magma and solid wall, and within the magma itself.

8. Except for a restricted zone along the northern margin of Unit III there is little field evidence for more than very minor interaction between silicate liquids and hosting metasedimentary wall rocks. Petrographic changes accompany cases of obvious sediment digestion.

10.1.2 GEOCHEMICAL OBSERVATIONS

9. The restricted range of rock types found for the three large plutons is reflected by their homogeneous chemistry. Although the entire range of SiO_2 contents is from 62.5 to 70.6 wt.%, about two-thirds of the exposed rock has between about 65 and 68 wt.% SiO_2.

10. Analyses of the major tonalites in general show strong covariation of all major elements. As SiO_2 increases, Ti, Al, Fe, Mn, Mg, Ca and P decrease; Na increase slightly with increasing SiO_2, then falls rapidly in the most felsic rocks. K shows considerable scatter, but with an overall trend to increases K at increased SiO_2.

11. Trace element variation is more complex. Sc, V, Cr, Zn, and Ga show apronounced linear decrease with increasing SiO_2. Sr and Zr

decrease slightly with increased SiO_2; Ba, Rb, Pb and Th increase. U, Nb, Y, La, Ce, Nd, Ni and Cu show no systematic correlation with changing SiO_2.

12. Mass balance shows that the bulk of the Sr is contained in plagioclase, and the bulk of the Rb is contained in biotite. Behaviour of these elements during high-level fractional crystallization should thus be controlled by precipitation of these two phases.

13. Rocks collected as probably representing felsic differentiates derived from in-situ fractional crystallization have the geochemical features expected for a system dominated by separation of plagioclase, biotite and quartz, notably relative enrichment in K, Rb, and Ba, and depletion of Sr.

14. There appears to be a dichotomy in geochemical features within these rocks. The more mafic tonalites, somewhat arbitrarily defined as those with $SiO_2 < 65.5$ wt.%, in general show linear interrelationships for most elements. Some of these relationships apparently imply that hornblende was an important phase in the processes producing the liquids from which these rocks formed, although hornblende is not a particularly significant phase in the rocks themselves. This implies that these geochemical characteristics were imposed on the liquids prior to their introduction into the exposed high-level magma chambers.

15. The more felsic rocks, including those analysed as probably representing the products of in-situ fractionation, have geochemical characteristics consistent with their derivation by such processes acting within the crystallizing magma chamber. Rocks of intermediate character

($65.5 < SiO_2 < 69.0$) have geochemical properties intermediate between the more mafic and more felsic rocks. However, there is not a continuous transition from the trace element features of the most mafic rocks to those of the most felsic. Rather, on an element-element diagram an approximately triangular data array commonly results, with the linear trend defined by the mafic tonalites forming the base, the data points for the felsic differentiates defining the apex, and the data points for other samples filling in the triangle thus defined.

16. The overlap of the chemical composition of each unit, and, in particular, the evidence that the most calcic plagioclase crystallizing from each unit had both similar anorthite and Sr content argues strongly that the mean composition of the liquids feeding each large chamber were very similar. Trace element abundances, Ca/(Ca + Na) and Mg/(Mg + Fe) argue against these liquids being in equilibrium with a residual assemblage containing olivine. This appears to rule out direct derivation from anything but highly modified mantle, and implies that the liquids may have undergone extensive modification (most probably by crystal fractionation) since their origin, presumably in the mantle. The REE data suggest that garnet was an important mineral either in the residue during partial fusion or during later crystal fractionation.

17. Rare earth element concentration data provided by L.P. Gromet (personal communication) show strong LREE enrichment relative to chondrites (Ce: 90 to 140 X), moderate enrichment in the MREE (Sm: 25 to 40 X), and only small enrichment in the HREE (Yb: 4 to 7 X). The less precise XRF data show that this behaviour is common to all samples from the major tonalites, and also applies for most of the early intrusives

as well.

These plutons show similar REE fractionation patterns and abundances to other tonalite and low-K granodiorite plutons from the central and eastern Peninsular Ranges batholith ("eastern REE zone" of Gromet, 1979).

18. The Rb-Sr data show geographic variation within individual plutons that mirrors the pattern found for the batholith as a whole by Silver and Early (1977), i.e., at a given Rb content Sr content increases to the northeast. This implies that mixing processes during magma generation, transport, emplacement and crystallization are not completely efficient.

19. Within Unit III, the largest and most complete of the major tonalite plutons, there is concentric zonation of rock types that is reflected by related patterns of element distribution. For instance, SiO_2 and K increase systematically inwards, away from the pluton margins, while elements such as Al, Mg, Fe, Ca and Sr decrease systematically with distance from the pluton margins.

20. Five analysed samples into which digestion of metasedimentary wall rocks has been relatively important show anomalously low Mg/(Mg + Fe) and Ti, high Ba, Zr and REE, and highly variable Al when compared to other analysed samples. These features are compatible with incorporation of the exposed metasedimentary host rocks, which tend to have REE and Zr, but suggest that processes other than simple mixing accompany sediment incorporation. The features listed above are not seen in any rocks for which there is no a priori evidence for sediment

incorporation.

10.1.3 ISOTOPIC DATA

21. The majority of analysed samples show a very restricted range of primary magmatic $\delta^{18}O$ values of from +10.0 to +10.4. The total range of primary $\delta^{18}O$ values observed for the common rock types (tonalites and low-K granodiorites) is much larger, from +9.0 to +10.6. A single sample of olivine gabbro has $\delta^{18}O$ = +7.8 per mil.

22. Primary $\delta^{18}O$ correlates negatively with Colour Index. Model calculations suggest that isotopic fractionation accompanying crystal fractionation involving the observed mineral proportions cannot explain this phenomenon, but crystallization of different proportions of phases from an isotopically homogeneous reservoir can. This latter process can account for an increase in $\delta^{18}O$ of 0.5 per mil as Colour Index falls from 25 to 10, in good agreement with the observed correlation.

23. The much larger total variation in primary $\delta^{18}O$ values of from +9.0 to +10.6 cannot be explained by such processes, and appear to reflect intial heterogeneity within liquids added to the magma chamber. The whole body of oxygen data thus implies that processes acting within the magma chamber were substantially able to homogenize initially quite heterogeneous liquids.

24. Because of a considerable contrast between the oxygen isotopic composition of the silicate liquids and their wall rocks, the oxygen isotope system is quite sensitive to the effects of interaction with these wall rocks. Except in cases where there is either field or petrographic evidence for such interaction, either by assimilation of

wall-rock or by exchange with a hydrothermal fluid, oxygen isotope effects attributable to such interaction is very minor.

25. The only large reservoir of oxygen recognized to date that has such high $\delta^{18}O$ values is that of rocks that have been affected by processes at or near the Earth's surface. These include sedimentary rocks, and the hydrothermally altered upper parts of the oceanic crust. The oxygen isotope data strongly implicate such materials as being important in the origin of the San Jacinto rocks.

26. A substantial variation in Sr_i (from 0.7057 to 0.7076) has been documented within the igneous rocks of the San Jacinto Mountains. Each of the large tonalite plutons shows much of this total observed range. Variation within each pluton appears geographically regular, though with a complex pattern of Sr_i distribution. This marked heterogeneity of Sr_i within individual plutons implies that processes acting within the inflating and crystallizing plutons were not capable of efficiently homogenize initial liquid variability. In a very general sense the pattern of Sr_i variation within the major tonalites reflects the regional gradient in Sr_i defined for the San Jacinto Mountains by the small early intrusives, and for the batholith by Early and Silver (1973).

This observation is in apparent contradiction of the interpretation from oxygen isotope data above that processes acting within the magma chamber <u>are</u> able to homogenize initially heterogeneous liquids, at least for this component.

27. Although the pattern of geographic distribution of Sr_i differs from the early intrusives to the late tonalites there is consid-

erable coherence in the data from both groups of rocks. The ranges of Sr_i overlap considerably, although it is difficult to tell to what extent processes within the magma chambers have diminished possibly larger original variation.

28. U-Pb isotopic data from zircons obtained from both minor early intrusives and the major tonalites obtained by L.T. Silver are interpreted as showing an almost complete absence of older inherited zircon within these rocks (L.T. Silver, personal communication).

10.1.4 REGIONAL CONSIDERATIONS

29. The apparent continuation of the batholithic pattern for the geographic variation of Sr_i into the early intrusives implies that the dominant source materials for the main Peninsular Ranges batholith and for the early San Jacinto Mountains intrusives are held in common.

30. The evidence for systematic south-west to north-east variation in Rb/Sr behaviour in Units I and III that parallels the behaviour shown for the rest of the batholith by Silver and Early (1977) implies that not only did the bulk source regions (for the main batholith and the San Jacinto rocks) have grossly similar chemistries, but probably similar mineralogy as well.

31. The relative lack of fractionation of REE between the two rocks for which data are available (L.P. Gromet, written communication, 1983) argue strongly for development of the distinctive REE patterns prior to injection of the liquids into upper crustal magma chambers. Gromet and Silver (1983) reached similar conclusions from considerations of REE fractionation between co-existing mineral phases in a granodiorite, and

from consideration of batholith-scale features of REE fractionation and mineral abundances.

32. The similarity of REE patterns for tonalites and low-K granodiorites from the main batholith and from the San Jacinto Mountains also implies similarities in both gross source composition and source mineralogy between the two areas (Gromet, 1979; L.P. Gromet, personal communication, 1983).

33. The close correspondence of major and trace element rock chemistry between rocks from the San Jacinto Mountains and rocks elsewhere in the batholith (Silver and Chappell, unpublished data) also argues for the operation of similar processes in both areas, although the isotopic data summarized above imply some differences in source compositions.

34. When compared to data obtained for the main part of the batholith to the south, the rocks from the San Jacinto Mountains show anomalous Sr_i-$\delta^{18}O$ relations. In particular, $\delta^{18}O$ at a given value of Sr_i is low by as much as 3.5 per mil when compared to the main batholith trend of Taylor and Silver (1978). Alternately, the San Jacinto rocks could be considered to have anomalously high Sr_i for a given value of $\delta^{18}O$. Consideration of the somewhat limited data available suggest that the anomalous component being added is mafic, has low $\delta^{18}O$, and slightly increased Sr_i. Slightly enriched old sub-continental lithosphere appears to satisfy the various geochemical and isotopic constraints. If this model is correct, it implies that as much as 25% (atom basis) of some of the San Jacinto rocks might be derived from such a source. However, the bulk of the igneous materials appear to have been derived from source materials similar to those generating the bulk of the batholith.

35. The appearance of complex geographic variation in Sr_i approximately coincides with the present-day position of the San Jacinto fault, and with the appearance of anomalous Sr_i-$\delta^{18}O$ behaviour in the plutonic rocks.

36. The metasedimentary sequences that crop out over much of the San Jacinto Mountains are of fundamentally different character from those described elsewhere in the batholith. They are much more quartz-rich, and apparently represent the metamorphosed remnants of a mature continental sequence.

37. Rb, Sr, and Sr isotopic data from the quartz-rich metasedimentary sequences of the San Jacinto Mountains allow differentiation from metasedimentary rocks elsewhere in the batholith on the basis of isotopic properties alone. In addition, they have lower $\delta^{18}O$ values than those reported for the bulk of the metasedimentary materials that crop out further to the west. The Sr isotopic data are most simply interpreted as indicating that these quartz-rich sequences are substantially older than is the Mesozoic graywacke-slate association exposed elsewhere in the batholith, perhaps as old as early Paleozoic or latest Precambrian.

The boundary between the two contrasting metasedimentary sequences coincides with other features indicative of an important boundary between the San Jacinto Mountain segment of the batholith, and the main mass of the batholith to the south and southwest. These other features are: the appearance of considerable complexity in the pattern of geographic variation of Sr_i, and anomalous Sr_i-$\delta^{18}O$ relations make an appearance in the San Jacinto Mountain rocks. These latter features apparently reflect a more complex source region for these rocks; if the

mature, apparently old, quartz-rich metasedimentary sequences of this area were deposited on stable continental crust, the combined data could be interpreted as indicating the southwestern margin of this old crustal material. This boundary is approximately coincident with the position of the Neogene San Jacinto fault.

CHAPTER 11

MAGMA CHAMBER PROCESSES

11.1 INTRODUCTION

The detailed re-examination of crystallization and solidification within the Skaergaard Intrusion in light of advances in the understanding of rheological and physical properties of magmas (McBirney and Noyes, 1979) has stimulated much interest in studies aimed at elucidating the dynamics of active magma chambers. McBirney and Noyes (1979, p.487) conclude that "solidification of large slowly cooled intrusions is a complex process entailing progressive changes of rheological properties as the crystallizing magma passes through successive stages between a viscous Newtonian fluid and a brittle solid rock." The prominent mineralogical layering of this classic intrusion is suggested by them to result from a double-diffusive process induced by the different rates of thermal and chemical diffusion during cooling. It is also suggested that double-diffusive systems operating in the gravitational field may lead to stratification of the cooling magma chamber, in a manner analogous to that demonstrated for salt solutions by Turner and Chen (1974).

Turner (1980) and McBirney (1980) have since modelled the expected situation for a calc-alkaline magma chamber, where residual liquids are less dense because of precipitation of more dense early crystallizing phases. This leads to a situation where a less dense cap overlies a more dense mass of liquid, and double-diffusive induced stratification may indeed follow.

A further complicating factor, the rate at which the magma chamber is filled, has been considered explicitly by Huppert and Sparks (1980a,b) and Huppert and Turner (1981, 1982), and, from a quite different viewpoint, by O'Hara (1977, 1980) and O'Hara and Mathews (1981). It is unlikely that a large magma chamber, such as those exposed in the San Jacinto Mountains, fills instantaneously, but rather must be filled over some considerable length of time. It is difficult to estimate at what rate these reservoirs were filled. Magma transport into the Kilaeau shield volcano is estimated to average 0.1 km^3yr^{-1} (Swanson, 1972); at this rate, it would take on the order of 10^4 years to fill the magma chamber for Unit III. Magma transport rates for the San Jacinto system might be considerably less. It appears unlikely that any plumbing system through which the growing magma chamber is fed would remain open for this length of time, but rather upward movement of liquid would be expected to be episodic as feeder dykes or conduits open and close in response to magmatic and lithostatic stresses. Periodic injection of liquid into the base of a cooling magma chamber can lead to a double diffusive situation (e.g., Huppert and Sparks, 1980b), and, depending on the rheological properties of the pre-existing liquids, may or may not initiate overturn of a large part of the system.

The efficiency of these various possible physical processes will, in turn, affect chemical processes within the crystallizing magma chamber. Element partitioning may be controlled by kinetic factors such as crystal growth rate and chemical diffusion rates, rather than by an "equilibrium" process (although surface equilibrium is attained). The amount of fractionation of any residual liquids will depend on the efficiency of separation of the liquid from crystallizing phases. Both hori-

zontal stratification and periodic replenishment could serve to isolate volumes of magma from each other, thus enabling initial variations in either geochemical or isotopic properties to be preserved in the solidified rock.

The data presented above for the rocks of the San Jacinto Mountains enable limitations to be placed on the importance of some of these possible processes. In particular, the Rb-Sr and Sr isotopic data demonstrate that each magma chamber did not act as a single, closed, rapidly convecting volume of silicate liquid, but rather as a number of more or less isolated volumes of material. This apparent isolation of one part of a crystallizing pluton from other parts of the same body could be in time as well as in space. The field data are interpreted as indicating that each magma chamber was filled by a large number of inputs of silicate liquids having a wide compositional range. The chemical and oxygen isotope homogeneity of the three major tonalite units argues, in apparent contradiction of the Rb-Sr and Sr isotope data, for relatively efficient homogenization of these various batches of liquid. The consistence of mineral chemistry throughout the three major plutons argues for consistency in physico-chemical conditions during crystallization; the plagioclase data in particular appear to require remarkable uniformity and stability in both the temperature and the partial pressure of water within the crystallizing liquids.

It is the purpose of this chapter to use the available chemical and physical data, both from this study and from the literature, to attempt to deduce the processes taking place within the San Jacinto magma chambers. A model for the origin of the chemical variations within

the three major tonalites is then developed, and although no single piece of data can be used to prove that this model is correct, it appears consistent with both all of the observations presented in the preceding chapters, and with the deductions as to likely magma chamber processes.

11.2 RHEOLOGICAL AND PHYSICAL PROPERTIES OF CRUSTAL MAGMA CHAMBERS

Density

The density of the melt equivalents of three rocks has been calculated using the partial molar volume data of Nelson and Carmichael (1979) and assuming 1) a temperature of 1000°C, 2) that the analyses represent liquid compositions at this temperature, 3) that all iron is present as FeO, and 3) that all samples contained 3.0 wt.% (10 mole %) water. The partial molar volume of water at 3.5 kb and 1000°C was calculated following Burnham et al., 1969. The liquid densities thus calculated are presented in Table 11.1, and agree favourably with experimentally determined densities of water-rich silicate liquids (e.g., Kushiro, 1978). These samples (a mafic xenolith, a mafic tonalite and a low-K granodiorite) encompass almost the entire compositional range of the major tonalites and their inferred more mafic "parental" liquids. As such, they encompass the entire range of physical properties of the liquids that may have been present in the magma chamber at some time during its evolution. The probable density differences between different composition liquids within the San Jacinto systems are small (≈0.1 gm cm^{-3}). Even the density of the liquids represented by the mafic xenoliths are not too different from that of their hosts. All these liquids would be capable of rising through the crust by buoyancy forces alone.

TABLE 11.1

CALCULATION OF LIQUID DENSITIES

COMPOSITIONS USED

	LTS 379	LTS 147	LTS 322	Crater Lake Andesite(1)
SiO_2	56.69	62.54	68.70	58.12
TiO_2	1.44	0.94	0.48	0.71
Al_2O_3	16.45	16.57	14.92	17.50
FeO(2)	7.12	4.41	2.28	5.16
MgO	3.11	1.72	0.79	3.63
CaO	6.76	5.21	3.28	6.31
Na_2O	3.74	3.79	3.55	4.13
K_2O	1.68	1.84	3.00	1.44
H_2O	3.00	3.00	3.00	3.00
CALCULATED DENSITY OF LIQUID AT 1000°C AND 3.5 KB(3)				
gm cm^{-3}	2.43	2.35	2.27	

(1) Composition of material studied by Kushiro *et al.*, 1976, recalculated on the basis of 3.0 wt.% H_2O

(2) Total iron as FeO. Also includes small amount of MnO, which is assumed to have comparable density and partial molar volume to FeO.

(3) Partial molar volume data from Nelson and Carmichael (1979); partial molar volume for water calculated from P,T relations of Burnham *et al.*, 1969. Calculated partial molar volumes (in cm^{-3}): SiO_2 (27.36); TiO_2 (20.20); Al_2O_3 (34.08); FeO (11.58); MgO (11.32); CaO (13.60); Na_2O (25.77); K_2O (40.75); H_2O (21.12) derived using the relationships:

$$\overline{V} = \overline{V}_o \exp\left[a(T-T_o) + \frac{b}{2}(T^2 - T_o^2)\right]$$

and

$$\alpha = \frac{1}{\overline{V}}\frac{(d\overline{V})}{(dT)} = a + bT, \quad T \text{ in Kelvins}$$

Viscosity

It is much more difficult to estimate other relevant physical and rheological properties of these rocks. Gill (1981) summarizes the available information on the viscosity of andesitic liquids. Experimentally determined near liquidus viscosities are of order 10^2 to 10^4 poise, depending on water content and confining pressure. Figure 11.1 shows the experimentally determined effect of temperature on the viscosity of andesite liquid. Kushiro (1978) shows that the addition of 3 wt.% water decreases viscosity by about two orders of magnitude. The liquids into the San Jacinto chambers probably had viscosities of order 10^3–10^5 poise, with the viscosity of liquid within each chamber increasing rapidly as crystallization progressed.

Yield Strength

McBirney and Noyes (1979) consider some of the implications of the presence of a finite yield strength within a magma. They also present experimental data on the yield strength of three silicate liquids, including one of andesitic composition. The effect of water on yield strength has not been studied, but increased water would probably tend to reduce yield strength. Figure 11.2 illustrates some of the effects of a finite yield strength. For gravitational separation the gravitational force acting on a crystal must exceed the yield strength of the liquid. For example, if the liquid has a yield strength of 100 dyne cm^{-2} and the density of LTS 147 (Table 11.1), then a hornblende crystal must grow to 6mm diameter before gravitational separation can begin. Similarly, a plagioclase crystal must be 20mm in diameter before it will begin to sink. Both experimental (McBirney and Noyes, 1979) and field (Shaw *et*

Viscosity of orogenic andesite magma. *Solid dots* are for an anhydrous melt at 1 atm for which the plagioclase liquidus and pyroxene-in temperatures are shown (Murase and McBirney 1973). The slope at $T < 1100°C$ yields 75 kcal for E_η. Data from Kushiro et al. (1976) and Kushiro (1978) are shown by *open symbols*, with pressure indicated. *Cross* is from Scarfe (1973)

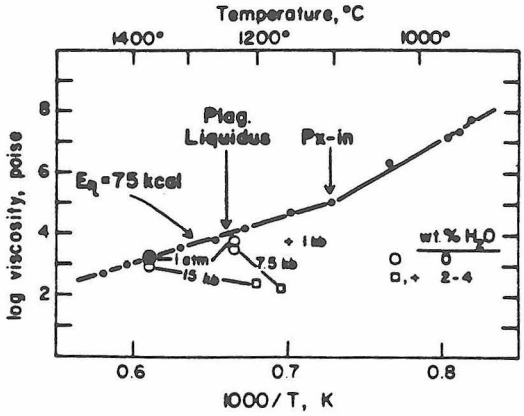

Figure 11.1. Viscosity of orogenic andesite magma as a function of temperature. From Gill (1981).

Figure 11.2. Relationship of particle radius, density contrast ($\Delta\rho$) relative to the value calculated for LTS 147 (2.35 gm cm^{-3}, Table 11.1), and yield strength. Diagonal lines give yield strength in dynes cm^{-2}. Field of probable lower limit to yield strength in naturally occurring silicate liquids is from Shaw et al., (1968) and McBirney and Noyes (1979); field of yield strength of multiply saturated andesite liquid is from McBirney and Noyes (1979). Probable ranges of density of minerals observed in the San Jacinto rocks are shown along the upper margin of the figure, along with estimated density contrasts for different composition silicate liquids and solid xenoliths.

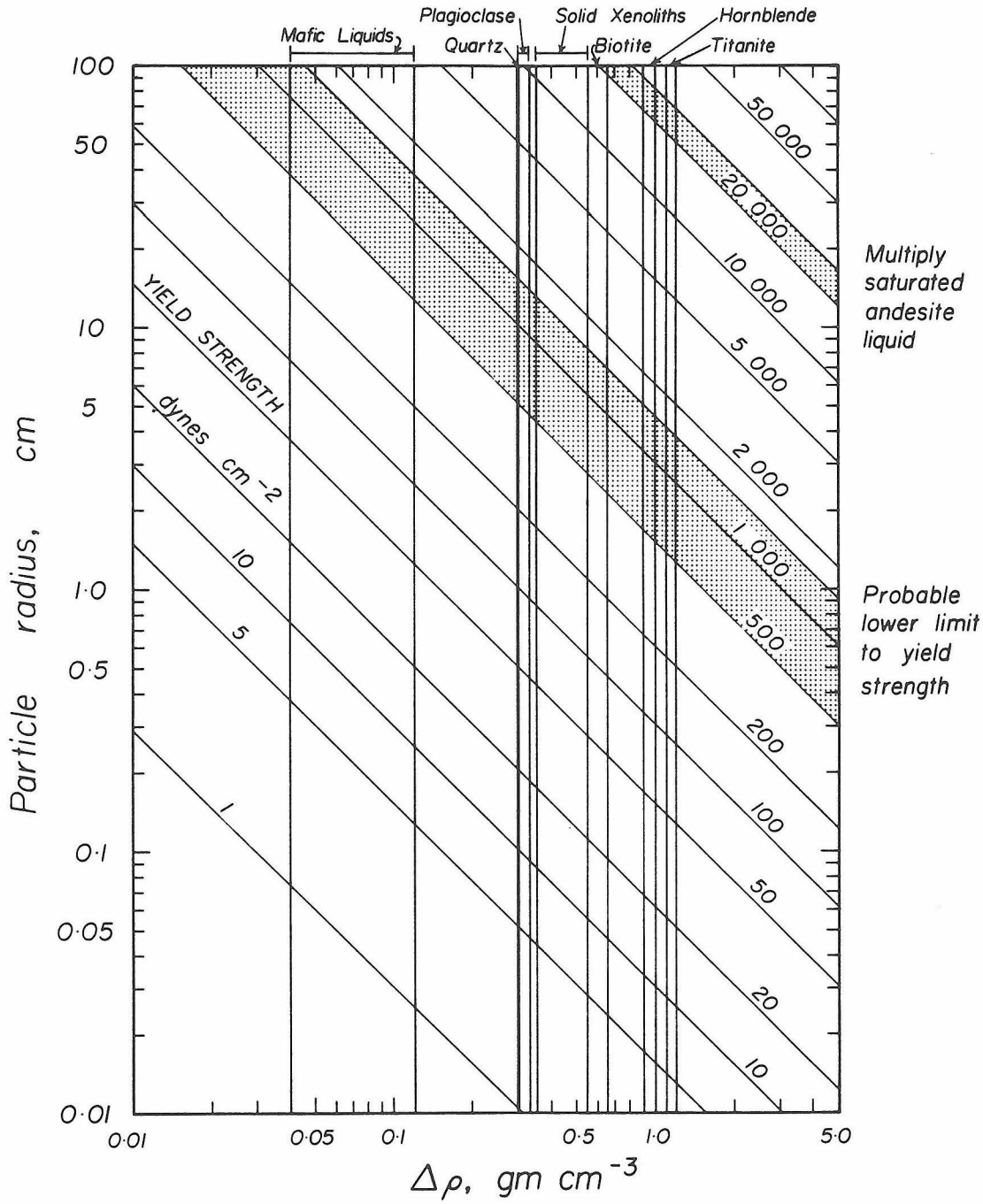
Mafic Liquids
Plagioclase
Quartz
Solid Xenoliths
Biotite
Hornblende
Titanite
100
50
10
5
1·0
0·5
0·1
0·05
0·01
Particle radius, cm
YIELD STRENGTH
dynes cm⁻²
50 000
20 000
10 000
5 000
2 000
1 000
500
200
100
50
20
10
10
5
1
Multiply saturated andesite liquid
Probable lower limit to yield strength
0·01
0·05
0·1
0·5
1·0
5·0
Δρ, gm cm⁻³

Figure 11.2

al., 1968) observations indicate that relatively anhydrous silicate liquid has a yield strength of ≈500-1500 dyne cm^{-2} at and just below its liquidus. Multiple saturation with crystallizing phases leads to rapid increase in yield strength to values of ≈25000 dynes cm^{-2} (McBirney and Noyes 1979). If these data are relevant to the San Jacinto system, they imply that 1) plagioclase is unlikely to separate gravitationally at any stage of the evolution of these bodies, 2) large crystals of mafic minerals [hornblende, biotite, titanite] may separate early in the crystallization process, and 3) after crystallization has proceeded to the point of multiple saturation even large (meter diameter) xenoliths will not be able to separate gravitationally from a stagnant liquid. Even lowering the yield strength by an order of magnitude or more would not greatly alter these conclusions. The relatively SiO_2-rich San Jacinto rocks (and inferred liquids) are likely to have greater, not lesser yield strength, making gravitational settling within the magma chamber even more unlikely. It appears that once material has reached the level of the exposed magma chamber flow differentiation (e.g., Bhattacharji and Smith, 1964) will be far more efficient at separating or concentrating phases than will gravity.

Rheological Considerations

Uncertainties in the values of several relevant parameters, notably viscosity, make rigorous evaluation of the rheological conditions pertaining during filling and solidification of the San Jacinto magma chambers impossible. The Rayleigh number, a dimensionless function, can be used to compare the relative stability of different systems with superimposed density gradients.

The Rayleigh number based on temperature is given by

$$Ra = \frac{\alpha \rho g \Delta T h^3}{\eta \kappa}$$

where ΔT is the temperature difference between the roof and floor of a magma chamber of thickness h, α is the coefficient of thermal expansion ($\approx 5 \times 10^{-5}$ deg^{-1}), κ is the thermal diffusivity (about 5×10^{-3} cm^{2}sec^{-1}), η the viscosity (in poises), and ρ and g are density and acceleration due to gravity, respectively. For the case under consideration h is large (10^5 cm or greater) and dominates the relationship; Ra is of order 10^{10} or greater.

Ra specifically considers the effects of density-driven instability related to the effects of an imposed thermal gradient. A superimposed chemical gradient may also produce a density gradient within a body of fluid. The effect of this may be to either stabilise or to destabilise a system with a concurrent temperature-induced density gradient, depending on the particular case. A Rayleigh number based on density difference can be defined (Richter and McKenzie, 1981)

$$R\rho = \frac{g\rho.(\Delta\rho/\rho).h^3}{\eta \kappa}$$

where $\Delta\rho$ is the (compositionally induced) density contrast over distance h, and ρ is the mean density of the system.

The ratio $Ra/R\rho$ [$= \alpha\Delta T(\rho/\Delta\rho)$] thus gives an indication of the relative importance of temperature versus chemically induced density gradients. Richter and Johnson (1974) suggest that if $Ra > \approx 10^4$ then the system will convect regardless of the value of $R\rho$. If (for $Ra > 10^4$) $R\rho > Ra$, then the system is likely to be broken into a series of layers with convection taking place <u>within</u> each layer; if $Ra > R\rho$, then the whole

system (of thickness h) will convect (Richter and McKenzie, 1981). Note that the ratio Ra/Rρ is independent of both h (magma chamber height) and η (liquid viscosity).

The consistency of mineral compositions throughout the crystallization history of the San Jacinto liquids suggests that there were not large long-lived temperature gradients within the magma chambers. The consistency of rock compositions imply that possible density contrasts within the liquid were also small. For $\Delta\rho = 0.025$ gm/cm^3, then a value of ΔT of $> 200^oC$ is needed or convection will be confined to thin layers of individual thickness $< h$. If $\Delta\rho = 0.1$ gm/cm^3, the value of ΔT needed before such a layered system will break up increases to 800^oC.

These considerations imply that the liquids within the San Jacinto magma chambers were probably convecting throughout much of their histories. The work of Richter and McKenzie (1981) is suggestive that this convective scheme may have been broken into a series of layers of considerable horizontal but limited vertical dimensions.

Rapidly increasing yield strength within a multiply-saturated crystal-rich magma may tend to damp out convective behaviour as crystallization procedes. Viscosity of the magma will also increase as crystallization procedes, but would need to increase to some 10^{10}–10^{11} poises before this factor alone would inhibit convection within a magma chamber of considerable vertical dimensions (1km or more) and with even a small superimposed temperature gradient (10^oC).

Any convective pattern is likely to have been influenced by the shapes of the magma chambers. In Unit III, in particular, the thin "wings" of the chamber edges would probably be quite effective in isolating

less than whole pluton scale convective cells from each other, even within a rapidly overturning system.

It appears likely that the yield strength of the liquid throughout crystallization would have been sufficient to suppress gravitational separation of all but the largest xenolithic blocks (>1 m diameter). The presence of a liquid with substantial yield strength could also affect the convective pattern operating in ways that cannot be evaluated with the available information. The presence of some convection is believed to be indicated by the ubiquitous schlieren, by apparent scour structures in the more marginal rocks of all major tonalite units, and by the dispersion of xenoliths away from their apparent source dykes. The presence of a liquid with finite yield strength is indicated by relations of the synplutonic dykes, which appear to have been emplaced into fractures within the crystallizing magma, but were then able to be deformed along with the enclosing magma. This suggests that under certain conditions of imposed stress the magma could behave in a brittle fashion, but under other conditions behaved more plastically, implying the presence of considerable yield strength.

11.3 PHYSICO-CHEMICAL CONSIDERATIONS

Possible kinetic control of trace element partitioning

The growth of a crystal from a melt is the net result of several processes. At the transport rates characteristic of cation diffusion in silicate liquids it is possible that the transfer of reactants or products to or from the crystal/liquid interface may be a significant factor in the rate of growth of a crystallizing phase. Similarly,

the incorporation into or exclusion of impurities from a growing crystal may be controlled by kinetic processes rather than equilibrium chemical processes. The incorporation of an impurity into a crystal can be characterized by a distribution coefficient, K. At equilibrium

$$K = \frac{C_s}{C_l}$$

where K = equilibrium distribution coefficient (for a particular element)

C_s = concentration of element in solid

C_l = concentration of element in liquid

The common occurrence of zoning in crystals suggests that equilibrium occurs only at the liquid/crystal interface, and the distribution coefficient is then given by

$$K(t) = \frac{C_s\ (0,t)}{C_l\ (0,t)}$$

where $C_i(0,t)$ refers to the concentration of the element in phase i at time t and distance x = 0 from the liquid/crystal interface. If $C_l(0,t) \neq C_l(\infty,t)$ the distribution coefficient, although an equilibrium parameter controlled by processes acting <u>at</u> the crystal/liquid interface cannot be simply used to calculate the history of a batch of magma.

Albarede and Bottinga (1972) show that the <u>apparent</u> distribution coefficient (K^A) measured (or used) with respect to the liquid some distance from the liquid/crystal interface is given by:

$$K^A(t) = \frac{\frac{1}{t}\int_0^t K(t).C_l(0,t')\,dt'}{\frac{1}{H}\int_0^H C_l(x,t)\,dx}$$

H is equal to half the mean distance between the centers of the crystals. Although this work was directed to the problem of the measurement of distribution coefficients using either natural or experimental systems, their treatment is also valid in the application of experimentally determined distribution coefficients (equilibrium or otherwise) to modelling natural systems. Their treatment was limited at the time by the paucity of data available on transport properties, specifically cation diffusivity and crystal growth rates in silicate liquids. Such data are now available, and their effects on K^A can be at least qualitatively evaluated.

Allegre and Minster (1978), following Burton et al., (1953) show that such transport-controlled processes are capable of controlling the trace element behaviour of a crystallizing silicate liquid. Burton et al., (1953) suggest that the distribution of an element may be described by an effective distribution coefficient, K^*, where

$$K^* = \frac{K}{K + (1 - K)\exp(- V\delta /D)}$$

and K = equilibrium distribution coefficient

V = crystal growth rate

D = diffusivity

δ = length scale parameter

δ is defined as the distance from the growing interface beyond which the concentration is uniformly $C_l(\infty,t)$. This uniformity can be the result of flow within the fluid [the case considered explicitly by Burton et al., 1953], or by other processes. Figure 11.3 illustrates diagramatically the dependence of K^* on the function $V\delta/D$. For the simple case presented, where $K = 4.0$, K^* falls from 4 (= K) to 1 over a variation of

Figure 11.3. Variation of apparent distribution coefficient (K*) with the function $V\delta/D$.

V = crystal growth rate (cm sec^{-1})

δ = length scale (distance from crystal/liquid interface at which concentration of element under consideration → concentration at infinite distance.

D = chemical diffusivity (cm^2 sec^{-1})

K = 4.0 is assumed

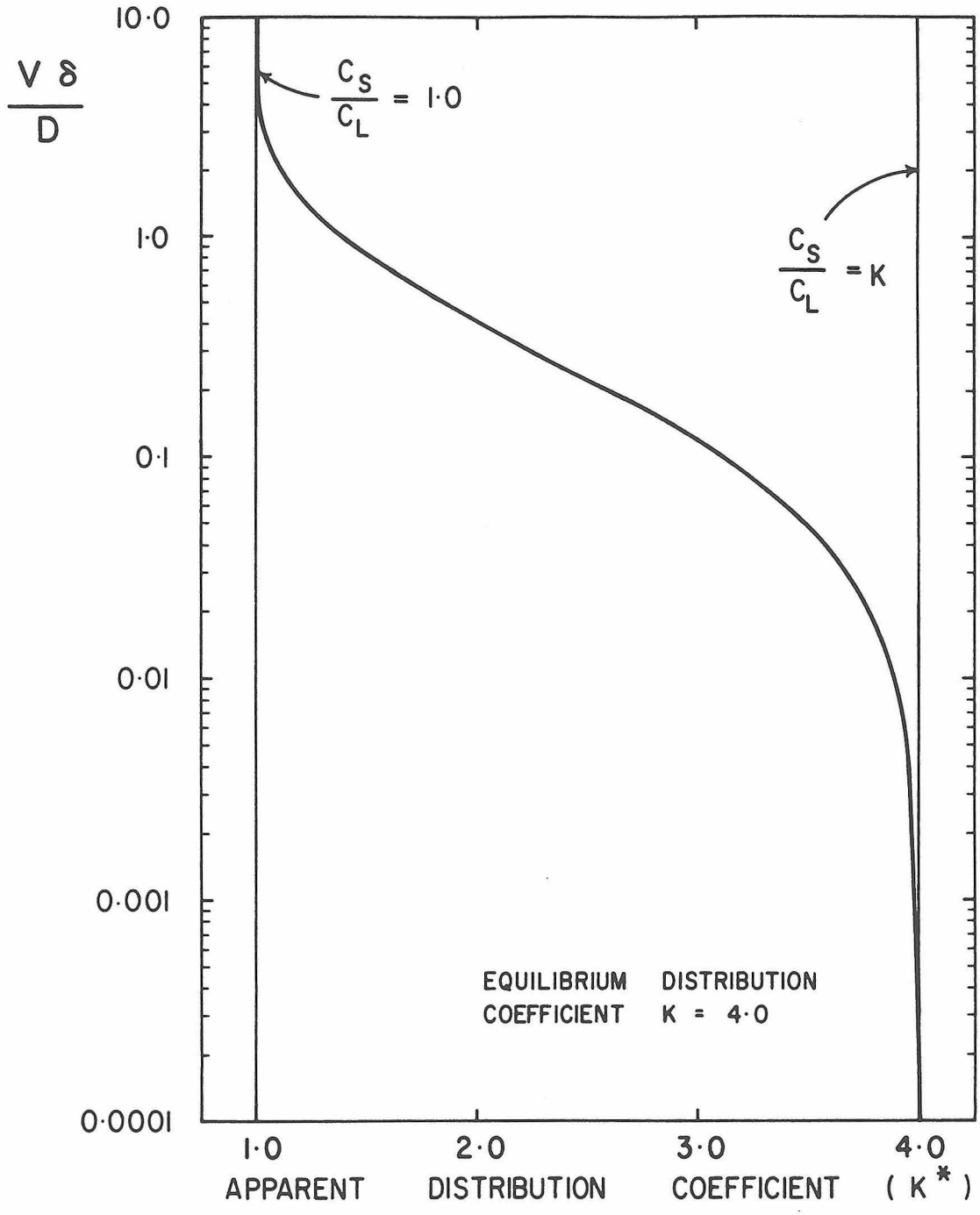
10·0
1·0
0·1
0·01
0·001
0·0001
V δ / D
Cs/CL = 1·0
Cs/CL = K
EQUILIBRIUM DISTRIBUTION COEFFICIENT K = 4·0
1·0
2·0
3·0
4·0
APPARENT DISTRIBUTION COEFFICIENT (K*)

Figure 11.3

less than three orders of magnitude in $V\delta/D$. Clearly, given the appropriate appropriate balance of these three parameters (crystal growth rate, length scale, and diffusivity) K^* can differ significantly from the "equilibrium" result where kinetic effects are insignificant.

Allegre and Minster (1978) consider the example of a plagioclase crystal growing in a basalt, and derive a value of about 1cm for δ [for the concentration of the element to be 90% of $C_l(\infty,t)$]. Here δ is a function of V, the crystal growth rate and D, the diffusivity. Equation 8 of Albarede and Bottinga (1972) can be used to approximate δ for the case where chemical transport due to fluid movement processes is slow compared to diffusion and crystal growth rates:

$$C_l(x,t) = C_l(\ ,t)\left[1 + \frac{1-K}{K}\exp\left(-\frac{V}{D}x\right)\right]$$

For the example considered by Allegre and Minster, $K^{*Sr}_{plag} = 1.5$, compared to $K^{Sr}_{plag} = 2.0$, a significant difference.

For the system under consideration in this study, the tonalitic plutons of the San Jacinto Mountains it is possible to use the geological, petrological and geochronological data available to consider the role of kinetic disequilibrium in some detail. To do this we need to be able to evaluate or make reasonable approximations for the crystallization rate, V; the diffusion coefficient for element i in the liquid, D^i; and the equilibrium distribution coefficient for element i and phase j, that is, K^i_j.

Crystallization rate

Several different approaches can be used to estimate limits for the crystallization rate pertinent to the San Jacinto system. Each gives a different result.

If crystallization largely proceeded inwards from the walls of the magma chamber, as appears to be the case, it is possible to use the geochronological data to obtain an estimate of the crystallization rate for this system. This method in effect assumes that a single crystal face was growing at any one time, and so gives a maximum value for V, the crystallization rate. The zircon U-Pb data are interpreted as indicating that the entire igneous construct was emplaced and crystallized within 2×10^6 years. Unit III may have crystallized over a maximum time interval of about 10^6 years. A reasonable estimate of the crystallization interval for Unit III is thus perhaps 10^5 to 10^6 years, giving, for a length scale of 10 km, crystallization rates of 3×10^{-8} to 3×10^{-7} cm yr^{-1} (Table 11.2).

Table 11.2. Estimates of Crystallization Rate for San Jacinto Unit III*

Crystallization Interval (years)	Crystallization Rate (V) (cm sec^{-1})
10^5	3×10^{-7}
10^6	3×10^{-8}

*for a length scale of 10 km

At the other extreme, all crystals within each chamber could have crystallized simultaneously. If the average grainsize is 3mm, a pluton 20 km across that cools in 10^5-10^6 years implies crystallization rates of order 10^{-13}-10^{-14} cm sec^{-1}.

Figure 11.4. Interrelationship of chemical diffusivity (D), apparent distribution coefficient and the function $V\delta/D$. 'Isotherms' calculated from the Arrhenius relationship and the data of Jambon (1982) for Sr (solid horizontal lines) and Rb (dashed horizontal lines). Limits of fields labelled "Sr" and "Rb" calculated using

$$C_l(x,t) = C_l(\infty,t)\left\{1 + \frac{1 - K}{K} \exp\left(-\frac{V}{D}x\right)\right\}$$

from Albarede and Bottinga (1972), the values of V listed in Table 11.2, and D estimated from the data of Jambon (1982). $C_l(x,t)$ is assumed to be 90% of $C_i(\ ,t)$, and the relationship solved for x (i.e., δ).

For further discussion, see text.

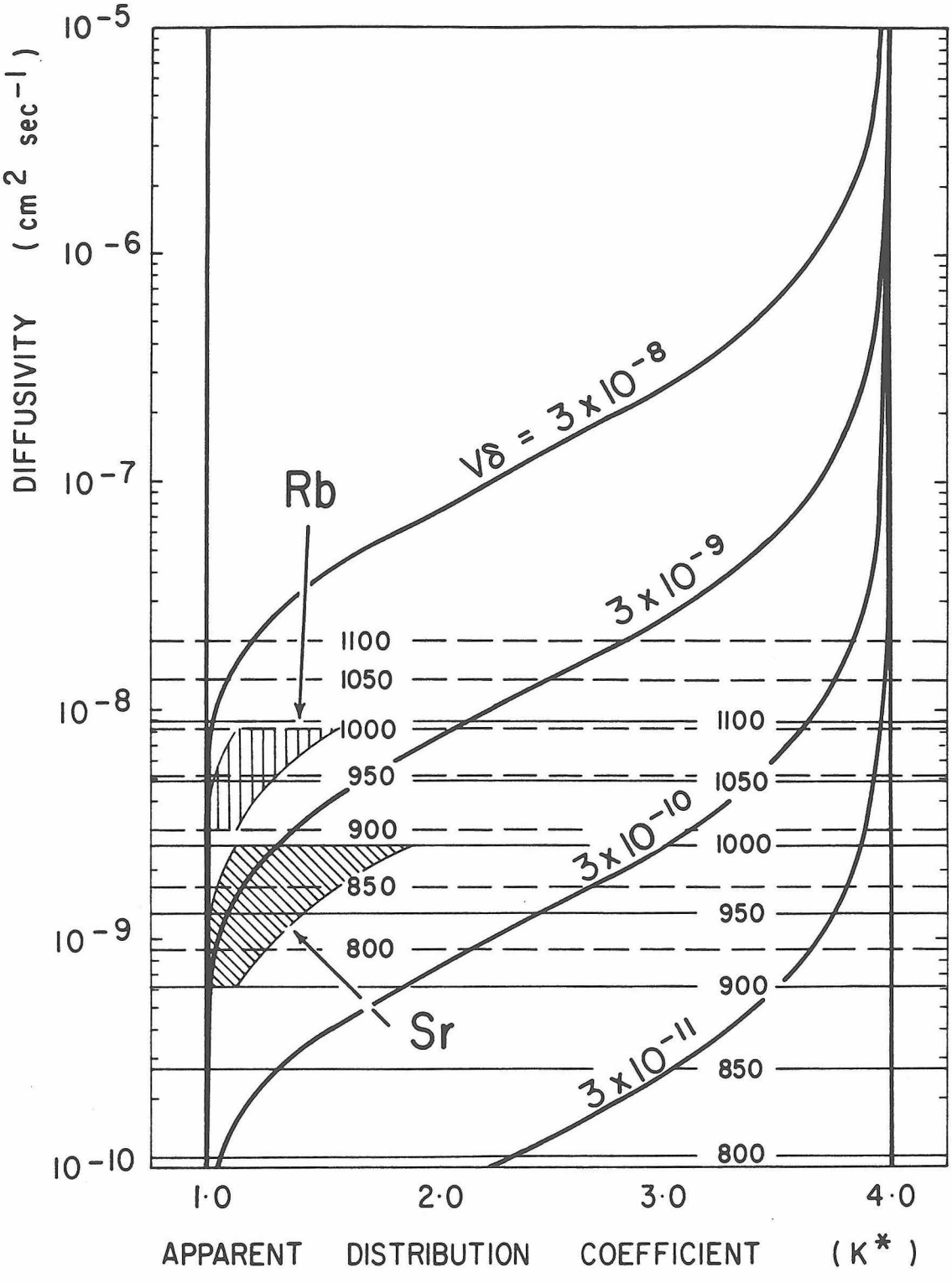
DIFFUSIVITY (cm² sec⁻¹)
10⁻⁵
10⁻⁶
10⁻⁷
10⁻⁸
10⁻⁹
10⁻¹⁰
Vδ = 3x10⁻⁸
3x10⁻⁹
3x10⁻¹⁰
3x10⁻¹¹
Rb
Sr
1100
1050
1000
950
900
850
800
1·0
2·0
3·0
4·0
APPARENT DISTRIBUTION COEFFICIENT (K*)

Figure 11.4

Experimental (e.g., Swanson, 1977) and model (e.g., Loomis, 1982) results suggest that crystallization rates for plagioclase in calc-alkaline plutons are of order 10^{-7}-10^{-8} cm sec^{-1} or less.

Diffusivity

Jambon (1982) presents details of tracer diffusion experiments for a number of elements in granitic (rhyolite obsidian) melts, adding to earlier work of Carron (1968) and Magaritz and Hofmann (1978a,b). He presents results for Na, K, Rb, Cs, Ca, Sr, Ba, Ce and Eu in the familiar Arrhenius form $D = D_o \exp(-E/RT)$, enabling the calculation of the diffusivity for these elements over a wide range of temperatures.

Experimental data on liquids of tonalitic composition (e.g., Wyllie, 1979) can be used to estimate magma temperatures of perhaps 900 to 1000 °C, giving probable diffusivities of 6×10^{-10} to 3×10^{-9} cm^2 sec^{-1} for Sr and 3×10^{-9} to 8×10^{-9} $cm^2 sec^{-1}$ for Rb in this liquid.

Equilibrium Distribution Coefficients

Distribution coefficients for Rb and Sr between silicate liquid (glass) and mineral have been determined for a number of phases, both empirically and experimentally. The empirically determined values in particular are likely to be limiting values only (minimum values for $K > 1$, maximum values for $K < 1$) because of the kinetic disequilibrium effects pointed out by Albarede and Bottinga (1972). In experimental studies such effects are potentially recognizable, and can be allowed for (e.g., Long, 1978).

Figure 11.4 compares the apparent distribution coefficient K^* to the diffusivity for a variety of values for $V\delta$, a function dominated by the effect of the crystallization rate. A value of K=4.0, appropriate for Sr in plagioclase or Rb in biotite is used to calculate K^*. The Arrhenius relationship and the data of Jambon (1982) are used to calculate "isotherms" for both Sr and Rb, and these are shown as the solid and dashed horizontal lines, respectively. For temperatures of 900 - 1000°C and for $V = 3 \times 10^{-7} - 3 \times 10^{-8}$ cm sec^{-1} (Table 11.2), δ has been calculated using Albarede and Bottinga's relationship, giving, for Sr a likely range of $V\delta$ of 1.2×10^{-9} to 5×10^{-9} cm^2 sec^{-1}. This range can be compared to the likely range of diffusivity of Sr (and/or T), yielding, for this case, an apparent distribution coefficient for Sr of from 1.0 to 1.9 as compared to the assumed value of 4.0. Similarly, for this model example, $K^{*Rb}_{biotite/liq}$ = 1.0 - 1.6 (Fig. 11.4).

This is, of course, only an illustrative example, but shows that within a tonalitic silicate melt trace element distribution may be controlled by kinetic factors rather than crystallization processes. The values of V used in this example probably approach maximum values allowable for this parameter. For Sr, as V decreases by two orders of magnitude (to 3×10^{-10} cm sec^{-1}) $K^* \rightarrow K$ (Fig. 11.4). The value used for D, the diffusion coefficient is probably accurate to within an order of magnitude or better (Jambon, 1982), although Long (1978) presents evidence that is suggestive that D may be two orders of magnitude faster in water-rich (approximately 9 wt % H_2O) silicate liquids than in the relatively water-poor but geologically reasonable matrices used in the tracer diffusion experiments. This leaves only effects on δ, the length-scale parameter, to be considered. For the simple model examined above, δ was itself

determined largely by diffusive processes. In practice, δ is more likely to be dependent to some degree on fluid flow within the melt.

The limited available mineral trace element data demonstrate that crystal-liquid partitioning in the San Jacinto magmas was accomplished under a close approach to "equilibrium" conditions. For instance, $K^{Rb}_{Bi/liq}$ appears to be approximately 6 to 7, and $K^{Sr}_{Plag-liq} \approx 1.5 - 2$. Unless the respective K's have numerically large values, inspection of Fig 11.4 shows that this implies either a slow crystallization rate, a small δ , or substantial sub-solidus re-equilibration of trace elements. The very slow rates of solid-state diffusion appear to limit the possible importance of the latter process. If crystallization rates are faster than about 10^{-9} cm sec^{-1}, relative fluid flow between crystals and liquid must be sufficiently rapid that the width of the boundary layer (δ) is substantially decreased from the diffusion-only case considered above. If crystallization rates are at least of this magnitude, then the apparent approach to "equilibrium" partitioning implied by the mineral data may be interpreted as indicating movement of crystals relative to the fluid from which they are precipitating, implying that the magma is convecting at some scale. This is consistent with the entirely independent argument for a dynamic magma chamber derived from consideration of the likely rheological behaviour of these liquids, and from the evidence for relative motions within the crystallizing liquids provided by field relations. Thus, the occurrence of convection within a cooling magma chamber tends to minimise possible kinetic effects in element partitioning, effects that may be expected to be substantial from a consideration of crystallization and diffusion rates alone.

For crystallization rates slower than about 10^{-10} cm sec^{-1}, $K^* \rightarrow K$, and the dimension of δ becomes unimportant. Trace element partitioning at slow crystallization rates is thus controlled by crystal-chemical processes rather than by kinetic effects.

These considerations suggest that kinetic factors were probably unimportant in influencing trace element partitioning for much of the history of the San Jacinto rocks. However, as crystallization procedes and both the viscosity and yield strength of the liquid increase, departure from "equilibrium" partitioning towards kinetic control of partitioning might have become more pronounced.

The discussion above suggests that values for "distribution coefficients" measured on crystal/liquid pairs in natural systems may well be influenced by kinetic factors, exactly as pointed out by Albarede and Bottinga from theoretical considerations and a very limited data set some time ago (Albarede and Bottinga, 1972). These considerations also suggest that experimentally determined values of "equilibrium" distribution constants may be of little use in modelling the behaviour of siliceous melt systems unless kinetic perturbations are explicitly accounted for (e.g., Long, 1978). Such kinetic perturbations do not appear to be important for the San Jacinto case.

11.4 MODELLING TRACE ELEMENT BEHAVIOUR IN SILICATE LIQUIDS

The application of trace element modelling to the elucidation of magmatic processes in isolation has been extensively reviewed by Allegre and Minster (1978) and Hanson (1978), among others. O'Hara (1977) pointed out that consideration of such simplified systems where

processes are treated in isolation could lead to misleading conclusions, and has subsequently developed the petrological and theoretical basis for understanding one set of interactive processes, those operating within a periodically replenished, periodically tapped, continuously fractionated magma chamber that is assimilating contaminant as it is inflated (O'Hara, 1977, 1980; O'Hara and Mathews, 1981). Taylor (1979) considered the isotopic, geochemical and thermal effects of contamination of a crystallizing (and fractionating) magma chamber. DePaolo (1981a) subsequently developed the analytical expressions that describe this process, and, among other things, noted explicitly that the cases of combined assimilation-fractional crystallization (AFC) and combined recharge-fractional crystallization (RFC) are mathematically similar.

The work on interactive systems has demonstrated that these more complex, and probably geologically more realistic situations yield geochemical and isotopic trajectories quite different from those obtained from simpler systems. In general, these effects are non-linear, meaning that extrapolated trends to not necessarily pass through the composition of either end-member. D.J. DePaolo and his co-workers (1981a,b; Farmer and DePaolo 1983) have demonstrated that for one simplified case (AFC) it is possible to model almost any data array by suitable variation of the model parameters. The mathematical similarity between the AFC and RFC processes thus implies that any <u>general</u> conclusions drawn for the AFC case must necessarily hold for the RFC case as well, with the obvious difference that the compositional and isotopic contrasts between chamber and added material will usually be much smaller for the latter (RFC) process.

11.4.1 MODELLING TRACE ELEMENT BEHAVIOUR DURING CRYSTALLIZATION

For a simplified model magma chamber where element concentrations are controlled solely by well-understood equilibrium processes (diffusion, crystal-liquid fractionation) and chamber dynamics are assumed to be completely efficient at homogenisation, we can write [in part, after DePaolo (1981a)]:

$$\frac{d\mu}{dt} = \dot{M}_a C_a + \dot{M}_r C_r - \dot{M}_c C_c - \dot{M}_e C_e = C_m \frac{dM_m}{dt} + M_m \frac{dC_m}{dt}$$

where the the subscripts m,a,r,c and e refer to magma, assimilation, recharge, cumulates (or crystallization) and eruptives, respectively. This can be rearranged to give:

$$\frac{dC_m}{dt} = \frac{\dot{M}_a}{M_m}(C_a - C_m) + \frac{\dot{M}_r}{M_m}(C_r - C_m) - \frac{\dot{M}_c}{M_m}(C_c - C_m) + \frac{\dot{M}_e}{M_m}(C_e - C_m)$$

For the model system under consideration $C_c = DC_m$ and $C_e = C_m$, so this simplifies to:

$$\frac{dC_m}{dt} = \frac{\dot{M}_a}{M_m}(C_a - C_m) + \frac{\dot{M}_r}{M_m}(C_r - C_m) - \frac{\dot{M}_c}{M_m} C_m(D - 1)$$

and the effect on the concentration of an element due to removal of material from the magma chamber is in the term $\dot{M}_m = \dot{M}_a + \dot{M}_r - \dot{M}_c - \dot{M}_e$.

For the completely general case, <u>all</u> parameters may be functions of t (time), and as the equation cannot be solved explicitly an iterative approach must be used.

O'Hara and Mathews (1981) point out that when all the likely possible sources of variation are taken into account then it is impossible to invert even the iterative relationships in order to deduce uniquely the magma chamber parameters or source compositions from study of the exposed products.

For the much simplified case of recharge and fractional crystallization only (RFC), we can write for the nth step

$$C_{l,n} = [C_{l,n-1}(1-X)^{K-1}](1-X) + XC_{l,n=0}$$

where $C_{l,n}$ is the concentration of the element in the liquid at the nth step, X is the fraction of liquid removed by crystallization (and then replenished) at each stage, and K is the solid/liquid partition coefficient for the element under consideration. The composition of the solid precipitated from the liquid at any point can be easily obtained using the relationship

$$C_{s,n} = K_{\bullet} C_{l,n}$$

In general, the amount of new liquid added need not exactly balance the amount of previous liquid removed as cumulates. This simple case serves, however, to illustrate some of the effects of combined recharge and fractional crystallization within a dynamic magma chamber. The complete treatment for the general case involving recharge, fractional crystallization, contamination and eruption is given by O'Hara and Mathews (1981). For the RFC process, deviation from the behaviour expected for the FC case becomes more pronounced as K departs significantly from unity. For a more complete discussion, see O'Hara and Mathews (1981).

11.4.2 LINEAR ELEMENT-ELEMENT COVARIATION IN CALC-ALKALINE ROCKS

The concept of combined recharge - fractional crystallization has potentially great importance in understanding chemical variation within calc-alkaline rock suites, where elements often show linear covariation. This feature of the calc-alkaline rock series has led many workers to suggest that mixing (or unmixing) is an important process in the generation of these rocks. It is becoming apparent that more than one process is involved in the generation of these linear relationships. B.W. Chappell and A.J.R. White and their co-workers in south-eastern Australia interpret linear element covariation as resulting from the incomplete unmixing of a mafic residuum ("restite") from a more felsic granitic or granodioritic liquid (e.g., Chappell, 1966, 1978; White and Chappell, 1977; Compston and Chappell, 1979). McBirney (1980) notes that one of the attributes of calc-alkaline rocks that serve to differentiate them from most other rock suites is the rectilinear variation of their various components. He proposes that these linear relationships result from the mixing of relatively unfractionated and relatively fractionated liquids near the top of a fractionally crystallizing magma chamber. In his model, precipitation of early formed crystals on the walls of a cooling pluton leaves a less dense residual liquid that rises and ponds at the top of the pluton, gradually mixing with the underlying unfractionated liquid. Crystallization of the various linearly related liquids then gives rise to linear relationships within the final solidified rocks.

There appears to be no doubt that such a mechanism can be quite efficient in developing a range of compositions within a cooling pluton, as shown by both experimental work (McBirney, 1980; Turner, 1980) and by the

study of exhumed natural examples (e.g., Wilcox, 1954; Bailey et al., 1976).

Combined recharge - fractional crystallization gives a third mechanism for developing rectilinear variation within a cogenetic suite of rocks. Here the mixing is between the fractionated liquid (or liquids) within the magma chamber and the new ("primitive") liquid (or liquids) being periodically added to the developing system.

These three processes need not operate in isolation; a pluton could develop a lid of less dense fractionated material at the same time as relatively dense "primitive" material is being added to the underlying liquids, and these "primitive" liquids could contain various amounts of restite, giving a final rock produced by mixing (or unmixing) at three different scales.

If volumes of liquid become isolated from the bulk of the magma chamber (by double-diffusive induced stratification, by magma chamber geometry, by a hiatus in the supply of new magma, or for some other reason), then a wide and complex range of variation may be expected in the final products of igneous activity.

One important feature of the RFC process is that, by continually adding new batches of "primitive" material it has the potential to buffer both the composition and physical conditions of the liquid to within a relatively narrow range. This could enable a large volume of material to crystallize from a liquid with a narrow compositional range, and at approximately uniform temperature.

11.5 APPLICATION TO THE SAN JACINTO IGNEOUS COMPLEX

Figure 11.5 shows how these processes can potentially explain the Rb-Sr covariation for the San Jacinto rocks described above (Ch. 9). The first solid crystallized from the initial batch of "primitive" liquid is assumed to have 620 ppm Sr, 45 ppm Rb, and $K^{Sr}_{solid/liq}$ = 1.2 and $K^{Rb}_{solid/liq}$ = 0.7 are assumed throughout. Simple fractional crystallization gives the solid trajectory labelled "SFC-Solid" for the evolving solid and the dashed trajectory labelled "SFC-Liquid" for the evolving liquid. Line "A" gives the composition of solids precipitating from the fractionated liquids for the RFC case where X = 0.9, and immediately prior to a new influx of magma. The line "A'" gives the composition of solids for this case (X = 0.9) immediately after each new batch of magma has been mixed with the liquid remaining from the previous stages of the process. Depending on the vagaries of crystallization, recharge and mixing, solids crystallized from this system would fall within the shaded area. Line B-B' shows a possible trajectory for a small volume of liquid, isolated from the main dynamic magma chamber, and having slightly different partition coefficients. Relatively small variations in the partition coefficients give markedly different slopes to the initial part of fractional crystallization trajectories.

The net result of such a system will be to give an approximately linear covariation of Rb and Sr (within the shaded area) except where pockets of liquid are isolated from the main volume of magma, or when recharge stops and the whole system stagnates. The solid triangles are the data points from Unit II. Slight variations in the Rb and Sr concentrations of the "parental" liquids would give rise to a broad

Figure 11.5. Illustration of an RFC model for Rb-Sr behaviour in the San Jacinto rocks. Distribution coefficients for Sr and Rb are shown for each curve. Shaded area gives compositions of solids attainable for an RFC process where X can reach 0.9, and there is considerable mixing of evolved liquids with newly added "primitive" liquids. Triangles are data points from Unit II. The curve B-B* shows a Simple Fractional Crystallization trajectory for slightly different values of D^{Rb} and D^{Sr}.

See text for further discussion.

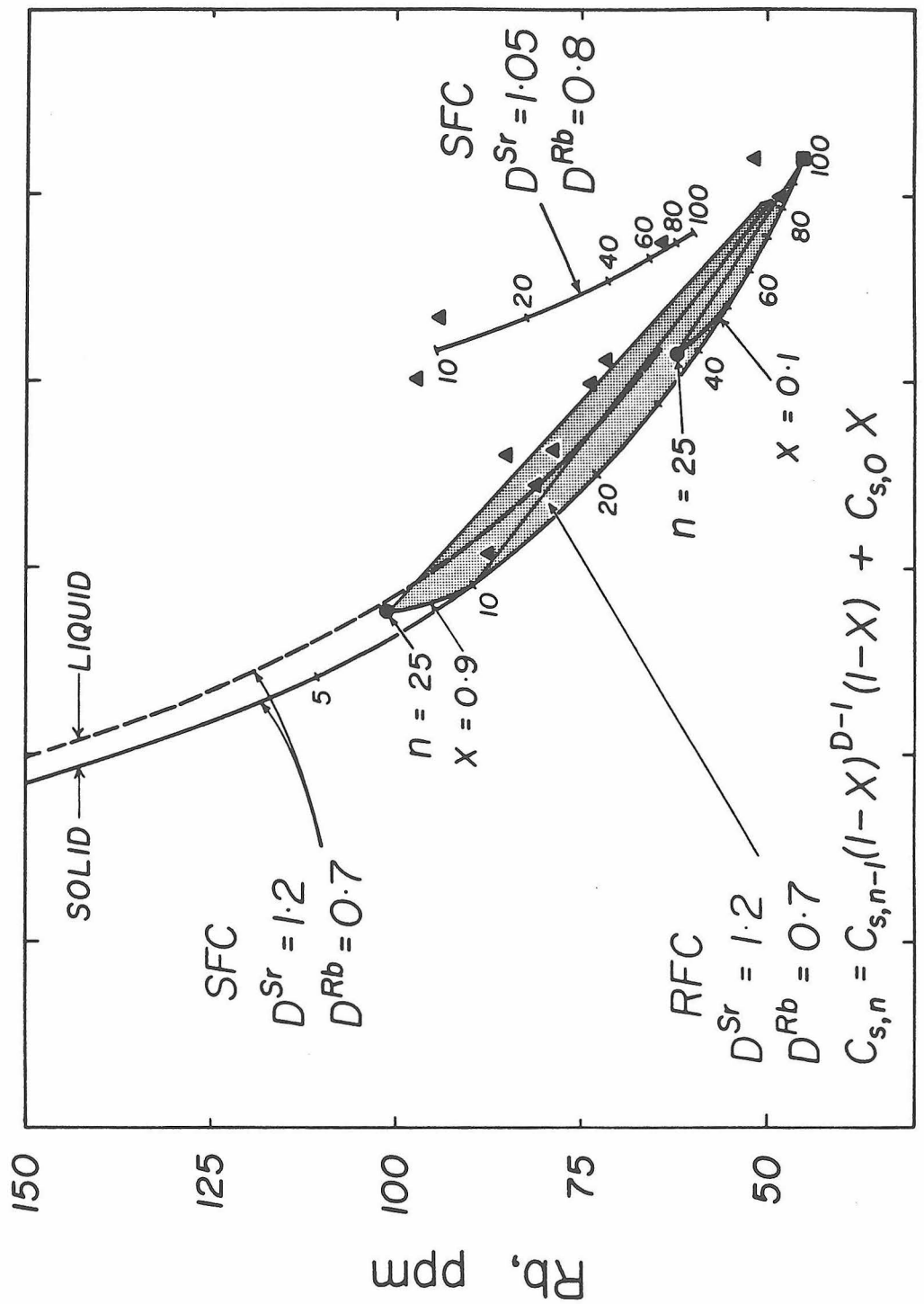
Rb, ppm
Sr, ppm
150
125
100
75
50
200
300
400
500
600
SOLID
LIQUID
SFC
D^{Sr} = 1·2
D^{Rb} = 0·7
SFC
D^{Sr} = 1·05
D^{Rb} = 0·8
RFC
D^{Sr} = 1·2
D^{Rb} = 0·7
$C_{s,n} = C_{s,n-1}(1-X)^{D-1}(1-X) + C_{s,0}X$
n = 25
X = 0·9
n = 25
X = 0·1
5
10
20
40
60
80
100

Figure 11.5

Figure 11.6a. Variation of Ce/Y with Ce, San Jacinto Mountains.

Filled symbols	-	"Mafic" tonalites
Open symbols	-	"Normal" tonalites
Squares	-	Unit I
Triangles	-	Unit II
Circles	-	Unit III
Plus signs	-	Felsic differentiates
Crosses	-	Mafic xenoliths
Asterisk	-	Mafic dike from Unit III
Diamonds	-	Granodiorite of Poppet Creek
Inverted traingles	-	Early intrusives

Figure 11.6b. As above, but showing diagramatically trajectories inferred for chemical evolution during in situ fractionation, followed by mixing of these evolved liquids with new mafic liquids added to the chamber.

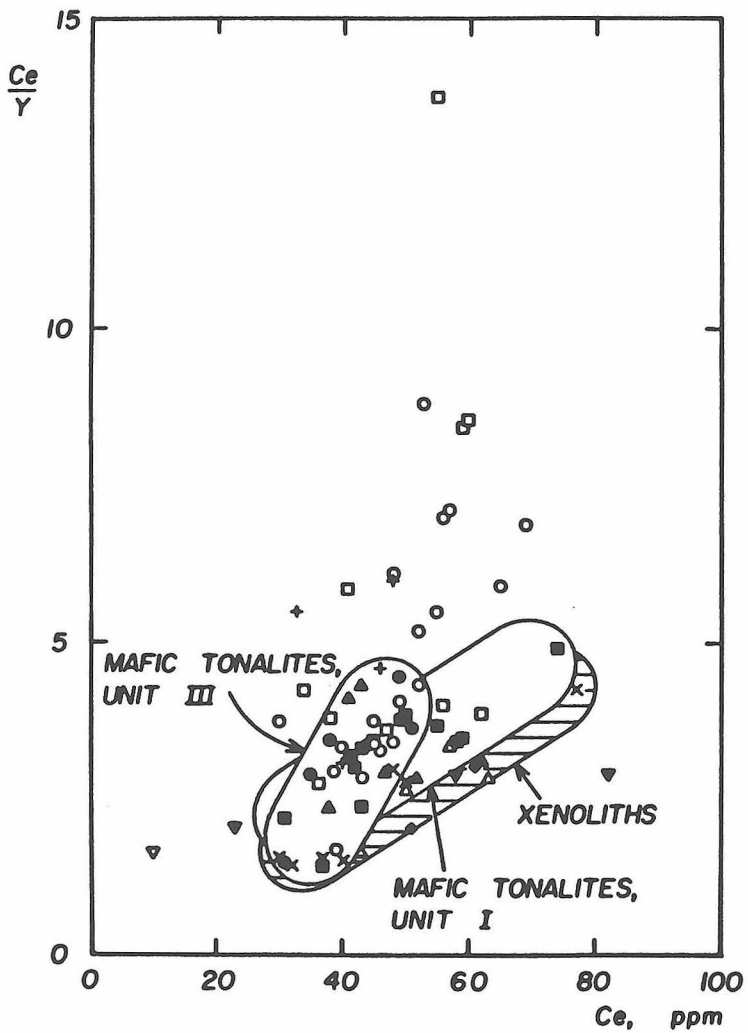

Figure 11.6a

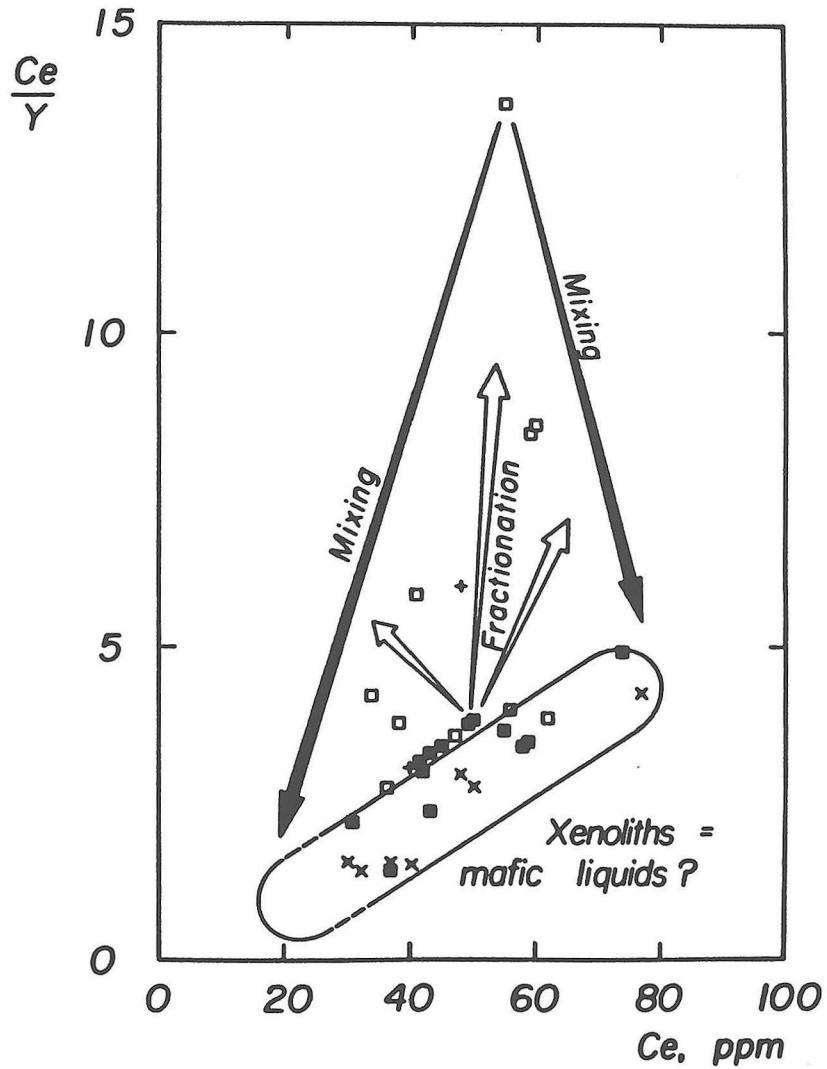

Figure 11.6b

spread on a Rb-Sr diagram. It is clear that the model described above is consistent with these available data.

One factor complicates a more quantitative evaluation of all of the available data - heterogeneity of the "primitive" liquids. The correlation of geography with Rb-Sr relations described above (Ch. 9) demonstrates that there was some variation in the composition of the liquids introduced into the magma chambers. The wide variation in the composition of the xenoliths, which are interpreted as samples of some of the more mafic of these introduced liquids, is also evidence for original liquid heterogeneity. A dynamic magma chamber such as that described above could be quite efficient at homogenizing the batches of various composition liquids added to the developing pluton. It cannot be completely efficient, however, because both trace element and isotopic heterogeneities remain.

The partition coefficients used in the model above (Fig. 11.5) were chosen so as to best fit the observed data array; they imply $K^{Sr}_{Plag/liq} \approx 2.4$, and $K^{Rb}_{Biotite/liq} \approx 5\text{-}6$. These values agree well with both both literature estimates and with estimates made from the limited mineral data presented above.

Many of the chemical features of the major tonalite units noted in Ch. 7 are also potentially explained by this model. Figure 11.6(a) shows the covariation of Ce abundance with an indicator of fractionation within the REE, Ce/Y. The more mafic rocks show a linear relationship of Ce/Y with Ce; however, as the rocks become more felsic, Ce/Y increases rapidly with little variation in Ce abundance. The triangular data array can be interpreted as resulting from mixing of "primitive"

liquids having a range of Ce and Ce/Y with fractionated liquids having highly variable Ce/Y but relatively unchanged Ce (Fig. 11.6). A large variation of Ce/Y within a cogenetic sequence of rocks has been suggested by Gromet and Silver (1983) to be a feature of in-situ fractionation where REE behaviour is controlled by minor phases (titanite, allanite, zircon), and this is precisely the situation for the San Jacinto rocks.

The K-Rb data (Fig. 11.7) can be similarly interpreted. The mafic rocks have K-Rb relations largely inherited from the "primitive" liquids. In-situ fractional crystallization leads to high K at relatively high Rb, and mixing of these fractionated liquids with either less fractionated liquids or with new volumes of "primitive" liquid gives the triangular data array of Fig. 11.7. It is not possible to easily determine from the chemical data alone whether the linear array defined by the mafic rocks results from fractionation processes prior to introduction of the liquids into the magma chamber, or from an efficient RFC process (i.e., one with X small) in a developing system. Either could explain the trace element data.

An active RFC system might be expected to homogenize original isotopic as well as geochemical variation as it develops. Figure 11.8 shows Sr_i plotted against an index of fractionation, K_2O, and thus also perhaps against some indication of the time that a volume of liquid has been within the magma chamber. Both the mafic tonalites and the xenoliths show a relatively restricted range in K_2O but a considerable range in Sr_i. The variation in Sr_i reflects, in part, geographical variation as is described above, with samples from the southwestern part of the San Jacinto block having, in general, lower values, and those from the northeast

Figure 11.7. K_2O versus Rb, showing inferred origin of K-Rb relations of San Jacinto rocks by mixing of newly introduced mafic liquids and more evolved liquids within a dynamic magma chamber. Symbols as for Fig. 11.6.

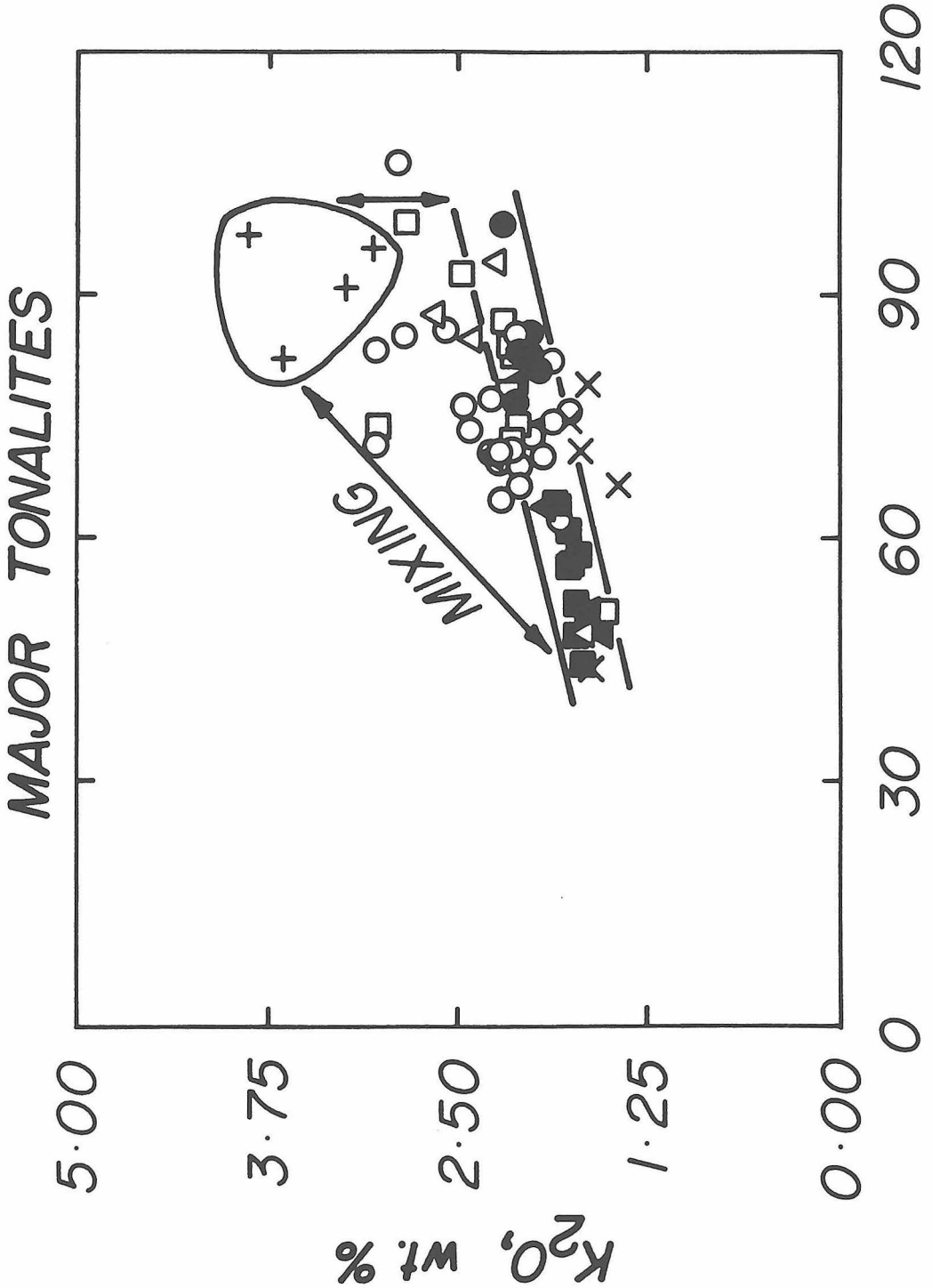
MAJOR TONALITES
MIXING
K_2O, wt %
5·00
3·75
2·50
1·25
0·00
0
30
60
90
120
Rb, ppm

Figure 11.8

Figure 11.8. Calculated initial $^{87}Sr/^{8}$ Sr versus K_2O, showing decrease in variability of initial $^{87}Sr/^{86}Sr$ as K_2O increases. Symbols as for Fig. 11.6.

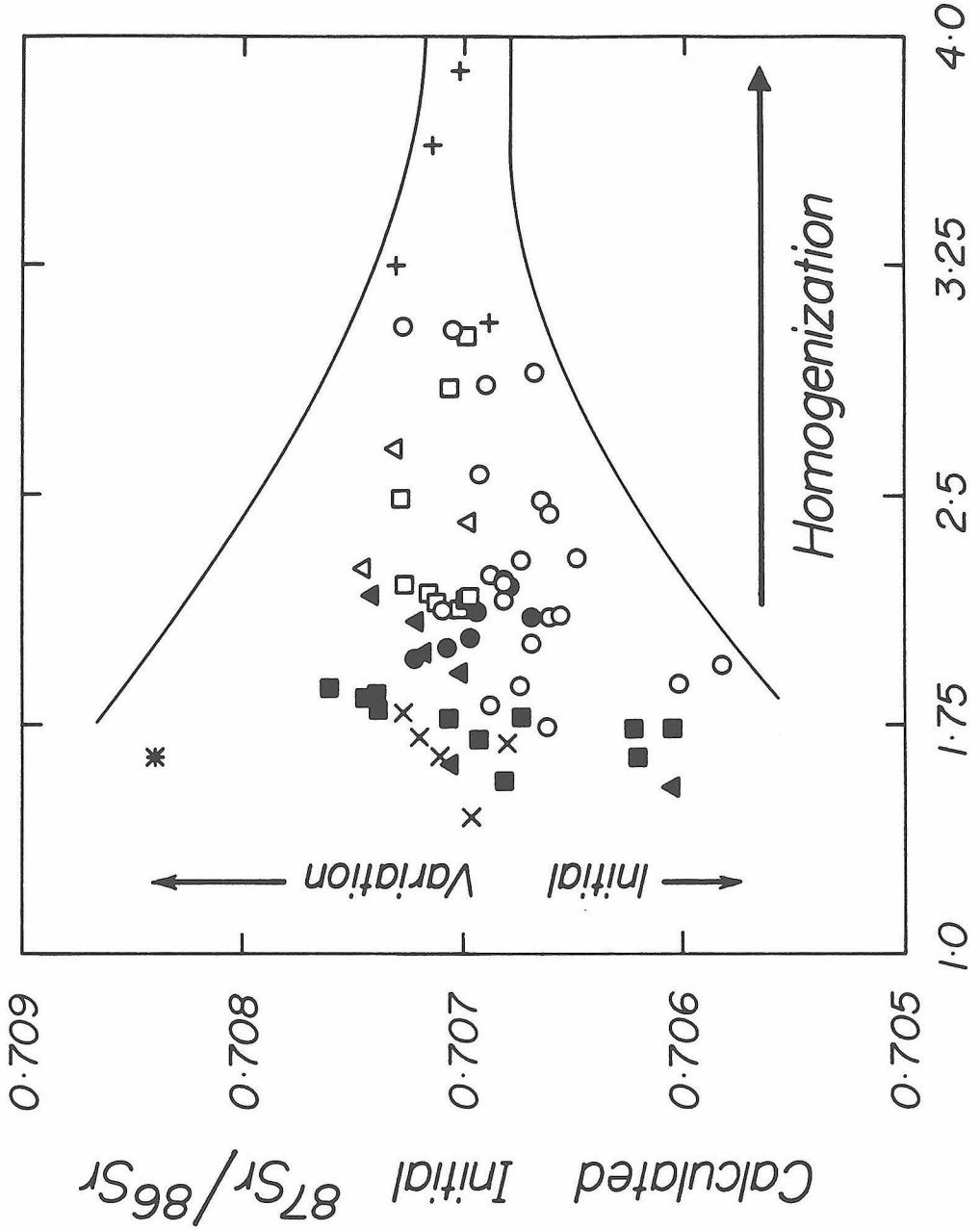
Calculated Initial $^{87}Sr/^{86}Sr$
0·709
0·708
0·707
0·706
0·705
Initial Variation
Homogenization
1·0
1·75
2·5
3·25
4·0
K_2O, wt %

Figure 11.8

Figure 11.9. Variation of calculated initial $^{87}Sr/^{86}Sr$ with Sr concentration. Variability in initial $^{87}Sr/^{86}Sr$ decreases as Sr abundance decreases. Symbols as for Fig. 11.6.

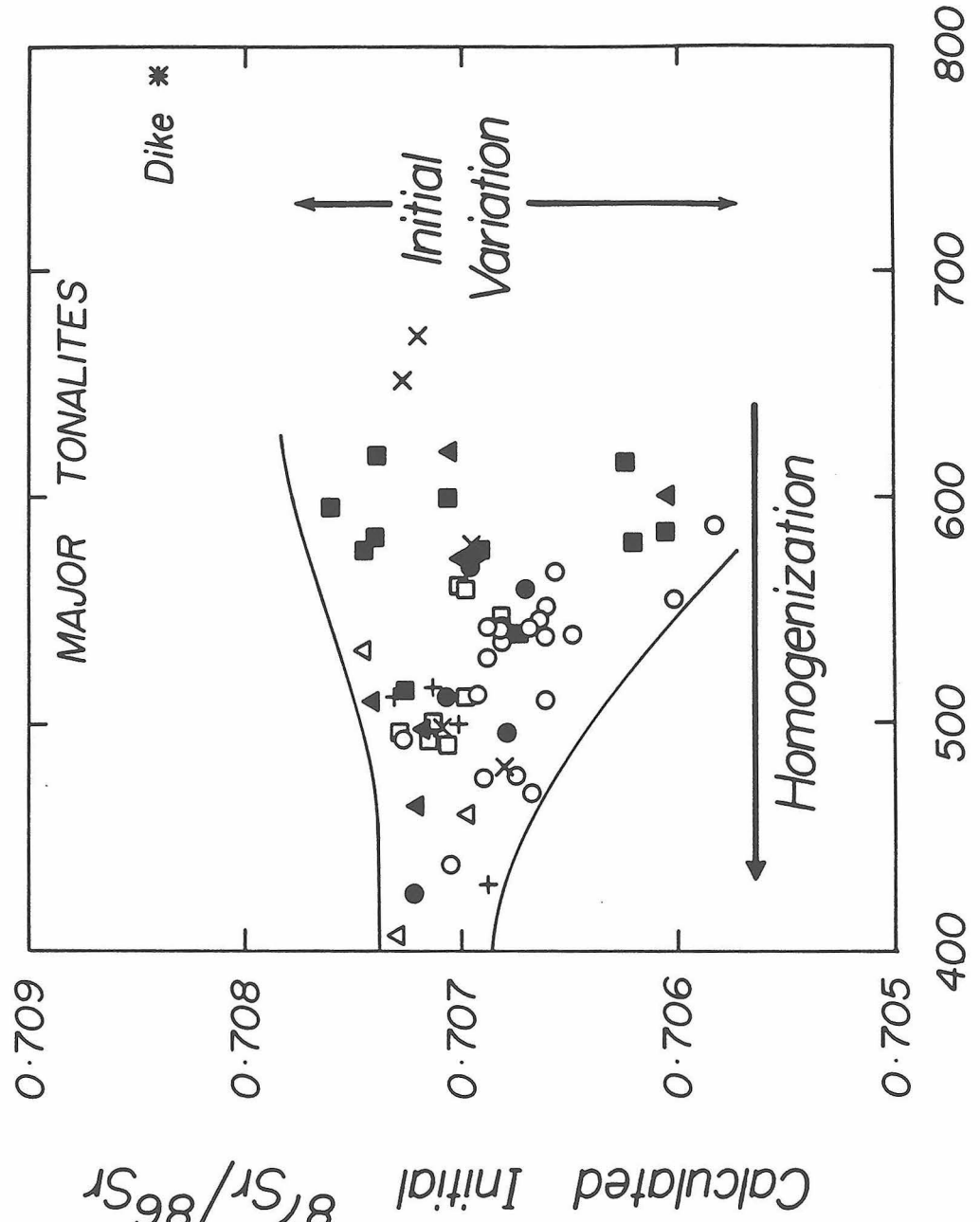
MAJOR TONALITES
Dike
Initial Variation
Homogenization
Calculated Initial $^{87}Sr/^{86}Sr$
0·709
0·708
0·707
0·706
0·705
400
500
600
700
800
Sr, ppm

Figure 11.9

having higher values. As fractionation increases the variation in Sr_i decreases markedly so that in the rocks collected as being representative of in-situ fractionation $\Delta\ Sr_i = 0.0004$ compared to a total range for the whole system of 0.0033.

Figure 11.9, a plot of Sr_i against Sr concentration shows much the same relationship, except that Sr is high in the more mafic rocks and decreases with increasing fractionation. The wide range of Sr concentrations shown by the xenoliths perhaps results from flow differentiation variously concentrating plagioclase within the dykes from which the xenoliths are derived.

Although oxygen isotopic data are more limited than strontium isotopic data, similar relations appear in the oxygen data. Figure 11.9 shows the combined $\delta^{18}O$-Sr_i data. The mafic rocks show considerable variability in both parameters; this variation must reflect original liquid variation to at least some degree. All of the more felsic rocks except one are from Unit III; as noted previously these samples (from Unit III) show a very restricted range in $\delta^{18}O$ values of 10.2 ± 0.2. Except for one sample from adjacent to the western contact of this unit, Sr_i for the more felsic rocks also shows a restricted range; this may reflect limiting sampling from a relatively restricted geographic area as much as it reflects homogeneity within the pluton. These data are consistent, however, with a model of partial homogenization of initially heterogeneous liquids within a dynamic long-lived magma chamber.

11.6 CONCLUSIONS

1. Estimation of rheological parameters likely to have been appropriate during filling and solidification of the San Jacinto magma chambers implies that each chamber probably supported a convective system operating in the laminar flow regime for at least part of its history. This is compatible with field evidence for dynamic magma chambers.

2. It appears likely that the magma had sufficient yield strength through most, if not all, of its history to suppress gravitational separation of solids from host liquid. This implies that relative accumulation of particular types of crystals (e.g., in schlieren) was accomplished by other processes, perhaps including flow differentiation

3. Simple models of trace element behaviour during crystallization, when combined with observed distribution patterns suggest that crystals were growing within a turbulent environment. Data obtained in the present study suggest that the depleted boundary layer around a growing crystal was thin, and far less extensive than expected from purely diffusional control of element transport. A simple model of kinetic control of trace component incorporation into a crystal growing in a moving fluid proposed by Burton et al., (1953) appears capable of observed trace element distributions, and implies that crystal growth took place in a dynamic environment. This is consistent with other evidence for convection within the magma chambers.

4. There appears to be a dichotomy between the composition of the mafic tonalites and the more chemically evolved felsic tonalites and minor granodiorites of the major plutons. "Normal" tonalites have

and minor granodiorites of the major plutons. "Normal" tonalites have intermediate properties. This dichotomy aapears to result from the operation of processes at different stages in the evolution of these systems. The more mafic rocks are interpreted as having crystallized from liquids that had largely acquired their geochemical characteristics prior to introduction into these relatively high-level magma chambers, while the most felsic rocks are interpreted as having crystallized from liquids that had undergone considerable chemical evolution within the magma chamber. Many of the chemical features of these systems can be interpreted as having resulted from mixing of these two types of genetically related liquids within a dynamic magma chamber.

5. Aspects of trace element characteristics of these rocks (Rb-Sr, K-Rb, Ce-Ce/Y) are compatible with an RFC (Recharge-Fractional Crystallization) process operating within a dynamic magma chamber.

6. Episodic recharge of a crystallizing magma chamber offers a mechanism for substantial buffering of the physico-chemical properties pertaining during solidification. Some such buffering appears required for the San Jacinto systems in order to explain the relative constancy of mineral composition throughout the crystallization interval.

7. Isotopic data can be interpreted as showing partial homogenization of initially heterogeneous liquids within an evolving magma chamber. In particular, the isotopic composition of both oxygen and strontium become much more homogeneous in the more evolved rocks, a point consistent with long residence times in the developing magma chambers and thus greater time for homogenization of the liquids parental to these samples.

CHAPTER 12

PETROGENESIS OF BATHOLITHIC ROCKS, SAN JACINTO MOUNTAINS

12.1 INTRODUCTION

The development of plate tectonics theory provided a mechanism by which the igneous rocks of the island arc and continental margin environment, on the one hand, and the oceanic and continental basalt provinces, on the other, could have such different chemical composition. The common basalt types, be they alkali or tholeiitic, are now widely interpreted as Mg-rich partial melts of near-anhydrous olivine-dominated mantle assemblages, often modified by extensive low-pressure crystal fractionation (e.g., O'Hara, 1977; Walker et. al., 1979; D.H. Green et. al., 1979; Jacques and D.H. Green, 1980). In contrast, the genesis of the volcanic rock associations of the island arcs and continental margins is intimately related to the consumption of oceanic crust in a subduction zone [see Gill (1981) for a recent summary] and appear to be the result of more complex petrogenetic processes. The involvement of water in the melting process, suggested by Poldervaart (1955) and O'Hara (1965) is now widely accepted as important (e.g., Wyllie, 1978, 1981; T.H. Green, 1980; Gill, 1981), largely on the basis of experimental studies. Also widely accepted is the apparent difficulty of deriving most (but not all) liquids of andesitic composition from a mantle assemblage leaving residual olivine (see D.H. Green et al., 1979; Wyllie, 1978, 1981; and Gill, 1981 for reviews). These and other authors stress that the genesis of the calc-alkaline rock series (including andesites) must involve some combination of varying source composition (and mineralogy), addition of volatile (and

perhaps silica and incompatible element)-rich fluids, varying physical conditions of melting, crystal fractionation and assimilation.

This chapter briefly summarizes some of the important points and conclusions relevant to the genesis of the calc-alkaline igneous rock suites made by these and other authors. The inferences made in the previous chapters about probable source properties (of the San Jacinto magmas) are then considered in the context of the regional data base for the Peninsular Ranges batholith developed by Silver and his co-workers, and also in the context of the experimental and observational data relevant to the problem of calc-alkaline rock genesis in general.

A model for the generation of the San Jacinto magmas is then developed using primarily the isotope data as constraints. The final part of the chapter considers some of the implications of this necessarily over-simplified model for several geochemical systems, in particular REE fractionation patterns. It is emphasised that this model is just that - a model. It is developed using currently available data, and future advances in particularly experimental petrology could necessitate major revision to this model. Most, if not all petrologic models can probably never be proven, only invalidated, and that offered here is no exception. The available data are consistent with, but do not prove the model.

12.2 REVIEW OF WORK PERTINENT TO UNDERSTANDING THE GENESIS OF THE CALC-ALKALINE ROCK SUITES

12.2.1 OCEANIC AND CONTINENTAL MARGIN ARCS

Following the advent of plate tectonics many workers sought to find unifying patterns within calc-alkaline rock suites from widely

scattered areas. Perhaps the best known is the work of Dickinson and Hatherton, who related K_2O content of erupted lavas to depth to the Benioff Zone beneath that volcano to give a generalized "K-h" relationship (Dickinson and Hatherton, 1967; Hatherton and Dickinson, 1969). Variation of total alkali content across specific arcs had been recognised much earlier (e.g., Indonesia: Van Bemmelen, 1949; Rittman, 1953; Japan: Tomita, 1935; Kuno, 1959; Sugimura, 1960: Pacific arcs: Tomkieff, 1949), and similar trends had been shown for large continental margin batholiths (e.g., Sierra Nevada batholith: Moore, 1959). The rapid accumulation of data on various calc-alkaline suites during the 1960's was followed by the proposal of generalized models that attempted to explain these apparently universal spatial-temporal-chemical patterns (e.g., Jakes and White, 1969, 1972; Jakes and Gill, 1970). Recent studies (e.g., Johnston et al., 1978; Arculus and Johnston, 1978) stress the uniqueness of each particular arc-trench system, and demonstrate that variation along the arc may be more significant in some systems than the oft-cited variation transverse to the arc.

In his extensive summary of orogenic andesites Gill lists 11 arcs or arc segments for which a systematic K-h relationship has been reported (Gill, 1981). Some of these data are open to more complex interpretation (Arculus and Johnston, 1978). Perhaps as significant is the location of these arc systems - 8 have almost certainly developed upon older continental crust, and for 2 of the remainder (Java, North Kuriles) the situation is equivocal. Only for the New Britain arc is there firm evidence for no old continental basement (Johnston, 1977). It may thus be argued that proximity to continental basement appears to be a significant factor in the development of the systematic geochemical

trends described by many workers.

This apparent contrast between the K-h relations of oceanic and continental calc-alkaline suites suggests that there may be other variations between the rocks of the two environments. Chemical data from variety of intra-oceanic and continental margin arc systems have been reviewed by Maaløe and Petersen (1981). They conclude that in general continental margin calc-alkaline rocks are richer in Na and K, and poorer in Fe and Ca than are intra-oceanic varieties. The relative proportions of other elements were thought to be similar, though it may be argued from their data (see particularly their Fig. 2) that Si and Al also tend to be more abundant in continental margin than in intra-oceanic arc rocks. With the exception of a lack of low Si (SiO_2 <58 wt.%) varieties, data from the Sierra Nevada batholith of California and the Coast Range batholith of British Columbia were found to overlap completely the data for the continental margin volcanic suites. These data suggest the involvement of sources or processes capable of enriching the continental margin rocks in the alkali feldspar components. An important corollary of these observations, and one previously made by many others (e.g., Hills, 1959; Branch, 1967; Wyborn et al., 1981) is that this overlap in the composition of continental margin volcanic and plutonic rocks indicate consanguinity. Chemical data from the Peninsular Ranges batholith (Silver and Chappell, unpublished data) show a strong coherence between spatially related volcanic and plutonic rocks, supporting inferences of consanguinity made earlier by other means (Silver et al., 1956, 1963, 1969). Consequently, the study of the petrogenesis of a batholith is more or less equivalent to the study of a volcanic arc that could have developed superjacent to that batholith. Some compositional differences between consanguineous

plutonic and volcanic suites may still remain, largely the result of different volatile contents or because of density filtering within crust. Such effects appear minor, however, so that inferences drawn from the study of volcanic suites should, in large part, be applicable to plutonic suites and vice versa.

A-, I-, and S-type granites

Workers in southeastern Australia have postulated a classification of granitic rocks into two major genetic groups. S-type granites are believed to have been derived by partial melting of a metasedimentary source region, while I-type granites are derived through partial melting of igneous source materials (Chappell and White, 1974; White and Chappell, 1977). By metasedimentary source is meant rocks having the geochemical characteristics of an evolved sedimentary rock, most notably low Na/(Na + K) and high Al/(Na + K + Ca)[implicit in Chappell and White, 1974; B.W. Chappell, personal communication, 1979]. A partial melt of a volcaniclastic sediment would thus, according to this geochemical classification, be I-type. A third grouping, the A-type contains rocks that are alkali-rich, anhydrous, and commonly are anorogenic, and are suggested to have formed by partial fusion of a near-anhydrous granulite, itself residual from an earlier crustal melting event. This granulite could have had either a meta-sedimentary or meta-igneous protolith (Loiselle and Wones, 1979; Collins et al., 1981).

With the exception of very minor hybrid varieties, all of the igneous rocks of the Peninsular Ranges so far studied in detail are I-type (Silver et al., 1979), and the origin of the other two types will not be considered further here.

Domains, Suites and Series - the case for uniqueness of segments of an arc

The uniqueness of each volcanic arc argued for by Arculus and Johnston (1978) receives ample confirmation from the plutonic environment. In fact, the recognition of inter- and intra-batholith variation argues for "uniqueness" on a much smaller scale than has so far been documented for volcanic systems. For instance, there are fundamental chemical differences between, say, the Cretaceous rocks of the adjacent Sierra Nevada and Peninsular Range batholiths of western North America (e.g., Larsen, 1948; Bateman and Dodge, 1970; Baird et al., 1974a,b, 1979; Silver et al., 1979), giving a large scale segmentation of a once-continuous magmatic arc (Silver, 1982, 1983). Work within each batholith has shown that finer-scale subdivision is possible, into the co-magmatic series of the Sierra Nevada batholith (Bateman and Dodge, 1970; Presnall and Bateman, 1973) or the domains of the Peninsular Ranges batholith (Silver and Early, 1977; Silver et al., 1979). Similar small-scale structure has been documented within the batholiths of south-eastern Australia (e.g., Chappell, 1966, 1978; Hine et al., 1978; Griffin et al., 1978) where chemically related plutons are grouped into suites. At least some of this chemical distinctiveness must reflect variation in the composition of the source material (e.g., Chappell and White, 1974; Chappell, 1978; Compston and Chappell, 1979; Silver and Early, 1977). Other factors that could contribute to such consistent intrabatholithic variation are numerous, and include variation in: subduction rates, the amount of fluid released from the slab, the rates at which ascending primary magmas fractionate, the nature of the tectonic environment in which magma genesis takes place, the residual assemblages present during either partial fusion or fraction-

ation, or interaction with the crust during ascent. The larger scale (inter-batholithic) variations are most reasonably interpreted as the result of tapping significantly different sources either within the crust or underlying mantle (the lithosphere)[e.g., Bateman and Eaton, 1967; Silver et al., 1979; Chappell and White, 1974]. These differences are probably related to the development of a particular segment of continental crust (e.g., Kistler and Peterman, 1973; White and Chappell, 1977; Compston and Chappell, 1979).

The development of the intra-oceanic arcs is free of this obvious relationship to older continental lithosphere, so that in the following review work on the intra-oceanic situation will be summarized first, and then differences between intra-oceanic and continental margin arcs noted.

12.2.2 GEOCHEMISTRY

Major and trace element abundance patterns

The chemistry of orogenic andesites from all environments has been extensively reviewed by Gill (1981). Figure 12.1, from Gill, shows diagramatically the range of chemistry observed for volcanic rocks of the calc-alkaline suite classified as "andesites". The boundaries at 53 and 63 wt % SiO_2 are arbitrary, and relate to Gill's definition of andesite. Andesites are distinguished from other rock suites suites by their low Ti, and by their relatively high Al, K, H_2O+ and Mg# [atomic $Mg/(Mg + Fe^{2+})$] at comparable SiO_2 content.

The water content of andesites is of particular interest. Gill reviewed several methods of estimating the water content of the liquid

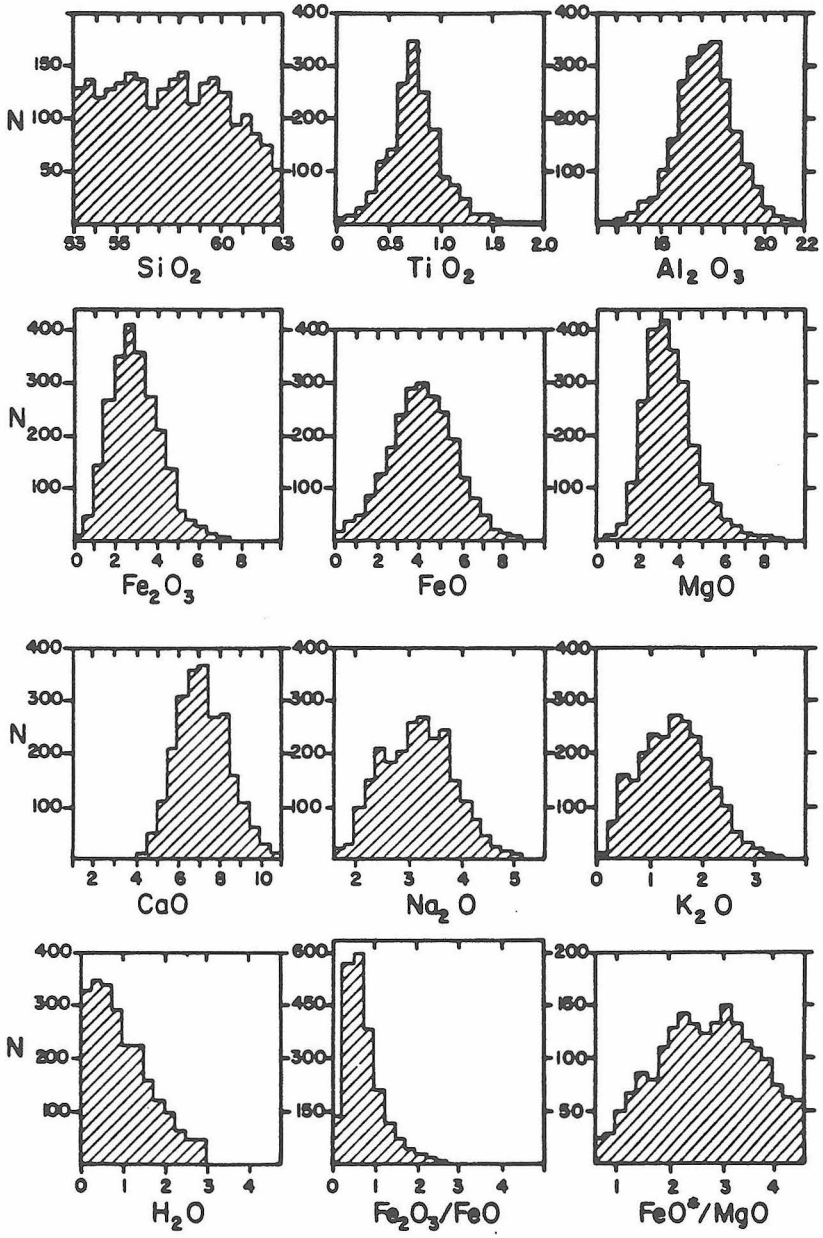

Histograms of the wt.% oxide compositions of the 2500 orogenic andesites, as defined in text, which are in electronic data file RKOC76 of F. Chayes. Analyses with more than 3 wt.% H_2O^+ were excluded

Figure 12.1. Chemical composition of andesite (from Gill, 1981).

portion of an andesite and concluded that, prior to eruption, they contained 1-5 wt.% H^2O. He also noted that the wt.% of water approximates or is greater than the wt.% of K_2O, and that even a water-rich andesite (5% H_2O) will be undersaturated with H_2O below about 5 km depth.

Trace element contents of andesitic rocks vary considerably, usually but not always in some relationship to changes in the major element chemistry. Perhaps most significant is the correlation of incompatible trace element abundances with K_2O (and SiO_2) content. In general, as K_2O (and SiO_2) increase, so do Rb, Cs, Ba, Th, U, Pb, Zr, Hf, Nb and Ta contents. Heavy rare earth element (HREE) abundances stay constant or perhaps decrease as K increases, while LREE abundances correlate strongly with K. As a consequence, indices of fractionation within the REE (such as La/Y, La/Yb, Ce/Yb) increase with increasing K.

Perhaps most useful for differentiating between conflicting genetic models are the compatible elements, especially Ni and Cr. Ni contents of most andesites are much too low for them to have been in equilibrium with mantle peridotite (e.g., Hart and Davis, 1978). Tatsumi and Ishizaka (1981) and Davis and Cameron (1983) report rare exceptions. Gill argues from Cr-Ni relationships that fractional crystallization is an important process in the genesis of many andesite suites, while fusion of either mantle peridotite or MORB-derived eclogite are disallowed by these data.

Given the wide range of chemistry found for the intra-oceanic suites it is probable that there is considerable overlap between the composition of intra-oceanic and continental margin calc-alkaline volcanic rocks and their plutonic equivalents. As mentioned above, continental

margin suites have generally higher Na and K (and perhaps Si and Al), and lower Fe and Mg. Trace element contents vary widely for continental margin suites also. The change in REE fractionation behaviour correlated with increasing K summarized by Gill has been observed within at least one batholith (Peninsular Ranges) in rocks of similar K_2O content (Gromet, 1979). This suggests that the increase in K_2O and the change in REE behaviour are controlled by independent processes that usually, but not always, act together.

Isotope Geochemistry

Strontium

The average $^{87}Sr/^{86}Sr$ of Quaternary andesitic suites from convergent plate boundaries lies between 0.703 and 0.704 (e.g., Gill, 1981). These data are summarized in Table 12.1 (from Kay et al., 1978). These values overlap the range of ocean island basalts and are significantly more radiogenic than normal unaltered mid-ocean ridge basalt (N-MORB)[range 0.7022 - 0.7035, mean 0.7029; Hofmann and Hart, 1978]. These data appear to rule out derivation of intra-oceanic andesites from unaltered N-MORB type crust, even crust that has aged for 200 m.y.. Addition of small amounts of sea-water Sr during hydrothermal exchange (e.g., Hart et al., 1974; Menzies and Seyfried, 1979 McCulloch et al., 1980) could raise the $^{87}Sr/^{86}Sr$ of the oceanic crust sufficiently for altered MORB-type crust to be a possible source for intra-oceanic andesites. The isotopic data also imply that the mantle sources of ocean island basalts are possible sources for intra-oceanic andesites, whilst those that generate the N-MORBs are not.

TABLE 12.1

Strontium isotopes in volcanic rocks from converging plate margins

	Location	$^{87}Sr/^{86}Sr$ Range (number of samples)	Average Value
a)	Aleutian Islands,	0.7028–0.7037 (24)	0.7032
	Alaska Peninsula (b-a)	0.7030–0.7034 (3)	0.7031
b)	Cascades -Washington (b,a,d)	0.7026–0.7041 (11)	0.7036
	-Oregon (b,a,d)	0.7027–0.7047 (19)	0.7038
	-California (b,a,d)	0.7030–0.7041 (18)	0.7036
	-California (a), Mt. Shasta	0.7030–0.7032 (5)	0.7030
c)	Japan - Hokkaido (b,a,d)	0.7027–0.7059 (46)	0.7038
d)	Caribbean - Monserrat-St. Kitts	0.7029–0.7035 (2)	0.7032
	- St. Lucia (b,a,d,r)	0.7035–0.7092 (10)	0.7063
	- St. Vincent (b,a,d)	0.7037–0.7043 (14)	0.7040
e)	South Sandwich Is. (b,a,d)	0.7031–0.7041 (11)	0.7037
f)	Solomon Is.-New Georgia (b,a,d)	0.7030–0.7043 (13)	0.7037
g)	Papua - New Britain (b,a,d,r)	0.7034–0.7037 (12)	0.7035
	- Various Islands (b,a,d)	0.7033–0.7043 (29)	0.7038
	- Mainland (b,a,d,r)	0.7036–0.7053 (10)	0.7042
h)	Mariana Arc (b,a)	0.7037–0.7038 (2)	0.7038
i)	Tonga (b,a,d)	0.7036–0.7043 (8)	0.7040
j)	Sunda Arc - tholeiites (b,a,d)	0.7040–0.7044 (9)	0.7042
	- calc-alkaline (b,a,d)	0.7039–0.7059 (67)	0.7047
k)	Eastern Sunda Arc (b,a,d)	0.7054–0.7091 (20)	0.7065
l)	New Zealand - Taupo region (b)	0.7041–0.7043 (4)	0.7042
	- Taupo region (a)	0.7045–0.7062 (12)	0.7055
m)	Greece - Santorini (b,a)	0.7045–0.7057 (6)	0.7050
n)	Peru - central (a,d)	0.7042–0.7051 (4)	0.7046
	-southern (Barroso)	0.7054–0.7068 (8)	0.7062
	-southern (Arequipa)	0.7067–0.7079 (16)	0.7074
o)	Chile - central, southern (b,a)	0.7038–0.7042 (6)	0.7040
	- northern (a,d)	0.7050–0.7070 (12)	0.7060
	- northern (r)	0.7052–0.7104 (8)	0.7080

All isotopic ratios normalized to 0.70800 (E and A standard) or 0.71022 (NBS 987

[From Kay et al., 1978, Table 2]

Correlations between $^{87}Sr/^{86}Sr$ and bulk chemistry have been noted for some arcs. For the New Guinea arcs $^{87}Sr/^{86}Sr$ tends to be higher in the more silicic rocks (Page et al., 1974; DePaolo and Johnston, 1979). $^{87}Sr/^{86}Sr$ may also correlate with Rb/Sr, giving linear arrays, called "pseudo-isochrons" by Brooks et al., 1976. Although age significance has been attached to the slope of these linear arrays, the justification for this has been much disputed (e.g., Roddick and Compston, 1977; DePaolo, 1981a).

$^{87}Sr/^{86}Sr$ of andesite suites developed upon thick crust of pre-Mesozoic age often lie outside the range given by the intra-oceanic rocks. Values commonly fall between 0.704 and 0.708. This is usually interpreted as implicating old continental lithosphere as an important factor in the genesis of these rocks. Continental margin batholiths may also have initial $^{87}Sr/^{86}Sr$ (Sr_i) of 0.703 or less (e.g., Peninsular Ranges batholith, 0.7026: Early and Silver, 1973; Sierra Nevada batholith, 0.7032: Kistler and Peterman, 1973), but commonly are much more radiogenic. Even when igneous rocks with obvious metasedimentary protoliths are excluded, Sr_i can still range to 0.710 or higher (Compston and Chappell, 1979).

Within the Peninsular Ranges batholith Sr_i increases regularly eastwards, from about 0.703 to 0.708 (Early and Silver, 1973; Silver and Early, 1977). Values of Sr_i range from 0.7027 to 0.706 in rocks from that part of the batholith for which there is no evidence for the existence of pre-Mesozoic continental crust (L.T. Silver, personal communication). Thus, any model that attempts to explain the origin of the rocks of the Peninsular Ranges batholith must be able to explain the presence of rocks

with quite radiogenic $^{87}Sr/^{86}Sr$ (≈0.706) in an area apparently devoid of pre-existing old (pre-Mesozoic) continental crust. This situation contrasts markedly with that of the Sierra Nevada batholith to the north, where there are relatively few Cretaceous igneous rocks having Sr_i between 0.704 and 0.706, and a huge volume of rock having Sr_i of 0.706 or more (Kistler and Peterman, 1973).

The San Jacinto Mountains appear to be underlain by pre-Mesozoic crust, presumably the southwestern-most extremity of the North American continent. As such they are analogous more to the Sierra Nevada batholith to the north than to the main volume of the Peninsular Ranges batholith to the south. Even here, however, in a place where the California batholith is apparently transitional from an intra-oceanic to a continental margin construct the data can be interpreted as showing that the vast bulk of the added igneous materials (80% or more) share similar source compositions. Put another way, it appears that the contribution to the San Jacinto igneous construct from old continental lithosphere is volumetrically minor.

Lead

The isotopic composition of lead from active orogenic andesitic arcs is summarized on Fig. 12.2.. Arc rocks tend to have higher $^{207}Pb/^{204}Pb$ for a given $^{206}Pb/^{204}Pb$ than do N-MORB, although some atypical MORB and some ocean island rocks overlap the arc associations. Data from northern Chile and Peru are interpreted as showing evidence for involvement of old high μ ($^{238}U/^{204}Pb$) material, generally interpreted to be continental crust or sediments derived there-from (Tilton, 1979; Tilton and Barreiro, 1979; McNutt *et al.*, 1979). Low μ material incorporation

Figure 12.2. Lead isotopic composition of selected Cenozoic andesite suites. Data from Sun, 1980. Field for Sierra Nevada batholith from Doe and Delevaux, 1973; Rubidoux leucogranite from Banks and Silver, 1964. Field for "Precambrian Leads" from L.T. Silver, unpublished data.

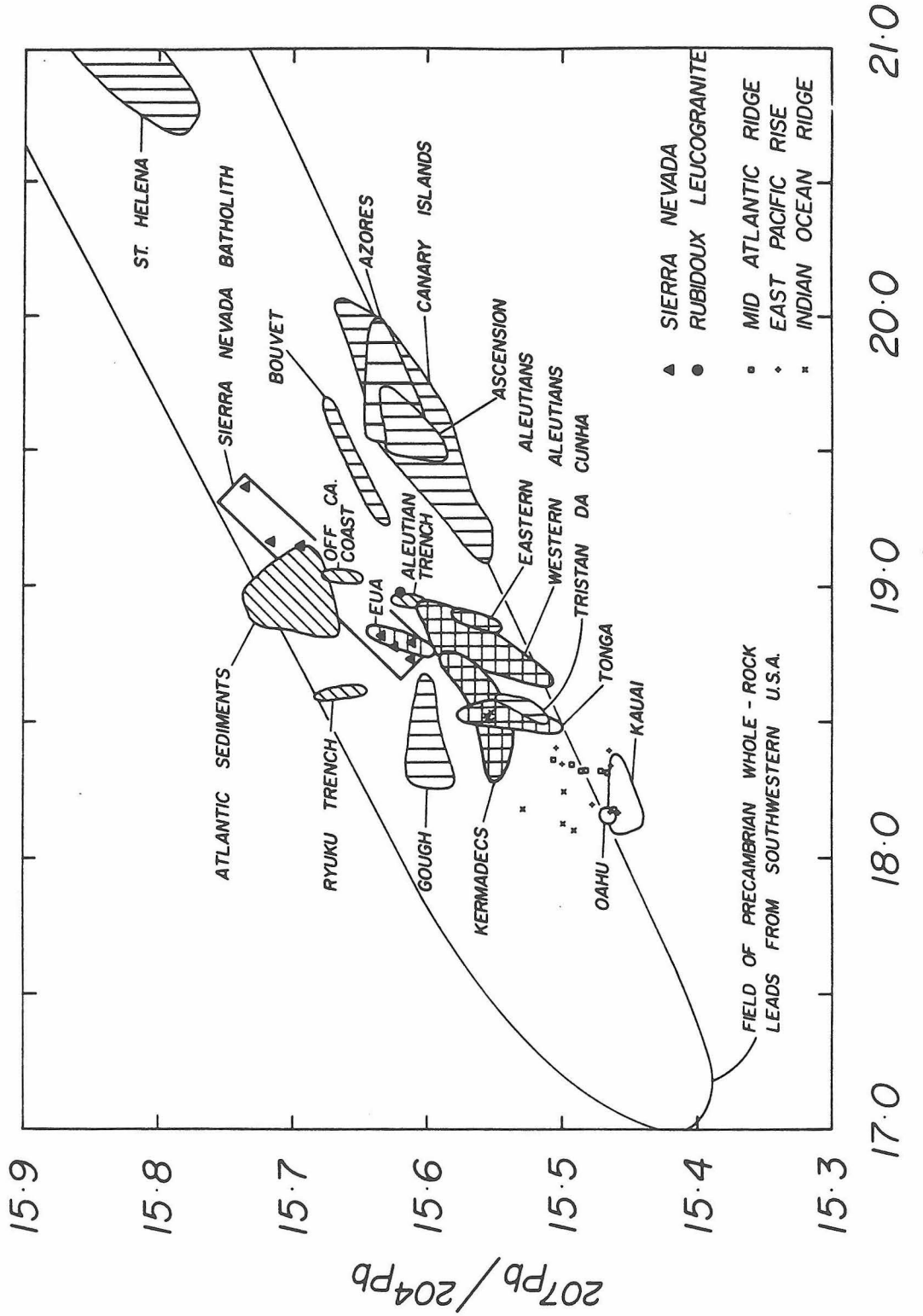
ST. HELENA
SIERRA NEVADA BATHOLITH
BOUVET
AZORES
CANARY ISLANDS
ASCENSION
ALEUTIANS
ATLANTIC SEDIMENTS
OFF CA. COAST
ALEUTIAN TRENCH
EUA
EASTERN ALEUTIANS
WESTERN ALEUTIANS
TRISTAN DA CUNHA
RYUKU TRENCH
TONGA
KAUAI
GOUGH
KERMADECS
OAHU
FIELD OF PRECAMBRIAN WHOLE - ROCK LEADS FROM SOUTHWESTERN U.S.A.
SIERRA NEVADA
RUBIDOUX LEUCOGRANITE
MID ATLANTIC RIDGE
EAST PACIFIC RISE
INDIAN OCEAN RIDGE
15·9
15·8
15·7
15·6
15·5
15·4
15·3
17·0
18·0
19·0
20·0
21·0
207Pb/204Pb
206Pb/204Pb

Figure 12.2

(granulites?) is indicated by data from one volcano (Tilton and Barreiro, 1979). The total data base can be interpreted as showing derivation from oceanic crust or mantle with minimal (<0.5%)[e.g.,Tonga-Kermadec: Oversby and Ewart, 1972], minor (≈ 2%)[Aleutians: Kay et al., 1978] or considerable [Andes: Tilton and Barreiro, 1979] incorporation of recycled continental crustal material. The role of possible enriched (high μ) subcontinental lithosphere in the genesis of the high $^{207}Pb/^{204}Pb$ suites is difficult to evaluate, although it is presumably not important for the intra-oceanic arcs. The apparently contradictory generalizations made from Pb isotopic data obtained from specific arc systems (cf., Oversby and Ewart, 1972, with Donnelly, 1971) serve to reinforce the conclusion that each arc segment is a unique product of its particular tectonic situation.

Published lead data for the Sierra Nevada batholith show a considerable range in $^{206}Pb/^{204}Pb$ (18.73-19.37) for a lesser variation in $^{207}Pb/^{204}Pb$ (15.61-15.71)[Doe and Delevaux, 1973]. These data define a linear array with an "age" of 2900 m.y., and are interpreted as indicating the involvement of old crustal materials in the generation of this batholith; the apparent "age" of 2900 m.y. is not thought to have geological significance (Doe and Delevaux, 1973). An analysis of a single leucogranite sample from the Peninsular Ranges batholith has slightly lower $^{207}Pb/^{204}Pb$ for a given $^{206}Pb/^{204}Pb$ than the Sierra Nevada samples (Banks and Silver, 1964). Work in progress (L.T. Silver, personal communication, 1983) indicates that the batholithic rocks from the San Jacinto Mountains have high $^{206}Pb/^{204}Pb$ (to 19.3), similar to that observed for other plutonic rocks from the eastern Peninsular Ranges batholith.

Neodymium

A steadily increasing number of $^{143}Nd/^{144}Nd$ analyses is demonstrating that rocks from intra-oceanic arcs have a restricted range of Nd isotopic composition, from +7 to +10 ε units (DePaolo and Wasserburg, 1976, 1977; O'Nions et al., 1977; Hawkesworth et al., 1977; DePaolo and Johnston, 1979). The available Nd data for modern volcanic rocks from a number of tectonic environments have been summarized by Shaw (1983)[Fig. 12.3]. The island arc data have been interpreted (e.g., DePaolo and Johnston, 1979) as indicating derivation from a mixture of sub-oceanic mantle and hydrothermally altered MORB. These authors note also that all of their well characterized samples spanning a considerable compositional range (SiO_2 = 49.2-75.6 wt.%; Mg# = 72-33) are thought to have undergone at least some fractional crystallization prior to eruption. No correlation exists between $^{143}Nd/^{144}Nd$ and composition, although these same samples show a positive correlation between $^{87}Sr/^{86}Sr$ and SiO_2.

The situation is not as simple within the continental margin rocks. Published ε_{Nd} for Quaternary volcanic rocks are as low as -7 (Hawkesworth et al., 1977). Values obtained for continental margin batholiths are as low (to -7.6 for the Sierra Nevada batholith and -6.4 for the Peninsular Ranges batholith: DePaolo, 1981b). Such low ε_{Nd} values have been generally interpreted as proving the incorporation of a large component of upper crustal material into these rocks (e.g., DePaolo, 1981b), but such interpretations are by no means unique (e.g., O'Nions et al., 1979; McCulloch et al., 1983). DePaolo (1981) presented Nd and Sr isotope data for 16 samples of igneous rock from the Peninsular Ranges batholith. ε_{Nd} varies from +8.2 to -6.4, and correlates negatively with

Figure 12.3. Isotopic composition of neodymium for rocks from various tectonic environments. From Shaw, 1983.

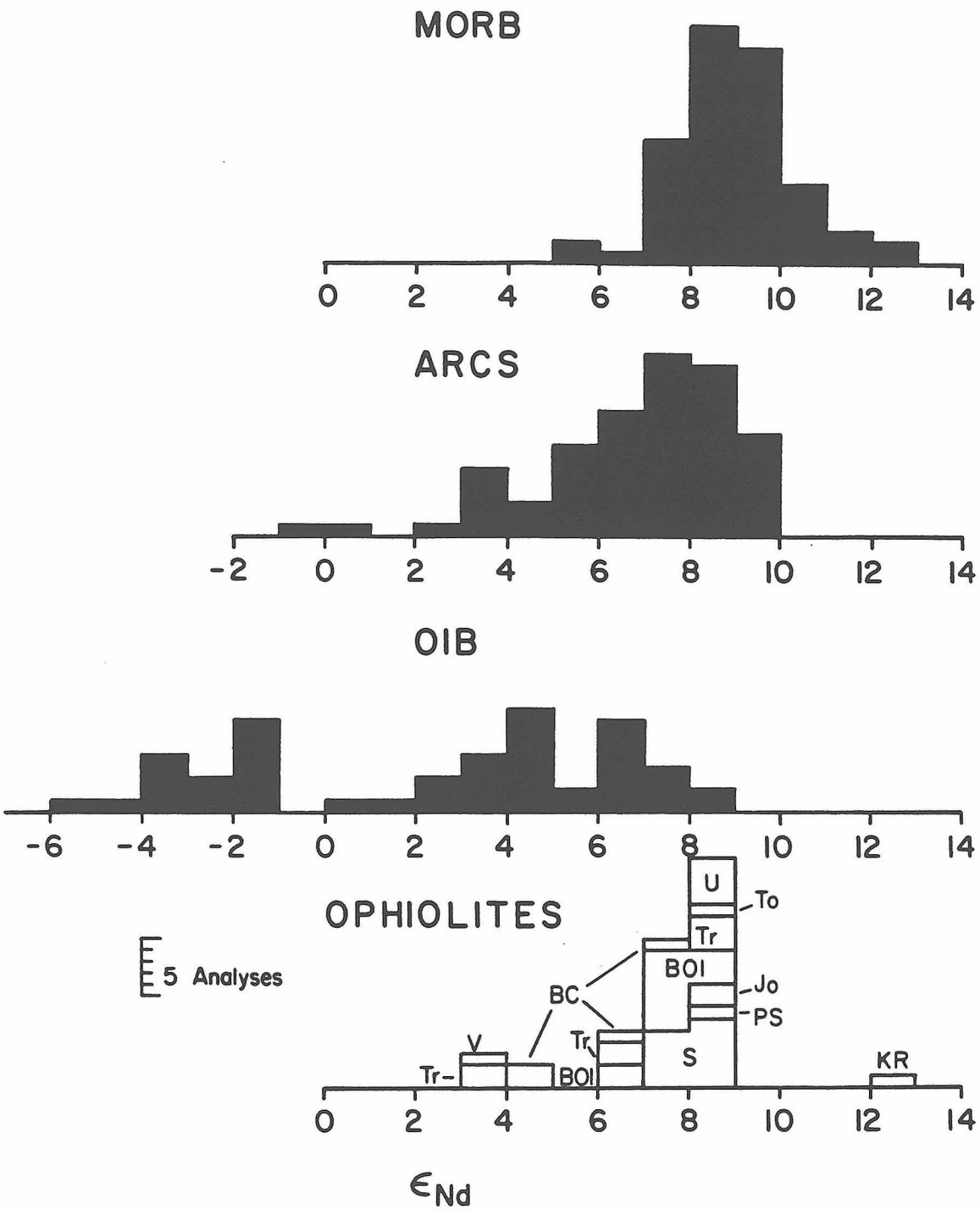
MORB
0 2 4 6 8 10 12 14
ARCS
-2 0 2 4 6 8 10 12 14
OIB
-6 -4 -2 0 2 4 6 8 10 12 14
OPHIOLITES
5 Analyses
U
To
Tr
BOI
Jo
PS
BC
V
Tr
Tr
BOI
S
KR
0 2 4 6 8 10 12 14
εNd

Figure 12.3

Figure 12.4. $\varepsilon_{Nd} - \varepsilon_{Sr}$ diagram for rocks from the Sierra Nevada and Peninsular Ranges batholiths. Data from DePaolo, 1981.

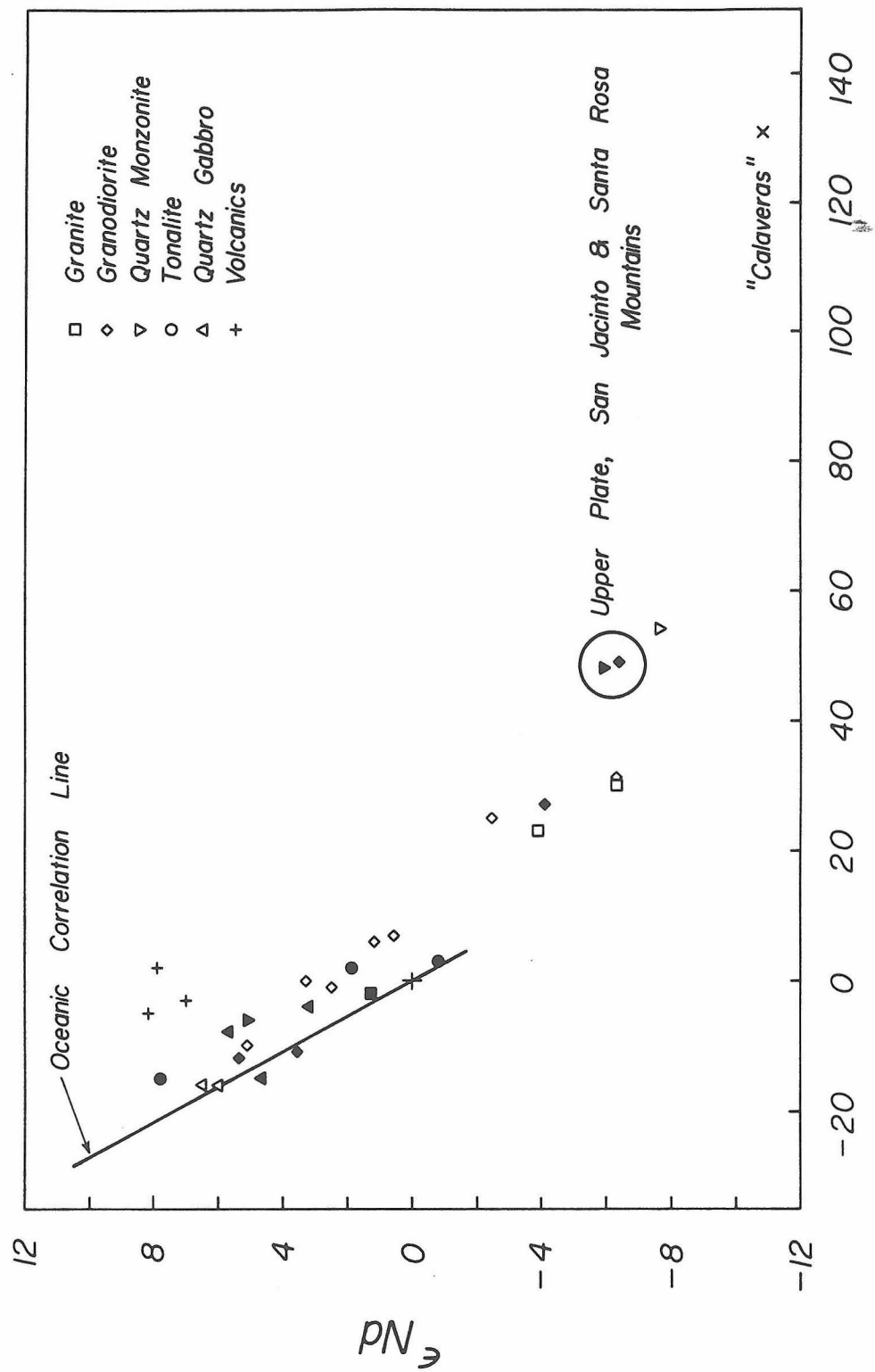
Granite
Granodiorite
Quartz Monzonite
Tonalite
Quartz Gabbro
Volcanics
Oceanic Correlation Line
Upper Plate, San Jacinto & Santa Rosa Mountains
"Calaveras"
12
8
4
0
-4
-8
-12
-20
0
20
40
60
80
100
120
140
ϵ_{Nd}
ϵ_{Sr}

Figure 12.4

ε_{Sr} (Fig. 12.4). DePaolo argued that these data proved the involvement of upper crustal material in the genesis of these rocks. The data break naturally into two groups, those that lie along the "mantle array" and those that have higher ε_{Sr} for a given ε_{Nd} than does the mantle array (Fig. 12.4). The three samples from the latter group are from within or above the post-batholithic eastern Peninsular Ranges mylonite zone (Sharp, 1979) and have been possibly transported some distance westward from an initial position east of the continental edge (Silver, 1982, 1983; see also Ch. 2). The plutons of the upper plate probably were intruded through Precambrian basement and its pre-Mesozoic cover (Taylor and Silver, 1978; Silver and Anderson, 1983; L.T. Silver, personal communication, 1983). The combined Sr-Nd isotope data for these samples are thus in accord with indications from other evidence ($\delta^{18}O$ values, traces of old inherited zircon, relatively K-rich chemistry: Taylor and Silver, 1978) that old continental materials have been involved in their genesis.

Interpretation of the data from the more westerly samples is more difficult. All samples plot along the mantle array, spanning the range from continental basalt to N-MORB sources. On the basis of the Sr-Nd isotope data these rocks could have been obtained from a mixture of mantle sources similar to those currently generating continental flood basalts and those generating N-MORB. Many other possibilities exist that can also explain this data array, so that the Sr-Nd isotopic data taken in isolation are inconclusive in constraining models for the genesis of the Peninsular Ranges batholith.

Oxygen

On an atomic basis oxygen is easily the most important element of almost any rock, including those of andesitic composition. It is now generally assumed that large variations in the ratio $^{18}O/^{16}O$ can only be produced in nature by low-temperature processes at the Earth's surface (e.g., Taylor, 1968). The small range of $\delta^{18}O$ values obtained from fresh basalts from all tectonic environments (approximately +5.4 to +6.2: Taylor, 1968; Muehlenbachs et al., 1973; Kyser et al., 1982) are interpreted as indicating a mantle with homogeneous oxygen and as showing that petrological processes within the mantle (partial melting, crystal fractionation, crystal-vapour equilibria) are not capable of changing $\delta^{18}O$ by more than a few tenths per mil. Theoretical and experimental studies (e.g., Muehlenbachs and Kushiro, 1974; Kyser et al., 1982) as well as studies of mantle-derived xenocrysts (Kyser and O'Neil, 1980) support these conclusions. Fractionation at lower but still magmatic temperatures (such as within the crust) also appears incapable of extensive modification of $^{18}O/^{16}O$. Most estimates suggest that the maximum amount of fractionation produced by low pressure crystal separation is 1.5 per mil or less (Taylor and Silver, 1978; Matsuhisa, 1979; Muehlenbachs et al., 1981; Chivas et al., 1983). Thus, unless there exists a significant mantle reservoir (for oxygen) that has not yet been characterized it appears that the maximum $\delta^{18}O$ value attainable in mantle-derived rocks that have undergone even extensive crystal-liquid fractionation before eruption at the surface is approximately +7.5. With the qualification noted above, it thus appears that $\delta^{18}O$ values of +8 or greater require the incorporation of oxygen that has had a prior low-temperature upper crustal history.

The $\delta^{18}O$ values of most intra-oceanic andesites fall between +5.5 and +7.0, within the range of values inferred for purely mantle-derived melts. Indeed, increase of $\delta^{18}O$ by low pressure crystal fractionation has been argued for several situations (e.g., Matsuhisa, 1979; Chivas et al., 1982), suggesting that other rocks with high $\delta^{18}O$ values formed similarly. If the mean $\delta^{18}O$ value of the entire oceanic crustal section is +5.7±0.2 (Gregory and Taylor, 1981) then incorporation of even large amounts of such material will not be detectable by its oxygen isotope signature.

Continental margin volcanic and plutonic arcs show more complex behaviour. Partial fusion of metasedimentary rocks within the crust gives derived liquids with high $\delta^{18}O$ values (>+10, O'Neil and Chappell, 1977). However, similarly high $\delta^{18}O$ values are obtained from batholiths where there is no chemical or mineralogical evidence for the involvement of a mature sedimentary component (e.g., Peninsular Ranges batholith, +6 to +13: Taylor and Silver, 1978; Sierra Nevada batholith, +6 to +12: Masi et al., 1981). High values (+7.0 to +9.2) have also been obtained for andesites from the Banda arc beneath which sialic crust is not expected (Magaritz et al., 1978). For the Banda arc situation incorporation of subducted continentally-derived sediment has been suggested (Magaritz et al., 1978). Depending on the oxygen isotopic composition of this sediment, something of the order of 10-20% of the oxygen could have been derived from such a source.

12.2.3 EXPERIMENTAL PETROLOGY

Recent reviews of experimental data pertinent to the problem of andesite genesis have been published by Wyllie (1978, 1981), T.H.

Green (1980) and Gill (1981). All agree that water has an important role in andesite genesis, both during partial fusion in the mantle and at higher levels by both suppressing plagioclase stability and by stabilizing amphibole (and biotite) as crystallizing phases. The presence of amphibole requires at least 3 wt.% water in the liquid (Eggler, 1972), and it is generally more abundant in plutonic than volcanic rocks, perhaps because exsolution of volatiles is limited by increased confining pressure (Burnham, 1975).

The work of several groups (Nicholls and Ringwood, 1973; Nicholls, 1974; D.H. Green, 1973, 1976; D.H. Green et al., 1979; Wyllie et al., 1976) argues against the derivation of liquids of andesitic composition by partial fusion of hydrous peridotite at depths >30 km. The experimental data do suggest that melting of water-rich peridotite generates high-Si high-Mg alkali-poor liquids with compositions akin to boninite and the clinoenstatite-bearing andesite from Cape Vogel, New Guinea (D.H. Green, 1973, 1976), or Ni-rich high Mg andesite from Teraga-Ike, Japan (Tatsumi and Ishizaka, 1981).

The partial melting of subducted oceanic crust has been explored experimentally by Stern and Wyllie (1978) and Sekine et al., (1981) at pressures corresponding to depths of about 100 km. This work demonstrated that siliceous liquids can be generated by melting of gabbroic (basaltic) composition with varying amounts of water present. Water-undersaturated siliceous liquids with compositions broadly similar to those of andesites coexist with residual eclogite through a wide temperature interval. These liquids generally have higher Ca/(Mg + Fe) than do andesites, and it was concluded that andesite cannot be a primary melt

of either dry or wet quartz eclogite (at 30 kb.). The closest match between andesite and the liquid obtained from partial fusion of a basaltic composition is for dry systems, but the pyroxene composition on the liquidus is incorrect, and there are systematic differences between the Ca/(Mg + Fe) of actual andesites and the Ca/(Mg + Fe) of the eutectic-like melts derived in the experimental system (Stern and Wyllie, 1978; Wyllie, 1978).

The fusion of amphibolite has been studied by Allen et al. (1975) and Allen and Boettcher (1978, 1983) who suggested that andesite magmas are produced by amphibole-melt reactions at pressures of approximately 20 kb and temperatures in excess of 950°C. Their more recent work (Allen and Boettcher, 1983) shows that amphibole is stable to much higher pressures than was indicated in the earlier work, and they conclude that the stability of amphibole in basaltic and andesitic compositions is limited by melting reactions at high temperatures, and by dehydration reactions (to give garnet-bearing assemblages) at high pressures. Silicate liquids obtained during the experimental runs were water-rich and variable in composition, but had low Mg/(Mg + Fe) and high Al and Si. No effort was made to match "phenocryst" compositions, as was done by Stern and Wyllie (1978), although compositional similarities (of garnet and glass) reported in the two studies suggest that the conclusions made by Stern and Wyllie outlined above might apply to the work of Allen and Boettcher as well. Clinopyroxene compositions reported by Allen and Boettcher (1983) are much less aluminous than those reported by Stern and Wyllie (1978), apparently the result of co-existence with an aluminous amphibole.

Burnham (1979) calculates that melting of an amphibolitized peridotite at 22-23 kb will produce a variety of melts ranging in composition from trondhjemitic (at 700°C) to dioritic (at 1050°C). This results from the thermally induced breakdown of amphibole to produce garnet peridotite plus hydrous melt, as demonstated experimentally. The recent work of Allen and Boettcher (1983) implies that revision of the pressure estimates are needed, but the main conclusions should remain.

Wyllie (1981) points out that the importance of the process suggested by these various workers (amphibole-breakdown induced melting) cannot be fully evaluated until a much better understanding of the thermal structure beneath the arc is available. In particular, it is critical to know whether the geothermal gradient allows for dehydration of amphibolite to eclogitic assemblages before the depth (pressure) for amphibole-breakdown induced melting is reached.

Wyllie, in a review of the experimental work on wet melting of rocks of gabbroic composition (Wyllie, 1981) concludes that given the very wide fusion interval of quartz eclogite in the presence of H_2O (some 700°C), it seems likely that any hydrous, siliceous magmas produced would leak from the subducting slab into the overlying mantle, as proposed by Nicholls and Ringwood (1973). The potential role of amphibolite is uncertain, depending on whether amphibole dissociates to an anhydrous mineralogy (eclogite) before it reaches the temperatures needed for amphibole-melt reactions. If amphibole dissociates before the onset of melting then the hydrous fluids thus produced could contain substantial amounts of dissolved SiO_2 (Nakamura and Kushiro, 1974), REE (Mysen, 1979) and alkalis and other incompatible elements (K: Stern and Wyllie, 1978; Rb, Cs, Ba,

well as on the composition of the fluid (e.g., Flynn and Burnham, 1978).

These details are important because such liquids [dubbed "IRS fluids" by Gill (1981)] could scavenge substantial amounts of radiogenic trace elements (Sr, Nd, Pb, U) or anomalous composition tracers (He, C, O, perhaps Be) from the downgoing slab.

12.2.4 MASS BALANCE CONSIDERATIONS

Obviously, the reservoirs from which it is proposed to derive andesites and their plutonic equivalents must contain sufficient of each species present in the observed rock that derivation is possible on a simple atom (or mass) balance basis. Various authors have attempted to demonstrate that a particular volcanic edifice can be obtained by the processing of only small proportions of the subducted oceanic crust beneath the structure (e.g., Francis and Rundle, 1976; Maaløe and Petersen, 1981). Such calculations usually concentrate on the surficial expression of magmatism (the volcano) and ignore those portions of the liquid that fail to reach the surface. They also generally consider only bulk volume considerations when tighter constraints may be possible using a particular species.

Consider the situation for potassium. Let us assume that the mean K_2O content of the upper 5 km of oceanic crust is 0.1 wt.% (e.g., McCulloch et al., 1980), that the mean density of this crust is 3.33 gm cm^{-3}, and that crust is being subducted at 80 km/m.y.. From this crust we wish to obtain a certain amount of liquid with the bulk composition of an andesite (K_2O = 2.0 wt.%, ρ = 2.67 gm/cm^3). With these parameters, it is possible to generate 15 km^3 of andesitic liquid/million years/km of

trench. How does this relate to the volume of some andesitic constructs?

Bristol Island, in the South Sandwich arc system, has a volume above sea level of 60 km^3, and was built in about 4 m.y.. Maaløe and Petersen (1981) estimate a production rate of ≈1.35 km^3/m.y./km trench, but this is just for that part of the island above sea level. Francis and Rundle (1976) estimated an eruption rate of 5 km^3/m.y./km trench for the central Andes, and Marsh (1979) estimates a similar total magma production rate for all island arcs. It thus appears that it is possible to match at least eruption rates with plausible generation rates if the source is entirely within the down-going slab.

The presence of linear batholiths that intrude contemporaneous volcanic ejecta (e.g., Silver et al., 1956, 1963, 1969) implies that the surficial constructs are not the only products of andesitic and related magmatism. The area now underlain by the Peninsular Ranges was described by Silver et al. (1956, 1963) as an "island archipelago", most of which apparently develped in Early Cretaceous time (Silver et al., 1979). The crust beneath the Peninsular Ranges is now some 30 to 35 km thick (Shorr and Raitt, 1958; Biehler in Elders et al., 1972; Oliver, 1980); metamorphic assemblages in the metasedimentary rocks of the central and eastern peninsula imply that perhaps 10 to 15 km of supracrustal materials have been removed during unroofing of the batholith (Schwarcz, 1969; Theodore, 1972; this work)). Geological considerations and analogy with both the western part of this batholith and with other batholiths suggest that much of the material removed may have been part of the whole igneous construct as well. If so, 20 km may be a conservative estimate for the thickness of crust formed during batholithic development.

If we assume that about half of the crust, say a layer 20 km thick, was added during Early Cretaceous time, what implications are there for magma genesis? The zircon data strongly suggest that igneous activity in the San Jacinto Mountains area was restricted to a very short period of time, perhaps 2 m.y.. During this time interval a 20 km wide belt of igneous materials developed; i.e., for every 1 km of trench, 1 x 20 x 20 km^3 of igneous rock was added to the crust (or 200 km^3/m.y./km trench). A similar width (and thus probably volume) of material was being added simultaneously in a north-northwest striking belt for at least several hundred kilometers to the south (Silver et al., 1979; L.T. Silver, personal communication, 1983), so that the San Jacinto Mountains do not appear to be an unusual situation. It was estimated above that completely efficient processing of oceanic crust being subducted at 80 km/m.y. could yield 15 km^3/m.y./km trench, so clearly either subducted oceanic crust is not the sole source for these magmas, or one or more of the assumptions made is in gross error. The trace element and isotopic data strongly suggest that the extent of lateral migration of rising igneous liquids has been minimal. The relatively high proportion of igneous to metasedimentary materials, and the continuous west to east progression of the locus of igneous activity within the (eastern) batholith (Silver et al., 1979) lends support to this conclusion, so that collection of magma from a horizontally continuous source region does not seem a viable mechanism to overcome the difficulty. Materials could have been added from the mantle as slab-derived liquids moved upward. If the underlying mantle contained, on average 100 ppm K, had a density of 3.33 gm/cm^3 and was 120 km thick each 1 km x 1 km vertical column could yield 0.45 km^3 of andesite (ρ = 2.67 gm/cm^3, K_2O = 2.0 wt.%), in this case in 2 m.y., or,

contained, on average 100 ppm K, had a density of 3.33 gm/cm^3 and was 120 km thick each 1 km x 1 km vertical column could yield 0.45 km^3 of andesite (ρ = 2.67 gm/cm^3, K_2O = 2.0 wt.%), in this case in 2 m.y., or, for a 20 km wide belt, 4.5 km^3/m.y./km trench. This figure could be doubled if lateral movement allows processing of an area twice as extensive as the surface expression of magmatic activity, and is obviously highly dependent on the K_2O content assumed for the mantle.

These calculations are most simply interpreted as suggesting the importance of a relatively K-rich source (or component in the source) compared to MORB or normal oceanic mantle. The coherence of the chemistry of the San Jacinto rocks (where enriched subcontinental lithosphere may have been present) with those from elsewhere in the batholith (where subcontinental lithosphere was probably absent) argues against this component having been enriched subcontinental lithosphere. The long-term depletion (in Rb relative to Sr, and Nd relative to Sm when compared with chondritic abundances) of the source for the western rocks indicated by both the Nd and Sr isotope data supports this conclusion.

It appears that, even within the constraints imposed by poorly known model parameters, that it is not possible to obtain the potassium for the San Jacinto igneous construct by completely efficient processing of <u>both</u> the basaltic component of down-going slab and the overlying mantle unless that mantle has highly anomalous composition [specifically, recent K (and presumably Rb, REE and other incompatible element) addition].

12.2.5 CONCLUSIONS

During the past few years consensus has developed on many aspects of andesite genesis, and, by implication, the genesis of contin-

compositions do not support the concept of primary magmas for andesites and associated lavas from mantle or subducted crust. Complex, multi-stage processes appear to be more likely which is consistent with recent interpretations of geochemical data." For intra-oceanic arcs the combined isotopic data are generally consistent with derivation from mixtures of different "types" of mantle material, perhaps with a slab-derived component in some areas. An important point is the potential for uniqueness of each arc segment - conclusions made from one area cannot be simply extended to the whole phenomenon. A small amount (≈2%) of subducted sediment is implicated in some situations (e.g., Antilles: Donnelly, 1971; Aleutians: Kay et al., 1978) but not in others (Tonga-Kermadec: Oversby and Ewart, 1972). The combined Sr and Nd isotope data suggest some involvement of altered oceanic crust, and there are indications that this is more important in the generation of more silicic rocks (e.g., Page et al., 1974; DePaolo and Johnston, 1979). Except in a few special cases (particularly the Banda arc: Magaritz et al., 1978) the oxygen isotope data are entirely in accord with mantle derivation.

Both experiment and calculation have been used to demonstrate that it is possible to proceed along the calc-alkaline compositional trends by fractional crystallization. In fact, most experimental work is interpreted as requiring the operation of fractional crystallization in the generation of andesitic liquids. At low SiO_2 contents olivine is the most important separating phase, at medium SiO_2 plagioclase, orthopyroxene, augite and magnetite dominate, and at higher SiO_2 or high H_2O amphibole and biotite may also become important (e.g., Gill, 1981). Other phases, such as garnet or perhaps high pressure hydrous phases (titanoclinohumite, titanochondroite) may be important under some conditions

phases, such as garnet or perhaps high pressure hydrous phases (titanoclinohumite, titanochondroite) may be important under some conditions (e.g., T.H. Green, 1980). Evidence for fractionation is supported by trace element covariance patterns, especially among compatible elements (Cr, Ni, V), by evidence from oxygen isotope systematics (e.g., Matsuhisa, 1979; Chivas et al., 1982), by the composition of glass inclusions in phenocryst phases (e.g., Anderson, 1976), and by least squares mixing calculations (e.g., Mertzman, 1977; Berman, 1981).

The situation for the continental margin arcs is less well clearcut, although there is nothing to suggest that the same processes that operate in the oceanic environment are not also operative here. The complications apparently come from the much more varied source materials present within the continental environment. The isotope data indicate the involvement of much more diverse source materials; oxygen isotope data appear to require that upper crustal rocks are important in the generation of at least some systems. Major involvement of subducted sediment is suggested for at least one arc (Banda: Magaritz et al., 1978) apparently developed on thin (oceanic?) crust but adjacent to thick continental crust both behind the arc and in the subducting plate.

Many batholiths emplaced into old continental terrains appear to have been developed largely by crustal reprocessing (e.g., White and Chappell, 1977; Compston and Chappell, 1979; Ben-Othman and Allegre, 1979; Farmer and DePaolo, 1983) with either metasedimentary or pre-existing igneous materials involved (Chappell and White, 1974). Even in areas of major crustal anatexis, the common occurrence of mantle-derived materials, particularly along graben-bounding faults, argues for at least some juvenile addition even if its major role is in heat transfer (e.g.,

Chappell and White, 1976; Cole, 1973, 1979).

The thicker low density crust that liquids traverse before crystallizing (compared with the intra-oceanic situation) will impede density-contrast-driven upward movement; this potentially increases the importance of low pressure crystal fractionation in modifying the composition of the original liquids. This thick crust could also act as a density filter, analogous to the situation suggested for the mid-ocean ridges (Sparks et al., 1980; Stolper and Walker, 1980), allowing less mafic and more water-rich rocks to move higher into the crust.

12.3 A MODEL FOR THE GENERATION OF THE IGNEOUS ROCKS OF THE SAN JACINTO MOUNTAINS

The various observations reviewed above seem to require a predominantly mantle source for the rocks of the Peninsular Ranges batholith. Interpretation of geochemical and experimental data suggest that direct derivation of large volumes of andesitic or tonalitic liquid from relatively unmodified mantle appears unlikely. This implies that significant amounts of crystal fractionation are important in the genesis of the liquids parental to the dominant tonalites of this area. Quantitative evaluation of the effects of such a process, particularly if largely occurring at mantle depths, is not possible with the available data.

Although the plutonic rocks of the San Jacinto Mountains show evidence for involvement of continental lithospheric (most probably subcontinental lithosphere) materials in their genesis, the amount of this component appears to be relatively small in comparison with the contributions of the other source materials. These other source components appear to be be unrelated to the presence of (presumably overlying)

"types", as well as materials derived from a down-going slab or materials injected into the mantle during some previous event.

A combination of three different components appears capable of at least qualitatively explaining the isotopic data reviewed above. These three components are 1) depleted mantle material, 2) subducted oceanic crust, and 3) subducted sedimentary materials. It is difficult to balance the various available isotopic constraints using only two of these components. A fourth component, such as slightly enriched old subcontinental lithosphere, is needed to fully explain the San Jacinto data array. However, in the development and discussion of the petrogenetic model below the effects of this component are initially ignored.

Figure 12.5 presents diagramatically a model for the generation of the igneous rocks of the San Jacinto Mountains. The primary liquids are derived from a combination of "normal" depleted mantle, slab-derived material, and subducted portions of the Mesozoic accretionary wedge by partial fusion within the mantle. These liquids rise, with crystal fractionation variously increasing SiO_2, alkalis (Na, K, Rb), Sr, and δ^{1} O, and decreasing Mg, Fe, Ca, Mg/(Mg + Fe) and Ca/(Ca + Na). Much of this fractionation may take place at or near the crust-mantle boundary, where the rate of ascent of buoyant magma will be slowed by the decreasing density contrast as it traverses first mantle in which earlier melts have been forced to crystallize (Marsh, 1979), and then relatively light crustal materials. The REE data of Gromet (1979; 1983, written communication) imply that garnet may be an important fractionating or residual phase. These fractionated liquids rise into the crust, where some may collect in large mid-crustal magma chambers. Within these large magma

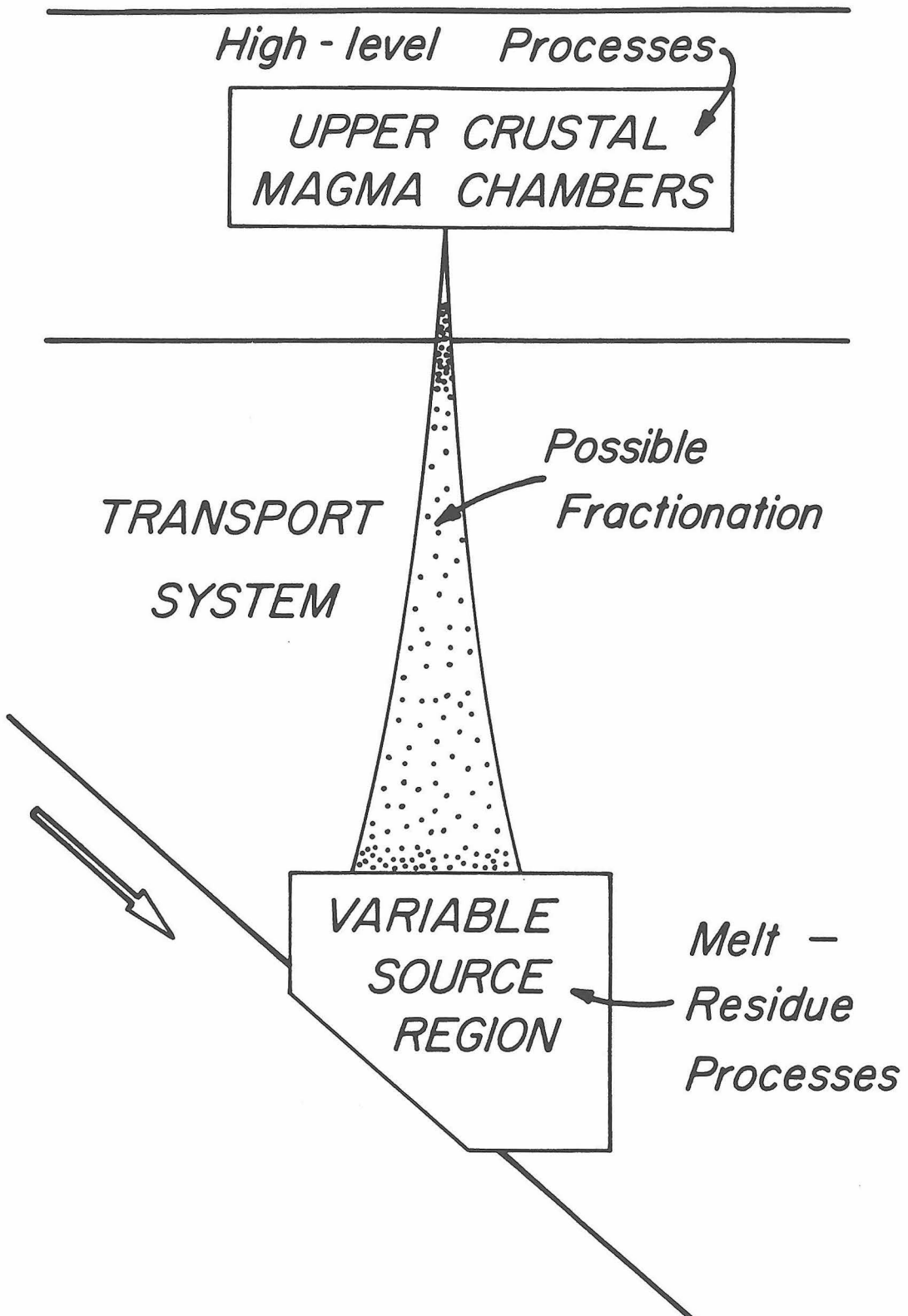

Figure 12.5. Diagram showing in cartoon form a model for the origin of the igneous rocks of the San Jacinto Mountains.

chambers crystallization is controlled by a balance between heat loss, magma and volatile loss (possibly including losses to volcanics), and episodic recharge. The most visible effect of such a dynamic reservoir is to buffer the composition of the precipitated solids that remain, giving a "perched" composition [in the sense of O'Hara, 1977] with monotonous chemical, mineral chemical and stable isotopic properties in an apparently fractionating system. The limited compositional variation within the bulk of the exposed rocks is largely the result of processes acting within this dynamic magma chamber.

Some of the implications for isotope systematics inherent in this model can be explored using Figure 12.6. The parameters used for the three components are listed in Table 12.2. The model depleted mantle is that of Jacobson and Wasserburg's (1979) 'Model II', with the isotope ratios calculated for 100 m.y. ago; the oceanic crust is from McCulloch et al., 1980, but with identical isotopic parameters to those used for depleted mantle. The error possibly introduced by this simplification is small, and should not affect any of the conclusions below. It has the advantage that it potentially allows the effects of sea-water interactions within the upper part of the oceanic crust to be recognized (e.g., McCulloch et al., 1980). A $\delta^{18}O$ value of +6 has been assumed for both depleted mantle and for the bulk composition of the oceanic crust. It is realised that $\delta^{18}O$ within oceanic crust is highly variable, depending on the amount and temperature of hydrothermal fluids that have interacted with a particular volume (Gregory and Taylor, 1981), and that this variability may be in part reflected in any liquids derived from this material.

Figure 12.6. $\varepsilon_{Nd} - \varepsilon_{Sr} - \delta^{18}O$ systematics for mixtures of model depleted mantle, ocean crust and subducted sediment. Numbered curves give $\delta^{18}O$ of mixtures. Peninsular Ranges batholith samples from DePaolo, 1981.

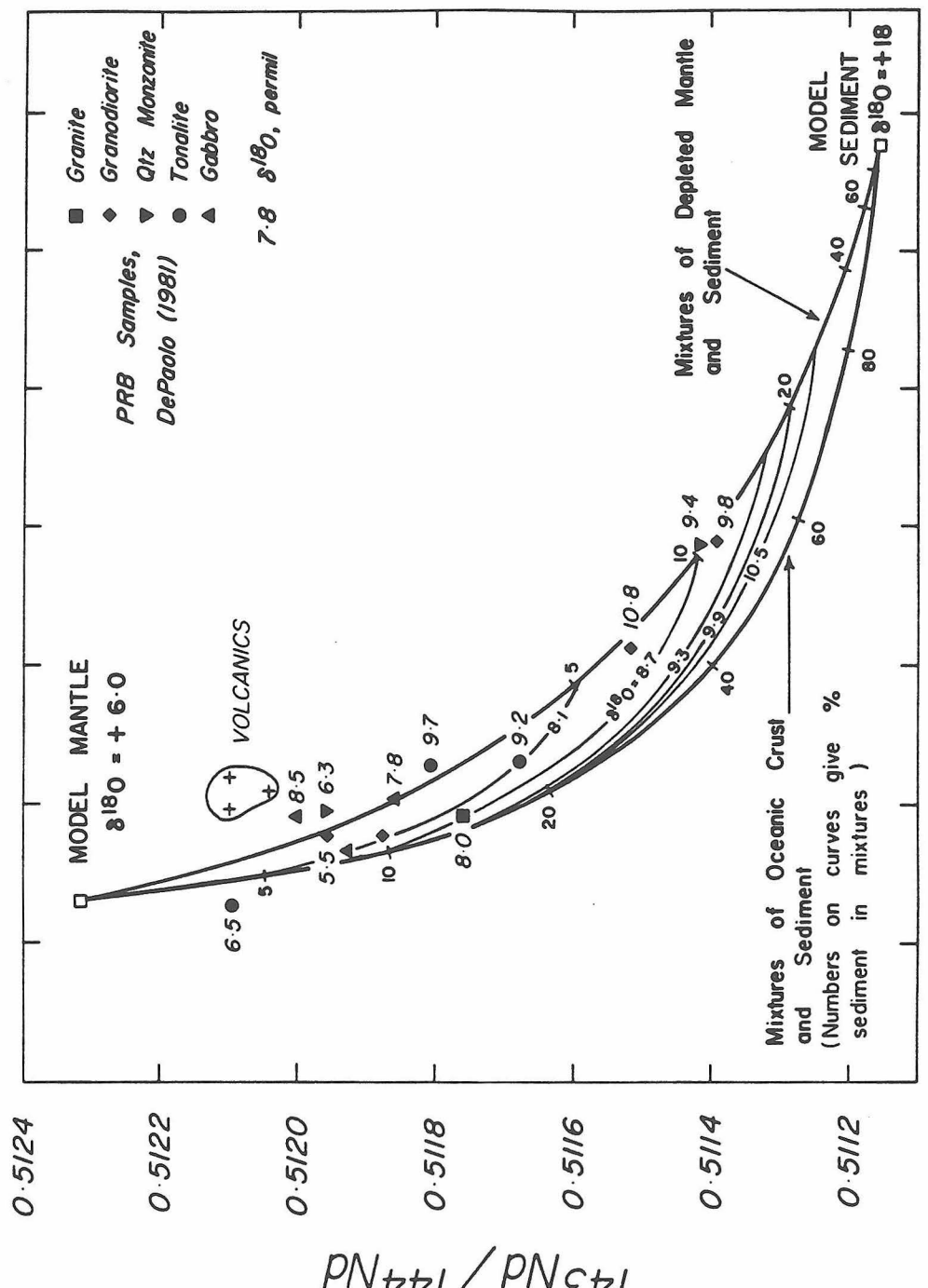
MODEL MANTLE
δ18O = + 6·0
VOLCANICS
PRB Samples,
DePaolo (1981)
Granite
Granodiorite
Qtz Monzonite
Tonalite
Gabbro
7·8 δ18O, permil
Mixtures of Depleted Mantle and Sediment
Mixtures of Oceanic Crust and Sediment
(Numbers on curves give % sediment in mixtures)
MODEL SEDIMENT
δ18O = + 18
δ18O = 8·7
0·5124
0·5122
0·5120
0·5118
0·5116
0·5114
0·5112
0·700
0·704
0·708
0·712
143Nd/144Nd
87Sr/86Sr

Figure 12.6

TABLE 12.2.

Parameters used in mixing model calculations

	DEPLETED[1] MANTLE	OCEANIC[2] CRUST	MODEL[3] SEDIMENT
K (ppm)	53	1100	21600
Rb (ppm)	0.041	0.85[4]	94.6
Sr (ppm)	14.5	160	109
Nd (ppm)	0.74	4.0	22.6
Sm (ppm)	0.29	1.6	4.26
$^{87}Rb/^{86}Sr$			2.511
$^{147}Sm/^{144}Nd$			0.114
$\varepsilon_{Sr}(0)$	-27	-27[5]	
$\varepsilon_{Nd}(0)$	+10	+10[5]	
$\delta^{18}O$	+6[6]	+6[6]	+18[7]
K/Rb	1300	1300[8]	230
Sr/Rb	355	190	1.2
Sr/Nd	19.6	40	4.8

1 Jacobson and Wasserburg (1979), Model II (continuous differentiation)
2 McCulloch *et al.*, (1980). Mean composition of oceanic crust calculated from measured values for the Samail ophiolite
3 Sample FD39('Calaveras' composite), Kistler and Peterman (1973) and DePaolo (1981)
4 Calculated assuming K/Rb = 1300
5 Assumed equal to depleted mantle i.e. no aging or alteration of oceanic crust
6 *e.g.*, Taylor (1968), Kyser and O'Neil (1980)
7 Silver *et al.* (1979). Approximate mean of sediment $\delta^{18}O$ values
8 From Jacobson and Wasserburg (1979), with assumption that there is no separation of K from Rb during formation of oceanic crust

The choice of suitable parameters for a possible subducted sediment component is not as straight-forward. Tectonic considerations that complicate understanding of the relationships of the various sedimentary sequences of western North America have been summarized above (Ch. 2). As well, there are no Nd isotopic data available for the metasedimentary host rocks to the batholith which are plausible candidates for such subducted material. These pre-batholithic rocks have been suggested to be part of an accretionary prism (e.g., Criscione et al., 1978), but may also represent pieces of displaced terranes juxtaposed against the continental margin prior to emplacement of the batholith. These Mesozoic sediments do, however, have age and lithological similarities with the Calaveras sequence of the Sierra Nevada foothills (Ch. 2).

DePaolo (1981) reports Nd data for a "Calaveras" composite collected by P.C. Bateman and P.C.W. Dodge, and analysed for K, Rb, Sr, and $^{87}Sr/^{86}Sr$ by Kistler and Peterman (1973). Recent workers (e.g., Schwieckart, 1981; Saleeby, 1981) subdivide rocks that have in the past been called "Calaveras", and this composite sample may unfortunately contain materials from both the "Calaveras sequence" (Saleeby, 1981), and the Lower Shoo Fly (Schwieckart, 1981), although the Sr isotope results are consistent with this sample being dominated by young (Mesozoic) rather than old materials (Kistler and Peterman, 1973; DePaolo, 1981). This sample has similar Rb, Sr, Sm and Nd concentrations to a composite from the French Valley formation collected by L.T. Silver (Early and Silver, 1973; Gromet, 1979; see Table 12.3), and has been used to model the subducted sediment. A $\delta^{18}O$ value of +18 has been used for this component (Turi and Taylor, 1971; Silver et al., 1979).

TABLE 12.3.

Comparison of sedimentary composites from French Valley formation, Peninsular Ranges, and 'Calaveras' composite, Sierra Nevada foothills

	French Valley formation PSCB-800	'Calaveras' composite FD-39
Collected by:	L.T. Silver	P.C. Bateman and P.C.W. Dodge
Rb (ppm)	137.5[1]	94.6[2]
Sr (ppm)	105.3[1]	109[2]
$^{87}Sr/^{86}Sr$	0.71949[1]	0.7171[2]
$^{87}Sr/^{86}Sr$(100 m.y.)	0.71411	0.71353
Sm (ppm)	7.24[3]	4.26[4]
Nd (ppm)	38.3[3]	22.6[4]
$^{143}Nd/^{144}Nd$		0.511230[4]

1 Early and Silver (1973)

2 Kistler and Peterman (1973)

3 Gromet (1979)

4 DePaolo (1981)

Geological and geochemical relations, particularly the lack of correspondence between pluton and wall-rock isotope properties (Early and Silver, 1973; Taylor and Silver, 1978; Silver et al., 1979; this work) suggest that if a sedimentary component is involved in the genesis of these rocks, then it is incorporated below the crust. Figure 12.6 shows graphically the range of isotopic compositions obtained by mixing various proportions of these three model components. A curvilinear field of possible compositions is obtained on the ε_{Nd}- ε_{Sr} diagram, and the samples analysed by DePaolo (1981) fall within or just outside this field. Contours of calculated $\delta^{18}O$ for the various mixtures are also shown on this figure. Fractionation could potentially increase the $\delta^{18}O$ of rocks obtained at the surface by as much as 1.5 per mil over source values (Taylor and Silver, 1978; Matsuhisa, 1979; Chivas et al., 1982). To allow for the possible effects of fractionation on the oxygen isotopic systematics the contours shown on Fig. 12.6 are of source $\delta^{18}O$ + 1.5 per mil. The actual $\delta^{18}O$ values of more fractionated liquids derived from combination of the three components considered here may well be slightly lower than the values thus assigned. Selective extraction of hydrothermally exchanged materials within the subducted oceanic crust would be expected to give variable and perhaps higher $\delta^{18}O$ and more radiogenic Sr at a given value of ε_{Nd}. DePaolo (1981) suggested that this may be the explanation for some of the high ε_{Nd} samples that lie to the right of the "Mantle Array". The closeness of the $\delta^{18}O$ contours, particularly for more than about 10% sediment involvement, the spread of ε_{Nd} for a particular ε_{Sr} (and vice versa), and the possibility of modification of $\delta^{18}O$ by fractionation en route to the surface imply that there need not be a correlation between the three isotope systems in

other than a general fashion.

The $\delta^{18}O$ of the San Jacinto rocks implies that some 10 - 25% of the oxygen of the source materials could have been derived from a subducted sediment with the oxygen isotopic composition assumed for this model case. The rest of the source would then be derived from various amounts of depleted mantle (perhaps 50%) and subducted oceanic crust (about 25%)[see Fig. 12.6]. Because the concentration of oxygen is approximately equal in all silicate rocks, these amounts are equivalent to mass fractions of each material processed. Because of different abundance levels in the different components, a mixture of 50:25:25 depleted mantle:oceanic crust:model sediment will have the trace element abundances of Table 12.4. Almost all of the K and Rb are contributed by the sedimentary component; two thirds or more of the LREE will be from the sediment also, whilst half of the Sr comes from the oceanic crust, a third comes from the sediment, and the rest is from depleted mantle. These values are significant as they imply a LREE-enriched source if significant (more than several percent) amounts of sediment are involved, and potentially remove the K mass balance problems outlined above. The need for an LREE-enriched source for the eastern part of the batholith (which includes the San Jacinto Mountains) has been concluded by Gromet (1979), and is reinforced by additional data including samples from the San Jacinto Mountains (L.P. Gromet, written communication, 1983).

This model, of course, grossly simplifies the actual situation. Variation of the parameters used for the depleted mantle and oceanic crust components within reasonable limits will change details but not the general patterns elucidated above. The neodymium, and to a lesser

TABLE 12.4.

Some geochemical parameters of, and relative contributions to, a 50:25:25 mixture of Depleted Mantle, Oceanic Crust, and Model Subducted Sediment

	Concentration (ppm)	Percentage of component derived from:		
		Depleted Mantle	Oceanic Crust	Subducted Sediment
K	5700	<1	5	95
Rb	23.9	<1	1	99
Sr	74.5	9	54	37
Sm	1.6	9	25	66
Nd	7.0	6	14	80
$\delta^{18}O$, permil	9.0	50	25	25
$^{87}Sr/^{86}Sr$	0.70659			
$^{143}Nd/^{144}Nd$	0.51138			

extent, the oxygen isotopic composition of the subducted sediment are believed to be the parameters most likely to be in error. The consistency of Rb, Sr, and Sr isotopic data obtained for samples of Mesozoic sediment (Ch. 2) suggests that these parameters may not be changed much. Solution of the Nd problem can only await more detailed work on the Mesozoic sedimentary rocks of western North America.

Perhaps more difficult to evaluate than juggling of model parameters are the effects of mantle processes that can separate elements from each other. For instance, if relatively large component from sedimentary rocks that appears required by the oxygen data comes, not directly from sedimentary rocks but from sediments that have been processed by prior melting events within the mantle then, depending on the residual mineralogy, Nd and Sr contents could differ greatly from those assumed in the calculations. If Nd and Sr contents of materials derived through pre-processing of subducted sedimentary rocks were increased by such a process, then the net effect would be to increase the curvature of the mixing lines on Figure 12.6. It is also assumed in the calculations that all of the oceanic crustal section contributes equally to the oceanic crustal component; this is almost certainly not true in detail.

It will probably never be possible to determine directly when the implicated sedimentary material was subducted. If it was subducted during Early Cretaceous time synchronous with batholith development, then why is it not seen more in rocks closer to the presumed position of the trench? There appears to be no simple answer to this question, suggesting that the sedimentary material had been introduced into the mantle prior to the initiation of early Cretaceous subduction. The Jurassic

rocks, interpreted as an accretionary prism (Criscione et al., 1978) may also be relict from an earlier Mesozoic subduction event, and provide tentative confirmation that such an event did occur.

12.3.1 IMPLICATIONS FOR TRACE ELEMENT ABUNDANCES OF DERIVATIVE LIQUIDS

This section discusses the implications of the model outlined above for the trace element characteristics of the ensuing melts. Table 12.5 lists REE abundances assumed for the three model end-members; Figure 12.7 presents these data graphically. Also shown on Figure 12.7 are REE patterns for various mixtures of these three model source components. A LREE-enriched pattern is indicative of a substantial proportion of sediment (≈>10%) in the mixture, though this is, of course, not the only way to obtain such a feature. The depleted mantle component effectively acts as a diluent, while an oceanic crustal component could contribute a significant fraction of the HREE.

Partial fusion of such a composition may yield a liquid with a quite different REE pattern to that of the source. The actual liquid composition depends heavily on the minerals residual to the fusion event. Figure 12.8(a) shows the effects of several different residual mineralogies on the composition of the derivative liquid, using the partition coefficients of Minster and Allegre (1977)[Table 12.6]. Residual hornblende and clinopyroxene yield very similar effects, while pronounced LREE enrichment results from residual garnet. Olivine and orthopyroxene effectively behave as diluents. A residue containing substantial hornblende is unlikely unless the water content of the source is extraordinarily high, and a residual composition containing substantial garnet and

TABLE 12.5.

ASSUMED RARE EARTH ELEMENT CONCENTRATIONS (IN PPM)

FOR MODEL COMPONENTS

	1. DEPLETED MANTLE	2. OCEANIC CRUST	3. MODEL SEDIMENT
Ce	0.74	3.86	42.2
Nd	0.74	4.0	22.6
Sm	0.29	1.6	4.26
Eu	0.118	0.63	0.71
Gd	0.45	2.33	3.37
Dy	0.58	2.93	1.85
Er	0.38	1.92	0.81
Yb	0.37	1.87	0.81

1., 2. Adjusted to give smooth patterns with flat HREE using Nd and Sm values from Table 12.2.

3. Adjusted to Nd and Sm abundances of Model Sediment (Table 12.2) using REE data from French Valley sedimentary composite (Gromet, 1979). See Table 12.3.

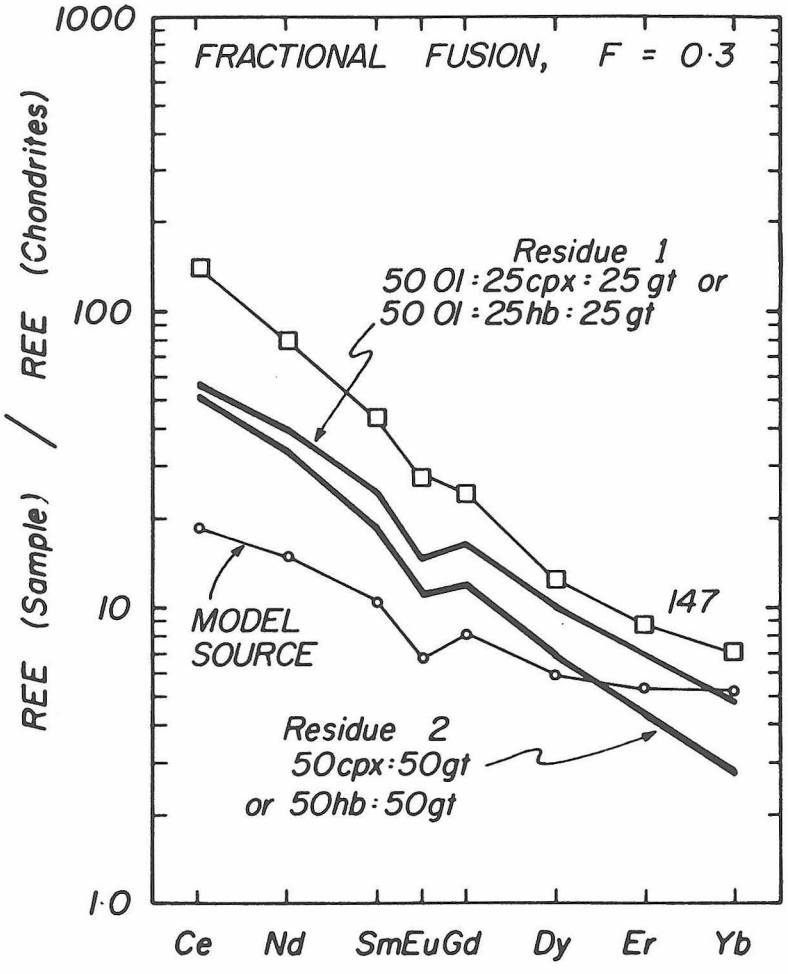

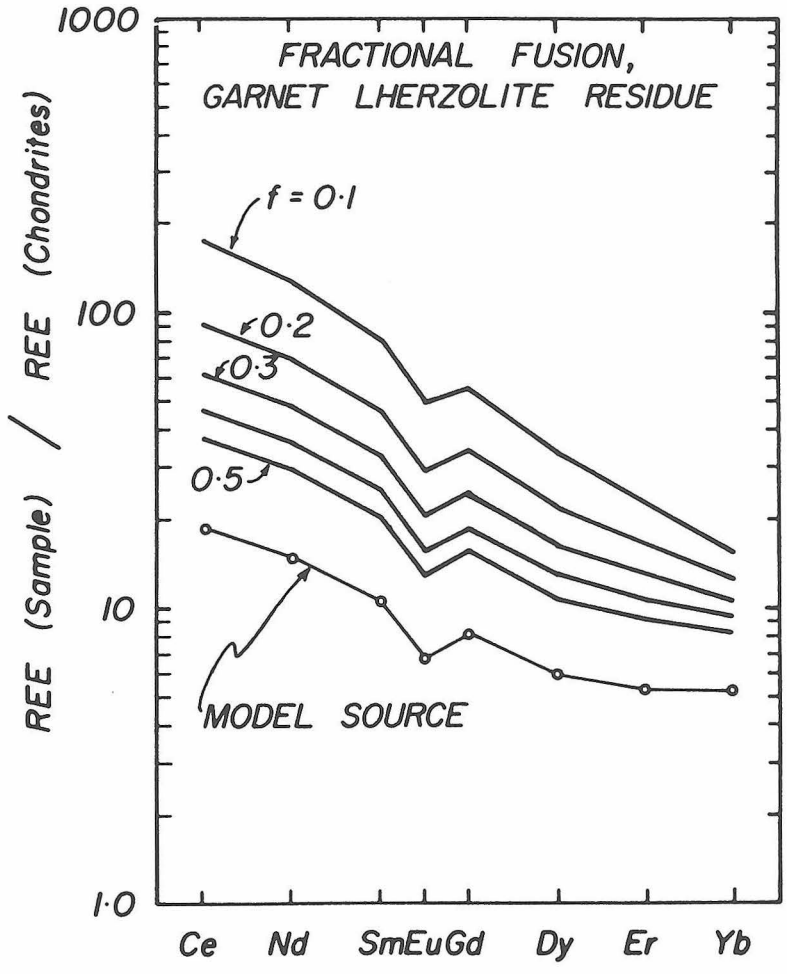

Figure 12.7a. (left) REE patterns for model source components (Table 12.2).
Figure 12.7b. (right) REE patterns for various mixtures of model source components.
DM = Depleted Mantle; OC = Oceanic Crust; SED = Sediment

Figure 12.8a. REE patterns of derivative liquids leaving noted residual assemblages.

Figure 12.8b. REE patterns of derivative liquids, garnet lherzolite residue. Numbers on curves give melt fraction.

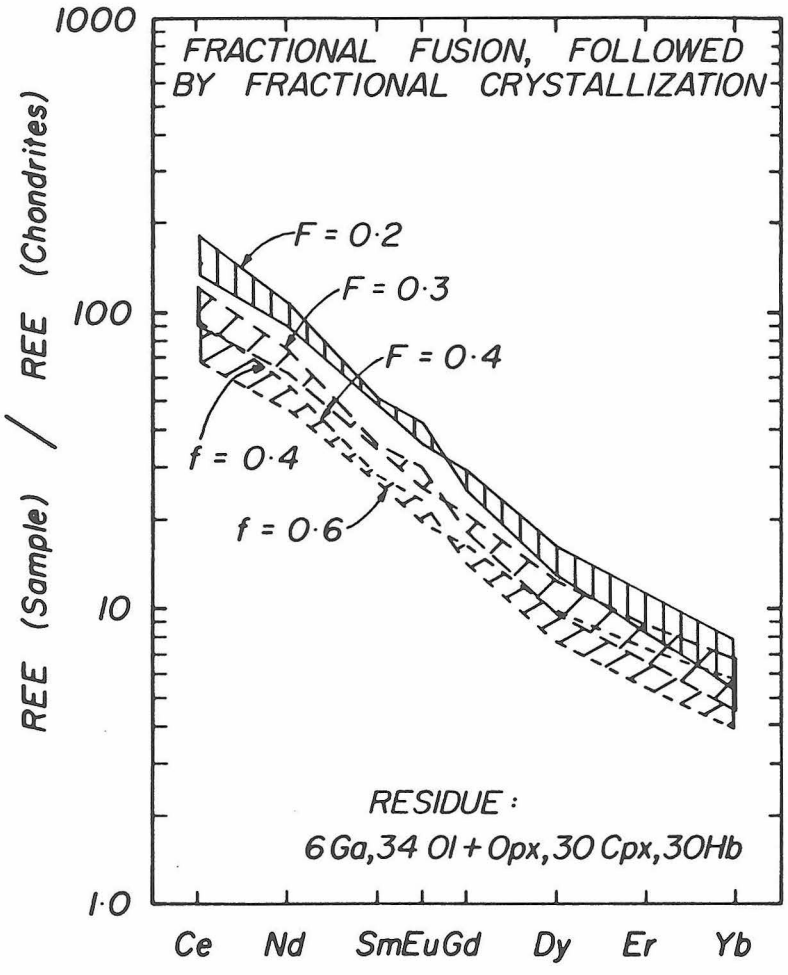

Figure 12.8a

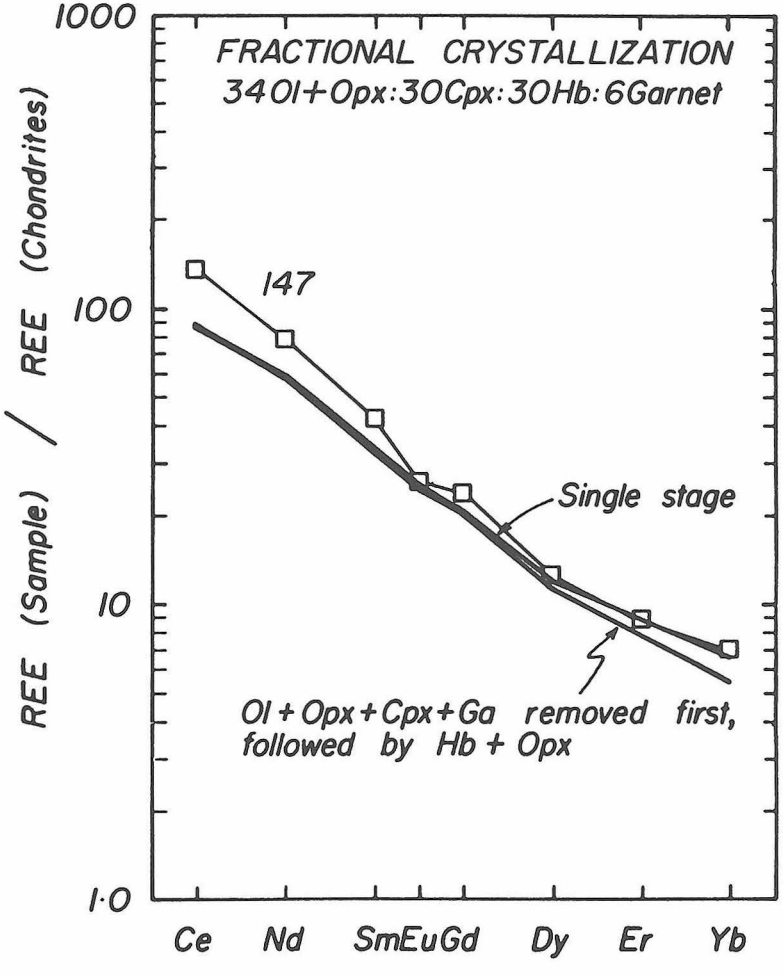

Figure 12.8b

TABLE 12.6.

Typical Values of Partition Coefficients

	ol, opx	cpx	gt	hb	plag	biot
			'Mantle' Values			
Ref.	(1)	(1)	(1)	(1)	(1)	
Ce	0.0040	0.15	0.02	0.20	0.10	
Nd	0.0045	0.30	0.09	0.35	0.085	
Sm	0.0055	0.50	0.22	0.52	0.07	
Eu	0.0058	0.53	0.32	0.59	0.8	
Gd	0.0065	0.56	0.50	0.63	0.06	
Dy	0.008	0.58	1.0	0.62	0.052	
Er	0.009	0.60	2.0	0.55	0.046	
Yb	0.010	0.60	4.0	0.49	0.040	
			'Crustal' Values			
Ref.	(2)	(3)	(4)	(5)		(5)
Ce	0.0069	0.508	0.03	0.35		0.034
Nd	0.0068	0.645	0.07	1.10		0.041
Sm	0.0067	0.954	0.29	2.01		0.051
Eu	0.0068	0.681	0.16	1.29		0.035
Gd	0.0077	1.35	0.97	2.82		0.062
Dy	0.0096	1.46	3.17	3.15		0.065
Er	0.011	1.33	6.56	3.17		0.069
Yb	0.014	1.30	11.5	2.84		0.071

References:

(1) Minster and Allegre (1977)
(2) Hanson (1978)
(3) Schnetzler and Philpotts (1972). Augite from basaltic andesite
(4) Gromet (1979)
(5) Gromet and Silver (1983). Calculated assuming total rock = liquid abundances.

clinopyroxene is unlikely unless the sediment component of the model source is very calcium-rich.

The effect of a more plausible residual mineralogy - garnet lherzolite - is shown on Figure 12.8(b). The liquid patterns mirror those of the source except that the LREE are enriched over the HREE (for F=0.3, Ce by 3.3x, Yb 2.1x; F = melt fraction). It is obvious that any change in the source composition will be directly reflected in the liquid composition for this type of residual mineralogy. For instance, the Eu anomaly in the derivative liquids is largely inherited from the model source composition.

Various authors (see Gill, 1981, for a summary) consider it unlikely for a mantle-derived liquid to reach the surface unaffected by crystal fractionation. The nature of the phases precipitating will vary as the liquid rises, and the partition coefficients for each phase will also change as the physico-chemical conditions of the liquid change. Given these factors it is almost impossible to deduce the nature and proportions of phases that may be removed during ascent. Hornblende and plagioclase appear to have been the major precipitating phases as liquids were injected into the evolving magma chamber. Residual phases from partial fusion are also likely fractionating phases. Trace element data presented above (Ch. 7) imply that hornblende was influential in the evolution of the San Jacinto liquids, and it may be difficult to resolve the effects of hornblende fractionation from those resulting from its presence as a residual phase during partial melting.

Figure 12.9(a) presents graphically the effects on the REE of removing 40-60% of material in the proportions 34% olivine+orthopyroxene:

Figure 12.9a. REE patterns showing the effects of combined fractional fusion and fractional crystallization. Melt fraction for fractional fusion, garnet lherzolite residue, given by F; fraction of liquid remaining after fractional crystallization given by f.

REE patterns produced by fractional melting of a LREE-enriched source, leaving a garnet lherzolite residue, followed by fractional crystallization of olivine, orthopyroxene, clinopyroxene and garnet gives patterns broadly similar to those of the eastern Peninsular Ranges batholith.

Figure 12.b. Comparative effects on REE patterns of a two-stage fractional crystallization model compared to the single-stage results. There is no substantive difference.

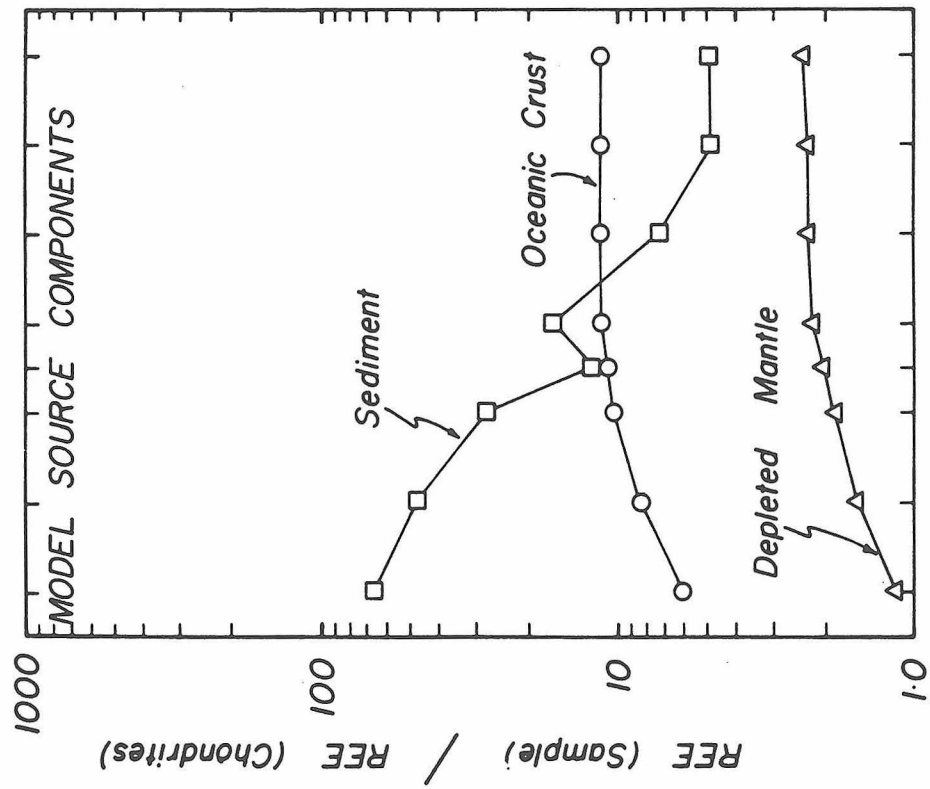

Figure 12.9a

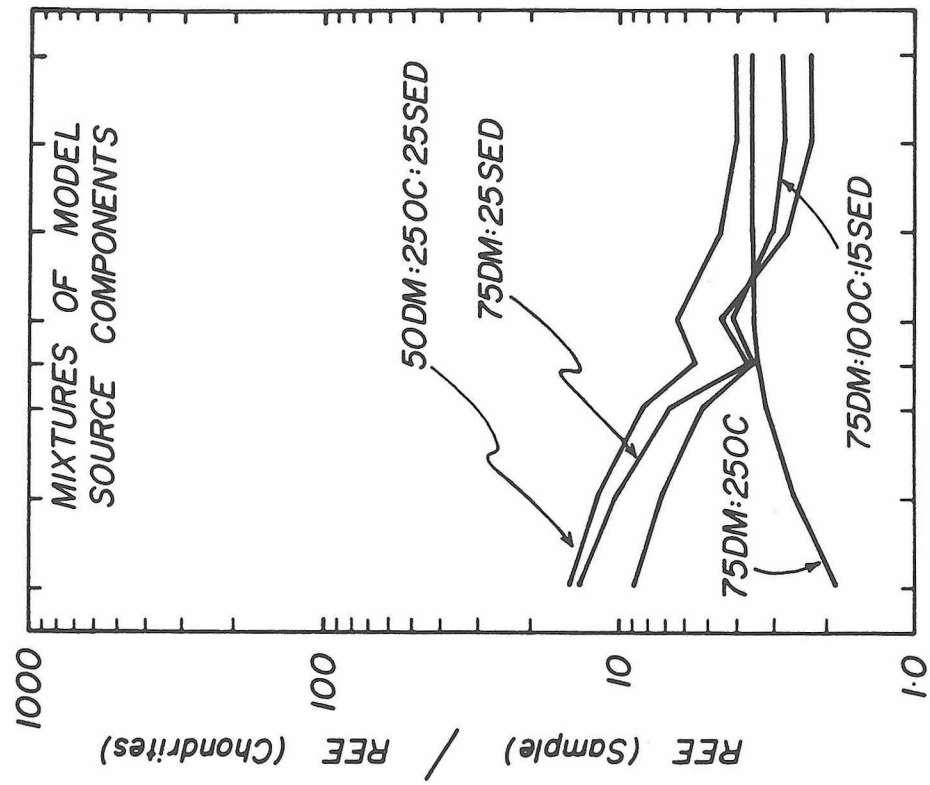

Figure 12.9b

30% hornblende: 30% clinopyroxene: 6% garnet for liquids derived by varying amounts of partial fusion (20 - 40%) of the model source, and using partition coefficients listed in Table 12.6. Given the possible permutations of fractionating phases and varying partition coefficients for each phase the match is surprisingly good. Figure 12.9(b) shows the effects of multi-stage fractionation; the total amount of each mineral removed is identical to the single-stage case described above, but the assemblage olivine + orthopyroxene + clinopyroxene + garnet is removed first, followed by the assemblage orthopyroxene + hornblende. Olivine and orthopyroxene act as diluents, and removal of other REE-poor phases (quartz, biotite, plagioclase except for Eu) would yield a similar result. There is little substantive variation between the single stage and two stage models.

12.4 CONCLUSIONS

In summary, a model for the formation of the rocks of the San Jacinto Mountains involving partial melting of a mixture of depleted mantle, subducted oceanic crust, and subducted sediment, followed by substantial crystal fractionation en route to the crust can, within the very broad constraints available, satisfy the observed isotopic and chemical properties.

Both isotopic and mass balance considerations strongly imply that the source material for these rocks cannot be simply undepleted mantle similar to that parental to MORB, of either normal or enriched type. Another component, enriched in ^{18}O, ^{87}Sr and incompatible elements such as K, Rb, Ba and the LREE, is needed. The oxygen isotope data are

most simply interpreted as indicating that at least part of this component is subducted sediment. If so, this sedimentary material may provide up to about 20% of the oxygen in the final magmas, implying the existence of a similar amount of crustal recycling. This sedimentary component also largely controls the REE behaviour, both in terms of concentration and in isotopic composition. A simple model suggests that some 80% of the Nd atoms in the derivative liquids could come from this source. The Sr data appear to neccessitate the involvement of a relatively Sr-rich component with low $^{87}Sr/^{86}Sr$; this could be subducted oceanic crust.

The role of other possible source components, particularly that of old subcontinental lithosphere, are less easy to evaluate. Regional and oxygen isotope considerations suggest that such a component is not particularly important on a volume basis, as the gross isotopic and chemical properties of the San Jacinto rocks are similar to those from elsewhere in the batholith where old continental lithosphere is thought to be absent. Such a component (or components) do appear to be in some way responsible for much of the observed complexity in the geographic distribution observed for $^{87}Sr/^{86}Sr$ in the San Jacinto Mountains, and for the apparently anomalously low $\delta^{18}O$ values found within these rocks. The oxygen isotope data may be interpreted to show that as much as 35% (atom basis) of some of the liquids reaching the upper crust in this region was derived from this assumed subcontinental lithospheric component.

Evaluation of the implications of the model described above shows that when observed chemical and isotopic features are used to attempt to model source properties it is possible that conclusions that

might be drawn from the study of one isotope system in isolation that differ significantly from conclusions made after consideration of several systems in conjunction. For instance, attempts to estimate the amount of crustal recycling using isotope systematics are very sensitive to the concentrations of the relevant elements chosen for the different possible source materials. Only oxygen is relatively free of this problem, and it appears that analysis of oxygen isotope data gives the best estimate of the importance of "crustal" involvement, even if that involvement is through injection into the mantle during subduction rather than through crustal-level processes such as assimilation or partial fusion. However, the oxygen isotopic composition may be significantly modified by fractionation during igneous processes (unlike the case for Sr, Pb, and Nd), so that the oxygen isotope ratio is not an extensive variable, but is rather the end product of a complex interplay of source and process characteristics.

It is believed that the observations and interpretation presented above show the value of a multi-faceted approach to an attack on a complex geological problem. Field observations provide a model for a dynamic magma chamber. The consequences of this model for the major and trace element geochemical data have been explored, and it has been suggested that the studied rocks show features related to these high-level processes as well as characteristics inherited from the liquids from which they crystallized. These characteristics derive from both source characteristics and the results of complex petrogenetic processes. The isotope data can be used to estimate the relative importance of likely candidates for these source materials, and geochemical data can be used to put limits on the importance of some plausible petrogenetic processes.

Taken alone, each type of information may give significant insight into a problem; however, it is the availability of the various types of complementary information for a well-characterized rock suite from an area where the regional setting is relatively well understood that has enabled the conclusions reached above to be made.

REFERENCES

de Albuquerque, C.A.R., 1975, Geochemistry of actinolite hornblendes from tonalitic rocks, Northern Portugal: Geochim. Cosmochim. Acta, 38, 789-803.

Albarede, F., and Bottinga, Y., 1972, Kinetic disequilibrium in trace element partitioning between phenocrysts and host lava: Geochim. Cosmochim. Acta, 36, 141-156.

Allegre, C.J., and J.F. Minster, 1978, Quantitative models of trace element behaviour: Earth. Planet. Sci. Lett., 38, 1-25.

Allegre, C.J., and Othman, D.B., 1980, Nd-Sr isotopic relationship in granitic rocks and continental crust development: a chemical approach to orogenesis: Nature, 286, 335-342.

Allen, C.R., 1957, San Andreas fault zone in San Gorgonio Pass, Southern California: Geol. Soc. Amer. Bull., 68, 315-350.

Allen, J.C., and Boettcher, A.L., 1983, The stability of amphibole in andesite and basalt at high pressures: Amer. Mineral., 68, 307-314.

Allison, E.C., 1955, Middle Cretaceous gastropoda from Punta China, Baja California, Mexico: Jour. Paleontol., 29, 400-432.

Anderson, A.T., 1976, Magma mixing: petrological process and volcanological tool: J. Volcanol. Geotherm. Res., 1, 3-33.

Anderson, T.H. and Silver, L.T., 1970, Reconnaissance survey of Precambrian rocks, northwestern Sonora, Mexico: Geol. Soc. Amer. Abstracts with Programs, 2, 484.

Anderson, T.H., and Silver, L.T., 1977, Geochronometric and stratigraphic outlines of the Precambrian rocks of northwestern Mexico: Geol. Soc. Amer. Abstracts with Programs, 9, 880.

Anderson, T.H., and Silver, L.T., 1979, The role of the Mojave-Sonora Megashear in the tectonic evolution of northern Sonora: in Anderson, T.H., and Roldan-Quintana, J., Geology of Northern Sonora: Guidebook - Field Trip #27, prepared for Geol. Soc. Amer. Annual Meeting, San Diego, 1979.

Arculus, R.J., and Johnston, R.W., 1978, Criticism of generalised models for the magmatic evolution of arc-trench systems: Earth Planet. Sci. Lett., 39, 118-126.

Armstrong, R.L., and Suppe, J., 1973, Potassium-argon geochronometry of Mesozoic igneous rocks in Nevada, Utah, and Southern California: Geol. Soc. Amer. Bull., 84, 1375-1392.

Arnold, R., 1918, Topography and fault system of the region of the San Jacinto earthquake: Seis. Soc. Amer. Bull., 8, 68-73.

Arriens, P.A., and Compston, W., 1968, A method for isotopic ratio measurement by voltage peak switching, and its application with digital output: Int. J. Mass Spectrom. Ion Phys., 1, 471-481.

Atwater, T., 1970, Implications of plate tectonics for the Cenozoic evolution of western North America: Geol. Soc. Amer. Bull., 81, 3515-3536.

Atwater, T., and Molnar, P., 1973, Relative motion of the Pacific and North American plates deduced from sea-floor spreading in the Atlantic, Indian, and South Pacific Oceans, in Kovach, R.L., and Nur, A., (eds.), Conf. on Tectonic Problems of the San Andreas Fault System: Stanford Univ. Pubs. Geol. Sci., 13, 136-148.

Axelrod, D.J., 1950, Studies in late Teriary paleobotany: Carnegie Inst. Wash. Pulication No. 590, 1-323.

Bailey, R.A., Dalrymple, G.B., and Lanphere, M.A., 1976, Volcanism, structure and geochronology of Long Valley Caldera, Mono County, California: J. Geophys. Res., 81, 725-744.

Baird, A.K., Morton, D.M., Woodford, A.O., and Baird, K.W., 1974a, Transverse Ranges Province: A unique structural-petrochemical belt across the San Andreas Fault System: Geol. Soc. Amer. Bull., 85, 163-174.

Baird, A.K., Baird, K.W., and Welday, E.E., 1974b, Chemical trends across Cretaceous batholithic rocks of southern California: Geology, 2, 493-496.

Baird, A.K., Baird, K.W., and Welday, E.E., 1979, Batholithic rocks of the northern Peninsular and Transverse Ranges, southern California: Chemical composition and variation: in Abbot, P.L., and Todd, V.R., (eds.), Mesozoic Crystalline Rocks, Manuscripts and road logs prepared for the Geol. Soc. Amer. Annual Meeting, San Diego, 1979: Dept. Geol. Sci., San Diego State University, 111-132.

Banks, P.O., and Silver, L.T., 1964, Material balance in the whole rock U-Pb system of a young granite: EOS (Trans. Amer. Geophys. Union), 45, 108.

Barker, F., Wones, D.R., Sharp, W.A. and Desborough, G.A., 1975, The Pikes Peak batholith, Colorado Front Range, and a model for the origin of the gabbro-anorthosite-syenite-potassic granite suite, Precamb. Res., 2, 97-160.

Barnes, D.A., and Berry, K.D., 1979, Jura-Cretaceous paleogeography: The Eugenia Group, western Vizcaino Peninsula, Baja California Sur, Mexico in Abbott, P.L. and Gastil, R.G., (eds.), Baja California Geology: Field guides and papers, Dept. Geol. Sci., San Diego State University, 53-64.

Bartholomew, M.J., 1970, San Jacinto fault zone in the Imperial Valley, California: Geol. Soc. Amer. Bull., 81, 3161-3166.

Bartlett, R.W., 1969, Magma convection, temperature distribution, and differentiation: Am. J. Sci., 267, 1067-1082.

Bateman, P.C., and Chappell, B.W., 1979, Crystallization, fractionation and solidification of the Tuolumne intrusive series, Yosemite National Park, California: Geol. Soc. Amer. Bull., 90, 465-482.

Bateman, P.C., and Dodge, F.C.W., 1970, Variations of major chemical constituents across the central Sierra Nevada batholith: Geol. Soc. Amer. Bull., 81, 409-420.

Bateman, P.C., and Nokleberg, W.J., 1978, Solidification of the Mount Givens Granodiorite, Sierra Nevada, California: J. Geol., 86, 563-579.

Bell, R.E., 1969, Geology of a plutonic-metamorphic terrain near Rancho Vallecitos, northwestern Baja California: San Diego State University undergraduate research reports, 14, pt. 1.

van Bemmelen, R.W., 1949, The geology of Indonesia, 2nd edition, Vol. 1: 732 p., The Hague Martinus Nijhoff.

Berman, R.G., 1981, Differentiation of calc-alkaline magmas: evidence from the Coquihalla Volcanic Complex, British Columbia: J. Volcanol. Geotherm. Res., 9, 151-179.

Berggren, W.A,. and Van Couvering, J.A., 1974, The Late Neogene: biostratigraphy, geochronology and paleoclimatology in the last 15 million years in marine and continental sequences, Palaeogeogr. Palaeoclimat. Palaeoecol., 16, 1-260.

Bhattacharji, S., and Smith, C.H., 1964, Flowage differentiation: Science, 145, 150-153.

Bigeleison, J., and Mayer, M.G., 1947, Calculation of equilibrium constants for isotopic exchange reactions: Jour. Chem. Phys., 15, 261-267.

Biscaye, P.E., and Dasch, E.J., 1971, The rubidium, strontium, strontium-isotope system in deep-sea sediments: Argentine Basin: Jour. Geophys. Res., 76, 5087-5096.

Black, L.P., Bell, T.H., Rubenach, M.J., and Withnall, I.W., 1979, Geochronology of discrete structural-metamorphic events in a multiply deformed Precambrian terrain: Tectonophysics, 54, 103-137.

Boettcher, A.L., and Wyllie, P.J., 1968, Melting of granite with excess water to 30 kilobars pressure: J. Geol., 76, 235-244.

Bofinger, V.M., Compston, W., and Gulson, B.L., 1970, A Rb-Sr study of the Lower Silurian State Circle Shale, Canberra, Australia: Geochim. Cosmochim. Acta, 34, 433-445.

Bond, G.C.,and others, 1977, Paleozoic-Mesozoic rocks of the Northern Sierra, Field Guide: Geol. Soc. America, 73rd Annual Meeting, Cordilleran Section, 35p.

Bottinga, Y. and Javoy, M., 1973, Comments on oxygen isotope geothermometry: Earth Planet Sci. Lett., 20, 250-265.

Bowen, N.L., 1913, Equilibrium diagram of the plagioclase feldspars: Am. J. Sci., 35, 579-599.

Bowen, N.L., 1928, Evolution of the Igneous Rocks: Princeton University Press.

Branch, C.D., 1967, Genesis of magma for acid calc-alkaline volcano-plutonic complexes: Tectonophysics, 4, 83-100.

Brooks, B, and Ellis, R., 1954, Geology of the Jacumba area, San Diego and Imperial Counties: Calif. Div. Mines Bull. 170, Map Sheet no. 23.

Brooks, C., James, D.E., and Hart, S.R., 1976, Ancient lithosphere: its role in young continental volcanism: Science, 193, 1086-1094.

Brown, A.R., 1968, Geology of a portion of the southeastern San Jacinto Mountains, Riverside County, California: Unpublished M.S. thesis, Univ. California, Riverside, 95p.

Brown, A.R., 1980, Limestone deposits of the Desert Divide, San Jacinto Mountains, California: in Fife, D.L., and Brown, A.R., (eds.), Geology and Mineral Wealth of the California Desert: South Coast Geological Society, Santa Ana, Calif., 284-293.

Brown, A.R., 1981, Structural history of the metamorphic, granitic and cataclastic rocks in the southeastern San Jacinto Mountains, in Brown, A.R., and Ruff, R.W., (eds.), Geology of the San Jacinto Mountains: South Coast Geological Society Annual Field Trip Guidebook No. 9, 100-138.

Brown, A.R., and Ruff, R.W., (eds.), 1981, Geology of the San Jacinto Mountains: South Coast Geological Society Annual Field Trip Guidebook No. 9, 219p.

Buddington, A.F., and Lindsley, D.H., 1964, Iron-titanium oxide minerals and synthetic equivalents: J. Petrol., 5, 310-357.

Burke, W.H., Denison, R.E., Hetherington, E.A., Koepnick, R.B., Nelson, H.F., and Otto, J.B., 1982, Variation of seawater $^{87}Sr/^{86}Sr$ throughout Phanerozoic time: Geology, 10, 516-519.

Burnham, C.W., 1975, Water and magmas: a mixing model, Geochim. Cosmochim. Acta, 40, 1077-1084.

Burnham, C.W., 1979, Magmas and hydrothermal fluids: in Barnes, H.L., (ed.), Geochemistry of Hydrothermal Ore Deposits, 2nd edition, John Wiley and Sons, Inc: 71-136.

Burnham, C.W., Holloway, J.R., and Davis, N.F., 1969, Thermodynamic properties of water to 1000^0C and 10,000 bars: Geol. Soc. Amer. Spec. Paper 132, 96p.

Burton, J.A., Prim, R.C., and Slichter, W.P., 1953, The distribution of solute in crystals grown from the melt: J. Chem. Phys., 21, 1987-1996.

Carmichael, I.S.E., and Stormer, J.C., 1971, Fluorine-hydroxyl exchange in apatite and biotite: a potential igneous geothermometer: Contrib. Mineral. Petrol., 31, 121-131.

Carron, J.P., 1968, Autodiffusion du sodium et conductivitie electrique dans les obsidiennes granitiques: C. R. Hebd. Seances Acad. Sci. Ser. D., 266, 854-857.

Cathles, L.M., 1977, An analysis of the cooling of intrusives by groundwater convection which includes boiling: Econ. Geol., 72, 804-826.

Chappell, B.W., 1966, Petrogenesis of the granites at Moonbi, New South Wales: Unpublished Ph.D. thesis, Australian National University.

Chappell, B.W., 1978, Granitoids from the Moonbi district, New England Batholith, eastern Australia: J. Geol. Soc. Aust., 25, 267-283.

Chappell, B.W., Compston, W., Arriens, P.A., and Vernon, M.J., 1969, Rubidium and strontium determinations by X-ray fluorescence spectrometry and isotope dilution below the part per million level: Geochim. Cosmochim. Acta, 33, 1002-1006.

Chappell, B.W., and White, A.J.R., 1974, Two contrasting granite types: Pacific Geology, 8, 173-174.

Chappell, B.W., and White, A.J.R., 1976, Plutonic rocks of the Lachlan Mobile Zone: 25th International Geological Conference, Excursion Guide No. 13C, Progress Press, Canberra, 40p.

Chen, J.H., and Moore, J.G., 1982, Uranium-lead isotopic ages from the Sierra Nevada batholith, California: Jour. Geophys. Res., 87, 4761-4784.

Chaudhuri, S., 1976, The significance of rubidium-strontium age of sedimentary rock: Contrib. Mineral. Petrol., 59, 161-170.

Chaudhuri, S., and Brookins, D.G., 1969, The Rb-Sr Whole-rock age of the Stearns Shale (Lower Permian), eastern Kansas, before and after acid leaching experiments: Geol. Soc. Amer. Bull., 80, 2605-2610.

Chivas, A.R., Andrew, A.S., Sinha, A.K. and O'Neil, J.R., 1982, Geochemistry of a Pliocene-Pleistocene oceanic-arc plutonic complex, Guadalcanal: Nature, 300, 139-143.

Clauer, N., 1973, Utilisation de la methode rubidium-strontium pour la datation de niveaux sedimentaires du Precambrien superieur de l'Adrar mauritanien (Sahara occidental) et la mise en evidence de transformations precoces des mineraux argileux: Geochim. Cosmochim. Acta, 37, 2243-2255.

Clauer, N., 1974, Utilisation de la methode rubidium-strontium pour la datation d'une schistosite de sediments peu metamorphises: Application au Precambrien II de la Boutonniere de Bou Azzer-El Graara (Anti-Atlas, Maroc): Earth Planet. Sci. Lett., 22, 404-412.

Clauer, N., Hoffert, M., Grimaud, D., and Millot, G., 1975, Composition isotopique du strontium d'eaux interstitielles extraites de sediments recents: un argument en faveur de l'homogeneisation isotopique des mineraux argileux: Geochim. Cosmochim. Acta, 39, 1579-1582.

Clayton, R.N., Grossman, L., and Mayeda, T.K., 1973, A component of primitive nuclear composition in carbonaceous meteorites: Science, 182, 485-488.

Clement, S., and Compston, W., 1969, The design and performance of a mass spectrometer using beam transport theory: Int. J. Mass Spectrom. and Ion Phys., 10, 323-342.

Cole, J.W., 1973, High-alumina basalts of Taupo Volcanic Zone, New Zealand: Lithos, 6, 53-64.

Cole, J.W., 1979, Structure, petrology and genesis of Cenozoic volcanism, Taupo Volcanic Zone, New Zealand - a review: J. Volcanol. Geothermal Res., 22, 631-657.

Collins, W.J., Beams, S.J., White., A.J.R. and Chappell, B.W., 1982, Nature and origin of A-type granites with particular reference to south-eastern Australia: Contrib. Mineral. Petrol., 80, 189-200.

Compston, W., and Chappell, B.W., 1979, Sr-isotope evolution of granitoid source rocks: in McElhinny, M.W., (ed)., The Earth: Its Origin, Structure, and Evolution: Academic Press, London, 477-426.

Compston, W., Chappell, B.W., Arriens, P.A., and Vernon, M.J., 1969, On the feasibility of NBS 70a K-feldspar as a Rb-Sr age reference sample: Geochim. Cosmochim. Acta, 33, 753-757.

Compston, W., Jeffrey, P.M. and Riley, G.H., 1960, Age of emplacement of granite: Nature, 186, 702-703.

Compston, W., and Pidgeon, R.T., 1962, Rubidium-strontium dating of shales by the total-rock method: Jour. Geophys. Res., 67, 3493-3502.

Compston, W., Crawford, A.R., and Bofinger, V.M., 1966, A radiometric estimate of the duration of sedimentation in the Adelaide Geosyncline, South Australia: Jour. Geol. Soc. Aust., 13, 229-276.

Compton, R.R., 1962, Manual of Field Geology: John Wiley & Sons, Inc. 378p.

Craig, H., 1961, Standard for reporting concentrations of deuterium and oxygen-18 in natural waters: Science, 133, 1833-1834.

Creasey, S.C., 1946, Geology and nickel mineralization of the Julian-Cuyamaca area, San Diego County, California: Calif. Jour. Mines and Geol., 42, 15-29.

Criscione, J.J., Davis, T.E., and Ehlig, P., 1978, The age of sedimentation/diagenesis for the Bedford canyon Formation and the Santa Monica Formation in southern California: A Rb/Sr evaluation, in Howell, D.G., and McDougall, K.A., (eds.), Mesozoic Paleogeography of the Western United States: Pacific Section, Soc. Econ. Palaeontologists and Mineralogists, Pacific Coast Paleogeography Symposium 2, 385-396.

Crowell, J.C., 1962, Displacement along the San Andreas fault, California: Geol. Soc. America Special Paper 71, 61 p.

Crowell, J.C., 1981, An outline of the tectonic history of south-eastern California: in Ernst, W.G. (ed.) The Geotectonic Development of California: Prentice Hall Inc., 284-305.

Crowell, J.C., and Ramirez, V.R., 1979, Late Cenozoic faults in south-eastern California: in Crowell, J.C. and Sylvester, A.G., eds., Tectonics of the juncture between the San Andreas fault system and the Salton trough, south-eastern California: Dept. Geol. Sci., U.C. Santa Barbara, 21-40.

Dalrymple, W., 1980, K-Ar ages of the Friant Pumice member of the Turlock Lake Formation, the Bishop Tuff, and the tuff of Reds Mountain, central California: Isochron West, 28, 3-5.

Dasch, E.J., 1969, Strontium isotopes in weathering profiles, deep-sea sediments, and sedimentary rocks: Geochim. Cosmochim. Acta, 33, 1521-1552.

Dasch, E.J., Hills, F.A., and Turekian, K.K., 1966, Strontium isotopes in deep-sea sediments: Science, 153, 295-297.

DePaolo, D.J., 1980, Sources of continental crust: Neodymium isotope evidence from the Sierra Nevada and Peninsular Ranges: Science, 209, 684-687.

DePaolo, D.J., 1981a, Trace element and isotopic effects of combined wall-rock assimilation and fractional crystallization: Earth Planet. Sci. Lett., 53, 189-202.

DePaolo, D.J., 1981b, A neodymium and strontium isotopic study of the Mesozoic calc-alkaline granitic batholiths of the Sierra Nevada and Peninsular Ranges, California: J. Geophys. Res., 86, 10470-10488.

DePaolo, D.J., and Wasserburg, G.J., 1976, Nd isotopic variations and petrogenetic models: Geophys. Res. Lett., 3, 249-252.

DePaolo, D.J., and Wasserburg, G.J., 1977, The sources of island arcs as identified by Nd and Sr isotopic studies: Geophys. Res. Lett., 4, 465-468.

DePaolo, D.J., and Johnson, R.W., 1979, Magma genesis in the New Britain island-arc: constraints from Nd and Sr isotopes and trace element patterns: Contrib. Mineral. Petrol., 70, 367-379.

Dibblee, T.W., Jr., 1954, Geology of the Imperial Valley region, California, in Jahns, R.W., (ed.), Geology of Southern California: Calif. Div. Mines Bull. 170, Ch. II, 21-28.

Dibblee, T.W., Jr., 1971, Regional geologic map of San Andreas and related faults in eastern San Gabriel Mountains, San Bernadino Mountains and San Jacinto Mountains, California: U.S. Geol. Survey Open-File Map.

Dibblee, T.W., Jr., 1981a, Geology of the San Jacinto Mountains and adjacent areas, in Brown, A.R., and Ruff, R.W., eds., Geology of the San Jacinto Mountains: South Coast Geological Society Annual Field Trip Guidebook No. 9, 1-47.

Dibblee, T.W., Jr., 1981b, Geologic map of the Perris (15-minute) quadrangle, California: South Coast Geological Society, Geologic Map SCGS-1.

Dibblee, T.W., Jr., 1981c, Geologic map of the Banning (15-minute) quadrangle, California: South Coast Geological Society, Geologic Map SCGS-2.

Dibblee, T.W., Jr., 1981d, Geologic map of the Palm Springs (15-minute) quadrangle, California: South Coast Geological Society, Geologic Map SCGS-3.

Dibblee, T.W., Jr., 1981e, Geologic map of the Hemet (15-minute) quadrangle, California: South Coast Geological Society, Geologic Map SCGS-4.

Dibblee, T.W., Jr., 1981f, Geologic map of the Idyllwild (15-minute) quadrangle, California: South Coast Geological Society, Geologic Map SCGS-5.

Dickinson, W.R., and Hatherton, T., 1967, Andesite volcanism and seismicity around the Pacific: Science, 157, 801-803.

Dockum, M.S., and Miller, R.H., 1982, Ordovician conodonts from the greenschist facies carbonates, western Imperial County, California: Geol. Soc. America Abstracts with Programs, 14, 160.

Dodge, F.C.W., and Ross, D.C., 1971, Co-existing hornblendes and biotites from granitic rocks near the San Andreas fault, California: J. Geol., 79, 158-172.

Dodge, F.C.W., Papike, J.J., and Mays, R.E., 1968, Hornblendes from granitic rocks of the central Sierra Nevada batholith, California: J. Petrol., 9, 378-410.

Dodge, F.C.W., Smith, V.C., and Mays, R.E., 1969, Biotites from granitic rocks of the central Sierra Nevada batholith, California: J. Petrol., 10, 250-271.

Doe, B.R., and Delevaux, M.M., 1973, Variations in lead-isotopic composition in Mesozoic granitic rocks of California: a preliminary investigation: Geol. Soc. Amer. Bull., 84, 3513-3526.

Dokka, R.K., and Frost, E.G., 1978, Fission-track ages from the Santa Rosa Mylonite and its protolith and their relation to the cooling history of the Southern California batholith: Geol. Soc. Amer. Abstracts with Programs, 10, 103

Donnelly, M., 1934, Geology and mineral deposits of the Julian district, San Diego County, California: Calif. J. Mines and Geology, 30, 331-370.

Donnelly, T.W., Rogers, J.J.W., Pushkar, P., and Armstrong, R.L., 1971, Chemical evolution of the igneous rocks of the eastern West Indies: an investigation of the thorium, uranium and potassium distributions, and lead and strontium isotopic ratios: Geol. Soc. Amer. Memoir 130, 181-224.

Durbin, T.J., 1975, Ground-water hydrology of Garner Valley, San Jacinto Mountains, California - a mathematical analysis of recharge and discharge: U.S. Geol. Surv. Open-File Report, 75-305.

Early, T.O., and Silver, L.T., 1973, Rb-Sr isotopic systematics in the Peninsular Ranges batholith of southern and Baja California: EOS (Trans. Amer. Geophysical Union), 54, 494.

Eggler, D.H., 1972, Amphibole stability in H_2O-undersaturated calc-alkaline melts: Earth Planet. Sci. Lett., 15, 28-34.

Eggler, D.H., and Burnham, C.W., 1973, Crystallization and fractonation trends in the system Andesite-H_2O-CO_2-O_2 at pressures to 10 kb.: Geol. Soc. Amer. Bull., 84, 2517-2532.

Elders, W.A., Rex, W.R., Meidav, T., Robinson, P.T. and Biehler, S., 1972, Crustal spreading in southern California, Science, 178, 15-24.

Engel, A.E.J., 1983, Antithetic Cenozoic tectonic events in southeastern California: Geol. Soc. Amer. Abstracts with Programs, 15, 438-439.

Engel, A.E.J., and Engel, C.G., 1982, Late Mesozoic and early Cenozoic tectonics along the Salton Trough - Peninsular Range boundary: Geol. Soc. America Abstracts with Program, 14, 162.

Engel, R., 1959, Geology and mineral deposits of the lake Elsinore quadrangle, California: Calif. Div. Mines Bull., 149, 9-58.

Evensen, N.M., Hamilton, P.J., and O'Nions, R.K., 1978, Rare-earth abundances in chondritic meteorites: Geochim. Cosmochim. Acta, 42, 1199-1212.

Fairbanks, H.W., 1893, Geology of San Diego County, also of portions of Orange and San Bernadino Counties: California State Mining Bur. Ann. Rept., 11, 76-120.

Farmer, G.L., and DePaolo, D.J., 1983, Origin of Mesozoic and Tertiary granite in the western United States and implications for pre-Mesozoic crustal structure, 1, Nd and Sr isotopic studies in the geosyncline of the northern Great Basin: J. Geophys. Res., 88, 3379-3402.

Faure, G., and Hurley, P.M., 1963, The isotopic composition of strontium in oceanic and continental basalts: Application to the origin of igneous rocks: J. Petrol., 4, 31-50.

Faure, G., Hurley, P.M., and Fairbairn, H.W., 1963, An estimate of the isotopic composition of strontium in rocks of the Precambrian shield of North America: Jour. Geophys. Res., 68, 2323-2329.

Ferry, J.M., and Spear, F.S., 1978, Experimental calibration of the partitioning of Fe and Mg between biotite and garnet: Contrib. Mineral. Petrol., 66, 113-117.

Fife, D.L., Minch, J.A., and Crampton, P.J., 1967, Late Jurassic age of the Santiago Peak Volcanics: Geol. Soc. Amer. Bull., 78, 299-304.

Finch, J.W., and Abbott, P.J., 1977, Petrology of a Triassic marine section Vizcaino Peninsula, Baja California Sur, Mexico: Sedimentary Geology, 19, 253-273.

Finlayson, D.N., Collins, C.D.N., and Denham, D., 1980, Crustal structure under the Lachlan Fold Belt, southeastern Australia: Phys. Earth Planet. Inter., 21, 321-342.

Forester, R.W., and Taylor, H.P., Jr., 1977, $^{18}O/^{16}O$, D/H and $^{13}C/^{1}C$ studies of the Tertiary igneous complex of Skye, Scotland: Amer. J. Sci., 277, 136-177.

Francis, P.W., and Rundle, C.C., 1976, Rates of production of the main magma types in the central Andes: Geol. Soc. Amer. Bull., 87, 474-480.

Fraser, D.M., 1931, Geology of San Jacinto quadrangle south of San Gorgonio Pass, California: Calif. Jour. Mines and Geology, 27, 491-540.

Frick, C., 1921, Extinct vertebrate faunas of the badlands of Bautista Creek and San Timoteo Canyon, southern California: Univ. Calif. Pub., Dept. Geol. Sci. Bull., 12, n. 5, 277-424.

Friedman, I., and O'Neil, J.R., 1977, Compilation of stable isotope fractionation factors of geochemical interest: U.S. Geol. Surv. Prof. Pap. 440-K.

Gast, P., 1960, Limitations on the composition of the upper mantle: J. Geophys. Res., 65, 1287-1297.

Gast, P., 1968, Trace element fractionation and the origin of tholeiitic and alkaline magma types: Geochim. Cosmochim. Acta, 32, 1057-1086.

Gastil, R.G., LeMone, D.V., and Stewart, W.J., 1973, Permian fusulinids from near San Filipe, Baja California: Amer. Assoc. Petroleum Geol., 57, 746-747.

Gastil, R.G., Phillips, R.P., and Allison, E.C., 1975, Reconnaissance Geology of the State of Baja California: Geol. Soc. Amer. Memoir 140, 170 p.

Gastil, R.G., Morgan, G.J., and Krummenacher, D., 1981, The tectonic history of peninsular California and adjacent Mexico: in Ernst, W.G., (ed.), The Geotectonic Development of California: Prentice Hall Inc., 284-305.

Gastil, R.G., and Miller, R.H., 1981, Lower Paleozoic strata on the Pacific Plate of North America: Nature, 292, 828-830.

Gastil, R.G., and Miller, R.H., 1983, Stratal-tectonic elements of the eastern Peninsular Ranges, Baja California, Mexico: Geol. Soc. Amer. Abstracts with Programs, 15, 439.

Gill, J., 1970, Geochemistry of Viti Levu, Fiji, and its evolution as an island arc: Contrib. Mineral. Petrol., 27, 179-203.

Gill, J., 1981, Orogenic Andesites and Plate Tectonics: Springer-Verlag Berlin.Heidelberg, 390p.

Gray, C.H., Jr., 1961, Geology and mineral resources of the Corona South quadrangle: Calif. Div. Mines and Geol. Bull., 178, 1-58.

Green, D.H., 1973, Experimental melting studies on a model upper mantle composition at high pressure under water-saturated and water-undersaturated conditions: Earth Planet. Sci. Lett., 19, 37-53.

Green, D.H., 1976, Experimental testing of "equilibrium" partial melting of peridotite under water-saturated, high-pressure conditions: Can. Mineral., 14, 255-268.

Green, D.H., Hibberson, W.O., and Jaques, A.L., 1979, Petrogenesis of mid-ocean ridge basalts: in McElhinny, M.W., (ed.), The Earth, Its Origin, Structure and Evolution, Academic Press, London, 265-299.

Green, T.H., 1980, Island arc and continent-building magmatism - a review of key geochemical parameters and genetic processes: Tectonophysics, 63, 367-385.

Gregory, R.T., and Taylor, H.P., Jr., 1981, An oxygen isotope profile in a section of Cretaceous oceanic crust, Samail ophiolite, Oman: Evidence for $\delta^{18}O$ buffering of the oceans by deep (>5km) seawater-hydrothermal circulation at mid-ocean ridges: J. Geophys. Res., 86, 2737-2755.

Griffin, T.J., White, A.J.R., and Chappell, B.W., 1978, The Moruya Batholith and geochemical contrasts between the Moruya and Jindabyne suites: J. Geol. Soc. Aust., 25, 235-247.

Gromet, L.P., 1979, Rare earths abundances and fractionations and their implications for batholithic petrogenesis in the Peninsular Ranges batholith, California, USA, and Baja California, Mexico: Unpublished PhD thesis, Calif. Inst. Technology, 337p.

Gromet, L.P., and Silver, L.T., 1977, Geographic variation of rare earth fractionations in plutonic rocks across the Peninsular Ranges batholith, southern California: EOS (Trans. Amer. Geophys. Union), 58, 532.

Gromet, L.P., and Silver, L.T., 1979, Zonation of REE characteristics in the Peninsular Ranges batholith, southern and Baja California, and their implications for magmatic arc petrogenesis: Geol. Soc. Amer. Abstracts with Programs, 11, 436.

Gromet, L.P., and Silver, L.T., 1983, Rare earth element distributions among minerals in a granodiorite and their petrogenetic implications: Geochim. Cosmochim. Acta, 47, 925-939.

Hall, C.A., Jr., 1981, Evolution of the Western Transverse Ranges Microplate: Late Cenozoic faulting and basinal development, in Ernst, W.G., (ed.), The Geotectonic Development of California: Prentice-Hall Inc., 559-582.

Hanna, M.A., 1926, Geology of the La Jolla quadrangle, California: University of California, Dept. Geol. Sciences Bull., 16, 187-246.

Hanson, G.N., 1978, The application of trace elements to the petrogenesis of igneous rocks of granitic composition: Earth Planet. Sci. Lett., 38, 26-43.

Hardee, R.C., and Larson, D.W., 1977, The extraction of heat from magmas based on heat transfer mechanisms: Jour. Volcan. and Geotherm. Res.,

2, 113-144.

Harland, W.B., Cox, A.V., Llewellyn, P.G., Pickton, C.A.G., Smith, A.G. and Walters, R., 1982, A geologic time scale, Cambridge University Press.

Hart, S.R., Erlank, E.J., and Kable, E.J.D., 1974, Sea floor basalt alteration: some chemical and Sr isotopic effects: Contrib. Mineral. Petrol., 44, 219- .

Hatherton, T., and Dickerson, W.R., 1969, The relationship between andesite volcanism and seismicity in Indonesia, the Lesser Antilles, and other island arcs: J. Geophys. Res., 74, 5301-5310.

Hawkesworth, C.J., O'Nions, R.K., Pankhurst, R.J., Hamilton, P.J., and Evensen, N.M., 1977, A geochemical study of island arc and back arc tholeiites from the Scotia Sea: Earth Planet. Sci. Lett., 45, 253-262.

Helz, R.T., 1973, Phase relations of basalt in their melting range at P_{H_2O} = 5 kb as a function of oxygen fugacity: J Petrol., 14, 249-302.

Helz, R.T., 1979, Alkali exchange between hornblende and melt: a temperature sensitive reaction: Amer. Mineral., 64, 953-965.

Haselton, H.,T., Jr., Hovis, G.L., Hemingway, B.S., and Robie, R.A., 1983, Calorimetric investigation of the excess entropy of mixing in analbite-sanidine solid solutions: lack of evidence for Na, K short-range order and implications for two feldspar thermometry: Amer. Mineral., 68, 398-413.

Henderson, L.H., 1939, Detailed geological mapping and fault studies of the San Jacinto tunnel line aicance of their displacements: Geol. Soc. Amer. Bull., 64, 443-458.

Hill, R.I., 1981a, Field, petrologic and isotopic studies of the intrusive complex of San Jacinto Mountain: in Brown, A.R., and Ruff, R.W., (eds.), Geology of the San Jacinto Mountains: South Coast Geological Society Annual Field Trip Guidebook No. 9, 76-89.

Hill, R.I., 1981b, Geology of Garner Valley and Vicinity: in Brown, A.R., and Ruff, R.W., (eds.), Geology of the San Jacinto Mountains: South Coast Geological Society Annual Field Trip Guidebook No. 9, 90-99.

Hill, R.I., Silver, L.T., and Taylor, H.P., Jr., 1982, $^{87}Sr/^{86}Sr$ and $^{18}O/^{16}O$ variations within a single intrusive unit of the Peninsular Ranges batholith, San Jacinto Mountains, southern California: in Abstracts of the Fifth International Conference on Geochronology, Cosmochronology, and Isotope Geology, Nikko, Japan, 141-142.

Hills, E.S., 1959, Cauldron subsidences, granitic rocks and crustal fracturing in S.E. Australia: Geol. Rdsch. 47, 543-561.

Hine, R., Williams, I.S., Chappell, B.W., and White, A.J.R., 1978, Geochemical contrasts between I- and S-type granitoids of the Kosciusko Batholith: J. Geol. Soc. Aust., 25, 219-234.

Hofmann, A.W., and Hart, S.R., 1978, An assessment of local and regional isotopic equilibrium in the mantle: Earth Planet. Sci. Lett., 38, 44-62.

Holdaway, M.J., 1971, Stability of andalusite and the aluminum silicate phase diagram: Am. J. Sci., 271, 97-131.

Holdaway, M.J., and Lee, S.M., 1977, Fe-Mg cordierite stability in high-grade pelitic rocks based on experimental, theoretical, and natural observations: Contrib. Mineral. Petrol., 63, 175-198.

Howell, D.G., and Vedder, J., 1981, Structural implications of stratigraphic discontinuities across the Southern California Borderland, in Ernst, W.G., (ed.), The Geotectonic Development of California: PrenticeHall Inc., 535-558.

Howell, D.G., Fuis, G.S., Haxel, G.B., and Keller, B.R., 1982a, Terrane accretion and dispersion, southern U.S. Cordillera: Geol. Soc. Amer. Abstacts with Programs, 14, 519.

Howell, D.G., Gibson, D., Fuis, G.S., Haxel, G.B., Keller, B.R., McCulloh, T.H., Sbar, M.L., Silver, L.T., Vedder, J.G., and Vedder, L., 1982b, Continent-ocean transect C-3, southern California to New Mexico: Geol. Soc. Amer. Abstracts with Programs, 14, 519.

Hudson, F.S., 1922, Geology of the Cuyamaca region of California, with special reference to the origin of the nickeliferous pyrrhotite: Univ. Calif. Dept. Geol. Sci. Bull., 13, 175-252.

Huppert, H.E., and Turner, J.S., 1981, Double-diffusive convection: J. Fluid Mech., 106, 299-329.

Huppert, H.E., and Sparks, R.S.J., 1980a, The fluid dynamics of a basaltic magma chamber replenished by influx of hot, dense ultrabasic magma: Contrib. Mineral. Petrol., 75, 279-289.

Huppert, H.E., and Sparks, R.S.J., 1980b, Restrictions of the compositions of mid-ocean ridge basalts: A fluid dynamical investigation: Nature, 286, 46-48.

Imlay, R.W., 1963, Jurassic fossils from Southern California: Jour. Paleontol., 37, 97-107.

Imlay, R.W., 1964, Middle and Upper Jurassic fossils from Southern California: Jour. Paleontol., 38, 505-509.

Jacobsen, S.B., and Wasserburg, G.J., 1980, The mean age of mantle and crustal reservoirs: J. Geophys. Res., 84, 7411-7427.

Jahns, R.H., 1954, Geology of the Peninsular Range province, southern California and Baja California, in Jahns, R.H., (ed.), Geology of Southern California: Calif. Div. Mines Bull., 170, Ch II, 29-52.

Jakes, P., and White, A.J.R., 1972, Major and trace element abundances in volcanic rocks of island arcs: Geol. Soc. Amer. Bull., 83, 29-40.

Jambon, A., 1982, Tracer diffusion in granitic melts: experimental results for Na, K, Rb, Cs, Ca, Sr, Ba, Ce, Eu to 1300^0C and a model of calculation: J. Geophys. Res., 87, 10797-10810.

Jaques, A.L., and Green, D.H., 1980, Anhydrous melting of peridotite at 0-15 kb pressure and the genesis of tholeiitic basalts: Contrib. Mineral. Petrol., 73, 287-310.

Johannes, W., 1978, Melting of plagioclase in the system Ab-An-H_2O and Qz-Ab-An-H_2O at P_{H_2O} = 5 kbars, an equilibrium problem: Contrib. Mineral. Petrol., 66, 295-303.

Johnson, R.W., 1977, Distribution and major-element chemistry of late Cainozoic volcanoes at the southern margin of the Bismark Sea, Papua, New Guinea: Bur. Miner. Resour. Aus. Rept. 188.

Johnson, W.R., MacKenzie, D.M., and Smith, I.E.M., 1978, Volcanic rock associations at convergent plate boundaries: reappraisal of the concept using histories from Papua New Guinea: Geol. Soc. Amer. Bull., 89, 96-106.

Jones, D.A., Miller, R.H., and Kling, S.A., Late Jurassic fossils from Santiago Peak volcanics, San Diego County, California: Geol. Soc. Amer. Abstracts with Programs, 15, 413.

Jones, D.L., Blake, M.C., and Rangin, C., 1976, The four Jurassic belts of northern California: their significance to the geology of the Southern California Borderlands, in Howell, D.G., (ed.), Aspects of the Geologic History of the California Continental Borderland: Pacific Section, Amer. Assoc. Petroleum Geologists Misc. Pub. 24, 343-362.

Jones, D.L., Cox, A., Coney, P., and Beck, M., 1981, The growth of western North America: Scientific American, 247, 70-84.

Joyce, A.S., 1973, Petrogenesis of the Murrumbidgee Batholith, A.C.T.: J. Geol. Soc. Aust., 20, 179-197.

Kay, R.W., Sun, S.-S., and Lee Hu, C.-N., 1978, Pb and Sr isotopes from the Aleutian Islands and Pribilof Islands, Alaska: Geochim. Cosmochim. Acta, 42, 263-273.

Kerrick, D.M., 1972, Experimental determination of muscovite+quartz stability with $P_{H_2O} < P_{tot}$: Am. J. Sci., 272, 946-958.

Kilmer, F.H., 1979, A geologic sketch of Cedros Island, Baja California, Mexico: in Abbott, P.L. and Gastil, R.G., (eds.), Baja California Geology: Dept. Geol. Sci., San Diego State University, 11-28.

Kistler, R.W., and Peterman, Z.E., 1973, Variations in Sr, Rb, K, Na and initial $^{87}Sr/^{86}Sr$ in Mesozoic granitic rocks and intruded wall rocks in central California: Geol. Soc. Amer. Bull., 84, 3489-3512.

Kistler, R.W., and Peterman, Z.E., 1978, Reconstruction of crustal blocks of California on the basis of initial strontium isotopic composition of Mesozoic granitic rocks: U.S. Geol. Surv. Prof. Paper 1071.

Kistler, R.W., Peterman, Z.E., Ross, D.C., and Gottfried, D., 1973, Strontium isotopes and the San Andreas fault: in Kovach, R.L., and Nur, A., (eds.) Proceedings of the conference on tectonic problems of the San Andreas fault system, Stanford Univ. Pubs. Geol. Sci., XIII, 339-347.

Krogh, T.E., 1973, A low contamination method for hydrothermal decomposition of zircon and extraction of U and Pb for isotopic age determinations: Geochim. Cosmochim. Acta, 37, 485-494.

Krumbein, W.C., and Sloss, L.L., 1963, Stratigraphy and Sedimentation, 2nd Edition: W.H. Freeman and Co., San Francisco, 660 p.

Krummenacher, D., Gastil, R.G., Bushee, J., and Doupont, J., 1975, K-Ar apparent ages, Peninsular Ranges Batholith, southern California: Geol. Soc. Amer. Bull., 86, 760-768.

Kuno, H., 1966, Review of pyroxene relations in terrestrial rocks in the light of recent experimental works: Mineral. J., 5, 21-43.

Kushiro, I., 1978, Density and viscosity of hydrous calc-alkaline magma at high pressures: Carnegie Inst. Wash. Yearb. 77, 675-677.

Kushiro, I., Yoder, H.S., and Mysen, B.O., 1976, Viscosities of basalt and andesite at high pressures: J. Geophys. Res., 81, 6351-6356.

Kyser, T.K., and O'Neil, J.R., 1978, Oxygen isotope relations among oceanic tholeiites, alkali basalts, and ultramafic nodules: U.S. Geol. Surv. Open-File Rept. 78-701, 237-240.

Kyser, T.K., O'Neil, J.R., and Carmichael, I.S.E., 1981, Oxygen isotope thermometry of basic lavas and mantle nodules: Contrib. Mineral. Petrol., 77, 11-23.

Kyser, T.K., O'Neil, J.R., and Carmichael, I.S.E., 1982, Genetic relations among basic lavas and ultramafic nodules: Evidence from oxygen isotope compositions: Contrib. Mineral. Petrol., 81, 88-102.

Laird, J., 1977, Phase equilibria in mafic schist and the polymetamorphic history of Vermont: Unpublished PhD thesis, Calif. Inst. Technology.

deLaeter, J.R., Vernon, M.J., and Compston, W., 1972, Revision of lunar Rb-Sr ages: Geochim. Cosmochim. Acta, 37, 700-702.

Lamb, T.N., 1970, Fossiliferous Triassic(?) meta-sedimentary rocks near Sun City, Riverside County, California: Geol. Soc. Amer. Abstracts with Programs, 2, 110-111.

Lanphere, M.A., Wasserburg, G.J., Albee, A.L., and Tilton, G.R., 1964, Redistribution of strontium and rubidium isotopes during metamorphism: Isotopic and Cosmic Chemistry, North-Holland Publishing Company, Amsterdam, 269-320.

Larsen, E.S., Jr., 1948, Batholith and associated rocks of Corona, Elsinore, and San Luis Rey quadrangles, Southern California: Geol. Soc. Amer. Memoir 29, 182 p.

Larson, P.A., Mudie, J.D., and Larson, R.L., 1972, Magnetic anomalies and fracture-zone trends in the Gulf of California: Geol. Soc. Amer. Bull., 83, 3361-2268.

Lawson, A.C., and others, 1908, The California earthquake of April 18, 1906: Carnegie Inst. Wash. Pub. 87, v. 1, 451p.

Lindgren, W., 1915, The igneous geology of the Cordilleran and its problems: in Problems of American Geology, New Haven, Yale University, Silliman Foundation, 234-286.

Lockwood, J.P., 1961, Geology of an area in the western Santa Rosa Mountains of southern California, with special emphasis on a previously unreported mylonite belt: Unpublished senior thesis, Univ. of California, Riverside.

Loiselle, M.C., and Wones, D.R., 1979, Characteristics and origin of anorogenic granites: Geol. Soc. Amer. Abstracts with Programs, 11, 468.

Long, P.E., 1978, Experimental determination of partition coefficients for Rb, Sr, and Ba between alkali feldspar and silicate liquid: Geochim. Cosmochim. Acta, 42, 833-846.

Lothringer, C.J., Gastil, G., and Miller, R.H., 1982, Lower Ordovician Carbonate-Quartzite sequence near Rancho San Marcos, Baja California: Geol. Soc. Amer. Abstracts with Programs, 14, 181.

Ludington, S.D., 1978, The biotite-apatite geothermometer revisited: Amer. Minerologist, 63, 551-553.

Ma, K., Li, H., and Xue, X., 1980, Isotopic ages of the Sinian in the East Yangtze Gorges: Bull. Chinese Acad. Geol. Sciences VIII, 1, 39-55.

Maaløe, S., and Petersen, T.S., 1981, Petrogenesis of oceanic andesites: J. Geophys. Res., 86, 10273-10286.

McBirney, A.J., 1980, Mixing and unmixing of magmas: J. Volcanol. Geotherm. Res., 7, 357-371.

McBirney, A.J., and Noyes, R.M., 1979, Crystallization and layering of the Skaergaard intrusion: J. Petrol., 20, 487-554.

McCulloch, M.T., Gregory, R.T., Wasserburg, G.J., and Taylor, H.P., Jr, 1980, A neodymium, strontium, and oxygen isotopic study of the Cretaceous Semail ophiolite and implications for the petrogenesis and seawater-hydrothermal alteration of oceanic crust: Earth Planet. Sci. Lett., 46, 201-211.

McCulloch, M.T., Gregory, R.T., Wasserberg, G.J., and Taylor, H.P., Jr., 1981, Sm-Nd, Rb-Sr, and $^{18}O/^{16}O$ isotopic systematics in an oceanic crustal section: evidence from the Semail ophiolite: J. Geophys. Res., 2721-2735.

McCulloch, M.T., Jaques, A.L., Nelson, D.R., and Lewis, J.D., 1983, Nd and Sr isotopes from kimberlites and lamproites from Western Australia: an enriched mantle origin: Nature, 302, 400-403.

McEldowney, R.C., 1970, Geology of the nothern Sierra Pinta, Baja California, Mexico: Unpublished M.S. thesis, San Diego State University, 78p.

McJunkin, R.D., Davis, T.E., and Criscione, J.J., 1979, An isotopic age for the Smartville ophiolite and the obduction of metavolcnaic rocks in the north-western Sierran foothills, California: Geol. Soc. Amer. Abstracts with Programs, 11, 91.

McKenzie, D.M., and Chappell, B.W., 1972, Shoshonitic and calc-alkaline lavas from the highlands of Papua New Guinea: Contrib. Mineral. Petrol., 35, 50-62.

McNutt, R.H., Clark, A.H., and Zentilli, M., 1979, Lead isotopic compositions of Andean igneous rocks, latitudes 26°-29°: petrologic and metallogenic implications: Econ. Geol., 74, 827-837.

MacKevett, E.M., 1951, Geology of the Jurupa Mountains, San Bernadino and Riverside Counties, California: Calif. Div. Mines Spec. Report 5.

Magaritz, M., and Hofmann, A.W., 1978a, Diffusion of Sr, Ba, and Na in obsidian: Geochim. Cosmochim. Acta, 42, 595-605.

Magaritz, M., and Hofmann, A.W., 1978b, Diffusion of Eu and Gd in basalt and obsidian: Geochim. Cosmochim. Acta, 42, 847-858.

Magaritz, M., Whitford, D.J., and James, D.E., 1978, Oxygen isotopes and the origin of high-$^{87}Sr/^{86}Sr$ andesites: Earth Planet. Sci. Lett., 40, 220-230.

Marsh, B.D., 1979, Island arc volcanism: American Scientist, 67, 161-172

Masi, U., O'Neil, J.R., and Kistler, R.W., 1981, Stable isotope systematics in Mesozoic granites of central and northern California and southwest Oregon: Contrib. Mineral. Petrol., 76, 116-126.

Matsuhisa, Y., 1979, Oxygen isotopic compositions of volcanic rocks from the East Japan island arcs and their bearing on petrogenesis: J. Volcanol. Geotherm. Res., 5, 271-296.

Matsuhisa, Y., Matsubaya, O., and Sakai, H., 1973, Oxygen isotope variations in magmatic differentiation processes of the volcanic rocks of Japan: Contrib. Mineral. Petrol., 39, 277-288.

Mattinson, J.M., and Hill, D.J., 1976, Age of plutonic basement rocks, Santa Cruz Island, California: in Howell, D.G., (ed.), Aspects of the Geologic History of the California Continental Borderland: Pacific Section, Am. Assoc. Petroleum Geologists Misc. Pub. 24, 53-59.

Menzies, M., and Seyfried, W.E., Jr., 1979, Basalt-seawater interaction: trace element and strontium isotopic variations in experimentally altered glassy basalt: Earth Planet. Sci Lett., 44, 463-472.

Merriam, R.H., 1946, Igneous and metamorphic rocks of the southwestern part of the Ramona quadrangle, San Diego, California: Geol. Soc. Amer. Bull., 57, 223-260.

Mertzman, S.A., Jr., 1977, The petrology and geochemistry of the Medicine Lake Volcano, California: Contrib. Mineral. Petrol., 62, 221-247.

Miller, W.J., 1944, Geology of the Palm Springs-Blythe strip, Riverside County, California: Calif. Jour. Mines and Geology, 40, 11-72.

Miller, W.J., 1946, Crystalline rocks of Southern California: Geol. Soc. Amer. Bull., 57, 457-542.

Minch, J.A., 1969, A depositional contact between the pre-batholithic Jurassic and Cretaceous rocks in Baja California, Mexico: Geol. Soc. Amer. Abstracts with Programs for 1969, part 3, 42-43.

Moore, D.G., 1969, Reflection profiling studies of the California continental borderland: Geol. Soc. Amer. Spec. Paper 107, 138p.

Moore, J.G., 1959, The quartz diorite boundary line in the western United States: Jour. Geology, 67, 197-210.

Moore, T.E., 1979, Geologic summary of the Sierra de San Andres ophiolite: in Abbott, P.L. and Gastil, R.G., (eds.), Baja California Geology, Dept. Geol. Sci., San Diego State University, 95-106.

Moran, A.I., 1976, Allochthonous carbonate debris in Mesozoic flysch deposits in the Santa Ana Mountains, California: Am. Assoc. Petroleum Geologists Bull., 60, 2038-2043.

Morton, D.M., 1972, Geology of the Lakeview-Perris quadrangles, Riverside County, California: Calif. Div. Mines and Geol. Map sheet 19, scale 1:24000.

Morton, D.M., Matti, J.C., and Cox, B.F., 1980, Geologic map of the San Jacinto wilderness, Riverside County, California: U.S. Geol. Surv. Map MF-1159-A, scale 1:62500.

Morton, D.M., and Long, L.E, 1982, Rb-Sr dating of the provenance and time of diagenesis of the Devonian Woodford Shale, West Texas: in Abstracts of the Fifth International Conference on Geochronology, Cosmochronology, and Isotope Geology, Nikko, Japan, 254-255.

Morton, D.M., and Gray, C.H., 1971, Geology of the northern Peninsular Ranges, southern California: Univ. of California, Riverside Campus Museum Contrib., 1, 60-93.

Moscoso, B.A., 1967, A thick section of "flysch" in the Santa Ana Mountains, southern California: Unpublished M.S. thesis, San Diego State University, 106 p.

Muehlenbachs, K., and Kushiro, I., 1974, Oxygen isotope exchange and equilibration of silicates with CO_2 or O_2, Carnegie Inst. Wash. Yearb. 73, 232-236.

Muehlenbachs, K., and Byerly, K., 1982, ^{18}O-enrichment of silicic magmas caused by crystal fractionation at the Galapagos spreading center: Cntrib. Mineral. Petrol., 79, 76-79.

Mueller, R.F., and Condie, K.C., 1964, Stability relations of carbon mineral assemblages in the Southern California batholith: Jour. Geology, 72, 400-411.

Mysen, B.O., 1979, Trace element partitioning between garnet peridotite minerals and water-rich vapor: experimental data from 5 to 30 kbar: Amer. Mineral., 64, 274-287.

Nakamura, Y., and Kushiro, I., 1974, Composition of the gas phase in Mg_2SiO_4-SiO_2-H_2O at 15 kbar: Carnegie Inst. Wash. Yearb. 73, 255-259.

Nelson, S.A., and Carmichael, I.S.E., 1979, Partial molar volumes of oxide components in silicate liquids: Contrib. Mineral. Petrol., 71, 117-124.

Nicholls, I.A., 1974, Liquids in equilibrium with peridotitic mineral assemblages at high water pressures: Contrib. Mineral. Petrol., 45, 289-316.

Nicholls, I.A., and Ringwood, A.E., 1973, Effect of water on olivine stability in tholeiites and the production of silica-saturated magmas in the island arc environment: J. Geol., 81, 285-300.

Nilsen, T.H., 1978, Late Cretaceous geology of California and the problem of the Proto - San Andreas Fault, in, Howell, D.G., and McDougall, K.A., (eds.), Mesozoic Paleogeography of the Western United States: Pacific Section, Soc. Econ. Palaeontologists and Mineralogists, Pacific Coast Paleogeography Symposium 2, 559-573.

Norrish, K., and Hutton, J.T., 1969, An accurate x-ray spectrographic method for the analysis of a wide range of geological samples: Geochim. et Cosmochim. Acta, 33, 431-453.

Norrish, K., and Chappell, B.W., 1977, X-ray fluorescence spectrometry: in Zussman, J., (ed.), Physical Methods in Determinative Mineralogy, 2nd edition, Academic Press, London, 201-272.

Norton, D., and Knight, J.E., 1977, Transport phenomena in hydrothermal systems: cooling plutons: Am. J. Sci., 277, 937-981.

Norton, D., and Taylor, H.P., Jr., 1979, Quantitative simulation of the hydrothermal systems of crystallizing magmas on the basis of transport theory and oxygen isotope data: an analysis of the Skaergaard Intrusion: J. Petrol., 20, 421-486.

Obradovich, J.D., and Peterman, Z.E., 1968, Geochronology of the Belt Series, Montana: Can. Jour. Earth Sci., 5, 737-747.

O'Hara, M.J., 1965, Primary magmas and the origin of basalts: Scottish J. Geol., 1, 19-40.

O'Hara, M.J., 1977, Geochemical evolution during fractional crystallization of a periodically refilled magma chamber: Nature, 266, 503-507.

O'Hara, M.J., 1980, Nonlinear nature of the unavoidable long-lived isotopic, trace and major element contamination of a developing magma chamber: Phil. Trans. Roy. Soc. Lond., A297, 215-227.

O'Hara, M.J., and Mathews, R.E., 1981, Geochemical evolution in an advancing, periodically replenished, periodically tapped, continuously fractionated magma chamber: J. Geol. Soc. Lond., 138, 237-277.

Oliver, H.W., (ed.), 1980, Interpretation of the gravity map of California and its continental margin: Calif. Div. Mines and Geology, Bull 205.

O'Neil, J.R., and Chappell, B.W., 1977, Oxygen and hydrogen isotope relations in the Berridale Batholith: J. Geol. Soc., 133, 559-571.

O'Nions, R.K., and Pankhurst, R.J., 1974, Petrogenic significance of isotope and trace element variations in volcanic rocks from the Mid-Atlantic: J. Petrol., 15, 603-634.

O'Nions, R.K., Carter, S.R., Evensen, N.M., and Hamilton, P.J., 1979, Geochemical and cosmochemical applications of Nd isotope analysis: Ann. Rev. Earth Planet. Sci., 7, 11-38.

Oversby, V.M., and Ewart, A., 1972, Lead isotopic composition of Tonga-Kermadec volcanics and their petrogenetic significance: Contr. Mineral. Petrol., 37, 181-210.

Owen, M., and Wyborn, D., 1979, Geology and geochemistry of the Tantangara and Brindabella area: Bur. Miner. Res. Aus. Bull. 204

Page, R.W., and Johnson, R.W., 1974, Strontium isotope ratios of Quaternary volcanic rocks from Papua New Guinea: Lithos, 7, 91-100.

Parcel, R.F., Jr., 1981, Structure and petrology of the Santa Rosa Shear Zone in the Pinyon Flat area, Riverside County, California, in Brown, A.R., and Ruff, R.W., (eds.), Geology of the San Jacinto Mountains: South Coast Geological Society, Annual Field Trip Guidebook No. 9, 139-150.

Pearce, J.A., and Norry, M.J., 1979, Petrogenetic implications of Ti, Zr, Y, and Nb variations in volcanic rocks: Contrib. Mineral. Petrol., 69, 33-47.

Perry, E.A., Jr., and Turekian, K.K., 1974, The effects of diagenesis on the redistribution of strontium isotopes in shales: Geochim. Cosmochim. Acta, 38, 929-935.

Peterman, Z.E., Hedge, C.E., Coleman, R.G., and Snavely, P.D., Jr., 1967, $^{87}Sr/^{86}Sr$ ratios in some eugeosynclinal sedimentary rocks and their bearing on the origin of granitic magma in orogenic belts: Earth Planet. Sci. Lett., 2, 433-439.

Pidgeon, R.T., and Compston, W., 1965, The age and origin of the Cooma granite and its associated metamorphic zones, New South Wales: J. Petrol., 6, 193-222.

Piwinskii, A.J., 1968, Experimental studies of igneous rock series, central Sierra Nevada batholith, California: J. Geol., 76, 548-570.

Platt, J.P., 1976, The significance of the Catalina schist in the history of the southern California Borderland, in Howell, D.G., (ed.), Aspects of the Geologic History of the California Continental Borderland: Pacific Section, Amer. Assoc. Petroleum Geologists Misc. Pub. 24, 47-52.

Poldervaart, A., 1955, Chemistry of the earth's crust: Geol. Soc. Amer. Mem. 62, 119-144.

Presnall, D.C., and Bateman, P.C., 1973, Fusion relationships in the system $NaAlSi_3O_8$-$CaAl_2Si_2O_8$-$KAlSi_3O_8$-SiO_2-H_2O and generation of granitic magmas in the Sierra Nevada Batholith: Geol. Soc. Amer. Bull., 84, 3181-3202.

Rangin, C., 1978, Speculative model of Mesozoic geodynamics, central Baja California to northeastern Sonora (Mexico), in Howell, D.G., and McDougall, K.A., (eds.), Mesozoic Paleogeography of the western United States: Pacific Section, Soc. Econ. Paleontologists and Mineralogists, Pacific Coast Paleogeography Symposium 2, 85-106.

Rayleigh, J.W.S., 1896, Theoretical considerations respecting the separation of gases by diffusion and similar processes: Philos. Mag., 42, 493.

Reed, B.L., and Lanphere, M., 1974, Chemical variations across the Alaska-Aleutian Range batholith: Jour. Res. U.S. Geol. Surv., 2, 343-352.

Rickard, M.J., and Ward, P., 1981, Paleozoic crustal thickness in the southern part of the Lachlan orogen deduced from volcano and pluton spacing geometry: Jour. Geol. Soc. Aust., 28, 19-32.

Riley, G.H. and Compston, W., 1962, Theoretical and technical aspects of Rb-Sr geochronolgy: Geochim. Cosmochim. Acta, 26, 1255-1281.

Rittman, A., 1953, Magmatic character and tectonic position of the Indonesian volcanoes: Bull. Volcanol., 14, 45.

Roddick, J.C.M., 1974, Responses of strontium isotopes to some crustal processes: Unpublished Ph.D. thesis, Australian National University, 350 p.

Roddick, J.C.M., and Compston, W., 1977, Strontium isotopic equilibrium: a solution to a paradox: Earth Planet. Sci. Lett., 34, 238-246.

Rogers, T.H., 1965, Santa Ana Sheet, Geologic Map of California: Calif. Div. Mines and Geology, Scale 1:250,000.

Rolfe, F., and Strong, A.M., 1918, The earthquake of April 21, 1918, in the San Jacinto Mountains: Bull. Seis. Soc. Amer., 8, 68.

Ross, R.J. Jr., Naeser, C.W., Izett, C.A., Obradovich, J.D., Bassett, M.G., Hughes, C.P., Cucks, L.R.M., Dean, W.T., Ingham, J.K., Jenkins, C.J., Richards, R.B., Sheldon, P.R., Toghill, P., Whittington, H.B., and Zalasiewicz, J., 1982, Fission-track dating of British Ordovician and Silurian stratotypes: Geol. Mag., 119, 135-153.

Saleeby, J.B., 1978, Kings River Ophiolite, southwest Sierra Nevada foothills, California: Geol. Soc. Amer. Bull., 89, 617-636.

Saleeby, J.B., 1979, Kaweah serpentinite melange, southwest Sierra Nevada foothills, California: Geol. Soc. Amer. Bull., 90, 29-49.

Saleeby, J.B., 1981, Ocean floor accretion and volcano-plutonic arc evolution of the Mesozoic Sierra Nevada: in Ernst, W.G., ed., The Geotectonic Development of California, Prentice-Hall Inc., 132-181.

Saleeby, J.B., 1982, Polygenetic ophiolite belt of the California Sierra Nevada - geochronological and tectonostratagraphic development: J. Geophys. Res., 87, 1803-1824.

Savage, D.E., Downs, T., and Poe, O.J., 1954, Cenozoic land life of southern California: in Jahns, R.H., (ed.), Geology of southern California: Calif. Div. Mines. Bull., 170, 43-58.

Scarfe, C.M., 1973, Viscosity of basic magmas at varying pressure: Nature, 241, 101-102.

Schwarcz, H.P., 1969, Pre-Cretaceous sedimentation and metamorphism in the Winchester area, northern Peninsular Ranges, California: Geol. Soc. Amer. Spec. Paper 100, 63 p.

Schweickert, R.A., 1981, Tectonic evolution of the Sierra Nevada Range : in Ernst, W.G., (ed.), The Geotectonic Development of California, Prentice-Hall Inc., 87-131.

Sekine, T., Wyllie, P.J., and Baker, D.R., 1981, Phase relationships at 30 kbar for quartz eclogite composition in CaO-MgO-Al_2O_3-SiO_2-H_2O with implications for subduction zone magmas: Amer. Mineral., 66, 935-950.

Sharp, R.V., 1967, San Jacinto Fault Zone in the Peninsular Ranges of Southern California: Geol. Soc. Amer. Bull., 78, 705-730.

Sharp, R.V., 1979, Some Characteristics of the Eastern Peninsular Ranges Mylonite Zone, in Proceedings of Conference VIII - Analysis of Actual Fault Zones in Bedrock: U.S.G.S. Open File Report 79-1239.

Sharp, R.V., 1981, Variable rates of strike slip on the San Jacinto fault zone: J. Geophys. Res., 86, 1754-1762.

Sharp, R.P., Allen, C.R., and Meier, M.F., 1957, Pleistocene glaciers on southern California mountains: Amer. Jour. Sci., 257, 81-94.

Shaw, H.F., III, 1983, Sm-Nd and Rb-Sr isotopic systematics of tektites and other impactites, Appalachian mafic rocks, and marine carbonates and phosphates: Unpublished Ph.D. thesis, California Institute of Technology.

Shaw, H.R., 1965, Comments on viscosity, crystal settling and convection in granite magmas: Am. J. Sci., 263, 120-152.

Shiro, Y., and Sakai, H., 1972, Calculation of the reduced partition function ratios of alpha-beta quartz and calcite: Japan Chem. Soc. Bull., 45, 2355-2359.

Shor, G.G., Jr., and Raitt, R.W., 1958, Seismic studies in the southern California borderland: Proceedings XX International Geological Congress, Mexico, 1956, Section IX, 243-249.

Shreiner, G.D.L., 1958, Comparison of the Rb^{87}-Sr^{87} ages of the Red Granite of the Bushveld Complex from measurements on the total rock and separated mineral fractions: Proc. Roy. Soc., A, 245, 112.

Silberling, N.J., Schoellhamer, J.E., Gray, C.H., Jr, and Imlay, R.W., 1961, Upper Jurassic fossils from Bedford Canyon Formation, southern California: Bull. Amer. Assoc. Petroleum Geologists, 45, 1746-1765.

Silver, L.T., 1971, Problems of crystalline rocks of the Transverse Ranges: Geol. Soc. Amer. Abstracts with Programs, 3, 193-194.

Silver, L.T., 1974, Precambrian and "Precambrian(?)" crystalline rocks of the southwestern Basin and Range province of California and Arizona: Geol. Soc. Amer. Abstracts with Programs, 6, 253-254.

Silver, L.T., 1982, Evidence and a model for west-directed Early to Mid-Cenozoic basement overthrusting in southern California: Geol. Soc. Amer. Abstracts with Programs, 14, 617.

Silver, L.T., 1983, Paleogene overthrusting in the tectonic evolution of the Transverse Ranges, Mojave and Salinian regions, California: Geol. Soc. Amer. Abstracts with Programs, 15, 438.

Silver, L.T., and Anderson, T.H., 1974, Possible left-lateral early to middle Mesozoic disruption of the southwestern North American craton margin: Geol. Soc. Amer. Abstracts with Programs, 6, 955-956.

Silver, L.T., and Anderson, T.H., 1983, Further evidence and analysis of the role of the Mojave-Sonora Megashear(s) in Mesozoic Cordilleran tectonics: Geol. Soc. Amer. Abstracts with Programs, 15, 273.

Silver, L.T., and Early, T.O., 1977, Rubidium-strontium fractionation domains in the Peninsular Ranges batholith and their implication for magmatic arc evolution: EOS (Trans. Amer. Geophysical Union), 58, 532.

Silver, L.T., Stehli, F.G., and Allen, C.R., 1956, Lower Cretaceous prebatholithic rocks of northern Baja California, Mexico: 20th Internat. Geol. Congr., Mexico City, Resumenes de los Trabajos Presentados, 30.

Silver, L.T., Stehli, F.G., and Allen, C.R., 1963, Lower Cretaceous prebatholithic rocks of northern Baja California, Mexico: Am. Assoc. Petroleum Geologists Bull., 47, 2054-2059.

Silver, L.T., Allen, C.R., and Stehli, F.G., 1969, Geological and geochronological observations on a portion of the Peninsular Ranges batholith of northwestern Baja California, Mexico: Geol. Soc. Amer. Spec. Paper 121, 279.

Silver, L.T., Early, T.O., and Anderson, T.H., 1975, Petrological, geochemical and geochronological asymmetries of the Peninsular Ranges batholith: Geol. Soc. Amer. Abstracts with Programs 7, 375-376.

Silver, L.T., Anderson, C.A., Crittenden, M., and Robertson, J.M., 1977, Chronostratigraphic elements of the Precambrian rocks of the southwestern and far western United States: Geol. Soc. Amer. Abstracts with Programs 9, 1176.

Silver, L.T., Taylor, H.P., Jr., and Chappell, B.W., 1979, Some petrological, geochemical and gechronological observations of the Peninsular Ranges batholith near the International border of the U.S.A. and Mexico: in Abbott, P.L., and Todd, V.R., (eds.), Mesozoic Crystalline Rocks, Manuscripts and road logs prepared for the Geol. Soc. Amer. Annual Meeting, San Diego. Dept. of Geol. Sciences, San Diego State University, 83-110.

Simpson, C., 1983, The Borrego Springs shear zone: a major west directed thrust zone: Geol. Soc. Amer. Abstracts with Programs, 15, 419.

Smith, J.P., 1898, Geographical relation of the Trias of California: Jour. Geol., 6, 776-787.

Smith, J.P., 1914, The Middle Triassic marine invertebrate faunas of North America: U.S. Geol. Surv. Prof. Pap., 83, 254.

Sparks, R.S.J., Meyer, P., and Sigurdsson, H., 1980, Density variation amongst mid-ocean ridge basalts: implications for magma mixing and the scarcity of primitive lavas: Earth Planet. Sci. Lett., 46, 419-430.

Spera, F.J., Yuen, D.A., and Kirshvink, S.J., 1982, Thermal boundary layer convection in silicic magma chambers: effects of temperature dependant rheology and implications for thermogravitational chemical fractionation: J. Geophys. Res., 87, 8755-8767.

Steiger, R.H., and Jaeger, E., 1977, Subcommision on geochronology: Convention on the use of decay constants in geo- and cosmochronology: Earth Planet. Sci. Lett., 36, 359-362.

Stern, C.R., and Wyllie, P.J., 1978, Phase compositions through crystallization intervals in basalt-andesite-H_2O at 30 kbar with implications for subduction zone magmas: Amer. Mineral., 63, 641-663.

Streckeisen, A.L., 1973, Plutonic rocks. Classification and nomenclature recommended by the IUGS Subcommission on the Systematics of Igneous Rocks: Geotimes: 18, 26-30.

Stolper, E., and Walker, D., 1980, Melt density and the average composition of basalt: Contrib. Mineral. Petrol., 74, 7-12.

Swanson, D.A., 1972, Magma supply rate at Kilauea Volcano, 1952-1971: Science, 175, 169-170.

Sydnor, R.H., 1975, Geology of the northeast border zone of the San Jacinto Pluton, Palm Springs, California: Unpublished M.S. thesis, Univ. California, Riverside.

Sun, S.-S., 1980, Lead isotopic study of young volcanic rocks from mid-ocean ridges, ocean islands and island arcs: Phil. Trans. Roy. Soc. Lond., A297, 409-445.

Tatsumi, Y., and Ishizaka, K., 1981, Existence of andesitic primary magma: an example from southwest Japan: Earth Plane. Sci. Lett., 53 124-130.

Tatsumoto, M., and Knight, R.J., 1969, Isotopic composition of lead in volcanic rocks from central Honshu, with regard to basalt genesis: Earth Planet. Sci. Lett., 38, 53-86.

Taylor, H.P., Jr., 1968, The oxygen isotope geochemistry of igneous rocks: Contrib. Mineral. Petrol., 19, 1-71.

Taylor, H.P., Jr., 1971, Oxygen isotope evidence for large-scale interaction between meteoric groundwaters and Tertiary granodiorite intrusions, western Cascade Range, Oregon: J. Geophys. Res., 76, 7855-7874.

Taylor, H.P., Jr., 1974, The application of oxygen and hydrogen isotope studies to the problem of hydrothermal alteration and ore deposition: Econ. Geol., 69, 843-883.

Taylor, H.P., Jr., 1977, Water/rock interactions and the origin of H_2O in granitic batholiths: Jl. Geol. Soc. Lond., 133, 509-558.

Taylor, H.P., Jr., 1978, Oxygen and hydrogen isotope studies of plutonic granitic rocks: Earth Planet. Sci. Lett., 38, 177-210.

Taylor, H.P., Jr., 1980, The effects of assimilation of country rocks by magmas on $^{18}O/^{16}O$ and $^{87}Sr/^{86}Sr$ systematics in igneous rocks: Earth. Planet. Sci. Lett., 47, 243-254.

Taylor, H.P., Jr., 1983, Oxygen and hydrogen isotope studies of hydrothermal interactions at submarine and subaerial spreading centers: Manuscript in preparation.

Taylor, H.P., Jr., and Epstein, S.E., 1962a, Relationship between $^{18}O/^{16}O$ ratios in co-existing minerals of igneous and metamorphic rocks, Part I: Principles and experimental results: Geol. Soc. Amer. Bull., 73, 461-480.

Taylor, H.P., Jr., and Epstein, S.E., 1962b, Relationship between $^{18}O/^{16}O$ ratios in co-existing minerals of igneous and metamorphic rocks, Part II: Geol. Soc. Amer. Bull., 73, 675-694.

Taylor, H.P., Jr., and Forester, R.W., 1971, Low-^{18}O igneous rocks from the intrusive complexes of Skye, Mull and Arndnamurchan, western Scotland: J. Petrol., 12, 465-497.

Taylor, H.P., Jr., and Silver, L.T., 1978, Oxygen isotope relationships in plutonic igneous rocks of the Peninsular Ranges batholith, southern and Baja California: in Zartman, R.E., (ed.), Short Papers of 4th International Conf. Geochronology, Cosmochronology, Isotope Geology, U.S. Geol. Surv. Open-File Report 78-701, 423-426.

Taylor, H.P., Jr., and Forester, R.W., 1979, An oxygen and hydrogen isotope study of the Skaergaard Intrusion and its country rocks: a description of a 55-M.Y. old fossil hydrothermal system: J. Petrol., 20, 355-419.

Taylor, S.R., 1967, The origin and growth of continents: Tectonophysics, 4, 17-34.

Taylor, S.R., 1979, Chemical composition and evolution of the continental crust: the Rare Earth Element evidence: in McElhinney, M.W., (ed.), The Earth: Its Origin, Structure and Evolution, Academic Press, London, 353-376.

Theodore, T.G., 1966, The fabric of a high-grade mylonite zone in Southern California: EOS (Am. Geophys. Union Trans.), 47, 491-492.

Theodore, T.G., 1970, Petrogenesis of mylonites of high metamorphic grade in the Peninsular Ranges of southern California: Geol. Soc. Amer. Bull., 81, 435-450.

Tilton, G.R., 1979, Isotopic studies of Cenozoic Andean calc-alkaline rocks: Carnegie Inst. Wash. Yearb. 78, 298-304.

Tilton, G.R., and Barreiro, B.A., Origin of lead in Andean calc-alkaline lavas, southern Peru: Science, 210, 1245-1247.

Todd, V.R., and Shaw, S.E., 1979, Structural, metamorphic and intrusive framework of the Peninsular Ranges batholith in southern San Diego County, California: in Abbott, P.L. and Todd, V.R., (eds), Mesozoic Crystalline Rocks, manuscripts and road logs prepared for the Geol. Soc. Amer. Annual Meeting, San Diego, 1979: Dept. of Geol. Sciences, San Diego State University, 177-231.

Tomita, T., 1935, On the chemical compositions of the Cenozoic alkaline suite of the circum-Japan Sea region: J. Shanghai Sci. Inst., Sect. II, 1, 227-306.

Tomkeiff, S.I., 1949, The volcanoes of Kamchatka, Bull. Volcanol., 8, 87.

Townley, S.D., 1918, The San Jacinto earthquakes of April 21, 1918: Bull. Seis. Soc. Amer., 8, 45-62.

Turi, B., and Taylor, H.P., Jr., 1971, An oxygen and hydrogen isotope study of a granodiorite pluton from the Southern California batholith: Geochim. Cosmochim. Acta, 35, 383-406.

Turner, J.S., 1980, A fluid dynamical model of differentiation and layering in magma chambers: Nature, 285, 213-215.

Unruh, M.E., and Ruff, R.W., 1981, History of gold mining in the south San Jacinto Mountains, Riverside County, California, in Brown, A.R., and Ruff, R.W., (eds.), Geology of the San Jacinto Mountains: South Coast Geological Society Annual Field Trip Guidebook No. 9, 219p.

Urey, H.C., 1947, The thermodynamic properties of isotopic substances: J. Chem. Soc., 1947, 562-581.

Walker, D., Shibata, T., and DeLong, S.E., 1979, Abyssal tholeiites from the Oceanographer Fracture Zone. II. Phase equilibria and mixing: Contrib. Mineral Petrol., 70, 111-125.

Walker, D.A., and Cameron, W.E., 1983, Boninite primary magmas: evidence from the Cape Vogel Peninsula, PNG: Contrib. Mineral. Petrol., 83, 150-158.

Wasserburg, G.J., Wetherill, G.W., and Wright, L.A., 1959, Ages in the Precambrian terrane of Death Valley, California: J. Geol., 67, 702-

Wasserburg, G.J., Papanastassiou, D.A., Nenow, E.V., and Bauman, C.A., 1969, A programmable magnetic field mass spectrometer with on-line data processing: Rev. Sci. Instruments, 40, 288-295.

Webb, R.W., 1939, Evidence of the age of a crystalline limestone in southern California: Jour. Geology, 47, 198-201.

White, A.J.R., and Chappell, B.W., 1977, Ultrametamorphism and granitoid genesis: Tectonophysics, 43, 7-22.

Wilcox, R.E., 1954, Petrology of Paricutin Volcano, Mexico: U.S. Geol. Surv. Bull. 965-C.

Willingham, C.R., 1981, Gravity anomaly patterns and fault interpretations in the San Bernadino Valley and western San Gorgonio Pass area, southern California: in Brown, A.R., and Ruff, R.W., (eds.), Geology of the San Jacinto Mountains: South Coast Geological Society Annual Field Trip Guidebook No. 9, 164-174.

Willis, B., 1912, Index to the stratigraphy of North America: U.S. Geol. Surv. Prof. Pap. 71, 894.

Wones, D.R., 1980, Contributions of crystallography, mineralogy and petrology to the geology of the Lucerne pluton, Hancock County, Maine: Am. Mineralogist, 65, 411-437.

Woodford, A.O., and Harriss, T.F., 1938, Geological reconnaissance across Sierra San Pedro Martir, Baja California: Geol. Soc. Amer. Bull., 49, 1297-1336.

Wright, L.B., 1946, Geology of Santa Rosa Mountains Area, Riverside County, California: Calif. J. Mines and Geology, 42, 9-13.

Wyborn, L.S., Chappell, B.W., and Wyborn, D., 1979, The Lachlan Fold Belt - Early Paleozoic links with Antarctica: Jour. Geol. Soc. Aust., 26, 277.

Wyborn, D., Chappell, B.W., and Johnson, R.M., 1981, Three S-type volcanic suites from the Lachlan Fold Belt, southeast Australia: J. Geophys. Res., 86, 10335-10348.

Wyborn, L.S., 1977, Aspects of the geology of the Snowy Mountains and their implications for the tectonic evolution of the Lachlan Fold Belt: Unpublished PhD thesis, Australian National University.

Wyllie, P.J., 1977, Crustal anatexis: an experimental review: Tectonophysics, 43, 41-71.

Wyllie, P.J., 1978, Water and magma generation at subduction zones: Bull. Volcanol., 41, 360-377.

Wyllie, P.J., 1981, Experimental petrology of subduction, andesites and batholiths: Trans. Geol. Soc. S. Afr., 82, 281-291.

Wyllie, P.J., Huang, W.L., Stern, C.R., and Maaløe, S., 1976, Granitic magmas: possible and impossible sources, water contents, and crystallization sequences: Can. Jour. Earth Sci., 13, 1007-1019.

Xenophontos, C., and Bond, G.C., 1978, Petrology, sedimentation, and paleogeography of the Smartville terrane (Jurassic) - bearing on the genesis of the Smartville ophiolite: in Howell, D.G., and McDougall, K.A., (eds.), Mesozoic Paleogeography of the Western United States: Pacific Section, Soc. Econ. Paleontologists and Mineralogists, Pacific Coast Paleogeography Symposium 2, 291-302.

Zhang, Z.C. Compston, W., and Page, R.W., 1982, The isotopic age of the Cambrian-Precambrian boundary from the Sinian-Lower Cambrian sequence in south China: in Abstracts of the Fifth International Conference on Geochronology, Cosmochronology, and Isotope Geology, Nikko, Japan, 411-412.

APPENDIX 1

ANALYTICAL PROCEDURES

Samples were analysed for Rb and Sr concentrations, and for $^{87}Sr/^{86}Sr$ by standard isotope dilution procedures. In general, a 60 - 100 mg of prepared powder was spiked appropriately, and washed into a cleaned teflon beaker with dilute HCl. The use of dilute acid is designed to prevent vigorous effervescence when the HF is added to carbonate-containing samples. All reagents were purified by sub-boiling distillation in a quartz still in this laboratory except for HF which was prepared by bubbling high-purity HF gas through sub-boiling distilled H_2O until saturation. Samples were dried down in a teflon tank flushed by high-purity nitrogen. When dry, 4 ml HF and 1 ml $HClO_4$ were added and allowed to stand in a nitrogen-flushed teflon tank for 6-8 hours. After evaporation to dryness a small amount of dilute HCl (2.5N) was added to the residue. This step was added to ensure complete conversion to chloride salts.

The chloride salt residue was dissolved in 2 ml 1N HCl, and added to a 20 x 1 cm column of Dowex AG50W-8X 100-200 cation exchange resin equilibrated to 2.5N HCl. Elution with 2.5N HCl followed. Rb and Sr fractions were collected in teflon beakers and dried down in nitrogen-flushed tanks. The Sr fraction was reprocessed to ensure complete separation of Sr from Rb.

Samples were loaded onto the side filamants of a degassed rhenium triple-filament assembly using distilled water. All analyses were performed on a 12 inch radius of curvature solid source mass spectrometer with magnetic peak switching and online data processing in

the laboratories of Prof. L.T. Silver in the Division of Geological and Planetary Sciences, California Institute of Technology, Pasadena.

For the Sr analysis, the center filament was initially run at 1,710°C and the current in the side filamants raised to 0.5 amp until the ^{85}Rb signal was negligible. The temperature of the center filament was then lowered to 890°C and current to the side filaments increased until a stable ^{88}Sr beam of $3x10^{-11}$ amp (±10%) was obtained. Data were collected for about 3 hours (100 $^{87}Sr/^{86}Sr$ ratios). For the Rb analysis the center filament was run throughout at 890°C, and side filament current adjusted to give a 3×10^{-11} amp ion beam for the larger Rb peak. Rb and Sr concentrations were calculated using atomic ratios recommended by Stieger and Jaeger (1977).

A total processing blank gave < 0.2 ng of both Rb and Sr; no blank corrections were needed for any samples (commonly, 5-10µg of Sr and 0.5-1.0µg). Multiple runs of a Sr concentration standard imply analytical reproducibility to ±0.2%. Reproducibility of analyses of aliquots of powder is about ±1%. It is expected that this may reflect sample heterogeneity as well as analytical effects.

The E&A $SrCO_3$ standard was run frequently to monitor machine drift. All analyses are reported corrected to a value of 0.70800 for this standard. Within a group of samples run together, the value obtained for the E&A standard generally gave agreement to ±0.00005 to ±0.00007 (2 σ n ≠0). Application of this machine correction adds a small but consistent error to the values for $^{87}Sr/^{86}Sr$ reported here.

APPENDIX 2

LOCATION AND DESCRIPTION OF METASEDIMENTARY ROCKS ANALYSED FOR RB, SR, AND $^{87}SR/^{86}SR$, NORTHERN PENINSULAR RANGES, SOUTHERN AND BAJA CALIFORNIA

1. Muscovite-biotite schist, French Valley Formation (PCSB-800), cutting for San Diego aqueduct west of Bachelor Mountain. Collected by L.T. Silver. Quartz, biotite, plagioclase, K-feldspar and opaque oxide in a fine-grained matrix of micas, opaques, and quartz. Cut by thin quartz veins.

2. Composite sample of reworked volcanic-lithic and crystal graywackes, Bedford Canyon Formation (Bedford Canyon Composite), Los Pinos Peak area, northern Santa Ana Mountains. Collected by L.T. Silver. Very approximately quartz (70%), chert+jasper fragments (15), plagioclase (10), K-feldspar (5) with minor biotite, zeolites, epidote or carbonate in some samples.

3. Biotite-sillimanite gneiss, eastern Lakeview Mountains (Lakeview Mtn. #6). Collected by L.T. Silver. Quartz (80), biotite (15), sillimanite (5).

4. Biotite quartzite, Sage (SCB 1712B). Quartz (65), biotite (25), irregular opaques (graphite?)(10) with minor plagioclase and very minor fibrolite.

5. Biotite-muscovite schist, roof pendant south of Banning (SCB 1725). Biotite (80) and muscovite (15), with sillimanite (fibrolite)(5) growing in micas; very minor quartz. Correlated with Desert Divide Group.

6. Biotite-muscovite schist, roof pendant south of Banning (SCB 1726). Biotite (40), muscovite (25), quartz (30), with sillimanite (fibrolite) (5) growing in micas; very minor K-feldspar. Correlated with Desert Divide Group.

7. Garnet-sillimanite gneiss, Thomas Mountain (SCB 779). Quartz (35), biotite(25), sillimanite (15), cordierite (10), K-feldspar (10), garnet (5); minor plagioclase. Cut by quartz+feldspar veins. Correlated with Desert Divide Group.

8. Garnet-sillimanite gneiss, Thomas Mountain (SCB 779A). K-feldspar (30), quartz (25), biotite (20), garnet (20), sillimanite (5); minor cordierite and plagioclase. Correlated with Desert Divide Group.

9. Quartzite, southeastern Thomas Mountain (SCB 746). Quartz (90), biotite (5), plagioclase (5). Correlated with Desert Divide Group.

10. Tourmaline schist, Desert Divide of southern San Jacinto Mountains (SCB 1729). Quartz (50), brown tourmaline (25), biotite (15) and

opaque (graphite?)(10); minor K-feldspar and plagioclase, very minor muscovite. Schist facies of Bull Canyon Formation, Desert Divide Grp.

11. Sillimanite gneiss, Desert Divide of southern San Jacinto Mountains. (SCB 1730. Quartz (35), K-feldspar (20), biotite (20), sillimanite (10), muscovite (5); minor plagioclase (An_{20}). Cut by veins of qtz+ +alkali-feldspar+whitemica (traces). Sample from schist facies of Bull Canyon Formation, Desert Divide Group.

12. Biotite-sillimanite gneiss, Red Tahquitz, San Jacinto Mountains (SCB 747A). Quartz (45), biotite (15), K-feldspar (15), cordierite (10), ilmenite (5), sillimanite (5), plagioclase (5). Lower part of Desert Divide Group.

13. Biotite-cordierite gneiss, Red Tahquitz, San Jacinto Mountains (SCB 747B). Quartz (70), biotite (10), cordierite (10), plagioclase (10); very minor muscovite. Lower part of Desert Divide Group.

14. Biotite-cordierite gneiss, Red Tahquitz, San Jacinto Mountains (SCB 747C). Quartz (70), plagioclase (15), biotite (10), cordierite (5); very minor muscovite. Lower part of Desert Divide Group.

15. Schist, Windy Point (SCB 1709A). Quartz (50), biotite (25), plagioclase (20), opaque (graphite?)(5); minor K-feldspar.

16. Calc-silicate, Windy Point (SCB 1709B-1). Diopside (35), quartz (20), plagioclase (15), biotite (15), brown hornblende (10), carbonate (5).

17. Biotite-rich layer from calc-silicate, Windy Point (SCB 1709B-2). Biotite (>75) with quartz, diopside, plagioclase, hornblende, and carbonate.

18. Plagioclase amphibolite, Windy Point (SCB 1709D). Quartz (40), brown amphibole (20), biotite (20), plagioclase (15), opaque (graphite?)(5); minor carbonate. Layered at the millimeter-scale; some layers contain >50% plagioclase.

19. Plagioclase amphibolite, Windy Point (SCB 1709E). Plagioclase (45), brown hornblende (25), biotite (15), quartz (15).

20. Quartzite, Terwilliger Valley (SCB 1724). Quartz (90), biotite (10); very minor muscovite, plagioclase, K-feldspar.

21. Layered gneiss, Vista Creek, near Ranchita (SCB 1720A). Quartz (40), K-feldspar (30), plagioclase (20), biotite (10); minor opaques, muscovite.

22. Layered gneiss, Vista Creek, near Ranchita (SCB 1720B). Quartz (30), K-feldspar (30), plagioclase (25), biotite (15); contains quartz-rich layers a few millimeters thick.

23. Gneiss, Lower Cottonwood Canyon (SCB 1716A). Quartz (50), plagioclase (40), biotite (10); minor K-feldspar.

24. Biotite-muscovite-cordierite gneiss, Box Canyon (SCB 1723). K-feldspar (20), quartz (20), biotite (20), plagioclase (15), muscovite (10), cordierite (5), sillimanite (fibrolite)(5).

25. Muscovite-biotite-cordierite gneiss, Garnet Mountain, Sunrise Highway (SCB 409A). Collected by L.T. Silver. Quartz (40), K-feldspar (20), muscovite (15), biotite (15), plagioclase (10).

26. Staurolite gneiss, Garnet Mountain, Sunrise Highway (SCB 409B). Collected by L.T. Silver. Quartz (30), plagioclase (20), K-feldspar (15), biotite (15), muscovite (15), staurolite (5).

27. Amphibolitic schist, Sunrise Highway south of Julian (SCB 1712). Amphibole (35), biotite (25), quartz (20), plagioclase (15), opaques (5); minor K-feldspar.

28. Muscovite-biotite schist, western Coyote Mountains (SCB 1717B). Muscovite (35), biotite (30), quartz (30), plagioclase (5), some minor ?andalusite.

29. Biotite gneiss, eastern Coyote Mountains (SCB 1718A). Quartz (50), muscovite (25), biotite (25); very minor tourmaline.

30. Biotite gneiss, eastern Coyote Mountains (SCB 1718B). Quartz (35), muscovite (30), biotite (30), andalusite (5); minor cordierite and garnet.

31. Fine-grained volcano-lithic siltstone, Alisitos Formation, south of Rancho Alisitos, Canon Santo Tomas, Baja California (BC-S-153). Collected by L.T. Silver. Plagioclase (20), larger opaques (5) and minor quartz in a matrix of chlorite, secondary oxides, and zeolites.

32. Volcanic-lithic sandstone, Alisitos Formation, northwest of Rancho Buenavista, foothills of the Sierra San Pedro Martir, Baja California (BC-S-9B). Collected by L.T. Silver. Altered volcanic-lithic clasts and abundant plagioclase phenocrysts in an altered matrix of carbonate, chlorite, zeolite and iron oxide minerals.

33. Biotite-muscovite schist composite sample from the roof pendant which underlies the National Astronomical Observatory, Sierra San Pedro Martir, Baja California (BC-S-401). Collected by L.T. Silver. Samples contain biotite, muscovite, quartz, plagioclase, K-feldspar, sillimanite and garnet, with minor tourmaline, sulphide, opaque oxide and graphite.

APPENDIX 3

USE OF GRID REFERENCES

Locations mentioned in the text can be found on the geological map (Plate 1) using the Grid References provided. These grid references are relative to the 1000-meter Universal Transverse Mercator grid, zone 11, 1927 North American Datum, and which is available on all recent topographic maps issued by the United States Geological Survey. This grid is superimposed on the geological map (Plate 1). A single six-digit number (e.g., G.R. 297414) gives the location of a particular location (in this case, San Jacinto Peak) to ±50 m. The first three digits give the east-west coordinates, the second three the north-south coordinates. Only the first two digits of the east-west and north-south coordinates are commonly shown on maps (these are the figures along the margins of Plate 1). The third digit is a decimal subdivision of this larger-scale grid, increasing from west-to-east and south-to-north.

For the example given above, San Jacinto Peak is 7/10 of the way between east-west grid numbers 29 and 30, and 4/10 of the way between north-south numbers 41 and 42.

APPENDIX 4

COMPARISON OF ALTERNATE METHODS (ISOTOPE DILUTION, X-RAY FLUORESCENCE SPECTROMETRY) FOR DETERMINATION OF RB AND SR CONCENTRATIONS

During the course of this project Rb and Sr concentrations have been determined on a substantial number of samples by two different analytical techniques, isotope dilution mass spectrometry (ID) and X-ray fluorescence spectrometry (XRF). The ID analytical data were obtained by the author in the laboratories of Prof. L.T. Silver in the Division of Geological and Planetary Sciences, California Institute of Technology, Pasadena. The XRF data were provided by Dr B.W. Chappell, and were obtained in his laboratories in the Department of Geology, Australian National University, Canberra. Comparative data for 97 samples of both igneous and metasedimentary rock are available. Analytical procedures are detailed elsewhere (ID: Appendix 1; XRF: Norrish and Hutton, 1969, Norrish and Chappell, 1977).

Figures A4.1 and A4.2 show graphically the percentage difference obtained for aliquots of a single sample by the two different techniques. Estimated precision for both elements is ± 5% by XRF and ± 1% by ID.

All the Sr data agree to much better than expected by a simple combination of the expected analytical errors estimated for the two different techniques.

The Rb data obtained by the two methods do not agree as well. The different symbols on Fig. A4.2 differentiate batches of samples

Figure A4.1. Comparison of isotope dilution (ID) and X-ray fluorescence (XRF) data for Sr for samples analysed in the present study.

Different symbols represent samples prepared at different times. See text for discussion.

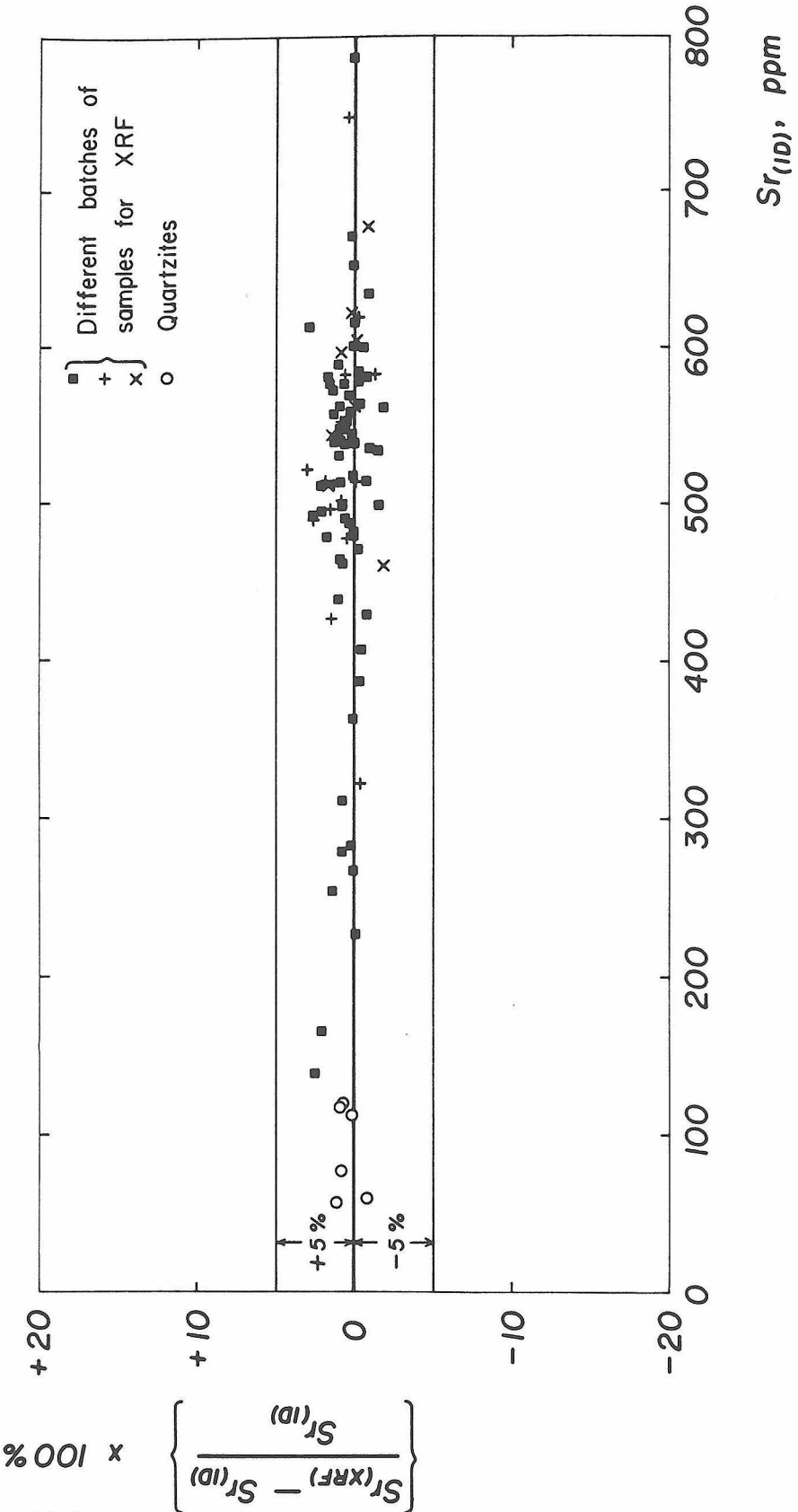
Different batches of samples for XRF
Quartzites
+5%
-5%
+20
+10
0
-10
-20
0
100
200
300
400
500
600
700
800
Sr(ID), ppm
{ (Sr(XRF) − Sr(ID)) / Sr(ID) } x 100%

Figure A4.1

Figure A4.2. Comparison of isotope dilution (ID) and X-ray fluorescence (XRF) data for Rb for samples analysed in the present study.

Different symbols represent samples prepared at different times. See text for discussion.

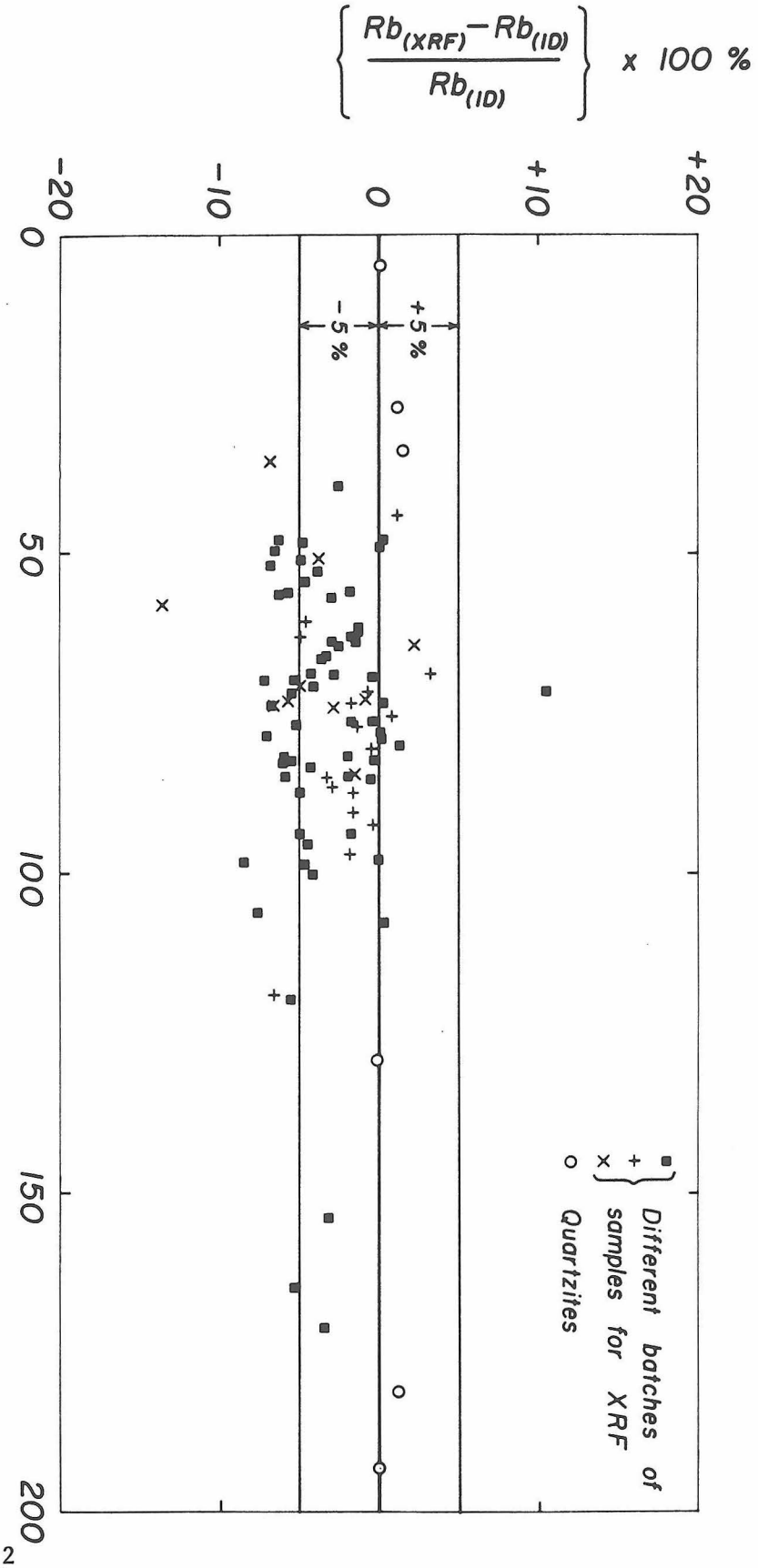
$\left\{\frac{Rb_{(XRF)}-Rb_{(ID)}}{Rb_{(ID)}}\right\} \times 100\ \%$
+20
+10
0
−10
−20
+5 %
−5 %
0
50
100
150
200
$Rb_{(ID)}$, ppm
Different batches of samples for XRF
Quartzites

Figure A4.2

prepared at different times using slightly different techniques. Samples represented by either (+) or (X) were not crushed for as long as samples represented by ( ) or (o). As a result, the earlier samples (+,X) may be somewhat coarser grained, and in particular contain relatively large flakes of biotite. This can lead to problems in either obtaining a representative aliquot of sample, or to matrix effects in the XRF analysis because of non-random orientation of grains in the pressed powder pellets used for the Rb and Sr determinations.

For example, if, for a rock containing 10 wt.% biotite the biotite flakes after crushing were circular sheets with a diameter of 1 mm and a thickness of 1 μ , sampling alone could give a variation ($\sqrt{n}$, n=number of biotite flakes) of ± 1.5%. If the sheets had a similar thickness but were 100 μ in diameter, the potential error in sampling falls to ± 0.2%.

Two other likely sources of error exist - imperfect analytical techniques, and differing standardization. An example of systematic bias resulting from standardization against a non-stoichiometric salt has been reported by de Laeter et al. (1973), who found that standardization against 'Specpure' RbCl gave systematic over-estimation of Rb by 1.7% relative to standardization against the stoichiometric salt (NBS Std. RbCl SRM #984).

The spikes used for the determination of Rb concentration in the present study were originally calibrated against an aliquot of NBS SRM #984 stoichiometric RbCl. The most likely cause of systematic bias in the isotope dilution analysis results from evaporation of the spike solution, leading to underestimation of the concentration of the element

in the sample. Two spike solutions of different Rb concentration were used randomly throughout the present work, and no systematic bias between the two solutions (compared to the XRF data) is apparent. The use of two different spike solutions should guard against the accidental contamination of one solution.

Replicate analyses of a standard Sr solution imply reproducibility in combined sample and spike delivery at the level of ± 0.2%. This suggests that the error introduced by a single spike delivery is ± 0.15%. Combined weighing errors (beaker,beaker+sample) are estimated to be of order ± 0.2% for a single sample, giving a combined estimate of reproducibility of ± 0.28% (combining errors as $s_T^2 = s_1^2 + s_2^2$). Spike solutions were delivered over a substantial range of temperatures, introducing another source of error of perhaps ± 0.15%. This error will cancel out in the determination of $^{87}Rb/^{86}Sr$, and in the analysis of standard solutions (E&A $SrCO_3$, NBS 987), but combines with the spiking and weighing errors to give an estimate of ± 0.3% (1σ) for a single concentration analysis. The sampling errors outlined above suggest that replication of aliquots of a particular sample are unlikely to be reproducible to this level.

XRF values are reported referenced to values of 523.3 ppm Rb for NBS 70a K-feldspar (B.W. Chappell, personal communication, 1983; Compston et al., 1969) and 660 ppm Sr for AGV-1 (B.W. Chappell, personal communication, 1983). Chappell et al., (1969) give further details on the analytical procedures used for Rb and Sr.

It is concluded that agreement for Sr between the two independent techniques in the two laboratories is excellent. There appears to

be a small unexplained bias between the two laboratories (the XRF values are consistently about 3% lower than the ID values). Excess scatter in the comparison of the Rb data probably reflects both sample heterogeneity and mica alignment within the pressed powder pellets used for the XRF analysis resulting from poor sample preparation (grinding).